ASA TECHNICAL
MEMORANDUM

NASA TM X-2509

ACE SHUTTLE AEROTHERMODYNAMICS CHNOLOGY CONFERENCE

lume IV - Operational Flight Mechanics

! at
s Resea: -h Center
ett Field, California
mber 15-16, 1971

ONAL AERONAUTICS AND SPACE ADMINISTRATION • WASHINGTON, D. C. • FEBRUARY 1972

1. Report No. NASA TM X-2509	2. Government Accession No.	3. Recipient's Catalog No.
4. Title and Subtitle SPACE SHUTTLE AEROTHERMODYNAMICS TECHNOLOGY CONFERENCE VOLUME IV - OPERATIONAL FLIGHT MECHANICS		5. Report Date February 1972
		6. Performing Organization Code
7. Author(s)		8. Performing Organization Report No. L-8136
		10. Work Unit No.
9. Performing Organization Name and Address NASA Langley Research Center Hampton, Va. 23365		11. Contract or Grant No.
		13. Type of Report and Period Covered Technical Memorandum
12. Sponsoring Agency Name and Address National Aeronautics and Space Administration Washington, D.C. 20546		14. Sponsoring Agency Code

15. Supplementary Notes

Held at NASA Ames Research Center, December 15-16, 1971.

16. Abstract

The conference encompasses four technology efforts, each published as a seprate volume.

Volume I - Flow Fields (NASA TM X-2506)

Volume II - Heating (NASA TM X-2507)

Volume III - Aerodynamics (NASA TM X-2508)

Volume IV - Operational Flight Mechanics (NASA TM X-2509)

17. Key Words (Suggested by Author(s))	18. Distribution Statement
Flow fields Heating Aerodynamics Operational flight mechanics Space shuttle Aerothermodynamics	Unclassified - Unlimited

19. Security Classif. (of this report)	20. Security Classif. (of this page)	21. No. of Pages	22. Price*
Unclassified	Unclassified	491	$6.00

*For sale by the National Technical Information Service, Springfield, Virginia 22151

PREFACE

A Space Shuttle Technology Conference on Flow Fields, Heat Transfer, Aerodynamics, and Operational Flight Mechanics was held at the NASA Ames Research Center on December 15 and 16, 1971. The objective of this conference was to review the broad base of aerothermodynamics technology developed for the space shuttle during the period of the Phase B studies and, thereby, help focus attention on the technology required for further space shuttle development. This publication is a compilation of the conference papers. It has been divided into four volumes, one for each of the sessions. Five papers which were omitted from the oral presentation at the conference are included in this publication. Contributing organizations include U.S. Aerospace Contractors, Universities, Canadian and European Space Agencies, in addition to NASA Research Centers.

CONTENTS

VOLUME II.- HEATING

VOLUME III.- AERODYNAMICS

VOLUME IV.- OPERATIONAL FLIGHT MECHANICS

GLOSSARY

ABES	air breathing engines
ACPS	attitude control propulsion system
AEDC	Arnold Engineering Development Center
AFB	air force base
AFFDL	Air Force Flight Dynamics Laboratory
ALT	altitude
APS	auxiliary propulsion system
AR	aspect ratio
ARC	Ames Research Center
ARDC	Air Research and Development Command
BECO	booster engine cutoff
BLOW	booster lift-off weight
BV	body-vertical tail
BW	body-wing
BWV	body-wing-vertical tail
CAL	Cornell Aeronautical Laboratory
CALCS	calculations
CAL HST	Cornell Aeronautical Laboratory hypersonic shock tunnel
CFHT	continuous-flow hypersonic tunnel
CG; C.G.; c.g.	center of gravity
CONFIG	configuration
CRT	cathode ray tube
Cyl	cylinder
2-D	two-dimensional
3-D	three-dimensional

DAC	Douglas Aircraft Company
DCM	data control management
DEX	exit diameter
DIA	diameter
DIAT	diatomic
DIF. REFL.	differential deflection
3DMoC	three-dimensional method of characteristics
DOD	Department of Defense
DOF	degrees of freedom
DWO	delta-wing orbiter
EHT	external hydrogen tank
EOHT	external oxygen-hydrogen tank
EPL	emergency power level
EST	estimated
ETR	eastern test range
F&M	force and moment
FAR; F.A.R.	Federal Aircraft Regulation
FBS	flyback system
F.D.	finite difference
F/O	fuel-oxygen ratio
FO/FS	fail operational/fail safe
FPR	flight performance reserve
FPRE	flat-plate reference enthalpy
FR	fully reusable
FREQ	frequency
GAC	Grumman Aerospace Corporation

GD	General Dynamics
GDC	General Dynamics Corporation
GD/C	General Dynamics/Convair
G.E.	General Electric Company
GLOW	vehicle gross lift-off weight
GTOP	general trajectory optimization program
GW	gross weight
H	hydrogen
HCF	highly compacted fibers
HCR	high cross range
HeT	Mach 20 helium tunnel
HO	hydrogen-oxygen system
H.W.T.	hypersonic wind tunnel
IAC	industrial air center
IBFF	impulse base flow facility
ICD	interface control drawing
IFR	instrument flight rules
ILRV	integral launch and reentry vehicle
ILS	instrument landing system
IND	industrial
IR	infrared
IRAD	Independent Research and Development
KSC	Kennedy Space Center
L.E.	leading edge
LEE	leeward
LH_2	liquid hydrogen

LMSC	Lockheed Missiles & Space Company
LO_2; LOX	liquid oxygen
LRC; LaRC	Langley Research Center
LRU	link retraction unit
MAC	mean aerodynamic chord
MAC Exp	exposed mean aerodynamic chord
MARK I, MARK II	shuttle configurations
MAX	maximum
MC	Monte Carlo
MCAIR	a low-speed wind tunnel
MCAS	Marine Corps Air Station
MDAC	McDonnell Douglas Astronautics Company
MDC	McDonnell Douglas Corporation
MIL SPEC	military specification
MIN	minimum
MM HWT	Martin Marietta Corporation hotshot wind tunnel
MOC	method of characteristics
MPL	minimum power level
MSC	Manned Spacecraft Center
MSFC	Marshall Space Flight Center
MT.	mountain
NA	North American
NAE; N.A.E.	National Aeronautical Establishment
NAR; NARC; NR	North American Rockwell Corporation
NAS	Naval Air Station
NASA	National Aeronautics and Space Administration

NO.; No.	number
NOZ	nozzle
NPL	normal power level
O/F	oxygen-fuel ratio
OLOW	orbiter lift-off weight
OMS	orbiting maneuvering system
P/L	payload
PM	pitching moment
RCC	reinforced carbon carbon
RCS	reaction control system
Ref	reference
REQD	required
RFP	request for porposals
RGAS	real gas
R.H.	right hand engine
RSI	reusable surface insulation
RTV	room-temperature vulcanizing rubber
S&C	stability and control
SCT	shock capturing technique
SF	stick force
S.L.; SL	sea level
SM	service module
SPEC	specification
SRM	solid rocket motors
SS	stainless steel
SSV	space shuttle vehicle
ST	straight

STAR	strings and array computer; self-testing and repair computer
STD	standard
STI	Systems Technology, Incorporated
STOL	short take-off and landing
SW	southwest
SYM	symbol
T/C	thermocouple
T.E.	trailing edge
T.E.D.	trailing edge down
TEMP	temperature
T.E.U.	trailing edge up
THEO	theoretical
TPS	thermal protection system
TRAJ	trajectory
TVC	thrust vector control
Typ	typical
UPWT	Unitary Plan wind tunnel
USAF	U.S. Air Force
VAC HVWT	Vought Aeronautics Company hypervelocity wind tunnel
VAFB	Vandenburg Air Force Base
VDT	variable density tunnel
VFR	visual flight rules
V/STOL	vertical and short take-off and landing
w/o	without
WT	weight
WWD	windward
YM	yawing moment

OPERATIONAL FLIGHT MECHANICS SESSION

INTRODUCTION

by

Victor L. Peterson

NASA Ames Research Center

The objective of this session is to present an overview of the technology program dealing with operational flight mechanics. Like the other technical areas discussed at this conference, part of the effort to be reported deals with applications of existing technology while the other part deals with the development of new technology. Existing technology is applied either to provide results upon which program decisions can be made or to uncover new problem areas needing attention. Of course, new technology must be developed when problems are uncovered that cannot be solved by existing techniques. In the area of flight mechanics, most of the effort currently is directed toward the "tooling up" for applying existing problem solving methods to the space shuttle system.

The first paper in the session presents results which clearly show that the use of an orbiter having external hydrogen and oxygen tanks would result in a shuttle system having development costs and technological risks substantially lower than for a system in which the propellant tanks are internal to the orbiter. The remaining papers treat flight-mechanics problems associated with ascent to orbit, abort staging, and booster and orbiter recovery.

VEHICLE PERFORMANCE IMPACT ON SPACE SHUTTLE DESIGN AND CONCEPT EVALUATION

By Mark K. Craig
NASA, Manned Spacecraft Center
Houston, Texas

INTRODUCTION

The continuing examination of widely varied space shuttle concepts makes an understanding of concept interaction with vehicle performance imperative. The estimation of vehicle performance is highly appurtenant to all aspects of shuttle design and hence performance has classically been a key indicator of overall concept desirability and potential. In this paper vehicle performance assumes the added role of defining interactions between specific design characteristics, the sum total of which define a specific concept. Special attention is given to external tank effects.

35

SPACE SHUTTLE CONCEPT EVOLUTIONARY PROCESS

(Figure 1)

The evolution of a space shuttle vehicle is by nature an iterative process. Each element driving the concept synthesis is highly dependent upon each other element. For convenience we may classify the principal synthesis drivers in three categories: cost, deployment, and design and performance. Of these three, we at this meeting are concerning ourselves with design and performance. It is appropriate, therefore, to subdivide the broad category design and performance into working groups which encompass specific engineering disciplines. To this end consider the groupings, which shall be designated shaping and protection, propulsion, and mission considerations.

Shaping and protection considerations subsume those aspects of the vehicle which must be introduced to protect the payload and to allow the vehicle to perform its mission potential in an acceptable fashion. Shaping and protection would include the vehicle's body, aerodynamic surfaces, and thermal protection.

Propulsion considerations are introduced by the requirement that the payload be physically transferred from one state to another. Thus all vehicle components necessary to produce a thrust acceleration are termed propulsive.

Mission considerations are those components of the vehicle system responsible for the successful completion of the prescribed system goal. Included, therefore, are the avionics and control systems. Man, as pilot, is essential to completion of the total mission so he, too, must be included.

The iterative nature of the shuttle evolutionary process is most visibly manifest in the interaction between the design and performance groupings listed above. This paper will identify, explain, and subsequently investigate the primary channels of these interactions.

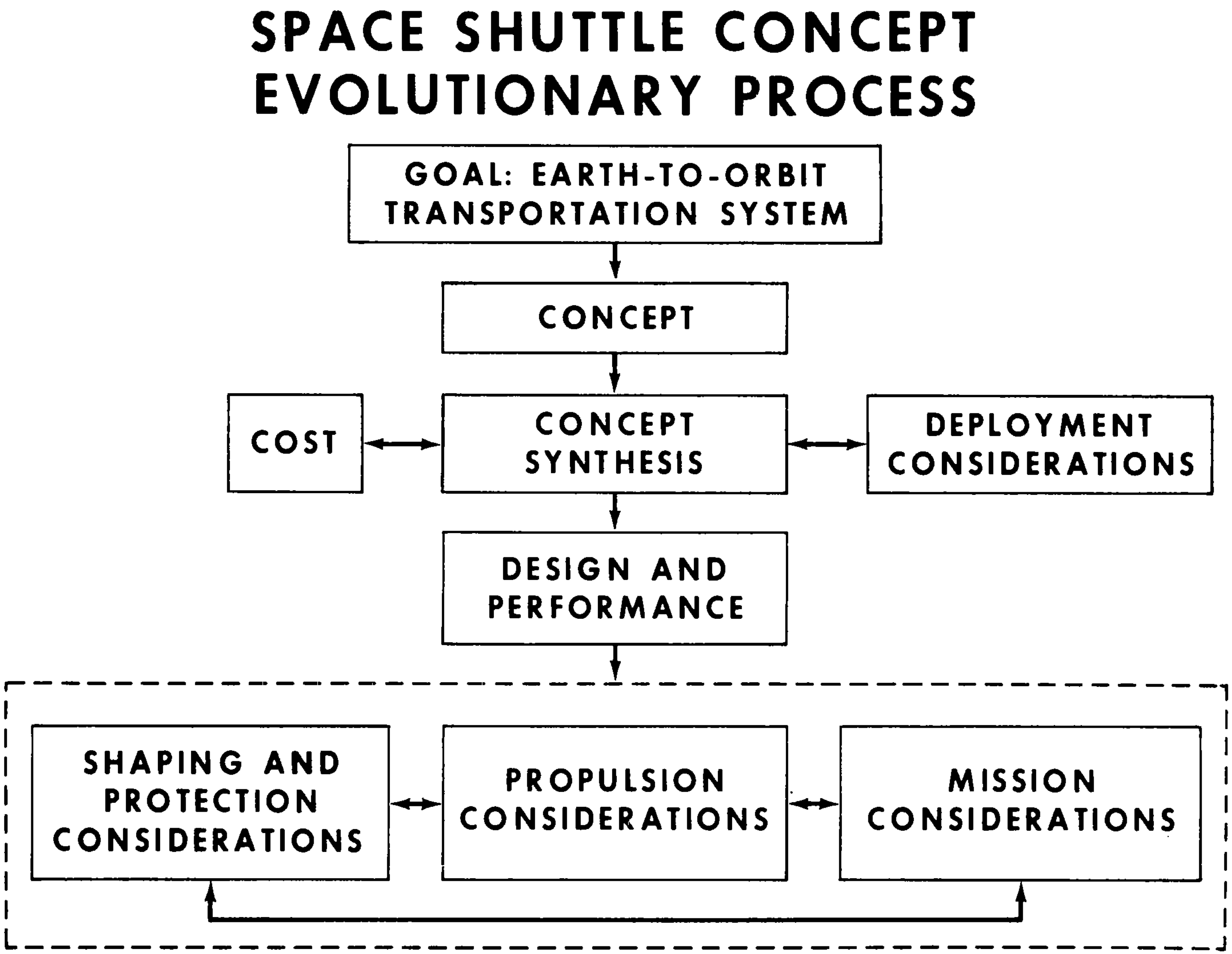
SPACE SHUTTLE CONCEPT EVOLUTIONARY PROCESS
GOAL: EARTH-TO-ORBIT TRANSPORTATION SYSTEM
CONCEPT
COST
CONCEPT SYNTHESIS
DEPLOYMENT CONSIDERATIONS
DESIGN AND PERFORMANCE
SHAPING AND PROTECTION CONSIDERATIONS
PROPULSION CONSIDERATIONS
MISSION CONSIDERATIONS

Figure 1

DESIGN AND PERFORMANCE PENALTY COMPONENTS

(Figure 2)

The logical abstraction of figure 1 can be formulated in an analytic sense by expressing dependencies in terms of physical parameters, the most obvious of which is weight. The relative magnitudes of the shaping and protection, the propulsion, and the mission penalties, for a typical vehicle, are given in figure 2. As is to be anticipated, the propulsion penalty is far greater than either of the other two, its predominance attributable to the large quantity of propellants. The impact of vehicle performance on design, then, will be concerned primarily with the variation of propellant loading with mission requirements and the resultant efficiency with which the propellants are contained.

DESIGN AND PERFORMANCE PENALTY COMPONENTS

PENALTY	SHAPING AND PROTECTION	PROPLUSION	MISSION
PENALTY COMPONENTS	BODY STRUCTURE WING TAIL TPS LANDING GEAR	MAIN ENGINES PROPELLANT SYSTEMS TANKS PROPELLANTS THRUST STRUCTURE ATTITUDE CONTROL SYSTEM ON-ORBIT PROPULSION	POWER SOURCE HYDRAULIC SYSTEM ENGINE GIMBAL AVIONICS ENVIRONMENTAL SYSTEM SURFACE CONTROLS PERSONNEL PROVISIONS ELECTRICAL SYSTEM PERSONNEL
PERCENT OF GROSS ORBITER WEIGHT (EXCLUDING PAYLOAD)	15	83	2

Figure 2

SIZING DEPENDENCE ON STRUCTURE FACTOR

(Figure 3)

A parameter essential to an understanding of the impact of vehicle performance on sizing is the stage structure factor, σ. The structure factor is defined as the stage gross weight, W_o, minus the propellant weight, W_p, minus the payload, W_{PLD}, divided by the gross weight minus the payload. The structure factor, then, is that fraction of the stage weight which is not usable propellant, and as such, it represents a propellant packaging efficiency. A high structure factor indicates that a particular vehicle is an inefficient propellant container.

Figure 3 indicates the degree to which stage gross weight is dependent on structure factor and stage characteristic velocity. A propulsion specific impulse of 459 seconds was assumed. At low characteristic velocities the difference between vehicle gross weights with different structure factors is small. As characteristic velocity increases, however, vehicles with higher structure factors begin to experience exponential growth in gross weight. Vehicles with lower structure factors approach exponential gross weight growth as the characteristic velocity continues to increase. The net effect of structure factor, then, is to determine the vehicle performance region in which gains in performance are offset by unacceptable gains in vehicle gross weight.

SIZING DEPENDENCE ON STRUCTURE FACTOR

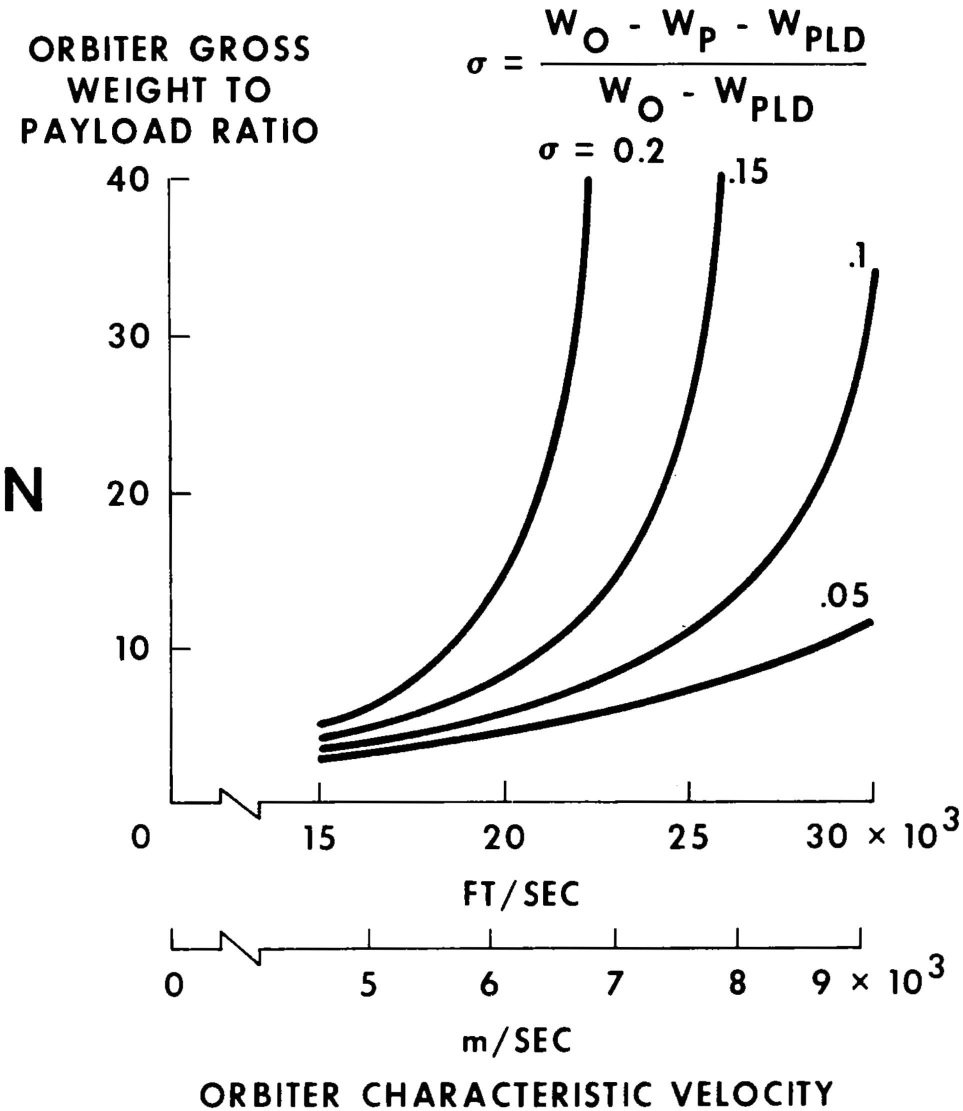

Figure 3

CONCEPT IMPACT ON VEHICLE DESIGN AND PERFORMANCE

(Figure 4)

The implications of stage structural factor can be illustrated in no better way than by examining the impact of three current orbiter concepts on system performance. The three concepts to be considered are internal propellant tanks, internal oxygen tank and external hydrogen tank (EHT), and external oxygen-hydrogen tanks (EOHT). Examples of these vehicles are the NR 161-C, the GAEC H-33, and the NASA 040A Mark II, respectively. All three vehicles are fueled by LOX-LH_2, have high chamber pressure engines, and have a 40,000 pound (18,144 kg) payload capability to polar orbit. The size of the payload bay in each is 15 x 60 ft (4.9 x 19.7 m).

External tanks diminish the structural factor by isolating those penalties to the vehicle structure which accrue from propellant storage. As a consequence of this penalty partitioning, weight savings are generated on two primary levels. Initially, because at least a major portion of the propellant volume is external, the physical size, and thus weight, of the core vehicle can be greatly reduced, as is readily apparent from figure 4. This initial reduction in size, coupled with the fact that the external tanks are jettisoned at orbit injection, prompts yet another weight savings. Once the vehicle jettisons its external tanks, the weight at which it performs certain mission sequences is much less than the weight of its internal tank counterpart. Thus mission sequence dependent weights, such as landing systems and on-orbit propulsion systems, are reduced.

Reduction of aggregate vehicle weight prompts an improvement in performance. Examination of the gross weight-characteristic velocity capabilities of the internal tank and external tank orbiters reveals that a 50% increase in performance from the internal tank to the EOHT vehicle has been achieved with a 30% increase in gross weight.

The internal tank vehicle having been shown to possess a relatively poor structural factor, with little outlook for improvement, a detailed study of the performance-design characteristics of external tank vehicles follows.

CONCEPT IMPACT ON VEHICLE DESIGN AND PERFORMANCE

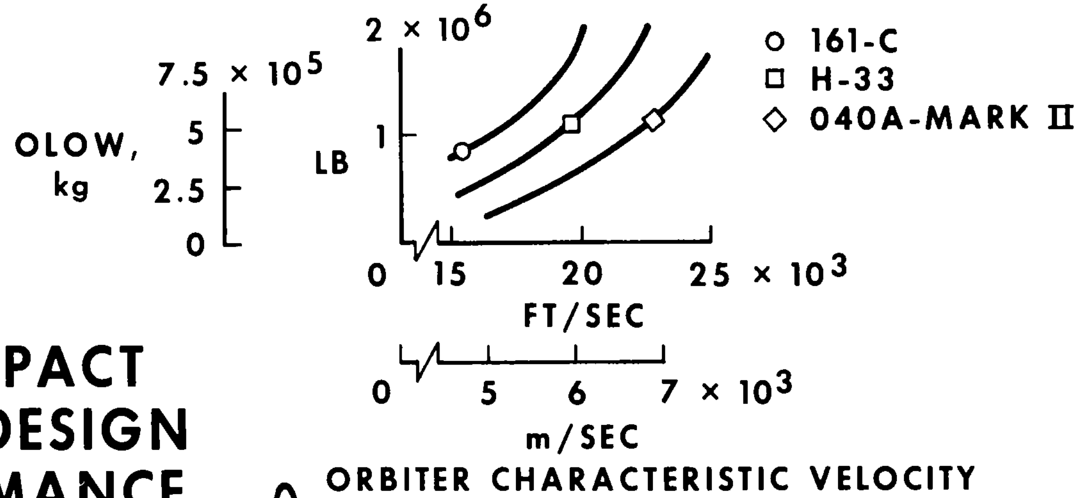

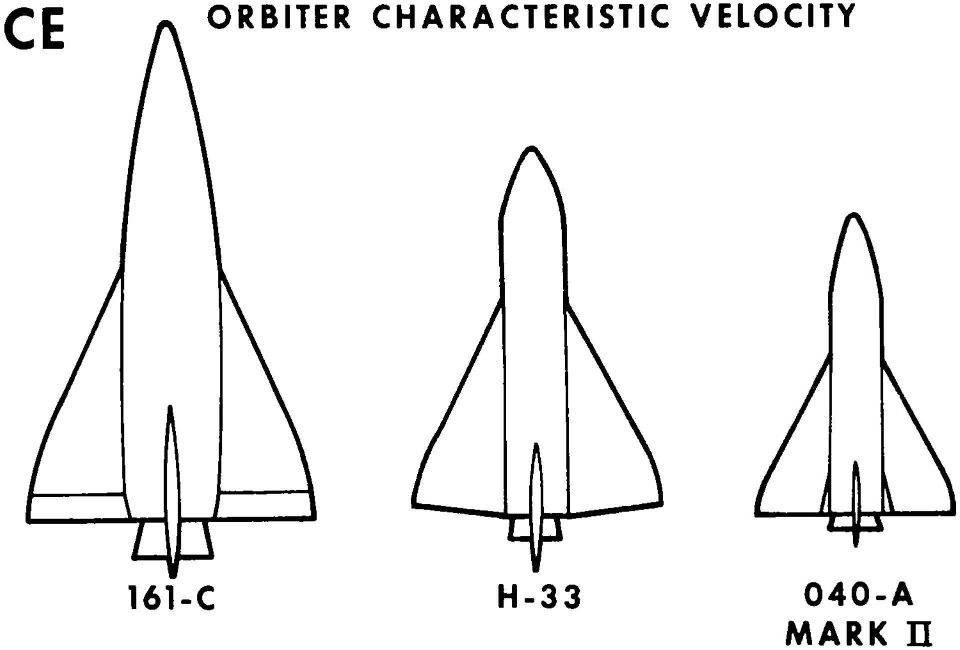

Figure 4

STUDY VEHICLE CHARACTERISTICS

(Figure 5)

In a study of the interactions of vehicle performance with system concept and design, a commonality of certain concept characteristics is desirable to assure consistent interpretation of the results. Allow this study to be premised, then, with the following primary assertions:

(1) orbiter propellant is liquid oxygen (LOX) and liquid hydrogen (LH_2);

(2) the orbiter has three high chamber pressure engines of variable thrust level, the specific impulses of which are 459 seconds;

(3) the vehicle is flown to a polar mission with insertion into a 50 x 100 n.m. (92.5 x 185 km) orbit;

(4) the orbiter is sized to carry 40,000 lb (18, 144 kg) payload both into orbit and back from orbit.

In addition to these, several secondary assumptions have been made:

(5) the orbiter has a cryogenic on-orbit propulsion system capable of a 650 ft/sec (198 m/sec) velocity increment;

(6) 1% flight performance reserve (FPR) propellant has been allotted to the orbiter.

STUDY VEHICLE CHARACTERISTICS

- LOX-LH_2 PROPELLANT
- 3 HIGH CHAMBER PRESSURE ENGINES
- POLAR MISSION
- 40,000 LB PAYLOAD UP/DOWN

Figure 5

ORBITER GROSS WEIGHT DEPENDENCE ON VELOCITY CAPABILITY

(Figure 6)

The orbiter lift-off weight (OLOW) here experiences the trends which were described previously. The EHT vehicle demonstrates a much higher sensitivity to characteristic velocity than the EOHT vehicle, the sensitivity a consequence of a higher stage structural fraction. One additional effect has been included here, however, and that is the effect of the orbiter vacuum thrust-to-weight ratio, T/W. As the thrust-to-weight ratio increases the stage structural fraction is made yet greater by the increasing propulsion system weights. Hence, the higher thrust-to-weight ratios are more performance-sensitive than the lower thrust-to-weight ratios for both the EHT and EOHT orbiters.

ORBITER GROSS WEIGHT DEPENDENCE ON VELOCITY CAPABILITY

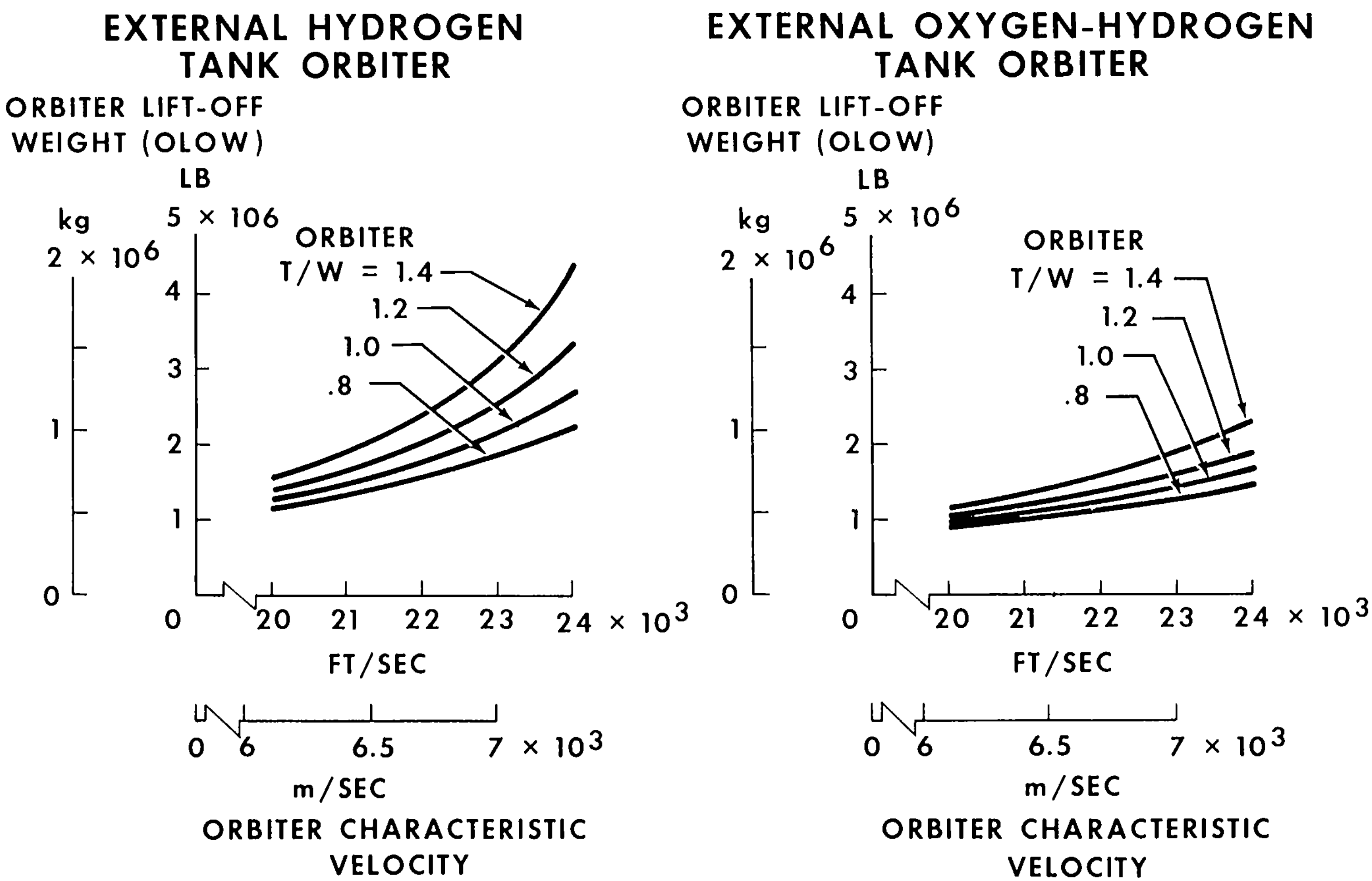

Figure 6

ORBITER INERT WEIGHT DEPENDENCE ON VELOCITY CAPABILITY

(Figure 7)

The orbiter core inert weight is the weight of the orbiter exclusive of all expendable propellants and the external tanks. Core inert weight sensitivity to characteristic velocity, then, relates trends in vehicle growth without explicit reference to the external tank growth characteristics. The structural factor of the EOHT vehicle is influenced only by the changing engine thrust level and its corresponding perturbation of propulsion system weights. The structure factor of the EHT vehicle, however, while influenced by the propulsion penalty, must also take into account the penalty associated with the internal oxygen tank. The resultant structure factor for the EHT vehicle is somewhat greater than that of the EOHT vehicle.

ORBITER INERT WEIGHT DEPENDENCE ON VELOCITY CAPABILITY

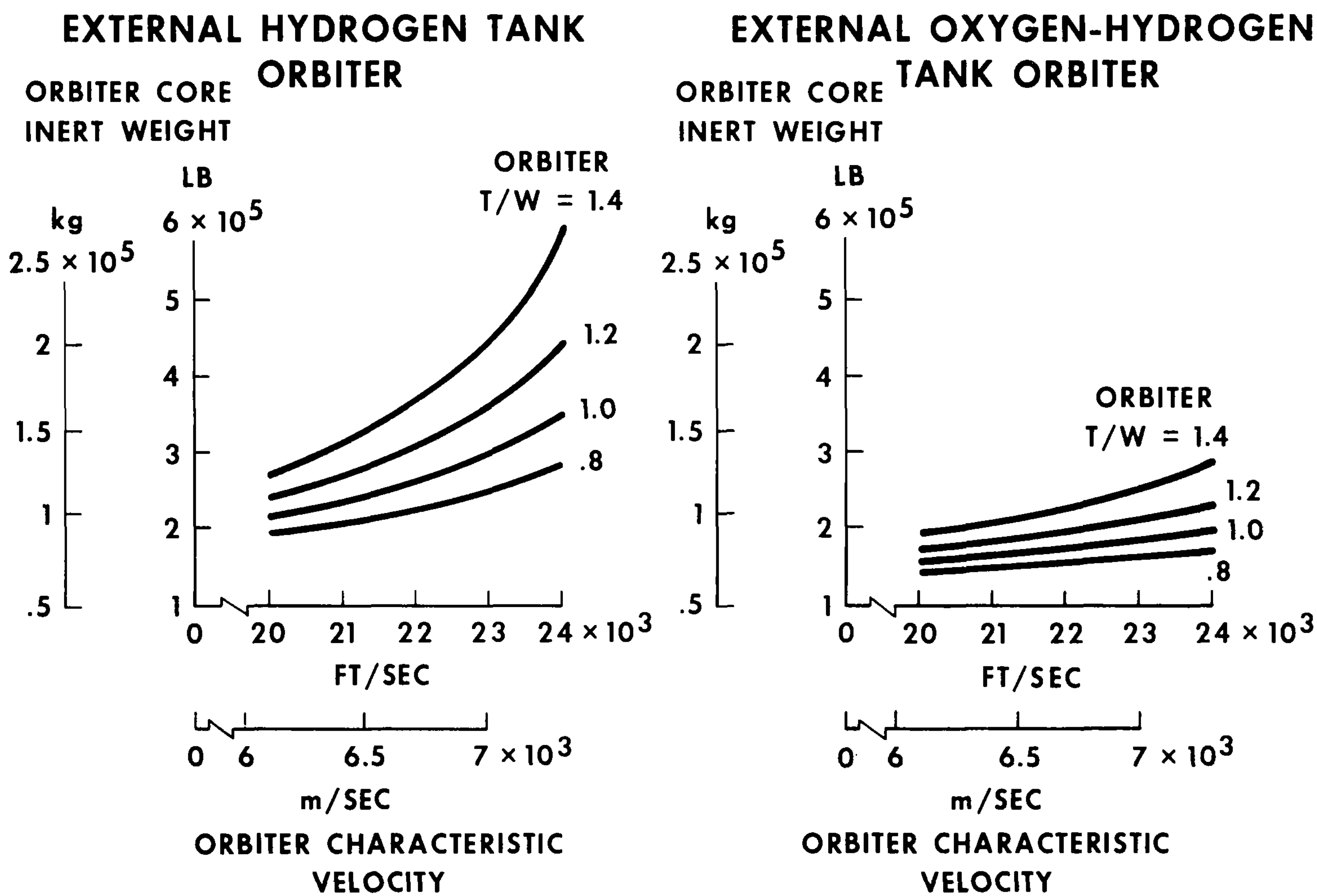

Figure 7

EXTERNAL TANK DRY WEIGHT DEPENDENCE ON VELOCITY CAPABILITY

(Figure 8)

The small weight differential between the external hydrogen tank and the external oxygen-hydrogen tank is deceiving. For a given characteristic velocity, the ratio of the propellant loading of the EHT vehicle to that of the EOHT vehicle is equal to the ratio of the gross weights (figure 6). For moderate thrust-to-weight ratios, the EHT vehicle has approximately 50% more propellant than the EOHT vehicle. Assuming an oxidizer-to-fuel ratio of 6:1, then, the EHT vehicle's external tank contains only 20% of the propellant, by <u>weight</u>, contained in the EOHT vehicle's external tank. The EHT vehicle's external tank, however, weighs 80% of the EOHT vehicle's tank.

This apparent anomaly is made clear when one recognizes the key role which propellant density, and thus tank volume, play in determing tank weight. Liquid oxygen, with a density 16 times greater than that of liquid hydrogen, can be contained in 1/16 the volume. Thus, while the EHT vehicle's external tank contains only 20% of the EOHT vehicle's propellant by weight, it may contain as much as 90% of the EOHT vehicle's propellant by volume.

At the higher orbiter thrust-to-weight ratios, and hence higher stage structural factors, the EHT vehicle propellant loadings are so much greater than the EOHT vehicle propellant loadings that the volume penalty for the storage of LH_2 becomes so prohibitive that the external oxygen-hydrogen tank is actually lighter than the corresponding external hydrogen tank.

EXTERNAL TANK DRY WEIGHT DEPENDENCE ON VELOCITY CAPABILITY

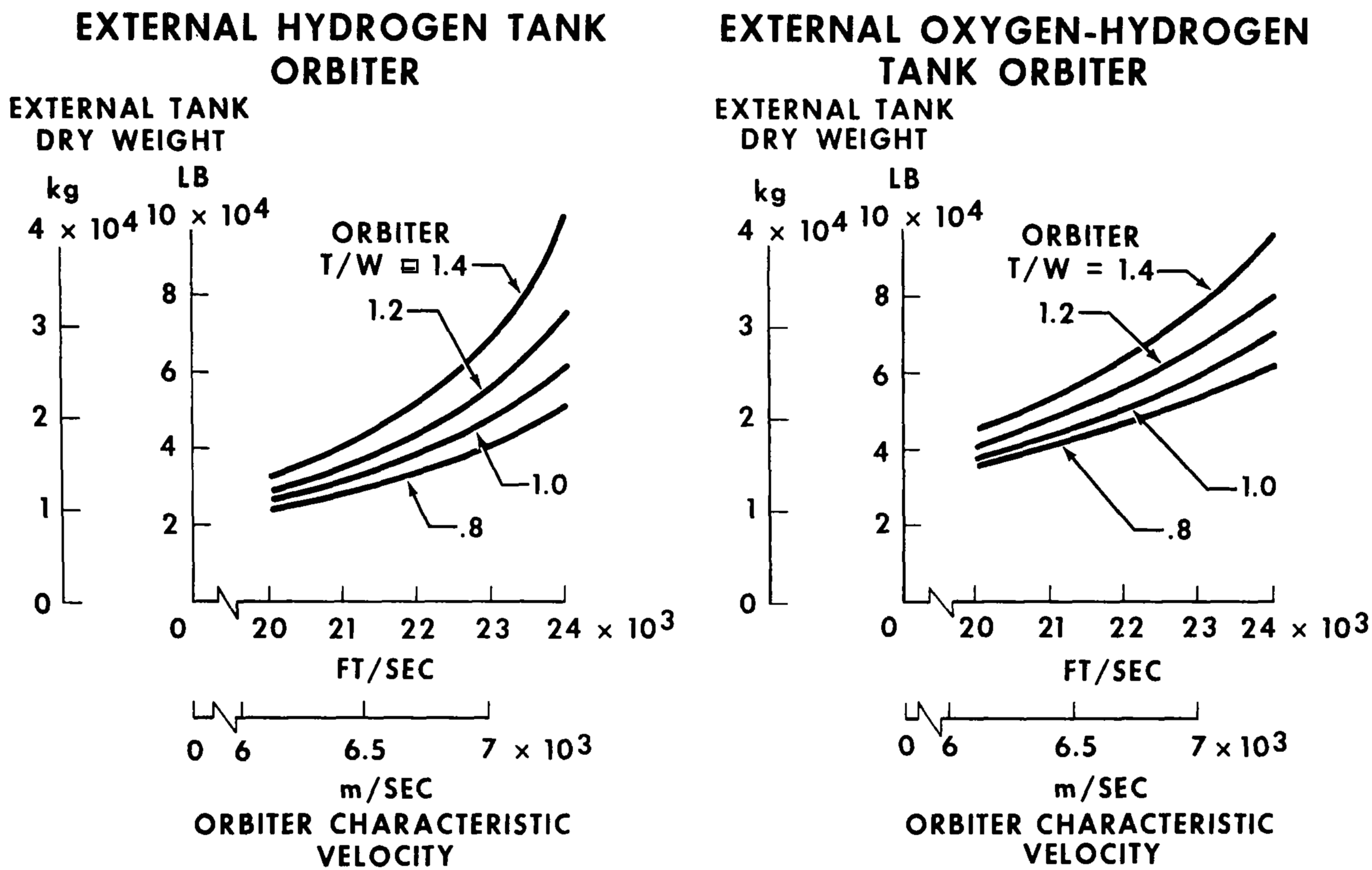

Figure 8

ORBITER CHARACTERISTIC VELOCITY DEPENDENCE ON STAGING VELOCITY

(Figure 9)

While orbiter characteristic velocity is an excellent reference from which to examine certain basic vehicle design and performance relationships, its limited scope does not bring to light certain other effects which must be examined. The introduction of gravity and steering losses to the characteristic velocity forms the generalized staging velocity curves of figure 9.

The orbiter thrust-to-weight ratio is introduced as a necessary third parameter. At low thrust-to-weight ratios the effect on characteristic velocity becomes quite marked as the burn time to orbit insertion, and thus the propellant loading, increase exponentially.

A 1% flight performance reserve (FPR) allocation is accounted for in these curves.

ORBITER CHARACTERISTIC VELOCITY DEPENDENCE ON STAGING VELOCITY

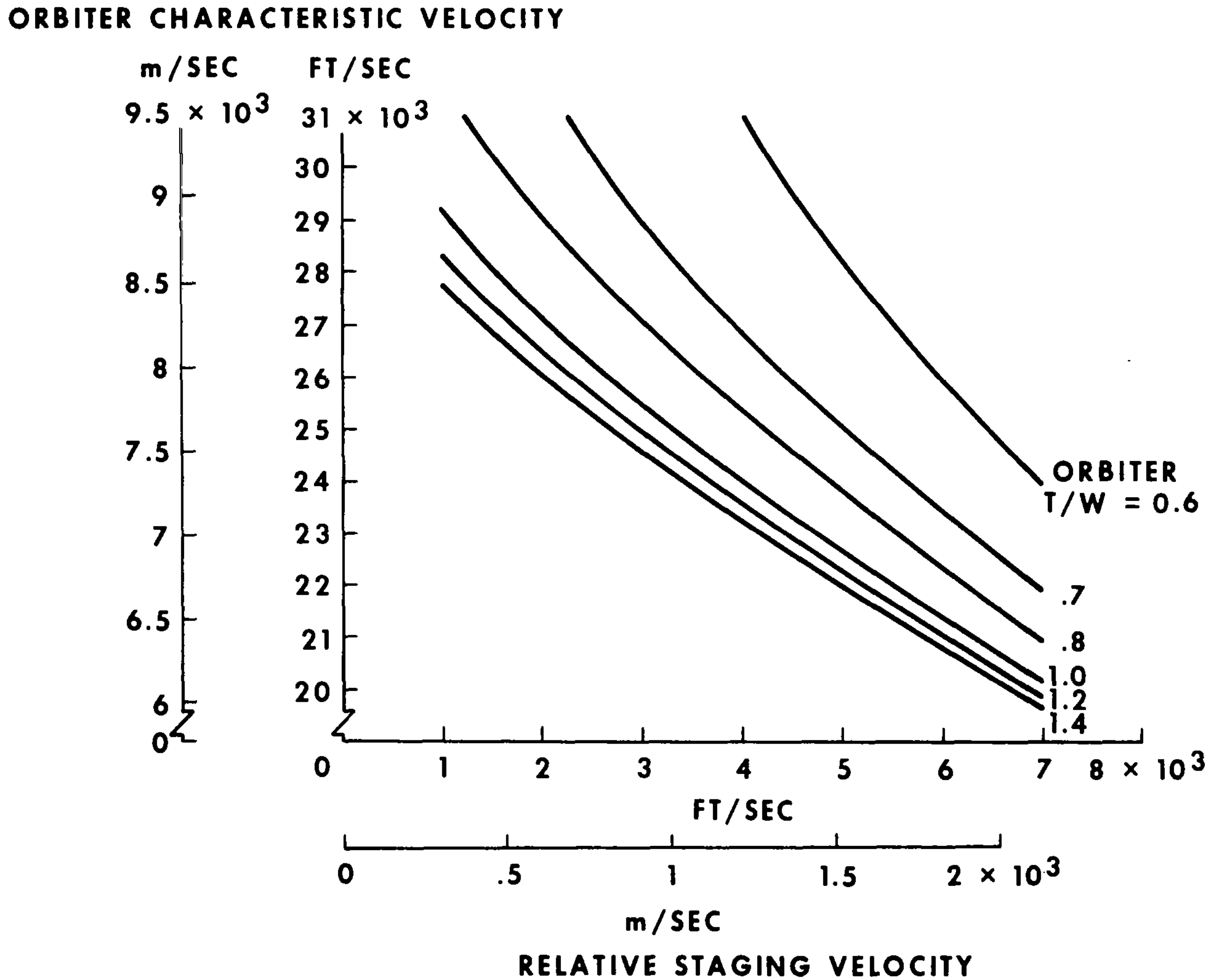

Figure 9

ORBITER GROSS WEIGHT DEPENDENCE ON STAGING VELOCITY

(Figure 10)

The low orbiter thrust-to-weight ratios which appeared attractive when considered only on the evidence of orbiter characteristic velocity, now appear rather undesirable. As was pointed out previously, low orbiter thrust-to-weight ratios increase the vehicle's burn time and thus the gravity losses which must be superimposed on the characteristic velocity requirement. There is a compromise, then, between sensitivities introduced by the increased propellant requirements of the low thrust-to-weight ratio vehicles and the increased propulsion system requirements of the high thrust-to-weight ratio vehicles. The optimum thrust-to-weight ratio is very near 1.0.

ORBITER GROSS WEIGHT DEPENDENCE ON STAGING VELOCITY

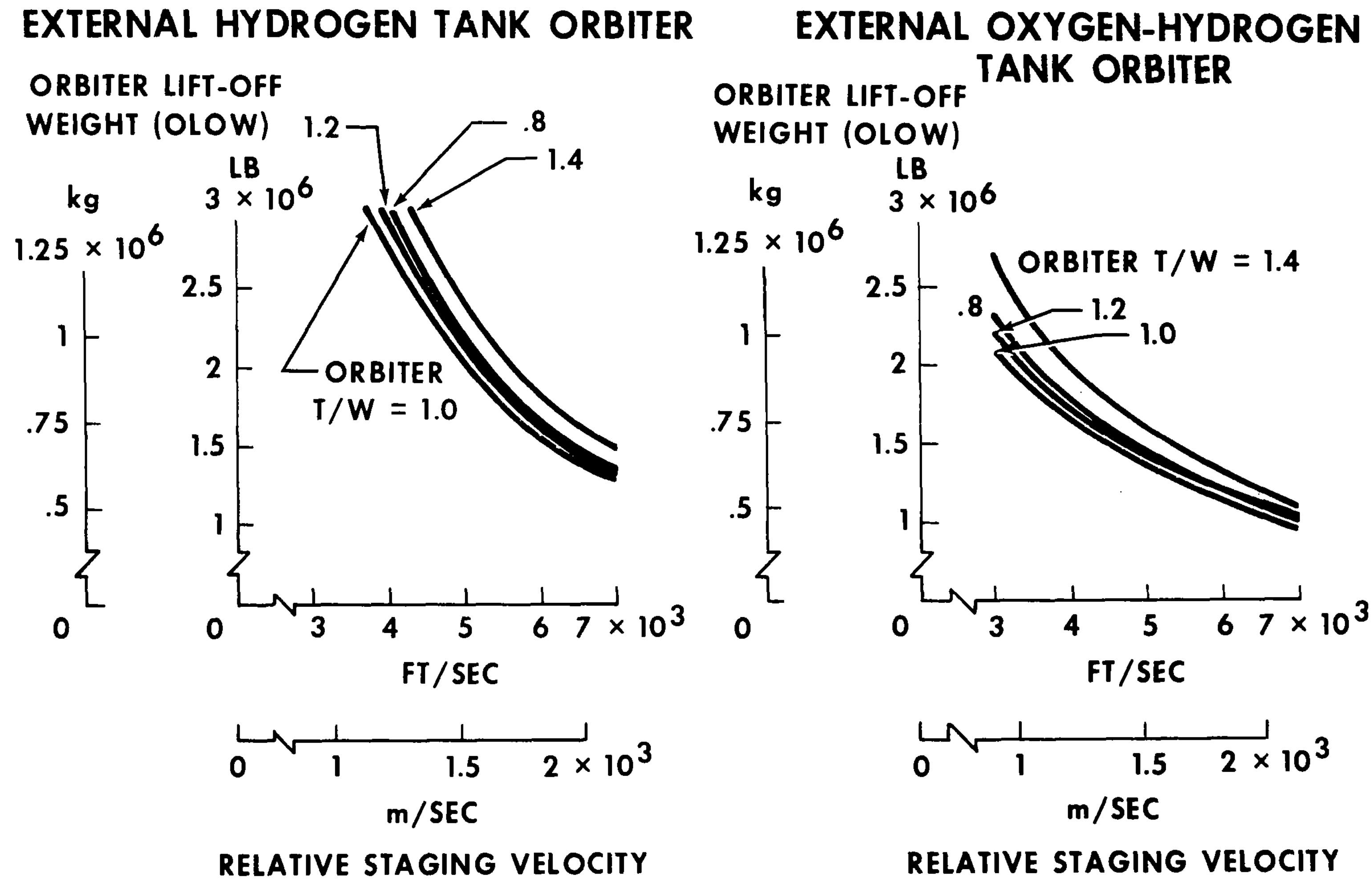

Figure 10

ORBITER INERT WEIGHT DEPENDENCE ON STAGING VELOCITY

(Figure 11)

Isolating the sensitivity of core inert weight to staging velocity clearly reveals the impact of the internal oxygen tank on the structure factor of the EHT vehicle. The diminished sensitivity of the inert weight of the EOHT vehicle is a result of that vehicle's lower structure factor, an advantage achieved by the divorce of propellants and tanks from the core vehicle.

ORBITER INERT WEIGHT DEPENDENCE ON STAGING VELOCITY

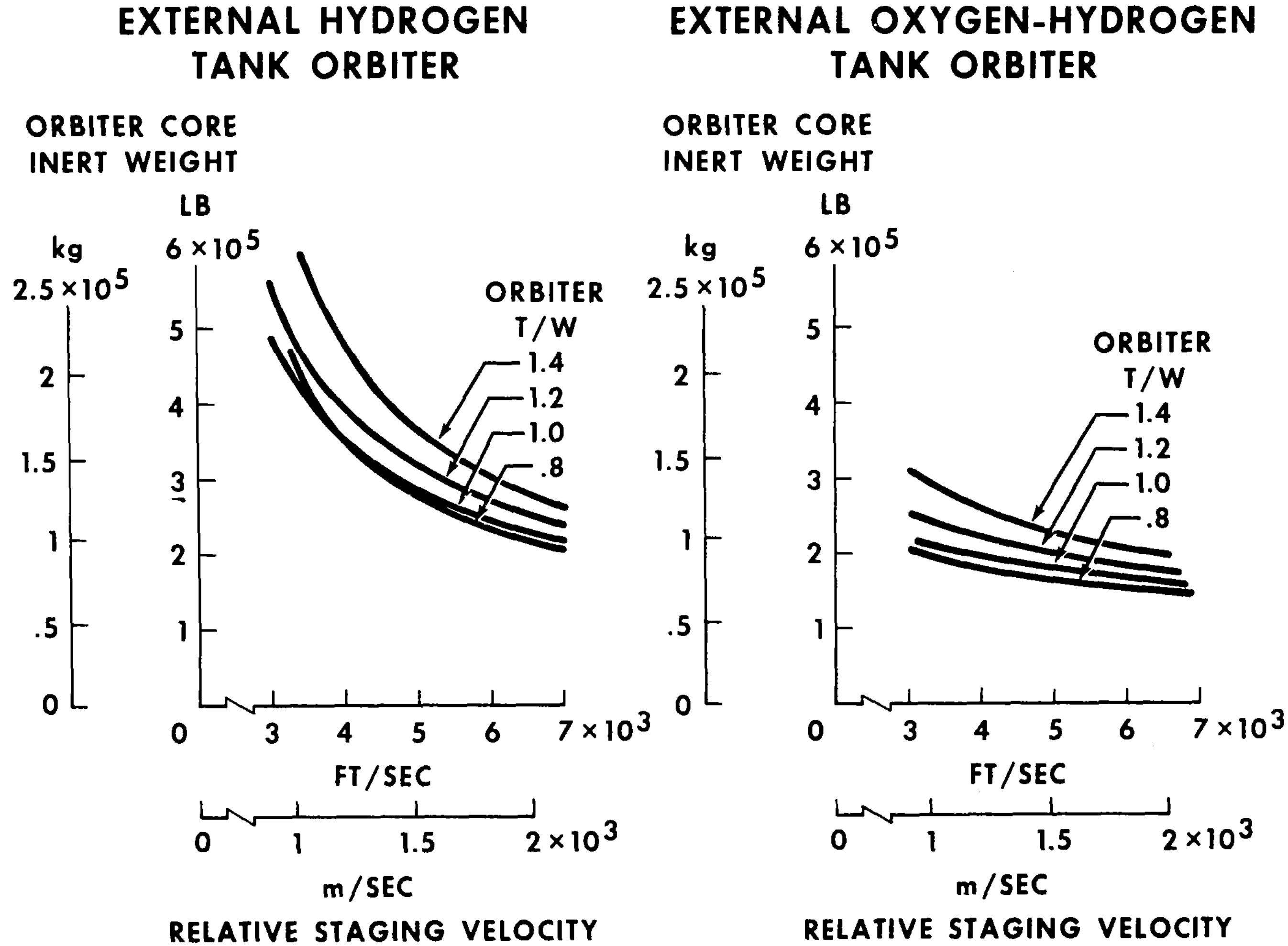

Figure 11

EXTERNAL TANK DRY WEIGHT DEPENDENCE ON STAGING VELOCITY

(Figure 12)

The reduction in orbiter core weight of the EOHT vehicle over that of the EHT vehicle displayed in figure 11 must be compensated for by a weight differential between the external oxygen-hydrogen tank and the corresponding external hydrogen tank. The magnitude of this differential, as collated with the EOHT vehicle core weight savings, determines the ultimate advantage or disadvantage of the EOHT concept in relation to the EHT concept.

At a representative staging velocity of 6000 ft/sec (1970 m/sec), the EOHT vehicle has a core inert weight which is 78,000 lbs (35,400 kg) less than that of the EHT vehicle. The corresponding external oxygen-hydrogen tank dry weight is, however, 12,000 lbs (5450 kg) greater than that of the external hydrogen tank. An orbiter thrust-to-weight ratio of 1.0 has been assumed. The net vehicle inert weight reduction attributed to the EOHT vehicle concept, under these circumstances, is thus seen to be approximately 66,000 lbs (30,000 kg).

EXTERNAL TANK DRY WEIGHT DEPENDENCE ON STAGING VELOCITY

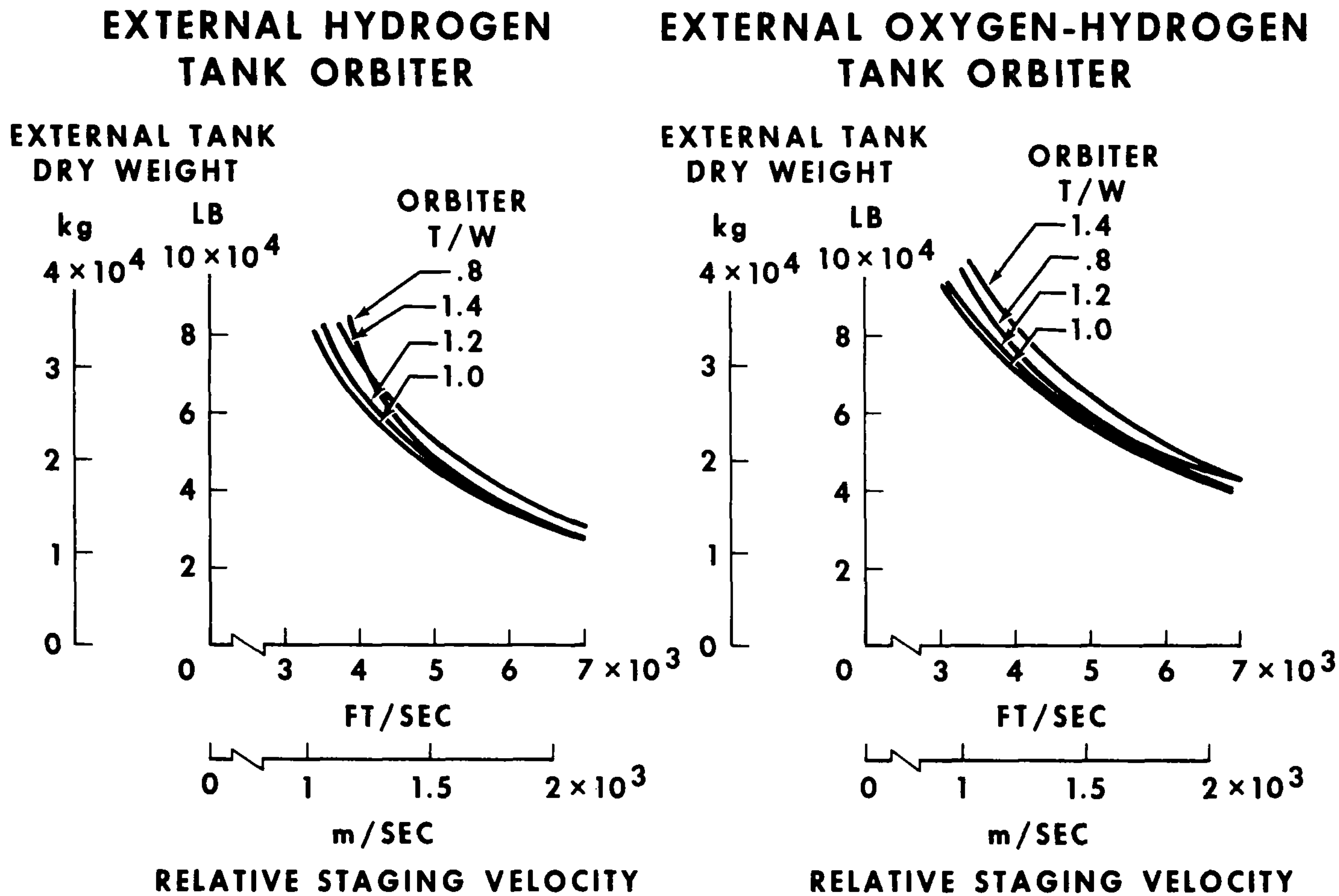

Figure 12

PRESSURE-FED LOX/PROPANE BOOSTER

(Figure 13)

The analysis of orbiter design and performance as a function of staging velocity takes on added significance when a representative booster vehicle is also matched to staging velocity. To this end, consider a booster having pressure-fed engines fueled by liquid oxygen and propane. Velocity losses attributable to drag, thrust-atmosphere effects, and gravity are summed in figure 13 to form the booster characteristic velocity as a function of staging velocity. A lift-off thrust-to-weight ratio of 1.2 was assumed.

PRESSURE-FED LOX/PROPANE BOOSTER

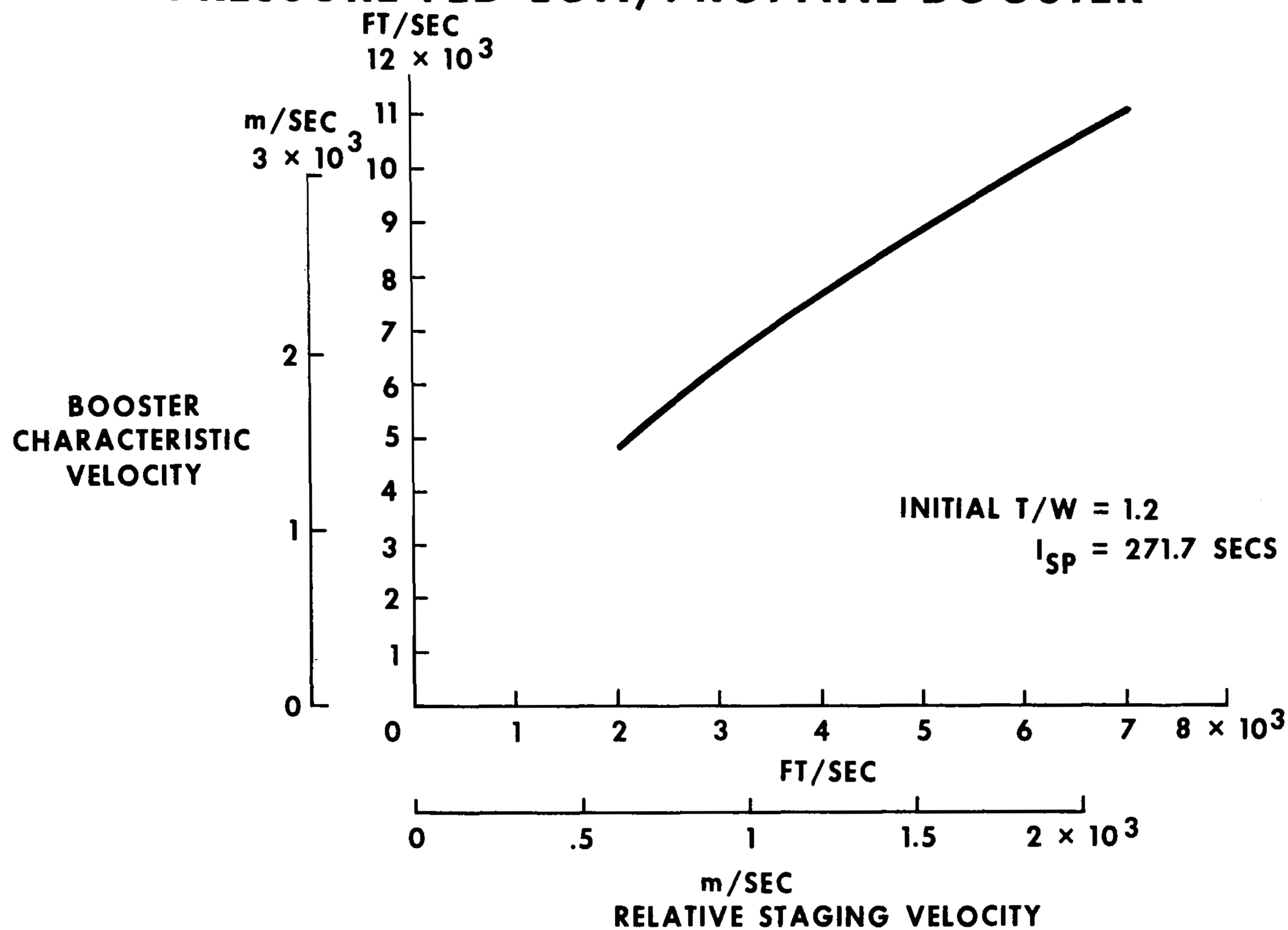

Figure 13

PRESSURE-FED BOOSTER GROSS WEIGHT

(Figure 14)

Penalties introduced to the orbiter design as a result of high stage structure factors are amplified when a booster is sized to be mission-compatible with the orbiter. At a staging velocity of 6000 ft/sec (1970 m/sec) the higher structure factor of the EHT orbiter translates into a 1,810,000 lb (820,000 kg) increase in booster gross weight when compared to the booster gross weight corresponding to an EOHT vehicle.

The net effect of the low EOHT orbiter structure factor is to induce in the system a preference for boosters smaller than those which would be desirable for EHT orbiters.

PRESSURE-FED BOOSTER GROSS WEIGHT

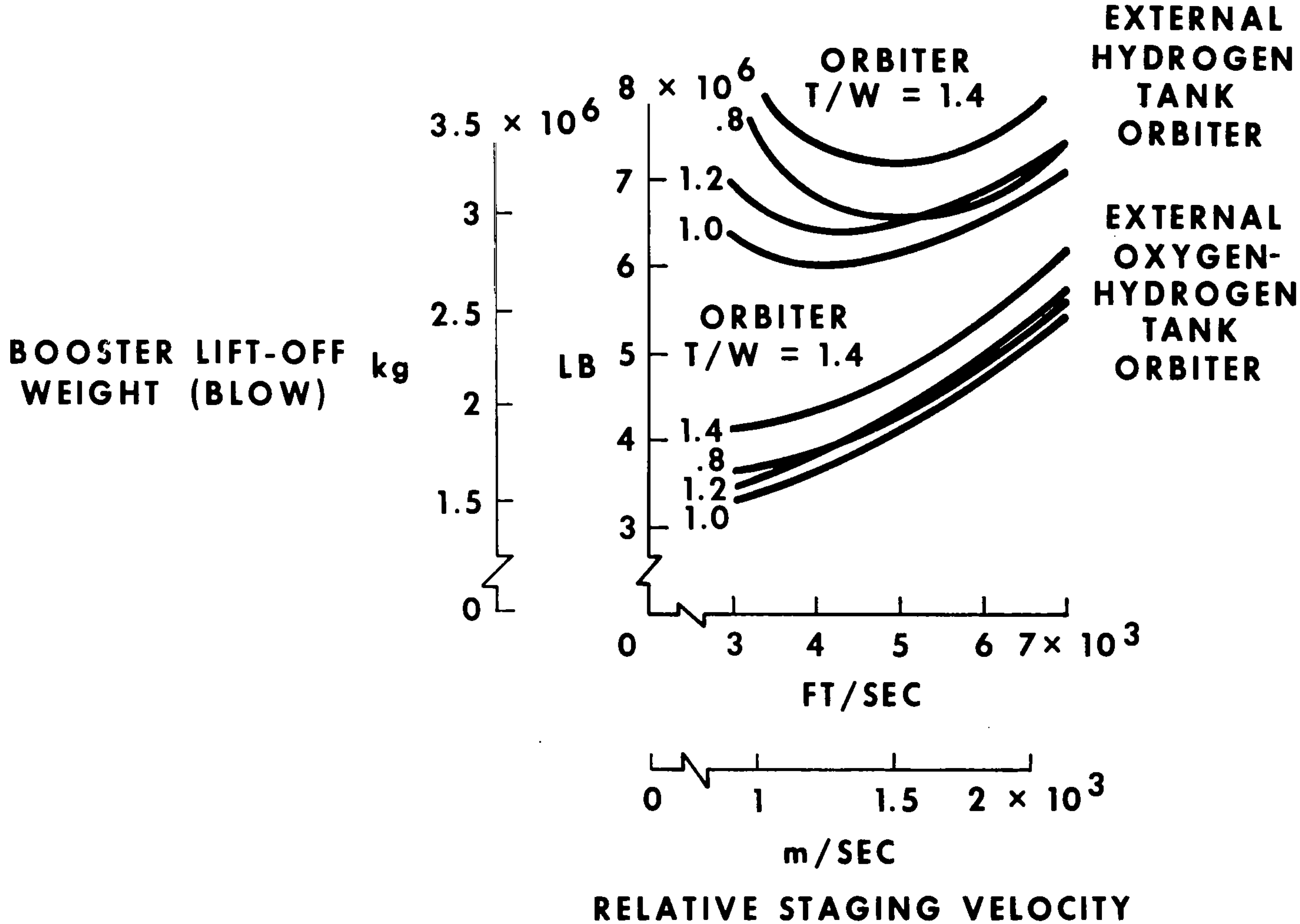

Figure 14

PRESSURE-FED BOOSTER/EXTERNAL TANK ORBITER GROSS VEHICLE WEIGHT

(Figure 15)

The superimposition of the booster/orbiter primary sizing trends is to be seen in the overall vehicle gross lift-off weight dependence on staging velocity. To recapitulate, these include:

(1) low orbiter thrust-to-weight ratios introduce excessive propellant penalties on orbiter performance;

(2) high orbiter thrust-to-weight ratios introduce excessive engine weight penalties on orbiter design;

(3) the best orbiter thrust-to-weight ratio for both EHT and EOHT orbiters is very near 1.0;

(4) the improved EOHT orbiter structure factor reduces the vehicle gross lift-off weight from that of the corresponding EHT orbiter;

(5) the improved EOHT orbiter structure factor and, hence, improved orbiter performance drive the system to smaller boosters and lower staging velocities.

PRESSURE-FED BOOSTER/EXTERNAL TANK ORBITER GROSS VEHICLE WEIGHT

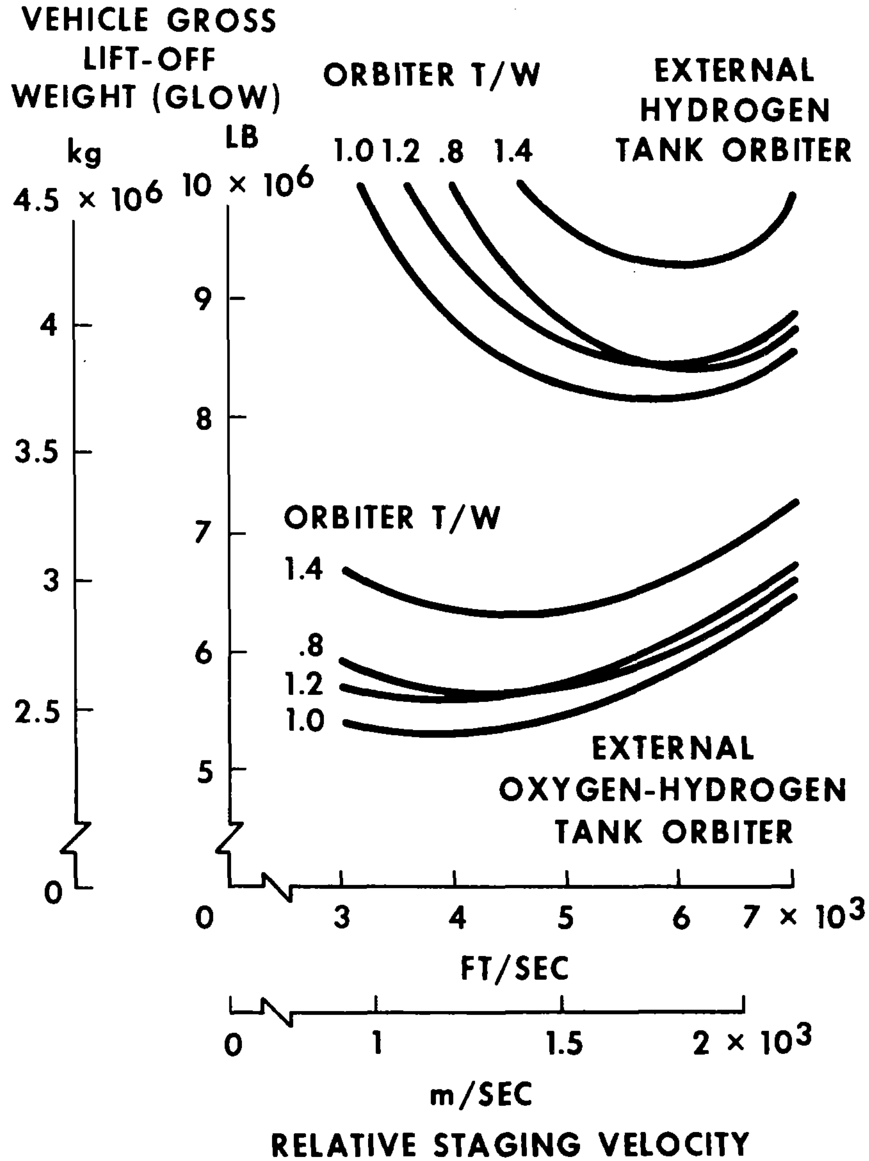

Figure 15

BOOSTER COMPARISON

(Figure 16)

It is of some interest to compare the pressure-fed booster of the previous discussion with the reusable, pump-fed, F-1 engine booster. The F-1 engine booster is fixed in weight and propellant loading so that its maximum capability is specified. To achieve below maximum capability propellant must be off-loaded. In figure 16, for an EOHT orbiter with thrust-to-weight ratio equal to 1.0, the booster gross lift-off weights of the pressure-fed and the F-1 engine boosters have been plotted as a function of staging velocity. The F-1 engine booster has been off-loaded to achieve the minimum thrust-to-weight ratio at lift-off of 1.25.

Use of the F-1 booster becomes advantageous when staging velocities greater than 6500 ft/sec (1980 m/sec) are considered.

BOOSTER COMPARISON

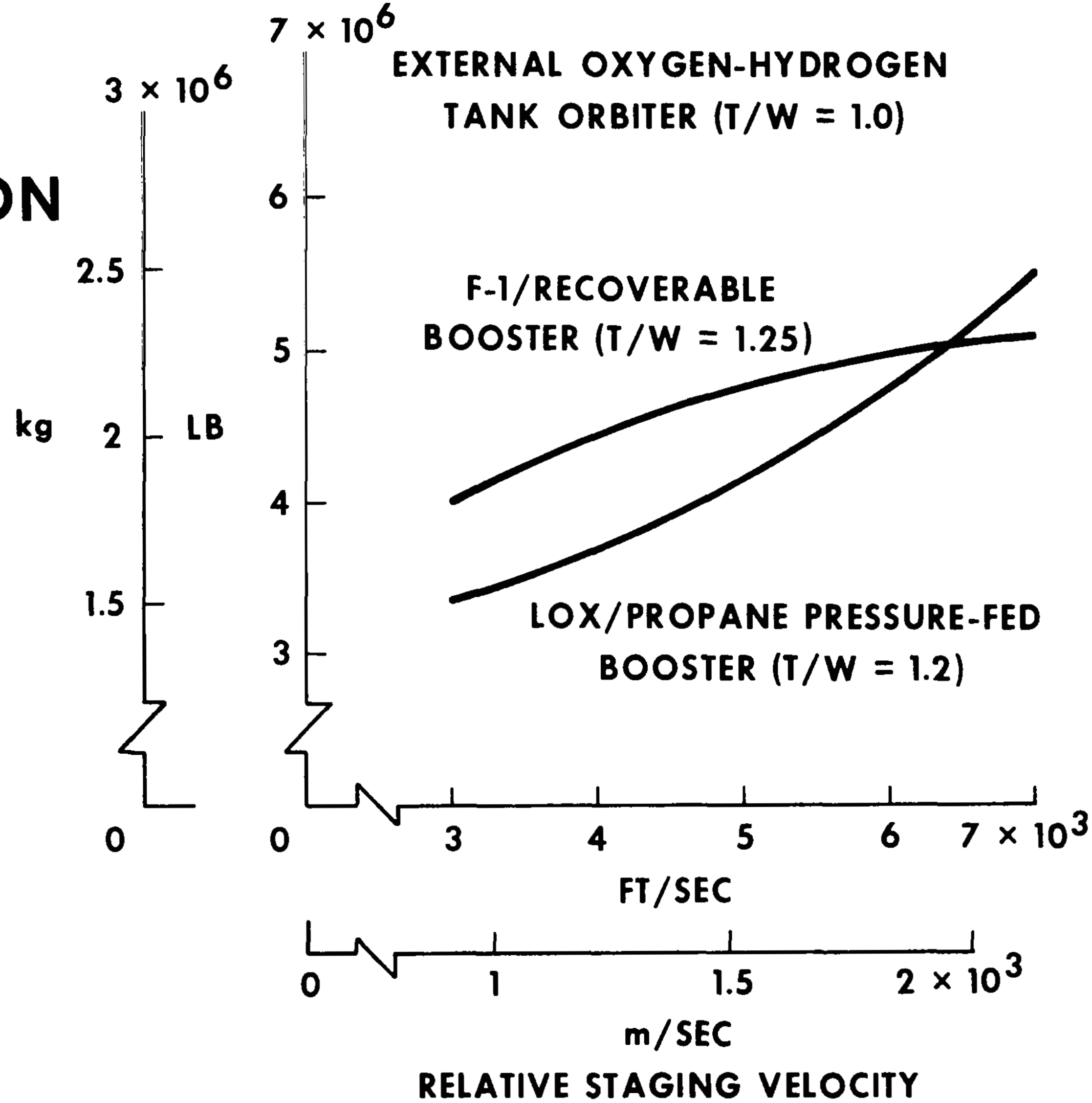

Figure 16

EHT/EOHT ORBITER INERT WEIGHT COMPARISON

(Figure 17)

Increases in the orbiter core inert weight attributable to the EHT orbiter, when compared to the EOHT orbiter, increase as the staging velocity decreases. At high staging velocities the core weight increases appear to level off at about 30%. An orbiter thrust-to-weight ratio at 1.0 was assumed.

EHT/EOHT ORBITER INERT WEIGHT COMPARISON

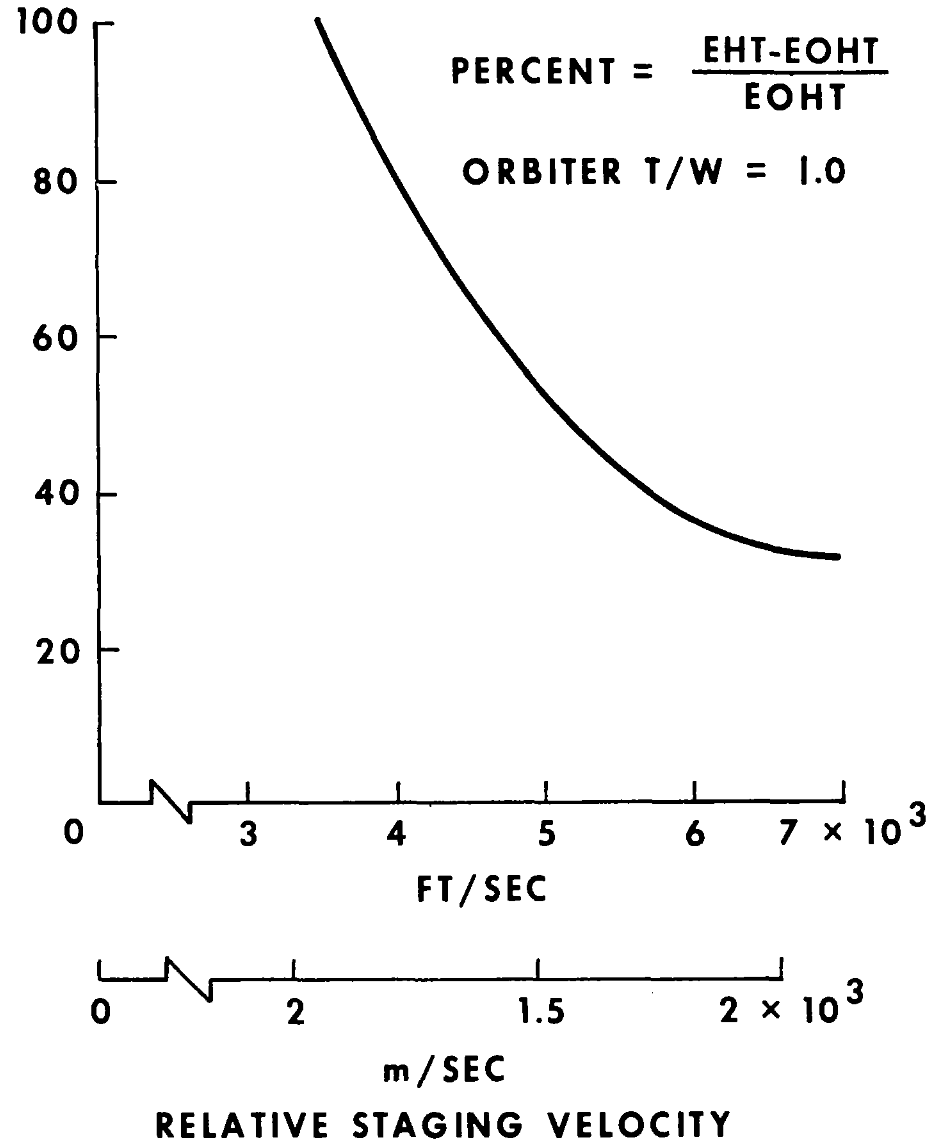

Figure 17

EHT/EOHT EXTERNAL TANK DRY WEIGHT COMPARISON

(Figure 18)

At low staging velocities the dry weight of the external tank is decreased by a few percent when only the hydrogen is placed in the external tank as opposed to placing both the oxygen and the hydrogen in the external tank. The large propellant penalties imposed by the EHT vehicle's higher structure factor are barely surpassed by the tank fraction penalty of including an oxygen tank in the external tank.

At high staging velocities the EHT vehicle's tank dry weight savings approach 30%.

EHT/EOHT EXTERNAL TANK DRY WEIGHT COMPARISON

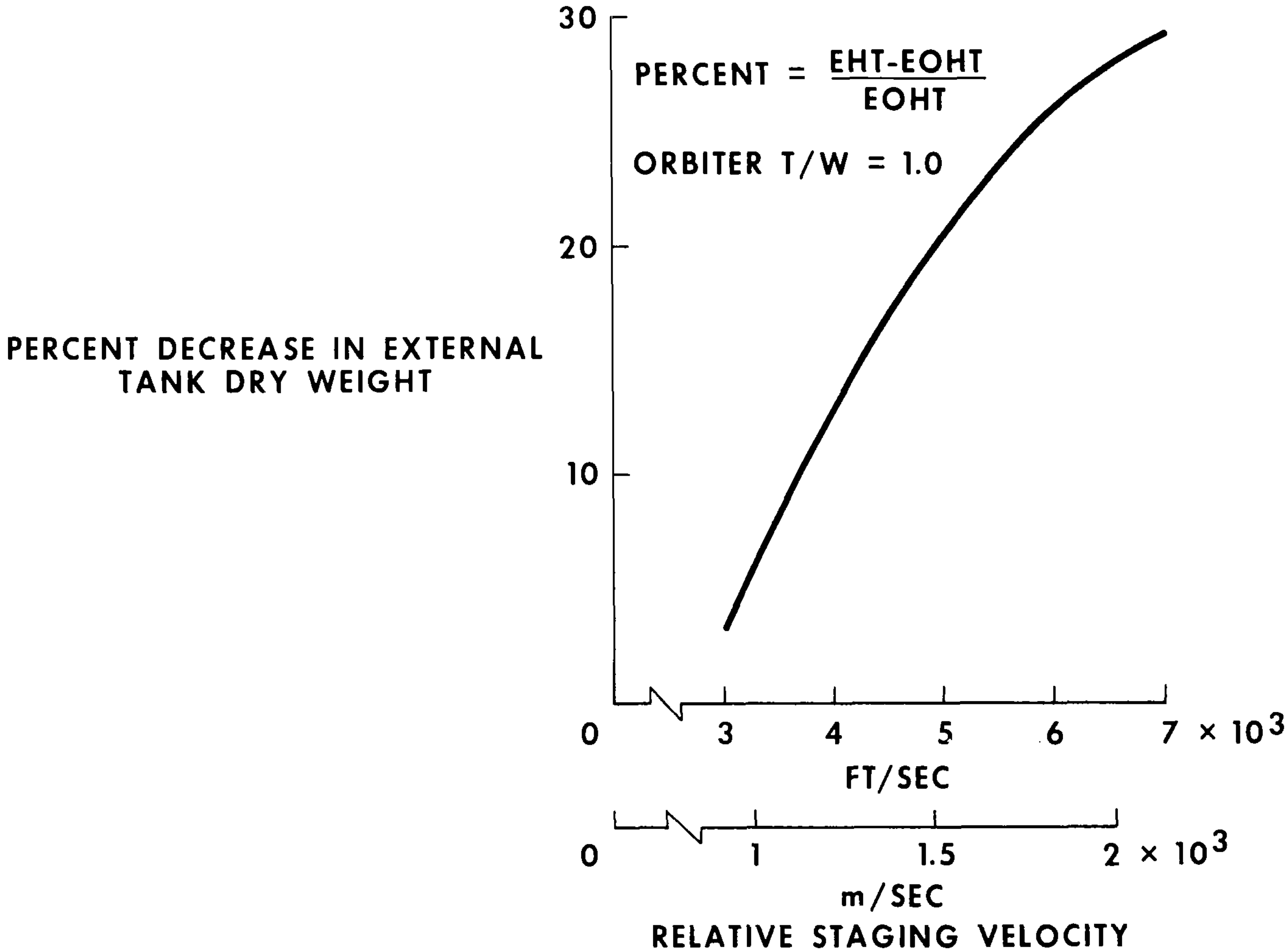

Figure 18

EHT/EOHT VEHICLE BOOSTER GROSS WEIGHT COMPARISON

(Figure 19)

Significant weight savings can be made in the pressure-fed booster gross weight by sizing it to an EOHT orbiter. At low staging velocities, where the EOHT orbiter is most compatible with this booster, a booster sized to an EHT orbiter would experience an increase in gross weight of approximately 90%. At higher staging velocities this increase approaches 30%.

EHT/EOHT VEHICLE BOOSTER GROSS WEIGHT COMPARISON

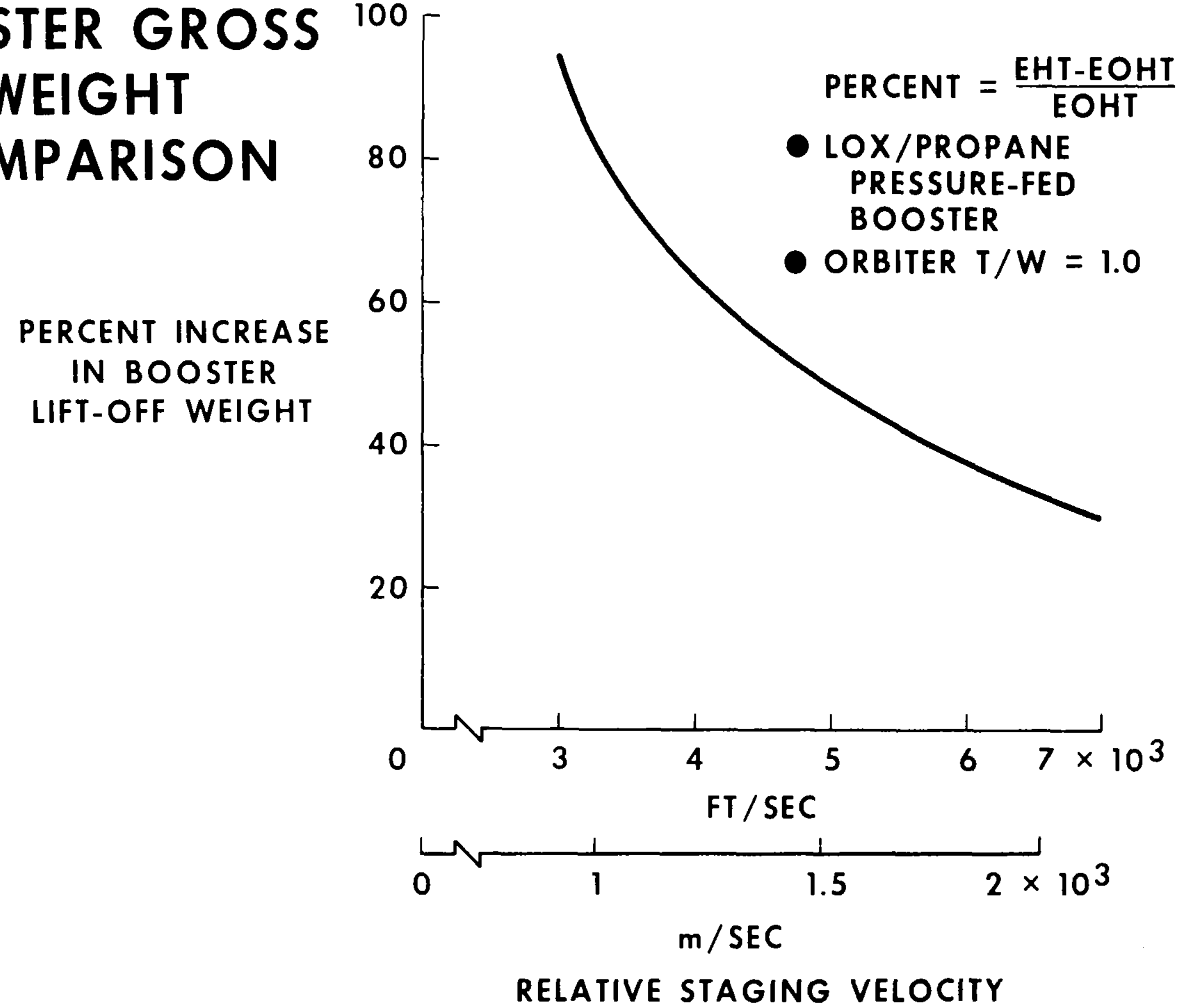

Figure 19

CONCLUSIONS

(Figure 20)

Based upon the general trending analysis of this paper the following conclusions can be reached:

(1) orbiter mass properties can be effectively decoupled from orbiter performance by using external oxygen-hydrogen tanks;

(2) at staging velocities of current interest, an EOHT orbiter has an inert weight which is approximately 40% lower than that of the corresponding EHT vehicle;

(3) a pressure-fed LOX/propane booster will have a 40% lighter gross weight if designed to an EOHT orbiter rather than an EHT orbiter.

CONCLUSIONS

- ORBITER MASS PROPERTIES CAN BE EFFECTIVELY DECOUPLED FROM ORBITER PERFORMANCE BY USING EXTERNAL OXYGEN-HYDROGEN TANKS

- FOR STAGING VELOCITIES OF CURRENT INTEREST AN EOHT ORBITER HAS AN INERT WEIGHT WHICH IS APPROXIMATELY 40 PERCENT LOWER THAN THAT OF THE CORRESPONDING EHT VEHICLE

- A PRESSURE FED LOX/PROPANE BOOSTER WILL HAVE A 40 PERCENT LIGHTER GROSS WEIGHT IF DESIGNED TO AN EOHT ORBITER RATHER THAN AN EHT ORBITER

Figure 20

SPACE SHUTTLE ATMOSPHERIC ASCENT FLIGHT DYNAMICS

by J. T. Patha, K. A. Noess, and M. V. Lines

The Boeing Company
Seattle, Washington

INTRODUCTION

An economical Space Shuttle is recognized to be the key to future space exploration. The Space Shuttle is envisioned to consist of a booster and orbiter with each having several flight phases. This paper is concerned with the atmospheric ascent flight phase of the mated composite booster and orbiter.

The composite recoverable Space Shuttle booster and orbiter exhibits unique flight control characteristics. This uniqueness results from large lifting surfaces and aerodynamic and structural assymetrics. An effective load relief technique reduces aerodynamic loads on both the booster and the orbiter. Reducing aerodynamic loads permits decreasing the structural weight of the lifting and stabilizing surfaces. An orbiter payload penalty is caused by trajectory deviations resulting from load relief. However, the net effect of an effective load relief technique is an increase in payload capability.

Atmospheric launch dynamics investigations have been carried out for different configuration types, which include expendable, straight wing, delta wing, and ballistic recoverable boosters.

FACTORS AFFECTING SPACE SHUTTLE ASCENT FLIGHT DYNAMICS

(Figure 1)

Factors that affect the ascent flight dynamics are vehicle mating geometry, vehicle aerodynamic and inertial characteristics, wind disturbances, maximum dynamic pressure, flexibility and slosh dynamics, rigid mode frequency and damping, aerodynamic control considerations, and the booster engine thrust vector actuation system. There also is an interaction between the ascent and entry flight dynamics. The vehicle ascent dynamics in terms of staging conditions have a strong influence on entry dynamics and control.

Typical mated vehicle design constraints are

- 95 percentile wind disturbances (Reference TMX-64589)[1]
- maximum dynamic pressure = 31,200 N/m^2 (652 lb/ft^2)(R-S-1C configuration)
- 3g maximum longitudinal load factor
- ± 5.15 deg TVC deflection
- ± 5 deg/sec nozzle deflection rate limit under loaded condition

(R-S-1C configuration)

- one engine out capability

FACTORS AFFECTING SPACE SHUTTLE ASCENT FLIGHT DYNAMICS

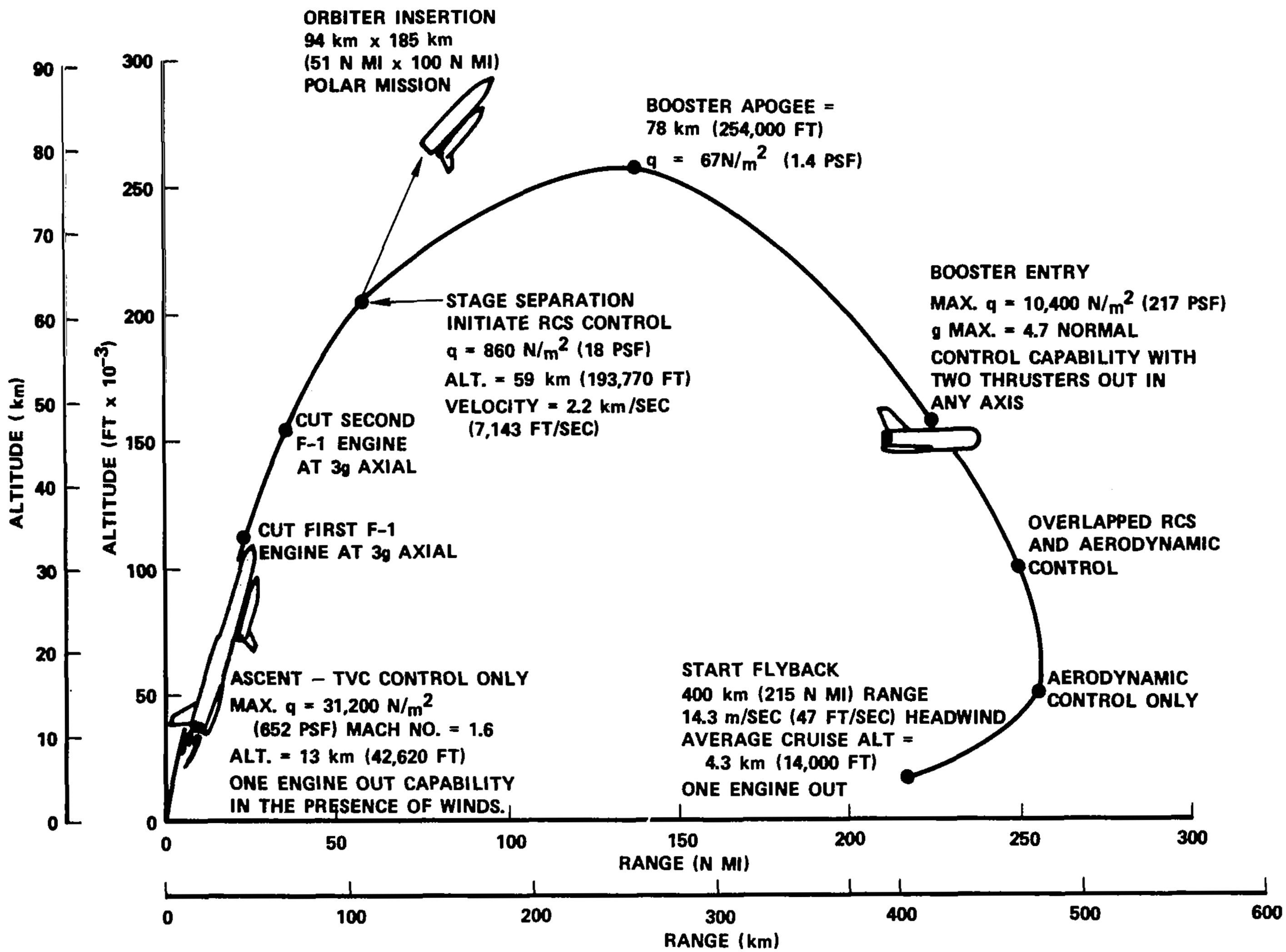

Figure 1

ASCENT FLIGHT DYNAMICS DESIGN OBJECTIVES

(Figure 2)

Stable flight dynamics and minimized system cost are design objectives for boost flight. The ability and need to satisfy these design objectives will vary for different space shuttle vehicle configurations. For example, if the design is not payload critical, then applying load relief to minimize booster structural weight would not be appropriate since this would unnecessarily increase the control system complexity. Also, if "off-the-shelf" hardware is available, then non-optimized but acceptable subsystem performance may be tolerated in order to reduce over-all system cost.

ASCENT FLIGHT DYNAMICS DESIGN OBJECTIVES

- CONFIGURATION MATING TO MINIMIZE LOADS AND NOZZLE DEFLECTIONS
- CONTROL LAW DEFINITION THAT MINIMIZES NOZZLE AND AERODYNAMIC CONTROL DEFLECTIONS AND RATES
- MAXIMIZE ORBITER PAYLOAD WEIGHT
- ADEQUATE RECOVERY FROM ACTUATOR AND ENGINE-OUT (MEET FAILURE CRITERIA)
- ADEQUATE ABORT CAPABILITY
- MEET FLEXIBILITY MODE STABILIZATION REQUIREMENTS
- SATISFY OTHER VEHICLE AND TRAJECTORY CONSTRAINTS

Figure 2

WIND DISTURBANCES

(Figure 3)

The wind disturbances during the booster ascent phase were derived from TMX-64589.[1] The magnitudes shown were used as head, tail, and cross winds. The Type I profiles are used in trajectory analyses because they result in the most severe flight path penalties. However, the Type II profiles (with back off shears) produce more severe control disturbances and are used to determine nozzle actuation system design requirements. A search with different gust altitudes is performed to establish where the trajectory, vehicle loads, and control system parameters are most sensitive. For a typical case the trajectory performance was found to be most sensitive with low altitude winds, i.e., approximately 1 km (3,280 ft.). Nozzle deflections were found to be most critical with cross winds at an intermediate altitude of 6 km (19,700 ft.), and vehicle loads were most critical for cross winds at an altitude of approximately 10 km (32,800 ft.).

WIND DISTURBANCES

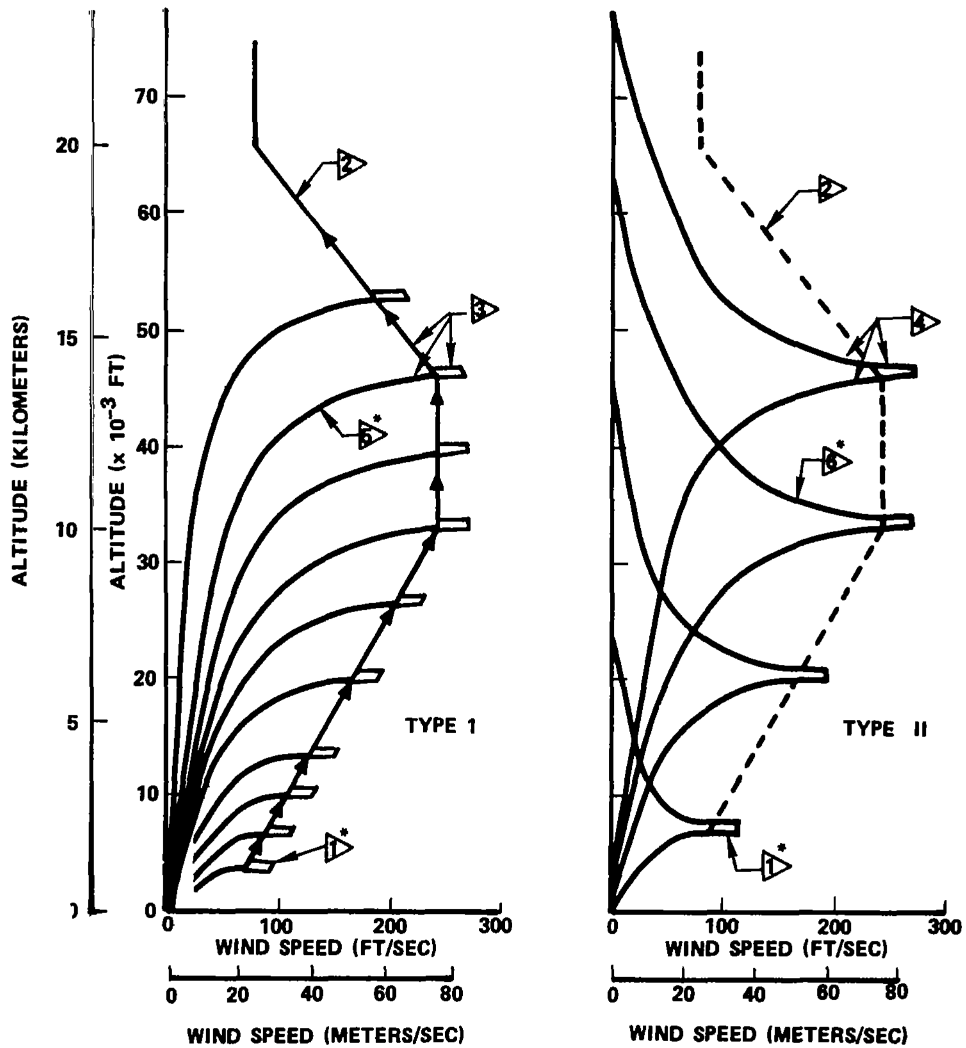

NOTES:

1. SUPERIMPOSED GUST (TYPICAL)
2. 95% DESIGN WIND SPEED ENVELOPE (ETR)
3. TYPE I PROFILE: BUILDUP SHEAR; SUPERIMPOSED GUST AND THEN FOLLOWS THE 95% ENVELOPE (TYPICAL)
4. TYPE II PROFILE: TYPE I WITH BACKOFF SHEAR (TYPICAL)
5. ADJUSTED *99% SHEAR BUILDUP ENVELOPE (TYPICAL)
6. ADJUSTED 99% SHEAR BACKOFF ENVELOPE (TYPICAL)

* 0.85 TIMES 99% VALUES.

Figure 3

LOAD RELIEF CONTROL LOGIC

(Figure 4)

An improved load relief technique which has the potential to increase orbiter payload is described for large boosters with lifting surfaces. This new innovation provides the optimum level of load relief with the minimum trajectory disturbance.

A logic scheme is utilized to limit maximum $q\alpha$ during composite boost and the technique is as follows: Equations (1) thru (3) are the control laws. The control gain λ_3 is a multiplier in the pitch attitude loop as shown in equation (1) and is varied as shown in the diagram. For small values of $q\alpha$, i.e. $\alpha < \alpha_1$, then λ_3 is set equal to 1.0. As $q\alpha$ becomes larger, λ_3, as shown is reduced in magnitude and can result in pure weathercock control if $\alpha > \alpha_2$ and $\lambda_5 = 0$. The variables α_1 and α_2 which are shown in the diagram are computed from equations (4) and (5). It can be shown the short period frequency is maintained approximately constant as λ_3 changes by equation (3). $q\beta$ is limited through λ_4 in equation (2) by a scheme similar to the above technique.

For analytical convenience, α and β have been utilized as the feedback quantities. The equivalent acceleration feedbacks may be used during mechanization. A large number of simulated load relief trajectories have been accomplished with this technique and the rigid mode exhibits good stability characteristics. The vehicle maximum rates when switching from one control mode to another are not excessive, i.e. < 3 deg/sec. The question of flexible mode filtering and slosh requirements with this technique of load alleviation must be analyzed before the final control logic and gains can be selected.

The new contribution to the art is the application of the non-linear gain technique to optimize load relief. The non-linear technique minimizes the time the load control law is utilized for any given gust, i.e. load relief is used only if the load exceeds a preselected level. This has the net effect of minimizing the trajectory deviation resulting from load relief and results in maximizing the payload capability.

NOTE:

λ_2 and λ_5 pre-set constants

δ Nozzle deflection

q Dynamic pressure

α Angle of attack

θ Attitude angle

K_α Computed for minimum drift law

LOAD RELIEF CONTROL LOGIC

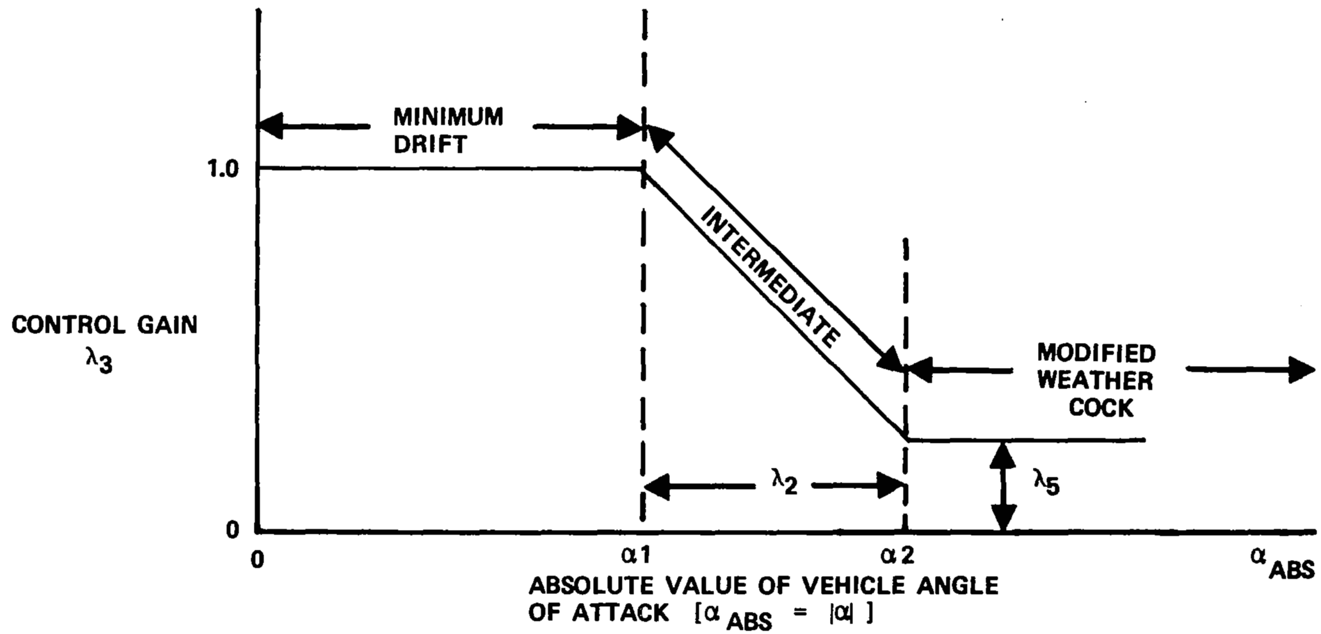

$\delta Y_C = \lambda_3 \; K_\theta \, (\theta - \theta_C) + K_{\dot\theta} \, \dot\theta + \bar{K}_\alpha \alpha$ (PITCH) (1)

$\delta Z_C = \lambda_4 \; K_\psi \, (\psi - \psi_C) + K_{\dot\psi} \, \dot\psi + \bar{K}_\beta \, \beta$ (YAW) (2)

$\delta X_C = K_\phi \, (\phi - \phi_C) + K_{\dot\phi} \, \dot\phi$ (ROLL) (3)

$\alpha_2 = \frac{(q\alpha)_{MAX}}{q}$ (4)

$\alpha_1 = \alpha_2 - \lambda_2$ (5)

$\bar{K}_\alpha = K_\theta \, (l - \lambda_3) + K_\alpha$ (6)

Figure 4

PAYLOAD SENSITIVITY TO LOAD INDICATOR

(Figure 5)

The sensitivity of orbiter payload weight to load parameters $q\alpha$ and $q\beta$ is shown for a typical large lifting vehicle. As $q\alpha$ and $q\beta$ are increased the payload penalty increases. The payload penalty results primarily from increased structural weight of booster and orbiter wings and tail surfaces. It is of interest to note the orbiter has the greater "payload lever." This is due to the fact that a weight reduction of about 5.45 kg (12 pounds) on the booster is required to gain 0.454 kg (one pound) of additional payload into orbit, while the ratio is 1 to 1 for the orbiter.

PAYLOAD SENSITIVITY TO LOAD INDICATOR

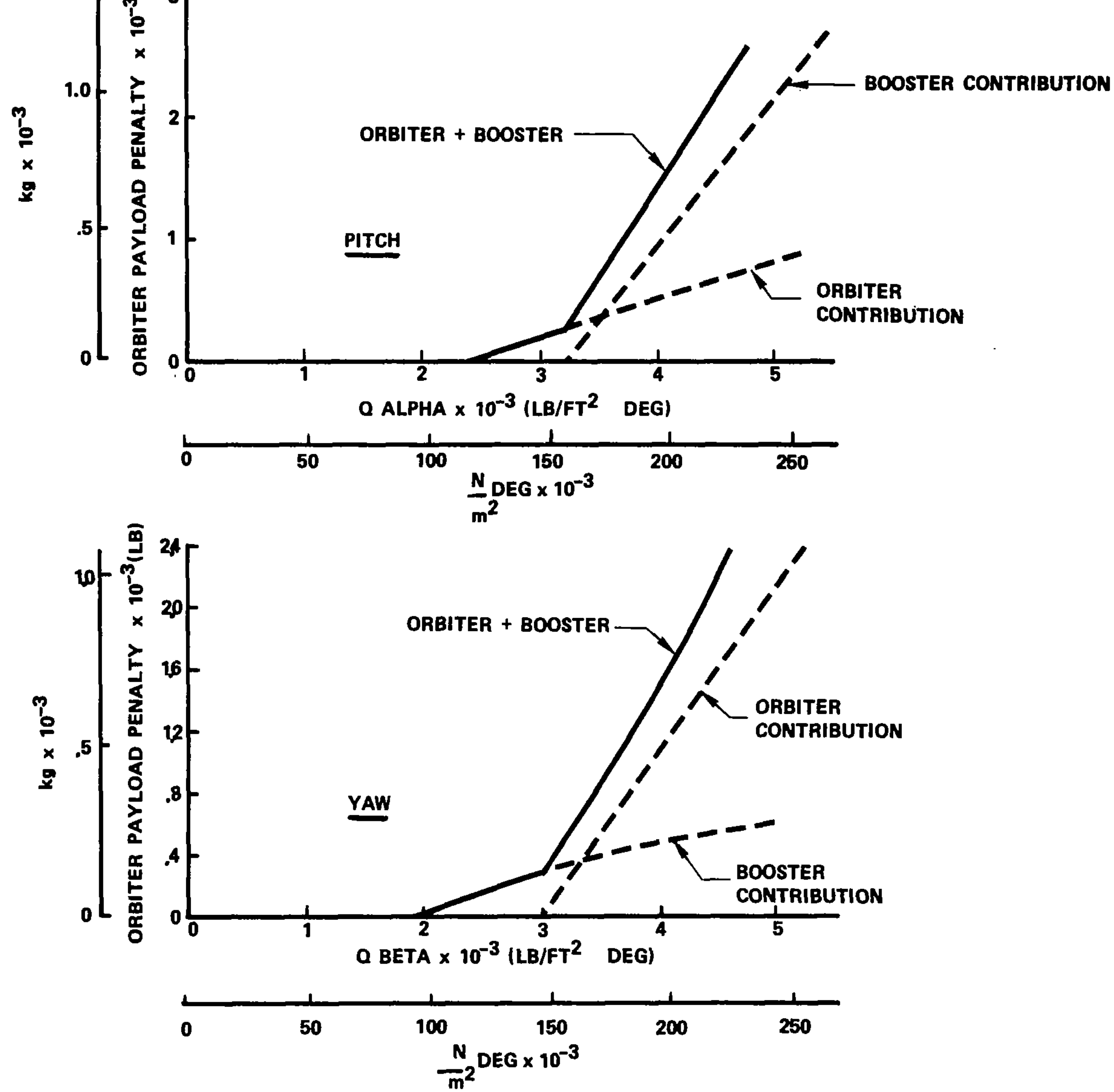

Figure 5

STRUCTURAL SAVING AND TRAJECTORY PENALTY
(Figure 6)

To find the optimum load relief level, Type I winds were investigated across the range of gust altitudes from 1 to 12 kilometers. A typical result from a 6 kilometer gust is shown. The structural weight saving results from the payload sensitivity to load indicator which was shown in Figure 5. The cross wind structural weight savings shown in Figure 6 is referenced to the maximum orbiter payload weight penalty without load relief which occurs for a Type I wind with a gust at 10 km altitude. This reference condition results in a maximum $q\beta$ of 201,000 N/m^2 (4200 psf deg) and a corresponding 863 kg (1900 lb) orbiter payload penalty shown in Figure 5. No load relief (0%) for the 6 km gust wind in Figure 6 results in approximately 180,000 N/m^2 (3750 psf deg) $q\beta$, which is an improvement of approximately 272 kg (600 lb) payload compared to the reference maximum $q\beta$. Further reduction of $q\beta$ in Figure 6, i.e. less than 180,000 N/m^2 (3750 psf deg $q\beta$), causes a further reduction in the orbiter payload penalty as shown in Figure 5 and results in the structural savings shown in Figure 6.

The trajectory penalty is a result of the energy required to compensate for the flight path deviation which results from rotating the vehicle into the wind to achieve load relief. The addition of the trajectory penalty and structural saving results in the net incremental increased or decreased payload to orbit. The cross wind disturbance causes the flyback range to be approximately 5.6 km (3 nautical miles) less. This has the effect of increasing the orbiter payload by the relatively small amount shown. The payload change is caused from the reduced flyback fuel. The effect of incremental changes in flyback range caused by head and tail winds during entry were also found to be equally small.

STRUCTURAL SAVING AND TRAJECTORY PENALTY (CROSSWIND)

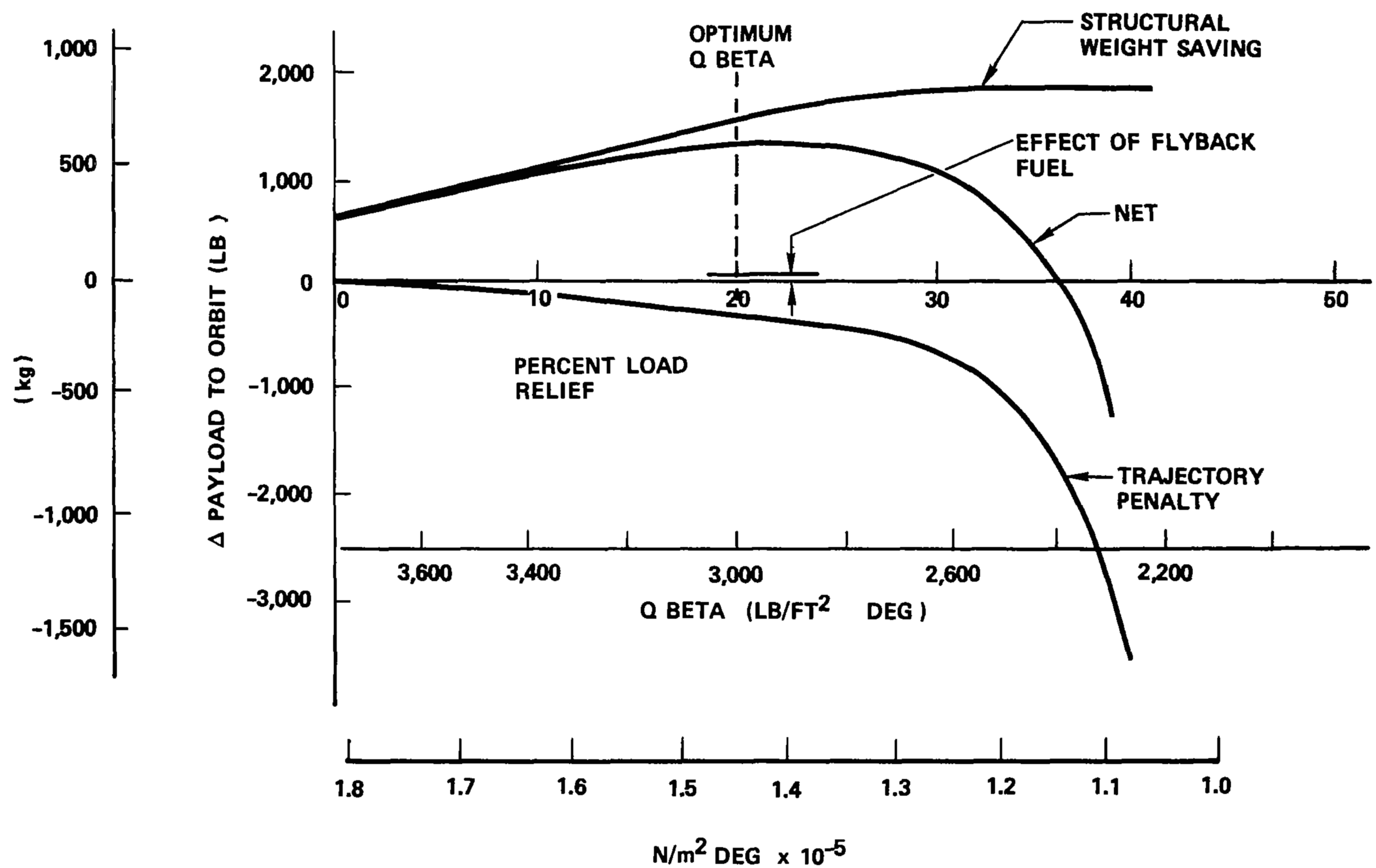

NOTE: 6 KILOMETER GUST

Figure 6

POTENTIAL PAYLOAD IMPROVEMENT FROM LOAD RELIEF

(Figure 7)

A summary of the load relief payload to orbit trade study is shown. For the case investigated, load relief gave a total payload improvement of 880 kg (1940 pounds). The net cross wind payoff of 500 kg (1100 pounds) resulting from structural improvement occurs at a $q\beta$ of 140,000 N/m^2 degree (2930 psf degree). A lesser payoff for head winds of 382 kg (840 pounds) occurs at approximately 110,000 N/m^2 degree (2300 psf degree) $q\alpha$. Load relief for a tail wind is not critical from a payload standpoint because considerable energy is added from the wind velocity component directed approximately parallel and with the same heading as the vehicle velocity vector. However, it is important to load relief to the same value of $q\alpha$ for tail winds as for head winds in order to take advantage of the structural weight savings for the head winds.

POTENTIAL PAYLOAD IMPROVEMENT FROM LOAD RELIEF

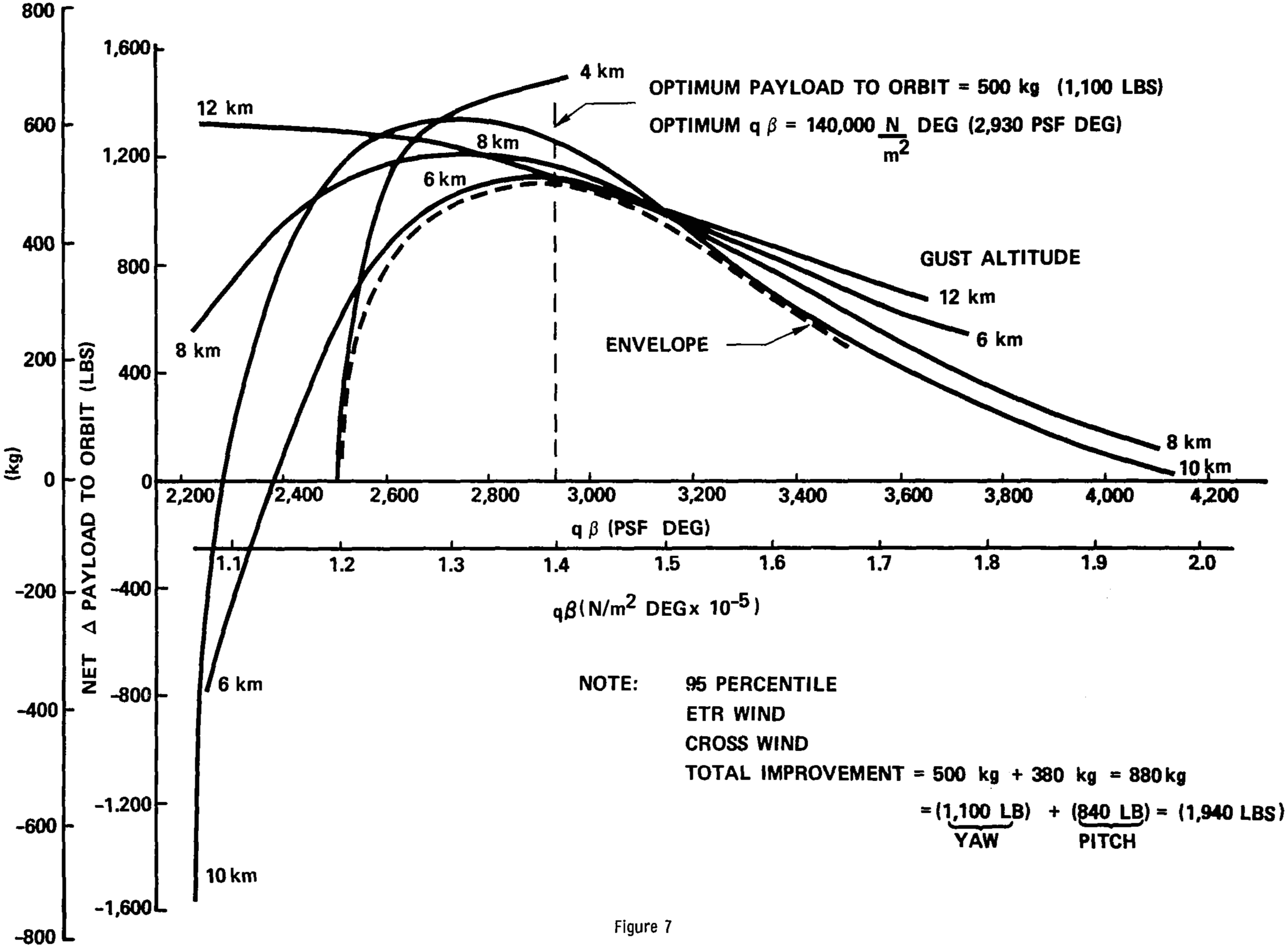

NOTE: 95 PERCENTILE
ETR WIND
CROSS WIND
TOTAL IMPROVEMENT = 500 kg + 380 kg = 880 kg

$= \underbrace{(1,100\ LB)}_{YAW} + \underbrace{(840\ LB)}_{PITCH} = (1,940\ LBS)$

Figure 7

LOAD RELIEF EFFECT ON BOOST TRAJECTORY

(Figure 8)

The effect of load relief on the trajectory is shown in Figure 8 for a cross wind with a gust occurring at 10 kilometers. When no load relief is employed the vehicle drifted to a large positive cross range. Then if excess load relief is employed, the vehicle went to a large negative cross range. When a near optimum load relief was employed the cross range was only 0.763 kilometers (2500 feet) at staging.

LOAD RELIEF EFFECT ON BOOST TRAJECTORY

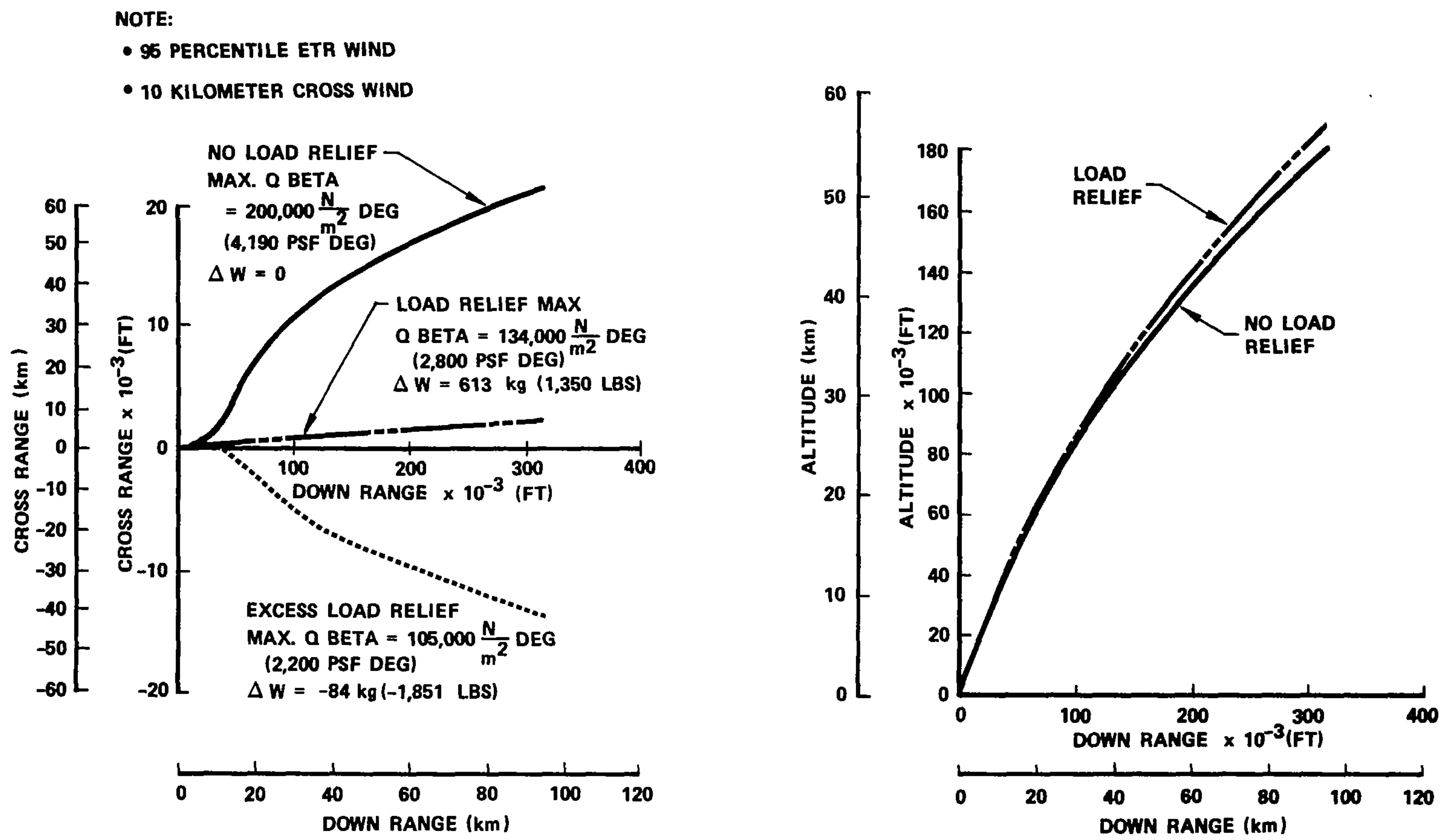

Figure 8

NOZZLE DEFLECTION DYNAMICS

(Figure 9)

Typical pitch and yaw plane gimbal requirements are shown. The nozzle deflection time histories with and without disturbances are shown. Engine shutdown results in unsymmetrical moments and the vehicle is retrimmed at about 150 seconds. The tail winds require the nozzle to deflect to the limit of -5.15 degrees, while the head winds require a maxim deflection of 4.0 degrees. The additional required nozzle deflection for one engine out and slosh and bending were added to the wind requirements to give the combined envelope. The elevons were set at -10 degrees. The elevons would be set more negative in a final analysis to center the wind deflection requirements in pitch.

The yaw nozzle deflection requirements are also shown. These data were developed in a manner similar to the pitch requirements.

As shown the requirements in pitch and yaw exceed 5.15 degrees with one engine out in the presence of 95 percentile winds. However, the vehicle is aerodynamically stable and the vehicle and trajectory transients are acceptable for the short time (less than 2 seconds) the nozzle deflection is saturated. Peak body axis rates during load relief transients are less than 3 deg/sec. Peak TVC nozzle rates are 5 deg/sec for a time period of less than 0.5 second.

NOZZLE DEFLECTION DYNAMICS

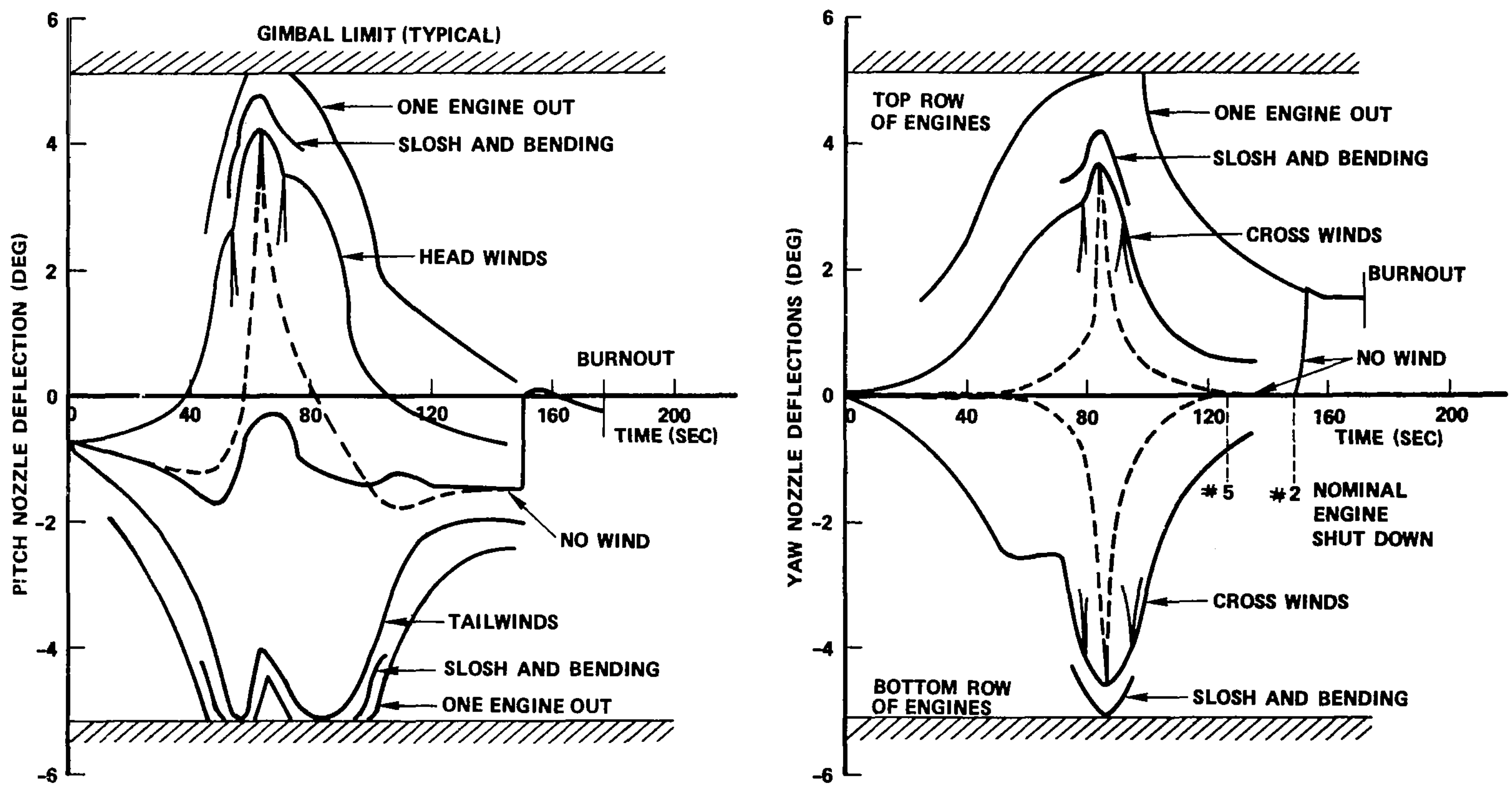

NOTE:
- 95 PERCENTILE ETR WIND
- NO AILERON CONTROL
- -10 DEG ELEVATOR

—— ENVELOPE OF TIME HISTORY
---- TYPICAL TIME HISTORY

Figure 9

CONCLUSIONS
(Figure 10)

To be complete, the atmospheric launch dynamics investigations of the composite vehicle must include integrated studies of: Wind Disturbance Definition; Load Indicator Comparison; Space Shuttle Ascent Simulation Requirements; Vehicle Mating; Analysis of Control Laws; Engine Gimbal Studies (including engine out and hydraulic failure); Control Sensitivity Study; Aerodynamic Sensitivity Study; Ascent Guidance Techniques; and Configuration Comparisons.

The developed load alleviation control law was found to have the potential to significantly improve payload to orbit capability. The dynamic interaction of the non-linear relief technique with slosh and vehicle flexibility must be investigated in detail in order to complete the analysis. It should also be noted that the importance of payload savings through load alleviation is highly configuration dependent. Some shuttle configurations are not payload critical and therefore the added complexity of load alleviation may not be warranted.

Of interest is that the maximum vehicle loads, nozzle deflections, and trajectory deviations occur at different gust wind disturbance altitudes.

It was also determined that a severe trajectory deviation with attendant payload loss will result if the vehicle has too much inherent aerodynamic stability, i.e., the vehicle "weathercocks" too much into the wind with a practical control authority.

CONCLUSIONS

- CRITICAL LOADS, NOZZLE DEFLECTION AND TRAJECTORY DEVIATIONS OCCUR AT DIFFERENT GUST WIND DISTURBANCE ALTITUDES.
- IF THE VEHICLE IS TOO AERODYNAMICALLY STABLE OR IF LOAD RELIEF IS OVER APPLIED – THEN A PAYLOAD LOSS WILL OCCUR FROM THE TRAJECTORY DEVIATION.
- THE NONLINEAR LOAD RELIEF TECHNIQUE IS DEMONSTRATED TO HAVE A POTENTIAL SIGNIFICANT SPACE SHUTTLE PAYLOAD TO ORBIT IMPROVEMENT 908 kg (2,000 LB) TYPICAL FOR CONFIGURATIONS WITH LARGE LIFTING SURFACES.
- PROPER ORBITER AND BOOSTER VEHICLE MATING MUST BE ACHIEVED BEFORE LOAD RELIEF CAN BE APPLIED ADVANTAGEOUSLY.
- SPACE SHUTTLE LOAD RELIEF REDUCES NOZZLE DEFLECTION REQUIREMENTS APPROXIMATELY 40 PERCENT.

Figure 10

REFERENCE

1. Daniels, Glenn E., ed.: Terrestrial Environment (Climatic) Criteria Guidelines for Use in Space Vehicle Development, 1971 Revision. NASA TM X-64589, 1971.

OPTIMAL LIFTING ASCENT TRAJECTORIES FOR THE SPACE SHUTTLE

By Timothy R. Rau and Jarrell R. Elliott
NASA Langley Research Center
Hampton, Virginia

INTRODUCTION

For many years trajectory analysts have been promoting the idea of using optimal lifting or optimal pointing trajectories as a way of improving the performance capabilities of boost-launch systems. However, prior to the space shuttle, the launch systems being built were not well suited to the use of such trajectories; the systems were incapable of producing substantial lift and were structurally incapable of withstanding the additional airloads brought about by optimal pointing of the thrust vector. Fortunately the space shuttle has these necessary capabilities and thus it provides the trajectory analyst with a new opportunity to demonstrate that the use of optimal lifting and pointing trajectories, as compared to ballistic trajectories, can materially increase the performance capabilities of boost-launch systems. Previous studies, such as reference 1, have parametrically studied the effect of adding wing areas to a boost-launch vehicle. This paper summarizes the performance gains which are possible through the use of optimal trajectories for a particular shuttle configuration and points out how these gains are produced.

CONFIGURATION STUDIED

A three-view drawing of the shuttle configuration studied is shown in figure 1. This is a fully reusable configuration in which the orbiter stage is mounted piggy-back style on the booster stage, both having delta wings. The distance from the nose of the orbiter to the tail of the booster is about 90 meters. The wing area of the orbiter is about 620 square meters while that of the booster is about 790 square meters. For comparison, the wing area of the Boeing 747 is about 520 square meters. Figure 2 shows a superposed planview of the shuttle over that of the Boeing 747.

Three basic missions are considered in the sizing of the shuttle: a polar orbit mission, a 55° orbit inclination mission, and a 28.5° orbit inclination mission. A polar orbit mission requirement of 18 140 kilograms (40 000 pounds) payload to a 50- by 100-nautical mile orbit sized the orbiter and booster elements. The weights of these two elements are as shown on figure 1 with the gross launch weight being around 2.29 million kilograms or about 5 million pounds.

SHUTTLE CONFIGURATION STUDIED

GROSS LIFT-OFF WEIGHT 2.29 MILLION kg
BOOSTER LIFT-OFF WEIGHT 1.90 MILLION kg
ORBITER LIFT-OFF WEIGHT 0.39 MILLION kg

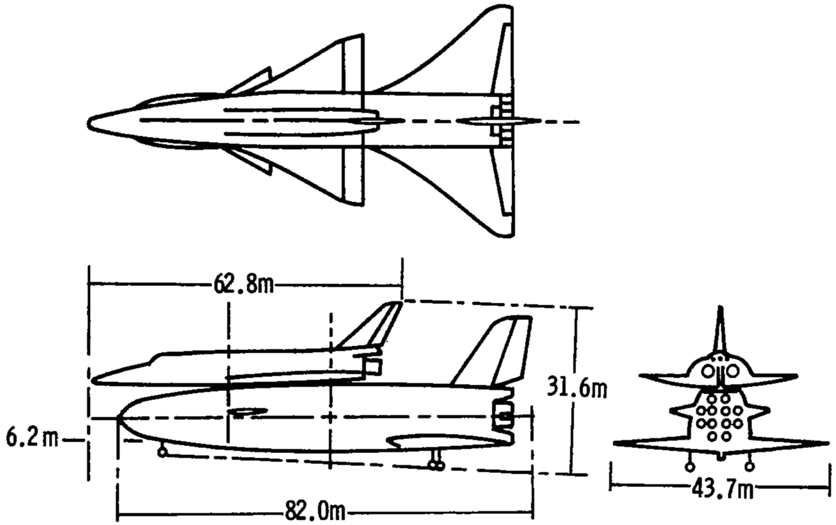

Figure 1

SHUTTLE-BOEING 747 COMPARISON

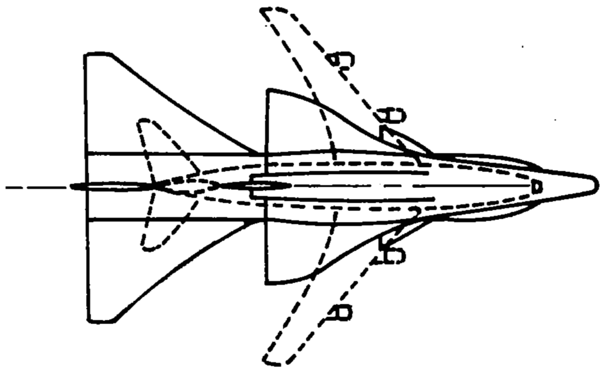

Figure 2

SHUTTLE CHARACTERISTICS

The thrust to weight ratios of the booster and orbiter at ignition are 1.3 and 1.5, respectively. In modeling this configuration for the trajectory computation program one of the ground rules followed was that the axial acceleration of the launch vehicle would not be allowed to exceed 3g. This required engine throttling in each of the stages. Typical thrust and weight time histories are shown in figure 3. Additional features of the shuttle configuration are presented in figure 4. Another ground rule followed was that the thrust axis be directed through the vehicle center of gravity.

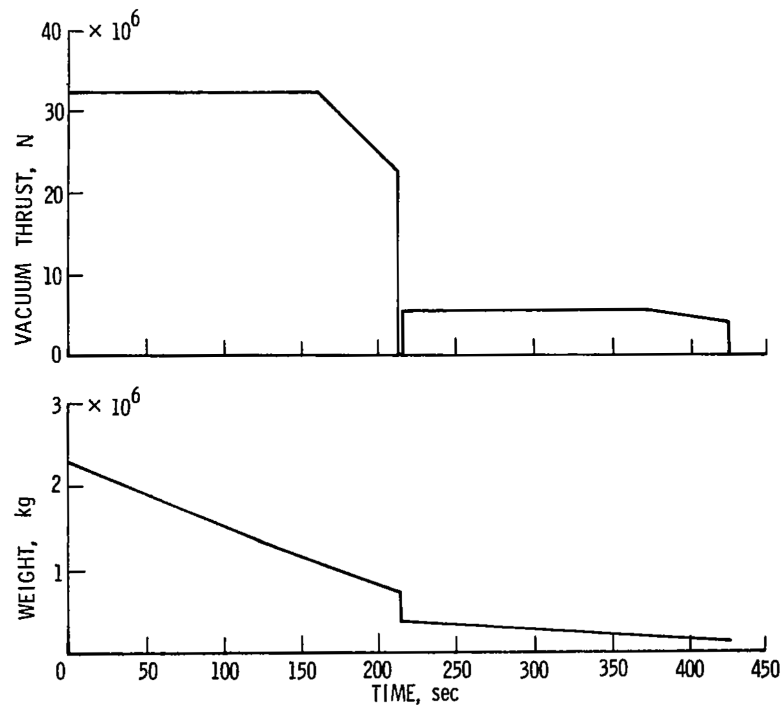

Figure 3

SHUTTLE CHARACTERISTICS

Characteristic	Stage	
	Booster	Orbiter
Number of engines	12	2
Specific impulse (vacuum), sec	439	459
Nozzle exit area, m^2	28.2	20.2
Aerodynamic reference area, m^2	785	618
Propellant weight, kg	1253×10^3	252×10^3
Landing weight, kg	290×10^3	122×10^3

Figure 4

LAUNCH CALCULATIONS

As described in figure 5, a point mass trajectory optimization program, based on the steepest ascent technique of iterative trajectory optimization, was used for calculating the trajectories. The program, described in reference 2, provided a fairly exact mathematical model of the shuttle. This program is quite versatile and is capable of optimizing and simultaneously satisfying a wide variety of constraints. Examples are to constrain certain portions of the flight to fly a specified angle-of-attack program or to constrain an airload parameter, the product of dynamic pressure and the angle of attack ($\bar{q}\alpha$), to be below a specified limiting value. The program was operated with various constraints for this study but was always operated to maximize the payload for a prescribed propellant loading. Vehicle launches were assumed to take place from Kennedy Space Center. The earth model used was a spherical rotating earth with the 1959 ARDC model atmosphere (reference 3).

LAUNCH CALCULATIONS

1. USED ITERATIVE STEEPEST ASCENT METHOD
2. CALCULATED THE MAXIMUM PAYLOAD FOR FIXED STRUCTURE AND FUEL LOADING
3. LIMITED THE AXIAL ACCELERATION TO 3g OR LESS
4. DIRECTED THE THRUST VECTOR THROUGH THE VEHICLE C. G.
5. IMPOSED $(\bar{q}\alpha)_{max}$ LIMITS ON LIFTING TRAJECTORIES

Figure 5

AERODYNAMIC DATA

Typical aerodynamic data in the form of lift coefficient plotted against drag coefficient for several Mach numbers are shown in figure 6. One of the characteristics of this configuration is that it has a positive aerodynamic lift coefficient at zero angle of attack so that it was necessary to program the angle of attack to obtain a ballistic, or nonlifting, trajectory during atmospheric flight for comparison with the lifting trajectories. This characteristic also casts some doubt upon the validity of using the airload parameter $(\bar{q}\alpha)_{max}$ as a basic parameter in structural considerations since appreciable lift is generated on a zero angle-of-attack trajectory. This will become more apparent in the results to follow.

1070

AERODYNAMIC DATA

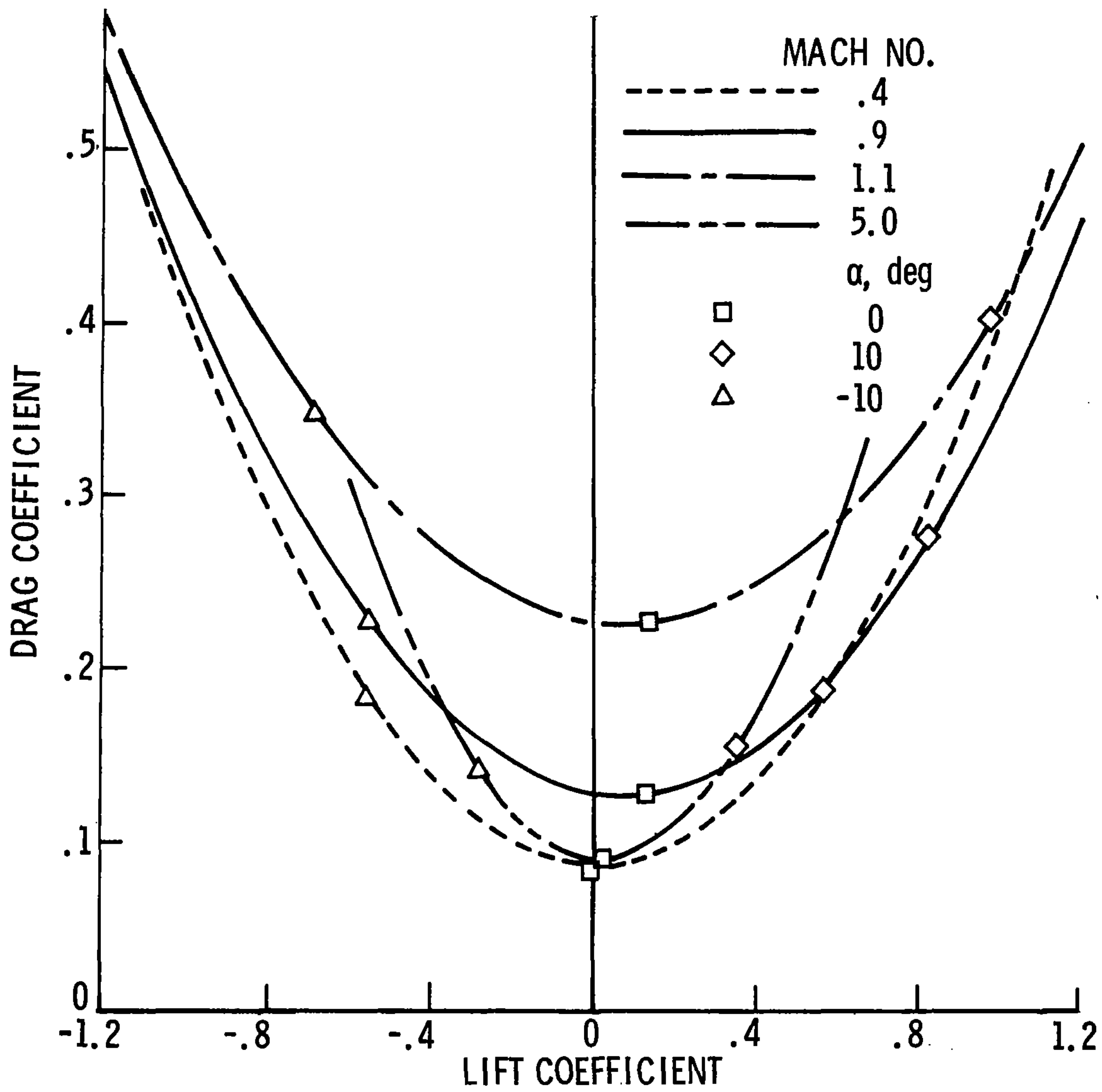

Figure 6

Payload improvements possible through the use of optimal lifting trajectories for the three different missions are shown in figure 7. The payload to a 50- by 100-nautical-mile orbit is plotted against mission in terms of the mission orbit inclination. Three curves are shown: the lower one for a nonlifting trajectory, the upper one for an unconstrained lifting trajectory, and the third for a lifting trajectory constrained to a maximum allowable $\bar{q}\alpha$.

Note that the polar mission, nonlifting data point indicates that 18 140 kilograms (40 000 pounds) payload can be orbited. The payload is roughly doubled by launching due east from Kennedy Space Center indicated at the 28.5° orbit inclination point.

For the unconstrained optimal-lifting polar trajectory, approximately 22 640 kilograms (50 000 pounds) payload can be orbited. This represents about 4500 kilograms (10 000 pounds) or a 25 percent increase in payload capability for this mission. For other missions, the payload improvement increases with decreasing orbit inclination to a maximum of 6000 kilograms (13 200 pounds) at 28.5° inclination.

The performance gain indicated by the unconstrained curve is probably impossible to achieve since it requires the vehicle to pitch down at very high pitch rates immediately after launch (a pitch attitude of about 50° at 15 seconds into flight is required). Also, the vehicle would have to be designed to withstand $\bar{q}\alpha$ airloads in excess of 345 000 deg-N/m^2 (about 7200 deg-psf), where current design values are 134 000 deg-N/m^2 (2800 deg-psf), and the wing body must be structured to carry up to 2.1 million kilograms (4.6 million pounds) of lift. This is probably too much to expect. However, it is possible to achieve a large part of the performance improvement by simply constraining the $(\bar{q}\alpha)_{max}$ to be below a specified value. The curve labeled "constrained" limited $(\bar{q}\alpha)_{max}$ to 134 000 deg-N/m^2 and, as can be seen for the polar design point mission, increased payload by about 3500 kilograms (7700 pounds) as compared to 4500 kilograms for the unconstrained trajectory. Similar results are shown for the other missions.

A part of these payload improvements may be attributable to the ability of the vehicle to efficiently use its lifting capability and a part to the ability to point the thrust vector in the optimum direction. Later in the paper the portion of the improvement due to lifting and the portion due to thrust pointing will be separately evaluated.

SHUTTLE MISSION PAYLOAD CAPABILITY

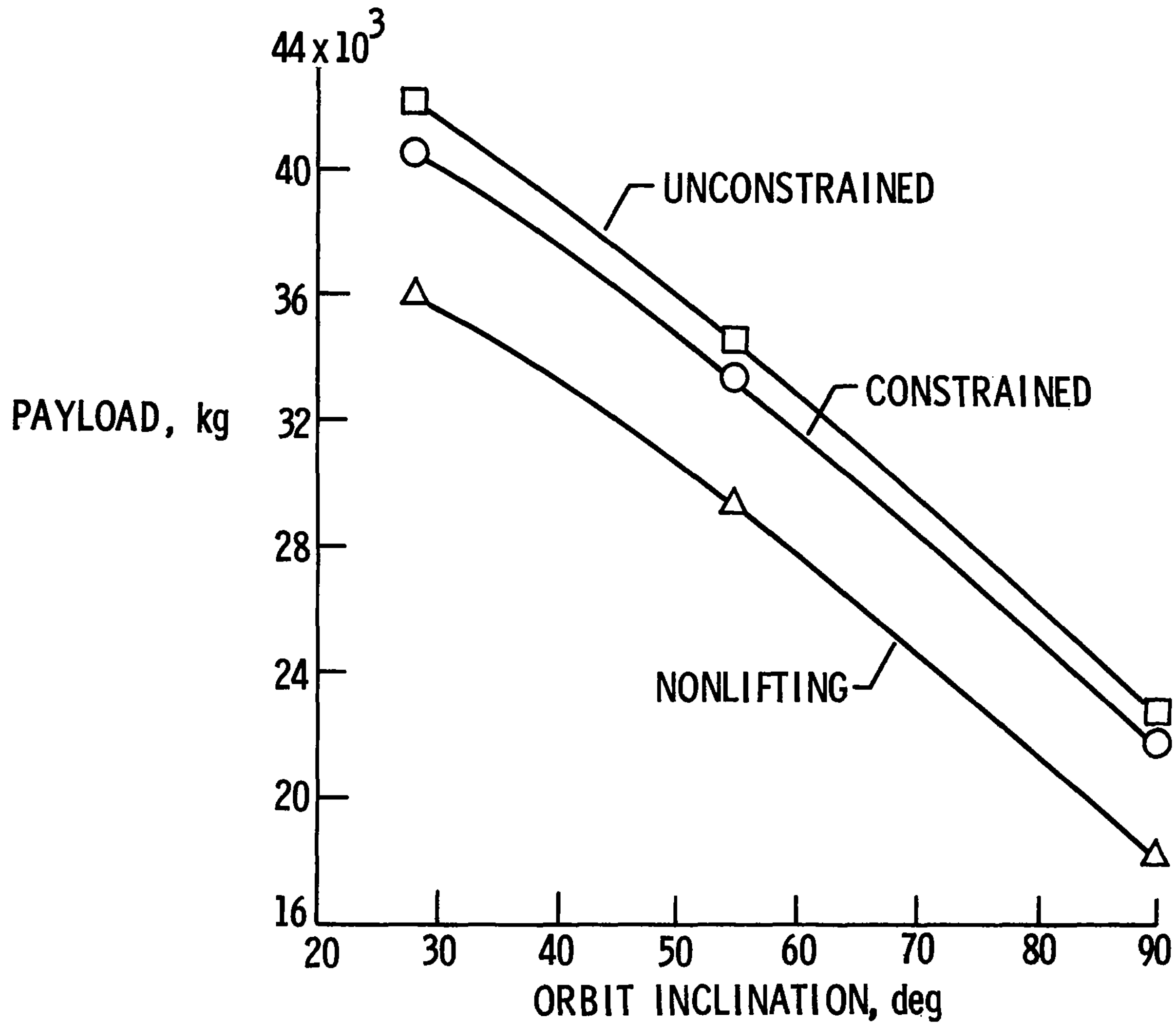

Figure 7

PAYLOAD FOR POLAR ORBIT

For the moment, however, the polar orbit mission will be examined in more detail. In particular, since $\bar{q}\alpha$ is used as a basic design parameter, the way that payload varies as maximum allowable $\bar{q}\alpha$ is increased will be shown. In figure 8 the payload to orbit for the polar mission is plotted against $(\bar{q}\alpha)_{max}$. Also shown on the plot is the payload injected using a nonlifting trajectory. As can be seen, the payload obtainable with $(\bar{q}\alpha)_{max} = 0$ shows a substantial payload increase over that of the nonlifting trajectory. This is because of the lift generated at zero angle of attack, as previously mentioned. An interesting characteristic of this curve is the bend in the vicinity of $(\bar{q}\alpha)_{max} = 55\,000$ deg-N/m^2. This indicates that perhaps a good design value of $(\bar{q}\alpha)_{max}$ for lifting trajectories, for this configuration, might be around 55 000 to 65 000 deg-N/m^2 (1200 to 1400 deg-psf) which is about half of the current design guideline. Of course, this number would have to be increased to provide for off-nominal trajectories, winds, and so forth. However, the horizontal wind shear problem is not as severe as one might think because the flight-path angles of the lifting trajectories are considerably lower in the region of maximum $\bar{q}\alpha$ than those of the ballistic trajectory. As a consequence, the lifting trajectories are less sensitive to horizontal wind shear.

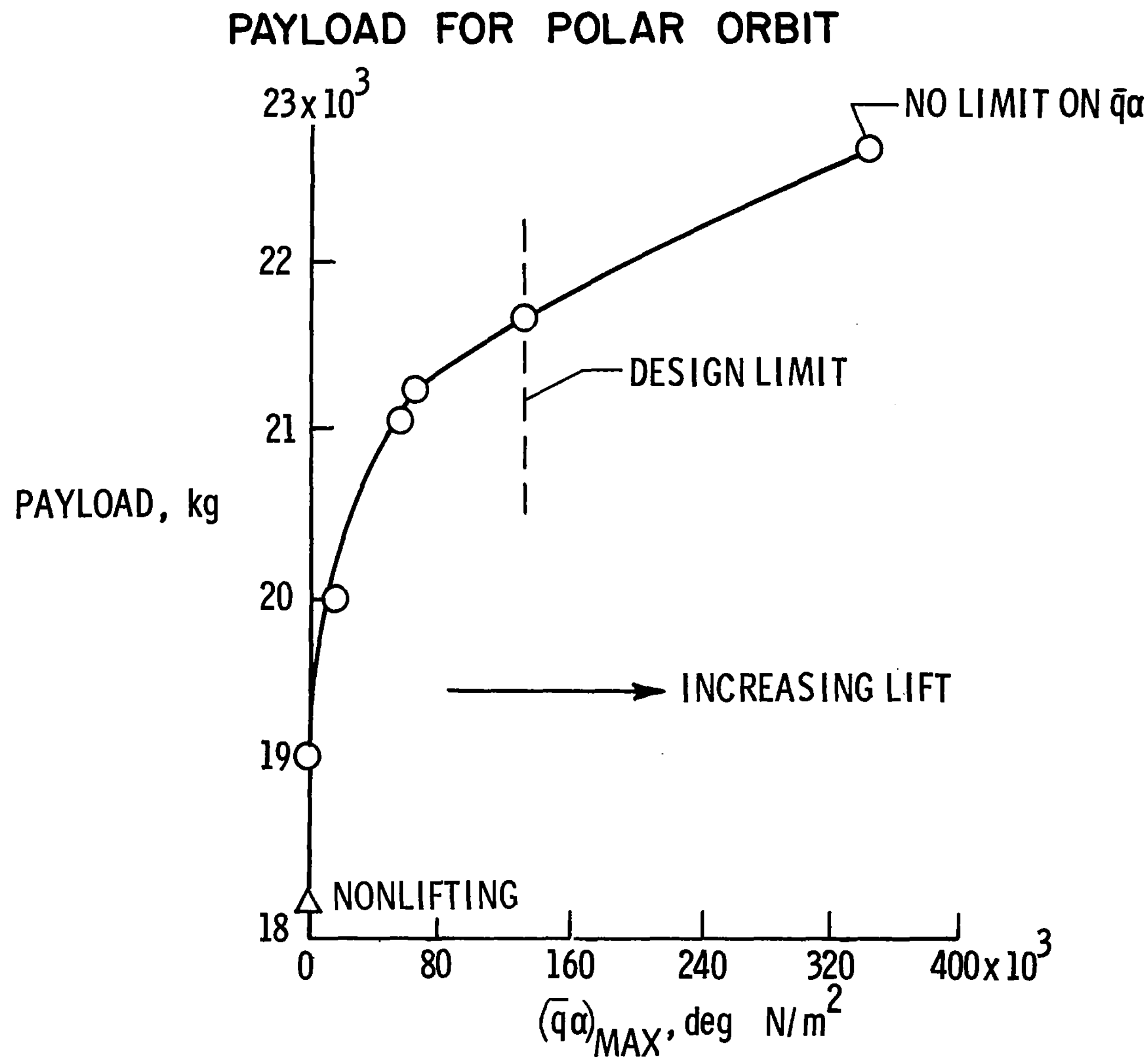
PAYLOAD FOR POLAR ORBIT
23 x 10^3
22
21
20
19
18
PAYLOAD, kg
NO LIMIT ON q̄α
DESIGN LIMIT
INCREASING LIFT
NONLIFTING
0
80
160
240
320
400 x 10^3
(q̄α)MAX, deg N/m^2

Figure 8

VELOCITY LOSSES

A part of the possible payload improvement shown is due to optimal pointing of the thrust vector and a part is due to optimal use of the lift capability of the configuration. Both of these factors are important in the reduction of the major source of velocity loss, that loss due to gravity. The major loss sources which prevent the realization of the ideal ΔV of a configuration are: gravity loss, drag loss, engine back pressure loss, and thrust vectoring loss. In order to show how these losses vary as the lift force changes, a new parameter is required. This new parameter is shown on the abscissa of figure 9 and is simply the integrated lift acceleration. The ordinate is the ΔV loss and the data points correspond to the non-lifting trajectory and a $(\bar{q}\alpha)_{max}$ of 0, 19 000, 67 000, 134 000, and 345 000 deg-N/m^2 moving from left to right. Both the back pressure loss and the thrust vectoring loss are relatively small, between 60 and 90 m/s, and are relatively insensitive to trajectory shaping so that not too much can be done about them. The gravity loss ΔV, however, is about 1290 m/s (about one-seventh of the ideal ΔV) for a ballistic trajectory and the drag loss is about 135 m/s. An optimal trajectory will tend to make the best use of thrust pointing and lift generation in order to reduce the total velocity loss. This is accomplished by reducing the gravity loss but is accompanied by increases in the drag loss. As shown on the total curve, the gravity loss decreases are just about equal to the increases in drag, back pressure, and thrust vectoring losses for large $(\bar{q}\alpha)_{max}$ values, indicating that no further payload increases are possible.

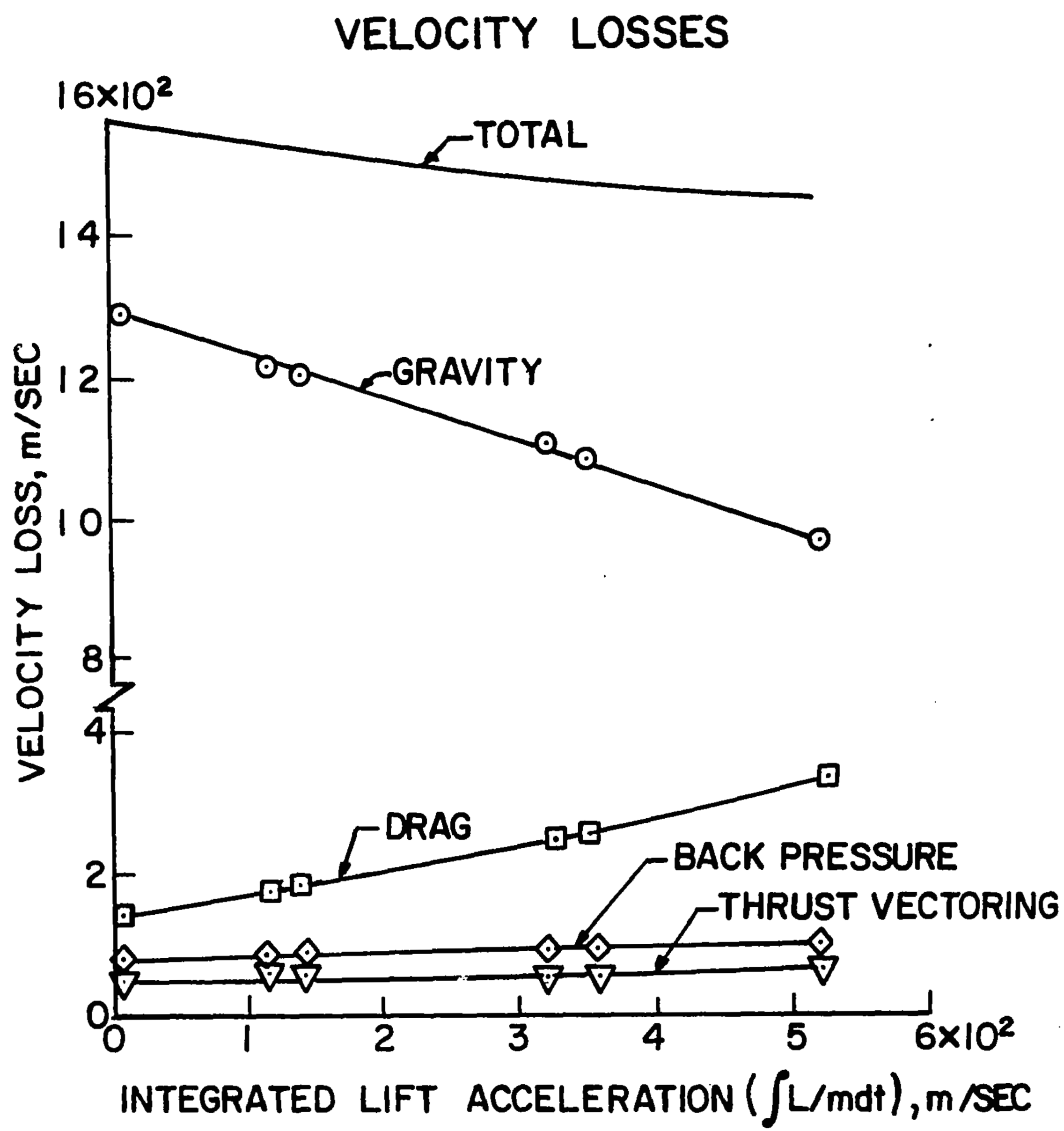
VELOCITY LOSSES
16X10²
TOTAL
GRAVITY
DRAG
BACK PRESSURE
THRUST VECTORING
VELOCITY LOSS, m/SEC
14
12
10
8
4
2
0
1
2
3
4
5
6X10²
INTEGRATED LIFT ACCELERATION (∫L/mdt), m/SEC

Figure 9

VELOCITY LOSS SOURCES

In order to further illustrate this mechanism, figure 10 shows time-history comparisons during booster burn between gravity loss acceleration ($g \sin \gamma$) and drag acceleration (D/m) for three trajectories: the nonlifting or ballistic, the constrained lifting, and the unconstrained lifting optimals. As can be seen in the time histories, since the gravity term is proportional to $\sin \gamma$, the tendency of the optimal lifting trajectories is to decrease the flight-path angle very quickly and thereby reduce the gravity acceleration as soon as possible. This is accomplished at some expense in the drag term.

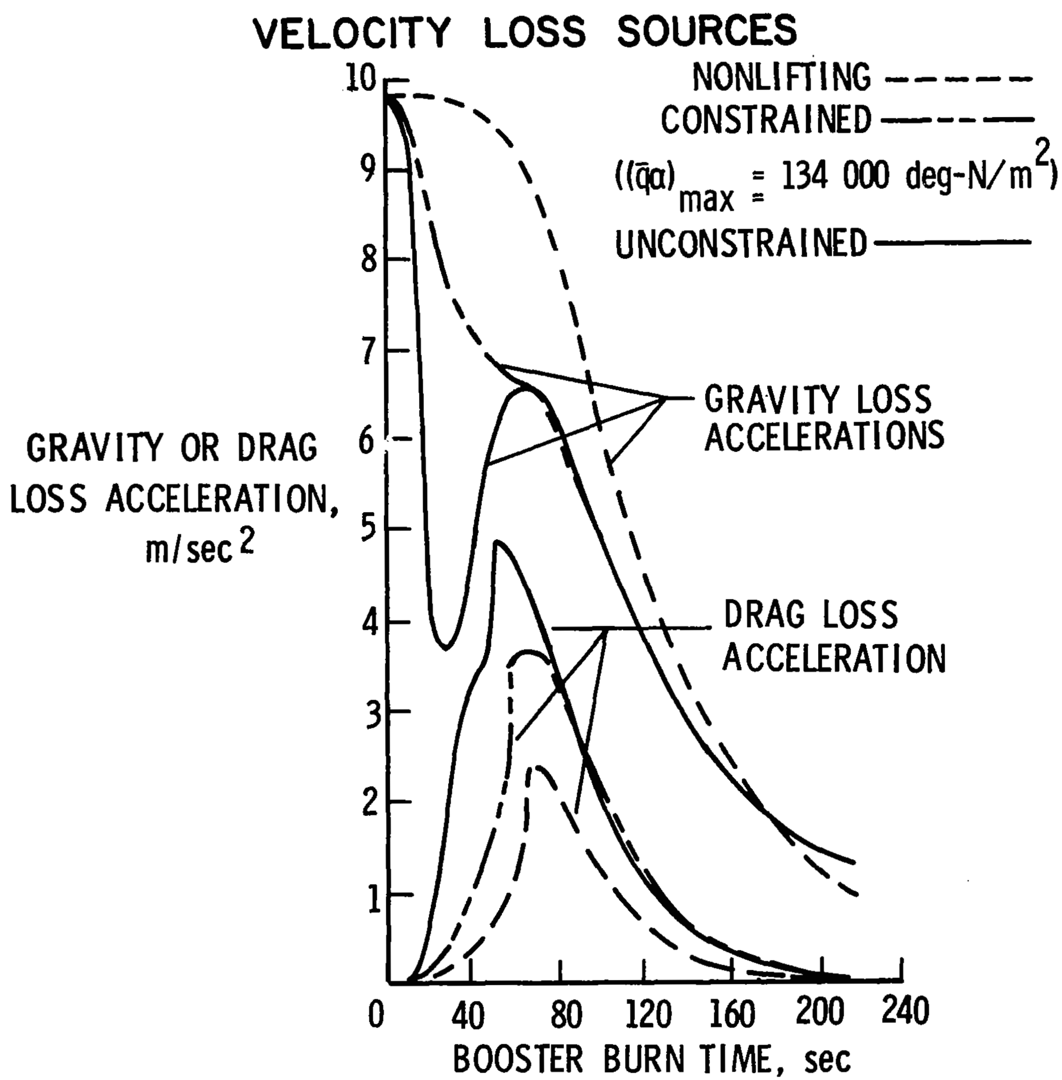
VELOCITY LOSS SOURCES
NONLIFTING
CONSTRAINED
$((\bar{q}\alpha)_{max} = 134\ 000$ deg-N/m^2)
UNCONSTRAINED
GRAVITY LOSS ACCELERATIONS
DRAG LOSS ACCELERATION
GRAVITY OR DRAG LOSS ACCELERATION, m/sec^2
10
9
8
7
6
5
4
3
2
1
0
40
80
120
160
200
240
BOOSTER BURN TIME, sec

Figure 10

LAUNCH TRAJECTORIES

In figure 11, flight-path angle, velocity, and altitude during booster burn are shown for each of the trajectories. As expected, the optimal lifting trajectories fly lower and faster than the nonlifting. Note also the much lower flight-path angles of the lifting trajectories which makes them less sensitive to horizontal wind shear during the period of $(\bar{q}\alpha)_{max}$, generally occurring around 40 seconds. In figure 12, time histories for lift, dynamic pressure, $\bar{q}\alpha$ during booster burn are shown. This figure shows an additional curve corresponding to the trajectory constrained to $(\bar{q}\alpha)_{max} = 67\ 000$ deg-N/m^2 (1400 deg-psf). This case remained on its $(\bar{q}\alpha)_{max}$ boundary for some time, and yet its peak lift of about 900 000 kilograms (2 million pounds) is about the same magnitude as that of the $(\bar{q}\alpha)_{max} = 134\ 000$ deg-N/m^2 case. In addition to the very high $\bar{q}\alpha$ peak for the unconstrained case as previously stated, note that the non-lifting case had fairly substantial negative values of $\bar{q}\alpha$ in order to maintain zero lift during booster burn. It should also be observed that for the lifting case $(\bar{q}\alpha)_{max}$ occurs before $\bar{q}_{max}$, while for the nonlifting case $(\bar{q}\alpha)_{max}$ and $\bar{q}_{max}$ occur at the same time.

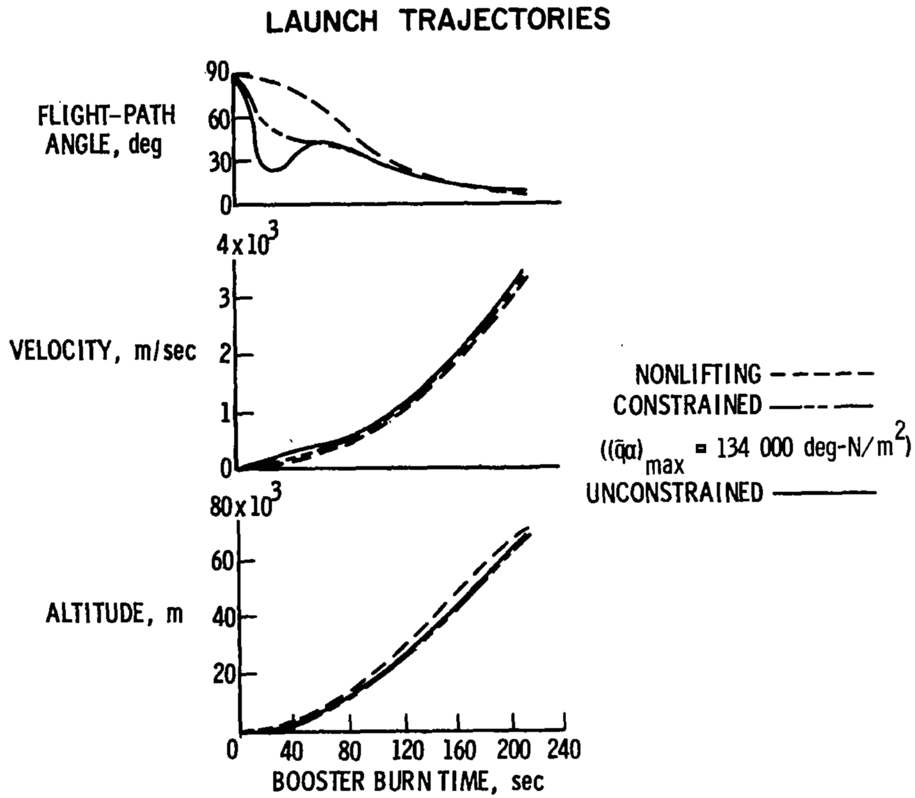

Figure 11

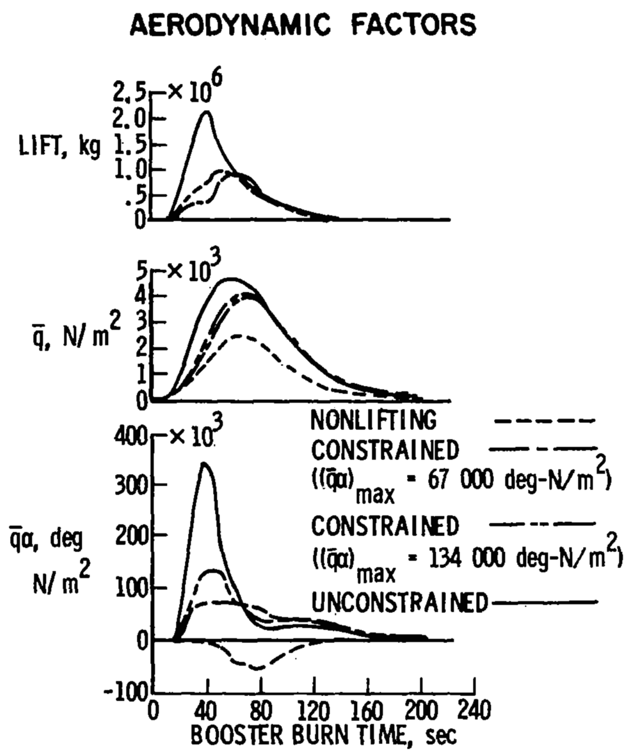

Figure 12

OPTIMAL POINTING-LIFTING

In order to separately evaluate the effects of lifting and thrust pointing, a brief computer study was conducted in which the allowable $\bar{q}\alpha$ was limited to 134 000 deg-N/m^2. For one trajectory, the effects of lift were eliminated by artificially setting the lift and induced drag coefficients to zero. As shown in figure 13, this case then showed a payload improvement of some 1700 kilograms over the nonlifting case, and yet showed some 1800 kilograms less than when the lift and induced drag effects were included in the computations. It is thus surmised that about 50 percent of the improvement was due to the ability to optimally point the thrust vector in relation to the path and that about 50 percent was due to the additional ability to utilize lift.

OPTIMAL POINTING—LIFTING

TRAJECTORY TYPE	PAYLOAD, kg	DELTA PAYLOAD, kg
$\alpha(t)$ FOR ZERO LIFT	18 100	—
OPTIMAL POINTING, NO LIFTING	19 800	1700
OPTIMAL POINTING AND LIFTING	21 600	3500

Figure 13

HEATING RATE

One of the factors which shuttle designers are concerned about, and which has not yet been mentioned, is the heating load experienced by the vehicle. One measure of the heating load is the laminar stagnation-point heat rate for a sphere of unit radius and its integral. The heat rate, in watts/m^2, is shown plotted against time in figure 14 for each of the cases previously mentioned. Tabulated values of the integral of this relation at booster and orbiter burnout times are given in the insert. Note that the heating rates during orbiter burn have been somewhat reduced by the use of lifting trajectories. The heating rates are increased during booster burn but those rates may not be a critical item in the booster. A close examination of the tabulated results shows that the orbiter stage experiences a slightly less severe environment on lifting trajectories than on nonlifting trajectories.

HEATING RATE TIME-HISTORY COMPARISON

TRAJECTORY	LINE TYPE	HEATING INTEGRAL IN JOULES/m^2 AT t = 214 sec	HEATING INTEGRAL IN JOULES/m^2 AT t = 426 sec
NONLIFTING	— — — — — —	8 115 000	29 275 000
CONSTRAINED	——— - - ———	12 150 000	31 935 000
UNCONSTRAINED	——————	12 285 000	31 710 000

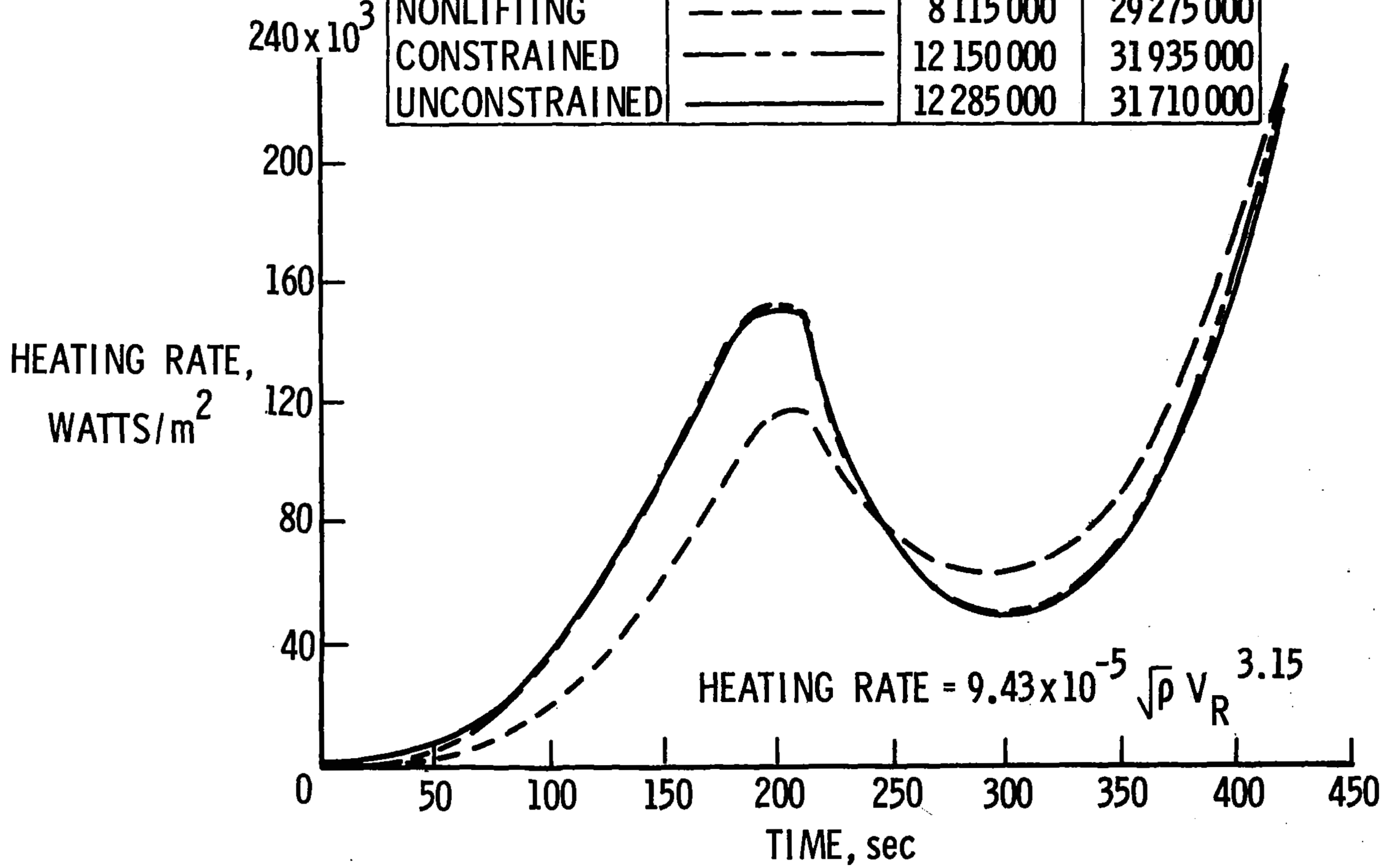

Figure 14

CONCLUDING REMARKS

During ascent the booster-orbiter configuration needs to create about 900 000 kilograms of lift. This should not be a factor of concern since the booster alone is structurally designed for lift loads of about 1.36 million kilograms (3 million pounds). For a configuration of this type, the inertia loads created by the orbiter on the booster during the lifting trajectories would require a more careful examination.

In summary, the use of lifting trajectories, with reasonable values of the airload parameter $(\bar{q}\alpha)_{max}$ can result in payload increases on the order of 15 to 20 percent without undue detrimental effect.

REFERENCES

1. Elliott, Jarrell R.; and Rau, Timothy R. Optimal Payload Trajectory Characteristics for Horizontally Launched Vehicle. J. Spacecraft Rockets, vol. 5, no. 2, Feb. 1968, pp. 218-220.

2. Stein, Laurence H.; Matthews, Malcolm L.; and Frenk, Joel W.: STOP - A Computer Program for Supersonic Transport Trajectory Optimization. NASA CR-793, 1967.

3. Minzner, R. A.; Champion, K. S. W.; and Pond, H. L.: The ARDC Model Atmosphere 1959. AFCRC-TR-59-267, U.S. Air Force, Aug. 1959.

OPTIMAL ASCENT TRAJECTORIES OF A TWO STAGE SPACE SHUTTLE VEHICLE

by R. A. Wilson
Space Division, North American Rockwell Corporation
Downey, California

INTRODUCTION

The Space Shuttle concept offers an interesting option to the traditional launch performance optimization problem in that the shuttle stages are equipped with lifting surfaces designed to withstand significant normal forces. Therefore, a natural question would be whether or not lift can substantially improve performance, thereby lowering total program costs.

Preliminary results obtained with the Phase B "piggy-back" configuration indicated at least quantitatively a potential 15% improvement in performance through the use of lift during mated ascent. Consequently, it is necessary to continually assess the importance of lift as the shuttle evolution progresses.

STUDY OBJECTIVE

(Figure 1)

The objective of this study is to determine the effects of lift on performance of a current space shuttle concept.

Groundrules necessary for the performance evaluation include: 1) Polar launch to a 50 x 100 nautical mile insertion; 2) Main propellant loadings are fixed for comparative purposes since off-loading the stages would result in an unnecessary payload loss; 3) Optimal steering is restricted to the pitch plane only; 4) The product of $q - \alpha$ is unconstrained, whereas axial load is limited to 3 g's in both stages and is achieved by throttling the main engines. The objective is to maximize performance for the given configuration.

STUDY OBJECTIVE

- DETERMINE EFFECTS OF LIFT ON PERFORMANCE CAPABILITY OF A TYPICAL SHUTTLE CONFIGURATION

GROUND RULES

- POLAR LAUNCH TO INSERTION AT 50 NAUTICAL MILES
- ASCENT PROPELLANT LOADINGS FIXED IN BOTH STAGES
- OPTIMAL STEERING RESTRICTED TO THE PITCH PLANE
- $q - \alpha$ UNCONSTRAINED
- AXIAL LOAD LIMITED TO THREE G'S
- MAXIMIZE PAYLOAD FOR GIVEN CONFIGURATION

Figure 1

PROGRAM DESCRIPTION

(Figure 2)

The performance program used in this analysis uses three-degrees-of-freedom to describe the trajectory of a point mass moving over a spherical rotating earth. The optimal thrust-vector angle (the angle between the free stream velocity vector and the thrust vector) is specified by the calculus of variation method. Other unique features of the program include the determination of booster flyback propellant requirements which are a function of staging conditions, and the thrust gimbal angle required to balance the aerodynamic moment. Thrust gimbal angle is referenced to the vehicle centerline such that during mated flight the thrust is generally vectored slightly above the reference axis whereas after separation the orbiter thrust is always pointing below the vehicle centerline. Vehicle aerodynamic coefficients are input in the body axis system and are a function of angle of attack and Mach number. Since the study purpose is to evaluate performance under nominal conditions, winds have been excluded. However, the effect of winds on performance and loads is a significant factor to consider in vehicle design.

PROGRAM DESCRIPTION

- 3 DOF EQUATIONS OF MOTION, SPHERICAL, ROTATING EARTH
- PARTICLE MASS
- OPTIMAL THRUST ATTITUDE SPECIFIED BY CALCULUS OF VARIATION METHOD
- BOOSTER FLYBACK PROPELLANT REQUIREMENTS DETERMINED FROM STAGING CONDITIONS
- AERO MOMENT BALANCED BY THRUST VECTOR
- AERO COEFFICIENTS FUNCTION OF ANGLE OF ATTACK & MACH NUMBER
- NO WINDS

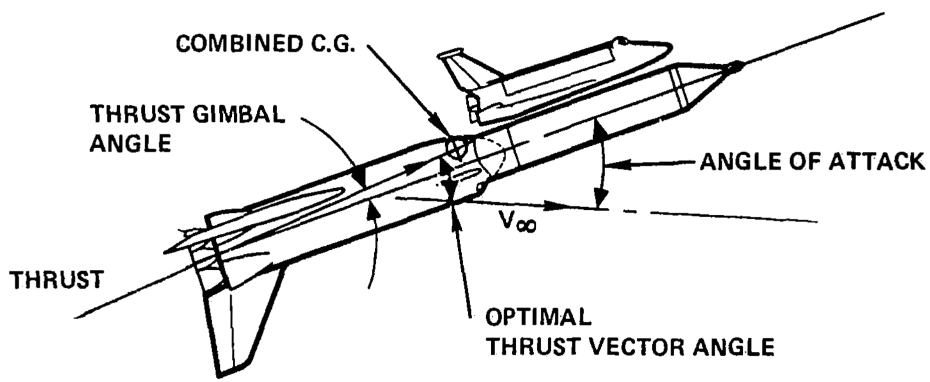

Figure 2

STUDY CONFIGURATION

(Figure 3)

The configuration selected for this study is representative of one of the shuttle concepts currently under investigation. This configuration consists of a reusable flyback booster and a tandem mounted all external tank orbiter. Both stages use liquid oxygen/liquid hydrogen for main ascent propellant. The orbiter main engines which are ignited at separation are canted approximately 8 degrees below the vehicle centerline in order to minimize the gimbal requirements during ascent to orbit.

STUDY CONFIGURATION
(AS OF SEPTEMBER 1, 1971)

GLOW = 3,111,000 (LBS), 1,411,000 KG

$(T/W)_O$ = 1.3

STAGING CONDITIONS

ALTITUDE, (FT), KM	(190,000), 57.9
VELOCITY, (FPS), M/SEC	(7,000), 2134
FLIGHT PATH ANGLE, DEG	13

ITEM	BOOSTER	ORBITER
GROSS STAGE WEIGHT, (K LB), KG	(2141), 971,000	(970), 440,000
ASCENT PROPELLANT, (K LB), KG	(1757), 797,000	(721), 327,000
SEA LEVEL THRUST, (K LB) KN	(4044), 17,990	–
VACUUM THRUST, (K LB), KN	(4441), 19,754	(1148), 5,106
VACUUM I_{SP}, SEC	439	453.2
ENTRY WEIGHT, (K LB), KG	(368), 167,000	(130), 59,000
NUMBER OF ENGINES	12	3

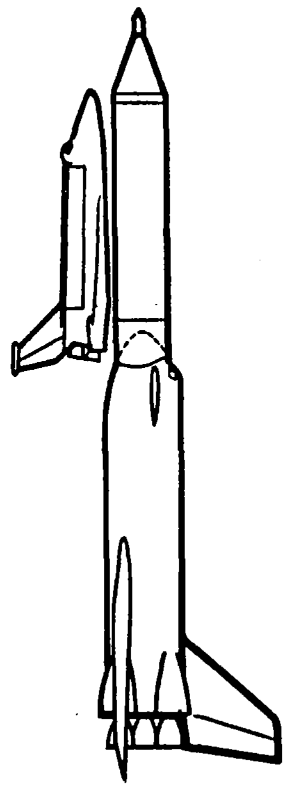

Figure 3

BASIC ASCENT MODES

(Figure 4)

The method for evaluating the effects of lift consisted of comparing the performance of two ascent modes. Case 1 represents the conventional zero alpha flight mode in which the vehicle ascends vertical for 10 seconds and subsequently performs a pitch-over maneuver for the next 20 seconds. From 30 seconds to staging the vehicle flies at zero angle-of-attack. After staging optimal thrust attitude steering directs the orbiter to insertion. Case 2 differs from case 1 in that optimal thrust attitude steering is prescribed from 30 seconds to orbit insertion.

BASIC ASCENT MODES

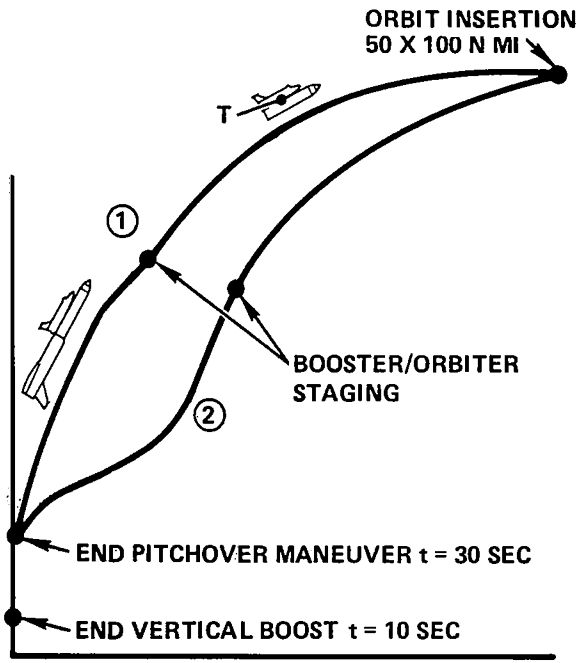

CASE	• EVENT
①	• VERTICAL BOOST FOR TEN SECONDS
	• PERFORM PITCHOVER MANEUVER FOR TWENTY SECONDS
	• ZERO ANGLE OF ATTACK POLICY TO STAGING
	• OPTIMAL PITCHPLANE STEERING TO INSERTION
②	• SAME AS CASE 1 FOR FIRST THIRTY SECONDS
	• OPTIMAL ANGLE OF ATTACK POLICY TO ORBIT INSERTION

Figure 4

ANGLE OF ATTACK TIME HISTORIES

(Figure 5)

Time histories of the angle of attack and thrust vector angle requirements are illustrated in this graph for the two flight modes. Note that the thrust angle requirements during orbiter burn do not represent actual gimbal requirements since the main orbiter engines are canted approximately 8 degrees below the vehicle centerline. As a result of this offset center of gravity, and the optimal thrust angle requirements, the angles-of-attack that the orbiter sees are quite large initially. This does not imply significant aerodynamic loads since dynamic pressure is relatively low at staging and continues to decrease to orbit insertion.

The thrust vector angle requirements during mated ascent of ± 2 degrees are attributed to the combined c.g. being essentially on the vehicle centerline.

THRUST VECTOR ANGLE & ANGLE OF ATTACK VS TIME FROM LIFT-OFF

CASE 1 ZERO ANGLE OF ATTACK

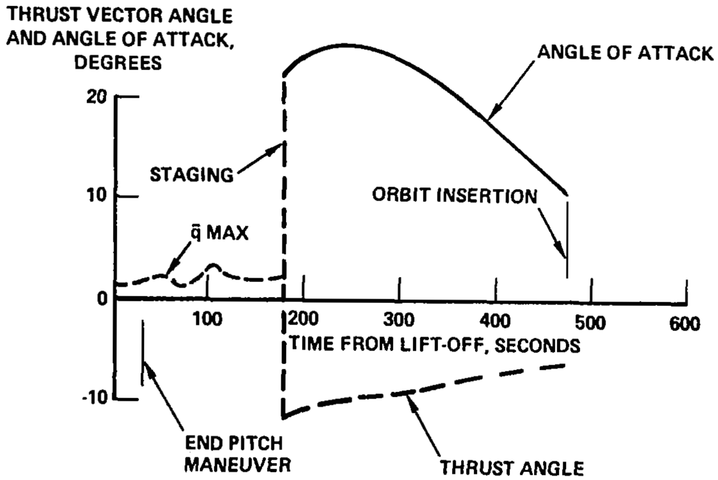

THRUST VECTOR ANGLE & ANGLE OF ATTACK VS TIME FROM LIFT-OFF

CASE 2 OPTIMAL STEERING

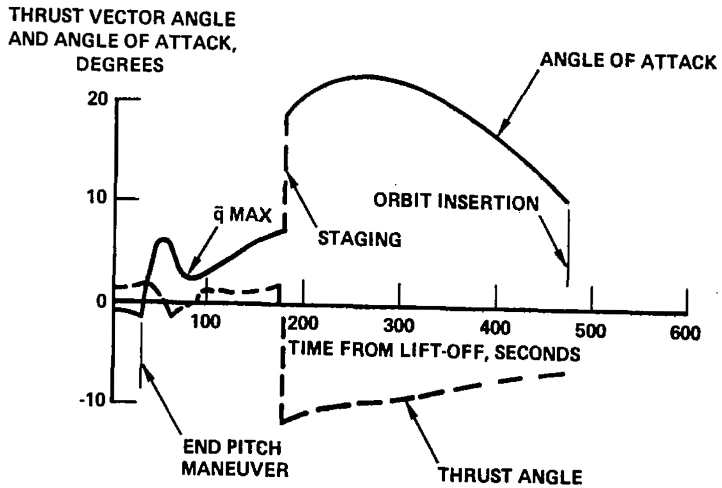

Figure 5

PERFORMANCE RESULTS

(Figure 6)

The performance results are summarized for the ascent modes investigated.

The zero alpha mode, case 1, resulted in a payload of 41,000 pounds with a corresponding maximum dynamic pressure of 518 psf and zero maximum $q - \alpha$ for a no wind condition. Case 2 resulted in a 2,000 pound performance gain over case 1; however, the maximum $\bar{q}$ increased to 644 psf and the product of $q - \alpha$ reached a maximum of 2711 psf degrees. No assessment of the effect of winds on loads was conducted. Nevertheless, it is anticipated that some structural redesign would be necessary to account for increased loads. Thus the potential advantage of mode 2 over mode 1 would diminish or completely disappear.

PERFORMANCE RESULTS

CASE	ALPHA POLICY	$Q_{MAX}/Q\text{-}\alpha_{MAX}$ (PSF)/(PSF-DEG) $N/M^2/N/M^2$-DEG	STAGING CONDITION			PAYLOAD (LBS) KG
			h (FT) KM	γ (DEG)	V (FT/SEC) M/SEC	
1	$\alpha = 0$ TO BOOSTER BURNOUT; OPTIMAL STEERING TO ORBIT INSERTION	(518)/(0) 24,802/0	(188,200) 57.4	13.0	(7085) 2160	(41,000) 18,600
2	OPTIMAL STEERING TO ORBIT INSERTION	(644)/(2711) 30,835/129,800	(182,400) 55.6	15.4	(7158) 2182	(43,000) 19,500

Figure 6

CONCLUSIONS

(Figure 7)

Optimal steering, mode 2, provides a small potential performance gain (approximately 5%) compared to a zero angle-of-attack mode. However, it is expected that the structural weight increase required to withstand increased loads due to winds would offset this potential gain. Consequently, this configuration does not appear to merit further investigation of the use of lift. Finally, significant improvements in performance through the use of lift appear to be configuration dependent, therefore the effects of lift cannot be generalized based on the results of this study.

CONCLUSIONS

- OPTIMAL STEERING RESULTS IN A POTENTIAL PERFORMANCE GAIN (2000 POUNDS) COMPARED TO A ZERO ALPHA ASCENT FOR THIS CONFIGURATION

- HIGHER MAX q-α WOULD RESULT IN STRUCTURAL WEIGHT INCREASE WHICH OFFSET POTENTIAL GAIN

- BENEFITS OF LIFT CANNOT BE GENERALIZED DUE TO CONFIGURATION DEPENDENCY

Figure 7

ABORT SEPARATION OF THE SHUTTLE

John P. Decker, LRC; Kenneth L. Blackwell, Joseph L. Sims, MSFC;
R. H. Burt, W. T. Strike, Jr., ARO;
C. Donald Andrews, L. Ray Baker, Jr., LMSC-Huntsville;
John M. Rampy, Northrop-Huntsville

ABORT

(Figure 1)

During the past year, the abort situation as applied to the Phase B shuttle concepts has been clarified somewhat. Many sub-systems were being designed to accept failures. Consequently, three distinct failure modes, catastrophic, critical, and non-critical, were defined. In the case of a catastrophic failure, both vehicles would be lost. Possibly the crew of each vehicle would be saved by some type of an escape system. For non-critical failures, the abort mode for the booster would be to deplete the excess propellant by burning the main propulsion engines and conducting staging operations near nominal conditions. The booster would return to the launch site after separation while the orbiter would have a trajectory tailored to abort once around and return to the launch site or a suitable downrange recovery site.

For critical aborts when mated flight would not be possible the stages would have to separate at off nominal conditions, that is, perform an abort separation maneuver in the sensible atmosphere. After separation both the orbiter and booster trajectories would be tailored so that both vehicles could land at a suitable site. The question here is, can the vehicles safely perform an abort separation maneuver at conditions from lift-off to nominal staging and if this is feasible, how does this influence the abort philosophy?

The abort separation work that will be discussed in this presentation has been an intercenter, interagency and intergovernmental effort and is the reason for the number of co-authors on the paper. In this paper the overall effort and what has been learned about abort separation of the shuttle will be discussed.

ABORT

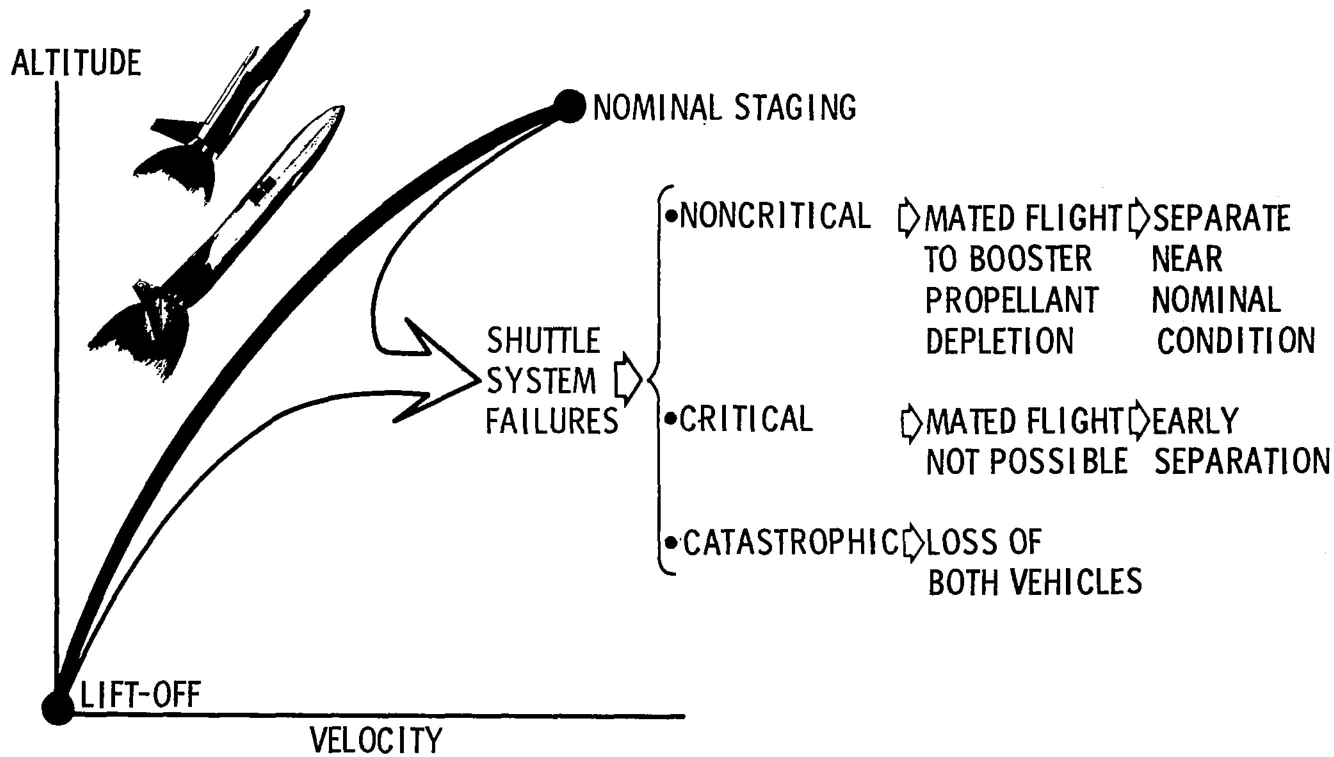

Figure 1

STAGING STUDIES DURING THE SIXTIES

(Figure 2)

Numerous staging studies (references 1 - 17) were conducted in the sixties on the vehicles shown in this figure. These staging studies were preliminary and consequently a clear answer to the question of parallel separation of two vehicles of similar size was not obtained. In fact, staging in the sensible atmosphere for most of these vehicle systems was generally avoided since some of the preliminary results indicated that staging in the sensible atmosphere would be difficult.

The parallel separation of two vehicles of similar size is different than the separation problem for any system designed up to the present. For the shuttle we are interested in the integrity of both vehicles at separation. For previous systems, only the integrity of the upper stage was involved at separation. Furthermore, the separation problem of the shuttle is also different than separating an external store from a parent vehicle such as the X-15 from the B-52. In the case of the separation of an external store, only the external store aerodynamic characteristics are disturbed from nominal conditions. For the parallel separation of two vehicles of similar size, both vehicles' aerodynamic characteristics are disturbed from nominal conditions.

STAGING STUDIES DURING THE SIXTIES

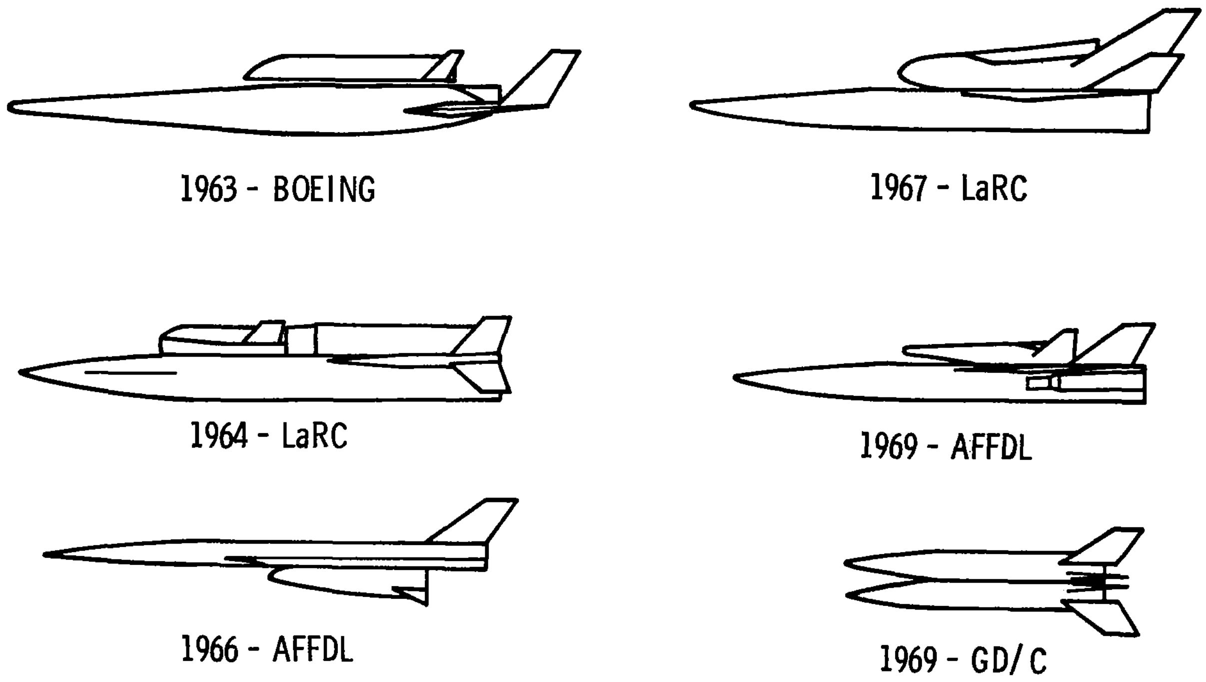

Figure 2

ABORT STAGING TECHNOLOGY CONSIDERATIONS

(Figure 3)

Many disciplines must be considered in an abort analysis and many iterations will take place between the disciplines before a workable abort procedure is completed. However, it is not necessary to close all these loops to accomplish the objectives of this study which were to perform a sensitivity analysis of factors which affect a successful abort maneuver and to provide guidelines for future studies.

The approach was to conduct wind tunnel tests using the best simulation techniques and data acquisition-analysis-dissemination procedures that were available within time and facility limitations. Static stability, dynamic stability and local loads investigations were conducted during this study. These results were extensively utilized in the dynamic simulation computer program which integrates the equations of motion for both vehicles (6 degrees of motion for each) and calculates their relative position and attitude. In the present effort only the longitudinal motion was studied in depth. Close coordination was maintained in planning and conducting of these tests to assure that data required for calculating separation trajectories would be available in an optimum format and on a timely schedule. Information from other disciplines such as mass characteristics, propulsion characteristics, mechanism kinematics, ascent conditions, and thrust vector control authority were obtained as open loop inputs from phase B studies while the aero control authority was looked at during the wind tunnel tests. The underlined items therefore are the items that were considered in the dynamic simulation program. The other items have been looked at to various degrees by other researchers.

ABORT STAGING TECHNOLOGY CONSIDERATIONS

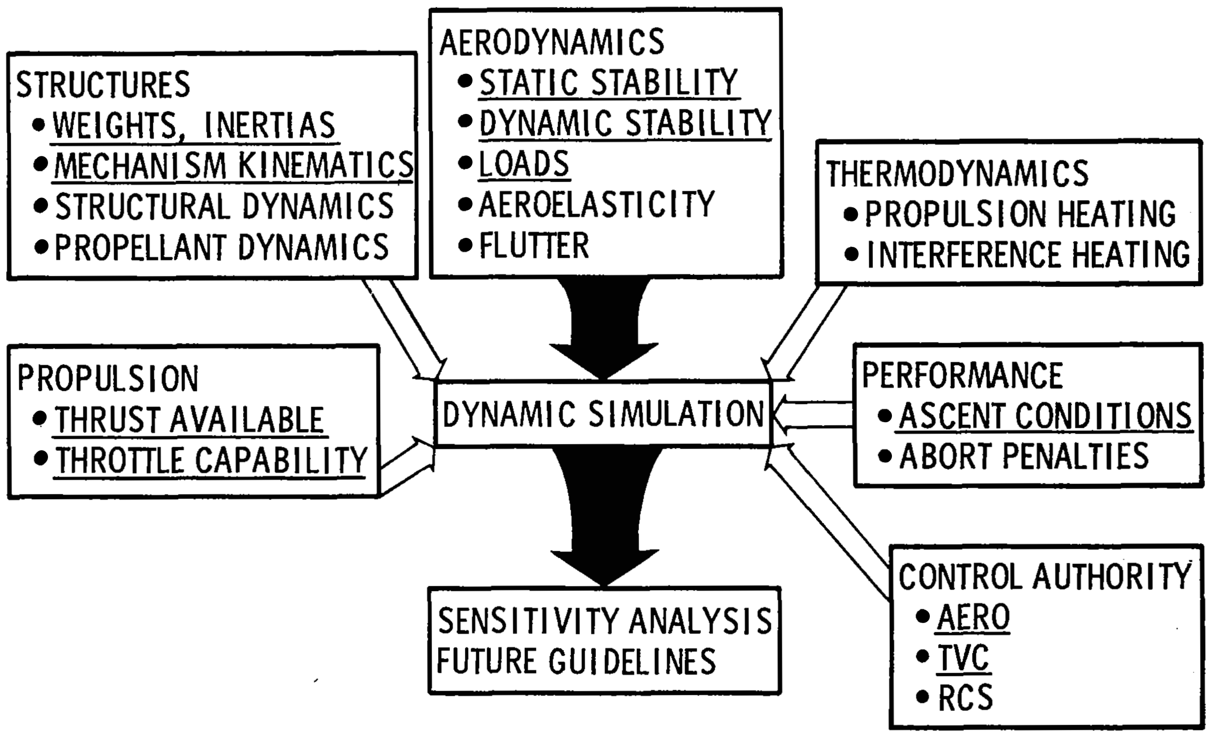

Figure 3

FORCE AND MOMENT TESTS AND PRESSURE DISTRIBUTION TESTS

(Figure 4)

Both the static stability and local loads investigations were conducted at Mach numbers from 2 to 6 in tunnel A of the von Kármán Gas Dynamics Facility at the Arnold Engineering Development Center. The vehicle system selected for these investigations was the McDonnell Douglas Corporation's Phase B shuttle concept. For the static stability tests, both stages were instrumented with strain gage balances to measure the forces and moments that occur on each vehicle when in proximity to each other. For the local loads investigation, the booster and orbiter were instrumented with pressure orifices to measure the local interference loads on the vehicles. All tests were conducted simulating the rocket exhaust plume from both the orbiter and booster. The two-engine orbiter arrangement and the twelve-engine booster arrangement were each simulated by a toroidal model nozzle, details of which are described in figures 6 - 9. The plume was simulated at various altitudes corresponding to the Mach number range investigated. The dynamic pressure for these conditions ranged from about 19,152 N/m^2 (400 psf) at $M = 2$ to 1,436 N/m^2 (30 psf) at $M = 6$.

Nominal staging conditions, references 18 and 19, have been looked at by Marshall Space Flight Center and Manned Spacecraft Center. The Mach number 1 regime has also been looked at in some depth by both Manned Spacecraft Center and General Dynamics/Convair. Other related staging data are shown in reference 20.

FORCE AND MOMENT AND PRESSURE DISTRIBUTION TESTS

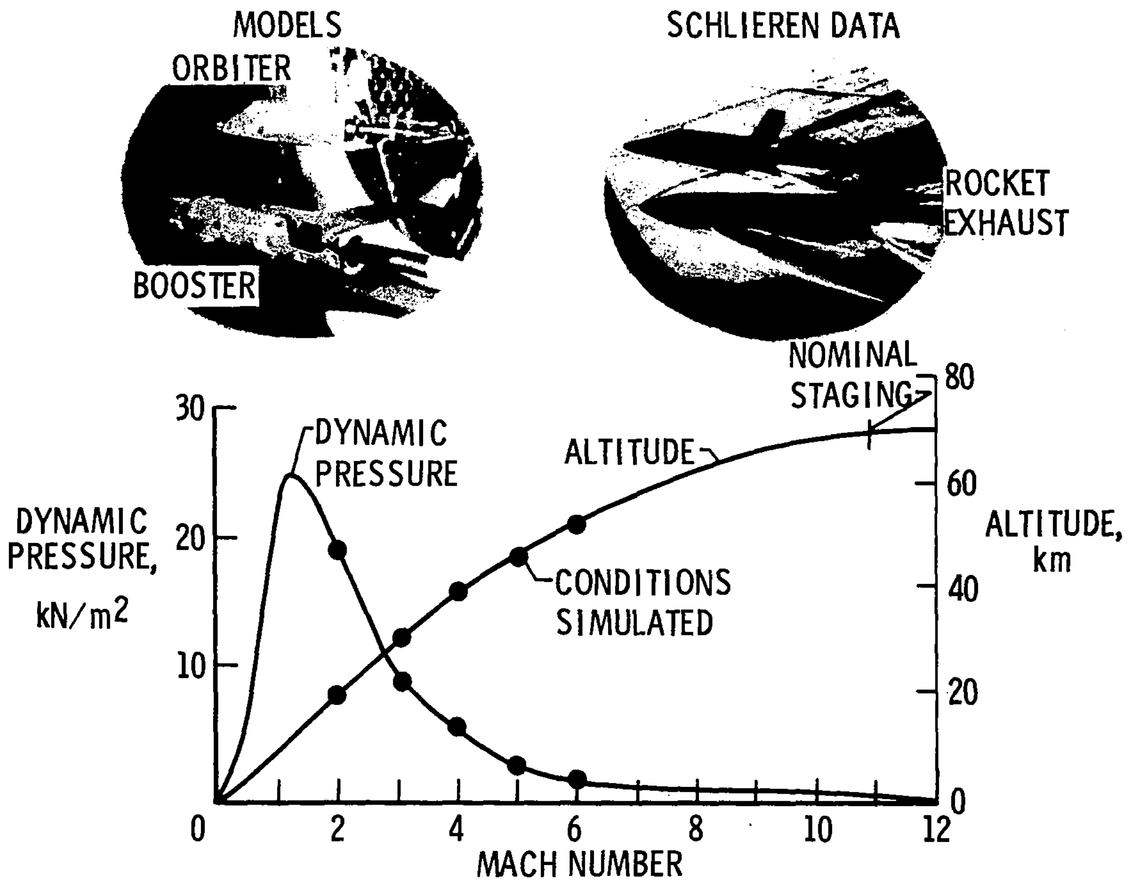

Figure 4

AERODYNAMIC DATA MATRIX

(Figure 5)

The matrix for which aerodynamic interference data was obtained is shown in this figure. Each dot represents the placement of the orbiter center of gravity with respect to booster center of gravity. An automatic control system allowed a series of orbiter positions to be programmed prior to a test run. This control system was integrated with the data recording system and angle-of-attack system so that model positioning, pitching, and data recording were completely automatic once a matrix was initiated. The orbiter and booster were pitched together as a unit from -10 to +10°. For the force and moment tests the data was recorded in a continuous pitch mode while for the pressure distribution tests the data was recorded in a pitch-pause mode. The orbiter incidence angle was varied by manual adjustment and incidences angles of 0°, ±5°, and ±10° were investigated. Orbiter thrust levels of 0%, 25%, 50%, and 100% and booster thrust levels of 0%, 50%, and 100% were investigated. By making use of the automatic control system 1850 pitch polars were obtained during the force and moment tests and 300 pitch polars were obtained during the pressure tests in 100 hr of tunnel occupancy time. All of the force and moment pitch polars were subsequently used in the dynamic simulation program.

AERODYNAMIC DATA MATRIX

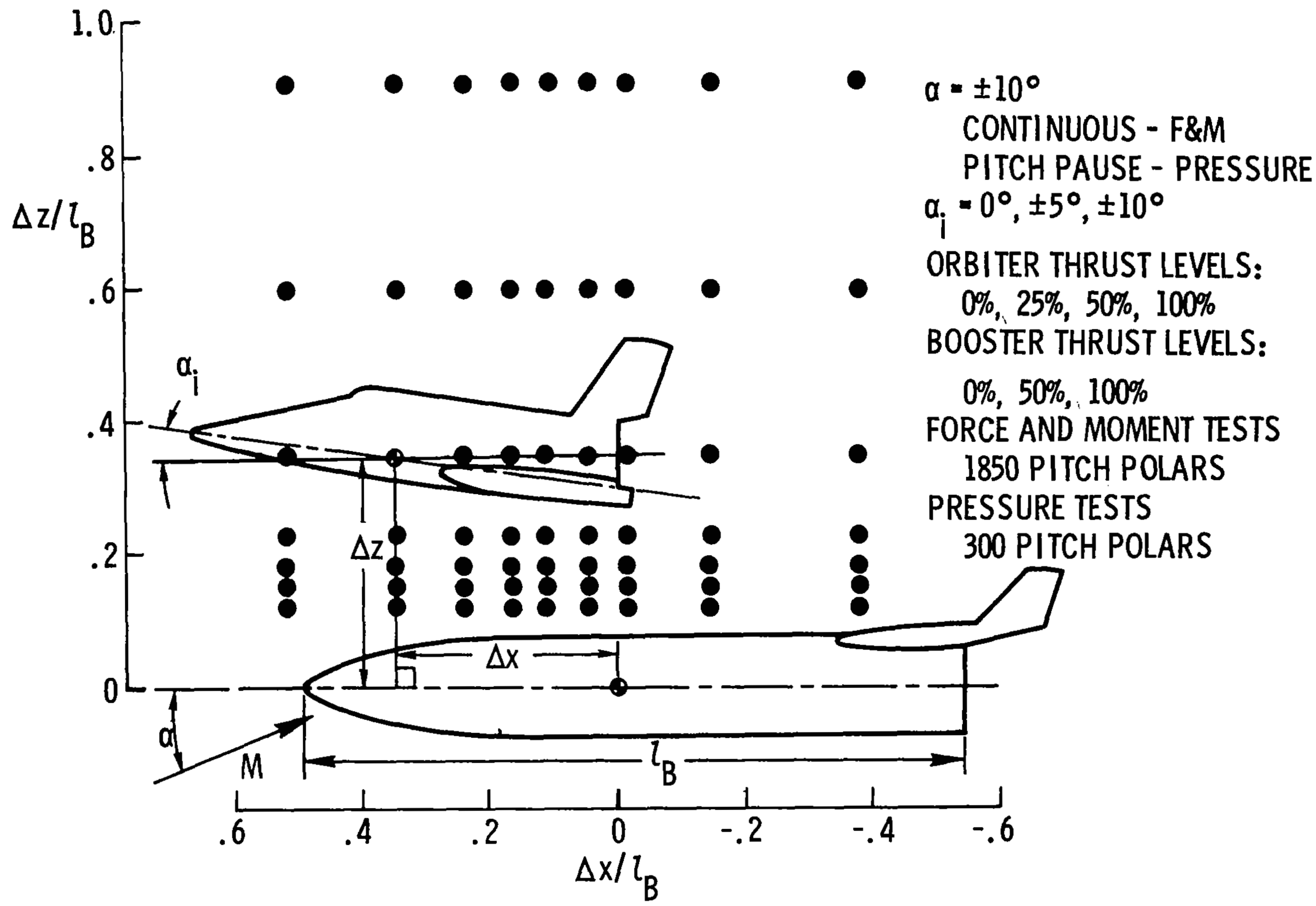

Figure 5

ROCKET EXHAUST SIMULATION

(Figure 6)

When a complex flow field such as a rocket's exhaust plume is to be modeled, it is usually impossible to simulate all of the gas dynamic parameters over the entire flow field if a different gas must be used. Thus, it is necessary to identify the important physical phenomena and the similarity parameters that control them. The two major effects of the plume on the flow field which need to be simulated are shown in this figure. These two effects are best simulated when the size and shape of the exhaust plume are scaled from the full scale plume. This is achieved by use of the similarity equations obtained from reference 21.

ROCKET EXHAUST SIMULATION

MAJOR PLUME EFFECTS TO BE MODELED

- AERODYNAMIC LOADS CAUSED BY THE PLUME GENERATED SHOCK LAYER
- LOADS CAUSED BY DIRECT PLUME IMPINGEMENT

PLUME PARAMETER SIMULATION TO ACHIEVE ABOVE RESULTS

- EXHAUST PLUME SIZE
- EXHAUST PLUME SHAPE

SIMILARITY EQUATIONS

$$\left(\frac{M_1}{\gamma}\right)_{MODEL} = \left(\frac{M_1}{\gamma}\right)_{FULL\ SCALE}$$

$$\left(\delta_J\right)_{MODEL} = \left(\delta_J\right)_{FULL\ SCALE}$$

$$\left(\theta_N\right)_{MODEL} = \left(\theta_N\right)_{FULL\ SCALE}$$

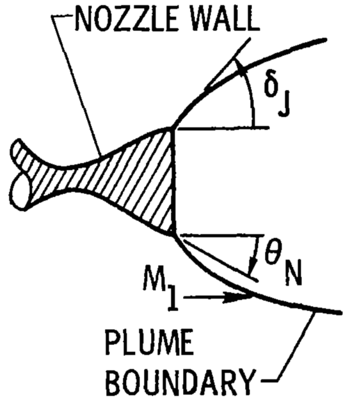

Figure 6

ESTIMATED FULL SCALE PLUME PARAMETERS

(Figure 7)

Two of the full scale plume parameters for the orbiter engine used in the similarity relationships are presented over the altitude range of interest. These two parameters are the plume boundary angle at the engine exit plane and the plume boundary Mach number. These results were computed for the combustion products of O_2/H_2 in thermodynamic equilibrium. The gas mixture has a variable ratio of specific heats over the range of temperatures in the nozzle and plume. Therefore, if the full scale similarity parameters are to be reproduced by a gas with a constant ratio of specific heats, the model nozzle area ratio will vary with altitude.

ESTIMATED FULL SCALE PLUME PARAMETERS

ORBITER ENGINE

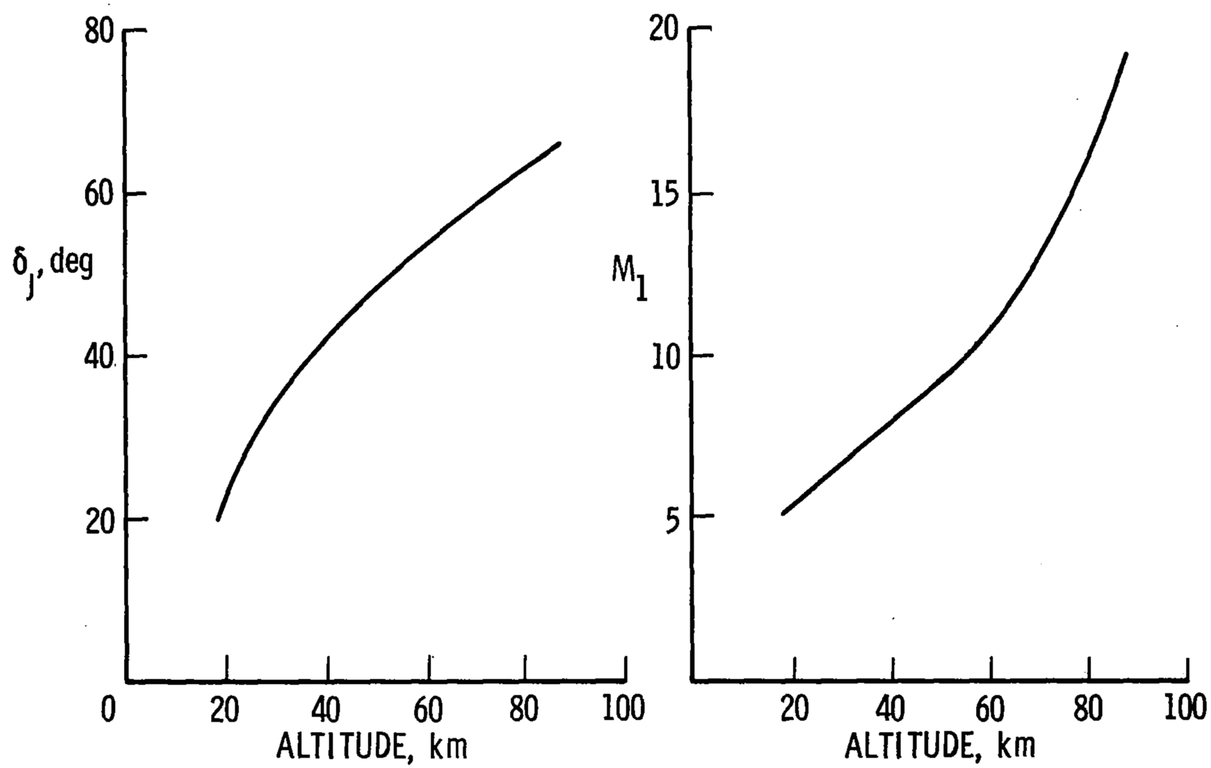

Figure 7

MODEL PLUME CHARACTERISTICS

(Figure 8)

The requirements for varying area ratio and hardware restraints imposed by the support stings led to the design of a toroidal model nozzle for both the orbiter and booster. Both nozzles were similar in detail. The support sting served as the center body of the nozzle and also as a conduit for the air supply to the nozzles. The nozzle area ratio, which is the ratio of the exit area to the throat area, could be varied by a longitudinal translation of the outer wall in relation to the inner body.

The required area ratio variation of the orbiter nozzle over this altitude range is shown. A calibration of the model nozzles was performed (reference 22) in order to establish the operating characteristics as a function of geometric setting. This was accomplished by computing the nozzle area ratio from exit plane static pressure data and from plume angles at the nozzle lip. These results are also shown and agree well enough so that we were confident that the required plumes would be generated by the nozzles.

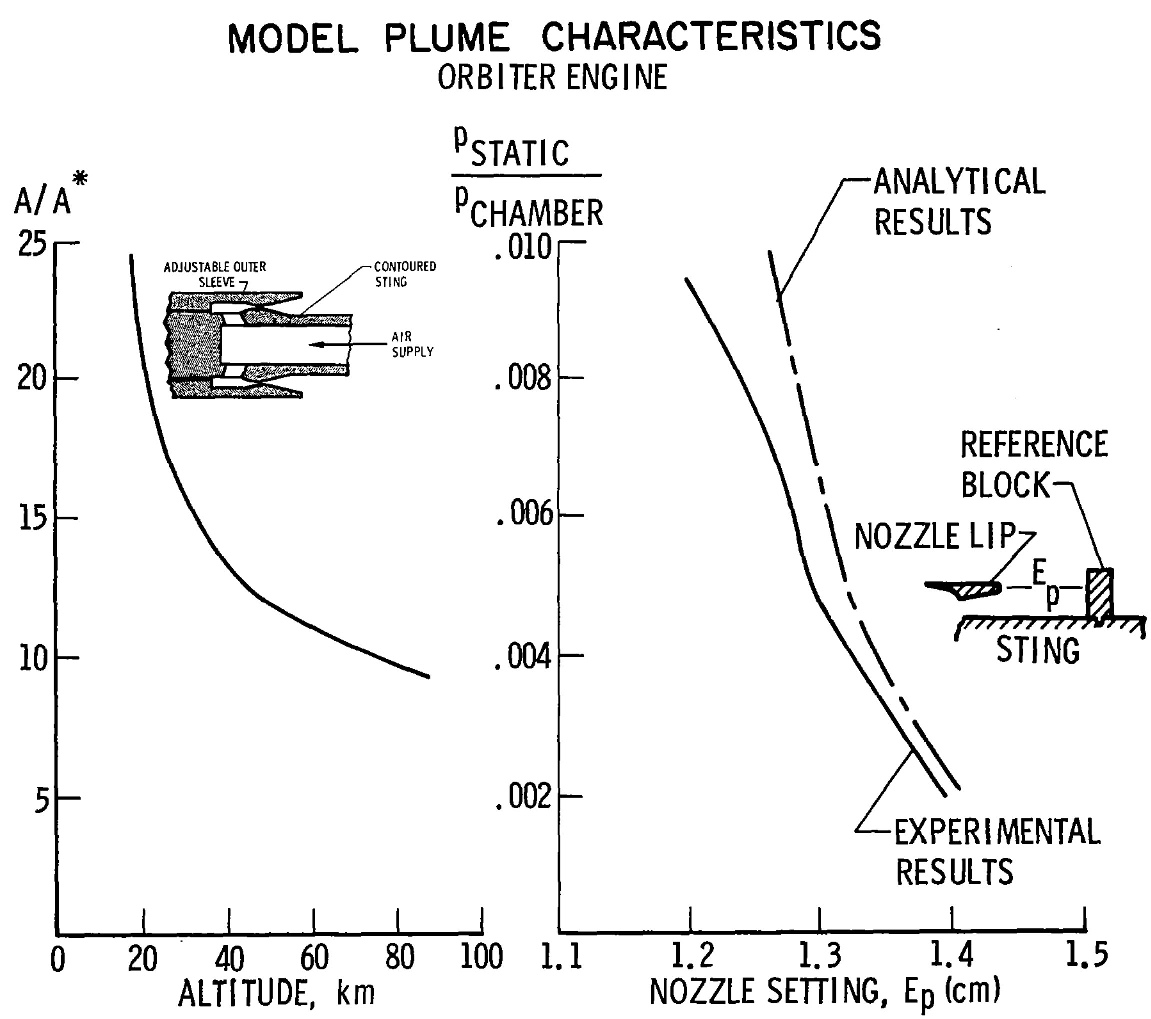
MODEL PLUME CHARACTERISTICS
ORBITER ENGINE
A/A*
25
20
15
10
5
0
20
40
60
80
100
ALTITUDE, km
ADJUSTABLE OUTER SLEEVE
CONTOURED STING
AIR SUPPLY
p STATIC / p CHAMBER
.010
.008
.006
.004
.002
1.1
1.2
1.3
1.4
1.5
NOZZLE SETTING, Ep (cm)
ANALYTICAL RESULTS
EXPERIMENTAL RESULTS
REFERENCE BLOCK
NOZZLE LIP
Ep
STING

Figure 8

EXTERNAL FLOW FIELD EFFECTS

(Figure 9)

To illustrate how the rocket exhaust influences the vehicles and also the importance of an external stream, representative data obtained during the pressure distribution tests are presented in this figure. Two plume impingement conditions are illustrated. One is where there is no external flow and the other is for an external Mach number 5 stream. The orbiter nozzle area ratio and chamber pressure are the same in both cases. The plume boundaries as viewed in the pitch plane of the vehicles did not differ by more than 5 or 6 percent at the orbiter nozzle exit.

The centerline peak pressures were nearly equal for the two cases illustrated and these peaks occurred at nearly the same booster model station. The important difference here is that the plume impingement disturbance propagates laterally or further outboard along the wing surface when the external stream is present. This is probably due to the combined wakes of the orbiter and booster interacting with the orbiter plume and causing the plume induced impingement pressure distribution to expand further in the yaw plane when the external Mach number 5 stream is present.

EXTERNAL FLOW FIELD EFFECTS

$\Delta x/l_B = 0.104$; $\Delta z/l_B = 0.150$; $\alpha = 0°$; $\alpha_i = 5°$; ORBITER POWER = 100%

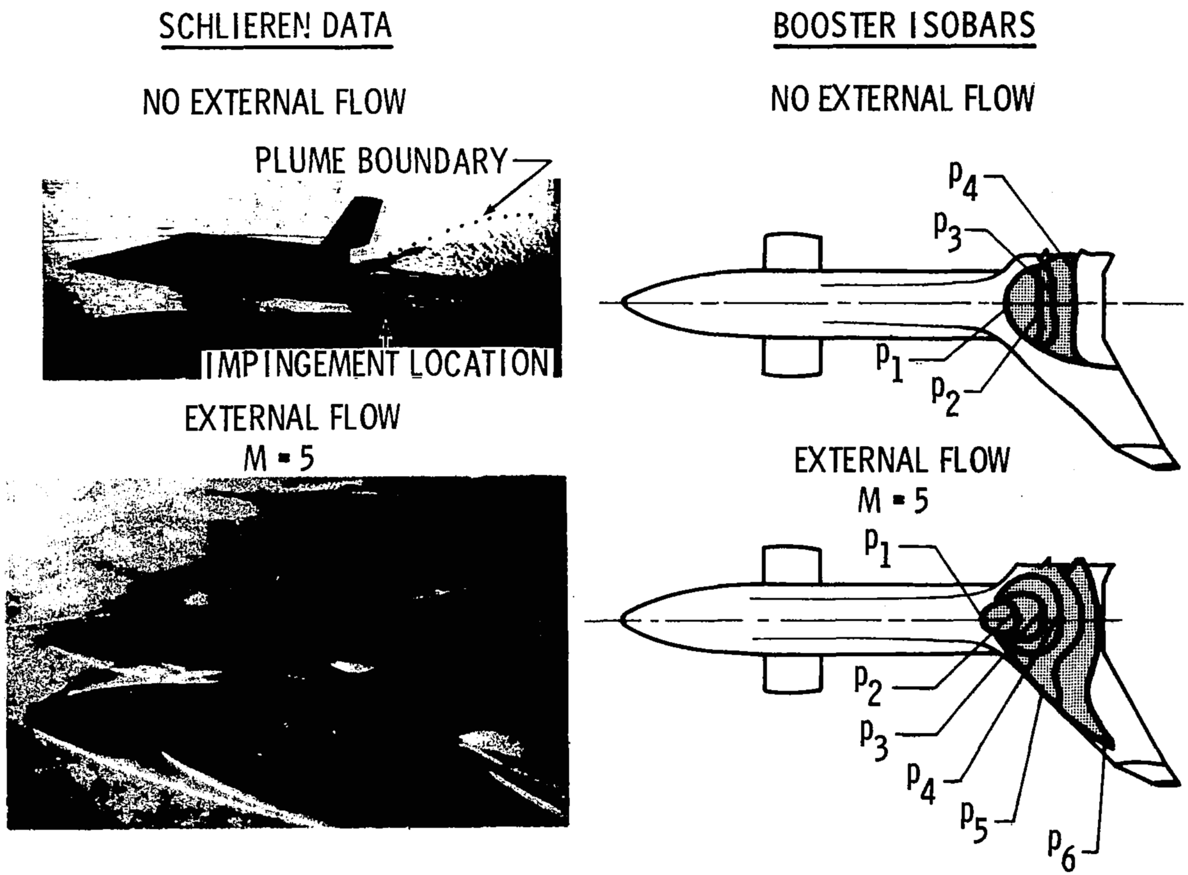

Figure 9

EFFECT OF ORBITER POWER LEVEL

(Figure 10)

An important feature learned about the use of simulated engine propulsion in conjunction with abort staging wind tunnel tests was that increments in aerodynamic coefficients for the booster as a function of orbiter engine power level were linear over large portions of the orbiter power range. This is illustrated in this figure where the increments on the booster aerodynamic coefficients for a representative position and attitude of the orbiter are shown as a function of orbiter power setting. The linearization of the curves is significant when considering application of the data to a flight dynamic simulation program where power transients must be considered. Data required for basic attitude and position variations for the separation envelope are already voluminous so the addition of another major variable requiring detailed definition would only complicate the study of abort staging and increase costliness of data acquisition. From what has been learned during this investigation it is envisioned that for final design data only a few (3, 4) power settings would be required to be tested for each of the other test condition variables.

EFFECT OF ORBITER POWER LEVEL

$M = 5; \Delta x/l_B = 0.104; \Delta z/l_B = 0.151; \alpha = 0°; \alpha_i = 5°$

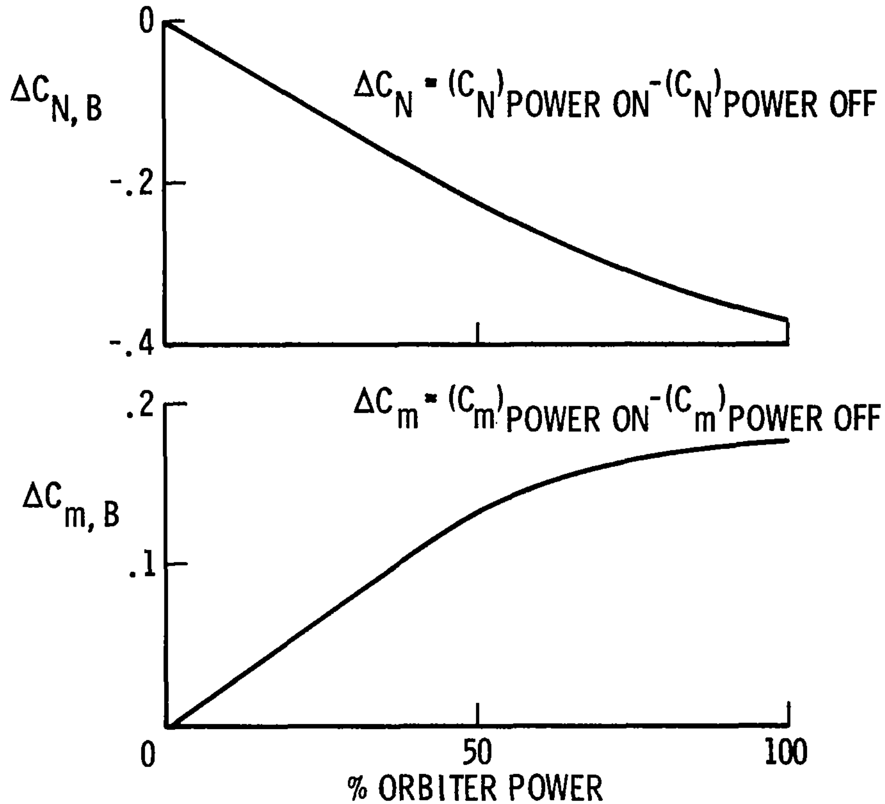

Figure 10

LOCUS OF MEASURED INTERFERENCE EFFECTS

(Figure 11)

The locus of measured interference effects as a function of the position parameters (figure 5) on the orbiter and booster due to the proximity of the other vehicle is illustrated in this figure at Mach numbers of 2, 3, and 5. The three interference conditions shown are an interference free condition, an aerodynamic interference condition where the interferences are due to mutual shock impingement on each vehicle, and a propulsive interference condition due to the impingement of the rocket exhaust plumes.

As the Mach number is increased, the region where the orbiter is at interference free conditions becomes larger due to the bow shock of the booster bending further towards the booster body. At the same time the region where the rocket exhaust from the booster impinges on the orbiter becomes larger since the plume of the booster becomes larger. Similar trends are also shown for the booster except that the regions are reversed as would be expected.

LOCUS OF MEASURED INTERFERENCE EFFECTS

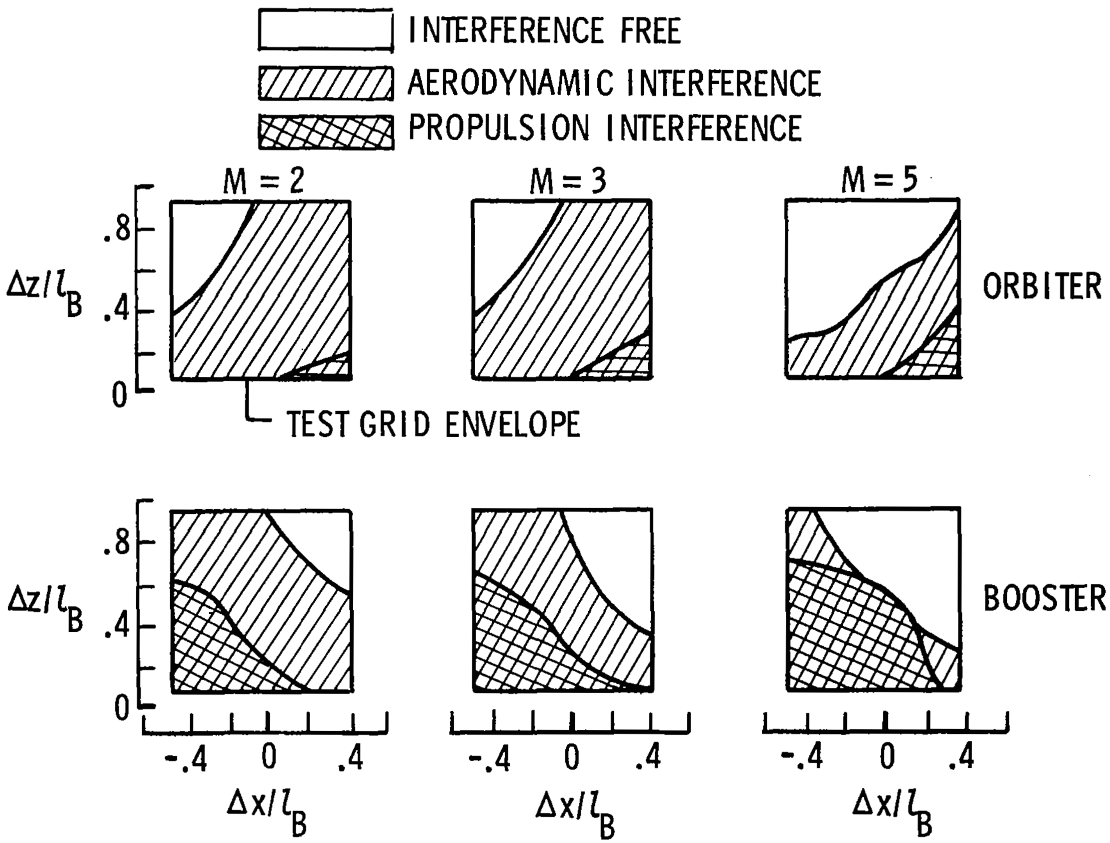

Figure 11

CENTERLINE PRESSURE DISTRIBUTIONS

(Figure 12)

The complexity of the flow fields is illustrated in this figure where the centerline pressure distributions on the orbiter and booster are shown as a function of distance from the nose of each vehicle. Two curves are illustrated. One is the interference free curve for the orbiter and booster and the other is for the orbiter in proximity to the booster and with the orbiter power level at 100% and the booster power level at 50%. The increase in centerline static pressures on the orbiter is due to the booster bow wave impingement and the canard bow wave impingement. No plume impingement is shown on the orbiter since for this case the orbiter is forward of the booster base. For the booster the increase in centerline static pressures is due to the orbiter bow wave impingement, the location of the booster canard, and the orbiter plume impingement. The important fact on this figure is the influence of the booster canard on the loadings of both the orbiter and booster and the orbiter plume effects.

CENTERLINE PRESSURE DISTRIBUTIONS

$M = 3$; $\Delta x/l_B = 0.227$; $\Delta z/l_B = .120$; $\alpha = 0^0$; $\alpha_i = 0^0$

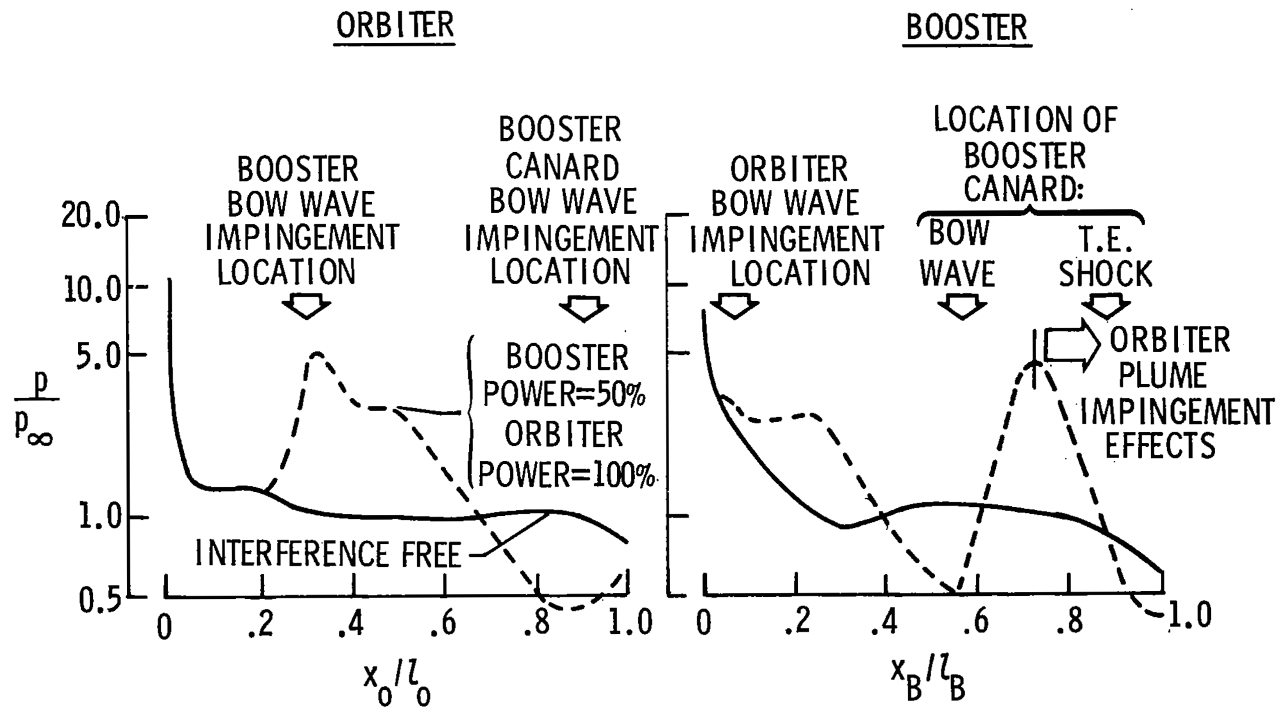

Figure 12

EFFECT OF BOOSTER CANARD

(Figure 13)

The effect of the booster canard on the proximity aerodynamics is shown in this figure at a Mach number of 3. The two curves illustrated are for the canard on and canard off and it is seen that the canard significantly changes the forces and moments on both vehicles, thus confirming that the proximity aerodynamic data is not only dependent on Mach number, rocket exhaust impingement, and relative position and attitudes of the stages, but also dependent on configuration.

EFFECT OF BOOSTER CANARD

$M = 3; \Delta x/l_B = 0.104; \Delta z/l_B = 0.120$

ORBITER POWER = 100%; BOOSTER POWER = 50%

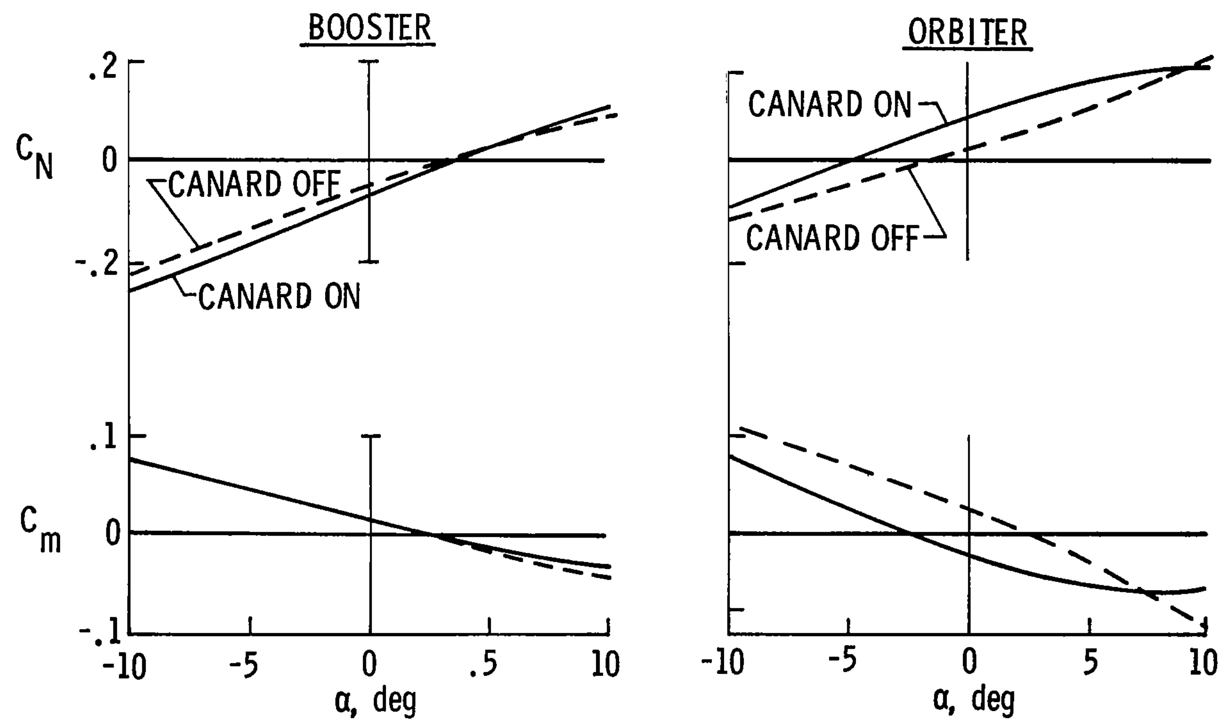

Figure 13

EFFECT OF INTERFERENCE AERODYNAMICS

(Figure 14)

To illustrate the importance of the interference aerodynamics typical dynamic simulation outputs at Mach number of 2 are presented in this figure. The trajectory data shown is with the orbiter power at 100% and the booster power at 50% at release. This would require the throttling of the 12 booster engines to 50%. The data on the left is a trajectory generated using the interference aerodynamics with plume simulation in the dynamic simulation program. The various pictures are shown at 1 second intervals from a release condition. The angle of attack and incidence angle at release were 0° and after 6 seconds the two vehicles are separating from each other. The data on the right is for a trajectory generated using just interference free aerodynamic data with plume simulation in the dynamic simulation program and for the same initial conditions. After about 3 seconds for this trajectory the two vehicles have collided. Consequently, not only is it important that the proper aerodynamic interference data be used in an abort separation dynamic program to obtain meaningful results, but also the interference aerodynamics at these conditions caused the two vehicles to separate.

EFFECT OF INTERFERENCE AERODYNAMICS

$M = 2$; $\alpha = 0°$; $\alpha_i = 0°$

ORBITER POWER = 100%; BOOSTER POWER = 50%

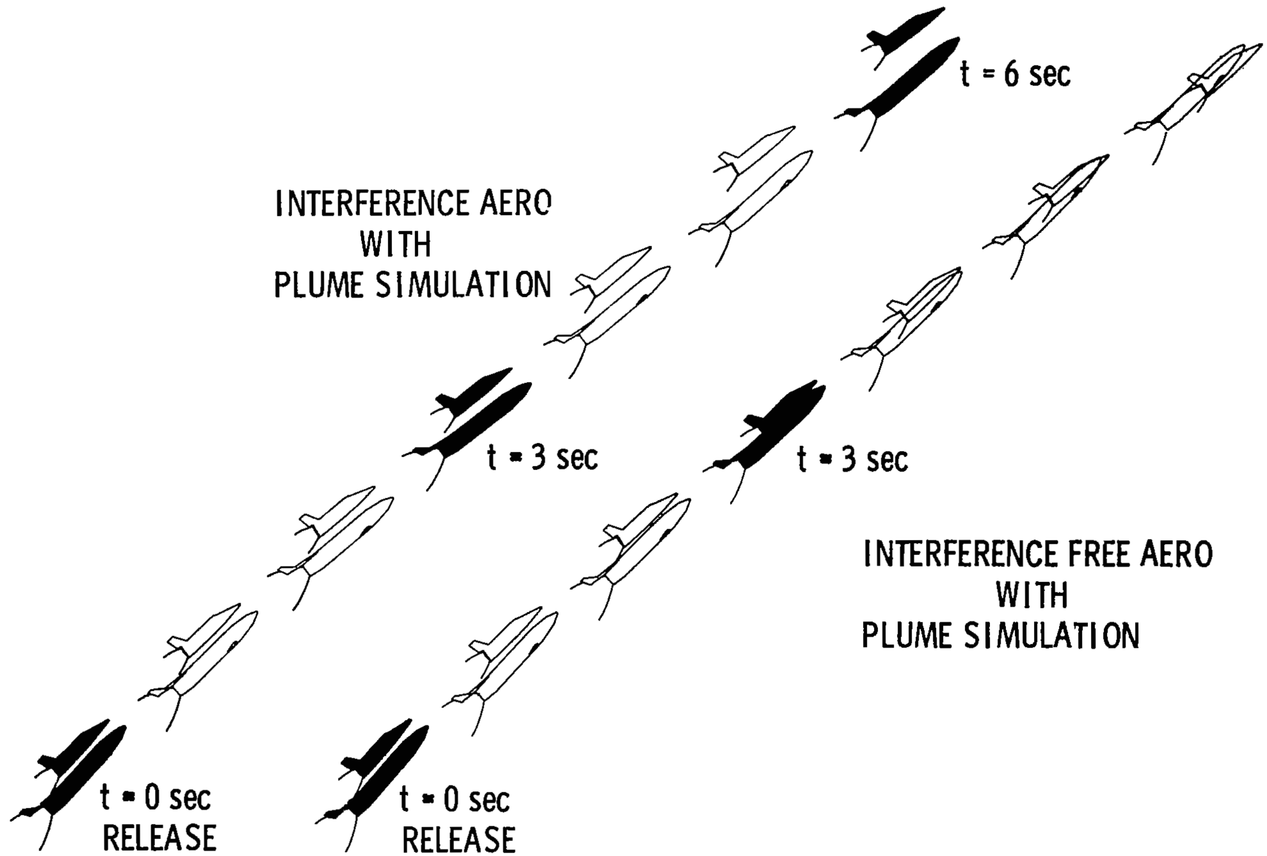

Figure 14

ROCKET EXHAUST INTERFERENCE EFFECTS

(Figure 15)

Figure 11 had shown that a large region of interference was caused by the rocket exhaust of the orbiter on the booster at M = 2. To illustrate how significant the rocket exhaust interferences were, some representative trajectories at Mach = 2 are shown. The trajectory on the left was obtained using aerodynamic wind tunnel data without the plume simulation in the dynamic simulation program while the data on the right was obtained using aerodynamic wind tunnel data with plume simulation in the dynamic simulation program. In both cases, however, the rocket thrust was included in the simulation. Both trajectories are very close to being the same. Consequently, the rocket exhaust impingement of the orbiter on the booster was not significant at the altitude and pressure ratio corresponding to the Mach number for which the rocket exhaust was simulated (see figures 4, 7, and 8). Future plume simulation would not be required if the rocket exhaust simulated in future testing generates the same size and shape plume as the rocket engines simulated at these conditions.

ROCKET EXHAUST INTERFERENCE EFFECTS

$M = 2; \alpha = 0°; \alpha_i = 0°$

ORBITER POWER = 100%; BOOSTER POWER = 50%

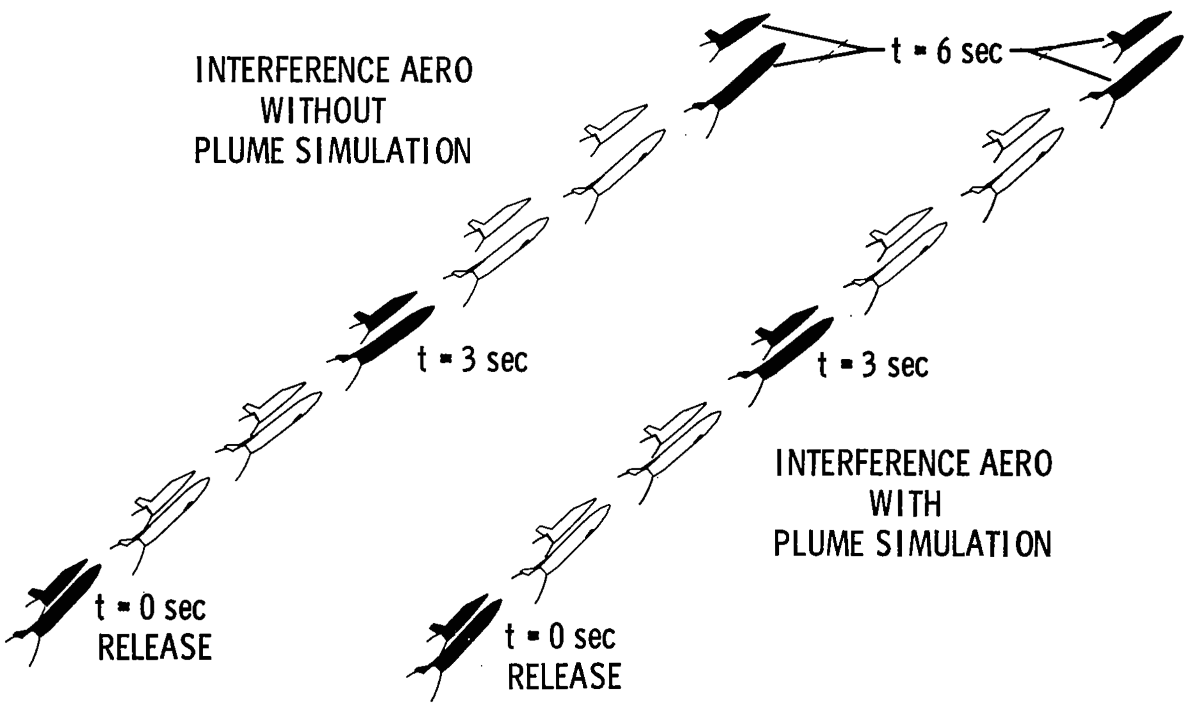

Figure 15

ROCKET EXHAUST INTERFERENCE EFFECTS

(Figure 16)

This figure shows the same type of results at $M = 3$ as was illustrated in figure 15 at $M = 2$. The data illustrated in this figure indicates that the orbiter plume impingement effects are important at the altitude and corresponding pressure ratio for which the rocket exhaust was simulated at this Mach number, since the trajectories are completely different when the aerodynamic wind tunnel data with and without plume simulation was used in the computer program. Consequently, future plume simulation would be required if the rocket exhaust simulated in future testing generates about the same size and shape plume as the rocket engines simulated at these conditions.

ROCKET EXHAUST INTERFERENCE EFFECT

$M = 3; \alpha = 0°; \alpha_i = 0°$

ORBITER POWER = 100%; BOOSTER POWER = 50%

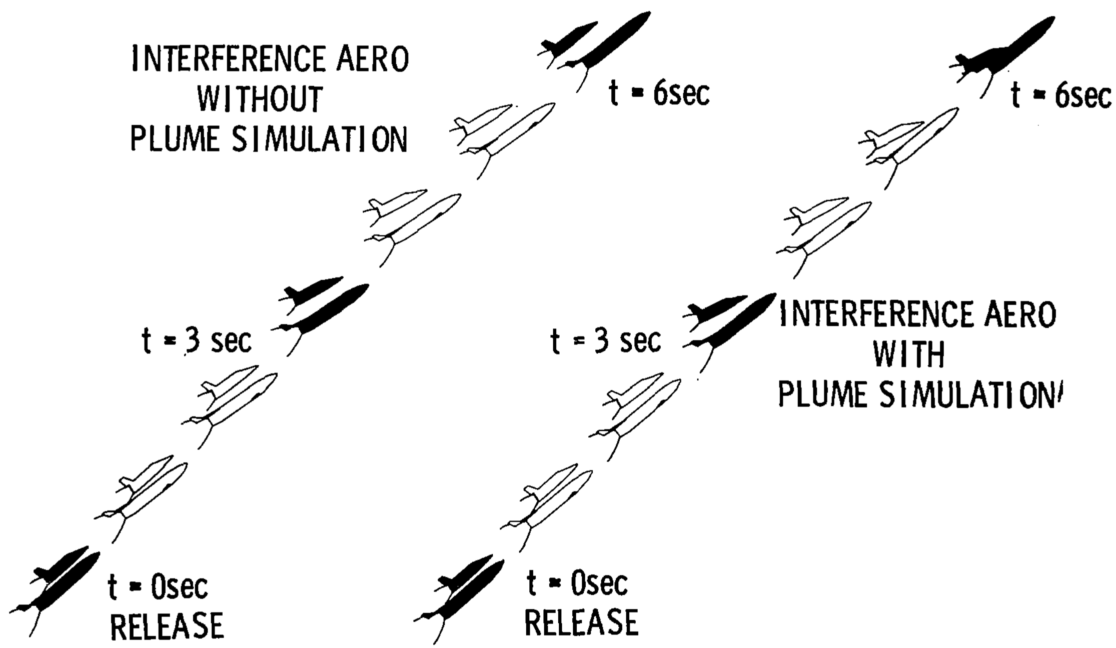

Figure 16

CONTROL EFFECTIVENESS

(Figure 17)

During the static wind tunnel tests some aerodynamic control effectiveness information was obtained for both the orbiter and booster. These results are summarized in this figure. It was found that both vehicles had control effectiveness even when in proximity to the other vehicle except for the booster at the higher Mach numbers when at interference free conditions the control effectiveness parameter, $C_{m_{\delta_e}}$, approached zero. The significance of the vehicles having control effectiveness at the lower Mach numbers is illustrated in figures 18 and 19.

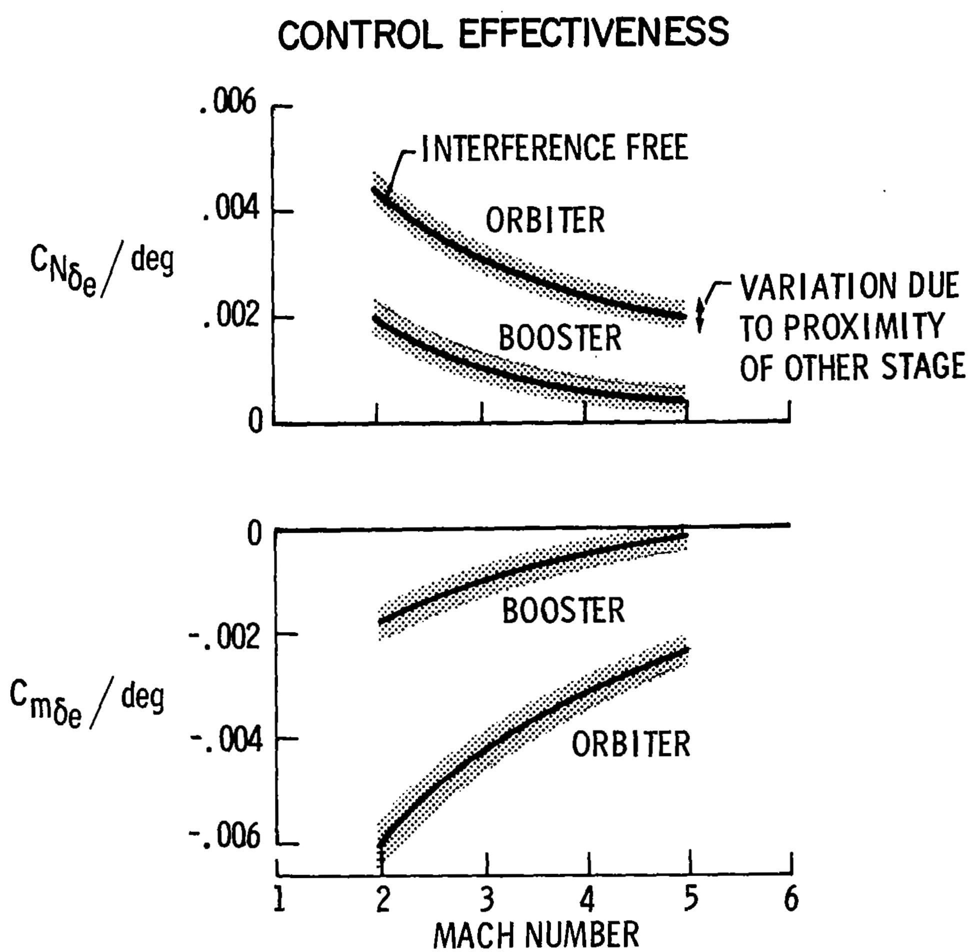
CONTROL EFFECTIVENESS
$C_{N_{\delta_e}}/\deg$
.006
.004
.002
0
INTERFERENCE FREE
ORBITER
BOOSTER
VARIATION DUE TO PROXIMITY OF OTHER STAGE
$C_{m_{\delta_e}}/\deg$
0
-.002
-.004
-.006
BOOSTER
ORBITER
1
2
3
4
5
6
MACH NUMBER

Figure 17

EFFECT OF AERO CONTROL

(Figure 18)

The importance of the aerodynamic control effectiveness for the orbiter is illustrated in this figure. The trajectory data illustrated is for a $M = 2$ condition and with the orbiter power level at 100% and the booster power level at 50% at release. For the case where the orbiter and booster controls are set at zero degrees it is seen that the vehicles collide after about 8 seconds. Deflecting the orbiter controls to -25° at release safely separates the vehicles at this condition.

EFFECT OF AERO CONTROL

$M = 2; \alpha = 0°; \alpha_i = 5°$

ORBITER POWER = 100%; BOOSTER POWER = 50%

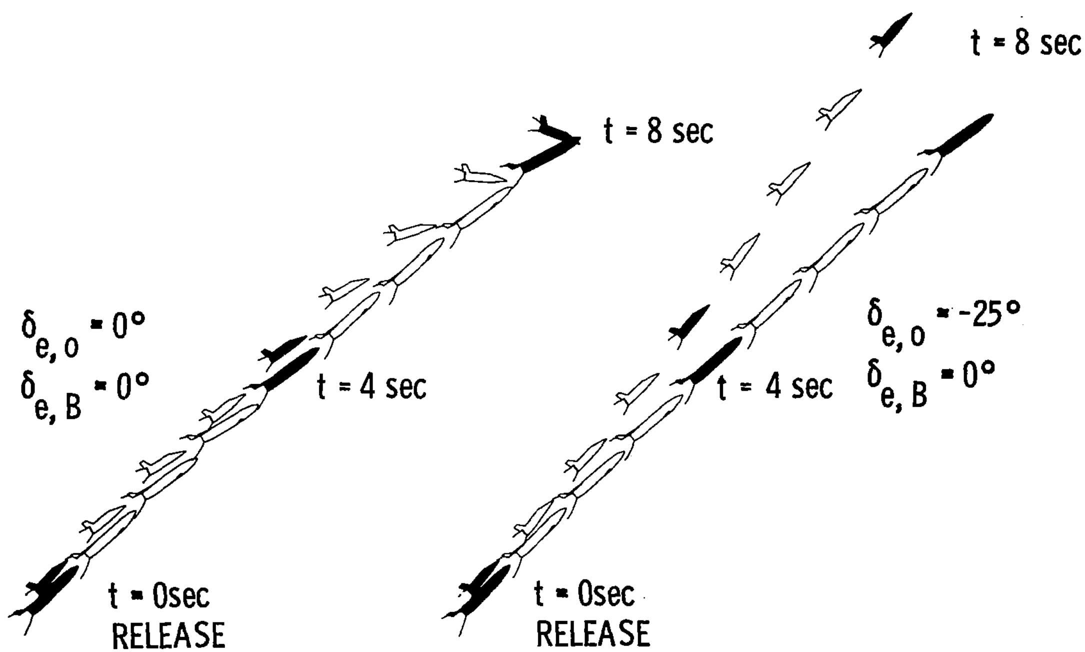

Figure 18

EFFECT OF AERO CONTROL

(Figure 19)

The importance of the aerodynamic control effectiveness for the booster is illustrated in this figure. The trajectory data shown is for a Mach number 3 condition and with the orbiter power level at 100% and the booster power level at 50% at release. For the case where the orbiter and booster controls are set at zero degrees it is seen that the vehicles collide after about 6 seconds. Deflecting the booster controls to 30° at release safely separates the vehicles at this condition.

EFFECT OF AERO CONTROL

$M = 3;\ \alpha = -5°;\ \alpha_i = 5°$

ORBITER POWER = 100%; BOOSTER POWER = 50%

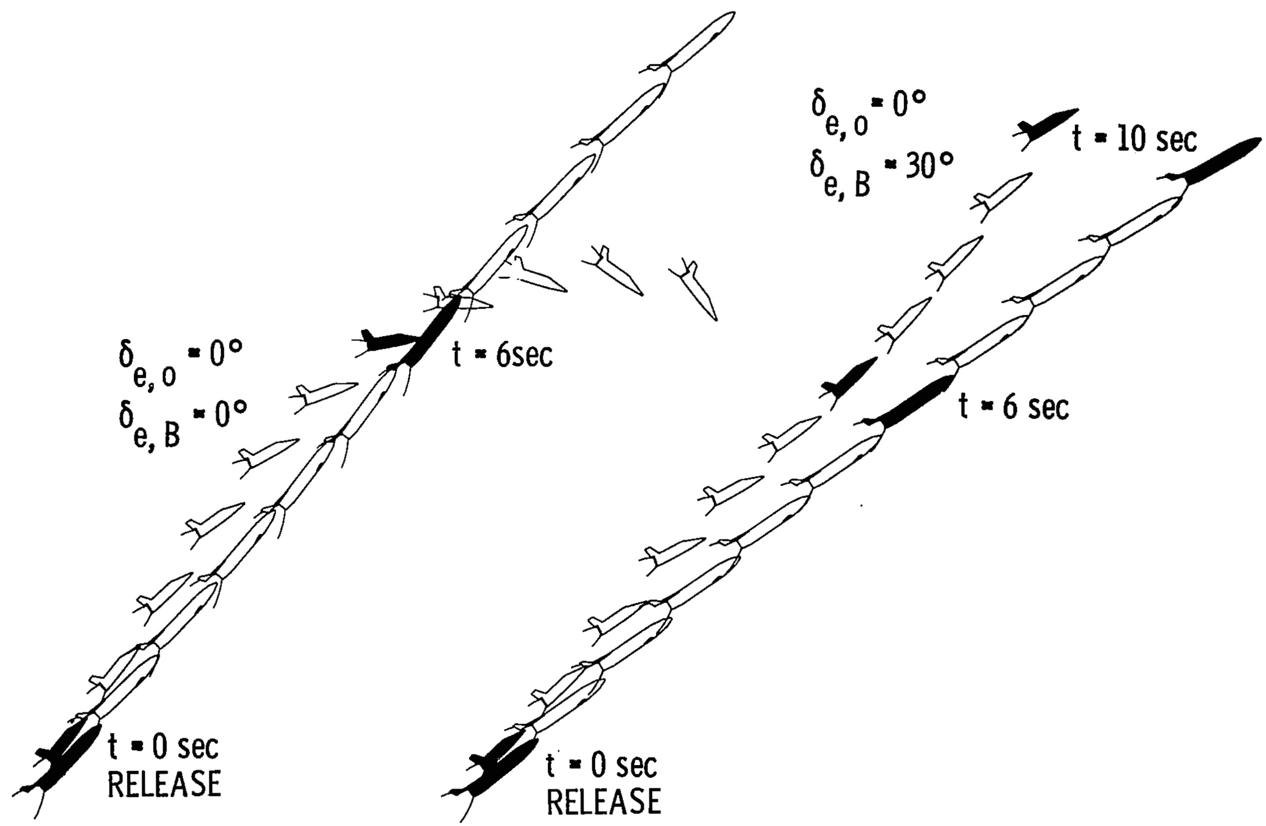

Figure 19

EFFECT OF THRUST VECTOR CONTROL ON BOOSTER

(Figure 20)

The use of thrust vector control in separating the vehicles is illustrated in this figure. This is a Mach number 5 condition with the orbiter power level at 100% and booster power level at 25% at release. Reducing the power level of the booster to 25% would require shutdown of 6 booster engines and throttling of the remaining 6 engines to 50%. As was shown in figure 17 the booster had very little aerodynamic control effectiveness at these higher Mach numbers and this would be a reason for utilizing the gimbal angle capability of the booster engines to safely separate the vehicles. For the case where the booster gimbal angle is set at 0° the two vehicles collide after about 5 seconds. However, gimbaling the booster engines to 2.5° at release allows the vehicles to safely separate. Although data is not presented in this paper for gimbaling the orbiter engines or for using the reaction control system on both the orbiter and booster, these control devices would also be useful in separating the vehicles.

EFFECT OF THRUST VECTOR CONTROL ON BOOSTER

$M = 5;\ \alpha = 0°;\ \alpha_i = 5°$

ORBITER POWER = 100%; BOOSTER POWER = 25%

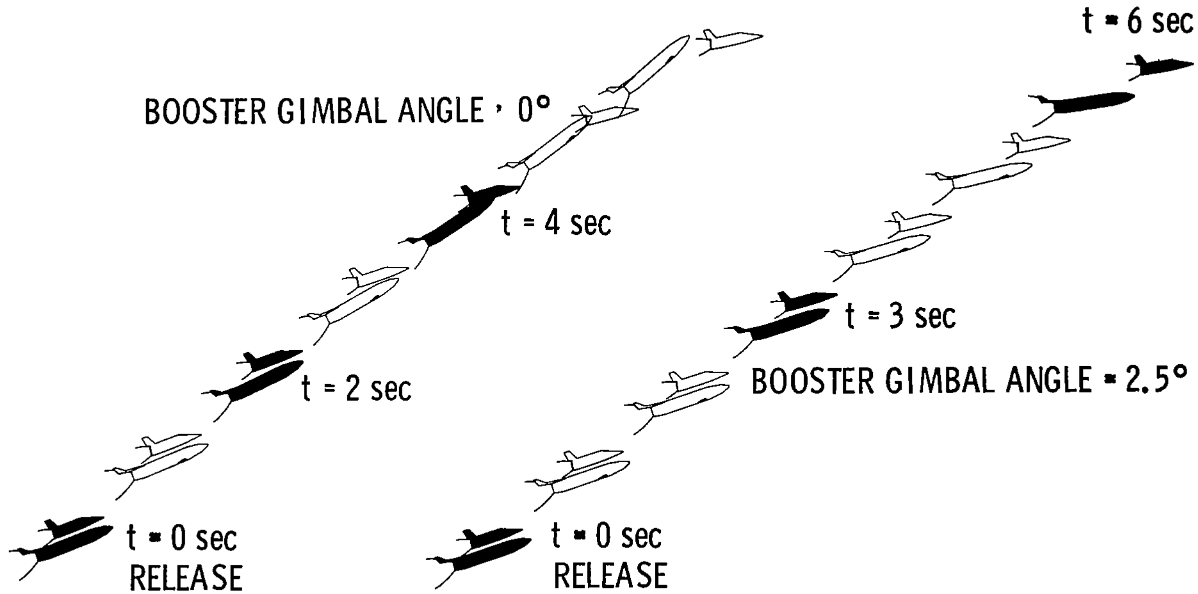

Figure 20

PITCHING MOMENT EQUATION

(Figure 21)

When considering the motion of a vehicle it is important to account for all factors which may influence the motion. The total pitching moment acting on a vehicle is composed of the sum of three distinct terms. The thrust term accounts for the canting of the thrust vector with respect to center of gravity and once the thrust level is known, the contribution to the total pitching moment is known. The static moment is also a known quantity which can be obtained from wind tunnel tests. If two bodies are involved as in the abort separation of the shuttle, this information is still obtainable from wind tunnel experiments. When the present study was started no information had been obtained on the dynamic damping contribution to the total pitching moment equation. Previous work was restricted to a single body and not two bodies in proximity to each other. The dynamic damping term plays a significant role mainly at the lower Mach numbers due to the velocity influence on the total moment. Because of a high degree of uncertainty with the dynamic damping contribution, investigations were initiated to determine if the dynamic damping term of either the orbiter or booster changed significantly when in proximity to the other vehicle.

PITCHING MOMENT EQUATION

$$\underbrace{M_Y}_{\text{TOTAL MOMENT}} = \frac{1}{2}\rho V_c^{\,2} S c \left(\underbrace{\frac{d_T}{c} C_T}_{\text{THRUST CONTRIBUTION}} + \underbrace{C_m}_{\text{STATIC MOMENT CONTRIBUTION}} + \underbrace{\frac{c}{2V_c} C_{m_{\dot{\theta}}} \dot{\theta}}_{\text{DAMPING-IN-PITCH CONTRIBUTION}} \right)$$

Figure 21

DYNAMIC STABILITY TESTS

(Figure 22)

These dynamic stability investigations, described in more detail in paper no. 31 by K. J. Orlik-Rückemann, J. G. LaBerge, and E. S. Hanff, are illustrated in this figure. Tests were conducted at the Arnold Engineering Development Center at M = 2 on the North American Rockwell/General Dynamics Phase B delta wing space shuttle concept, reference 23, at the National Aeronautical Establishment, Canada at M = 1.8 on the North American Rockwell/General Dynamics straight wing space shuttle concept, reference 24, and at the National Aeronautical Establishment at M = 1.8 on the McDonnell-Douglas Phase B space shuttle concept, references 25 and 26. In the early portion of these tests either the orbiter or booster would be fixed and the other vehicle would be oscillated to obtain the damping-in-pitch derivative. Conducting the experiment in this fashion indicated that the interference effects on the damping-in-pitch derivative of either the orbiter or booster due to the stationary presence of the other vehicle were relatively small. However, when both vehicles were oscillated the damping-in-pitch derivative changed significantly when a phase shift occurred between the orbiter and booster. The largest increase and largest decrease in the damping-in-pitch parameter occurred when the orbiter and booster were out of phase with each other by 90° and 270° respectively. Most of the separation trajectories obtained during the present study showed that both the orbiter and booster were almost in phase with each other and oscillating with the same frequency.

DYNAMIC STABILITY TESTS

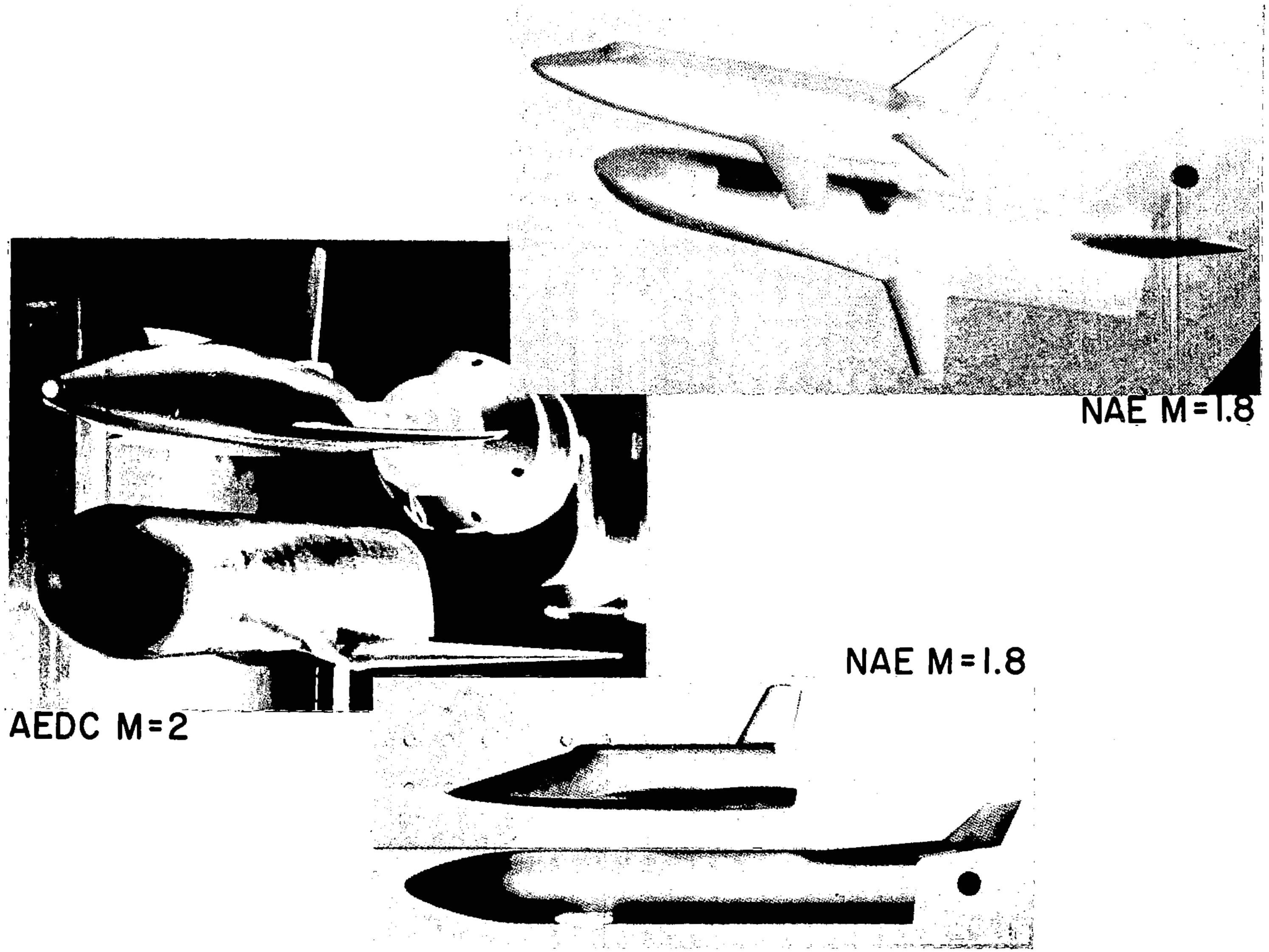

Figure 22

EFFECT OF DYNAMIC DAMPING DERIVATIVES

(Figure 23)

The implication of the change in magnitude of the damping-in-pitch derivative is illustrated in this figure. The results illustrated are at a Mach number of 2 and with the orbiter power at 100% and the booster power at 50% at release. The trajectory on the left is with the controls sct at 0° deflection and with nominal values of the damping in pitch parameter for both the orbiter and booster. As can be seen, the vehicles are separating from each other after about 10 seconds. The trajectory in the center is again with the controls on the booster and orbiter set at 0° but with the damping in pitch parameters for both the orbiter and booster increased to -40/rad. It is seen here that the vehicles collide after 5 seconds. The fact that the damping-in-pitch parameter can be increased does not mean that the vehicles cannot be safely separated. Instead this is a fact for which a workable abort solution may have to be designed To illustrate this, the abort trajectory on the right is for the damping in pitch parameters for the orbiter and booster still increased to -40/rad. To safely separate the vehicles, however, the orbiter controls are set to -20° and the booster controls to +20°. Consequently, it is important to know the interference effects on the damping-in-pitch derivatives. However, as was illustrated in this figure, a safe abort separation can be obtained by properly using controls already envisioned for the vehicles.

EFFECT OF DYNAMIC DAMPING DERIVATIVES

$M = 2$; $\alpha = 0°$; $\alpha_i = 0°$

ORBITER POWER = 100%; BOOSTER POWER = 50%

$\delta_{e,o}$	= 0°	0°	-20°
$\delta_{e,B}$	= 0°	0°	20°
$\left(\bar{C}_{m_{\dot{\theta}}}\right)_o$	= -3/ rad	-40/ rad	-40/ rad
$\left(C_{m_{\dot{\theta}}}\right)_B$	= -1/ rad	-40/ rad	-40/ rad

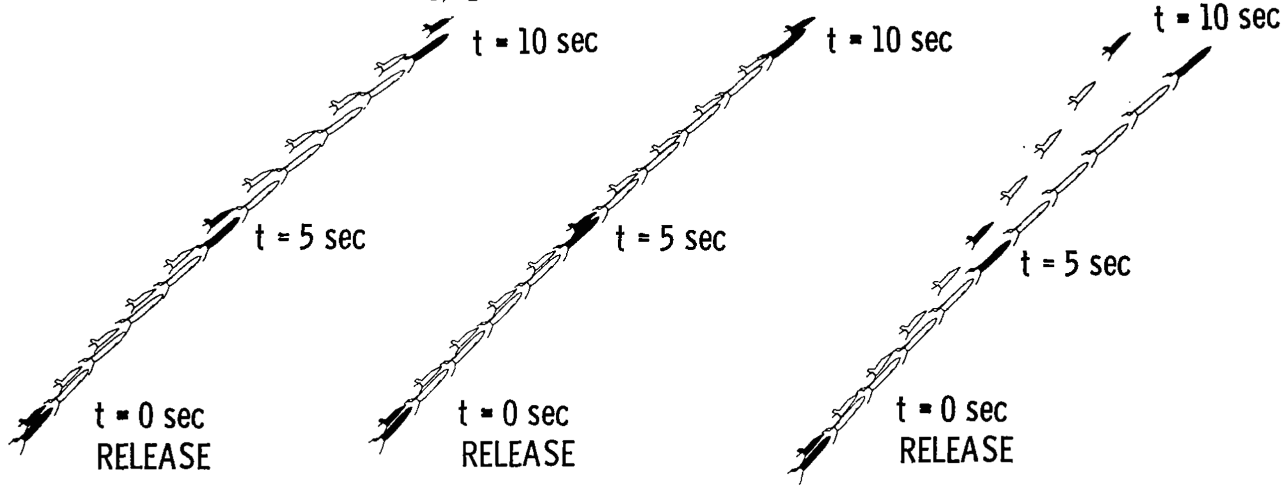

Figure 23

EFFECT OF SEPARATION MECHANISM

(Figure 24)

The potential effect of designing a separation mechanism to impart certain rotational motions to the vehicles at release is illustrated in this figure. The trajectory data on the left is for no pitch rotation imparted to the vehicles at release and it is seen that the two vehicles collide after about 4 seconds. The trajectory data on the right is for a condition where the separation mechanism has imparted a nose up pitch rotation to the orbiter of 6 deg/sec and a nose down pitch rotation to the booster of -6 deg/sec. It is seen that a safe separation trajectory is obtained.

EFFECT OF SEPARATION MECHANISM

$M = 5; \alpha = 0°; \alpha_i = 0°$

ORBITER POWER = 100%; BOOSTER POWER = 50%

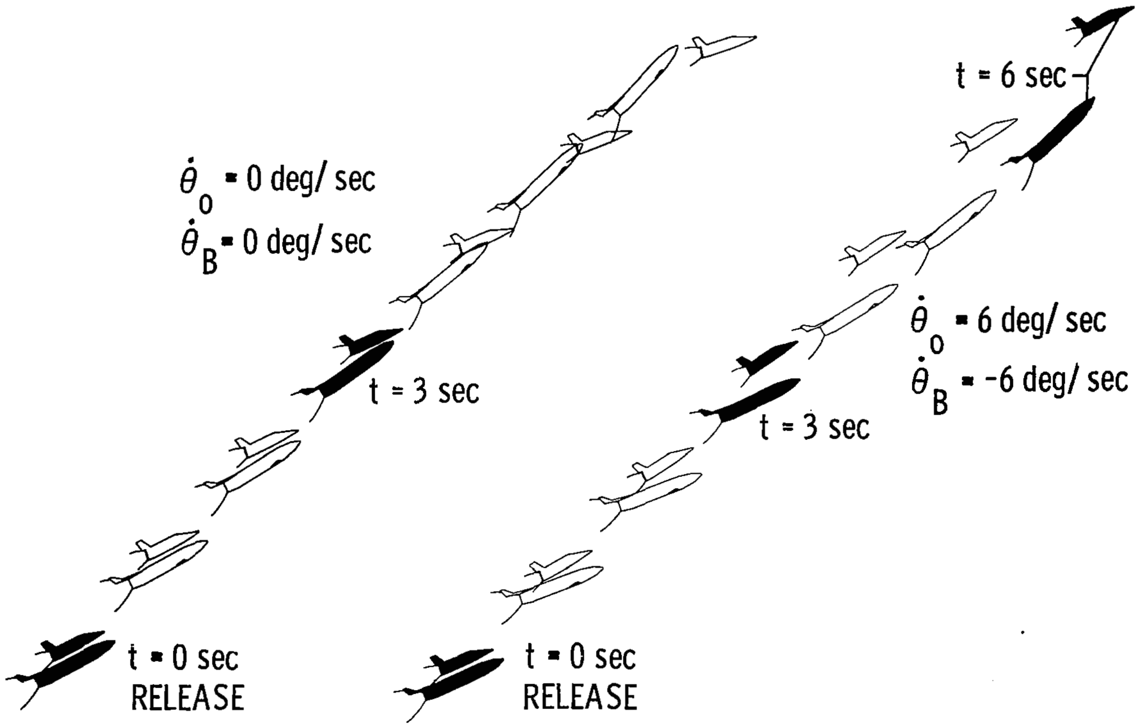

Figure 24

EFFECT OF ORBITER LOCATION

(Figure 25)

The dependency of abort separation trajectories on the location of the orbiter on the booster is shown in this figure at M = 2. One trajectory is for the nominal launch position and the other is for a parallel burn launch position. A safe abort separation is obtained when the vehicles are separated from the nominal launch position and the vehicles collide when they are separated from the parallel burn launch position. This does not imply that the nominal position is a better position than the parallel burn position since safe separation trajectories have been obtained from this position also. Instead it indicates that separation is a function of position of the orbiter on the booster.

EFFECT OF ORBITER LOCATION

$M = 2; \alpha = 0°; \alpha_i = 0°$

ORBITER POWER = 100%; BOOSTER POWER = 50%

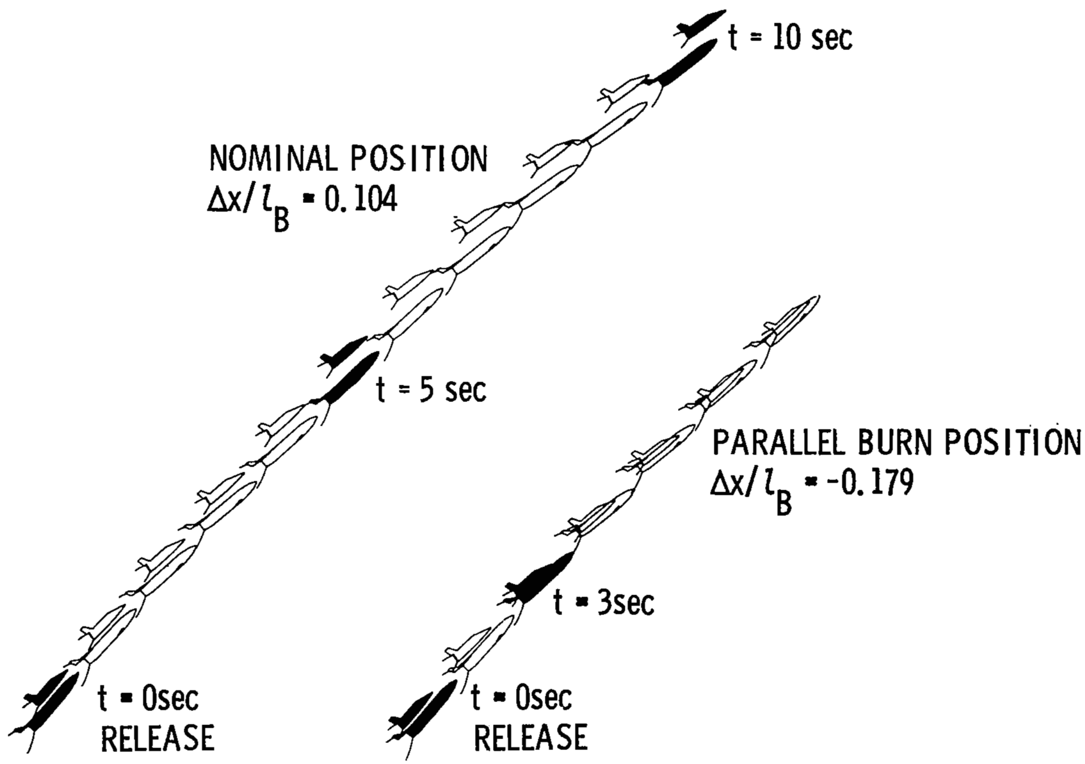

Figure 25

TECHNOLOGY IMPLICATIONS
(Figure 26)

As a result of the study to date, some observations pertinent to future studies are made.

Approach to Study Abort Staging

Close Coordination Between Technical Disciplines.- Aerodynamic staging testing could be extremely costly if the project is not well organized due to the complexity of testing and the data volume required. It is imperative that close coordination be maintained between the various technical disciplines during planning and conducting the test and during data analysis to reduce the cost and to insure that optimum use of the data is obtained.

Since the propulsion simulation requires matching of Mach number and altitude (so that the proper plume size and shape is obtained) the nominal trajectory for the system to be investigated should be well established. If excursions from the nominal trajectory are expected to be large then additional tests would be required to determine altitude effect.

Obtain Data by Grid Method.- In order to gain maximum utilization from the data, the method of obtaining aerodynamic coefficients as a function of a grid position and attitude is preferred. The captive trajectory approach might be desirable after vehicle design is firmed, but during the design phase, this approach limits data usability since only one unique trajectory can be obtained or at least a limited number fixed to certain trajectory and mass conditions.

In order to minimize amount of testing and to assure that most important interference regions are included, detailed layouts of the models and their estimated shock and plume boundaries should be made. Grid densities will then be a function of Mach number and relative location of the vehicle components such as nose, wing, canard, etc.

Automated Data Acquisition.- Completely automated data acquisition equipment which gets the man out of the loop is necessary to insure that the quantities of data required for abort analysis can be obtained quickly, efficiently, and economically. The system should be capable of automatically positioning the models at as many grid points as possible at a given set of tunnel conditions.

Another facet of data acquisition is the importance of reducing the data to orderly arrays that are amenable to being used in flight mechanic programs, plotting programs, and other programs which may be necessary for use in analysis or application of scaling parameters. The volume of data obtained from these type tests is so massive that it is prohibitive to take a manual approach or fragmented computerized approach in analysis and dissemination of test results. As much as possible, data handling analysis and dissemination should be done with computers through a totally integrated approach.

Flow Visualization.- Because of the complex flow fields caused by shock interaction and engine plume interference, analysis and understanding of resulting force and moment data requires the use of extensive flow visualization. Schlierens, shadowgraphs or interferograms should be obtained for as many conditions as practical.

Technology Concerns

Plume Simulation.- The method used to simulate the rocket exhaust of the orbiter and booster in the present study appears to be adequate. However, there are certain gray areas which need clarification to ascertain the degree of sophistication required in the simulation. Tests are needed to evaluate the effect of hot flow, momentum match and multiple nozzle arrangements.

Wind Tunnel Facilities.- For a shuttle system such as considered during the present investigation, certain facility improvements would be needed to provide final design aerodynamic data. A fully automatic twelve degree of freedom system would be desirable; however, a system which only has mixed automatic-manual capability would be acceptable for operation under a grid data acquisition mode. Although only the longitudinal motion was studied in-depth in the present study, a captive trajectory system which has eleven or twelve degrees of motion would be desirable in evaluating the out-of-plane forces and moments as they influence the separation trajectories. Definitely more degrees of motion need to be simulated in future testing.

Support hardware is needed to minimize strut and sting interference effects. For instance a ceiling or floor-mounted mechanism might be required for extreme forward orbiter to booster positions while conventional sting mounts might be acceptable for other positions.

Reynolds Number Scaling.- When conducting wind tunnel tests where the rocket exhaust is simulated, tunnel operating pressures are low to provide the back pressure necessary for the proper plume simulation. This can be minimized by using high engine model chamber pressures but only within limits of structural integrity and simulated gas supply pressures. Low tunnel pressure, however, is opposite to that desired when considering Reynolds number scaling. This can result in laminar boundary layers on the model in areas where shocks of one vehicle intersect another.

Although during this investigation we saw no adverse effects such as major flow separation, there have been other investigations where this did occur, references 27 - 30. Also, the magnitude of the effect of shocks intersecting a laminar boundary layer is unknown. The sensitivity of these effects, once obtained, needs to be assessed as they influence the abort separation trajectories.

TECHNOLOGY IMPLICATIONS

APPROACH TO STUDY ABORT STAGING

- CLOSE COORDINATION BETWEEN TECHNICAL DISCIPLINES
- OBTAIN DATA BY GRID METHOD
- AUTOMATED DATA ACQUISITION
- FLOW VISUALIZATION

TECHNOLOGY CONCERNS

- PLUME SIMULATION
  - HOT FLOW
  - MULTI-NOZZLE
  - MOMENTUM MATCH
- WIND TUNNEL FACILITIES
  - 12-DEGREE OF MOTION SIMULATION (CAPTIVE AND GRID)
  - SUPPORT HARDWARE TO MINIMIZE STING EFFECTS
- REYNOLDS NUMBER SCALING

Figure 26

CONCLUDING REMARKS

(Figure 27)

Abort separation investigations have been conducted at Mach numbers from 2 to 6 and at both high and low dynamic pressures. The investigations have included static stability, dynamic stability, and pressure distribution tests. Both the static stability and pressure distribution tests were conducted simulating the rocket exhaust from both the orbiter and booster. The data from these investigations have been utilized in a dynamic simulation program which calculates the motion of the vehicles during an abort separation maneuver. Within the scope of this study, parallel abort separation appears possible at both high and low dynamic pressures. In this study only rigid body aerodynamic data was obtained and consequently such things as scale effects and aeroelastic effects need to be considered.

Both aerodynamic and thrust vector control have been shown to be useful as an aid in the separation of the two stages. Other types of control devices such as the reaction control system for the orbiter and booster, although not considered in the present study, should also be useful to separate the vehicles. Consequently, the flight control systems presently envisioned for the shuttle vehicles appear adequate to separate the vehicles during abort conditions.

The results of this study confirm that abort separation is dependent on configuration, Mach number, rocket exhaust impingement, and relative position and attitude of the stages. Furthermore, abort separation procedures will not just depend on the configuration selected but also the concept selected.

Many different concepts are presently being considered for the shuttle system. However, the testing technology developed during this study as well as the dynamic simulation program is applicable to the separation problems for any of these concepts - for example, the separation of the external HO tank from the orbiter and even the HO tank-orbiter combination from the booster. Consequently, the abort separation methodology developed during this study is applicable to current shuttle concepts.

CONCLUDING REMARKS

- WITHIN THE SCOPE OF THIS STUDY, PARALLEL ABORT SEPARATION APPEARS POSSIBLE AT BOTH HIGH AND LOW DYNAMIC PRESSURES
- FLIGHT CONTROL SYSTEMS PRESENTLY ENVISIONED FOR THE SHUTTLE VEHICLES APPEAR ADEQUATE TO SEPARATE THE VEHICLES DURING ABORT CONDITIONS
- THE RESULTS OF THIS STUDY CONFIRM THAT ABORT SEPARATION IS DEPENDENT ON CONFIGURATION, MACH NUMBER, ROCKET EXHAUST IMPINGEMENT, AND RELATIVE POSITION AND ATTITUDE OF THE STAGES
- THE ABORT SEPARATION METHODOLOGY DEVELOPED DURING THIS STUDY IS APPLICABLE TO CURRENT SHUTTLE CONCEPTS

Figure 27

REFERENCES

1. Donaldson, J. C.: Aerodynamic Interference Effects of Parallel Delta Wings and Cone-Cylinder Bodies in Close Proximity: Force Tests at Mach Numbers 2, 5, and 10. AEDC-TDR-64-135, U.S. Air Force, July 1964. (Available from DDC as AD 351 435.)

2. Sayano, S.; Erickson, C. R.; and Murphy, J. S.: Aerodynamic Interference Associated With Two Parallel Bodies in Close Proximity in Hypersonic Flow. AFFDL-TR-64-158, U.S. Air Force, Dec. 1964. (Available from DDC as AD 357 000.)

3. Donaldson, J. C.: Aerodynamic Interference Effects of Parallel Delta Wings and Cone-Cylinder Bodies in Close Proximity: Pressure Tests at Mach Numbers 5 and 10, Heat-Transfer Tests at Mach Number 10. AEDC-TDR-64-172, U.S. Air Force, Sept. 1964. (Available from DDC as AD 353 390.)

4. Spurlin, C. J.: Aerodynamic Interference Effects of Delta Wings in Close Proximity: Pressure Tests at Mach 8. AEDC-TR-66-215, U.S. Air Force, Nov. 1964. (Available from DDC as AD 376 887.)

5. Decker, John P.; and Pierpont, P. Kenneth: Aerodynamic Separation Characteristics of Conceptual Parallel-Staged Reusable Launch Vehicles at Mach 3 to 6. NASA TM X-1051, 1965.

6. Decker, John P.: Aerodynamic Abort-Separation Characteristics of a Parallel-Staged Reusable Launch Vehicle From Mach 0.60 to 1.20. NASA TM X-1174, 1965.

7. Decker, John P.: Experimental Aerodynamics and Analysis of the Stage Separation of Reusable Launch Vehicles. Conference on Hypersonic Aircraft Technology, NASA SP-148, 1967, pp. 63-77.

8. Jones, Jerry H.: Force Tests on the Two Stages of an Aerospace Plane Configuration as the Stages Separated at Mach 3. AEDC-TR-67-45, U.S. Air Force, May 1967. (Available from DDC as AD 380 971.)

9. Decker, John P.; and Gera, Joseph: An Exploratory Study of Parallel-Stage Separation of Reusable Launch Vehicles. NASA TN D-4765, 1968.

10. Jenson, Richard; Dahlem, Valentine, III; and Schnabel, Charles W.: Hypersonic Aerodynamic Interference Analysis of Parallel Staged Blunt Delta Wings. AFFDL-TR-68-116, U.S. Air Force, Nov. 1968.

11. Matthews, M. L.: Stage Separation of Two Stage Reusable Vehicles. Doc. No. D2-90661-1, Boeing Co., July 15, 1965.

12. Decker, John P.: An Exploratory Experimental and Analytical Study of Separating Two Parallel Lifting Stages of a Reusable Launch Vehicle at Mach Numbers of 3 and 6. M.A.E. Thesis, Univ. of Virginia, 1968.

13. Decker, John P.: Aerodynamic Interference Effects Caused by Parallel-Staged Simple Aerodynamic Configurations at Mach Numbers of 3 and 6. NASA TN D-5379, 1969.

14. Flaherty, Jack I.; and Dahlem, Valentine, III: A Prediction Technique for Estimating Interference Effects During a Parallel Staged Separation Maneuver at Supersonic Speeds. AFFDL-TR-70-21, U.S. Air Force, June 1970.

15. Lanfranco, M. J.: Wind-Tunnel Investigation of the Separation Maneuver of Equal-Size Bodies. J. Spacecraft Rockets, vol. 7, no. 11, Nov. 1970, pp. 1300-1305.

16. Jenke, Leroy M.; and Lutz, Ronald G.: Force Tests of a Hypersonic Recoverable Booster in Proximity to the Second-Stage Vehicle at Mach Number 10. AEDC-TR-70-70, U.S. Air Force, May 1970.

17. Decker, John P.; McGhee, Robert J.; and Pierpont, P. Kenneth: Abort Separation Including Aerodynamic, Dynamic, Propulsive, and Trajectory Influences. Space Transportation System Technology Symposium, NASA TM X-52876, Vol. I, 1970, pp. 67-97.

18. Fossler, Ivy; and Prozan, Robert: Plume Impingement During Separation of a Two-Stage Space Shuttle Vehicle. NASA Space Shuttle Technology Conference, Vol. I, NASA TM X-2272, 1971, pp. 393-421.

19. Penny, Morris M.; and Ring, Larry R.: Definition of the Preliminary Impingement Forces and Moments for the MDAC and GD/C Booster Configurations. TM 54/20-317, LMSC-HREC-D225155 (Contract NAS9-11758), Lockheed Missiles and Space Co., July 1971.

20. Andrews, C. Donald: A Space Shuttle Parallel Staging Feasibility Study in the NASA-MSFC 14 x 14-Inch Trisonic Wind Tunnel. TM 54/20-319, LMSC-HREC D225158 (Contract NAS8-20082), Lockheed Missiles & Space Co., July 1971.

21. Herron, R. D.: Investigation of Jet Boundary Simulation Parameters for Underexpanded Jets in a Quiescent Atmosphere. AEDC TR-68-108, U.S. Air Force, Sept. 1968.

22. Baker, L. Ray, Jr.: Calibration of Propulsion Simulation Nozzles for Space Shuttle Booster and Orbiter Models for the Abort/Separation Staging Experimental Program. TM 54/20-320, LMSC-HREC D225144 (Contract NAS8-20082), Lockheed Missiles & Space Co., July 1971.

23. Uselton, Bob; and Wallace, Arthur R.: Dynamic Stability Testing of Space Shuttle Configurations During Abort Separation at Mach Numbers 1.76 and 2. AEDC-TR-71-198, U.S. Air Force, Oct. 1971.

24. Orlik-Rückemann, K. J.; and LaBerge, J. G.: Dynamic Stability Experiments on Straight Wing Space Shuttle Abort Separation at M = 1.80. Lab. Tech. Rep. LTR-UA-16, Nat. Res. Counc. Can. (Ottawa), May 1971.

25. LaBerge, J. G.: Dynamic Stability Experiments on Delta Wing Space Shuttle in Abort Separation at M = 1.80. Lab. Tech. Rep. LTR-UA-17, Nat. Res. Counc. Can. (Ottawa), July 1971.

26. Orlik-Rückemann, K. J.; and LaBerge, J. G.: Dynamic Interference Effect on Dynamic Stability of Delta-Wing Shuttle in Abort Separation at M = 2.0. Lab. Tech. Rep. LTR-UA-18, Nat. Res. Counc. Can. (Ottawa), Nov. 1971.

27. Fong, Michael C.; and Ehrlich, Carl F., Jr.: Propulsion Effects on Aerodynamic Characteristics of Lifting Reentry Vehicles. AFFDL-TR-70-12, U.S. Air Force, Mar. 1970.

28. McGhee, Robert J.: Jet Plume Induced Flow Separation on a Lifting Entry Body at Mach Numbers From 4.00 to 6.00. NASA TM X-1997, 1970.

29. Strike, W. T., Jr.: Jet Plume Simulation at Mach Number 10. AEDC-TR-70-118, U.S. Air Force, Aug. 1970.

30. McGhee, Robert J.: Some Effects of Jet Pluming on the Static Stability of Ballistic Bodies at a Mach Number of 6.00. NASA TN D-3698, 1966.

BOOSTER RECOVERY FOLLOWING PREMATURE SPACE SHUTTLE STAGE SEPARATION

M. J. Hurley, Design Specialist
Flight Technology, Space Shuttle

Convair Aerospace Division of General Dynamics
San Diego, California

INTRODUCTION

Abort criteria necessary to satisfy Space Shuttle program requirements include intact vehicle abort capability. Intact abort implies the ability of the booster and orbiter to separate and both continue flight to a safe landing, with a full payload aboard the orbiter. Obviously, the requirement to separate early along the ascent trajectory presupposes critical operational problems that are probably booster problems and may preclude booster recovery. On the other hand, some critical problems while mated can become manageable when separated (e.g., major loss of booster thrust) and should result in full booster recovery. All critical orbiter problems fall into this category; since stage separation without orbiter thrust is a capability of some separation system concepts, booster stage recovery following separation is a requirement.

40

STUDY CONFIGURATION

The study configuration is the North American Rockwell delta-wing orbiter and the General Dynamics B-9S delta-wing booster. The orbiter is launched piggyback on the booster and is located slightly ahead of the booster nose. Previous studies (e.g., Ref. 1 – 3) have demonstrated the ability of a modified four-bar linkage system to separate the stages anywhere along the ascent trajectory with a modest weight penalty. The capacity for booster recovery after separation was the objective of this study. It should be noted that the study results are equally applicable to the current, tandem-staged Space Shuttle concepts, providing that (1) stage separation does not require booster engine cutoff, and (2) the basic booster design parameters (e.g., wing loading and aerodynamic balance) are comparable.

STUDY CONFIGURATION

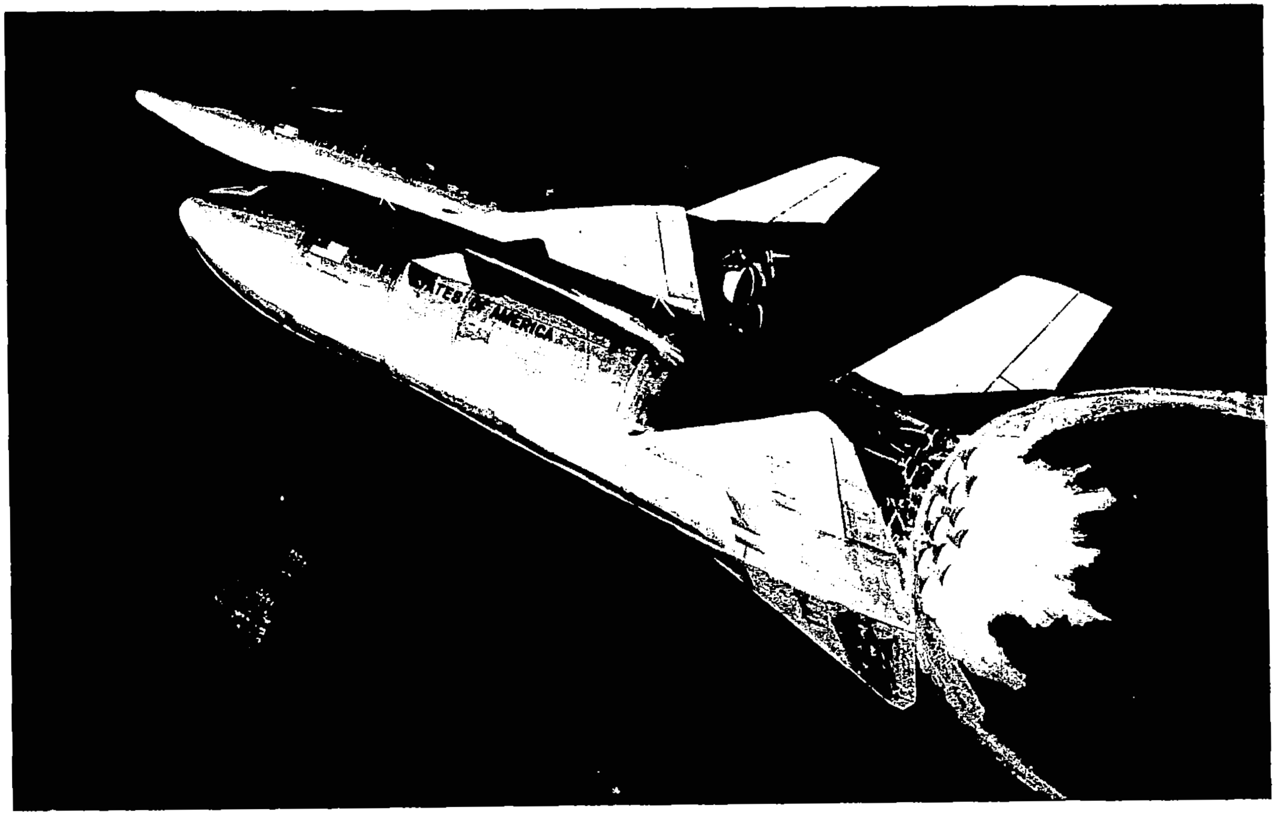

Figure 1

BURNOUT AND APOGEE CONSTRAINTS

Several recovery problem areas can be immediately uncovered in even a cursory overview of the postseparation physics. Without the orbiter mass in which to "sink" the energy derived from thrust acceleration, the resultant burnout conditions could* be at a much higher energy state, resulting in much more severe entry heating and loading problems, as well as downrange recovery problems due to the added velocity. The alternative of engine cutoff with substantial propellants still remaining in the booster tanks creates insurmountable problems on entry and landing. Even deviations from the nominal ascent trajectory immediately result in a host of off-nominal flight conditions (e.g., heating, loading) that must be carefully evaluated to ensure that design constraints are not appreciably** violated. In some instances, these constraints are not readily apparent and can be easily violated; for example, the thermal protection system and the cruise flyback systems are designed for the worst recovery trajectory – namely, the nominal trajectory – and any trajectory that substantially exceeds it in burn duration or velocity-time will be unacceptable.

This trajectory constraint diagram exhibits two of the major constraints on the apogee. Also presented is the nominal trajectory through the 200.4-second burnout point. Any apogee (γ = 0) point would violate either (or both) the entry heating or loading capabilities of the booster. It should be noted that the coast to apogee beyond the 200.4-second burnout condition will put the apogee point directly on the 4g boundary (the nominal condition). Velocity-time constraints (e.g., exceeding booster flyback range) cannot be included on velocity x altitude constraint space.

**Abort just before nominal separation (where the burnout conditions are near nominal) are also considered.*

***In a probabilistic sense, it is conceivable to use the design margin of the various subsystems in event of an independent failure, since the probability of a marginal subsystem (already a partial failure) and a primary critical failure is very small by design intent.*

TRAJECTORY CONSTRAINT DIAGRAM

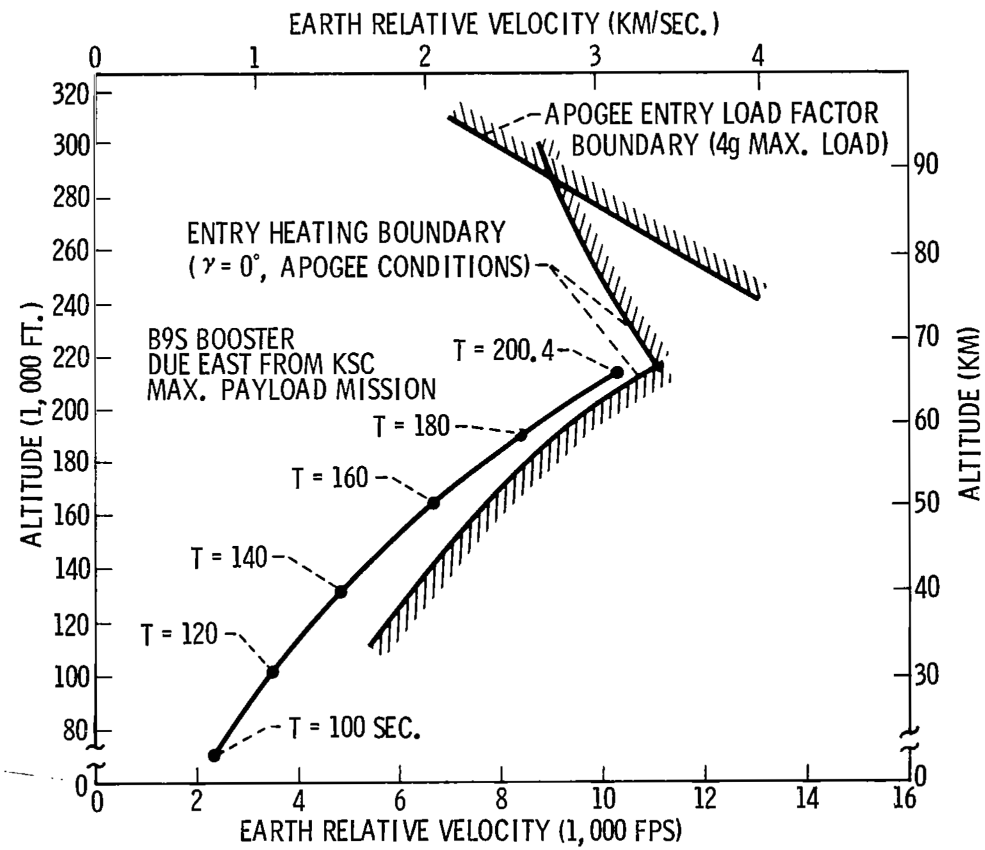

Figure 2

A secondary problem is with the engine system. To maintain a maximum of 3g longitudinally during engine firing as the booster approaches an empty condition, a number of engines must be throttled or cut off. The problem with cutting off one engine in the proximity of others that are still firing is illustrated opposite and is serious enough to require scrapping the engine bell after booster recovery. Since this procedure does not jeopardize vehicle recovery, it is an accepted mode of operation in event of an abort.

BOOSTER ENGINE BELL HEATING, ENGINE OUT CONDITIONS

NO ENGINE DEFLECTION

ESTIMATED HEATING RATE: 114 - 285 KW/M^2 (10 -25 BTU/SQ.FT.-SEC.)

EQUIVALENT RADIATION EQUILIBRIUM TEMPERATURE 1,217°– 1,517° K (1,730°– 2,270° F)

BASED ON ENGINE MANUFACTURER QUOTED LIMIT OF 1,356°–1,422° K (1,980°F–2,100°F) CONDITION IS MARGINAL & REQUIRES DETAILED ANALYSIS

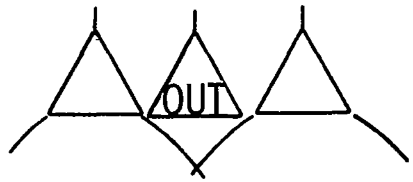

EFFECT OF ENGINE DEFLECTION

HEATING RATE = 794 KW/M^2 (70 BTU/SQ.FT.-SEC.) BASED ON SATURN V/S-II STAGE TESTING

EXPECTED HEATING RATE IS TOO SEVERE FOR THE SHUTTLE ENGINE

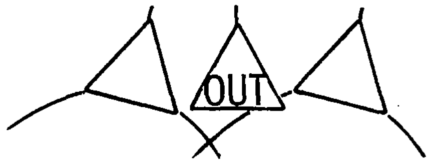

Figure 3

The general effect of aerodynamic heating can best be seen in this figure. The majority of heat transfer to the booster lower surfaces occurs during the entry phase; internal temperatures (e.g., the LH_2 and LO_2 tanks in the figure) tend to peak shortly thereafter. It was reasoned that if a loiter maneuver could be employed within the constraint region shown earlier so that the velocity vector magnitude was not increased and the altitude was increased (if desired) to reduce the prevailing heat transfer rate, then a recovery trajectory could be conceived that would result in temperatures lower or on the same order as the nominal trajectory.

TYPICAL BOOSTER LOWER SURFACE TANKAGE TEMPERATURE AND HEAT TRANSFER RATE HISTORIES

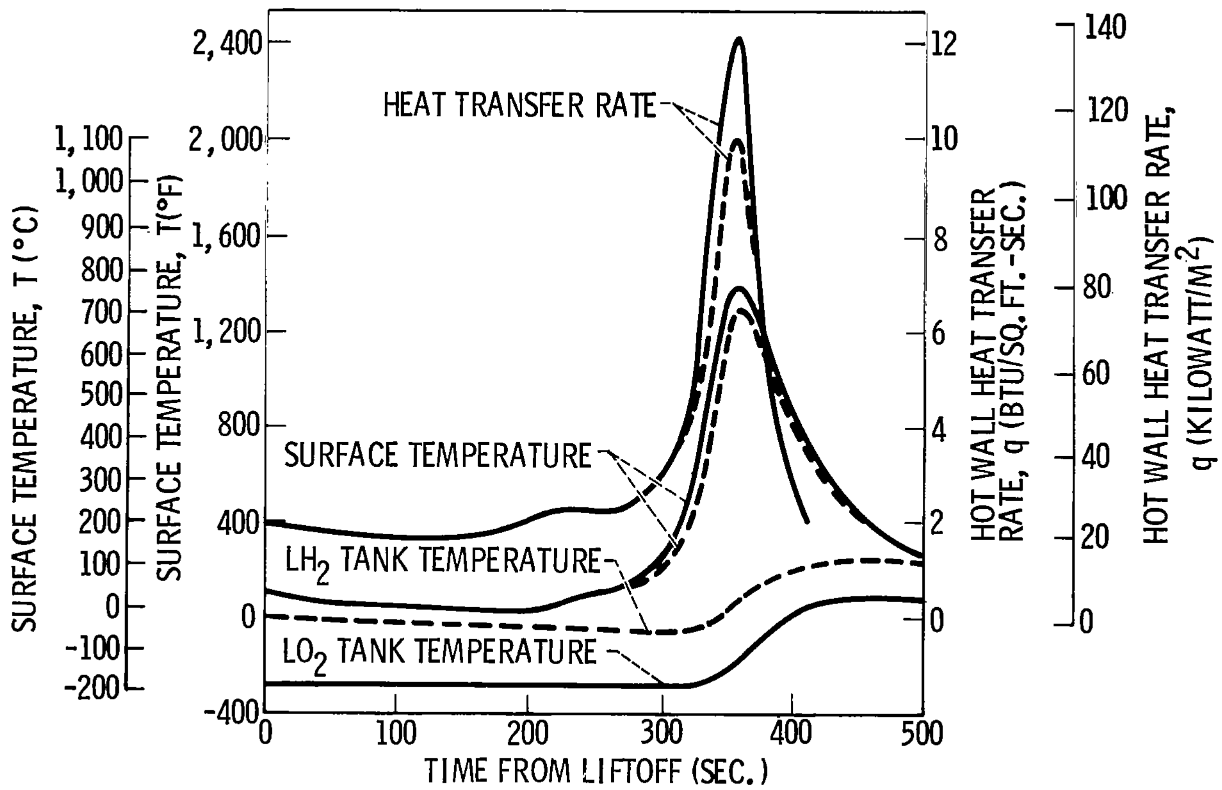

Figure 4

RECOVERY CONCEPT

Such a recovery trajectory is shown on this figure. Following abort separation (1), the booster continues on the nominal ascent trajectory until arriving within the constrained region. At that point (2), it departs from the nominal trajectory by (3) rolling 90 degrees counterclockwise about its longitudinal axis, (4) pitching 90 degrees nose-up to a 90 degree angle of attack, and (5) modulating the yaw angle with respect to the local horizontal to add to or detract from the gravity vector, thus controlling the vertical velocity component. By modulating the yaw angle, various higher altitudes may be achieved or altitudes in the near vicinity of the trajectory departure point (2) may be held. Once the flight path angle (γ) falls to zero, a vertical acceleration vector $\dot{V}_v = g$ could be achieved (by changing the yaw angle) so as to maintain the desired altitude. The component of thrust acceleration that lies in the horizontal plane will serve to torque the velocity vector to the left (back toward continental United States, if Kennedy Space Center is the launch site), thus both reducing downrange (by vectoring this into cross-range) and not adding to the initial departure velocity V_i. Since $\gamma > 0$, the final velocity attained at $\gamma = 0$ is $V_f < V_i$ due to the component of gravity that detracts from velocity. The resulting loiter trajectory (5) is a constant-altitude, constant-velocity powered (cruise) turn until burnout. At burnout (γ near 0), the booster begins its entry trajectory (8) at that apogee altitude and cruise velocity (V_f). Since the velocity is being continuously turned with the horizontal thrust acceleration vector component, the range plot will lie within the nominally provided flyback range. (An important feature is that entry loading and heating will also be less severe.) Following deployment of its airbreathing engines, the booster returns to the launch site (9) and lands (10).

BOOSTER RECOVERY TRAJECTORY FOLLOWING ABORT SEPARATION

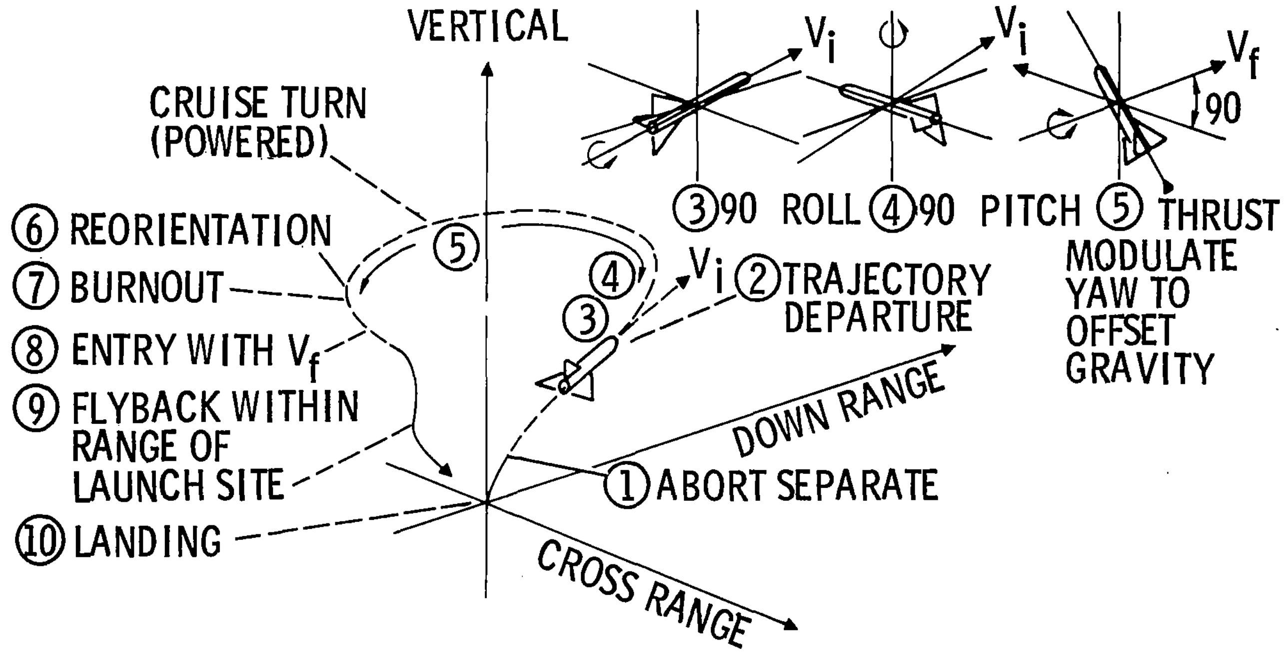

WITHIN CONSTRAINTS
UP TO 30% THROTTLING OR CUTOFF ENGINES
BURN TIME ≤100 SEC. OVER NORMAL

Figure 5

ABORT TRAJECTORY CONSTRAINTS

Flying at 90 degrees relative to the free stream can produce additional problems to be resolved. The figure presents the wing loading constraint at 90 degrees angle of attack and is seen to completely enclose the constrained region. (Note that for the configuration investigated, the control constraint line to hold 90 degrees angle of attack fell just below the wing loading constraint.) Thus, if an abort resulted in stage separation before 130 seconds into the flight, the procedure would be to proceed along the nominal trajectory until the 130-second point is reached before departing from the nominal trajectory in accordance with the recommended recovery procedure (preceding figure). If an abort occurred after 130 seconds and resulted in stage separation, trajectory departure would occur immediately.

The requirements of a booster recovery following stage separation can now be simply expressed:

1. Stay within the nominal ascent trajectory until the sensitive regions (e.g., Mach 1.0 and maximum q) have passed, thus avoiding excessive aerodynamic loading and heating at maneuvering angles of attack. This requirement implies delaying trajectory departure until after 130 seconds into the flight.
2. Avoid high velocities when possible to avoid excessive heat transfer during the burn to propellant depletion.
3. Avoid holding inertial velocity orientations for appreciable durations so as not to aggravate the downrange problem during the burn to propellant depletion.
4. Minimize, when possible, the entry loading and heating so as not to aggravate a possibly crippled booster.
5. Maneuver, when possible, into a region that will put the intended landing site in close proximity.

ABORT TRAJECTORY CONSTRAINT DIAGRAM

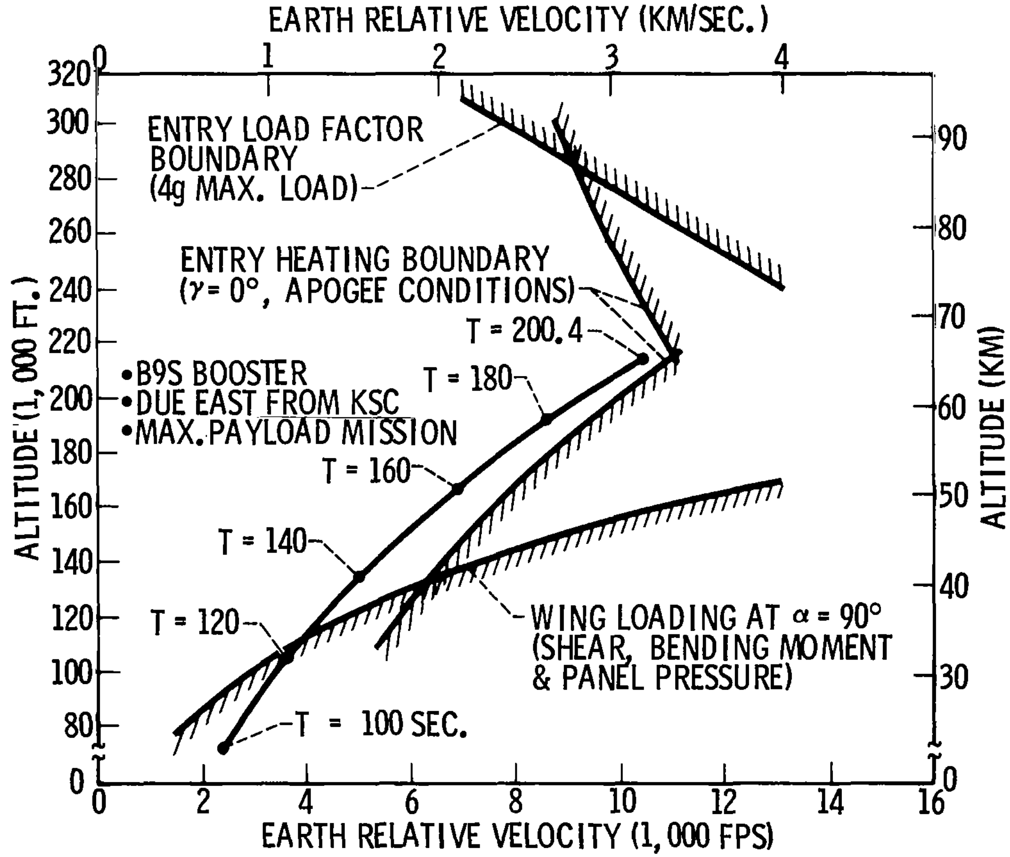

Figure 6

This figure presents the additional burn time beyond the nominal 200.4-second burnout condition due to the propellant remaining, which was to have been spent carrying the orbiter. This time ranges from a maximum of 92 seconds when the orbiter is dumped at liftoff, to a minimum of zero seconds for an abort at booster engine cutoff (BECO). Up to 92 seconds additional burn time might be required if separation occurs before 130 seconds, depending upon the actual time of separation. However, should separation occur after 130 seconds, the additional burn time can be read directly from the figure and will be less than 54 seconds.

ADDITIONAL BURN TIME VERSUS ABORT INITIATION

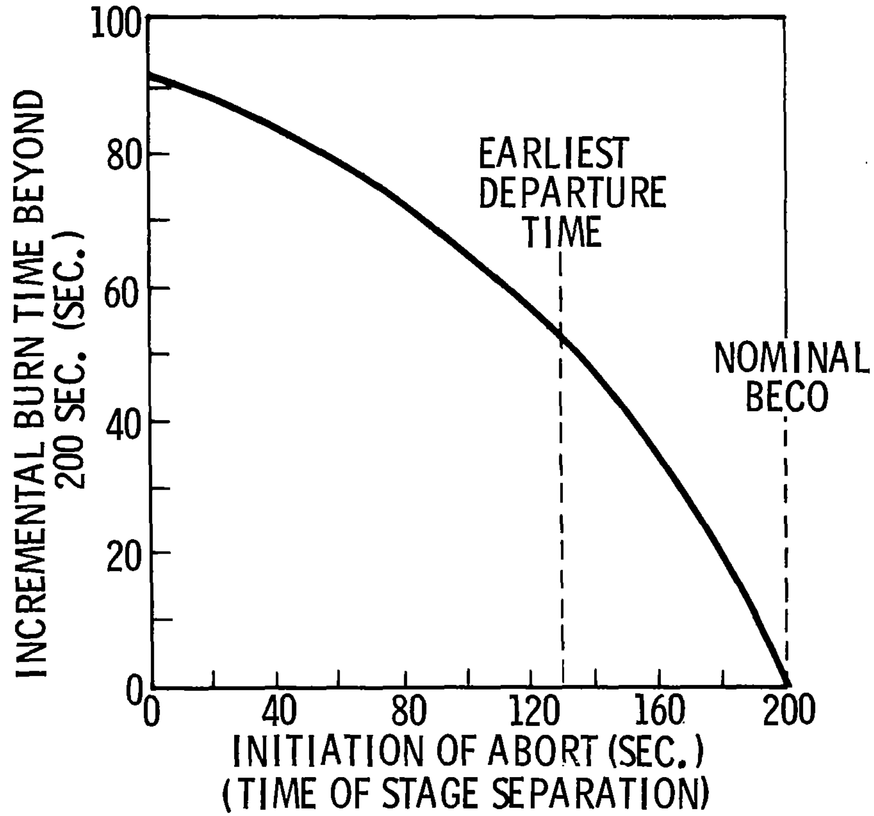

Figure 7

Two easily achievable operating procedures (using the recovery technique outlined) are superimposed on the constraint diagram. One procedure selects and maintains a constant yaw angle (no modulation), which produces burnout at apogee ($\gamma = 0$). The second procedure accomplishes continuous modulation of yaw angle to attain an altitude hold in the vicinity of the trajectory departure point. These procedures are merely extremes of trajectory management capability inherent in the recovery technique. Three distinct points (shown as "X") were selected at representative points in the region for detailed aerothermal analysis during the loiter and subsequent entry.

ABORT TRAJECTORIES FOR T DEPARTURE >130 SECONDS

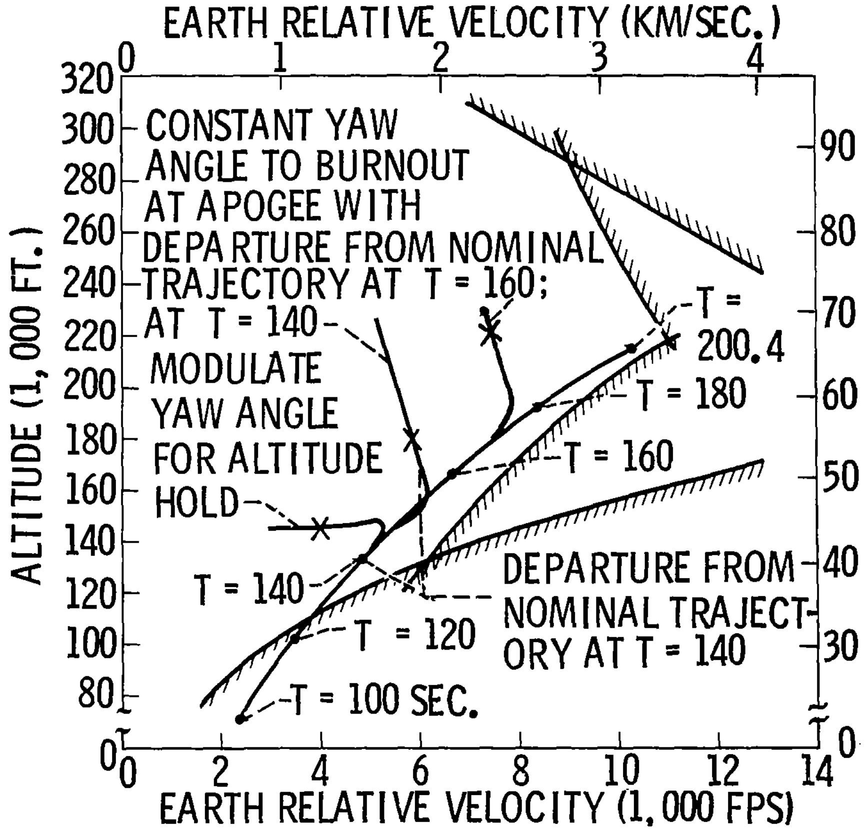

Figure 8

This figure demonstrates that the lower surface of the wing skin panel (Node 12) is lower in temperature than the nominal ("no abort") condition shown as a solid line. The aeroheating analysis included the ascent trajectory, a maximum-duration loiter at the "X" points, and subsequent entry heating. The results assumed an abort separation at time zero (post-liftoff) and included the full 92-second added burn time (beyond nominal burn) to propellant depletion; as such, the results are overly conservative. Although the 1,219-mps loiter is applicable to an abort separation at time zero and a trajectory departure of t = 140 seconds (see previous figure), the higher loiter velocities would generally be a consequence of abort separation after the earliest possible departure time (130 seconds) and the resulting loiter time would be correspondingly shorter.

LOWER SURFACE SKIN PANEL TEMPERATURES

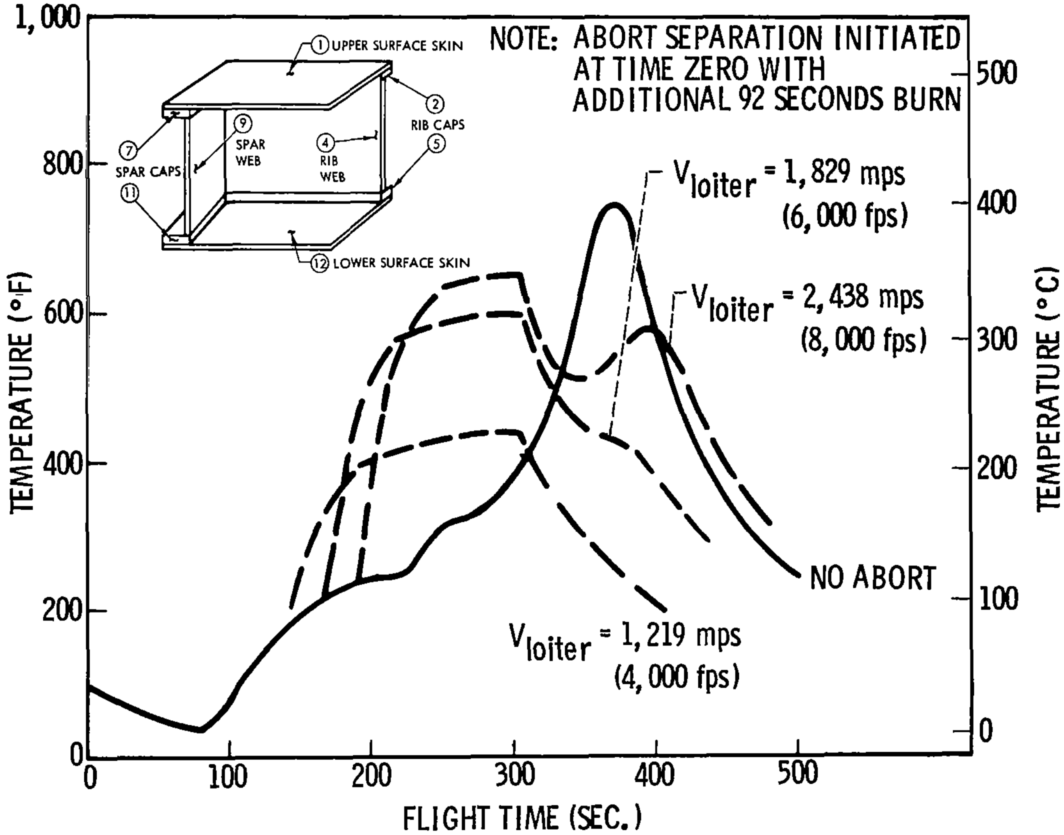

Figure 9

This illustration shows lower surface spar cap temperatures (Node 11) corrected to reflect the anticipated additional burn time commensurate with the indicated departure velocities. Again, it may be seen that the maximum spar cap temperature during abort is lower than in the "no abort" case.

LOWER SURFACE SPAR CAP TEMPERATURES

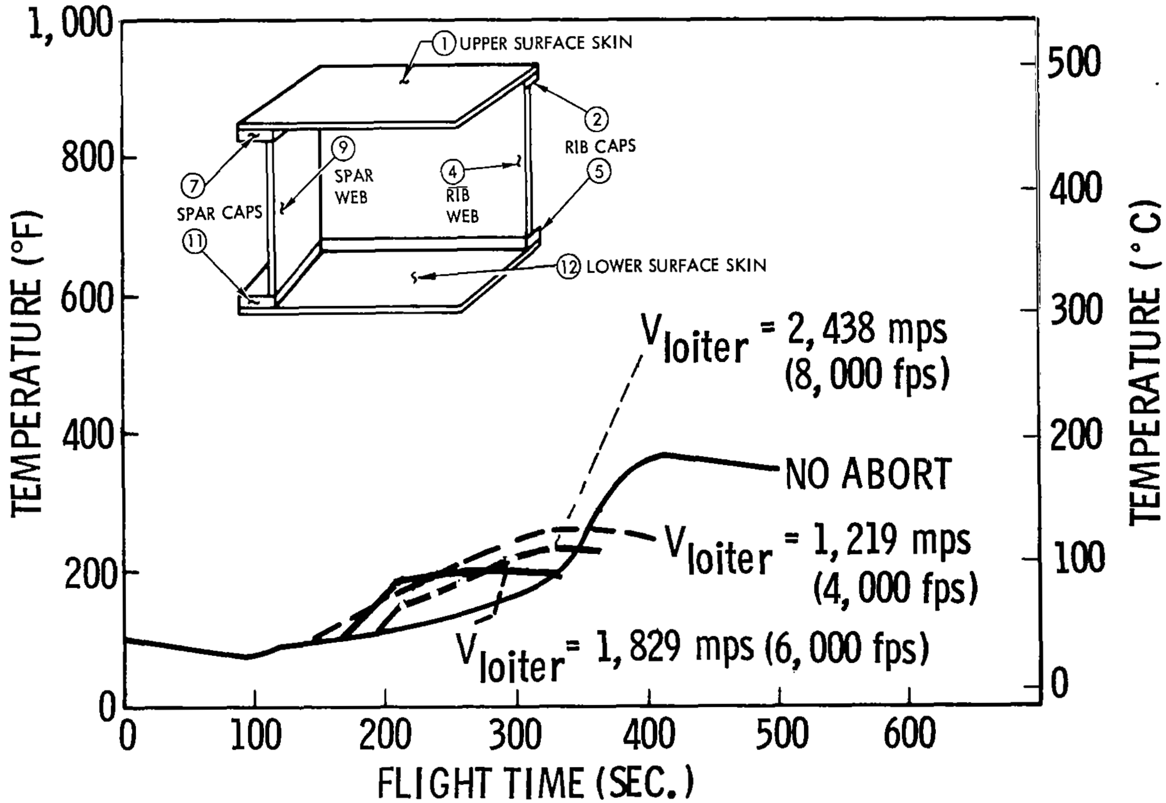

Figure 10

STUDY RESULTS

Separation times of T_{abort} = 40, 80, 100, 160, and 190 seconds were simulated and the resulting trajectories plotted. The trajectories illustrate that the abort recovery procedure is well within the established flight constraints, except for abort separation near nominal BECO.

ABORT TRAJECTORIES FOR CONSTANT YAW ANGLES

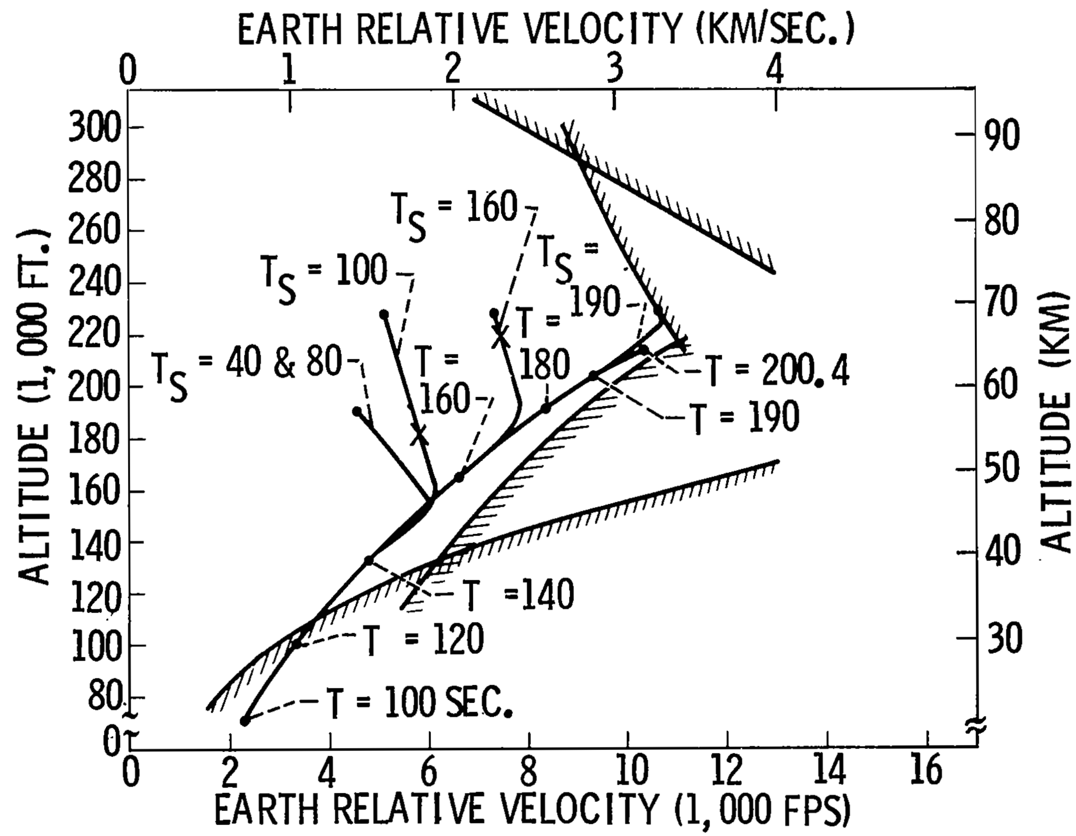

Figure 11

After deployment of its airbreathing engines, the booster returns to the launch site. The figure compares post-recovery flyback distance with time of abort separation. The reference flyback range is also shown. Except for abort separation immediately before normal staging, enough burn time remains to restrict the flyback range to within the baseline capability. Beyond 180 seconds into the trajectory, insufficient time is available to redirect the velocity vector; however, the excess energy is expended nearly colinearly with the velocity vector at separation, placing the booster beyond its design flyback range. An alternative landing site may be required for this condition.

REFERENCES

1. M.J. Hurley and M.J. Lanfranco, "Separation Dynamics of Multibody Clusters of Hinged and/or Linked Lifting-Entry Vehicles," presented to the Seventh Space Congress, Cocoa Beach, Fla., April 1970.
2. G.W. Carrie and M.J. Hurley, "Space Shuttle Separation System Analysis, A Capability Assessment," Convair Aerospace Report 76-549-4-172, 15 June 1971.
3. M.J. Hurley and G.W. Carrie, "Stage Separation of Parallel-Staged Shuttle Vehicles, A Capability Assessment," (to be published in proceedings of NASA Space Shuttle Aerothermodynamics Technology Conference, 15 and 16 Dec. 1971).

FLYBACK DISTANCE VERSUS TIME OF ABORT SEPARATION

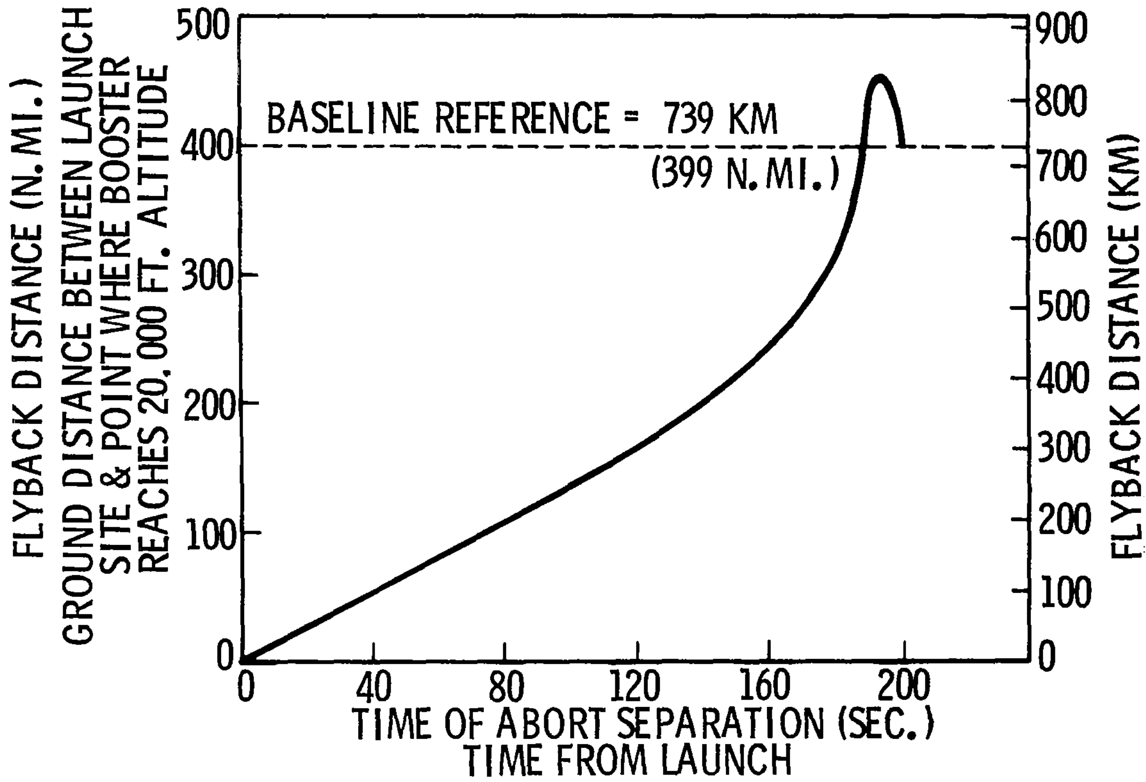

Figure 12

EFFECT OF COMMERCIAL AND MILITARY PERFORMANCE REQUIREMENTS FOR TRANSPORT CATEGORY AIRCRAFT ON SPACE SHUTTLE BOOSTER DESIGN AND OPERATION

R. A. Bithell and W. A. Pence, Jr.
Convair Aerospace Division of General Dynamics
San Diego, California

INTRODUCTION

The operating rules under which an aircraft performs affect every phase of flight from takeoff to landing and help determine engine requirements by setting critical thrust levels for various flight modes. The effect of two such sets of performance requirements, commercial and military, on the design and operation of the Space Shuttle booster is evaluated according to the following documents: Part 25 and Part 121 of the Federal Aviation Regulations (FAR) for commercial transport category aircraft; and MIL-C-5011A performance requirements for military aircraft.

Critical thrust levels are established according to both sets of operating rules for the takeoff, cruise, and go-around flight modes, and the effect on engine requirements determined. Both flyback and ferry operations are considered. The impact of landing rules on potential shuttle flyback and ferry bases is evaluated. Factors affecting reserves are discussed, including winds, temperature, and nonstandard flight operations. Finally, a recommended set of operating rules is proposed for both flyback and ferry operations that allows adequate performance capability and safety margins without compromising design requirements for either flight phase.

INTRODUCTION

- FLYBACK PERFORMANCE
  - THRUST REQUIREMENTS
    - CRUISE
    - GO-AROUND
  - LANDING RULES
  - RESERVES
    - ATMOSPHERE
    - WINDS
    - ENGINE-OUT
    - GO-AROUND
  - RECOMMENDED OPERATING RULES

- FERRY OPERATIONS
  - FERRY ROUTES
  - THRUST REQUIREMENTS
    - CRUISE
    - GO-AROUND
    - TAKEOFF
  - LANDING PERFORMANCE
  - RESERVES
  - RECOMMENDED OPERATING RULES

BOOSTER CONFIGURATION

Configuration geometry for a representative Space Shuttle booster is presented. The vehicle shown is an LO_2/RP booster with delta wing/canard geometry. The flyback engines are low bypass ratio turbofans burning JP-5; they are installed within the wing and deploy beneath it while in operation.

Details of the booster performance are based on this configuration.

BOOSTER CONFIGURATION

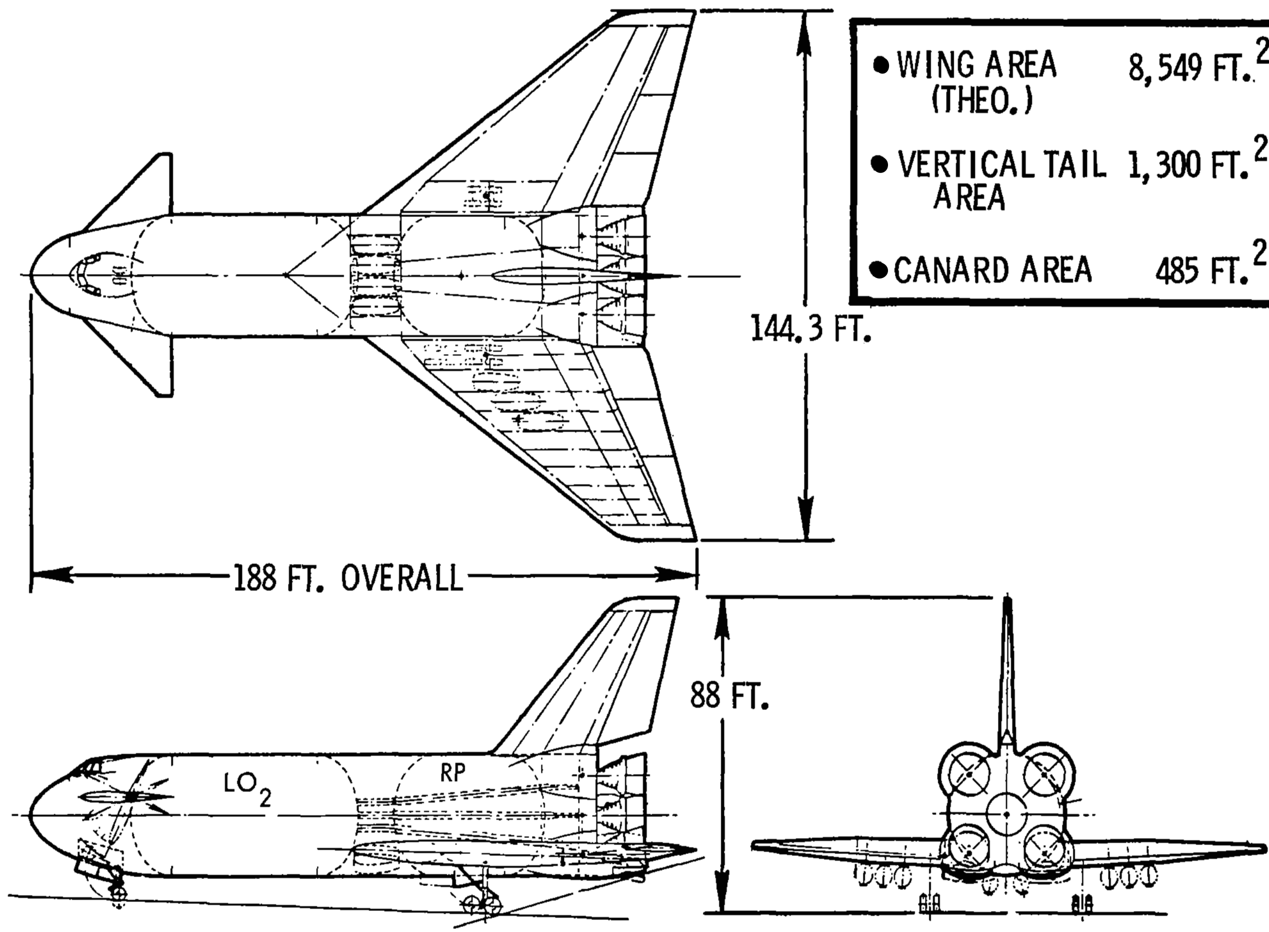

• WING AREA (THEO.)	8,549 FT.^{2}
• VERTICAL TAIL AREA	1,300 FT.^{2}
• CANARD AREA	485 FT.^{2}

CANDIDATE LANDING SITES

Two landing sites for the baseline configuration are considered for flyback because of their current launch vehicle capability: Kennedy Space Center, Florida, and Vandenberg Air Force Base, California. The elevation for both locations is near sea level.

At the present time, no landing facility exists at KSC, but field lengths over 3,050 meters (10,000 feet) are being planned. The 2,440-meter (8,000-foot) runway at Vandenberg may not be adequate to accommodate booster landings at heavy gross weights under wet field conditions, and extension of the runway may have to be considered.

CANDIDATE LANDING SITES

KENNEDY SPACE CENTER, FLORIDA
ALTITUDE: 3 M (10 FT.)
FIELD LENGTH: MORE THAN 3,050 M (10,000 FT.)

VANDENBERG AIR FORCE BASE, CALIFORNIA
ALTITUDE: 112 M (368 FT.)
FIELD LENGTH: 2,440 M (8,000 FT.)

CRUISE OPTIMIZATION

The number of operating engines required to minimize flyback systems weight was determined for still-air, standard day conditions and Eastern Test Range 95 percentile headwind conditions on a MIL-STD-210A hot day for cruise ranges from 185.2 kilometers (100 nautical miles) to 555.6 kilometers (300 nautical miles). Flyback systems weight, defined here as engine weight plus fuel weight, is presented as a function of the number of operating engines.

For still-air, standard-day conditions, the optimum number of operating engines resulting in the minimum flyback systems weight for a given range increases from 6.2 engines for 185.2 kilometers (100 nautical miles) to 10 engines for 555.6 kilometers (300 nautical miles). As the flyback range increases, fuel weight becomes the dominant factor in the total flyback systems weight. Increasing the number of cruise engines with flyback range results in higher cruise altitudes and improved cruise efficiency, thereby minimizing flyback fuel. For short cruise ranges of approximately 185.2 kilometers (100 nautical miles) or less, for which fuel weights are small, the optimum cruise altitude occurs below sea level, since engine weight now becomes the driving factor. Sea level, however, is the limiting minimum altitude.

Flyback on a hot day against the ETR 95 percentile headwind results in an optimum cruise altitude of sea level for all flyback ranges from 185.2 kilometers (100 nautical miles), to 555.6 kilometers (300 nautical miles), and optimum engine numbers from 7.1 to 7.9. Although the cruise ceiling increases with increasing flyback range because of improved cruise efficiency at higher altitudes, the effect of the ETR headwind tends to drive the optimum altitude to sea level, where headwinds are a minimum. The increase in fuel flow at this altitude is more than offset by the increase in ground speed, resulting in a net improvement in cruise efficiency.

Flyback range for the baseline booster is approximately 370.4 kilometers (200 nautical miles). Since eight operating engines are optimum at sea level on a hot day against the NASA ETR 95 percentile headwind, a total of 10 engines is considered adequate to meet engine sizing design requirements under these conditions, taking into account the large number of engines and the possibility of more than one engine failure. This is equivalent to cruising at 1,525 meters (5,000 feet) on a hot day with one engine inoperative or at 3,050 meters (10,000 feet) on a standard day with one engine inoperative at maximum continuous power. If two-engine-out, hot-day emergency operation is required, intermediate power can be used to increase the cruise altitude to safe operating elevations above sea level.

CRUISE OPTIMIZATION

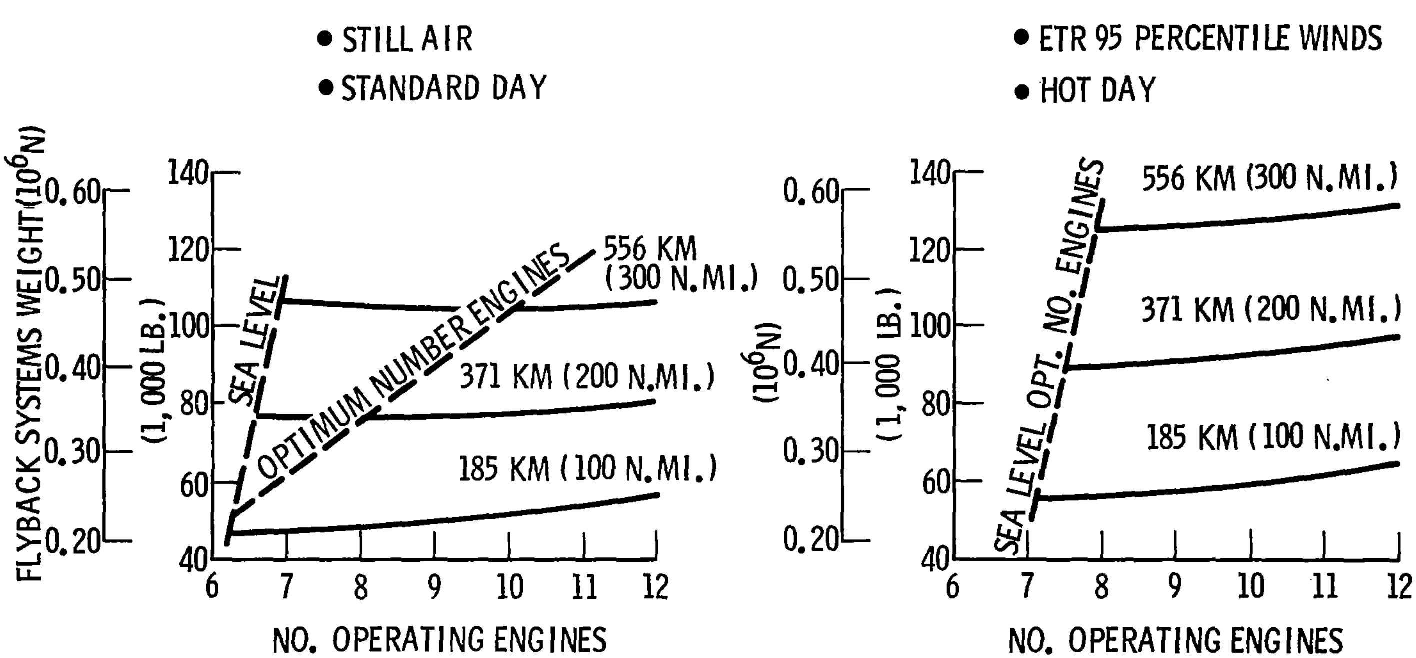

GO-AROUND CLIMB GRADIENTS

The commerical and military climb gradient requirements for the landing and approach configurations are presented. The Federal Aviation Regulations (FAR) Part 25 requires that compliance with specified climb gradients must be shown at each weight, altitude, and ambient temperature within the operational limits of the aircraft for both the landing and approach configurations. These configurations are generally selected by the applicant seeking certification. The approach configuration for the booster is defined by the approach canard setting (+10 degrees), with elevons set for trim and landing gear retracted. The landing configuration is defined by the landing canard setting (+15 degrees), with elevons set for trim and landing gear down and locked. In addition, the stall speed (V_S), or minimum speed, for the approach configuration cannot exceed 110% of the stall speed for the related landing configuration.

Compliance with the climb gradients shown is required for four-engine aircraft with all engines operating in the landing configuration, or one engine out in the approach configuration. Climb gradients for turbine-engine-powered vehicles with more than four engines, such as Space Shuttle, are not specifically covered in FAR Part 25.

No specified climb gradient is required by MIL-C-5011A in the landing and approach configuration. However, climb performance must be calculated with all engines operating and one engine inoperative.

GO-AROUND CLIMB GRADIENT

FAR PART 25

FOR EACH OPERATIONAL WEIGHT, ALTITUDE, & TEMPERATURE –

- LANDING CLIMB – GRADIENT $\geq$ 0.032
  - LANDING CONFIGURATION
  - ALL ENGINES OPERATING
  - TAKEOFF POWER
- APPROACH CLIMB – GRADIENT $\geq$ 0.027
  - APPROACH CONFIGURATION
  - ONE ENGINE OUT
  - TAKEOFF POWER

MIL-C-5011A

- NO SPECIFIED CLIMB GRADIENT

GO-AROUND THRUST REQUIREMENTS

The thrust required to meet the FAR Part 25 landing and approach climb gradients is presented as a function of landing gross weight, together with that required to maintain a positive climb gradient. Engine requirements are determined for the critical hot-day conditions at sea level. In the landing configuration for a gross weight of 2.85×10^6 N (640,000 pounds), with gear down and canard set at +15 degrees, 10 engines are required to maintain the FAR climb gradient of 0.032; nine engines are needed to maintain a positive gradient. In the approach configuration at the same gross weight, with gear up and canard set at +10 degrees, 10 engines are necessary to meet the required FAR climb gradient of 0.027, whereas nine are needed to maintain a positive gradient. All engines are operating in the landing configuration, with one engine inoperative for approach. Throttles are at takeoff power.

Because of the large number of engines required on the baseline booster, it is felt that allowance should be made for more inoperative engines than is required by Part 25 of the FAR. Increasing the number of inoperative engines from none to one for the landing configuration, and from one to two for the approach configuration, while maintaining a positive climb gradient, provides for safe operation in both flight modes. For the baseline configuration, this results in 10 flyback engines, or the same number required to maintain the FAR gradients.

GO-AROUND THRUST REQUIREMENTS

LANDING CLIMB

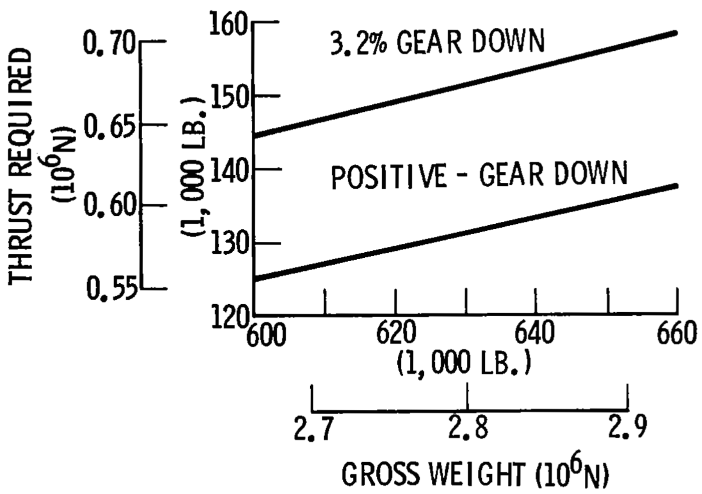

- GW = 2.84×10^6 N (640,000 LB.)
- SEA LEVEL — HOT DAY
- TAKEOFF POWER
- ALL ENGINES OPERATING

GRADIENT	NO. ENGINES
0.032	10
POSITIVE	9

APPROACH CLIMB

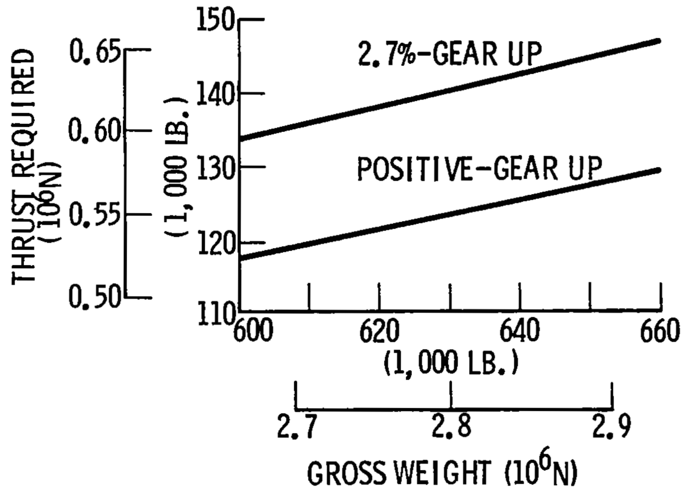

- GW = 2.84×10^6 N (640,000 LB.)
- SEA LEVEL—HOT DAY
- TAKEOFF POWER
- ONE ENGINE OUT

GRADIENT	NO. ENGINES
0.027	10
POSITIVE	9

LANDING RULES

Landing rules according to the Federal Aviation Regulations and MIL-C-5011A are presented. Part 25 of the FAR includes the threshold speed requirements; Part 121 covers the stopping distance requirements for wet and dry field operation. Landing performance must be determined for each weight and altitude within the operational limits of the aircraft and for standard temperatures.

Landing performance according to MIL-C-5011A must be determined for each operational weight, altitude, and temperature. The distances are not factored to determine required field length. However, coefficient of friction values must be representative of actual runway conditions.

LANDING RULES

FAR PART 25 & PART 121

- ALL OPERATIONAL WEIGHTS & ALTITUDES
- STANDARD TEMPERATURES
- LANDING CONFIGURATION
- $V_{OBS} = 1.3\ V_{MIN}$
- DISTANCE MEASURED FROM POSITION 15.3 M (50 FT.) ABOVE LANDING SURFACE TO STOPPING POINT
- REQUIRED FIELD LENGTH FOR DRY SURFACE LANDINGS DEFINED AS ACTUAL LANDING DISTANCE DIVIDED BY 0.6
- REQUIRED FIELD LENGTH FOR WET SURFACE LANDINGS DEFINED AS 1.15 TIMES REQUIRED DRY SURFACE FIELD LENGTH

MIL-C-5011A

- ALL OPERATIONAL WEIGHTS, ALTITUDES, & TEMPERATURES
- LANDING CONFIGURATION
- $V_{OBS} = 1.2\ V_{MIN}$
- COEFFICIENT OF FRICTION (μ) = 0.30 FOR DRY SURFACES
- DISTANCE MEASURED FROM POSITION 15.3 M (50 FT.) ABOVE LANDING SURFACE TO STOPPING POINT
- COEFFICIENT OF FRICTION (μ) VALUES REPRESENTATIVE OF ACTUAL RUNWAY CONDITIONS

LANDING PERFORMANCE

Landing performance is presented according to FAR and MIL-C-5011A requirements. Threshold speed is determined as a function of landing gross weight at sea level for standard and hot-day conditions. The FAR requirements state that the vehicle must cross the threshold at a speed not less than 1.3 V_{min}, while MIL-C-5011A requires a threshold speed not less than 1.2 V_{min}.

The FAR landing distances presented are based on a dry runway coefficient of friction of 0.35. This value was arbitrarily selected as being representative of the shuttle braking system, since Part 25 of the FAR does not specify a dry coefficient of friction to be used in landing distance calculations. MIL-C-5011A specifies that a coefficient of friction of 0.30 be used for dry surface landings; a wet value of 0.10 was arbitrarily selected as representative of average wet runway conditions. Required landing distances less than 2,590 meters (8,500 feet) can be obtained under FAR rules for dry field operation at heavy gross weights at sea level, while field lengths less than 3,050 meters (10,000 feet) are required for wet operations. The corresponding distances under MIL-C-5011A rules are less than 1,680 meters (5,500 feet) for hot-day, dry-field operation at sea level, and 3,050 meters (10,000 feet) for hot-day, wet-field operation. All distances over the 15.25-meter (50-foot) obstacle are based on a three-degree glide path – the typical ILS glide-slope angle.

Recommended landing procedures for shuttle operations consist of threshold speeds that are based on 120% of the minimum speed in the landing configuration, and coefficient of friction values that are representative of actual runway conditions. Lower threshold speeds result in shorter stopping distances; representative friction coefficients ensure realistic field lengths under all weather conditions.

On the basis of landing considerations, a field length of 3,050 meters (10,000 feet) is sufficient to meet Space Shuttle requirements for hot-day, wet-field operations at sea level. Consequently, the runway at Vandenberg Air Force Base must be increased 610 meters (2,000 feet) if it is to be considered a potential Space Shuttle launch and recovery site.

LANDING PERFORMANCE

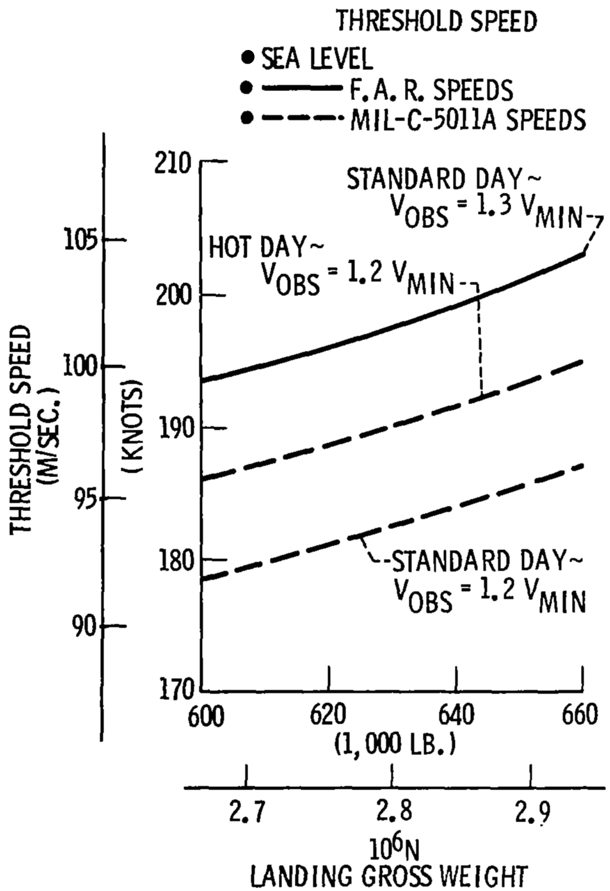

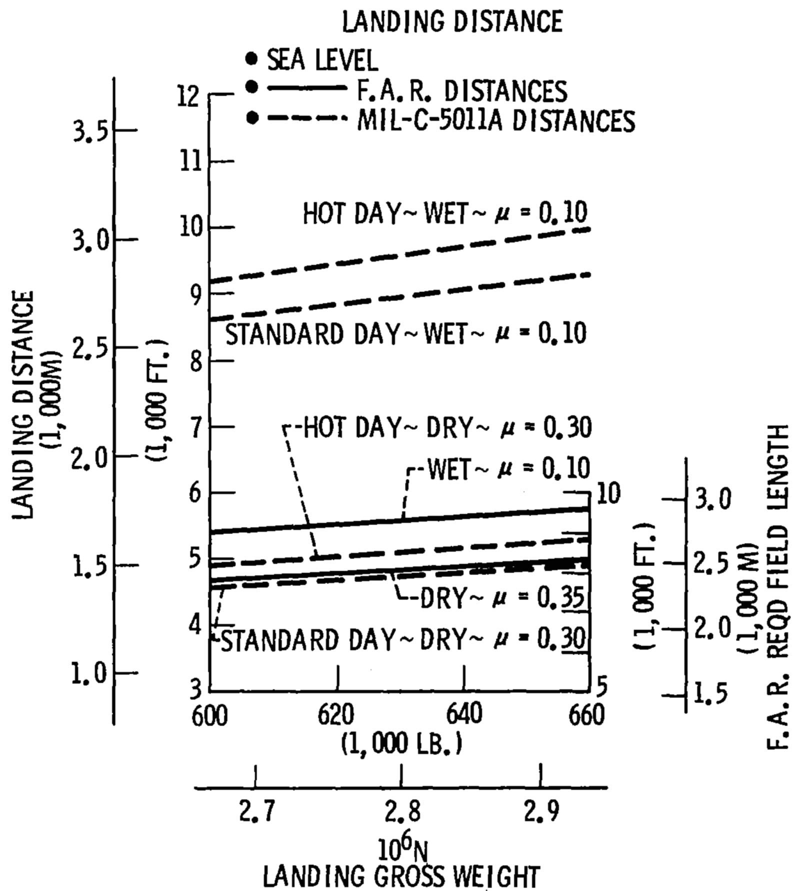

RESERVES

The various factors affecting fuel reserve requirements are presented, together with their respective fuel increments for a 10-engine vehicle having a flyback range of 370.4 kilometers (200 nautical miles). Allowance for all of these "contingencies" requires a fuel increment of 149,000 N (33,500 pounds).

Also presented are the military and commercial reserve requirements. Commercial requirements are clearly unnecessary and performance-penalizing for the shuttle vehicle, while the MIL-C-5011A requirements are inadequate for long flyback ranges and too severe for the very short ranges.

Recommended reserves for flyback include allowance for the ETR 95 percentile headwind and go-around, the two most severe "contingencies" from a fuel increment standpoint. Fuel reserves to cover these conditions can also include any of the following occurrences: (1) ETR winds and go-around; (2) ETR winds, hot day, and two engines out; or (3) go-around, hot day, and two engines out.

RESERVES

R = 371 KM (200 N.MI.) — 10 ENGINES

FACTORS AFFECTING FUEL REQUIREMENTS		FUEL INCREMENT
• ATMOSPHERE	HOT	2,224 N (500 LB.)
• WINDS	ETR 95 PERCENTILE	64,500 N (14,500 LB.)
• NO. OF OPERATING ENGINES	TWO OUT	20,000 N (4,500 LB.)
• GO-AROUND	LANDING/APPROACH CONFIG.	62,200 N (14,000 LB.)
• TOTAL		148,924 N (33,500 LB.)

RESERVES

- MIL-C-5011A – 106,800 N (24,000 LB.)
  - 5% INITIAL FUEL
  - 30 MINUTES AT MAXIMUM ENDURANCE AT SEA LEVEL
- COMMERCIAL – 369,000 N (83,000 LB.)
  - 45 MINUTES AT MAXIMUM ENDURANCE
  - FUEL FOR 371 KM (200 N.MI.) AT LONG-RANGE CRUISE
- RECOMMENDED – 126,600 N (28,500 LB.)
  - ETR 95 PERCENTILE WINDS
  - GO-AROUND

FLYBACK OPERATING RULES

The recommended operating rules for flyback are summarized. On the basis of cruise and go-around thrust requirements, 10 engines are necessary to meet the proposed operating rules. From a landing performance consideration, the runway at Vandenberg Air Force Base must be increased to 3,050 meters (10,000 feet) to accommodate shuttle landings at heavy gross weights under wet-runway, hot-day conditions. Allowances for ETR 95 percentile headwinds and go-around provide an adequate reserve margin for flyback.

RECOMMENDED FLYBACK OPERATING RULES

R = 371 KM (200 N.MI.) 10 ENGINES

CRUISE –

- 5,000 FT.
- HOT DAY
- MAX. CONTINUOUS POWER
- ONE ENGINE OUT

GO-AROUND –

- LANDING CLIMB –
  POSITIVE GRADIENT, ONE ENGINE OUT, SEA LEVEL, HOT DAY
- APPROACH CLIMB –
  POSITIVE GRADIENT, TWO ENGINES OUT, SEA LEVEL, HOT DAY

LANDING – (MIL-C-5011A)

- $V_{THRESHOLD} = 1.2\ V_{MIN}$
- DISTANCE DETERMINED FOR ALL OPERATIONAL WEIGHTS, ALTITUDES & TEMPERATURES
- COEFFICIENT OF FRICTION (μ) VALUES REPRESENTATIVE OF ACTUAL RUNWAY CONDITIONS

RESERVES –

- ETR 95 PERCENTILE WINDS
- GO-AROUND

APPLICATION OF BASELINE VEHICLE TO FERRY OPERATIONS

The baseline Space Shuttle booster is designed for a flyback mission with limited range and altitude requirements. In adapting the vehicle to cross-country ferry operations, its capability must be improved to meet the range and altitude necessary for transcontinental flight. In addition, thrust improvements may be necessary to ensure adequate takeoff capability from candidate airfields. However, any improvements in aerodynamic efficiency and thrust capability needed for ferry flight must not compromise the design of the baseline vehicle.

APPLICATION OF BASELINE VEHICLE TO FERRY OPERATIONS

- LIMITED RANGE
- LIMITED ALTITUDE CAPABILITY

TRANSCONTINENTAL FERRY ROUTE

A representative ferry route across the continental United States from Vandenberg Air Force Base, California, to Kennedy Space Center, Florida, is presented. Because of the booster's size and weight, only airfields capable of supporting B-52 aircraft operations are considered. The DOD Flight Information Publication IFR–Supplement United States was the principal source of information on candidate airfields. Distances between airfields were obtained by scaling from standard USAF jet navigation charts. Existing runway lengths and field elevations are presented in meters, and the distances between airfields in kilometers, for the most conveniently spaced suitable airfields.

TRANSCONTINENTAL FERRY ROUTE

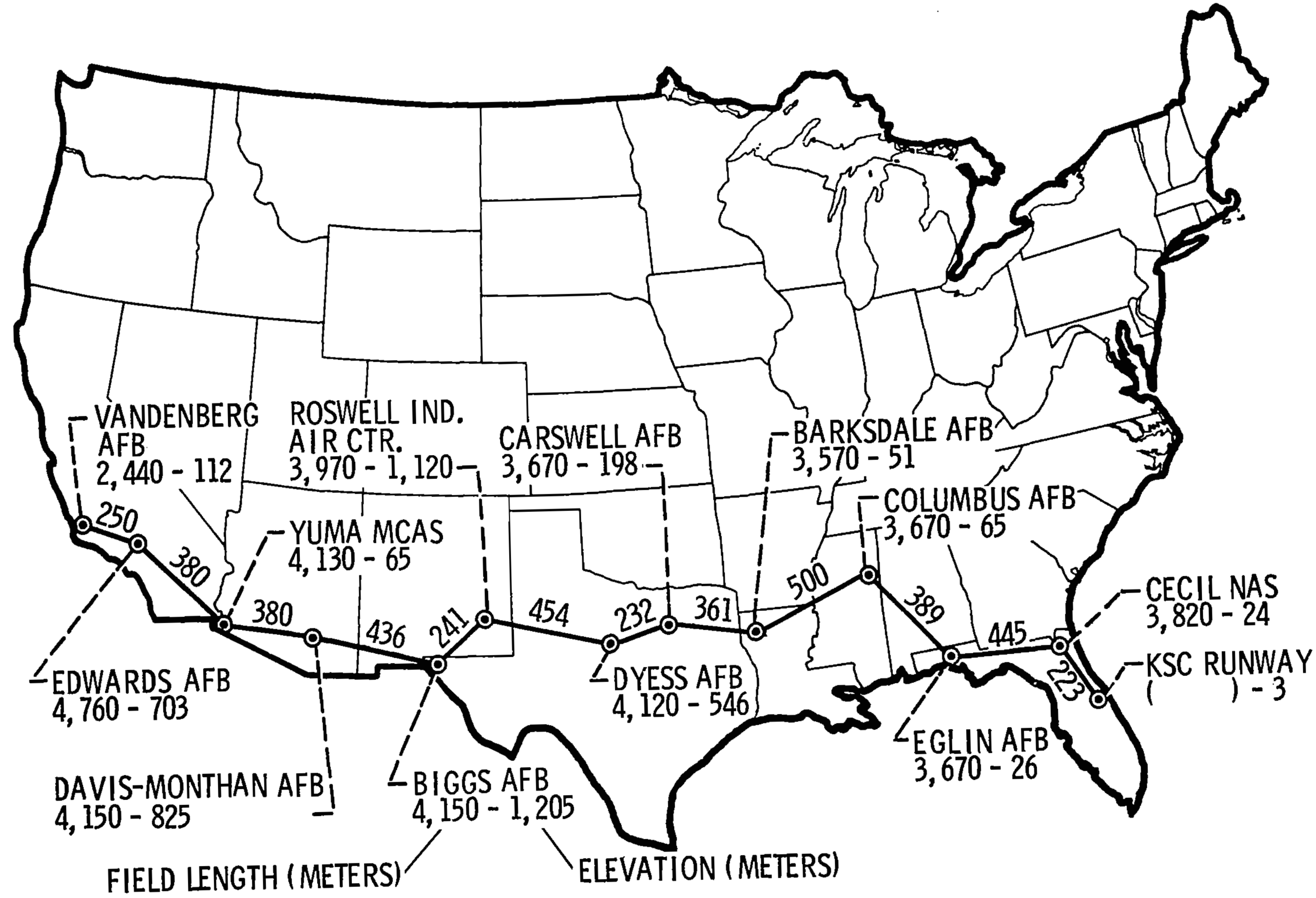

FERRY ROUTE TERRAIN ELEVATIONS

Terrain elevations along the proposed ferry route are shown. Because of the booster's low cruise ceiling, consideration was given to terrain heights within 18.5 kilometers (10 nautical miles) of the direct course between airfields and along the lowest practical route between airfields. A flight altitude of at least 2,135 meters (7,000 feet) is required to clear terrain along the entire route. However, except for terrain elevations east of Davis-Monthan Air Force Base and west of Roswell Industrial Air Center, a flight altitude of 1,525 meters (5,000 feet) is sufficient to meet terrain requirements along low-level routes between points.

FERRY ROUTE TERRAIN ELEVATIONS

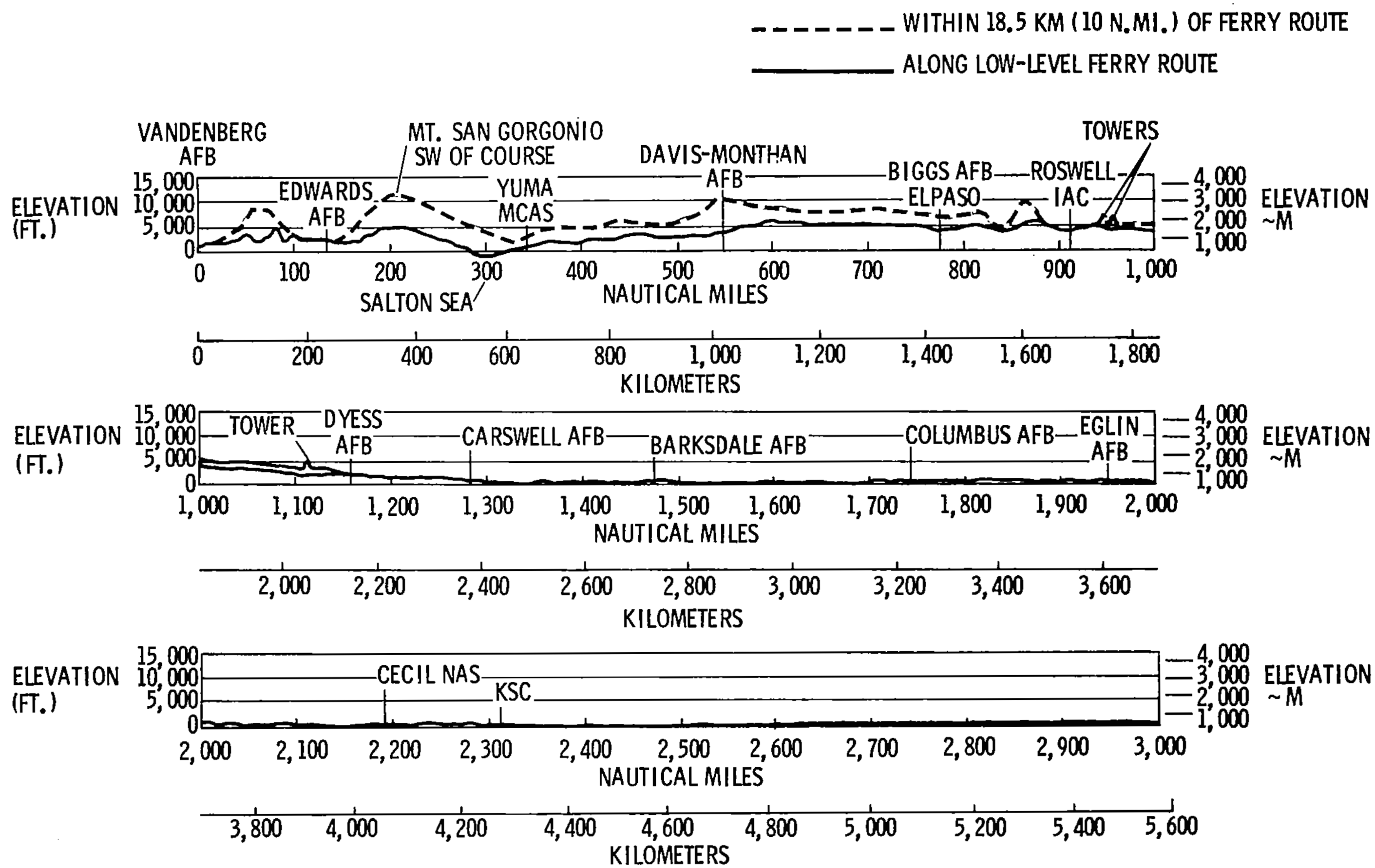

THRUST REQUIRED

The thrust required to meet the FAR Part 25 climb gradients for the baseline ferry configuration is presented together with that needed to maintain a positive gradient for the landing and approach configuration. The thrust necessary to maintain minimum drag levels is also presented for the clean configuration ($L/D_{max} = 6.40$) as a function of gross weight.

The thrust levels for the same requirements are also presented for the baseline vehicle, with the addition of a tailcone fairing over the base. Since almost 50% of the booster subsonic drag is base drag, the addition of a tailcone aft of the vehicle base which produces a faired fuselage results in a considerable decrease in vehicle drag levels and improved aerodynamic efficiency (L/D_{max} = 10.10).

THRUST REQUIRED

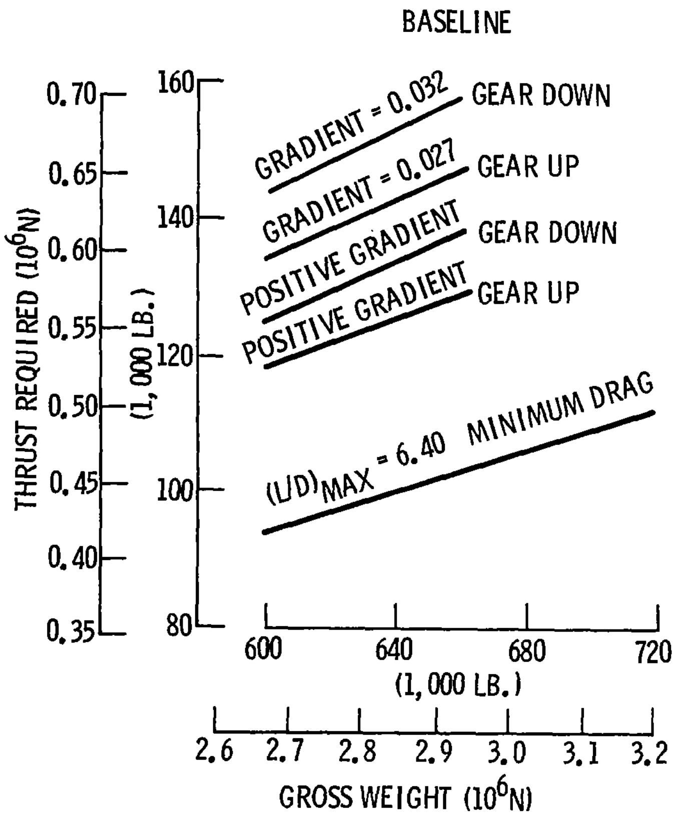

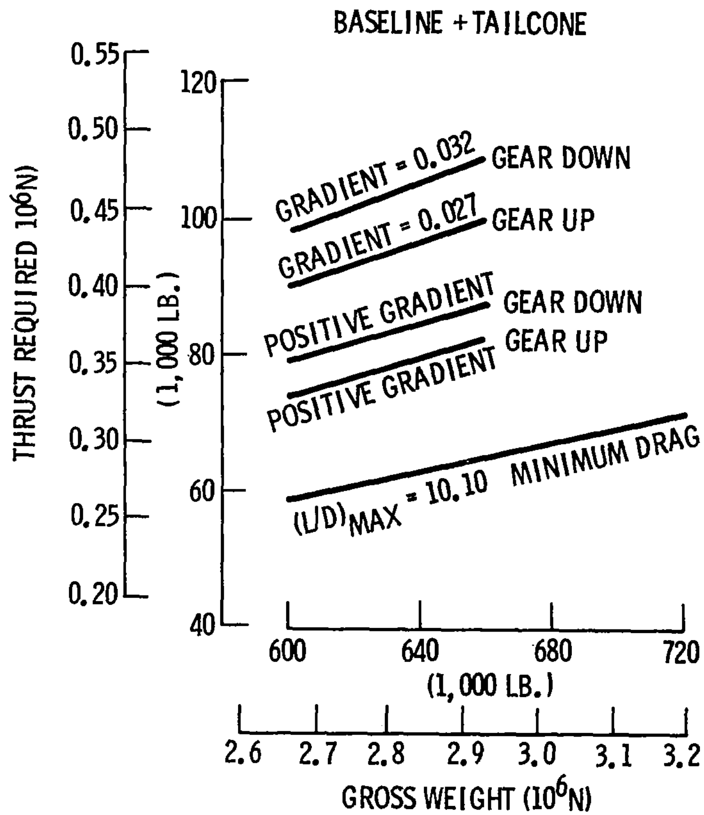

REQUIRED NUMBER OF ENGINES

The effect of the decreased vehicle drag levels resulting from the addition of a tailcone fairing is shown by the reduced number of cruise engines required to maintain adequate cruise and go-around performance. The baseline configuration with tailcone reduces by three the number of engines necessary to maintain hot-day cruise performance at 1,525 meters (5,000 feet) and 3,050 meters (10,000 feet) and hot-day go-around performance at 1,220 meters (4,000 feet). This is a distinct advantage of the tailcone modification under ferry flight operating conditions that necessitate increased thrust capability to the baseline vehicle and hence additional engines.

Recommended operating conditions and engine requirements for cruise and go-around are also presented. Because of the low minimum cruise altitude (1,525 meters or 5,000 feet) along the ferry route, the high temperatures expected to be encountered in the southern United States, and the large number of required engines, an absolute ceiling capability of 1,525 meters (5,000 feet) on a hot day with two engines inoperative at maximum continuous power is recommended for cruise. Under these emergency conditions, when additional altitude capability is required to clear terrain east of Davis-Monthan and west of Roswell, intermediate power may be used. As for flyback, recommended go-around operating rules increase the number of inoperative engines specified by FAR Part 25 from none to one for the landing configuration, and from one to two for the approach configuration because of the large number of engines. Performance must be calculated at 1,220 meters (4,000 feet) elevation on a hot day to cover the range of airfield elevations and expected temperatures. A positive climb gradient capability is considered sufficient under these emergency conditions.

Eleven engines are required for the baseline vehicle to meet these recommended operating rules; this is one more than the baseline requirement for flyback. The addition of the tailcone reduces this number to eight engines, well within the flyback limit of 10.

REQUIRED NUMBER OF ENGINES

	NO. ENGINES BASELINE	NO. ENGINES TAILCONE
CRUISE – 3.11×10^6 N (700,000 LB.)		
• 3,050M (10,000 FT.), HOT DAY, ONE ENGINE OUT	11	8
• 1,525 M (5,000 FT.), HOT DAY, ONE ENGINE OUT	10	7
GO-AROUND – 2.89×10^6 N (650,000 LB.) 1,220M (4,000 FT.) HOT DAY		
• LANDING CLIMB – ALL ENGINES OPERATING		
FAR PART 25 – GRADIENT = 0.032	11	8
POSITIVE CLIMB GRADIENT	10	7
• APPROACH CLIMB – ONE ENGINE OUT		
FAR PART 25 GRADIENT = 0.027	11	8
POSITIVE CLIMB GRADIENT	10	7
RECOMMENDATIONS –		
• CRUISE – 1,525 M(5,000 FT.), HOT DAY, TWO ENGINES OUT	11	8
• GO-AROUND – 1,220 M (4,000 FT.), HOT DAY		
LANDING CLIMB – POSITIVE CLIMB GRADIENT, ONE ENGINE OUT	11	8
APPROACH CLIMB – POSITIVE CLIMB GRADIENT, TWO ENGINES OUT	11	8

FERRY RANGE

Vehicle ferry range is presented as a function of takeoff gross weight for the baseline vehicle and the baseline with a tailcone. The improved aerodynamic efficiency of the tailcone configuration not only results in reduced engine requirements because of lower drag levels, but also increased cruise range for a given takeoff gross weight.

Recommended operating rules for flight planning are presented. Fuel for taxi, takeoff, and acceleration to climb speed is five minutes at normal rated power (maximum continuous) at sea level. Taken from MIL-C-5011A requirements for transport aircraft, this is adequate for shuttle ferry operations. Recommended cruise operation consists of flight against a 25.7 meters-per-second (50-knot) headwind with all engines operating at the optimum cruise altitude to the point of no return on a standard day, loss of one engine, and one-engine-out cruise from the point of no return to the destination. A 25.7 meters-per-second (50-knot) headwind is commonly used by airline operators for transcontinental flight planning purposes and is considered satisfactory for shuttle ferry flight planning. The point of no return is defined as that point on the flight trajectory from which the vehicle can return to the takeoff site or continue to the destination using all of the remaining cruise fuel on board. A fuel allowance for one aborted landing attempt and go-around in the landing configuration is recommended for flight reserves.

FERRY RANGE

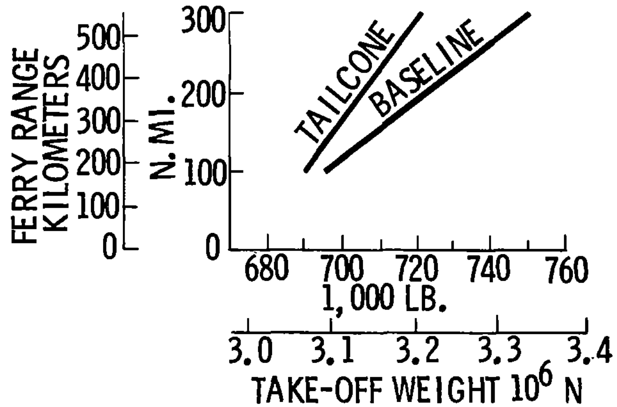

OPERATING RULES

TAXI, TAKEOFF & ACCELERATE TO CLIMB SPEED – FUEL FOR 5 MIN. AT NORMAL POWER AT SEA LEVEL – MIL-C-5011A

CRUISE – ALL ENGINES OPERATING AT OPTIMUM CRUISE ALTITUDE AGAINST 25.7 M/SEC. (50KT.) HEADWIND TO POINT OF NO-RETURN – ONE ENGINE OUT CRUISE AGAINST 25.7 M/SEC. HEADWIND TO DESTINATION

LANDING & RESERVES – FUEL ALLOWANCE FOR GO-AROUND

CRITICAL ROUTES

The critical routes for the transcontinental ferry operation are presented. These flight segments are considered critical because of their limited field length capability for the takeoff gross weights required to meet the specified ranges.

CRITICAL ROUTES

	TAKEOFF WEIGHT — 10^6 N (LB.)	
	BASELINE	TAILCONE
SEA LEVEL		
• VAFB TO EDWARDS	3.14	3.09
RUNWAY: 2,440 M (8,000 FT.) DISTANCE: 250 KM (135 N.MI.)	(705,500)	(694,500)
• BARKSDALE TO COLUMBUS AFB	3.30	3.19
RUNWAY: 3,570 M (11,700 FT.) DISTANCE: 500 KM (270 N.MI.)	(743,000)	(716,000)
4,000 FT. ALTITUDE		
• BIGGS AFB TO DAVIS-MONTHAN AFB	3.26 (733,000)	3.16 (710,500)
RUNWAY: 4,150 M (13,600 FT.) DISTANCE: 436 KM (235 N.MI.)		
• ROSWELL IAC TO DYESS AFB	3.27 (736,000)	3.17 (712,500)
RUNWAY: 3,970 M (13,000 FT.) DISTANCE: 454 KM (245 N.MI.)		

TAKEOFF RULES

The takeoff operating rules required by FAR Part 25 and MIL-C-5011A are presented. Because of the large number of cruise engines on the booster vehicle, 115% of the all-engines operating distance is greater than the FAR balanced field takeoff distance, with the critical engine made inoperative during the ground roll. According to FAR Part 25, the greater of the two distances is the required takeoff distance.

The critical FAR takeoff condition resulting in the greatest thrust requirement is the takeoff segment with landing gear retracted with a required climb gradient of 0.030. However, the number of engines necessary to meet this gradient is less than the number required to meet the final takeoff gradient of 0.017 with landing gear retracted, since the throttle setting for the latter is maximum continuous power.

The takeoff distance as defined by MIL-C-5011A is determined from start of ground roll to a point 15.25 meters (50 feet) above the takeoff surface with all engines operating. Engine-out takeoff performance is required if requested by the procuring agency. No climb gradient after liftoff is specified. However, the takeoff gross weight is limited by a 0.508 meters-per-second (100 feet-per-minute) rate-of-climb capability at sea level on a hot day with one engine inoperative.

TAKEOFF RULES

FAR PART 25

TAKEOFF DISTANCE GREATER OF:

- 115% OF ALL-ENGINES-OPERATING DISTANCE FROM START OF TAKEOFF TO POINT 10.7M (35 FT.) ABOVE TAKEOFF SURFACE
- BALANCED FIELD TAKEOFF DISTANCE FROM START OF TAKEOFF TO POINT 10.7M (35 FT.) ABOVE TAKEOFF SURFACE — CRITICAL ENGINE CUT AT V_1

TAKEOFF CLIMB GRADIENTS — OUT OF GROUND EFFECT, 4-ENGINE AIRCRAFT

- LANDING GEAR EXTENDED, ONE ENGINE OUT, TAKEOFF POWER, GRADIENT ≥ 0.005 AT V_{LOF}, TAKEOFF CONFIGURATION
- LANDING GEAR RETRACTED, ONE ENGINE OUT, TAKEOFF POWER, GRADIENT ≥ 0.030 AT V_2, TAKEOFF CONFIGURATION
- FINAL TAKEOFF, LANDING GEAR RETRACTED, ONE ENGINE OUT, MAX. CONTINUOUS POWER, GRADIENT ≥ 0.017 AT 1.25 V_S, ENROUTE CONFIGURATION

MIL-C-5011A

- TAKEOFF DISTANCE DETERMINED FROM START OF TAKEOFF TO POINT 15.3M (50 FT.) ABOVE TAKEOFF SURFACE, ALL ENGINES OPERATING
- ENGINE-OUT PERFORMANCE AS REQUESTED BY PROCURING AGENCY

TAKEOFF PERFORMANCE

Baseline

The thrust required to meet the FAR Part 25 critical takeoff climb gradients is presented as a function of vehicle takeoff gross weight for the baseline configuration, together with the thrust necessary to meet a positive gradient. For the critical 1,200-meter (4,000-foot) elevation, hot-day condition, 13 engines are needed to meet the FAR final takeoff gradient of 0.017 with one engine inoperative; whereas only 11 engines are needed to maintain a positive gradient with gear down. This is still one more engine than is required for baseline flyback operations.

The baseline vehicle takeoff performance along the critical ferry routes further reveals the inadequate thrust capability of the baseline booster for ferry operations. Under hot-day conditions, with all engines operating, 14 engines are needed to meet takeoff requirements from Vandenberg Air Force Base, California; 12 engines are needed to meet requirements from the remaining three airfields.

TAKEOFF PERFORMANCE – BASELINE

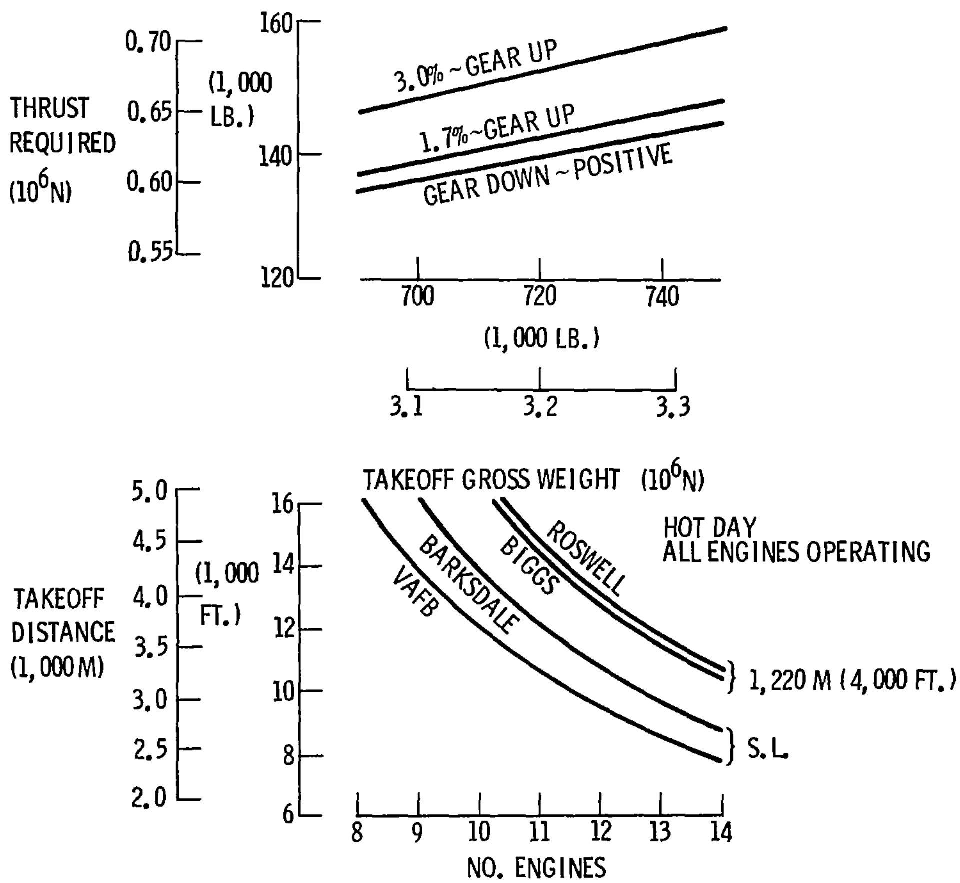

3.27×10^6 N (736,000 LB.)
1,220 M ELEVATION (4,000 FT.)
HOT DAY
ONE ENGINE OUT

GRADIENT	NO. ENGINES
0.030	12
0.017	13
POSITIVE	11

LOCATION	NO. ENGINES
VAFB	14
BARKSDALE	12
BIGGS	12
ROSWELL	12

TAKEOFF PERFORMANCE
Baseline with Tailcone

The tailcone configuration thrust requirements to meet the FAR Part 25 critical takeoff climb gradients and a positive climb gradient are presented as a function of takeoff gross weight. The addition of the tailcone fairing reduces the number of required engines to meet the FAR final takeoff climb gradient of 0.017 from 13 for the baseline vehicle to nine, with one engine inoperative. Only seven engines are needed to maintain a positive climb gradient with gear down.

Tailcone configuration takeoff performance is presented for the critical ferry routes as a function of number of operating engines for hot-day conditions with all engines operating. Thirteen engines are needed to meet takeoff requirements from Vandenberg Air Force Base, California, whereas 10 are required for the remaining critical routes.

TAKEOFF PERFORMANCE – BASELINE + TAILCONE

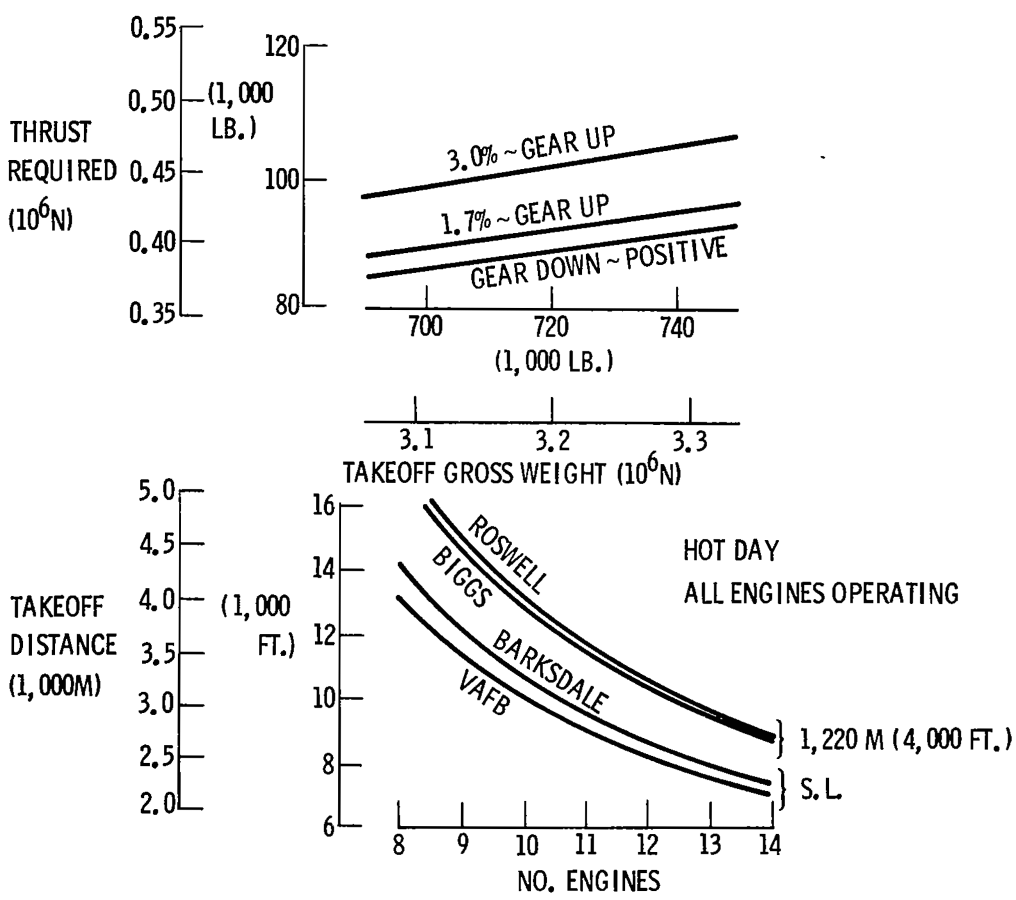

3.17×10^6 N (712,500 LB.)
1,220 M ELEVATION (4,000 FT.)
HOT DAY
ONE ENGINE OUT

GRADIENT	NO. ENGINES
0.030	8
0.017	9
POSITIVE	7

LOCATION	NO. ENGINES
VAFB	13
BARKSDALE	10
BIGGS	10
ROSWELL	10

FERRY PERFORMANCE
Baseline with Tailcone

Takeoff and landing performance for the baseline vehicle with a tailcone is presented. Balanced field takeoff performance according to FAR Part 25 is recommended for shuttle operations to maintain satisfactory safety margins without unnecessarily penalizing vehicle performance. A balanced field takeoff is one in which the distance required to complete the takeoff equals the distance necessary to decelerate and stop the vehicle when the critical engine is suddenly made inoperative. The speed at which this occurs is defined as the critical engine failure speed, V_1.

Balanced field length is presented for a 10-engine vehicle as a function of takeoff gross weight for standard and hot-day conditions at sea level and at 1,220 meters (4,000 feet). All runway lengths are adequate for standard-day operation from the critical locations along the transcontinental ferry route. However, Vandenberg Air Force Base is approximately 747 meters (2,450 feet) short of the required field length for hot-day operation at sea level, and Roswell Industrial Air Center is 183 meters (600 feet) short of its required field length for hot-day operations at 1,220 meters (4,000 feet). Runway extensions at both these fields must be considered if balanced field takeoff requirements are to be met without the addition of engines to the baseline vehicle.

Recommended landing performance is calculated for an obstacle speed of 1.2 V_{min}. Landing distance is presented as a function of landing gross weight for standard-day, dry, and hot-day, wet conditions at sea level and 1,220 meters (4,000 feet). Only Vandenberg Air Force Base falls short of the hot-day, wet landing distance requirements; all other locations have adequate field lengths to meet these requirements.

FERRY PERFORMANCE — BASELINE + TAILCONE

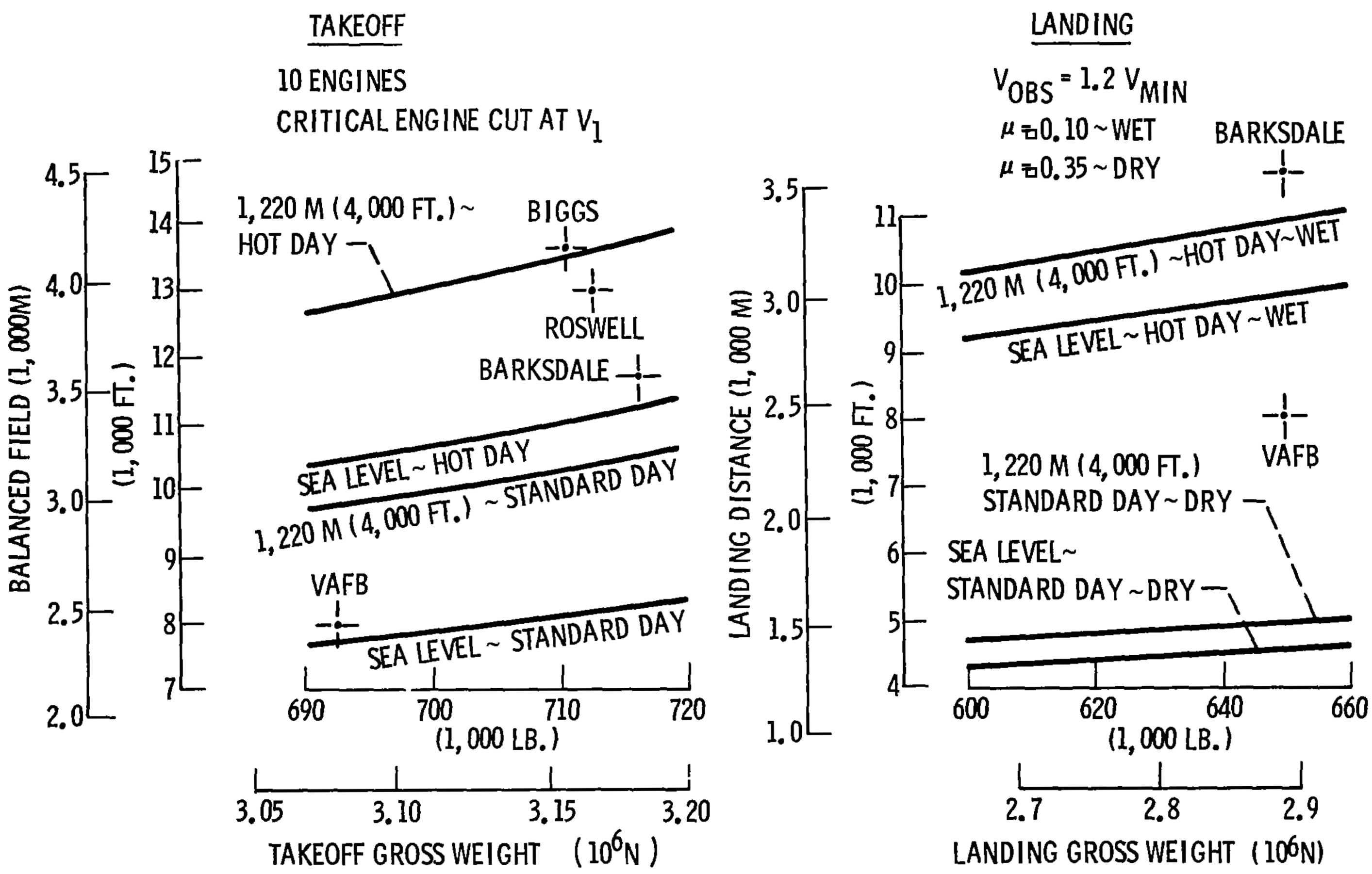

FERRY PERFORMANCE

Operating Rules

The recommended operating rules for ferry performance are summarized. These rules are compatible with those for the baseline flyback mission, insofar as they do not necessitate major design changes to the vehicle, yet ensure adequate safety margins. The addition of the tailcone fairing provides performance capability for ferry with the same number of engines required by flyback operating rules, with modifications required to only two candidate airfields along the proposed ferry route under hot-day conditions.

Means other than a tailcone fairing for improving ferry performance were considered, i.e., additional engines and engines with afterburners. However, the additional expense and maintenance time required for these modifications do not warrant their consideration for ferry operations, when compared to the procedure of adding a tailcone fairing.

RECOMMENDED FERRY PERFORMANCE OPERATING RULES

R_{MAX} = 500 KM (270 N.MI.)

10 ENGINES + TAILCONE

TAKEOFF

- BALANCED FIELD, POSITIVE CLIMB GRADIENT AFTER LIFTOFF
- FUEL ALLOWANCE 5 MINUTES AT NORMAL POWER AT SEA LEVEL (MIL-C-5011A)

CRUISE

- ALL ENGINES OPERATING AT OPTIMUM CRUISE ALTITUDE TO POINT OF NO RETURN
- 25.7 M/SEC. HEADWIND (50 KT.)
- ONE ENGINE OUT TO DESTINATION
- 1,525 M (5,000 FT.) ALTITUDE CAPABILITY, TWO ENGINES OUT, HOT DAY – MAX. CONTINUOUS POWER

GO-AROUND

- LANDING CLIMB – POSITIVE GRADIENT, ONE ENGINE OUT, 1,220 M (4,000 FT.) HOT DAY
- APPROACH CLIMB – POSITIVE GRADIENT, TWO ENGINES OUT, 1,220 M (4,000 FT.) HOT DAY

LANDING (MIL-C-5011A)

- $V_{THRESHOLD} = 1.2\ V_{MIN}$
- DISTANCE DETERMINED FOR ALL OPERATIONAL WEIGHTS, ALTITUDES, & TEMPERATURES
- COEFFICIENT OF FRICTION (μ) VALUES REPRESENTATIVE OF ACTUAL RUNWAY CONDITIONS

RESERVES

- ALLOWANCE FOR GO-AROUND

SUMMARY

A set of flyback and ferry operating rules have been recommended that provide safe flight operations and adequate reserves. Of prime importance, the recommended ferry rules do not compromise design of the baseline vehicle. For the configuration investigated herein, 10 engines are required to meet the flyback operating rules. Addition of a tailcone fairing and extension of two of the runways along the transcontinental ferry route are the only modifications necessary to meet the recommended ferry operating rules. No additional engines are required.

SUMMARY

FLYBACK OPERATING RULES

- SAFE OPERATIONS
- ADEQUATE RESERVES

FERRY OPERATING RULES

- SAFE OPERATIONS
- ADEQUATE RESERVES
- NO COMPROMISE TO BASELINE DESIGN

SPACE SHUTTLE ORBITER HANDLING QUALITY CRITERIA APPLICABLE TO TERMINAL AREA, APPROACH, AND LANDING

By

Gordon H. Hardy
NASA Ames Research Center, Moffett Field, California

INTRODUCTION

(Figure 1)

The requirement for satisfactory handling qualities of the space shuttle vehicle (SSV) may have a major impact on the vehicle and control system configuration. The present military specification for the flying qualities of piloted airplanes (MIL-F-8785B) has been developed to specify the requirements for satisfactory handling qualities for piloted military aircraft. While much of this specification for piloted aircraft is applicable to the SSV during terminal area, approach, and landing, there are some aspects of the SSV that are not satisfactorily covered (e.g., unpowered approach and landing).

Consequently, the NASA Ames Research Center (ARC) contracted (Contract NAS2-6057) with Systems Technology, Incorporated, to derive handling qualities criteria for the SSV orbiter during the terminal phases of flight using MIL-F-8785B as a point of departure. The study combined the results of an analytical pilot-vehicle systems analysis with the results of an extensive simulation conducted simultaneously at ARC. The purpose of this paper is to present some results of this study. The complete results will be reported in a low number NASA contractor report in the near future.

Several areas of MIL-F-8785B were initially identified as needing additional or modified criteria. These are listed in figure 1. Each of these areas will be discussed and criteria recommended. Two problem areas were also identified and are listed in figure 1. They will also be discussed.

SPACE SHUTTLE ORBITER HANDLING QUALITY CRITERIA APPLICABLE TO TERMINAL AREA, APPROACH, AND LANDING

- AREAS OF MIL-F-8785 B IDENTIFIED AS NEEDING ADDITIONAL OR MODIFIED CRITERIA
  - FLIGHT-PATH STABILITY AND CONTROL
  - PITCH ATTITUDE CONTROL
  - HEADING CONTROL
  - LONGITUDINAL PILOT INDUCED OSCILLATIONS
  - MISCELLANEOUS TOPICS
- PROBLEM AREAS IDENTIFIED
  - PITCH TRIM CHANGES DURING FINAL APPROACH
  - LATERAL RIDE QUALITY PROBLEM DURING FINAL APPROACH

Figure 1

UNPOWERED APPROACH AND LANDING TRAJECTORY
(Figure 2)

Before getting into the specific problem areas, a look at the various phases of an unpowered approach and landing trajectory is desirable. Figure 2 depicts a trajectory for that portion of the SSV trajectory considered in the present study. There are three fairly separate phases.

The high altitude maneuvering phase of flight extends from end of reentry (assumed for the study to be 30,000 m altitude and Mach = 3) down to capturing the initial approach path (3000 - 6000 meters). It is characterized by flight near maximum L/D using roll maneuvers for energy management. While most current SSV configurations have quite poor HQ characteristics (caused by high α, supersonic-transonic aerodynamics, etc.) the HQ requirements during this phase are quite low since precise maneuvering is not required.

The straight-in, constant flight path angle (10-20 degrees), initial approach phase usually starts at about 3000 - 6000 meters and extends down to the initial flare (200 - 600 m). Flight during this phase is characterized by fairly precise maneuvering. The vehicle is usually flown at a fairly constant equivalent speed (subsonic) 20-50% in excess of that for maximum L/D.

The constant flight path angle (about 3°) final approach extends from the initial flare down to final flare and touchdown. This phase of flight is one of the most critical for the SSV, requiring very precise maneuvering. The vehicle is decellerating from the equilibrium speed of the initial approach down to touchdown near the speed for maximum L/D.

UNPOWERED APPROACH AND LANDING TRAJECTORY

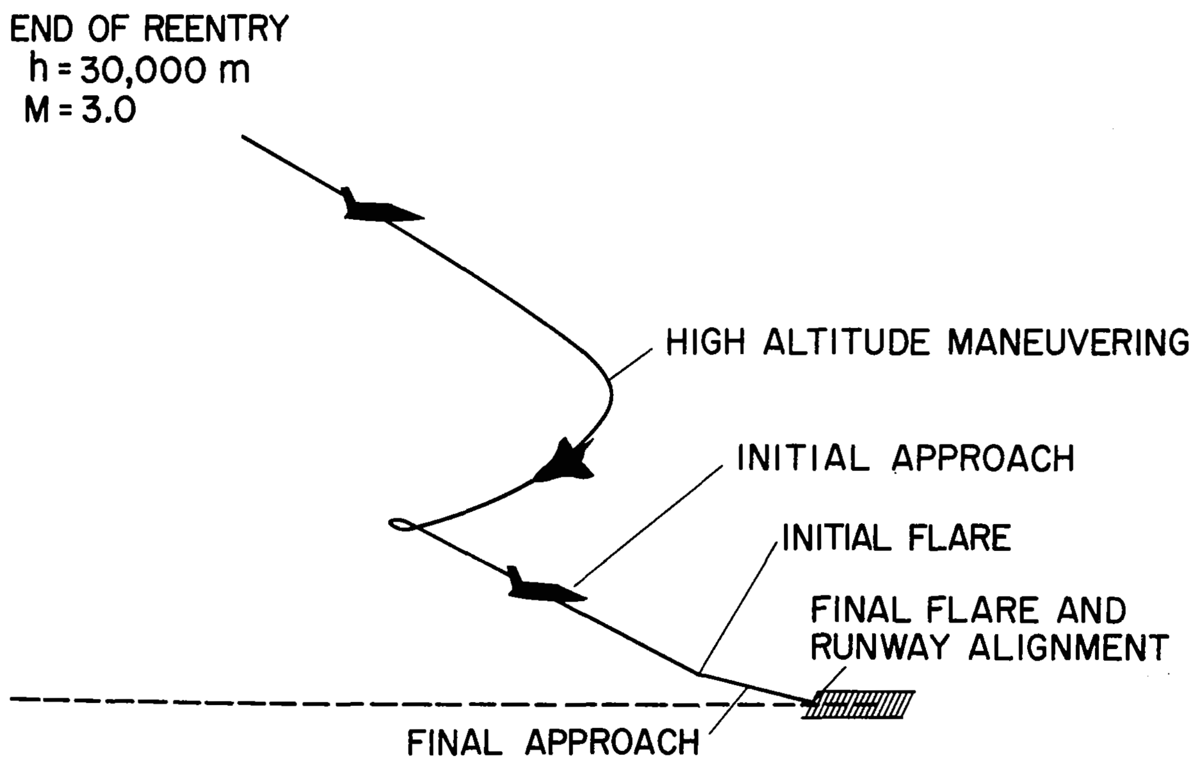

Figure 2

FLIGHT PATH STABILITY AND CONTROL FOR AN UNPOWERED APPROACH AND LANDING
(Figure 3)

Flight path stability and control is a measure of the vehicles capability to be controlled to the desired flight path assuming satisfactory attitude control. The main difference for flight in the approach and landing phase between a conventional airplane and the SSV is, of course, that the SSV may be unpowered. For a conventional powered approach, the present study recommends using the criteria of MIL-F-8785B. For an unpowered approach, new criteria are needed.

As mentioned earlier, the initial approach is made at essentially a constant flight path angle and equivalent airspeed. This phase should be made on the frontside of the drag curve (i.e., at speeds greater than that for maximum L/D). The problem was to define how far on the frontside was necessary. A considerable amount of effort was unsuccessfully spent attempting to define such a criteria. There appeared to be no handling quality problem per se as long as the approach was on the frontside of the drag curve. The only problems were of a performance nature, that is whether or not the pilot had sufficient maneuver capability to compensate for initial errors and winds. The pilots did object if the initial approach was too steep because of the high decent rates and large flight path angle change required during initial flare.

During the final approach phase, very precise flight path control is necessary. To ensure this a limit value on the flight path time constant, T_{θ_2}, was selected. T_{θ_2} is the time constant in the response of flight path to a pitch attitude change.

(Continued on next page.)

FLIGHT PATH STABILITY AND CONTROL

- RECOMMENDED REQUIREMENTS
  - INITIAL APPROACH ANGLE $\leq 20°$
  - FLIGHT PATH TIME CONSTANT, T_{θ_2}, ≤ 2.5 sec
  - FINAL APPROACH FLOAT TIME $\geq 6\ T_{\theta_2}$

- TYPICAL SSV CHARACTERISTICS

CONFIGURATION	T_{θ_2}, sec
MDAC HCR	2.0
040 A	1.9

- IMPACT ON VEHICLE CONFIGURATION

$$T_{\theta_2} \doteq \frac{-1}{Z_w} = \frac{-1}{\frac{C_{z_\alpha} S\bar{q}}{2mV}}$$

Figure 3

FLIGHT PATH TIME CONSTANT

(Figure 4)

(Continued from previous page.)

Figure 4 shows a typical variation of pilot rating (Cooper-Harper) for different values of T_{Θ_2} during the final approach. From data of this type, it is recommended that the maximum value of T_{Θ_2} up until the runway threshold be limited to 2.5 seconds. Since the magnitude of T_{Θ_2} is approximately inversely proportional to Z_ω, the rate of change of normal force with plunge velocity, it can be seen that this criteria can have a significant effect on the air frame configuration. Values for two candidate SSV configurations are shown in figure 3 and are seen to be satisfactory.

Assuming the flight path time constant is satisfactory, the pilot still needs a certain minimum time to settle down on the shallow glide slope and get set up for final flare and touchdown. The recommended value for float time (measured from completion of initial flare to runway threshold) is 6 times the flight path time constant or about 12 seconds for the particular SSV configurations noted.

The requirement for being on the front side of the drag curve during initial approach is not necessary for the final approach.

It should be noted that during the simulation studies to develop the present criteria, part of the final approach and the landing was done VFR, but the cockpit display also included raw ILS data. The limiting values of $1/T_{\Theta_2}$ and final approach float time may change for different display conditions. The requirements for IFR may be more stringent; and use of a flight director display might ease the requirements. There were also some indications of a possible effect of L/D on the criteria; however, the effect cannot be defined from the current data.

EFFECT OF FLIGHT PATH TIME CONSTANT

FLOAT PHASE $V_{L/D_{MAX}} = 220$ knots $T_{FLOAT} = 30$ sec

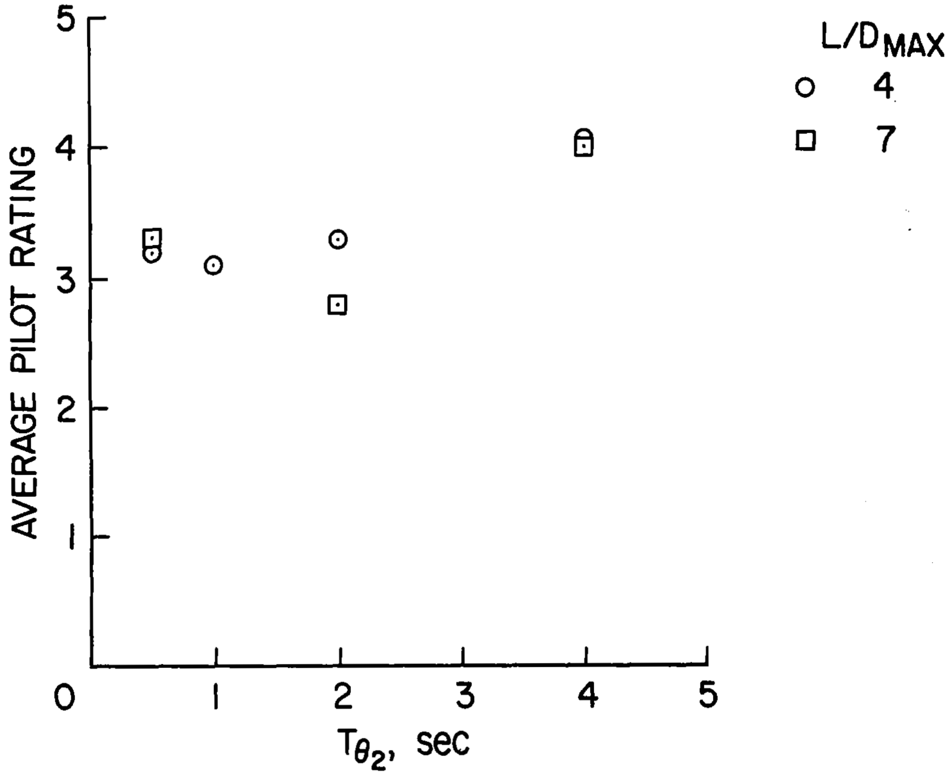

Figure 4

FINAL APPROACH AND LANDING PITCH ATTITUDE CONTROL

(Figure 5)

The recommended criteria for the SSV for pitch attitude control during final approach and landing is based on an earlier study by Systems Technology, Incorporated, sponsored by the Air Force (STI TR-189-1).

Figure 5 shows the MIL-F-8785B criteria and that recommended for the SSV for a typical flight condition during the final approach. The abscissa is the equivalent pitch short period damping, $2\zeta_{SP}\,\omega_{SP}$, while the ordinate is the equivalent short period natural frequency, ω_{SP}. The Level 1 and 3 flying qualities boundaries are shown. Insufficient data existed to adequately define the lower left corner of the recommended SSV Level 3 criteria. Level 1 corresponds to clearly adequate flying qualities (Cooper-Harper pilot rating < 3-1/2) while Level 3 corresponds to flying qualities such that the vehicle can be controlled safely, but pilot workload is excessive (Cooper-Harper pilot rating < 6-1/2). Characteristics for two typical unaugmented SSV's are shown, the McDonnel/Douglas HCR Phase B configuration (model 050B) and the NASA 040A configuration (from a Lockheed Missiles and Space Company report, LMSC EM L4-02-01-M7-3, based on a September 1971 data package). The 040A configuration is shown at two angles of attack as there was a break in the static stability curve near the trim condition chosen.

For Level 1 flying qualities, the MIL-F-8785B criteria for piloted airplanes and the criteria recommended for the SSV are quite similar while for Level 3, the SSV criteria is much less restrictive.

If it is desired to fly the SSV unaugmented or with minimum augmentation, this new Level 3 criteria may be significant.

It should be noted that some difficulty was experienced in verifying the recommended criteria of figure 5 on the NASA ARC SSV simulation. It was concluded that most of the problem could be attributed to a longitudinal trim problem associated with the particular side arm controller used (discussed later) and that while the recommended criteria was primarily based on piloted aircraft results, it was probably applicable to the SSV.

FINAL APPROACH AND LANDING PITCH ATTITUDE CONTROL

V_e = 180 knots $n/\alpha \doteq 5.0$ g'S / rad $1/T_{\theta_2} \doteq 0.53 \text{ sec}^{-1}$

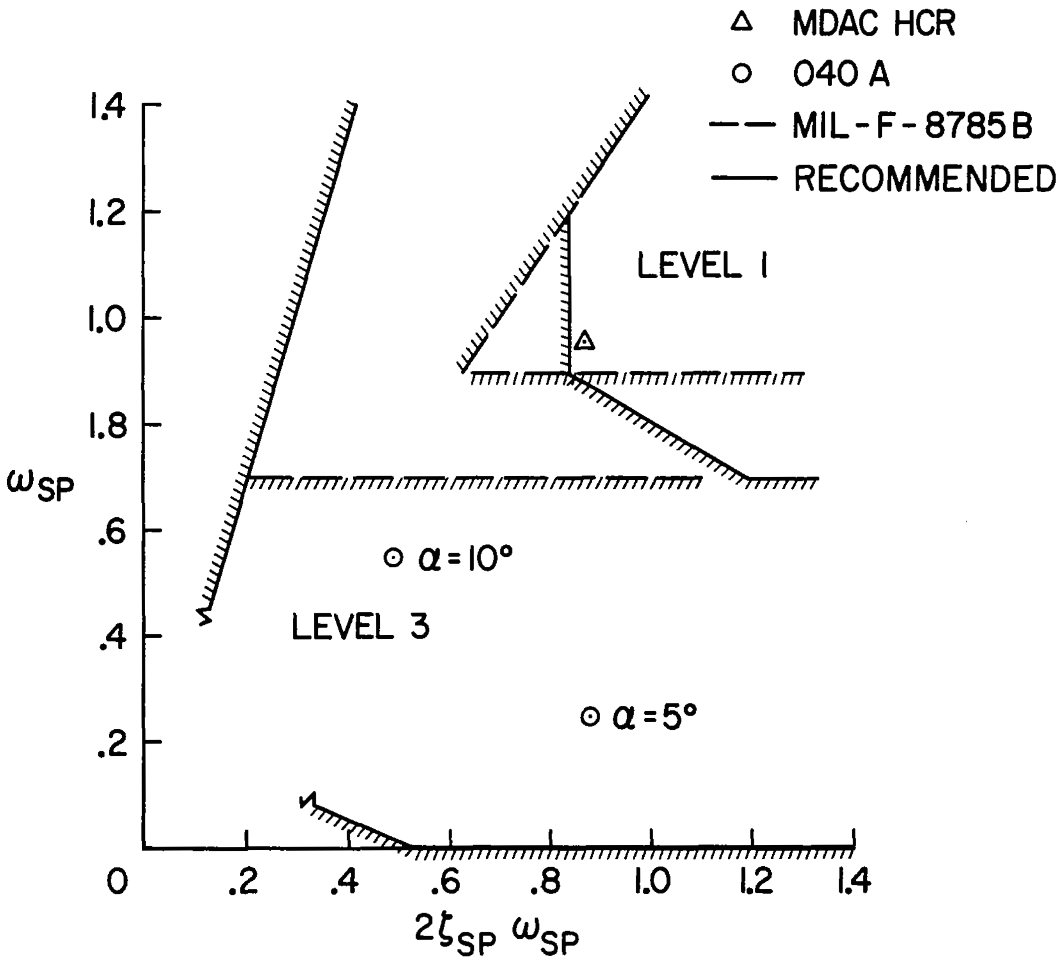

Figure 5

HEADING CONTROL
(Figure 6)

The military flying quality specification for piloted aircraft, MIL-F-8785B, has no direct criteria on heading control. It attempts to insure adequate heading control by restricting the amount of sideslip in aileron-alone turns. Because of the importance of adequate heading control in the final approach, the present study attempted to develop a heading control criterion.

The recommended criterion is based on the aileron-to-rudder crossfeed which would be required to coordinate turns, i.e., keep sideslip equal to zero. The criterion involves two parameters and is shown in figure 6. One is the ratio of yaw acceleration to roll acceleration due to aileron, $N'_{\delta_a}/L'_{\delta_a}$, measured in stability axes, divided by dutch roll frequency squared. The second parameter, μ, defines the shape of the required crossfeed in the frequency domain. This parameter is computed as follows:

- Compute the ideal rudder/aileron crossfeed, Y_{cf}, required to keep zero sideslip. This computation can be based on the measured or estimated sideslip/stick and sideslip/rudder pedal frequency responses, i.e.,

  $$Y_{cf} = -\frac{\text{sideslip/stick frequency response}}{\text{sideslip/rudder pedal frequency response}}$$

  where the frequency responses are those of the airplane plus appropriate augmentation systems.

- Over the frequency range 0.2-5 rad/sec, approximate the ideal crossfeed by a filter of the form

  $$\frac{-N_{\delta_a}}{N'_{\delta_a}} \frac{(s + z)}{(s + p)}$$

- μ is given by

  $$\mu = \frac{z}{p} - 1$$

The value of μ and $N'_{\delta_a}/L'_{\delta_a}\omega_d^2$ should then fall within the contours shown in figure 8.

(Continued on next page.)

(Figure 6)

(Continued from previous page.)

For $\mu = 0$ the ideal crossfeed would be a pure gain; rudder into the turn for adverse yaw and rudder opposite to the turn for proverse yaw. For $\mu = -1$ the ideal crossfeed low frequency characteristics or D.C. gain would equal zero with the high frequency crossfeed characteristics still requiring rudder into or opposite to the turn for adverse or proverse yaw respectively. For values of $\mu < -1$ the ideal crossfeed required rudder reversals while for $\mu > 0$ large amounts of D.C. gain are required.

The MDAC HCR vehicle is shown for several subsonic flight conditions (no calculations made for the NASA 040A configuration).

It was found that the above criteria is not appropriate if the magnitude of aileron-yaw becomes quite small. Then the yaw due to roll rate is the critical parameter. It is, therefore, recommended that if $|N'_{\delta_a}/L'_{\delta_a}| \leq 0.04$, the following be used instead of figure 7 (N'_p also measured in stability axes):

$$-0.25 < N'_p - \frac{g}{U_o} < 0.15 \text{ sec}^{-1}$$

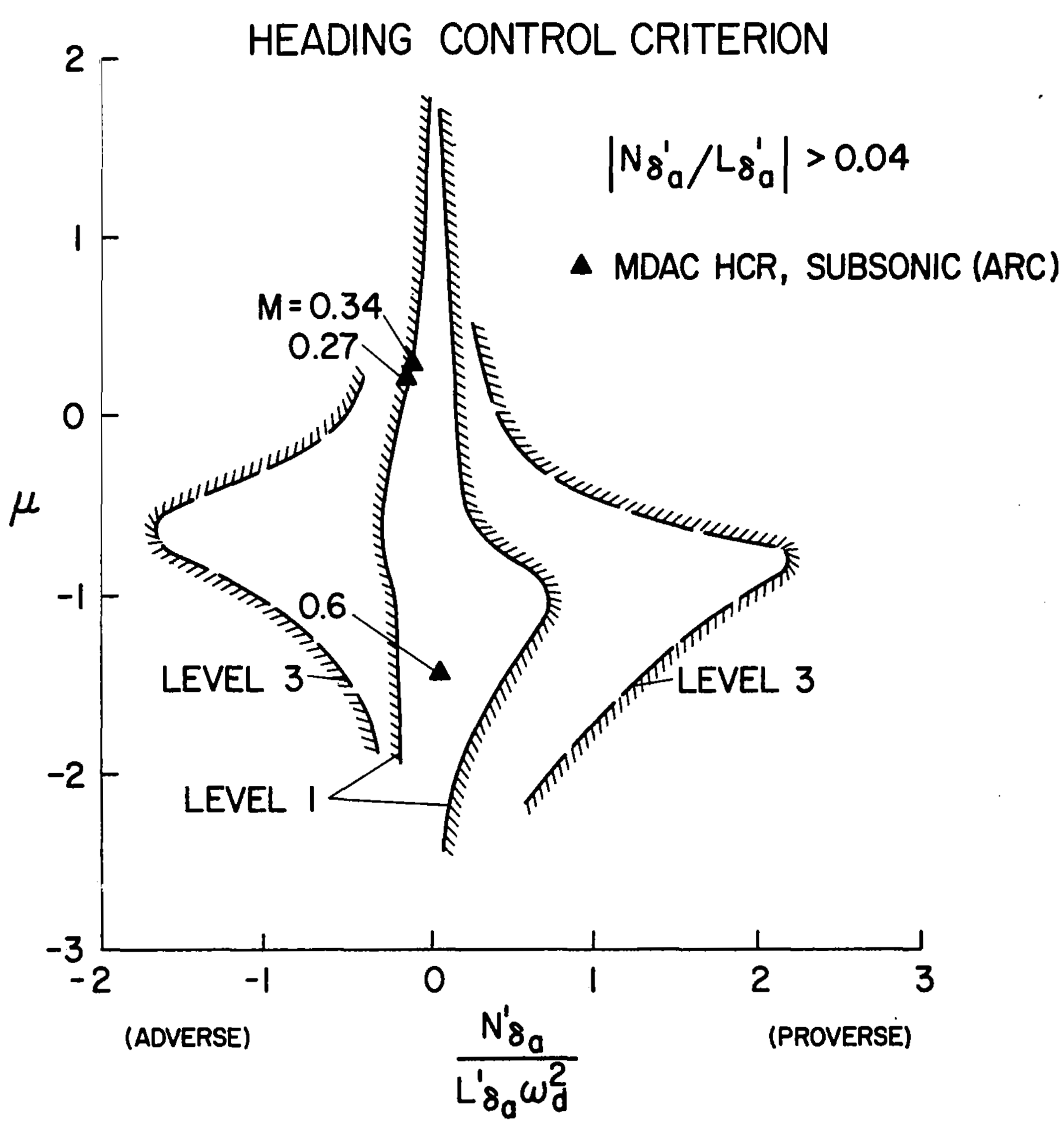
HEADING CONTROL CRITERION
$|N'_{\delta_a}/L'_{\delta_a}| > 0.04$
▲ MDAC HCR, SUBSONIC (ARC)
M = 0.34
0.27
0.6
LEVEL 3
LEVEL 3
LEVEL 1
μ
2
1
0
-1
-2
-3
-2
-1
0
1
2
3
(ADVERSE)
$\frac{N'_{\delta_a}}{L'_{\delta_a}\omega_d^2}$
(PROVERSE)

Figure 6

LONGITUDINAL PILOT-INDUCED OSCILLATIONS
(Figure 7)

MIL-F-8785B merely prohibits pilot-induced oscillations (PIOs) without providing any quantitative guidance. For the orbiter, the recommended criteria is based on STI TR 189-1. This criteria applies only for tasks which require tight attitude control.

Figure 7 shows the pilot/vehicle model of the pitch attitude loop used for analysis and the resulting root locus. The system elements are the pilot, the effective control system, and the effective air frame. Each of these components are represented by an appropriate simple transfer function form which identifies the key factors contributing to the closed-loop stability of the system. These are the pilot gain, K_P, the control system lag, τ_C; and the effective airframe dynamics, ζ'_P ω'_{S_P}, and $1/T_{\theta_2}$.

(Continued on next page.)

LONGITUDINAL PILOT - INDUCED OSCILLATIONS

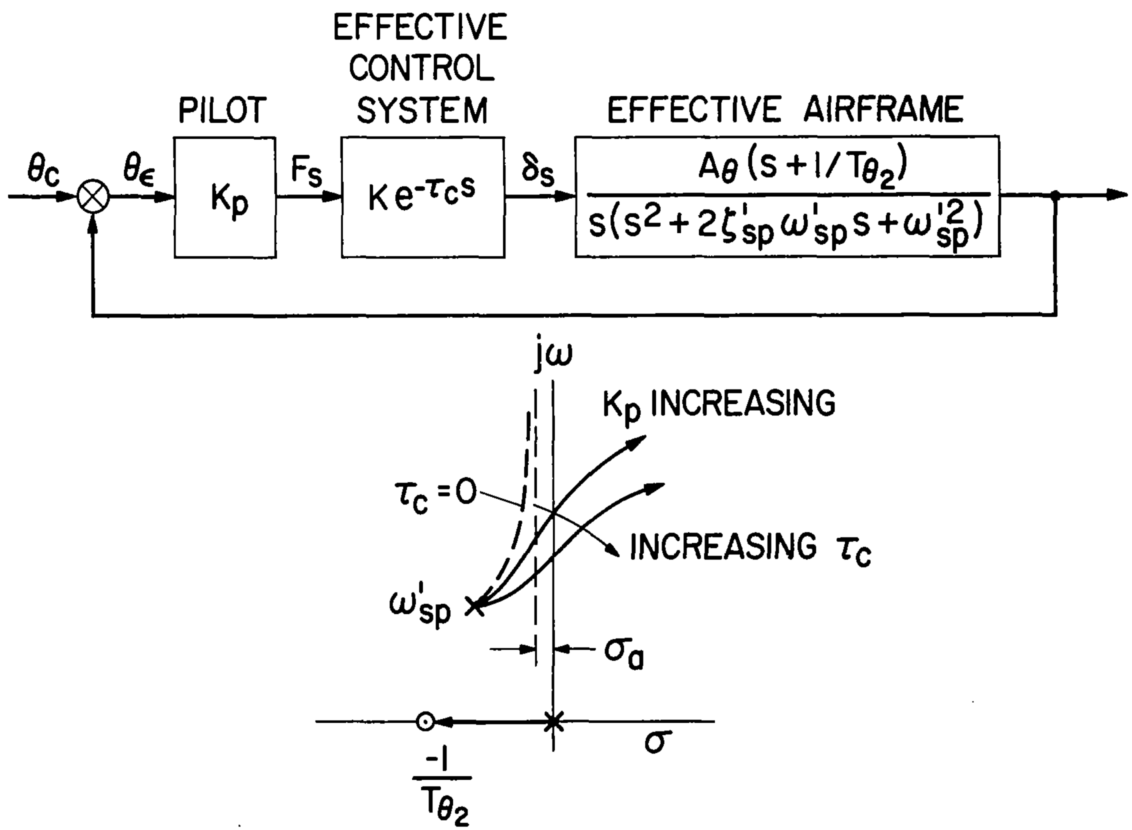

Figure 7

REQUIREMENT FOR AVOIDANCE OF LONGITUDINAL PILOT-INDUCED OSCILLATIONS (Figure 8)

(Continued from previous page.)

The PIO criteria shown in figure 8 is expressed in terms which are related to these factors. The abscissa of figure 8 is based on the root locus high gain asymptote parameter, σ_a, which is functionally related to the factors of figure 7 (i.e., $\sigma_a = 2\zeta'_{SP}\,\omega'_{SP} - 1/2\ 1/T_{\theta_2}$). The ordinate represents the effective control system lag contribution to the phase angle measured at the effective airframe short-period frequency (i.e., $\phi \doteq \tau_C\,\omega_{SP}$).

The unaugmented vehicle dependent characteristic, σ_a, for the two SSV configurations discussed previously, is also shown on figure 8 for a typical landing approach condition (Category C). It can be seen that even with no control system lag, the unaugmented vehicle may be marginal for Level 1 flying qualities but will probably be acceptable for Level 3. This result was generally verified on the NASA ARC simulation of the MDAC HCR vehicle where pilot comments indicated that the vehicle seemed lightly damped but no PIO problem per se.

REQUIREMENTS FOR AVOIDANCE OF PILOT-INDUCED OSCILLATIONS

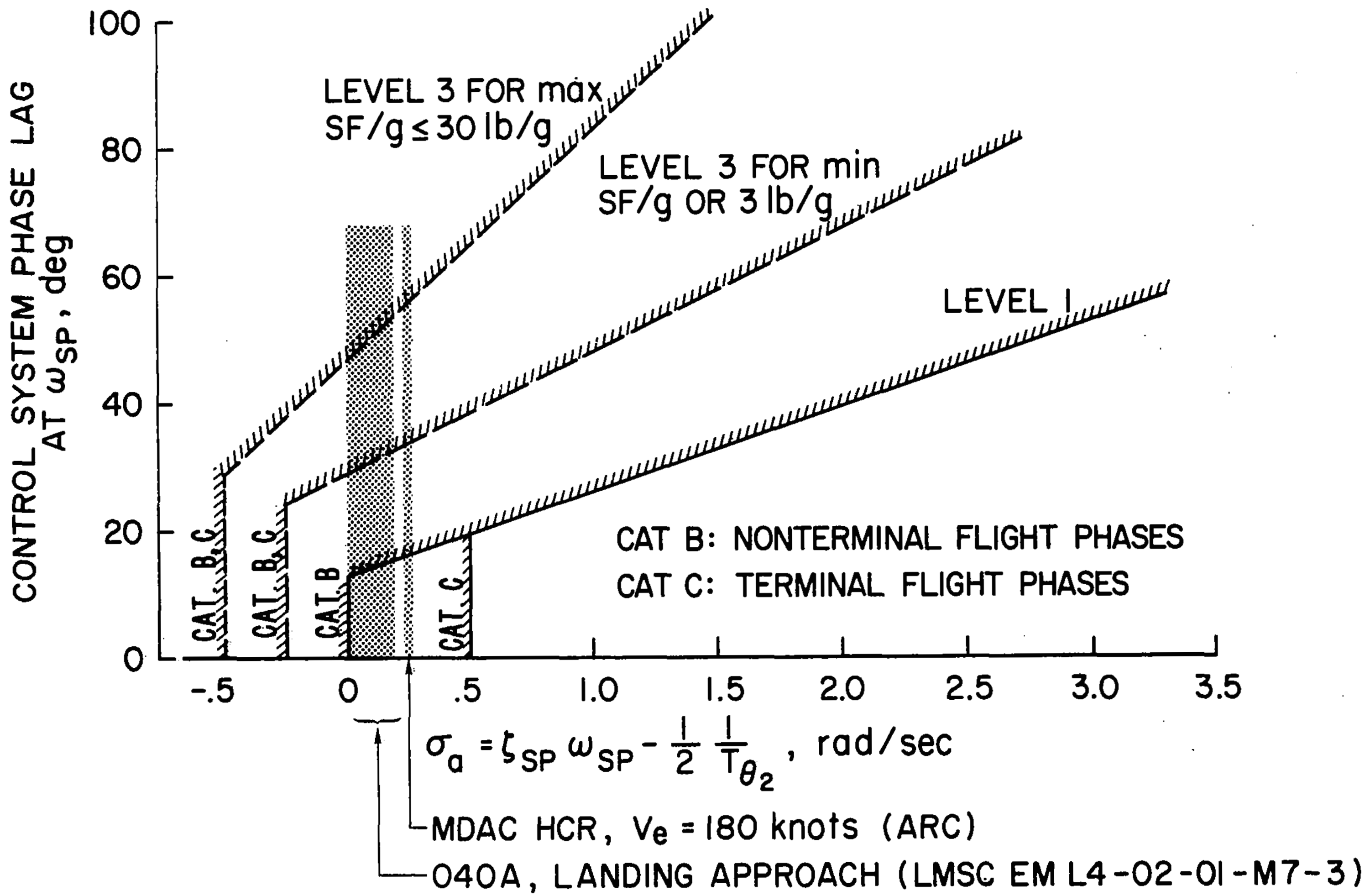

Figure 8

MISCELLANEOUS TOPICS

(Figure 9)

Three additional areas will be discussed briefly.

The first deals with the dynamics of the primary flight control system. MIL-F-8785B specifies the allowable control system lag from cockpit control force input to control surface motions. Based on STI TR 189-1, it is recommended for the SSV Level 1 requirement that the total phase lag from cockpit control force or displacement to vehicle attitude be specified as less than 135 degrees, at 1 rad/sec.

MIL-F-8785B limits rudder pedal forces for zero side slip in rolls. It is felt that this is overly restrictive and a SSV HQ criteria should limit rudder pedal forces to keep sideslip less than some finite value.

The only MIL-F-8785B criterion for rudder power is to ensure adequate rudder power for steady sideslips in crosswind approaches. It is recommended that adequate rudder power be provided the SSV to rapidly decrab the vehicle for runway alignment at touchdown.

MISCELLANEOUS TOPICS

- PRIMARY FLIGHT CONTROL SYSTEM DYNAMICS
    - MIL-F-8785 B SPECIFIES ALLOWABLE PHASE LAG IN CONTROL SYSTEM
    - PRESENT STUDY SPECIFIES TOTAL PHASE LAG FROM COCKPIT TO VEHICLE ATTITUDE
    - RECOMMENDED LEVEL I CRITERIA: 135° AT 1 rad/sec
- RUDDER PEDAL FORCES DURING ROLLS
    - MIL-F-8785 B LIMITS FORCES FOR ZERO SIDESLIP IN ROLLS
    - PRESENT STUDY RECOMMENDS LIMITING FORCES FOR FINITE VALUES OF SIDESLIP
- RUDDER POWER FOR DECRAB
    - MIL-F-8785 B SPECIFIES RUDDER POWER FOR STEADY SIDESLIP DURING CROSSWIND APPROACH
    - PRESENT STUDY RECOMMENDS ADDITIONAL CRITERIA FOR DECRAB NEEDED

Figure 9

PROBLEM AREAS

(Figure 10)

While much additional work needs to be done on the areas of research considered, two new problem areas developed during the course of the study. Because of time limitations, the present study didn't fully resolve these.

The first problem area encountered was trouble with longitudinal trim during the final approach with the particular side arm controller and trim system used in the NASA ARC simulation. As mentioned earlier, the final approach is characterized by a constant flight path angle and constantly decreasing equivalent airspeed. The decreasing airspeed requires that the vehicle be constantly retrimmed. The side arm controller used has a very light force gradient and a series trim wheel. Several symptoms were noted: (1) because of the light force gradient, it was possible to forget to trim resulting in inadequate elevator for flare; (2) it was difficult to coordinate stick motion while retrimming; and, (3) it was difficult to get full required elevator and still maintain the trim sensitivity at a reasonably low value. Based on the experience obtained, it appears that a comprehensive investigation needs to be conducted before a specification can be made for side arm controllers.

The other problem relates more to ride, rather than handling qualities. It was experienced during the simulation runs in support of the heading control work discussed earlier. With a large aircraft approaching at high angles of attach the pilot can be situated several feet above the stability axes. If the aircraft is coordinated, it will roll about the velocity vector or stability X axis. This can produce highly objectionable side accelerations at the cockpit, especially if the aileron roll acceleration is high. The only solutions are to reduce the aileron power below what is normally considered desirable or to degrade the degree of coordination. Both have deleterious effects so a design compromise must be made. The outcome of the proper compromises needs further investigation and definition.

PROBLEM AREAS

- PITCH TRIM CHANGES DURING FINAL APPROACH DICTATES A GOOD PITCH TRIM SYSTEM
- LATERAL RIDE QUALITY PROBLEM DURING FINAL APPROACH – CAUSED BY HIGH α AND HIGH ROLL POWER

Figure 10

AREAS NEEDING FURTHER RESEARCH
(Figure 11)

Further research is also needed in several of the areas investigated.

Additional research in the area of flight path control criteria is considered essential because of the potential impact of the criteria on basic vehicle parameters and trajectory limitations. If an unpowered Orbiter is selected, the criteria proposed here need to be extended. The effects of IFR flight and the effects of adding a flight director display should be assessed. The potential influence on the criteria of variations in L/D also needs further investigation. If a powered Orbiter is selected, a better flight path control criterion than that of 8785B may be desirable.

Further verification of the recommended pitch attitude control criteria is needed. The proposed criteria is mainly based on results from conventional aircraft. Because of the longitudinal trim problem discussed earlier, it was not possible to conclusively verify the proposed criteria for the SSV on an unpowered trajectory. This was especially true for the Level 3 flying quality boundary.

Further research on heading control criteria is also considered important but of lower priority than the subjects noted above. The criterion proposed appears to be a significant advancement, but additional verification, and possible refinement, is highly desirable.

FURTHER RESEARCH NEEDED

- PITCH FLIGHT PATH CONTROL
  - UNPOWERED
  - POWERED
- PITCH ATTITUDE CONTROL
- HEADING CONTROL

Figure 11

ORBITER ENTRY TRAJECTORY CONSIDERATIONS

By John J. Rehder and Paul F. Holloway

NASA Langley Research Center

INTRODUCTION

Any space shuttle trajectory-shaping optimization study must consider the vehicle's thermal environment and the resulting requirements of the thermal protection system (TPS). Optimization studies have been conducted at the NASA Langley Research Center, yielding results which are generally applicable to shuttle orbiters and are independent of evolution and redirection of the space shuttle program. This paper presents the work of two investigations of optimal trajectory shaping, in which different methods of considering the thermal environment are used.

The first approach defines a nominal trajectory which achieves a desired cross range by assuming a simple control history with an appropriate TPS design. Trajectory optimization is then used to maximize cross range with minimal impact on the nominal TPS. Heating analysis illustrates the effect of the optimization on surface temperatures and heat-load distribution along the bottom center line of the vehicle. This approach indicates the mission flexibility and growth potential in terms of cross-range capability which may be realized through trajectory shaping.

The goal of the second study is to determine if payload gains for an all-ablative TPS Mark I orbiter can result from entry trajectory optimization. Since the ablative TPS weight is primarily a function of heat load, the total stagnation-point heat load is minimized for various values of cross range and deorbit propellant weight. The effects on total weight (ablator + propellant) are summarized.

The aerodynamic characteristics in both studies are typical of delta-wing orbiter configurations. Entry is initiated from an equatorial orbit at an altitude of 185.2 km at 0° latitude and longitude. Entry into the atmosphere occurs at 121.9 km.

SYMBOLS

C_L lift coefficient

$f(\alpha)$ experimentally determined boundary layer transition onset prediction as a function of angle of attack

I_{sp} specific impulse

L length of vehicle

M Mach number

Q_{total} total heat load

Re_θ	Reynolds number based on momentum thickness
S	reference area
T	temperature
V	velocity
W	weight of vehicle
x	distance along center line of vehicle with the nose as origin
α	angle of attack, deg
μ	coefficient of viscosity
ρ	density
ϕ	bank angle, deg

Subscripts:

e	edge of boundary layer
max	maximum

1267

MAXIMIZING CROSS RANGE WITH MINIMAL IMPACT ON AERODYNAMIC HEATING AND TPS

During space shuttle operations, it may be desirable to obtain a cross range greater than the design nominal with minimal impact on TPS weight or material. The approach followed defines a nominal entry trajectory for the initial operational period of the orbiter. A simple control history – constant angle of attack and simple bank-angle variation – and an appropriate TPS are assumed. The optimal angle-of-attack and bank-angle histories are then determined which will maximize cross range with the maximum heat rate and total heat load at the stagnation point constrained to those of the nominal.

In all trajectories the maximum deceleration was limited to 3g (1g = 9.8 m/sec^2). The vehicle characteristics, which are typical of fully reusable orbiter designs, include a weight of 102 060 kg and a reference area of 565.2 m^2. An entry angle of -1.6° and entry velocity of 7450 m/sec were assumed.

HEATING ASSUMPTIONS

A heating analysis along the bottom center line of the vehicle for all trajectories was conducted using the MINIVER computer program developed by the McDonnell Douglas Astronautics Company (MDAC). Laminar and turbulent heat-transfer calculations for a flat plate were based on the Eckert reference enthalpy method and Spalding and Chi method, respectively. Sharp-cone conditions (oblique shock entropy) were used to determine shock angle and local flow conditions.

The onset of boundary-layer transition was predicted using both the current MDAC and North American Rockwell Corporation (NAR) criteria. For the MDAC criteria, transition onset occurs when $\frac{Re_\theta}{M_e}\left(\frac{\rho_e V_e}{\mu_e}\right)^{-0.2}$ lies on the experimentally determined curve $f(\alpha)$. The NAR criteria predicts transition onset when $\frac{Re_\theta}{M_e} = 225$. For both cases, fully turbulent flow was assumed to occur at a length Reynolds number double that at transition onset. The Baranowski crossflow correction accounts for the effects of streamline divergence on a delta-wing configuration in a real gas. The calculation of thin-skin surface temperatures was based on the material characteristics of coated columbium.

ENTRY TRAJECTORY CONTROL HISTORIES — LOW CROSS RANGE

The nominal trajectory was flown at a constant angle of attack of 53° at $C_{L,max}$. The vehicle banks at pull-out, and the bank angle decreases at a constant rate. The nominal trajectory obtains a cross range of 240 n.mi. (See fig. 1.)

The optimal trajectory begins the bank program earlier and maintains a steeper bank throughout most of the entry. Once the vehicle has decelerated sufficiently, the angle of attack is modulated downward to increase range without violating the heating-rate constraint. The steeper bank angles also result in a more efficient heading-angle change which is the primary factor in increasing the cross range to 571 n.mi.

The quantitative increase in cross range is not important, since this percentage is governed by the selection of the nominal entry profile. The results do establish qualitatively, however, that significant increases in ranging are possible through optimal trajectory shaping.

ENTRY TRAJECTORY CONTROL HISTORIES
LOW CROSS RANGE

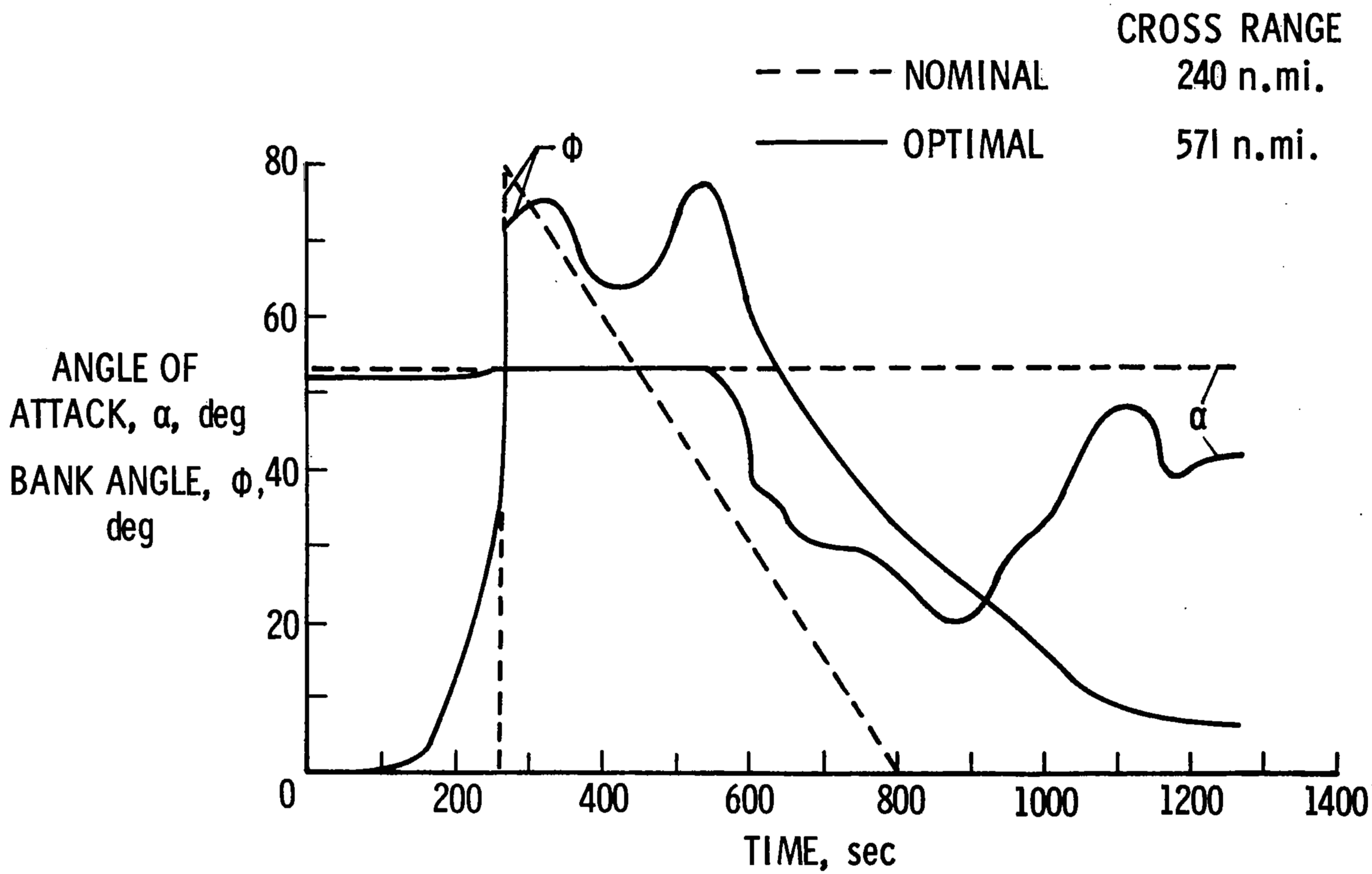

Figure 1

ALTITUDE AND VELOCITY HISTORIES — LOW CROSS RANGE

A comparison of the nominal and optimal altitude and velocity time histories is given in figure 2. The earlier and steeper bank-angle history of the optimal trajectory results in quicker deceleration yielding a lower altitude profile at slower speeds at any time over most of the entry.

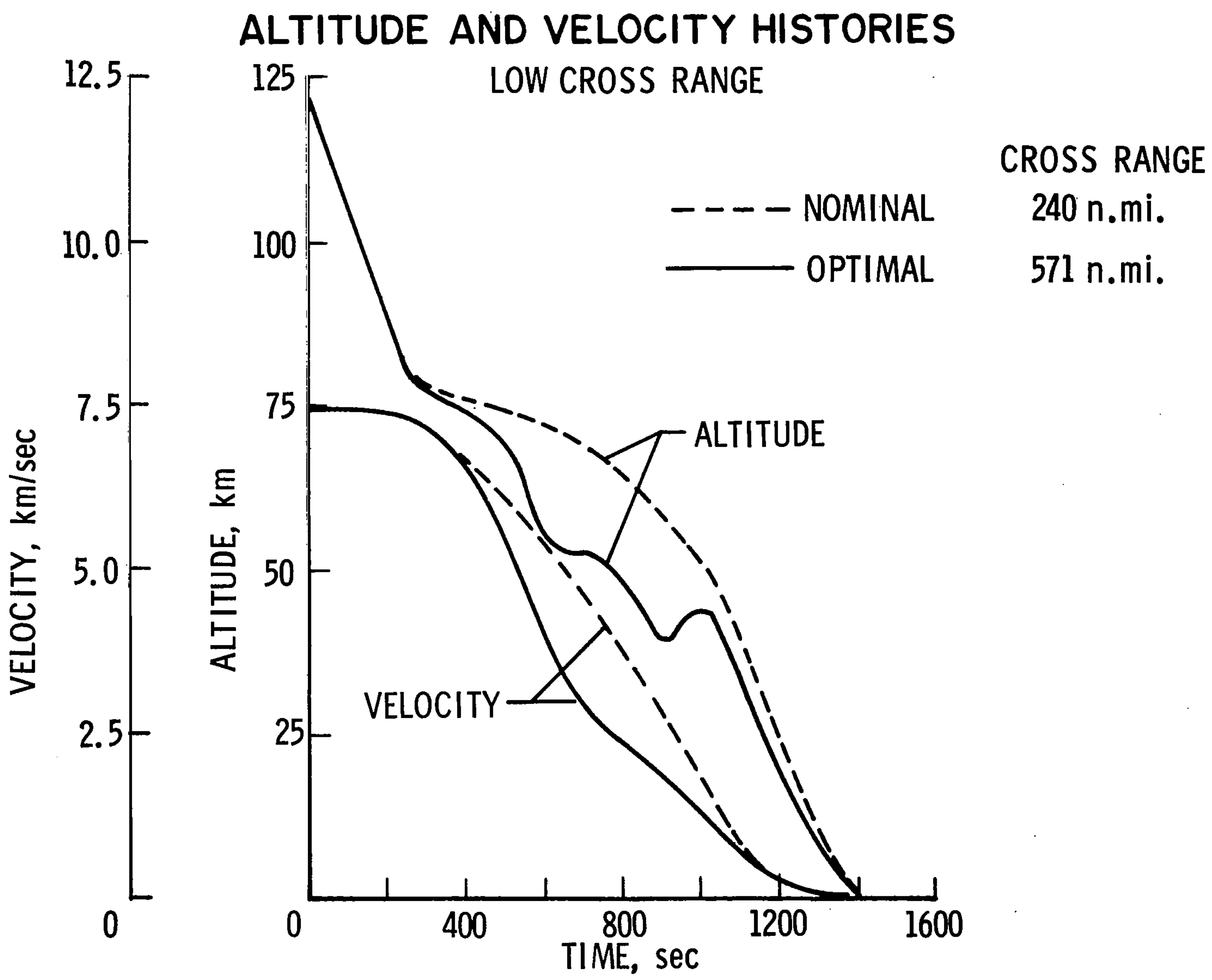
ALTITUDE AND VELOCITY HISTORIES
LOW CROSS RANGE
CROSS RANGE
NOMINAL
240 n.mi.
OPTIMAL
571 n.mi.
ALTITUDE
VELOCITY
VELOCITY, km/sec
12.5
10.0
7.5
5.0
2.5
0
ALTITUDE, km
125
100
75
50
25
0
400
800
1200
1600
TIME, sec

Figure 2

STAGNATION-POINT HEATING SUMMARY – LOW CROSS RANGE

The results of the stagnation-point heat constraints are shown in figure 3. The heat rate for the optimal case remains near the maximum value for a longer period of time. Later in the entry, however, the optimal heat rates are less than those of the nominal so that the integrated heat loads are virtually the same for both cases.

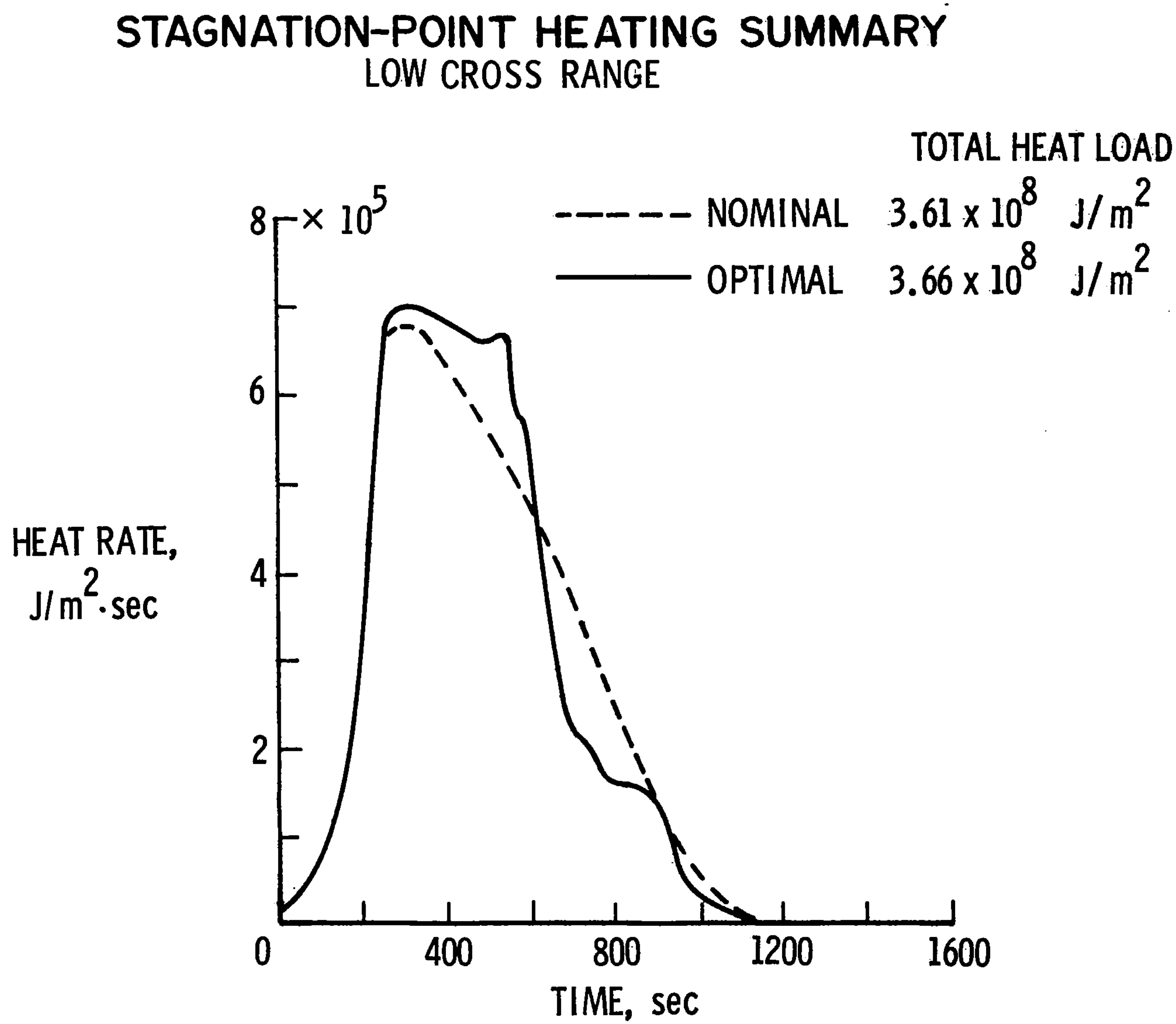
STAGNATION-POINT HEATING SUMMARY
LOW CROSS RANGE
TOTAL HEAT LOAD
NOMINAL 3.61 x 10^8 J/m^2
OPTIMAL 3.66 x 10^8 J/m^2
HEAT RATE, J/m^2·sec
8 × 10^5
6
4
2
0
400
800
1200
1600
TIME, sec

Figure 3

MAXIMUM BOTTOM CENTER-LINE TEMPERATURES – LOW CROSS RANGE

A comparison of the maximum surface-temperature distributions for the nominal and optimal trajectories is shown in figure 4 for both the MDAC and NAR boundary-layer transition criteria. The temperature limits for several candidate materials for reusable TPS designs are indicated on the right of the figure. The difference between the maximum temperatures for the MDAC transition criteria is 100° K or less over most of the vehicle with the optimal case having the higher temperatures. For the NAR criteria, there is no difference in maximum temperatures over the forward portion of the body, while the maximum temperatures encountered during the optimal trajectory on the rearward portion are about 400° K greater than those in the nominal trajectory. For the Haynes material, assuming MDAC criteria, and for the superalloys, assuming NAR criteria, optimal entry would not require a new surface material.

MAXIMUM BOTTOM CENTER-LINE TEMPERATURES

LOW CROSS RANGE

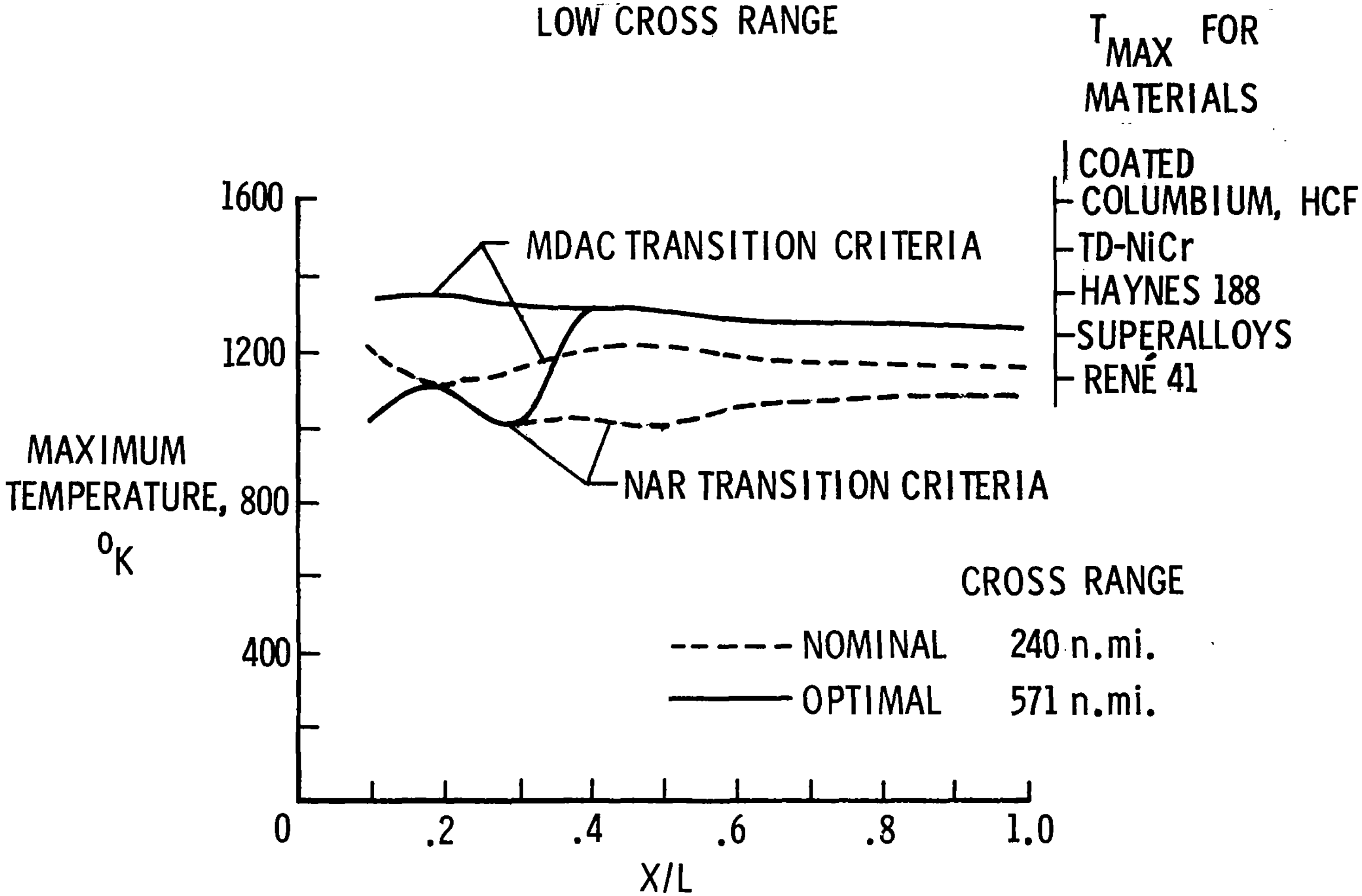

Figure 4

BOTTOM CENTER-LINE CONVECTIVE HEAT SUMMARY — LOW CROSS RANGE

Significant differences in the total-heat-load distribution levels are indicated as a result of transition criteria. (See fig. 5.) Comparisons between the optimal and nominal trajectories indicate that the optimal heat load is slightly higher than the nominal over the forward portion of the vehicle using the MDAC transition criteria. Using the NAR criteria, the trend is reversed with the heat load for the nominal trajectory higher than that for the optimal trajectory on the forward portion of the body and lower on the rearward portion.

It should also be noted that the differences in heat load between the optimal and nominal entries predicted for either transition criteria are considerably less than the differences caused by the two criteria for a particular trajectory.

BOTTOM CENTER-LINE CONVECTIVE HEAT SUMMARY

LOW CROSS RANGE

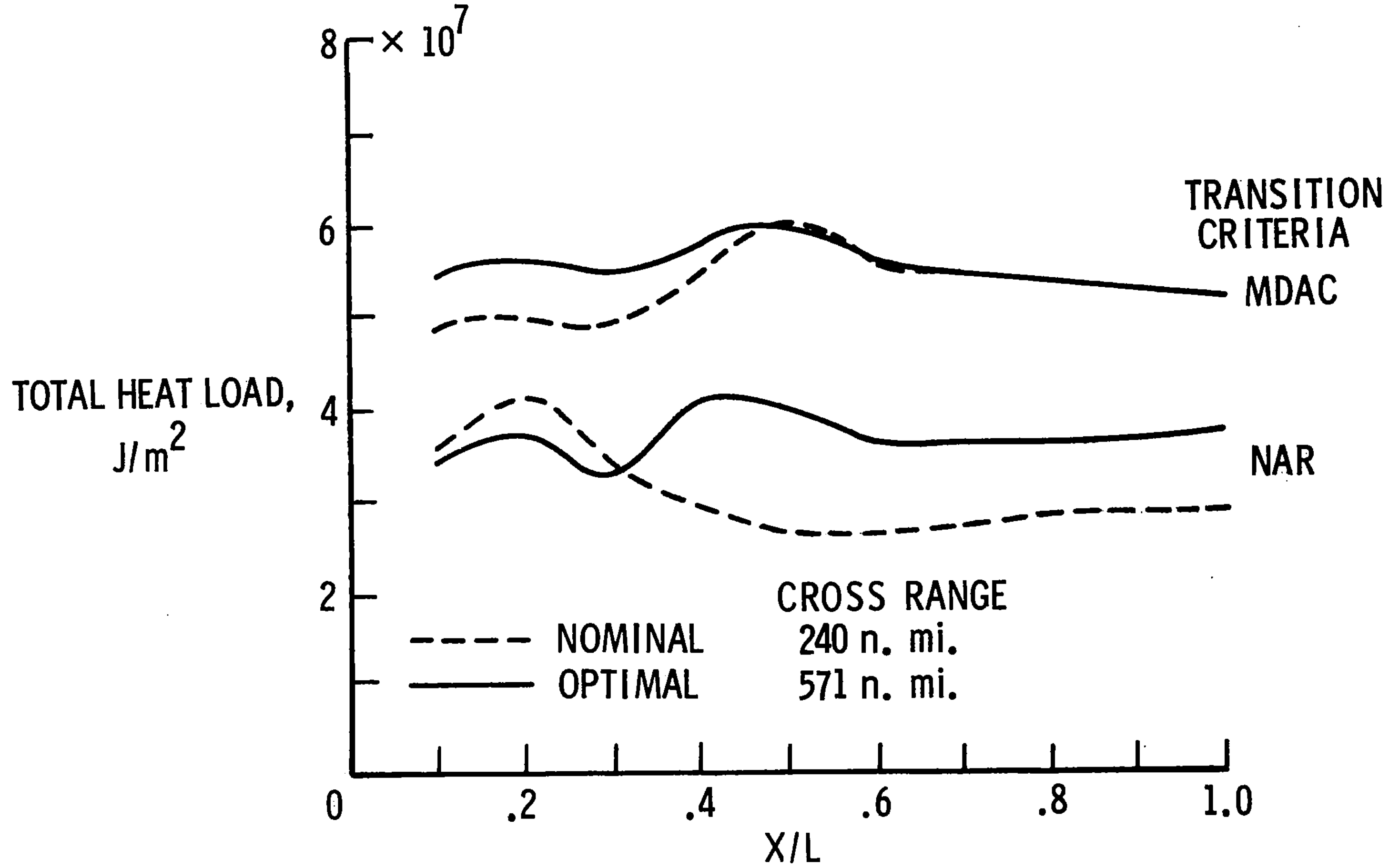

Figure 5

ENTRY TRAJECTORY COMPARISON — MEDIUM CROSS RANGE

A medium cross range nominal entry trajectory was generated using a constant angle of attack of 40° and another simple bank angle history. An optimal trajectory, maximizing cross range, was determined using the same technique previously described. The angle of attack, bank angle, altitude, velocity, and stagnation-point heat-rate histories, shown in figure 6, indicate the same characteristics as the low cross range case. Using the MDAC transition criteria, the maximum center-line temperature profiles were very similar to those shown previously, while the total heat load, in this case, is higher for the optimal trajectory across the entire bottom center line.

ENTRY TRAJECTORY COMPARISON—MEDIUM CROSS RANGE

	CROSS RANGE	TOTAL HEAT LOAD AT STAGNATION POINT
NOMINAL	587 n. mi.	- - - - - - 5.12×10^8 J/m^2
OPTIMAL	1014 n. mi.	———— 5.19×10^8 J/m^2

MDAC TRANSITION CRITERIA

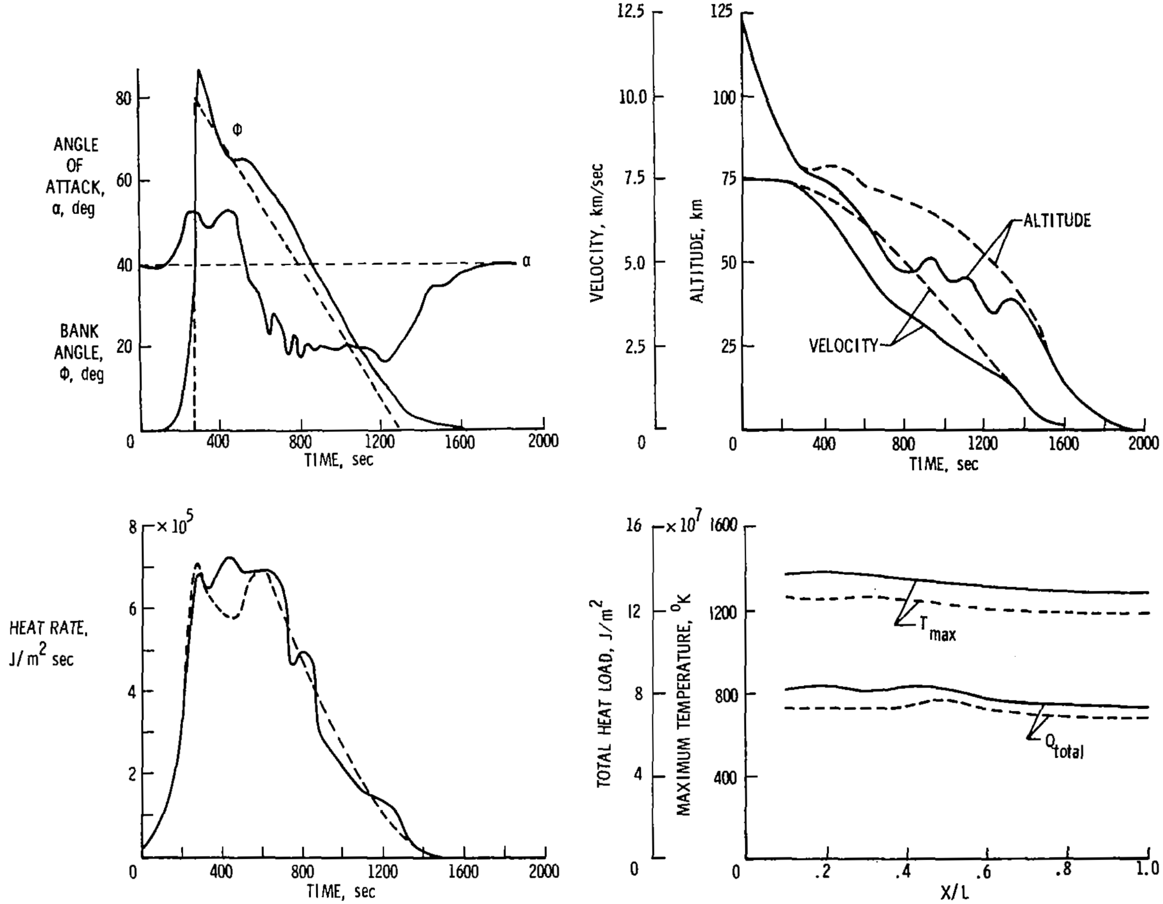

Figure 6

ENTRY TRAJECTORY COMPARISON – HIGH CROSS RANGE

The same process was followed using a nominal trajectory with a constant angle of attack of 30° and another simple bank-angle history. The improvement in cross range was not as great in this case. Otherwise the results, shown in figure 7, are entirely similar to those of the low cross range case.

ENTRY TRAJECTORY COMPARISON—HIGH CROSS RANGE

	CROSS RANGE	TOTAL HEAT LOAD AT STAGNATION POINT
NOMINAL	1107 n. mi.	- - - - - - 8.33×10^8 J/m^2
OPTIMAL	1470 n. mi.	——— 8.28×10^8 J/m^2

MDAC TRANSITION CRITERIA

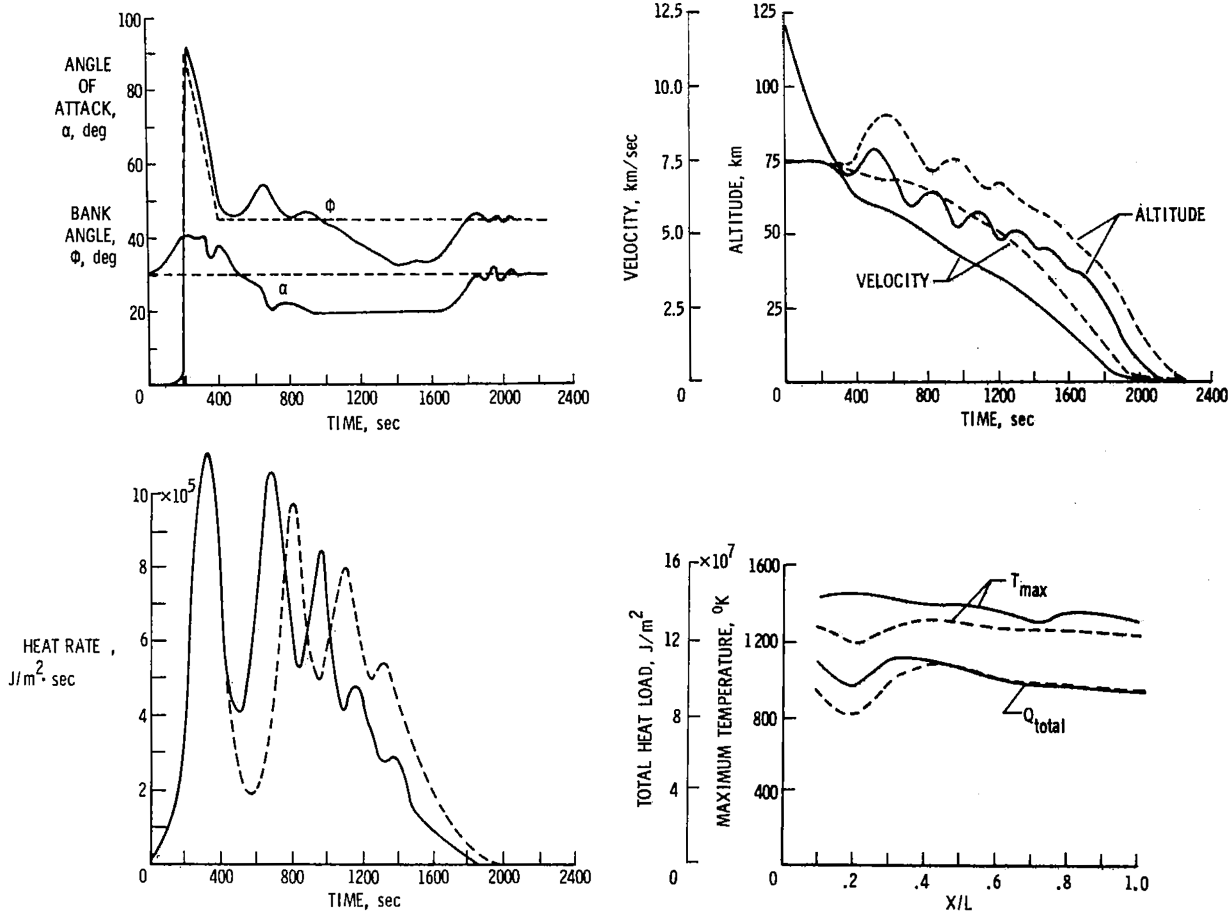

Figure 7

ENTRY TRAJECTORY OPTIMIZATION FOR SHUTTLE ORBITER WITH ABLATIVE TPS

The second objective of this study is to examine the possibility of gaining payload for a Mark I orbiter design through trajectory optimization for an all-ablative TPS. (See fig. 8.) In this analysis, minimum total stagnation-point heat-load trajectories are calculated for various values of cross range from 300 to 1500 n.mi. Since entry angle, or deorbit ΔV, plays a major role in determination of the total heat load, these effects are also investigated. In addition, an alternate entry mode using negative lift to steepen the flight path is evaluated.

Aerodynamic characteristics, weight, and reference area compatible with current Mark I orbiter designs are assumed. As in the preceding analysis, entry is initiated from an equatorial orbit at an altitude of 185.2 km at 0° latitude and longitude. Maximum deceleration was limited to 2.5g for all trajectories.

ENTRY TRAJECTORY OPTIMIZATION FOR SHUTTLE ORBITER WITH ABLATIVE TPS

PURPOSE

- DETERMINE MINIMUM TOTAL STAGNATION-POINT HEAT LOAD TRAJECTORIES AT VARIOUS CROSS RANGES AND ENTRY CONDITIONS FOR MARK I ORBITER
- STUDY EFFECT OF DEORBIT ΔV ON THE ENTRY WEIGHT OF THE VEHICLE
- INVESTIGATE ALTERNATE ENTRY MODES TO OBTAIN MINIMUM VEHICLE WEIGHT

ASSUMPTIONS

- MARK I ORBITER - ALL–ABLATIVE TPS
- WEIGHT = 68 267 kg
- REFERENCE AREA = 310.7 m^2

Figure 8

EFFECT OF ENTRY ANGLE ON STAGNATION-POINT HEATING

It is well known that for a given vehicle entering the atmosphere at a given angle of attack, the maximum stagnation-point heat rate increases as the entry angle increases, while the total heat load decreases because of lower flight time. (See fig. 9.)

Since an ablative TPS allows a relaxation of maximum heat-rate constraints, the possibility of reducing total heat load, thereby reducing TPS weight, by entering at a higher entry angle is investigated as a potential means of reducing vehicle weight and/or improving payload capability.

EFFECT OF ENTRY ANGLE ON STAGNATION–POINT HEATING

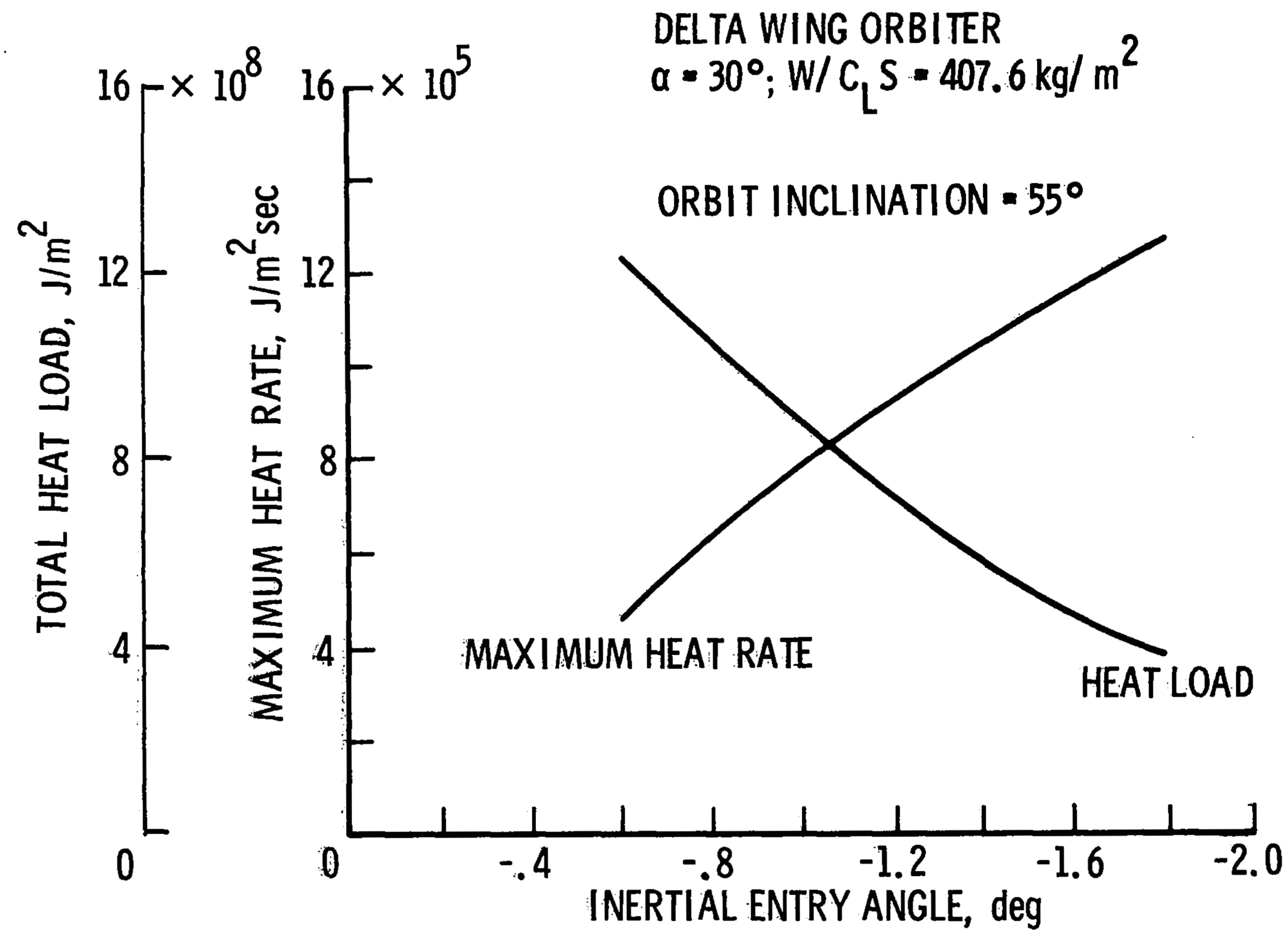

Figure 9

HORIZONTAL IMPULSIVE DEORBIT ΔV REQUIREMENT

To get the desired steeper entry mentioned previously, a greater deorbit ΔV capability is required. Shown in figure 10 is the horizontal impulsive deorbit ΔV requirement for the orbit of interest. The trade between reduced TPS weight and greater deorbit ΔV capability must be investigated.

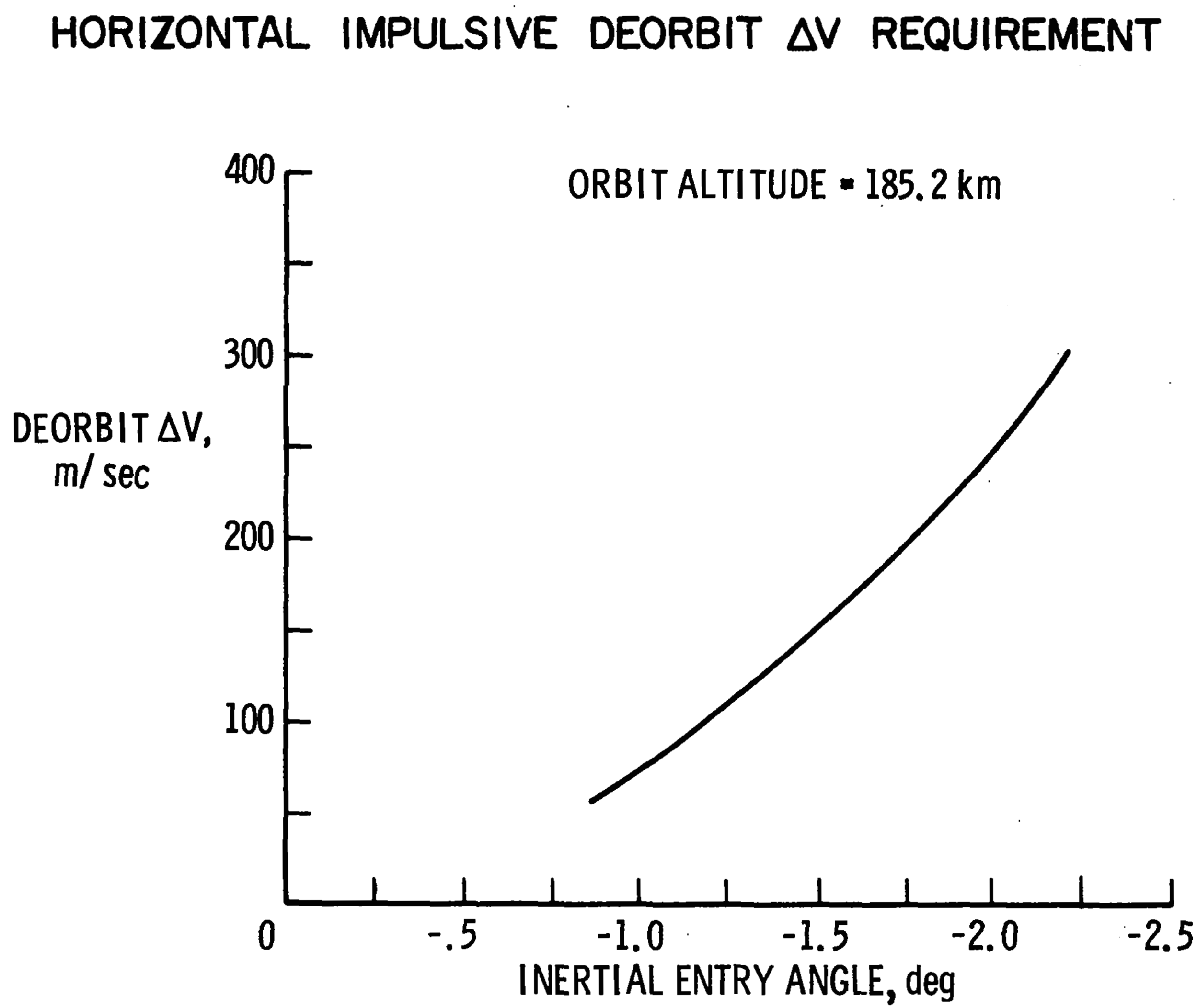
HORIZONTAL IMPULSIVE DEORBIT ΔV REQUIREMENT
ORBIT ALTITUDE = 185.2 km
DEORBIT ΔV, m/ sec
400
300
200
100
0
-.5
-1.0
-1.5
-2.0
-2.5
INERTIAL ENTRY ANGLE, deg

Figure 10

EFFECT OF DEORBIT ΔV ON TOTAL STAGNATION-POINT HEAT LOAD

Minimum total stagnation-point heat-load trajectories were determined for a range of values of deorbit ΔV and cross range. A constant angle of attack was assumed for each cross range, while bank angle was used to optimize the trajectories. As shown by the solid curves in figure 11, the total heat load decreases with increasing deorbit ΔV, for an initial bank angle of 0°.

An alternate approach to achieving the benefits of steeper entry without paying the penalty of increasing deorbit ΔV is the use of negative lift through bank-angle control. That is, by banking the vehicle 180° at entry, the aerodynamic lift forces are utilized to steepen the flight path. The symbols on the figure illustrate the reductions in total heat load resulting from negative lift which can be achieved for one value of ΔV with cross ranges of 300 and 700 n.mi. The total heat loads are reduced by about 20 percent over that for 0° bank angle entries. In effect, the negative lift is equivalent to about 75 m/sec of deorbit ΔV.

EFFECT OF DEORBIT ΔV ON TOTAL STAGNATION-POINT HEAT LOAD

MINIMUM TOTAL HEAT TRAJECTORIES; INITIAL BANK ANGLE = 0^0

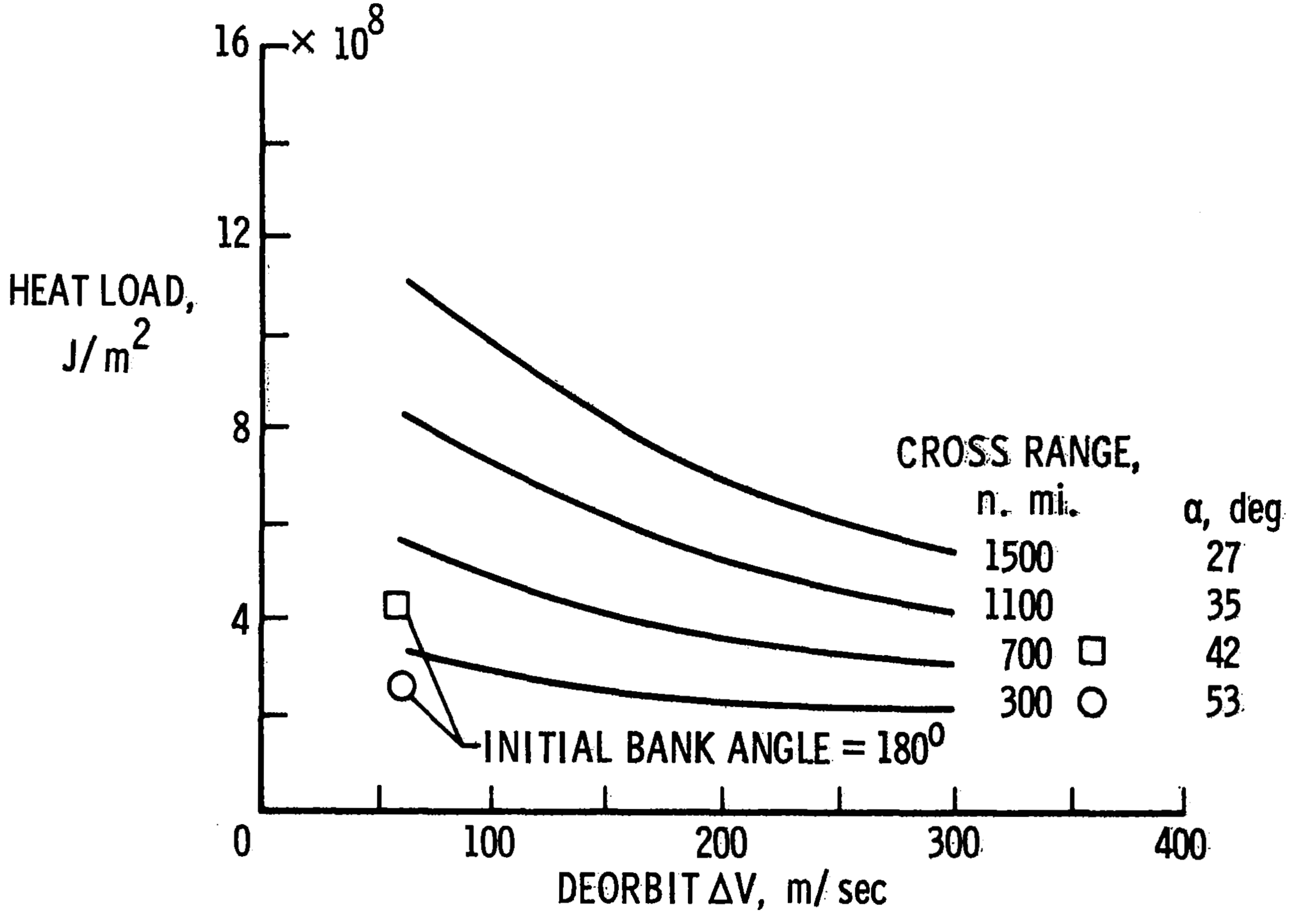

Figure 11

BOTTOM-SURFACE ABLATOR WEIGHT

A preliminary study of the bottom-surface ablator weight for the Mark I orbiter was performed by W. D. Brewer at the Langley Research Center. A heating distribution over the lower surface of a typical delta-wing orbiter was used assuming laminar flow throughout the optimal trajectories determined previously. For the lower values of heat load, a potential for significant ablator-weight savings is seen. (See fig. 12.)

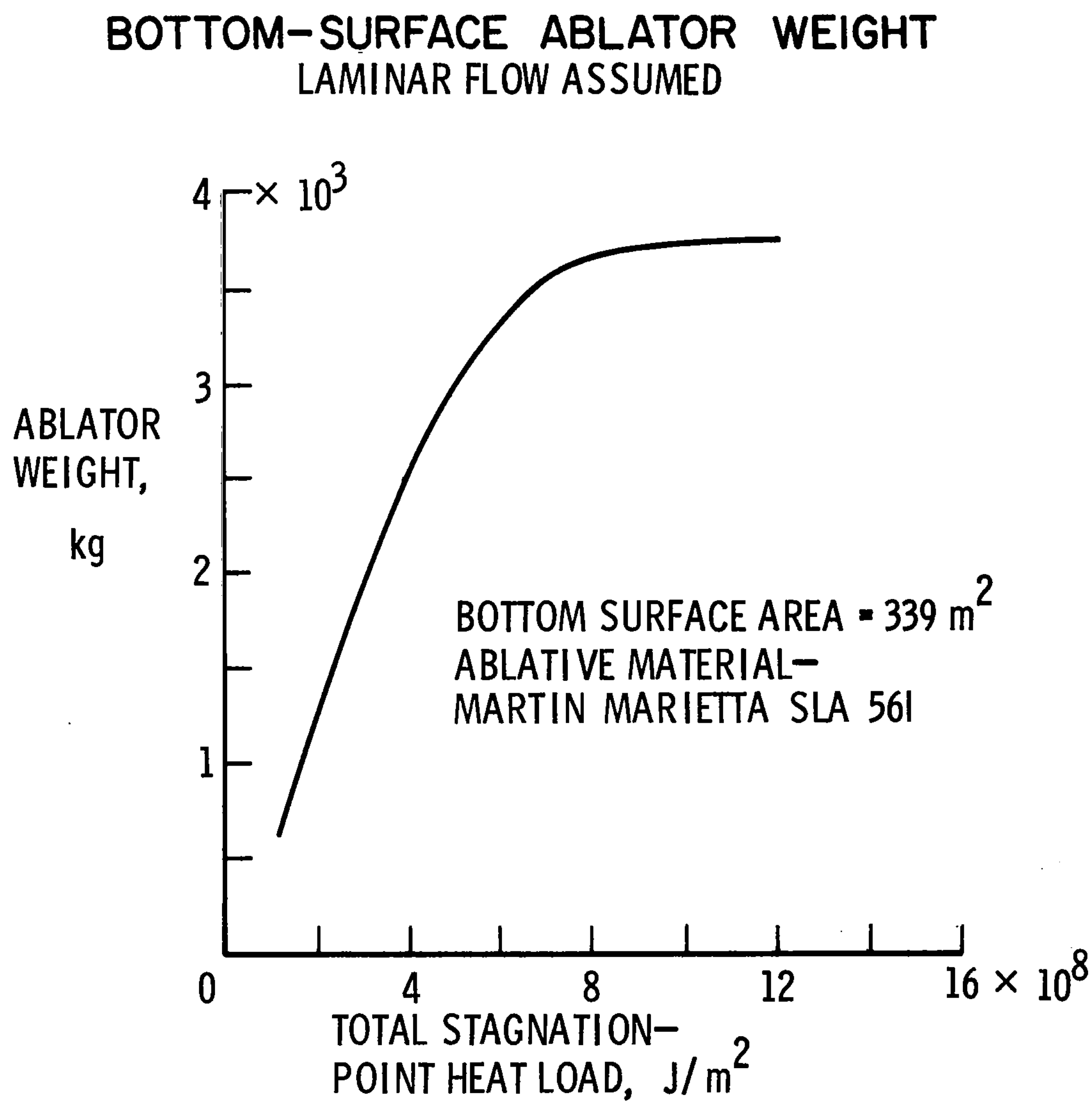
BOTTOM-SURFACE ABLATOR WEIGHT
LAMINAR FLOW ASSUMED
ABLATOR WEIGHT, kg
× 10^3
0
1
2
3
4
4
8
12
16 × 10^8
TOTAL STAGNATION-POINT HEAT LOAD, J/m^2
BOTTOM SURFACE AREA = 339 m^2
ABLATIVE MATERIAL–
MARTIN MARIETTA SLA 561

Figure 12

EFFECT OF DEORBIT ΔV ON BOTTOM-SURFACE ABLATOR WEIGHT

By using the total stagnation-point heat load from the optimal trajectories and the results of the preliminary weight study presented in figures 11 and 12, respectively, the effect of deorbit ΔV on the ablator weight is shown in figure 13. For all the values of cross range considered, the bottom-surface ablator weight decreases with increasing ΔV. The greater weight savings occur for the lower values of cross range and ΔV.

EFFECT OF DEORBIT ΔV ON BOTTOM-SURFACE ABLATOR WEIGHT
MINIMUM TOTAL HEAT TRAJECTORIES

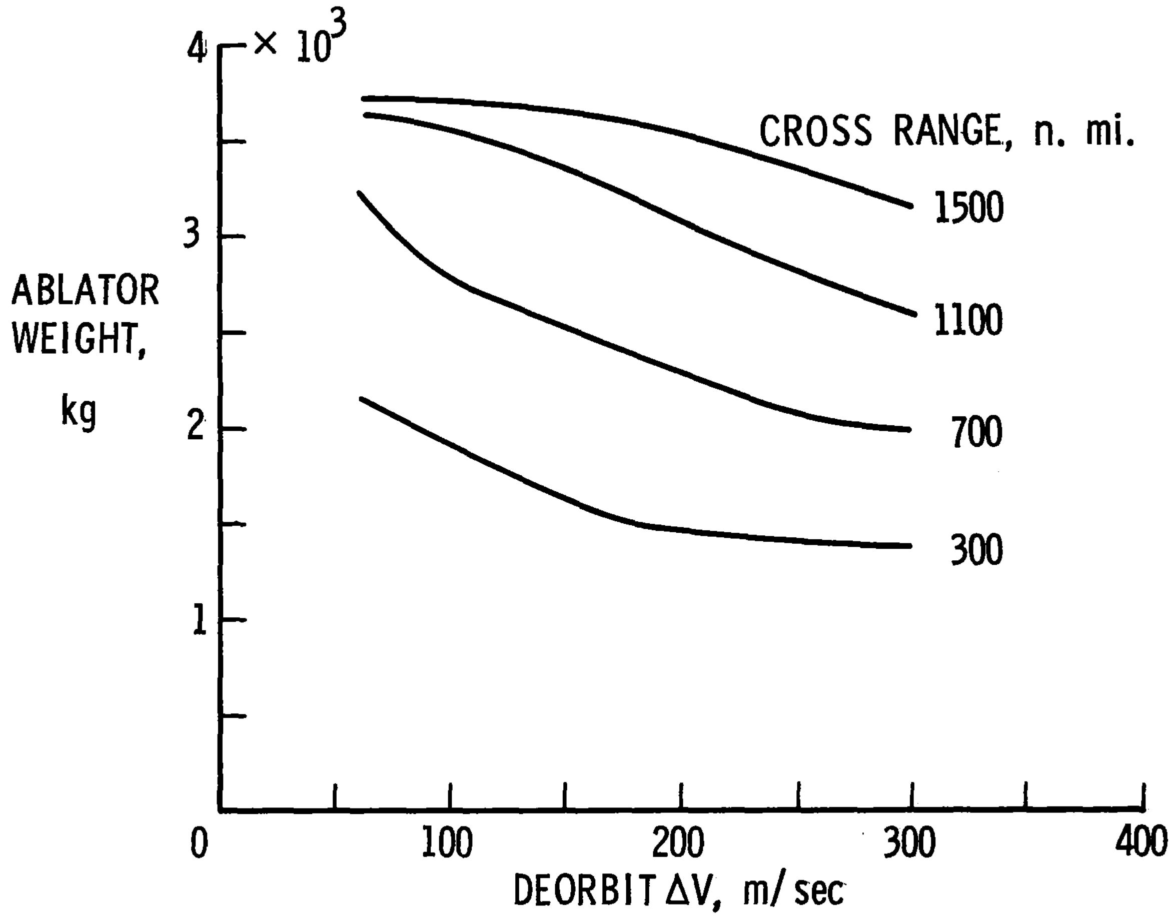

Figure 13

DEORBIT PROPELLANT WEIGHT SUMMARY

While it has been shown that ablator weight is reduced by increasing deorbit ΔV, a propellant weight penalty must be payed for the additional ΔV capability required. Shown in figure 14 is the weight of propellant required to obtain various values of ΔV for a typical orbiter deboost engine. Propellant weight increases with deorbit ΔV at a rate of approximately 17 $\frac{kg}{m/sec}$.

DEORBIT PROPELLANT WEIGHT SUMMARY

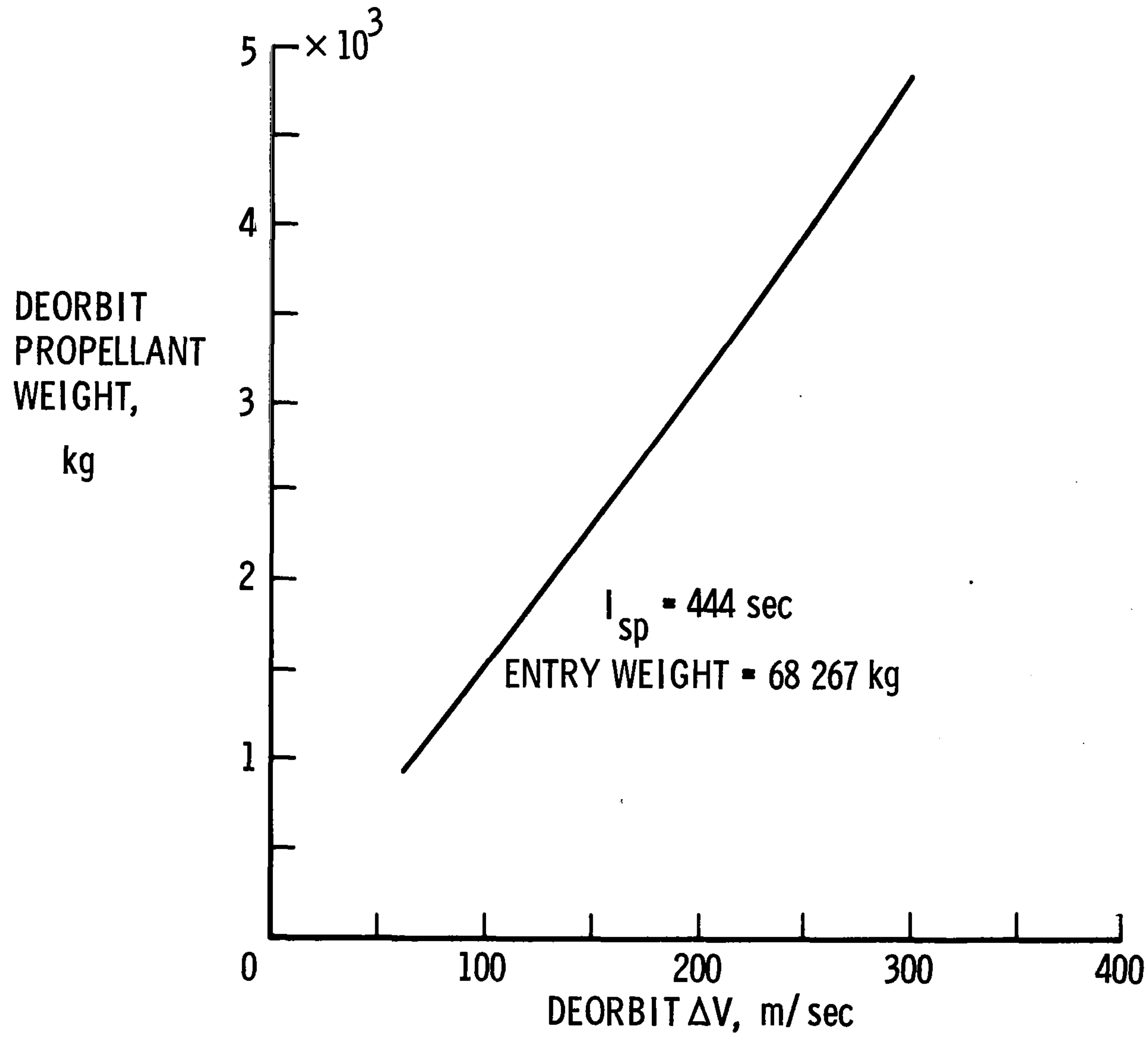

Figure 14

EFFECT OF DEORIBT ΔV ON THE TOTAL OF ABLATOR WEIGHT + DEORBIT PROPELLANT WEIGHT

To find a minimum of the total of the ablator and deorbit propellant weights, the results of figures 13 and 14 are added. As shown by the curves in figure 15, this total weight strictly increases with increasing deorbit ΔV for all values of cross range. Therefore, the vehicle requires only a minimum of deorbit ΔV propellant to achieve the lowest weight even though the advantage of a steeper entry for reducing ablator weight is lost.

To capitalize on the advantage of steeper entry while retaining the low ΔV requirement, the results of entering with the vehicle banked at 180° to achieve a steeper entry by negative lift are also shown in figure 15. The result, denoted by the symbols in the figure, was a 15 percent reduction in the total weight using this entry mode for cross ranges of 300 and 700 n.mi. without violating the 2.5g maximum deceleration limit.

EFFECT OF DEORBIT ΔV ON THE TOTAL OF ABLATOR WEIGHT + DEORBIT PROPELLANT WEIGHT

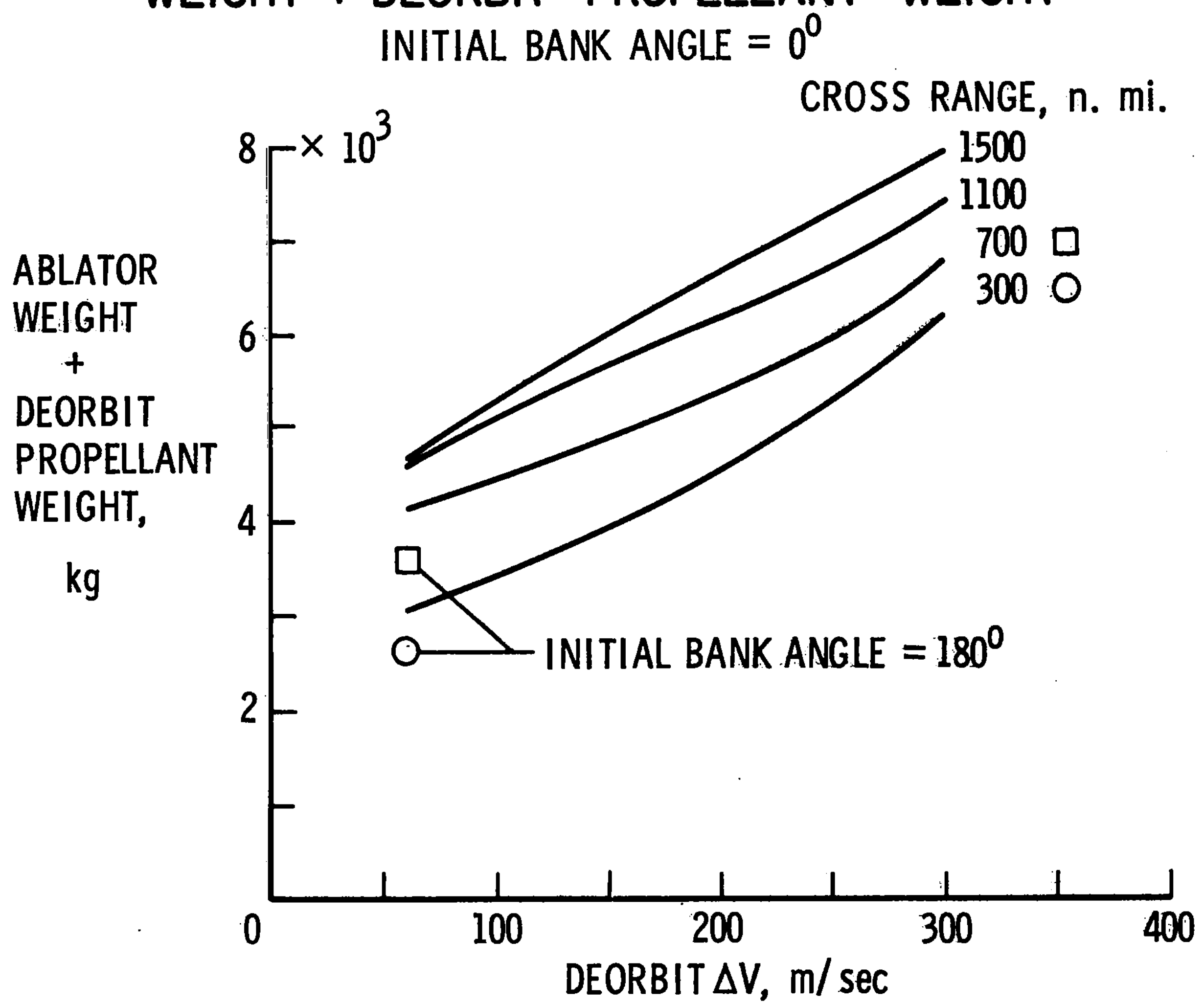

Figure 15

CONCLUDING REMARKS

From a chosen nominal trajectory, significant improvement in shuttle orbiter cross range can be made with no increase in the values of heat load and maximum heat rate at the stagnation point. However, along the bottom center line of the vehicle, a uniform increase of about 10 percent in the values of maximum temperature and total heat load results when using the MDAC boundary-layer transition criteria. Also, the magnitudes of these parameters predicted by the MDAC and NAR criteria were significantly different.

Although the first study considered only a reusable TPS for the orbiter, the results are equally applicable to an ablative TPS. Additional cross-range capability could be obtained with a minimal increase in ablator weight.

While total stagnation-point heat load for the Mark I orbiter can be reduced by increasing deorbit ΔV, the resulting decrease in ablator weight is overcome by the increase in deorbit propellant weight. However, a small deorbit ΔV combined with negative lift in the initial phase of entry results in significant ablator-weight reductions. Negative-lift entry offers a means of saving ablative TPS weight through steepening the entry without a deorbit propellant penalty. The effective reduction of deorbit ΔV obtained using the negative-lift entry mode is equivalent to about 1300 kg of deorbit propellant.

A more detailed ablative heat shield weight study is needed which includes the effects of boundary-layer transition and angle of attack on heating, and structure and insulation weights.

STAGE SEPARATION OF PARALLEL-STAGED SHUTTLE VEHICLES, A CAPABILITY ASSESSMENT

M. J. Hurley, Design Specialist
Flight Technology, Space Shuttle

G. W. Carrie, Senior Design Engineer
Vehicle Design & Structures, Space Shuttle

Convair Aerospace Division of General Dynamics
San Diego, California

INTRODUCTION

Stage separation has long been recognized as a major Space Shuttle problem area. The parallel-staged or "piggyback" arrangement precludes use of separation techniques developed for tandem vehicle stages. Also, since most shuttle configurations are not symmetrical (thereby complicating interactions), experience gained from Titan IIIC solid motor separation is not directly applicable. Unlike present-day launch vehicle stage separation, the depleted Space Shuttle booster is as massive as the orbiter element and large intervehicular interaction is probable. Abort separation is likely to yield the most severe separation condition, since aerodynamic loading is significantly higher during the abort regime. Aerodynamics, including interference effects, will dominate the separation dynamics for all but the lowest dynamic pressures.

Convair Aerospace has been conducting detailed analytical and experimental studies of multibody staging directly related to Space Shuttle for three years (Ref. 1 through 10). In support of these studies, one of the most comprehensive multibody separation simulations in existence today was developed on Independent Research and Development (IRAD) funds (Ref. 3). This simulation, in its various stages of development, was the analytic basis for the various analytical studies performed to date.

This paper is essentially self-contained; it reviews the genesis of the forward link separation concept, evolves the stage separation system from its initial concept through detailed preliminary design, and presents major conclusions and results of supporting analyses. The paper contains all pertinent material generated as a consequence of the Space Shuttle Phase B study which was documented in June of 1971. In some areas, the approach differs from our Phase B baseline and reflects results from more current analyses; these differences are not always noted in the text that follows.

STAGE SEPARATION CONCEPTUAL ANALYSIS

This table presents 16 qualitative measures used to perform a preliminary evaluation of various separation system concepts so that a few of the better concepts might survive. The first three of these "measures" were in actuality merely categories used to label the various candidates. These categories were useful in ensuring that the candidates to be considered adequately span or exhaust the conceptual possibilities of systems that can perform the separation function. The remainder were measures intending to reject obviously poor candidates so that a select few may be looked at in detail in a subsequent design-oriented evaluation. A brief discussion of each should serve to illustrate its intent.

By commonality (see table) we mean the degree to which the separation system does not duplicate the functions of other systems – e.g., the support and release (of these supports) functions of the interstage attachment system. Complexity is an obvious factor influencing design (nonrecurring) costs, qualification testing (nonrecurring) costs, maintenance (recurring) costs and even reliability. As such, complexity cannot be considered an independent measure, but its ease of determination makes it a valuable qualitative measure. Further, complexity has a direct bearing on the risk that such a conceptual approach might cost considerably more than expected to design and qualify or, worse, must eventually be scrapped in favor of an alternative approach.

Dispersion sensitivity is meant to measure the degree to which the system concept can tolerate the inevitable variability of contributing factors; e.g., engine thrust rise and thrust decay uncertainties, aerodynamic load variations, variations in mass properties, sequence timing uncertainties, etc. It is a general consequence of constraints that systems properly employing constraints will be less dispersion sensitive (other things being equal), since the separation trajectory is restrained from entering an undesirable clearance-critical region.

Reliability and safety are also not independent. Reliability is the certainty that the system will perform as designed when called upon to do so, including known variability (and its probability) in its operation. Safety is how safe the concept itself might be and embodies the consequence of potential (i.e., probable) failures in terms of the loss of life and equipment.

Maintainability is the ease of maintenance of the system in operation and includes the system turnaround requirement. Nonrecurring costs are distinguished from recurring costs in that the former is a one-time cost (development, testing, and initial procurement) and the latter a cost per operation (per flight).

Some separation concepts can be used only with "belly-to-belly" or "belly-to(booster's) back" parallel arrangements (clusters) and imply operational restructions. All concepts investigated applied to parallel (as opposed to tandem) arrangements.

The factors of separation system performance and equivalent (booster) weight are estimates of the adequacy of the envisioned system in performing its intended function efficiently. The final category brings out the degree to which the candidate concepts can be extended into the abort regime where the booster mass is substantially increased and aerodynamic loading becomes a major problem.

QUALITATIVE EVALUATION FACTORS FOR CANDIDATE SEPARATION SYSTEM CONCEPTS

ENERGY SOURCE	MAINTAINABILITY
ENERGY CONVERSION	NONRECURRING COST
NUMBER OF CONSTRAINTS	RECURRING COST
COMMONALITY	BELLY-TO-BELLY MOUNT
COMPLEXITY	BELLY-TO-BACK MOUNT
DISPERSION SENSITIVITY	SEPARATION PERFORMANCE
RELIABILITY	EQUIVALENT WEIGHT
SAFETY	EXTENDABILITY TO ABORT

Figure 1

QUALITATIVE EVALUATION SUMMARY

This table is a condensed summary of the conceptual systems as they evolved from a system with no (or zero) constraints to systems that constrain the relative trajectory to all but motion along the "guide's" arc. Energy sources considered ranged from separate systems (solid-propellant rockets or pneumatic sources) to systems using the energy (acceleration) available through vectoring the orbiter or booster main propulsion acceleration.

The table indicates that additional reliability and cost improvements accrue through using the main propulsion system on either the orbiter or booster as the energy source. This follows, since (1) these systems are already provided and are designed to be highly reliable, (2) qualification testing is already provided, and (3) the booster propulsion system (even in case of abort) is in operation and instantly ready to perform the separation function. It is this last consideration (continuity) that makes the forward or reversed four-bar linkage system such an attractive candidate. Before separation, the four-bar linkage is transmitting the main propulsion loads into the orbiter in the role of reversed "drag" links. These links are already in compression and (in the event of an immediate release) reacting full booster thrust (as could occur for an immediate abort), providing a remarkable degree of continuity as these links begin to accelerate angularly along their arc. This continuity can mitigate impact loading and substantially reduce link-load overshoot while still providing a high acceleration component into the orbiter (i.e., the elastic structure is already "deformed").

Again, it should be observed that dispersion sensitivity can be reduced through constraints by restraining the separation trajectory from entering an undesirable region and providing good separation system velocities at restraint release. This technique is what gives the forward linkage system such a good evaluation in this regard.

The table indicates that two concepts definitely should be pursued: lateral rockets and the four-bar linkage (particularly the linkage using booster thrust). If abort separation is a requirement, the linkage using booster thrust appears to be the best candidate system.

QUALITATIVE EVALUATION SUMMARY

FACTORS UNDER CONSIDERATION	LATERAL ROCKETS	PNEUMATIC PISTONS	DUAL RAIL SYSTEMS FORWARD	DUAL RAIL SYSTEMS REARWARD	FOUR-BAR LINKAGE SYSTEMS REARWARD	FOUR-BAR LINKAGE SYSTEMS FORWARD
ENERGY SOURCE	ROCKETS	GHe^2	ORBITER ENGINES	BOOSTER ENGINES	ORBITER ENGINES	BOOSTER ENGINES
ENERGY CONVERSION	THRUST	4 PISTONS	2 RAILS	2 RAILS	4 LINKS	4 LINKS
NUMBER OF CONSTRAINTS	0	3	5	5	5	5
COMMONALITY	EXCELLENT	GOOD	GOOD	GOOD	VERY GOOD	VERY GOOD
COMPLEXITY	VERY LOW	HIGH	HIGH	HIGH	LOW	LOW
DISPERSION SENSITIVITY	LOW	MEDIUM	HIGH	HIGH	MEDIUM	VERY LOW
RELIABILITY	HIGH	FAIR	GOOD	FAIR	GOOD	VERY GOOD
SAFETY	GOOD	POOR	FAIR	FAIR	FAIR	EXCELLENT
MAINTAINABILITY	VERY GOOD	POOR	POOR	POOR	EXCELLENT	EXCELLENT
NONRECURRING COST	VERY LOW	VERY HIGH	HIGH	HIGH	MODERATE	MODERATE
RECURRING COST	HIGH	NEGLIGIBLE	MODERATE	MODERATE	NEGLIGIBLE	NEGLIGIBLE
BELLY-TO-BELLY MOUNT?	YES	YES	YES	YES	YES	YES
BELLY-TO-BACK MOUNT?	YES	YES	YES	NO	YES	YES
SEPARATION PERFORMANCE	GOOD	EXCELLENT	FAIR	POOR	GOOD	EXCELLENT
EQUIVALENT WEIGHT	LOW	MODERATE	HIGH	VERY HIGH	LOW	LOW
EXTENDABILITY TO ABORT	LOW	VERY LOW	FAIR	GOOD	FAIR	EXCELLENT

Figure 2

SPACE SHUTTLE SEPARATION SYSTEM TRADE STUDY RESULTS

The objective of this study (Ref. 7) was to develop and evaluate several candidate concepts and to select a design that best met the requirements of withstanding all flight loads of the mated configuration during ascent, while providing capability for safe separation from liftoff to normal staging.

Candidate concepts were evaluated based on separation characteristics during normal staging, maximum αq, and immediately off the pad.

NORMAL STAGING – Capability for safe separation considering the system tolerance to off-nominal design conditions of booster and orbiter thrust, release time, and attitude control were evaluated. The rocket and piston concepts were the heaviest of the alternatives studied, due principally to coast-time propellant requirements. The links using booster thrust and the rocket concepts are the most tolerant of these off-nominal conditions. The links-using-booster-thrust concept provides the best separation distance versus time. The rocket and piston concepts investigated require zero g engine start capability for the orbiter for safe operation. Because they react ahead of the booster cg, the pistons, rails, and links using the orbiter-thrust concept gave high post-separation pitchdown rates to the booster.

MAXIMUM αq – The concepts that use orbiter thrust to provide lateral acceleration are totally inadequate in supplying safe separation due to the low T/W of the orbiter. The piston and rocket concepts incur significant weight penalties over that required for normal staging. Additionally, the piston reaction ahead of the booster cg pitches the booster into higher aerodynamic loading. The links-using-booster-thrust concept provides satisfactory separation with minor weight penalty.

ABORT IMMEDIATELY OFF THE PAD – The reduced booster thrust required for all the concepts except the links-using-booster-thrust results in unsatisfactory booster attitude control (actually maneuvering). Piston and rocket concepts incur additional weight penalties due to the heavier booster.

CONCEPT COMPARISON

EVENT	ROCKET	PISTON	RAILS	LINKS, USING ORBITER THRUST	LINKS, USING BOOSTER THRUST
NORMAL STAGING					
WEIGHT KG (LB.*)	10,251 (22,600)	10,569 (23,300)	8,256 (18,200)	7,303 (16,100)	8,165 (18,000)
SEPARATION DISTANCE	GOOD	GOOD	POOR	POOR	GOOD
POSITIVE g FOR ORBITER ENGINE START	NO	NO	YES	YES	YES
BOOSTER PITCHDOWN RATE	LOW	HIGH	HIGH	MEDIUM	LOW
FAILURE TOLERANCE	GOOD	POOR	POOR	POOR	GOOD
ABORT - MAXIMUM α q					
BOOSTER THRUST	43%	43%	0	0	100%
SEPARATION TRAJECTORY	GOOD	GOOD	NOT ACCEPTABLE	NOT ACCEPTABLE	GOOD
BOOSTER ATTITUDE CONT.	PARTIAL	NOT ACCEPTABLE	NOT ACCEPTABLE	NOT ACCEPTABLE	FULL
ΔWEIGHT PENALTY KB (LB*)	2,722 (6,000)	7,484 (16,500) (2,000 ORBITER, 4,500 BOOSTER)	HIGH	HIGH	LOW
ABORT - OFF THE PAD					
BOOSTER THRUST	65%	65%	58%	58%	100%
RELATIVE FORWARD/AFT ACCELERATION	GOOD	NOT ACCEPTABLE	POOR	POOR	GOOD
ΔWEIGHT PENALTY KM (LB.*)	2,722 (6,000)	7,484 (16,500) (2,000 ORBITER 4,500 BOOSTER)	HIGH	HIGH	LOW

*TOTAL MATING/SEPARATION SYSTEM ESTIMATED WEIGHTS EXPRESSED AS EQUIVALENT BOOSTER WEIGHT.

Figure 3

SEPARATION TRAJECTORY COMPARISON, NORMAL STAGING

The links-using-booster-thrust concept was recommended as being the most failure tolerant, providing the best separation characteristics for normal staging, having the greatest potential for safe separation at maximum αq and immediately off the pad, and for satisfying all other abort conditions.

The figure illustrates the clearance versus time achieved for each candidate at normal staging.

SEPARATION TRAJECTORY COMPARISON, NORMAL STAGING

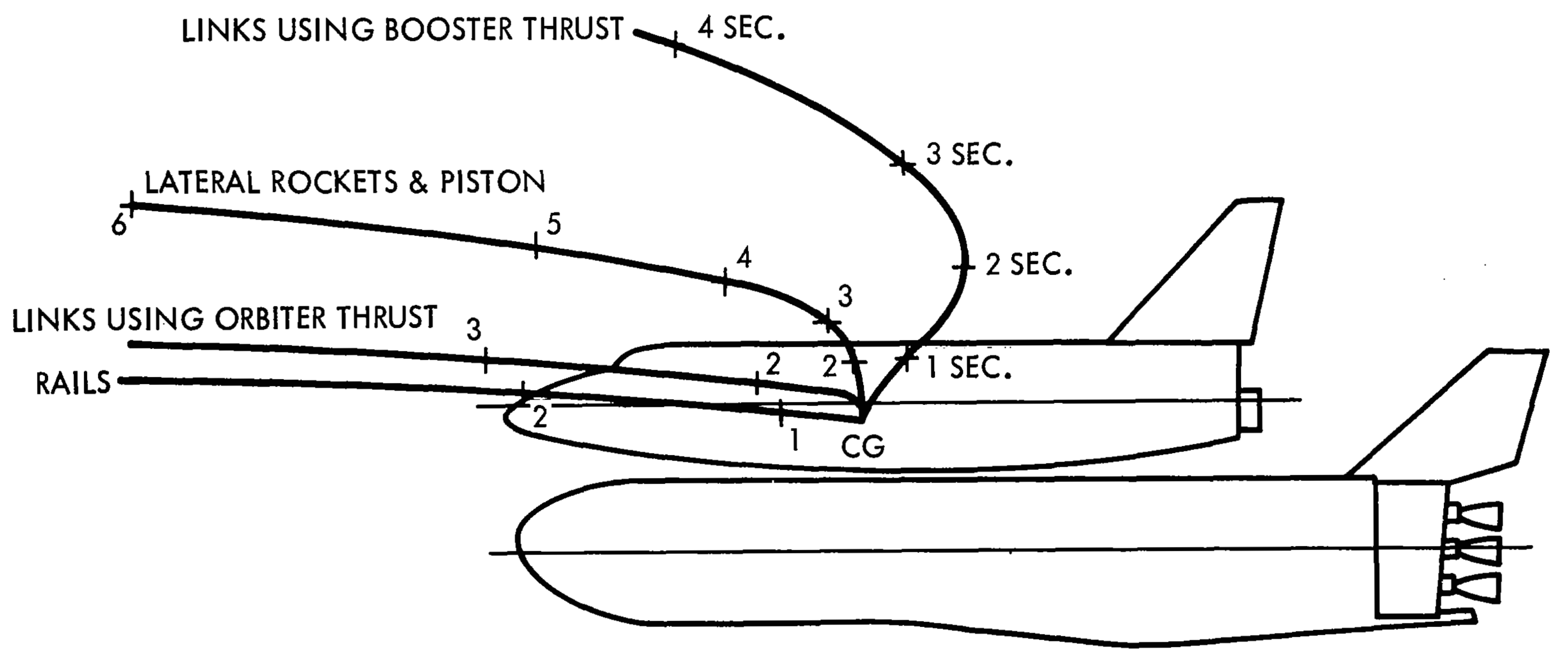

Figure 4

ABORT CRITERIA

Abort criteria necessary to satisfy the program requirements included intact vehicle abort capability. Intact abort implies the capability of the booster and orbiter to separate and both continue flight to a safe landing, with a full payload aboard the orbiter. In addition, a vehicle performance Level II requirement specified, "a single main engine out on the booster shall permit nominal mission continuation; on the orbiter, a safe abort capability," The FO/FS subsystem design criterion was specified to reduce the likelihood of an abort occurring, whereas the fail-safe level of subsystems operation is, in fact, an abort operating procedure.

Failure conditions are classified in one of three categories as a function of the time-criticality of the situation, as illustrated in the table. Noncritical failures are those that (by definition) allow continued safe mated flight to propellant depletion. Examples of this type of failure are detection of minor leaks or loss of any subsystem to the FS level. Noncritical failures typically jeopardize mission continuance but not mated flight. Both vehicles are expected to be recovered successfully.

Critical failures are defined as those in which continued mated flight to booster propellant depletion are either deemed not possible or not advisable. Examples of this type of failure are a fire or localized explosion, significant loss of booster thrust and/or thrust vector control capability, or major leaks that could easily result in a fire, explosion, or significant loss of booster thrust. Critical failures typically jeopardize mated flight and early, safe stage separation is advised. The time-criticality is principally at issue for critical failures. Required reaction time can range from a few seconds to a minute or more before stage separation must be accomplished. Following stage separation, both vehicles are required to be recoverable if possible; that is, stage separation itself shall not jeopardize vehicle recovery.

Catastrophic failures are defined as those for which there is insufficient time to effect stage separation or, following separation, insufficient time to recover the vehicles and/or crew. Examples of this type of failure are near-immediate explosions, major primary structural failure, or major loss of thrust shortly after liftoff. This latter condition is catastrophic because insufficient time is available following separation to obtain the required separation clearance before the booster impacts in the vicinity of the launch complex and destroys itself and the orbiter. No design requirements were provided for this type of failure. (Crew ejection seats were to be provided during the development flight test program because of initial flight uncertainties and a greater risk of failures occurring. The ejection seats in the booster and orbiter were to be removed for the operational phase.)

ABORT FAILURE CATEGORIES

CATEGORY	FAILURE CLASS	EFFECT	ABORT ACTION
NONCRITICAL	MINOR LEAK LOSS OF ANY SUBSYSTEM TO FS LEVEL	CAN RECOVER VEHICLES AND CREWS	ABORT MISSION (CONTINUE MATED FLIGHT)
CRITICAL	FIRE/LOCAL EXPLOSION SIGNIFICANT LOSS OF THRUST AND CONTROL CAPABILITY MAJOR LEAK	SUFFICIENT TIME TO RECOVER VEHICLE AND RESCUE CREW WHERE BOTH ARE IN DANGER OF CATASTROPHIC LOSS	ABORT MATED FLIGHT (INTACT RECOVERY)
CATASTROPHIC	EXPLOSION MAJOR STRUCTURAL FAILURE LOSS OF BOOSTER THRUST SHORTLY AFTER LIFTOFF	INSUFFICIENT TIME TO RECOVER VEHICLE AND/OR CREW	NONE

Figure 5

MATED ASCENT ABORT PROCEDURES

The abort procedure for noncritical failures is to fly the mated configuration to booster propellant depletion (low q), separate, and fly the booster back to the primary landing site. The orbiter then has three options: (1) continue the mission from the normal staging velocity, if attained; (2) continue the mission with the orbiter engines throttled up to 109% EPL to make up booster velocity losses (if less than 50 fps); or (3) return to continental United States when the velocity losses exceed the mission requirements. The separation system at nominal staging conditions was to be designed for loss of thrust or thrust vector control (TVC) from any two booster engines and loss of thrust or TVC from any one booster and one orbiter engine.

After a noncritical failure, the flight to propellant depletion can be along the nominal trajectory if mission completion is still possible or can be along an alternative trajectory if mission completion is not possible. The staging velocity associated with noncritical normal separation conditions is related to the time of failure, loss of TVC, or engine thrust. With the loss of orbiter injection velocity capability, alternative ascent trajectories are required to minimize downrange flyback of the booster and orbiter.

In the event of a critical failure, preseparation maneuvers would be desirable, if possible, to put the mated configuration in a more favorable condition for separation, such as lower dynamic pressure. For early separation during mated flight, two conditions had to be satisfied: (1) a positive head for orbiter engine start-to-mainstage thrust must be provided, and (2) separation subsystem must function, considering inadvertent booster engine cutoff signals and the maximum booster thrust level required for safe booster recovery. The induced vehicle loads and control conditions had to be within the design capability of the baseline vehicles.

Following an early stage separation, it is required that both vehicles be recovered if at all possible. Since neither can enter or land safely with any significant main propellants onboard, it is necessary to dispose of these propellants, which was to be accomplished by burning them through the main engines.

MATED ASCENT ABORT PROCEDURES

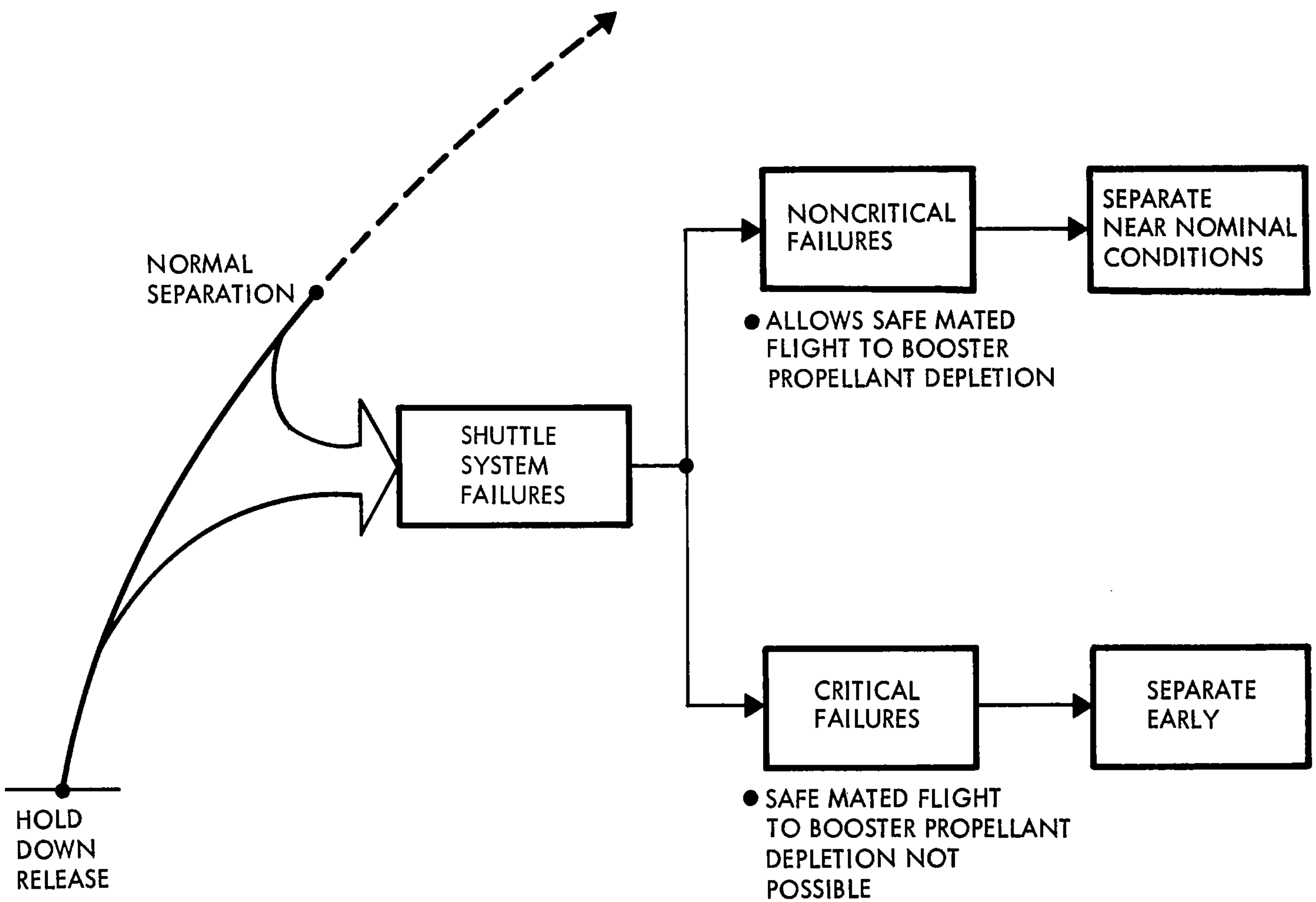

Figure 6

STUDY CONFIGURATION

The study configuration consists of the North American Rockwell 161C delta-wing orbiter and the General Dynamics B-9U delta wing booster. The orbiter is launched piggyback on the booster and located slightly ahead of the booster nose. Previous studies (e.g., Ref. 2, 4, and 8) had investigated the proximity aerodynamics and determined these effects must be included for any realistic study of stage separation capability in a high aerodynamic pressure regime.

The capability of booster recovery following separation had been previously analyzed (Ref. 9 and 10) and determined to be feasible. What remained was to assess the ability of the parallel-staged shuttle to separate at various points along its ascent trajectory.

It should be noted that this study is directly applicable to many of the tandem-staged shuttle arrangements should it be desired to stage the orbiter from its external propellant tanks, leaving them with the booooster.

STUDY CONFIGURATION

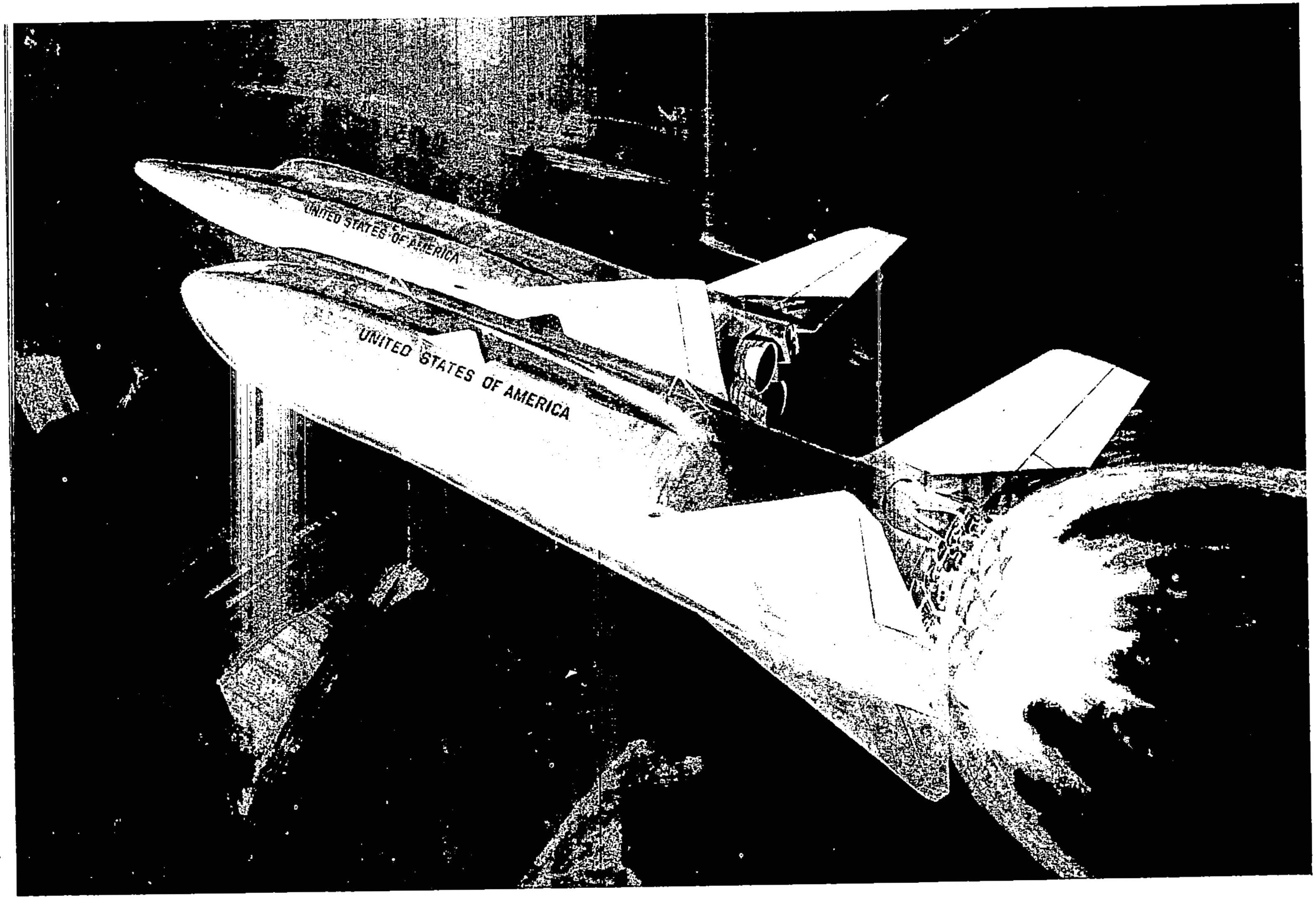

INVESTIGATIVE REGION FOR ABORT SEPARATION

This figure illustrates the regions under investigation and the range of parameter encompassed. Included in the study was pre-liftoff separation of the orbiter from the booster while the latter remained on the launch pad. Also included was an investigation of normal staging with dispersions in system parameters and loss of either or both orbiter main propulsion engines.

INVESTIGATIVE REGION FOR ABORT SEPARATION

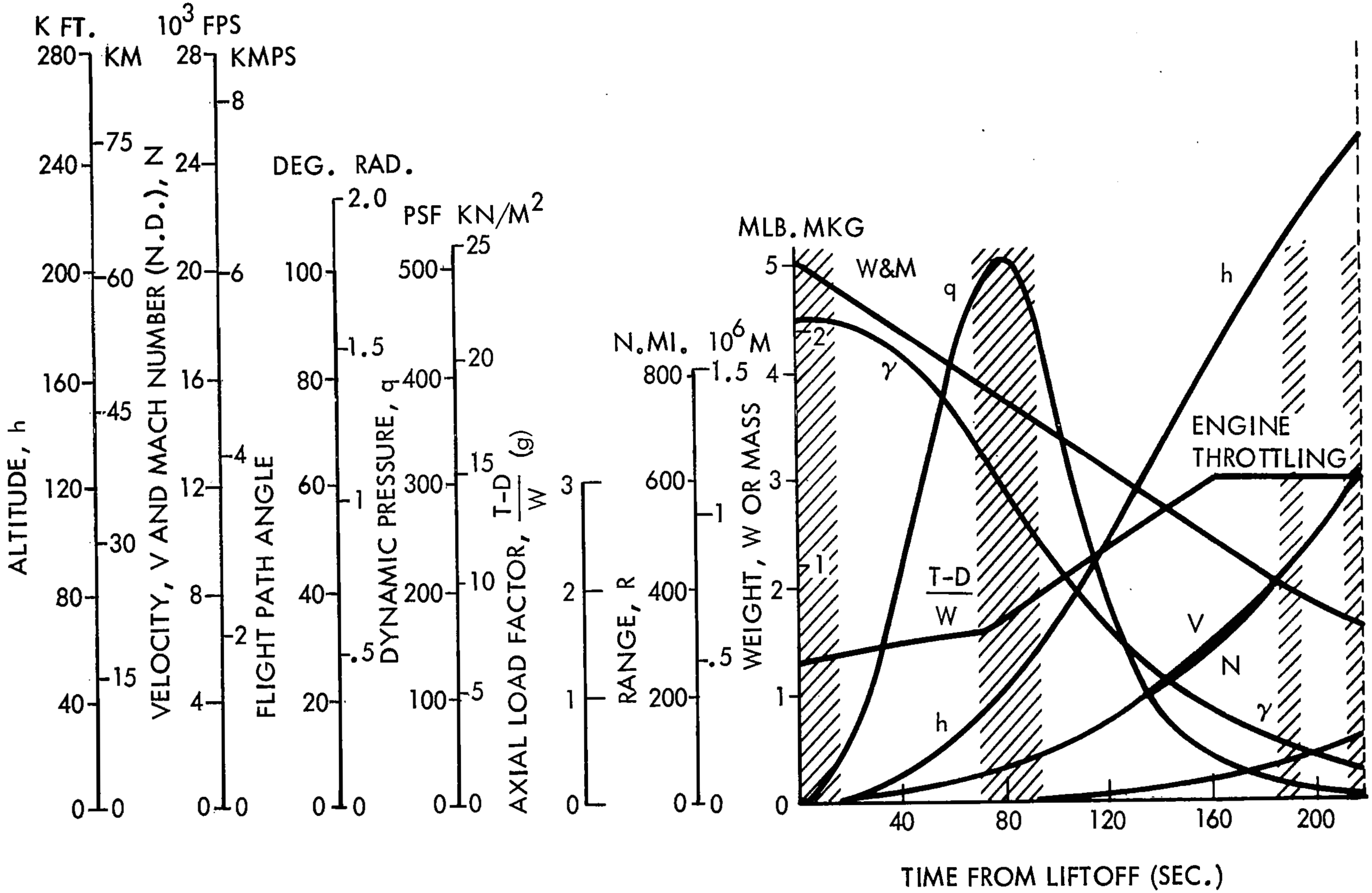

INCORPORATION OF AERODYNAMIC INTERFERENCE EFFECTS

Perhaps the most extensive task was the incorporation of detailed interference aerodynamics obtained from tests run by Convair Aerospace in August 1970 (Ref. 8) and by NASA/MSC in January 1971.
This figure presents the data obtained in graphic form and requires some explanation. Both tests were run with a delta-winged orbiter and a delta-winged booster; however, these used different models and were conducted in different wind tunnels. Neither test was representative of the current baseline configuration.

The Convair Aerospace test (left half of figure) collected appreciable data for only one Mach condition (1.6) and only in the pitch plane. For given angles of attack for the booster and orbiter (pairs α_B α_O on upper left in figure), the sting-mounted booster model was maneuvered in the proximity of the fixed-sting orbiter model while data was continuously being collected. The trajectories (or "traverses," as they were called) were run parallel to the orbiter's longitudinal body axis at preselected vertical displacements normal to its longitudinal axis (lower left of figure). Vertical displacement ranged from the mated position (at closest approach) to 0.25 booster body length. Longitudinal displacements ranged from 0.3 booster body length forward (booster ahead) to 0.7 booster body length aft. Although the region of interest was booster ahead, tunnel limitations prevented better coverage.

In contrast, the MSC test (right half of figure) collected data in both pitch and yaw planes for Mach 0.6, 0.9, 1.1, and 1.4. In this test, the procedure was reversed. For a given location in proximity of the booster (pairs X/ℓ_B, Z/ℓ_B on the lower right figure) and a given angle of attack of the booster, the orbiter angle of attack was continuously swept (while data was being recorded) through ±10 deg. (upper right of figure). This was done for booster angles of attack of -5, 0, and +4 deg. and at 15 selected points in the proximity. These runs constituted the majority of the test and were made at zero angle of sideslip for both models. The test was then repeated for an angle of sideslip of +5 deg. on the booster while the orbiter was swept through ±6 deg. This beta test was run at zero angle of attack for both models. As in the Convair Aerospace test, the region of interest (booster ahead) obtained rather limited coverage.

INCORPORATION OF AERODYNAMIC INTERFERENCE EFFECTS

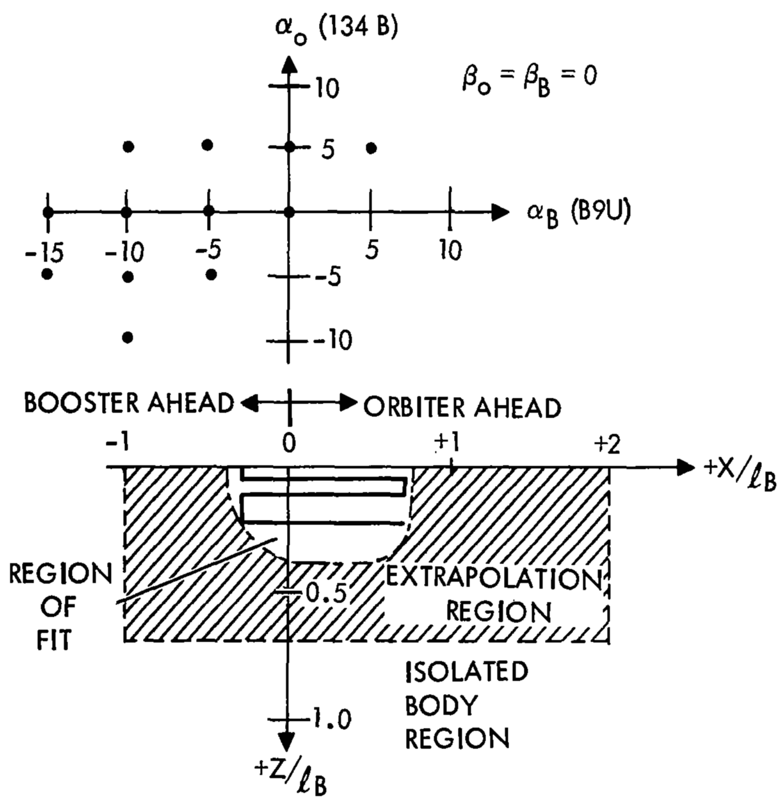

CONVAIR TEST 304, AUG. 1970
DELTA/DELTA CONFIGURATIONS
MACH 1.6

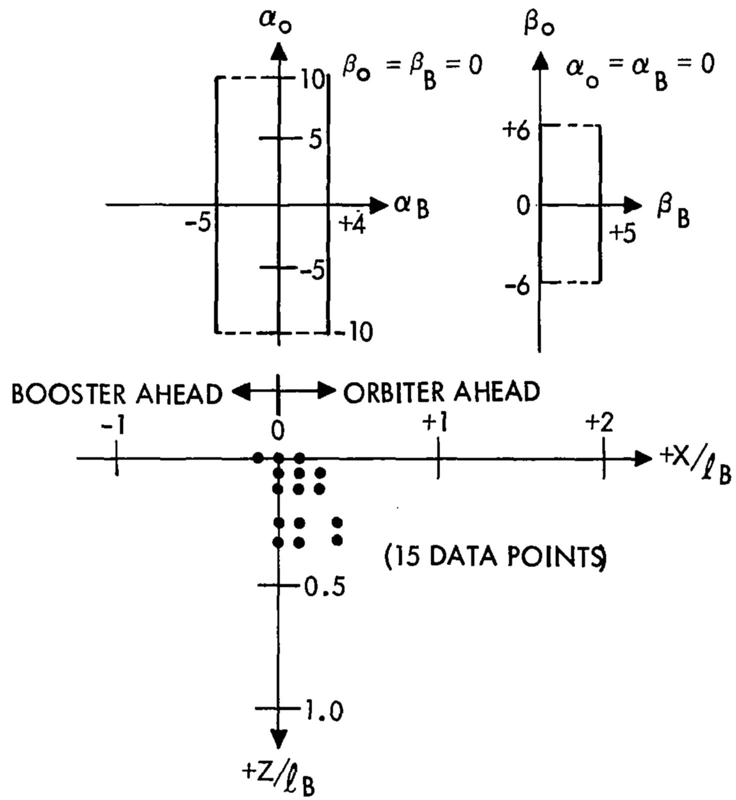

NASA/MSC TEST 401 JAN, 1971
DELTA/DELTA CONFIGURATIONS
MACH 0.6, 0.9, 1.1 AND 1.4

NOTE: FOLLOWING ABORT SEPARATION THE BOOSTER MOVES AHEAD (REGION OF LEAST DATA)

INTERFERENCE EFFECT ON PITCH MOMENT MULTIPLIER

The aerodynamic interference effects were derived from this data and were then fit using an existing polynominal fitter and computer graphics. Use of computer graphics allowed human interaction in the decision process, thereby avoiding the pitfalls of relying solely on analytical measures (such as "least squares" rms value). Since the data is primarily trigonometric rather than polynomial in form, distinct compromises were made in order to use the polynomial fitter. This figure presents a portion of the sweep data from Convair Aerospace Test 304 and illustrates the trigonometric form. The figure is also indicative of the large data range; here the pitch moment multiplier varies between +1.35 and -0.61 (i.e., between +35% and -161%.

The select polynominal fits were generally poor; however, every effort was made to ensure that the resulting fits were conservative so that conclusions arising from this study would not change adversely when more comprehensive data and better fits became available. It should however be noted that data obtained from these tests is of unusually good quality. The difficulties fitting the data arose principally from the sparsity of data and data coverage, and from the use of the simple polynomial fitter.

INTERFERENCE EFFECT ON PITCH MOMENT MULTIPLIER

$$K_{m_B} = (C_{m_B})_{\text{measured}} / (C_{m_B})_{\text{isolated body}}$$

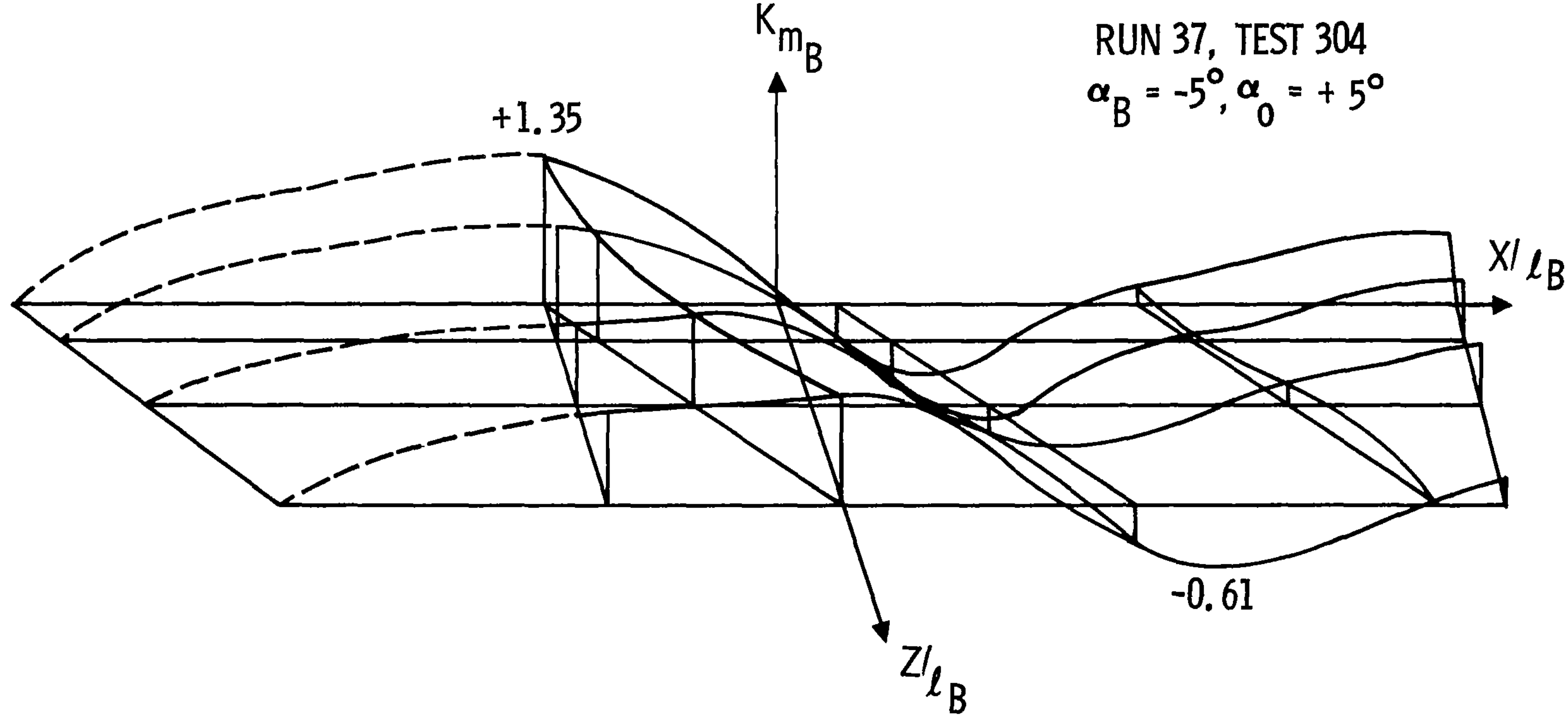

STAGE SEPARATION SYSTEM DESCRIPTION

A common feature of all separation systems, regardless of concept, is the interstage attachment structure to support the orbiter. This structure must hold the orbiter securely and rigidly during ascent from liftoff through staging. Longitudinally, the orbiter experiences a maximum of 3g during ascent.

Large lift loads due principally to the angle of attack of the wings are transferred through the interstage attachment structure and distributed (through frames, stiffeners, etc.) into each vehicle. Although not as large, aerodynamic side loads must also be reacted. In addition, the structure must be sufficiently rigid to prevent control system and/or aeroelastic interaction. These considerations dictate that the attachments be heavy structure.

Early in the study, it became apparent that the aerodynamic/inertia loads occurring during mated flight required heavy fittings, frames, and longerons in both booster and orbiter. Since the structural attachment has to be broken during separation, there is a strong interface between the attachment structure components and the separation system.

The highest load occurs at maximum longitudinal acceleration of the booster. This load could be taken at either the forward or the aft attachment. Because the orbiter is six times more sensitive to weight growth than the booster, however, it is lighter to transfer this load at the forward attach point since it is close to the liquid oxygen tank (and hence the cg) of the orbiter.

The main axial load (orbiter mass times 3g) is reacted in the forward attachment structure between the hydrogen and oxygen tank to simplify the tank design and minimize weight. The internal bulkheads are quite deep to handle the kick load and the attachment fittings are axially spread to transfer the high axial load to the booster structural skins.

SEPARATION SYSTEM FORWARD AXIAL LINK ATTACHMENTS

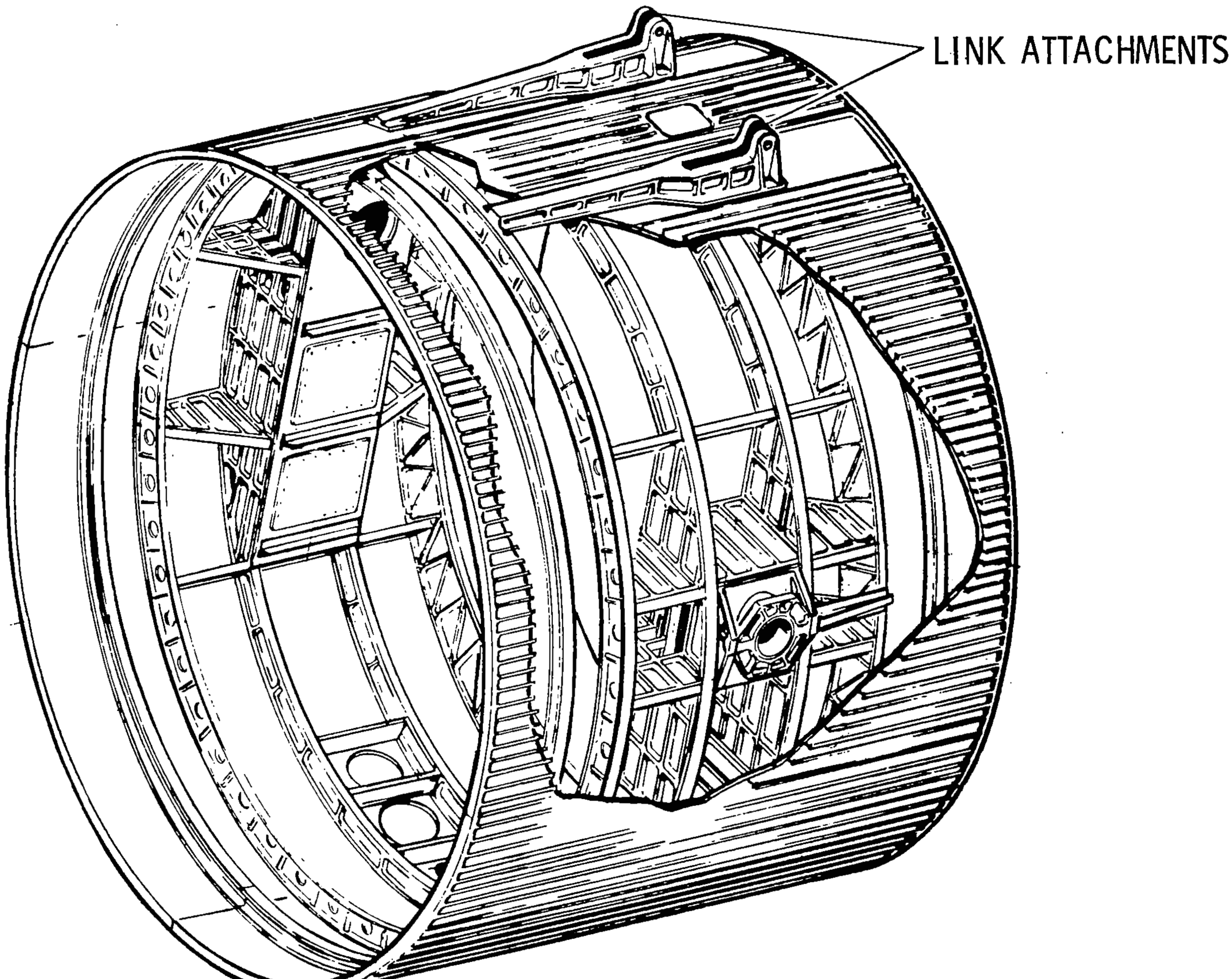

SEPARATION SYSTEM FORWARD VERTICAL LINK ATTACHMENTS

The maximum load normal to the waterline of the vehicles was tension at the front attachment. Shown here is the internal and external structure required in the LO_2 tank to react this load requirement.

SEPARATION SYSTEM FORWARD VERTICAL LINK ATTACHMENTS

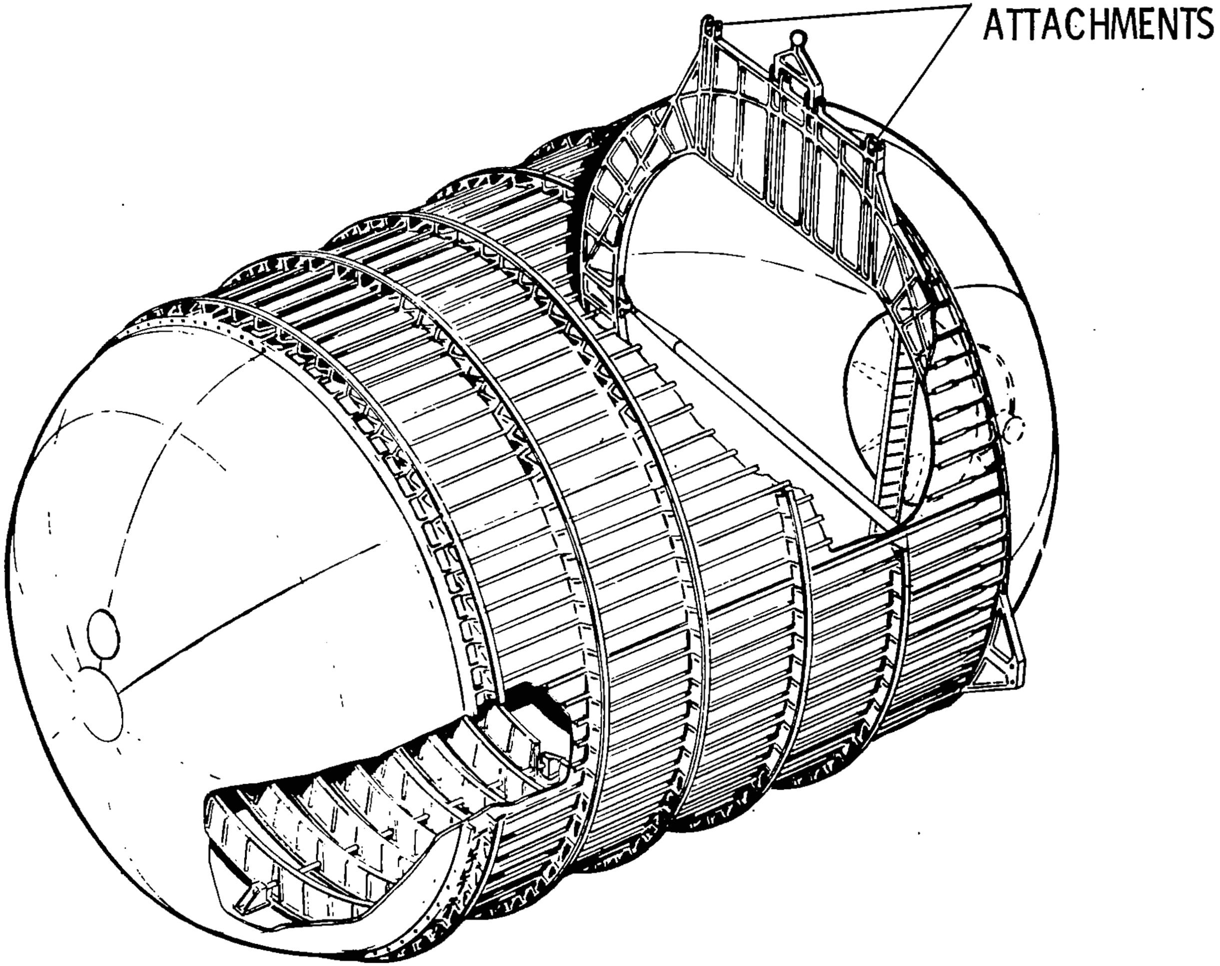

1325

SEPARATION SYSTEM AFT LINK ATTACHMENTS

The aft attachment was determined by the best location compatible with the orbiter location – the forward logical position was between tanks – but here we must facilitate the orbiter. Shown are the bulkheads required to react both the vertical load during ascent and the separation load during normal staging.

SEPARATION SYSTEM AFT LINK ATTACHMENTS

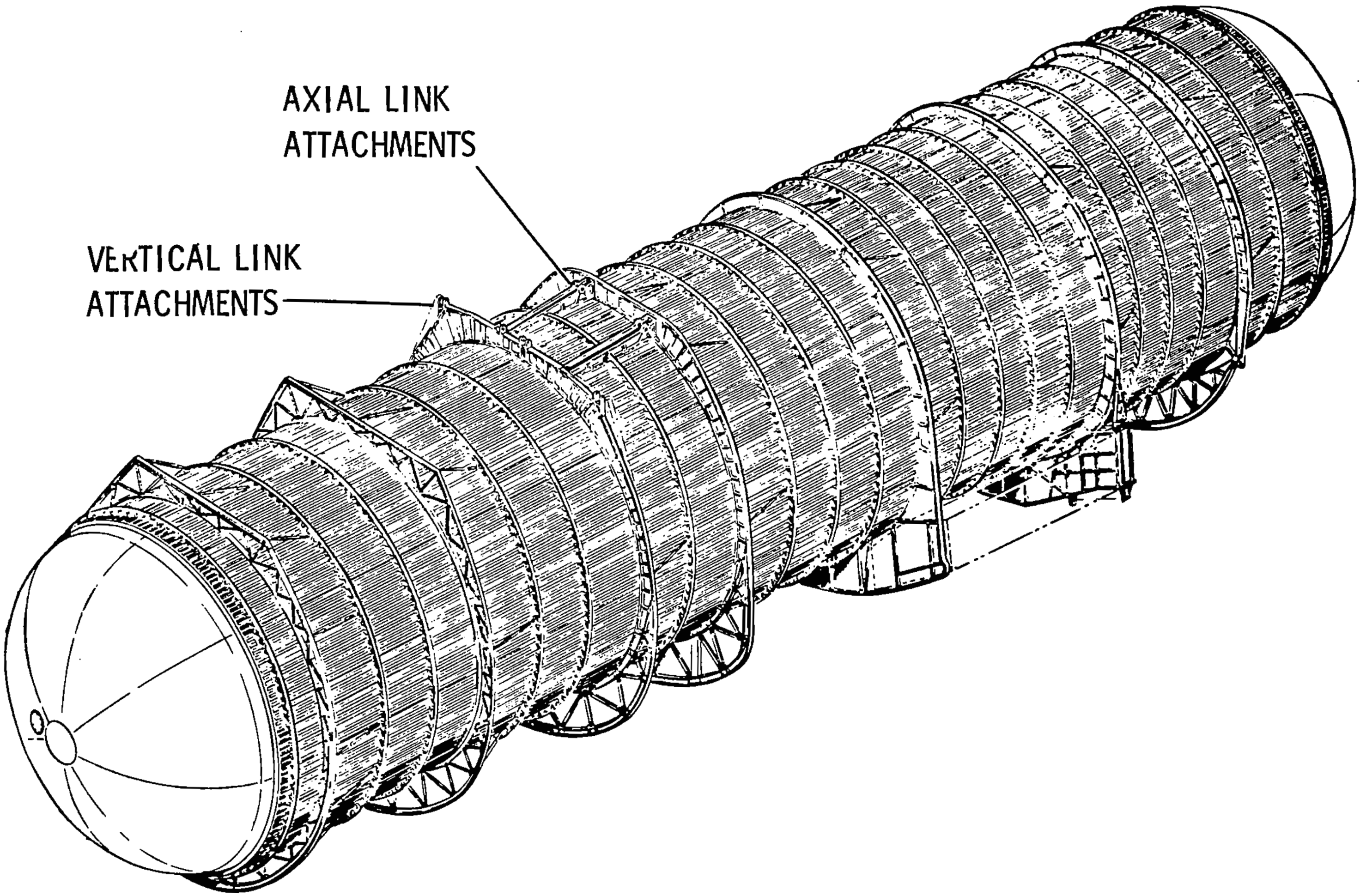

FORWARD AND AFT SEPARATION LINKS

The mating/separation system general arrangement consists of sets of vertical, side, and drag links located forward and aft. The links are designed to react all flight loads and are configured to provide the mechanics for separating the orbiter from the booster.

Separation is accomplished by using the booster thrust to accelerate the orbiter transversely. The forces for transverse acceleration are transmitted through rotating drag links located at the forward and aft attach points.

FORWARD AND AFT SEPARATION LINKS

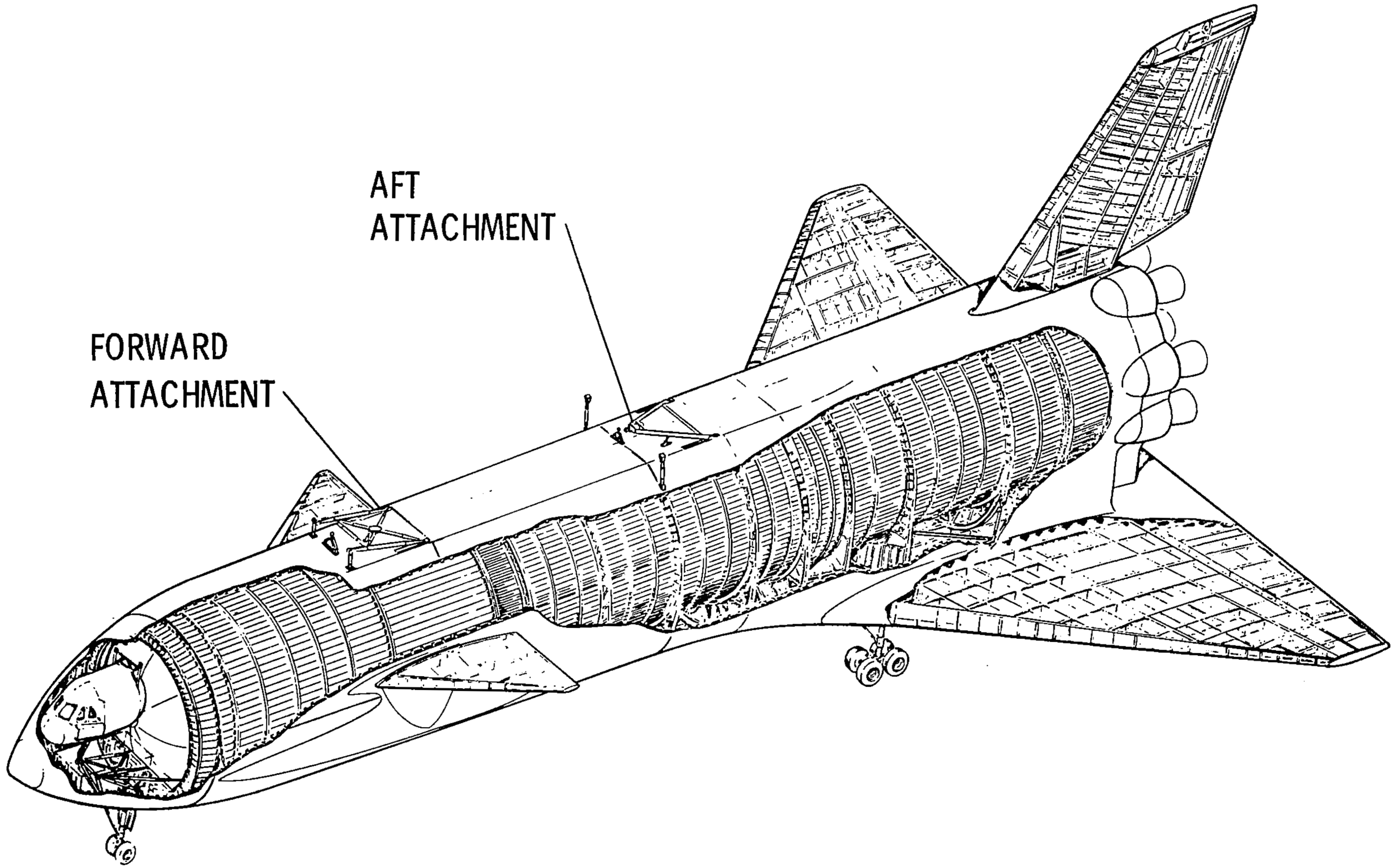

FORWARD LINK ARRANGEMENT

The forward attachments consist of: (1) Frame A, which reacts the total axial load in the mated configuration, reacts side loads, and imparts a transverse acceleration force to the orbiter as it rotates aft during the separation sequence; (2) Link B, which reacts the vertical loads during ascent, a portion of the roll moment, and the vertical component of the axial load; and (3) Fitting C, which reacts side loads during ascent.

Frame A and Link B are pin-jointed. A spherical end located on Fitting C at the centerline of the vehicle fits into a bored hole in the bottom of the orbiter. During ascent, side loads are carried through this fitting directly from the orbiter bulkhead to the booster bulkhead. The spherical end, in conjunction with the fitting pin-jointed to the booster, accommodates misalignments and relative motion between the booster and orbiter.

Spherical bearings at the pin joints of the bulkhead attachments provide the adjustment required to facilitate installation of the links during the mating operation and to compensate for structural deflections during mated flight. Snubber/retractor actuators snub the rotating links after separation has been achieved and retract them to a stowed position.

FORWARD LINK ARRANGEMENT

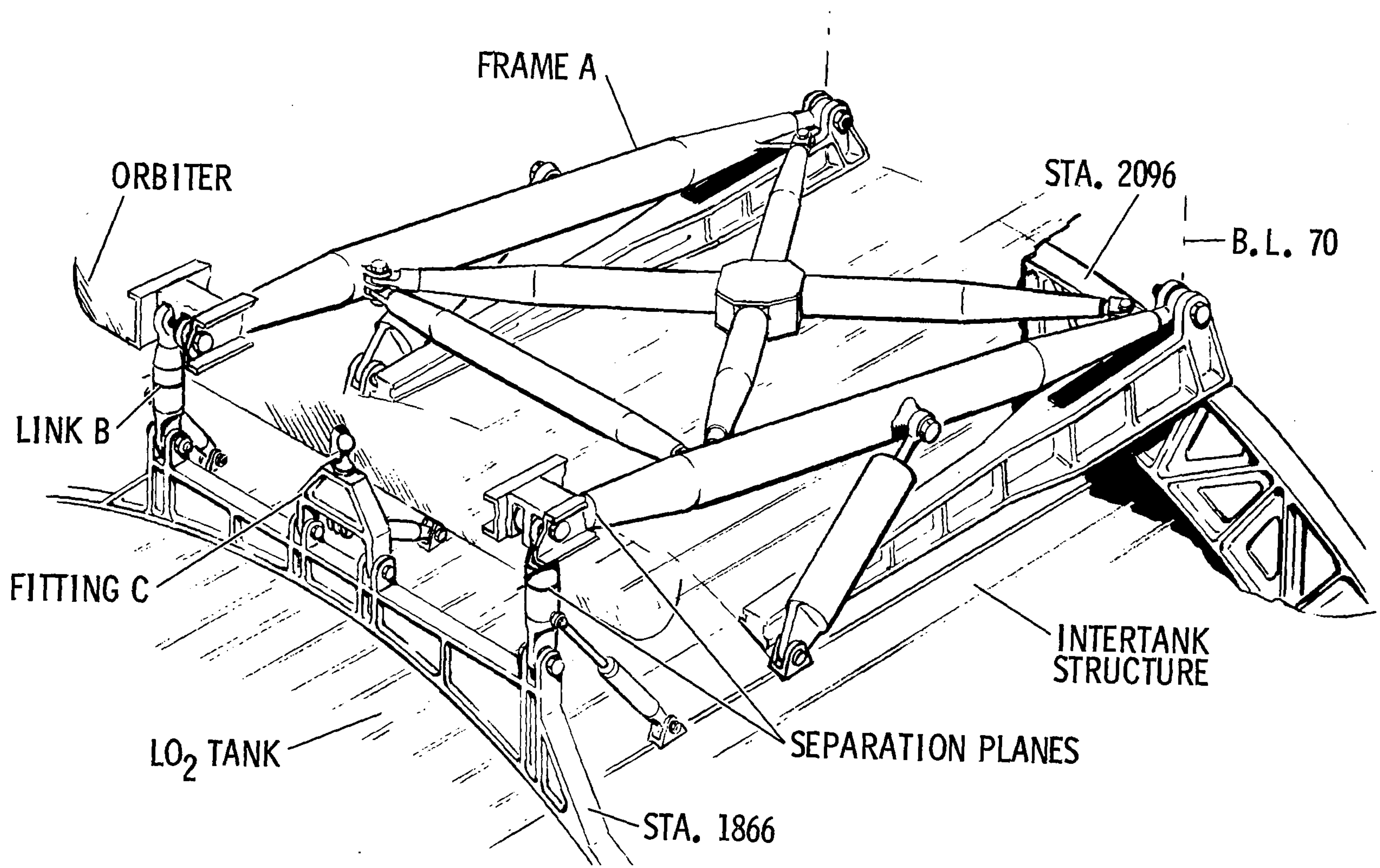

AFT LINK ARRANGEMENT

Aft attachments consist of: (1) Link D, which reacts vertical loads and a portion of the roll moment during ascent; (2) Frame E, which reacts side loads and axial loads as it guides the aft end of the orbiter during separation rotation; (3) Member F, which reacts side loads during ascent; and (4) Expansion Unit G, which accommodates forward/aft thermal expansion and precludes introducing axial loads into Frame E during mated flight. Member D and Frame E are pin-jointed to accommodate differential movement between orbiter and booster due to thermal expansion.

AFT LINK ARRANGEMENT

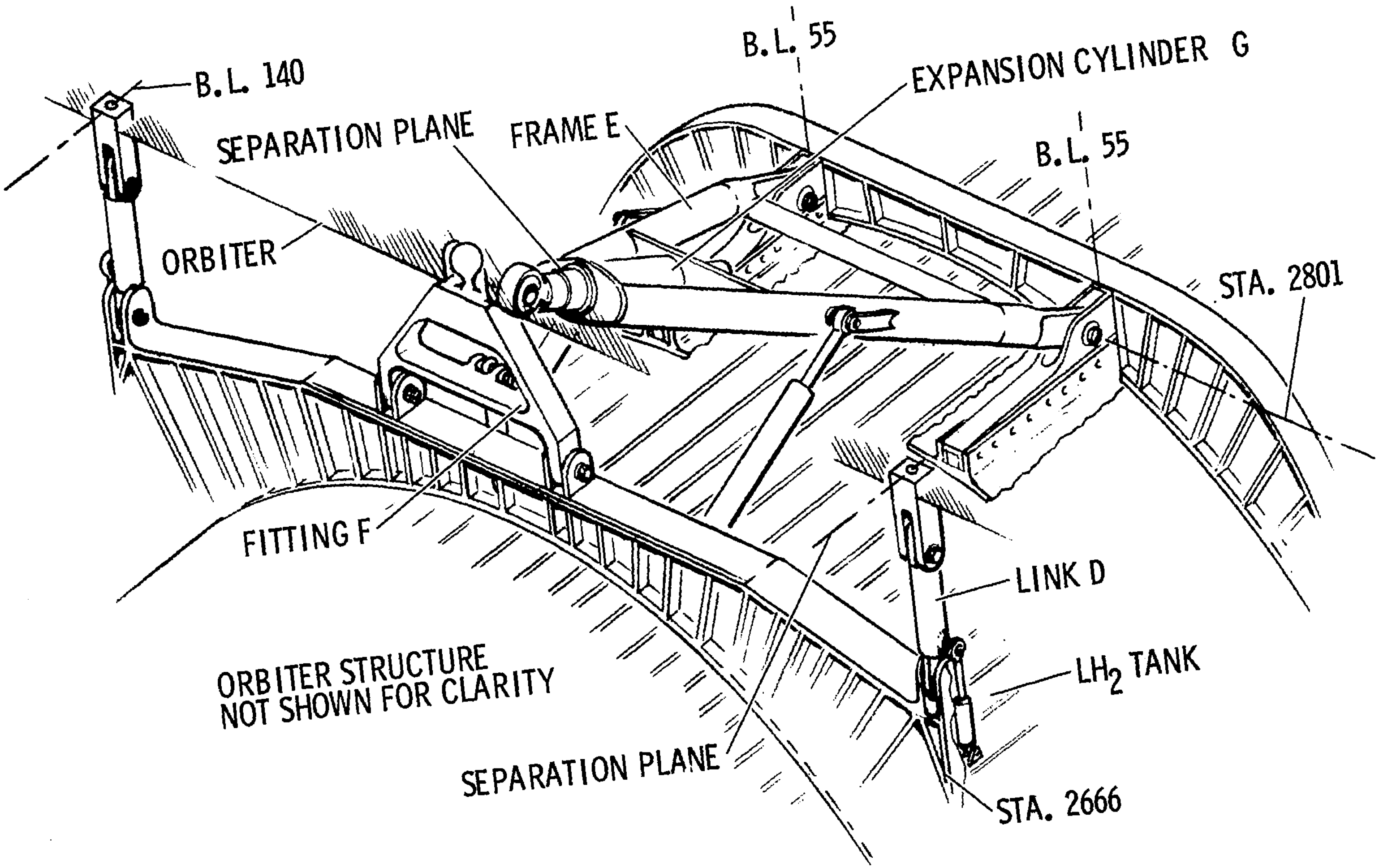

TYPICAL PYROTECHNIC BOLT ARRANGEMENT

Pyrotechnic bolts are used at the vertical connections and between the orbiter and rotating link for separating the orbiter from the booster. These low-shock, energy-absorbing pyrotechnic separation bolts are quite similar to those used on the LEM. The two bolt initiators receive an electrical impulse from the orbiter and/or the booster. All initiators are supplied from independent power sources. When the main charges on each end of the bolt are ignited, the pressure moves the pistons and compresses the rubber, causing a shear failure in a 45-deg. plane on the annular outside diameter at the center of the bolt, creating separation. Redundancy is achieved by providing dual pistons, four main charges, and four initiators. Housings on the attach fittings contain any loose pieces.

TYPICAL PYROTECHNIC BOLT ARRANGEMENT

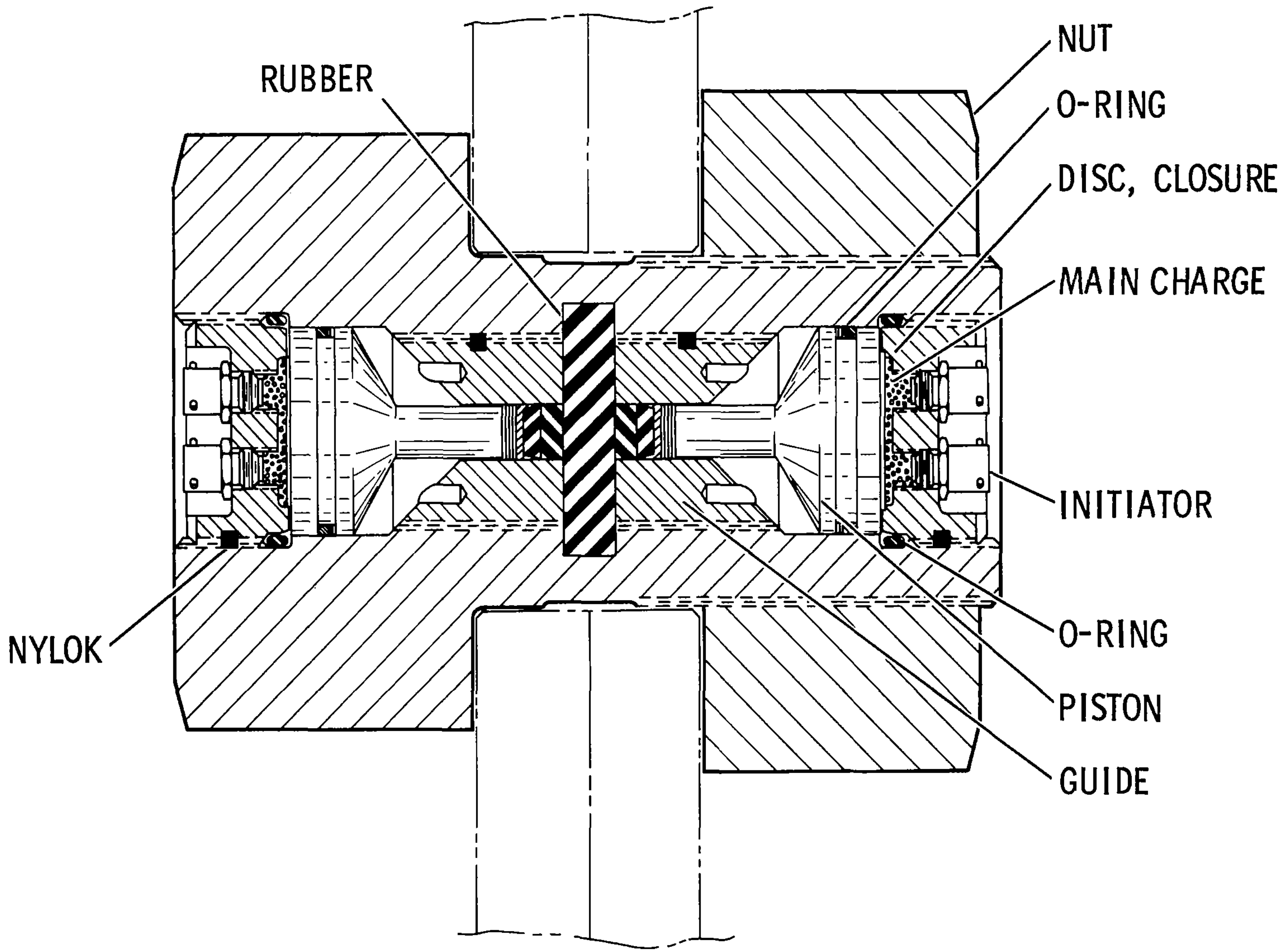

SEPARATION SEQUENCE

The figure shows booster and orbiter sequencing, illustrating the release of the disconnects for normal staging. A signal from the booster propellant depletion sensors initiates throttling of the booster engines to 50% thrust and, concurrently, starts the orbiter engines and brings them to 50% thrust. When the orbiter engines have reached 50% thrust, pyrotechnic bolts on the four vertical members are fired, releasing the vertical restraint of the orbiter. At the same time, the expansion unit in the aft rotating frame is actuated, locking the frame to the orbiter; 0.10 second later, the booster engines are shut off. Axial aft forces acting on the orbiter due to the greater booster thrust rotates the links aft, providing a transverse acceleration to the orbiter. After a 0.50-second time delay, the pyrotechnic bolts restraining the orbiter to the rotating links are fired, freeing the orbiter from the booster. Immediately upon orbiter release, the snubber/retractor actuators are activated and the rotating links are returned and locked into their stowed positions.

SEPARATION SEQUENCE

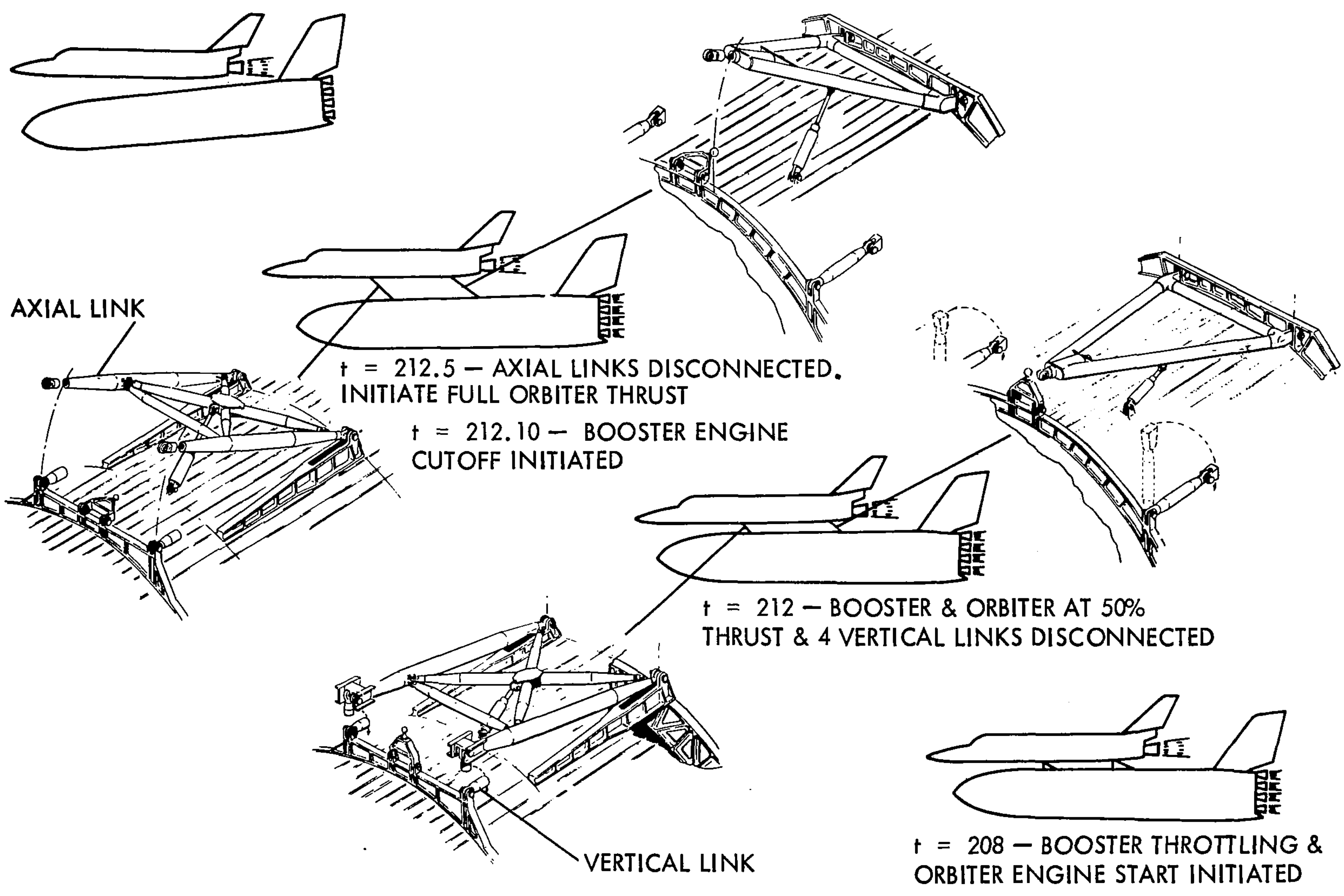

SEPARATION SUBSYSTEM FUNCTIONAL SCHEMATIC

The separation subsystem functional schematic is shown to illustrate the reliability and control interface associated in the separation system sequence. The controller initiates the separation sequence from the LO_2 depletion signal. Redundancy for orbiter and booster separation is ensured by dual separation controllers and subsystems and individual separation bolt planes in both orbiter and booster.

SEPARATION SUBSYSTEM FUNCTIONAL SCHEMATIC

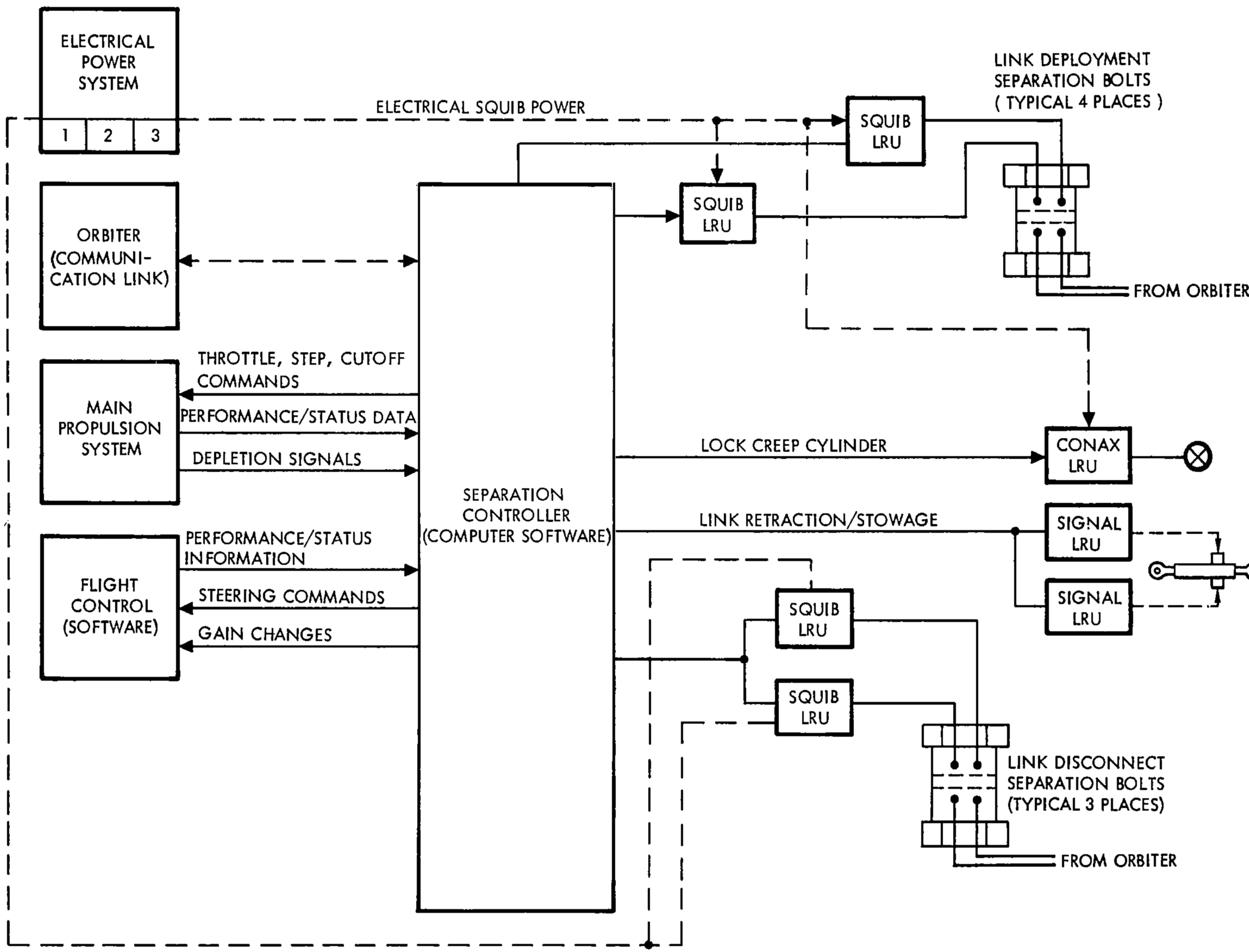

LIQUID OXYGEN DEPLETION SUBSYSTEM

It is at normal staging (and only there) that the booster engines are cut off before separation is complete. An understanding of the booster propellant-depletion system is necessary to an understanding of the separation sequence.

The booster is designed to go into LO_2 depletion 98.4% of the time. The design approach is dictated by the much higher density of LO_2 as compared to LH_2 (about 16 to 1). LH_2 depletion sensors provide a backup to prevent LH_2 starvation; i.e., the LH_2 depletion sensors start the separation sequence 1.6% of the time. Both sensors are wet-dry indicators with response times on the order of one millisecond. A discussion of the LO_2 depletion subsystem will suffice to describe them both.

This figure illustrates the operation of the LH_2 depletion subsystem from the point of initial breakthrough through thrust termination. The depletion or "shutdown commit" sensors are located in the supply ducts sufficiently downstream to allow settling of the two-phase layer developed during breakthrough. These same sensors initiate the stage separation sequence and must be located sufficiently upstream to allow time to start the orbiter engines before separation. As now envisioned, each of four supply ducts will contain a five-element vertically oriented rake and associated remote electronics. Each element will give a "Wet" indication when covered and a "Dry" indication together with a Time Code indication at the instant they become uncovered. The individual response from each element will provide an accurate prediction of the true point of depletion, enabling compensation if required (adaptability – a reliability consideration). The predominate failure mode of the sensors is Wet; by voting, any two Dry indications together with any two lines will initiate the separation sequence and controlled shutdown. If necessary (e.g., orbiter engines Ignition Complete signal delay), the engines can thrust to LO_2 starvation without jeopardizing the mission or vehicle; however, the engines may have to undergo overhaul upon vehicle recovery.

LIQUID OXYGEN DEPLETION SUBSYSTEM

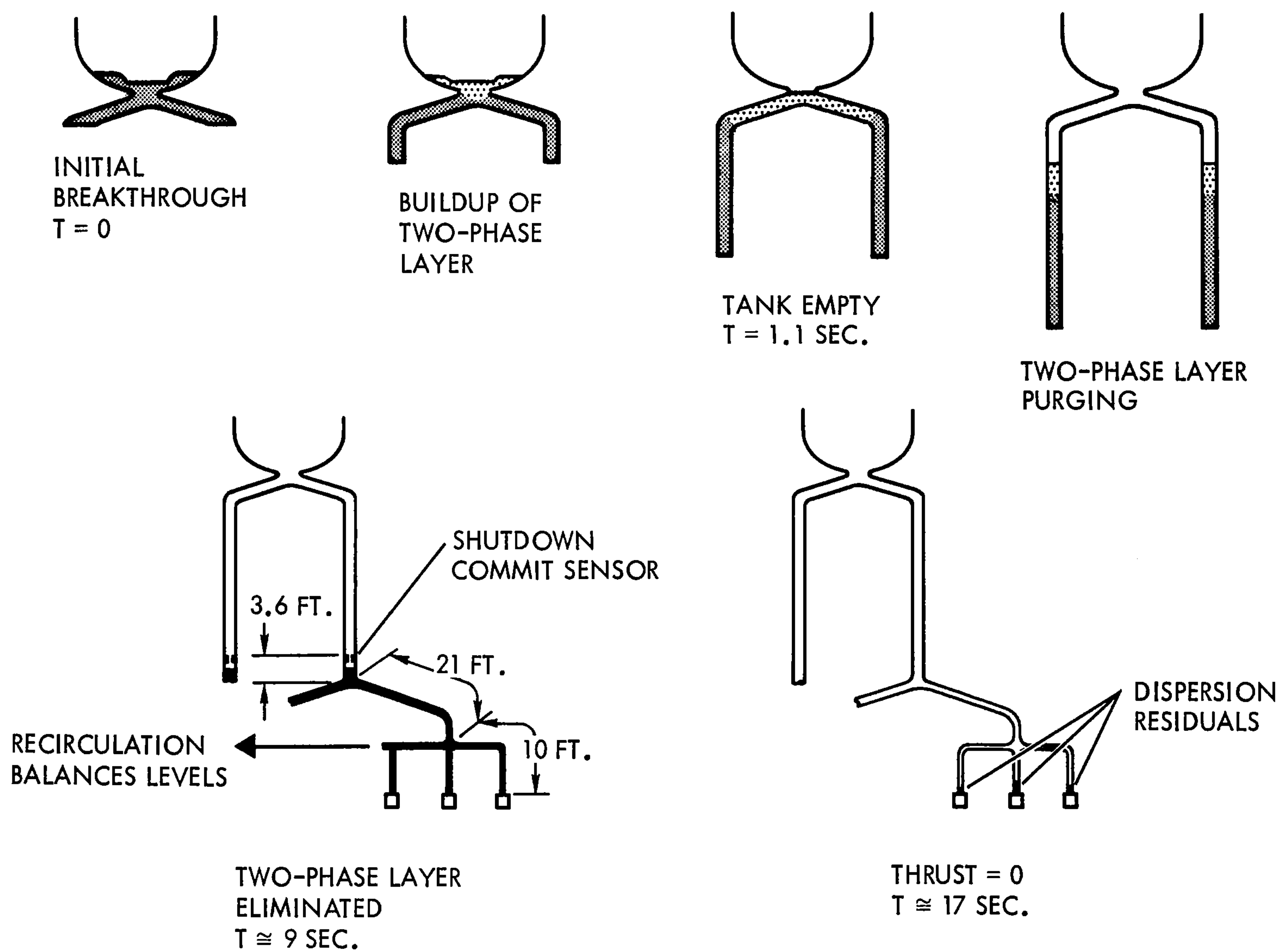

NORMAL STAGING SEQUENCING, TWO ORBITER ENGINES

The normal staging booster and orbiter thrust sequencing is shown. The separation sequence is initiated at 208.5 seconds by a signal from the propellant depletion system. At this time, the booster staircase steps to 50% thrust (minimum power level, MPL) as the orbiter engines are ignited and build up thrust. At 210.5 seconds, an Ignition Complete signal is received from the two orbiter engines. The booster reaches MPL (50% thrust) at 211.5 seconds and is held until BECO. The orbiter engines have been accelerating to MPL (50%) and hold at 212 seconds. Motion of the links is now initiated by activation of the pyrotechnic separation bolts on all four of the vertical attachment members and the orbiter is held at MPL (50%) until 212.5 seconds. The orbiter is held at this plateau to allow equalization of engine thrust at separation to minimize the following.

THRUST CONTROL EFFECTS – While there is motion on the links and without equallizing dwell, the thrust differential could be 100%. This would certainly tend to increase the plume pressure across the vertical stabilizer, which would introduce roll of the booster and additional side loads during separation.

PLUME IMPINGEMENT – The plateau at orbiter MPL thrust reduces the time of exposure of the vertical stabilizer at 100% orbiter thrust by 50%. To remove this plateau would definitely result in a weight increase, as the leading edge of the vertical stabilizer is designed by normal staging.

TRAJECTORY DEGRADATION – The differential in actual and assumed orbiter thrust without the dwell would have considerable effect on the orbiter trajectory as shown in the engine ICD: 50% thrust can be achieved in 2.4 to 4.4 seconds; 100% thrust can be achieved in 3.2 to 4.9 seconds. The effect would be especially felt with only one orbiter engine operative. Presently, the trajectories for one and two engines are quite similar and acceptable but because of the tolerance band the sequence for both would have to be different. They are currently identical except for removal of the 0.5-sec. dwell.

At 212.1 seconds, BECO occurs and at 212.5 seconds the vehicles are separated by a signal to the three remaining separation bolts in the axial links. The orbiter then accelerates to 100% thrust (normal power level or NPL) and holds to achieve maximum clearance and minimize coast. By 213.5 seconds, booster thrust is essentially zero.

NORMAL STAGING SEQUENCING, TWO ORBITER ENGINES

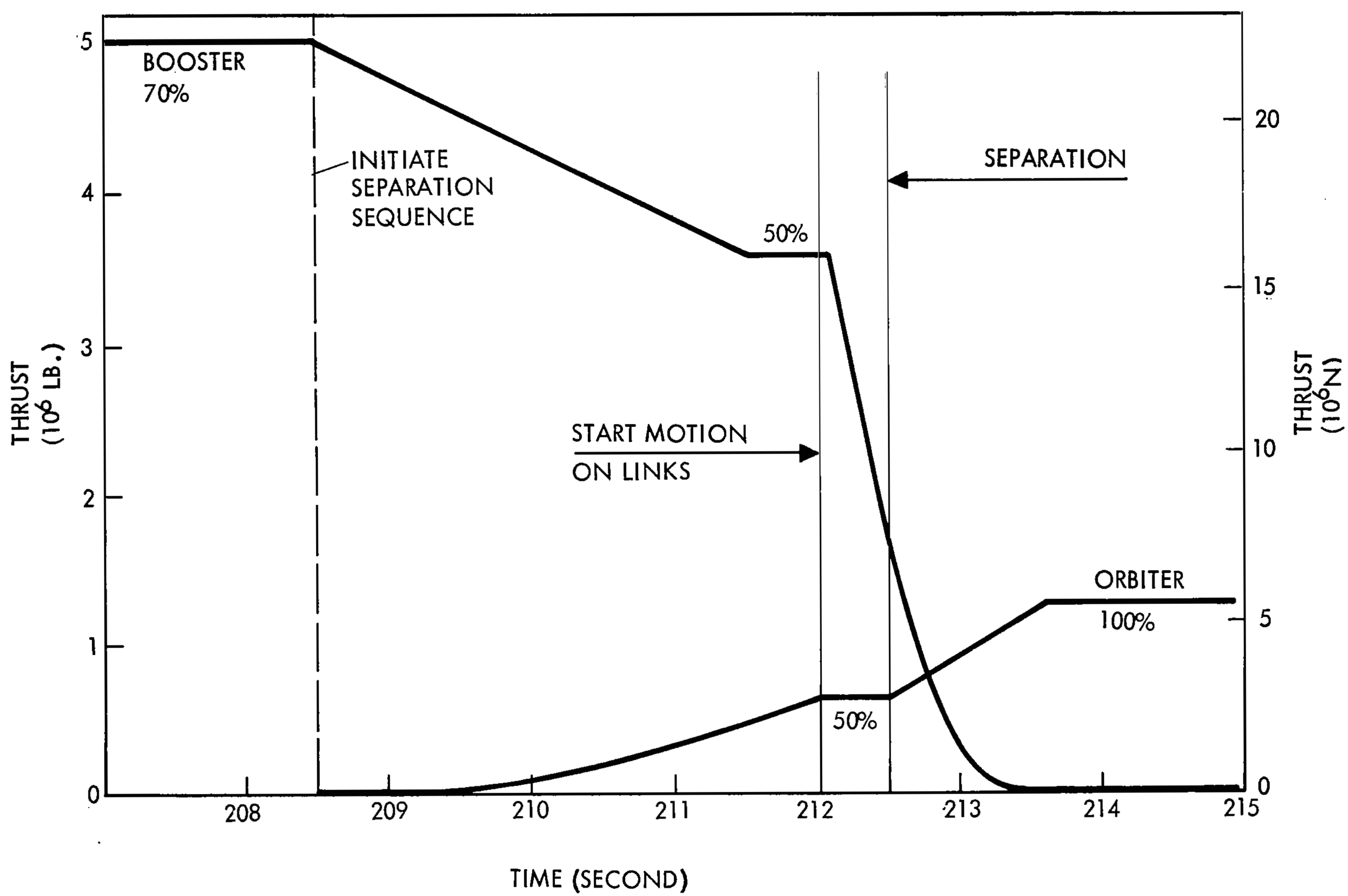

ABORT SEPARATION CAPABILITY, AN ASSESSMENT

Specific tasks associated with the abort trade studies as they related to the separation system were:

1. Determine the capability of the baseline linkage system for immediate stage separation at any time during mated ascent. Define limitations and constraints.
2. Determine the capability of both the booster and orbiter to maintain control and limit environmental loads to a safe level following immediate stage separation.
3. Determine the capability to immediately separate under conditions of loss of booster thrust including the (highly unlikely) total loss of booster thrust. Assess warning time, thrust decay characteristics, and desirability of immediate separation.
4. Determine the capability of the baseline linkage system to provide stage separation and orbiter flyaway while the booster remains on the pad.
5. Define system modifications and weight penalties (if any) associated with providing immediate stage separation capability from pre-liftoff through normal staging.

This figure illustrates the five investigative regions: pad flyaway, post-liftoff, maximum q, pre-BECO, and BECO (booster engine cutoff). Shown on this figure are the achieved separation trajectories.

SEPARATION TRAJECTORY ENVELOPE

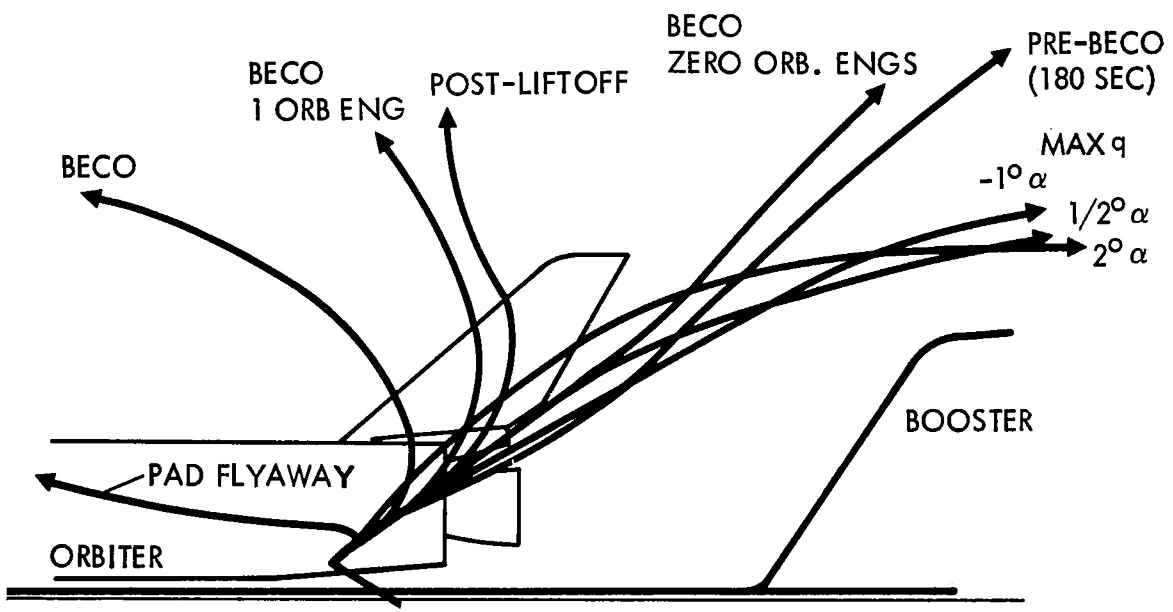

SEPARATION DISTANCE AT BECO WITH 1 OR 2 ORBITER ENGINES FUNCTIONING

Abort separation at normal staging is basically a condition where one or both orbiter engines are not functioning; this is generally not known until after the separation sequence has begun. For this purpose, the orbiter engine transmits a Ignition Complete signal to the Data Control Management (DCM) computer two seconds after the start of the separation sequence. This signal specifies that two, one, or zero orbiter engines have started; it occurs at 210.5 seconds. The figure shows the separation achieved when one or two orbiter engines are functioning, thereby creating maximum vehicle separation in the least amount of time. (This figure is in a coordinate frame fixed to the booster.)

SEPARATION DISTANCE AT BECO WITH 1 OR 2 ORBITER ENGINES FUNCTIONG

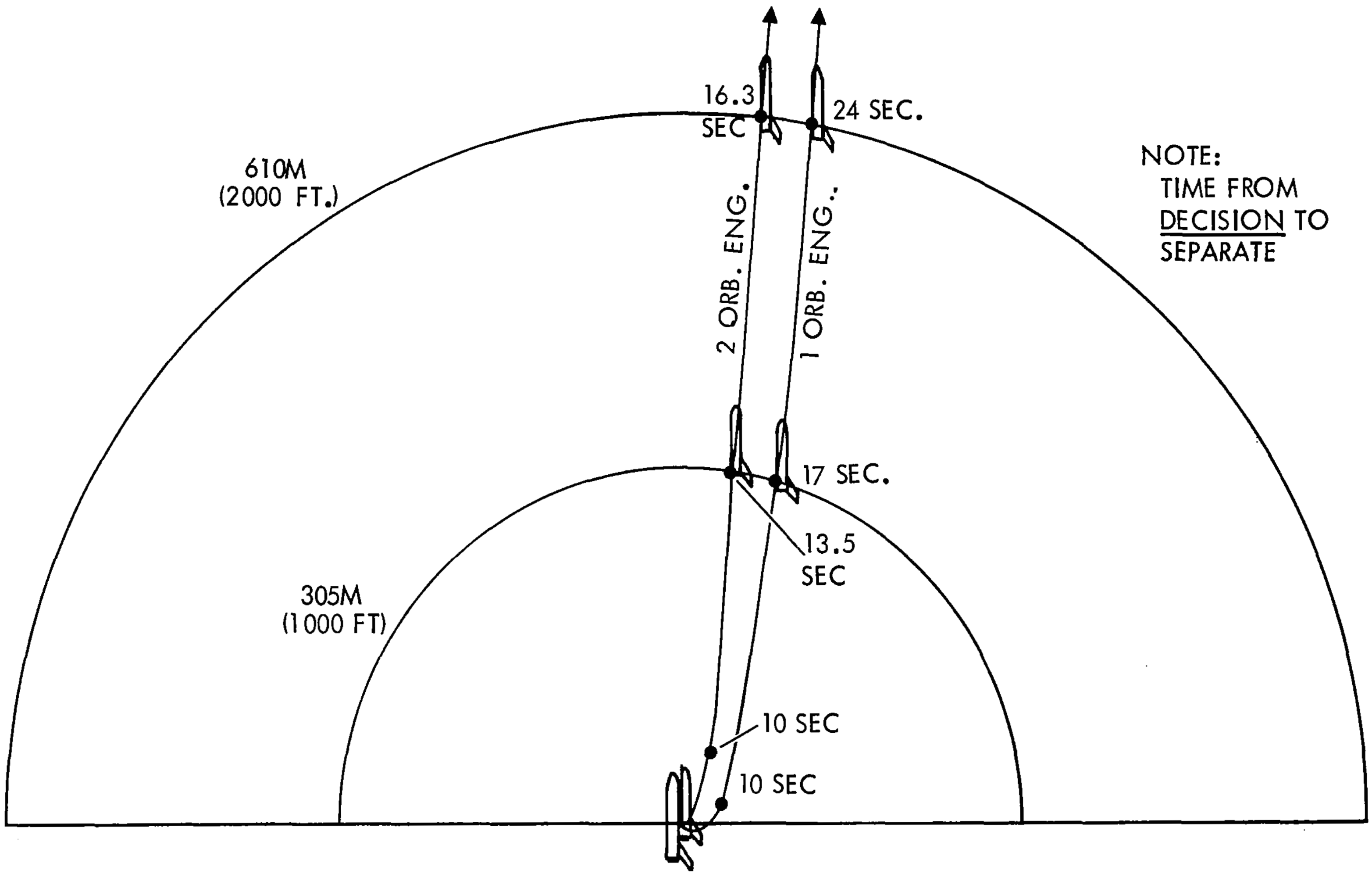

TRAJECTORIES AT BECO, ONE ORBITER ENGINE

The sequence and trajectory shown with one orbiter engine is similar to normal separation with one basic exception; the orbiter engine dwell for 0.5 second at 212.0 seconds is bypassed and the engine is accelerated to NPL (100% thrust). This produces a separation trajectory with maximum clearance similar to that for normal staging. The BECO tolerance band is shown at +0.03 second, with little effect on the trajectory.

The trajectory for one orbiter engine operation is shown both with and without the effect of the orbiter plume. As the engine moves aft and passes close to the booster vertical tail, a very large turning moment is created as the tail acts like a sail, causing the booster to heel over and build up large booster residual rates following disconnect. As shown the change in the vertical trajectory is minor but the booster residual roll rate has increased from a negligible value (for nominal separation) to more than 4.5 deg. per second. Although the booster ACPS is sized to handle these residual rates adequately, some slight additional propellant margin will be required to offset this condition.

TRAJECTORIES AT BECO, ONE ORBITER ENGINE

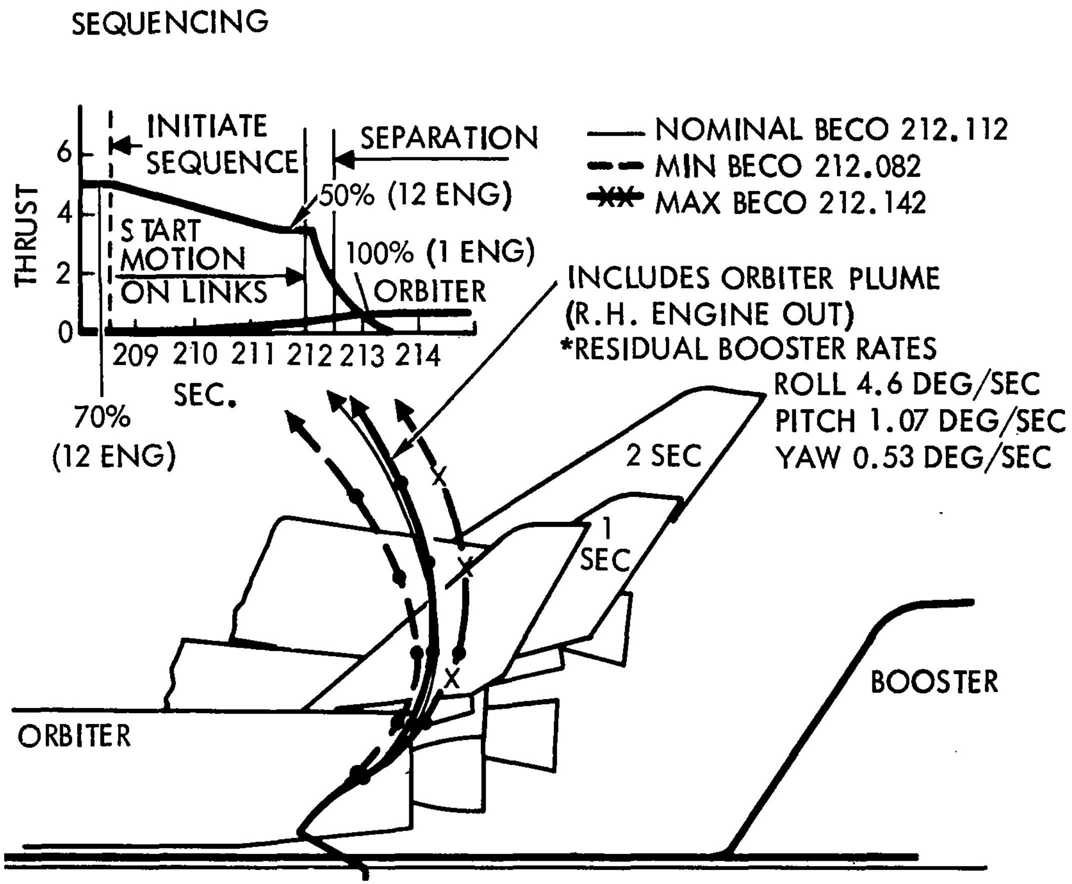

*HAND CALCULATED

PITCH RATE AND ATTITUDE AT BECO, ONE ORBITER ENGINE

The guidance command shown is identical to normal staging for the booster but is changed slightly for the orbiter at separation to aid separation clearance and minimize orbiter control system overshoots.

PITCH RATE & ATTITUDE AT BECO, ONE ORBITER ENGINE

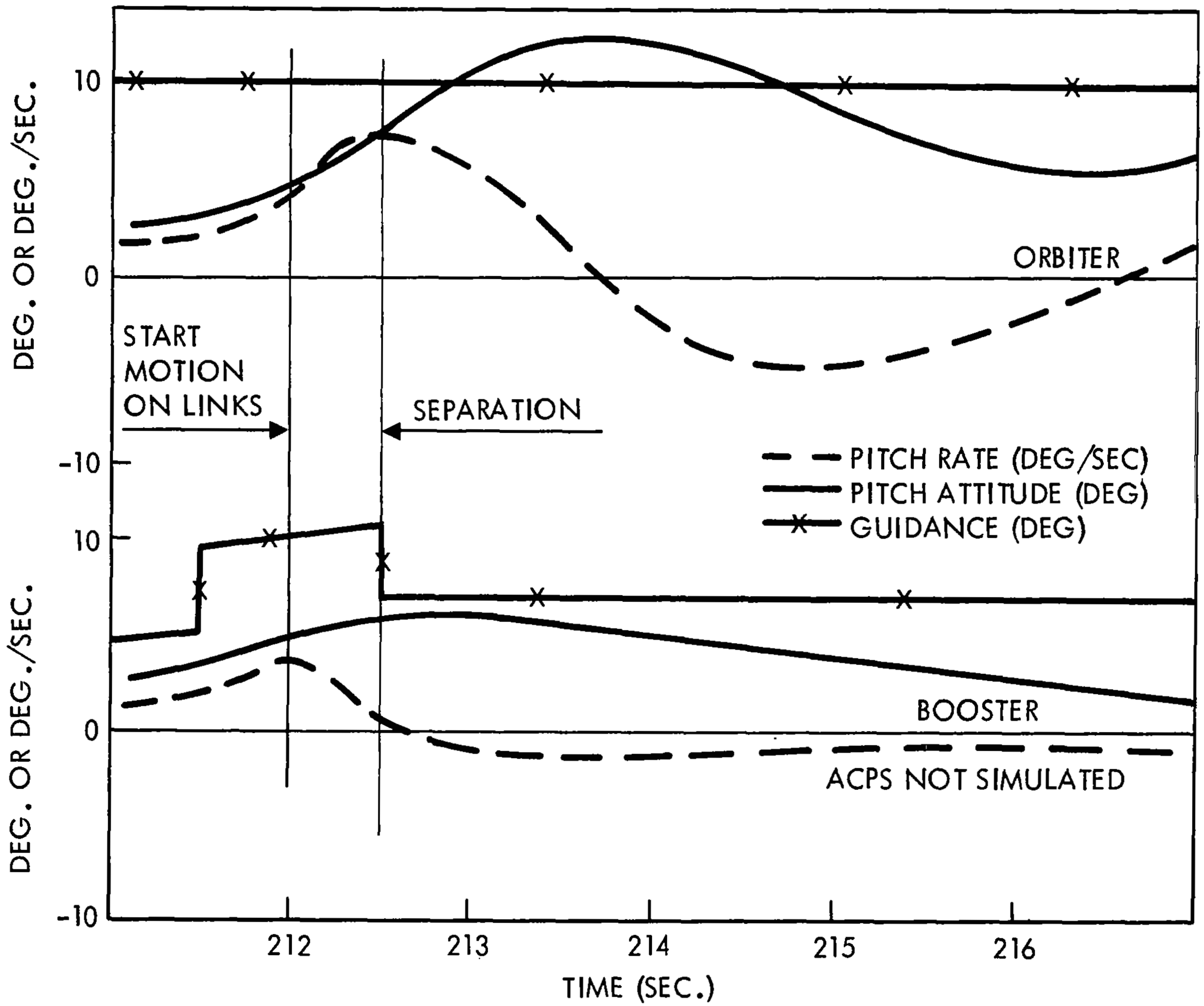

TRAJECTORIES AT BECO, ZERO ORBITER ENGINES

The two-orbiter-engine-out condition is shown. When the No Engines Operative signal is received from the orbiter at 210.5 seconds, four booster engines are automatically shut down, the remaining eight engines are stepped to MPL (50% thrust), and normal sequencing occurs. The trajectories for all conditions are shown with slight upward curvature; this is due to the controls and guidance introduced in the booster. Before start of motion on the links, the guidance is the same as normal, but at this point a hard-over, nose-up gimbal command is introduced into the booster engine control system. This command creates a pitch-up attitude in both vehicles and improves tail clearance. The booster then proceeds into normal recovery. The orbiter ignites its orbit maneuvering system (OMS) engines and further attempts ignition of its main propulsion engines. Failure to achieve main engine ignition will result in loss of the orbiter.

TRAJECTORIES AT BECO, ZERO ORBITER ENGINES

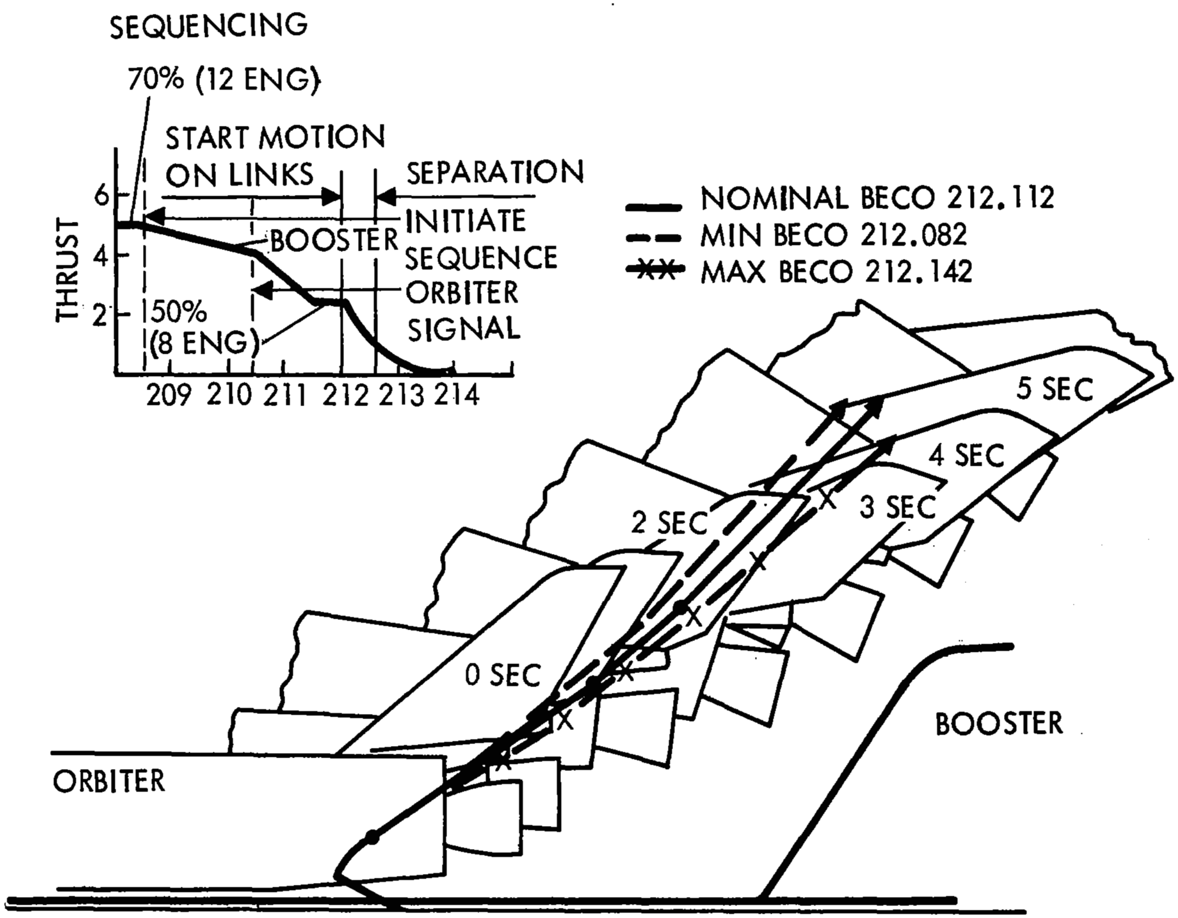

TRAJECTORIES AT ABORT, t = 180 SEC., TWO ORBITER ENGINES

Pre-BECO separation offers many interesting conditions not common to any other area in the trajectory. First, the orbiter is at the point of no return and must proceed once around to continental United States for recovery. The booster cannot go into BECO due to the residual propellants that must be used up, as the booster has no dump capability and cannot land with substantial residuals. The booster, being relatively light at this time with high thrust, must shut off engines and step the remaining engines to MPL (50%) in order not to exceed the 3g design axial limit on the booster. (This means automatic loss of the engine bell due to overheating caused by surrounding engines firing in the near proximity.) It is quite obvious that maximum separation distance can be achieved by using the booster 3g capability.

Four of the booster's twelve engines are shut down before motion on the links. The orbiter engines are locked at a 3-deg. nose-up attitude (nearly on the center of gravity) before and for 10 seconds after start of motion of the links. The booster is preprogrammed for 2 deg./sec. pitch rate to attain a 4-deg. nose-up attitude before motion on the links, then a hard 10-deg. nose-up command during and after motion on the links.

TRAJECTORIES AT ABORT, t = 180 SEC., TWO ORBITER ENGINES

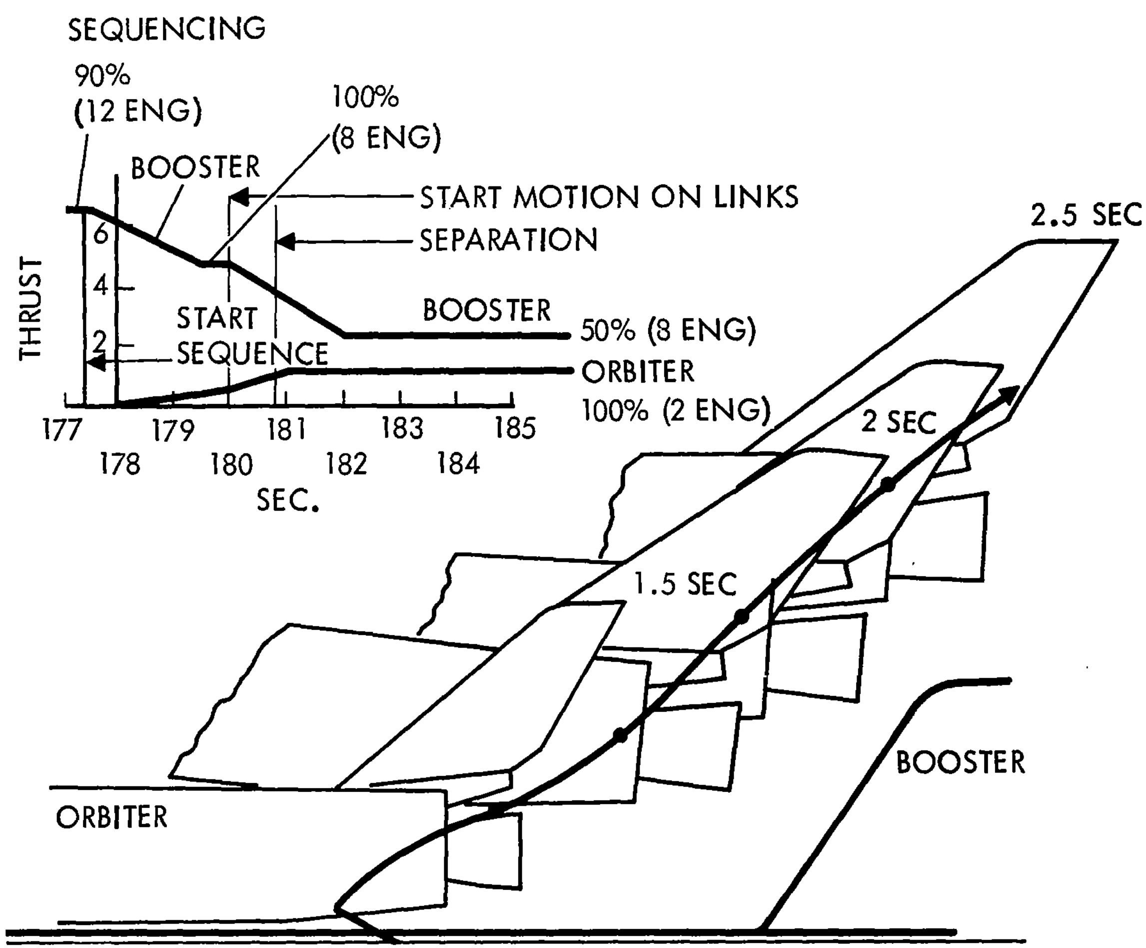

HISTORY OF ANGLE OF ATTACK BEFORE SEPARATION

Maximum aerodynamic conditions set for the current mission trajectory were established as $q_{max.} = 560$ psf with an angle of attack +5 deg. for headwinds and $q_{max.} = 470$ psf with an angle of attack of -6 deg. for tailwinds. Using this data, simulations were made for abort separation at these conditions – separation was not successful. The design limit of $|\alpha q| \leq 2{,}800$ psf-deg. was exceeded for both headwinds and tailwinds.

An examination was then made of the angle of attack history in the region of maximum q (80 seconds). Simulation studies using load-relief-type logic had demonstrated that the angle of attack could be held at any commanded low value ±1.5 deg. This uncertainty resulted from the dynamic lag of the booster/orbiter cluster in response to wind shears and gusts (prevalent in this altitude region) plus the uncertainties associated with onboard measurement of angle of attack. Using the indicated $\pm 3\sigma$ tolerance band, a spectrum of simulations was made and successful separation was achieved for conditions of angle of attack from -1 through +2 deg. Using this data, the sequence and limitations were established as follows.

An abort command is actuated (e.g., by the crew). This then sends a control command to the DCM computer which will supply a new trajectory for the cluster; i.e., to hold at +0.5 deg. alpha and 0 deg. beta (centerline of booster to the relative velocity vector). Alpha, beta, and dynamic pressure can be computed from trajectory (guidance) information in the DCM computer or be determined using the air data sensors on the nose of both the orbiter and booster. The computation from trajectory information is likely to yield more accurate steady-state values, whereas the air data sensors will yield superior rate of change ($\dot{\alpha}$ and $\dot{\beta}$) values necessary to provide anticipatory and damping signal components.

The derived reorientation command will correct within two seconds of initiation, during which the orbiter engines are ignited. After separation, guidance will command new trajectories to both vehicles to maximize clearance in minimum time, while maintaining vehicle loading with design limits. The maximum q abort shows a capability of 610 meters (2,000 feet) of separation in 13.1 seconds from the point of decision to abort.

HISTORY OF ANGLE OF ATTACK BEFORE SEPARATION

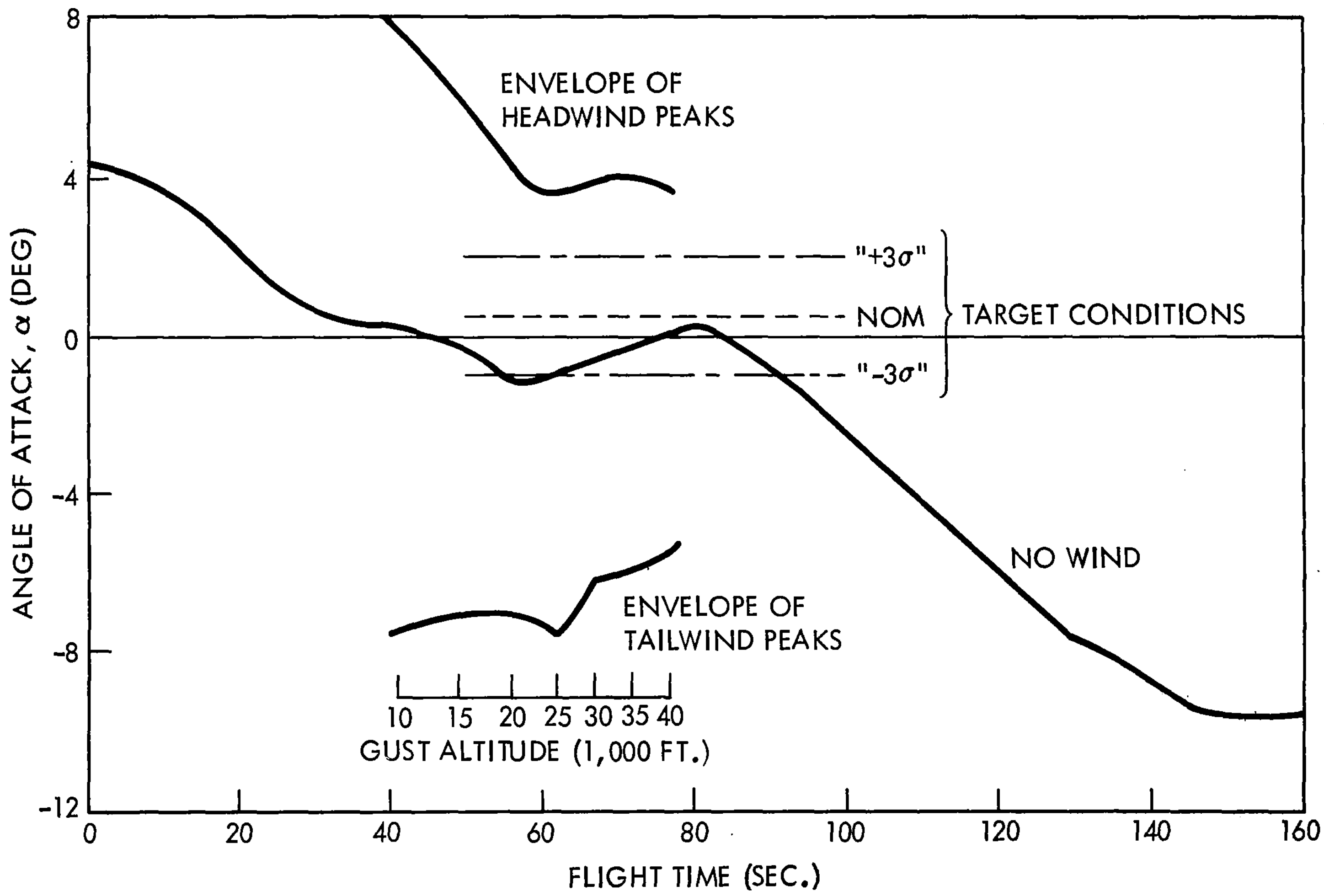

TRAJECTORY AT ABORT, TWO ORBITER ENGINES

The maximum q separation sequence is similar to the pre-BECO conditions. Booster thrust is stepped to near MPL (50%) from NPL (100%) at the start of motion on the links. The 100% thrust at the beginning is required to supply the maximum vertical separation to the system; the reduction of thrust to 55% slows the booster to further improve the separation trajectory. Finally, the booster is stepped back to NPL (100% thrust) to maximize vehicle separation versus time.

The orbiter thrust is built up to MPL (50%) at separation and held. An increase in orbiter thrust to NPL (100%) at this time creates a slower separation in the critical region of maximum interference aerodynamics.

The one- and two-orbiter-engine-out conditions at maximum q separation indicated little or no change in the separation trajectory due to orbiter thrust (or lack of it).

TRAJECTORY AT ABORT, MAX. q, - 0.5-DEG. α, TWO ORBITER ENGINES

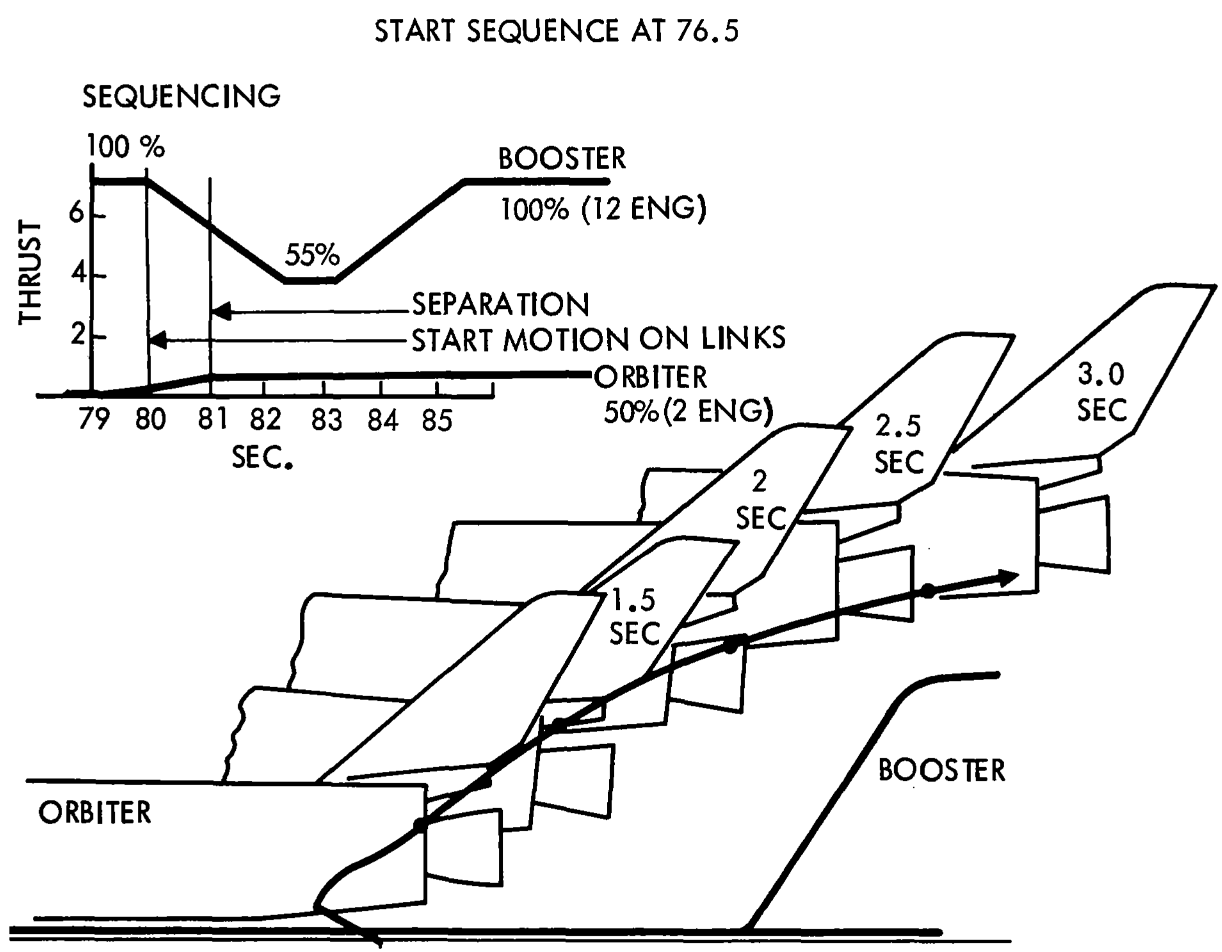

PITCH RATE AND ATTITUDE AT ABORT, TWO ORBITER ENGINES

Shown is the pitch rate and attitude during separation for both the orbiter and booster at 0.5-deg. alpha. The only guidance input is in the orbiter in the form of the engines locked at the nose-up pitch gimbal limits; this is required if any orbiter thrust is used. The pitch rate and attitude of the vehicles show a complementary trend with a very stable booster at a low pitch angle. The orbiter also shows a relatively low pitch angle and acceptable pitch rate with a pronounced oscillatory effect at approximately 3.0-second intervals. This oscillatory response is more evident where the orbiter attitude is directly related to α and q, to produce the high alpha-q conditions. High alpha-q is required for effective separation; it is a combination of this and the booster thrust effect that produces acceptable separation trajectories. However, care must be taken to ensure that the response does not exceed the αq design limits of the wings.

PITCH RATE AND ATTITUDE AT ABORT, MAXIMUM q, 0.5-DEG. α, 2 ORBITER ENGINES

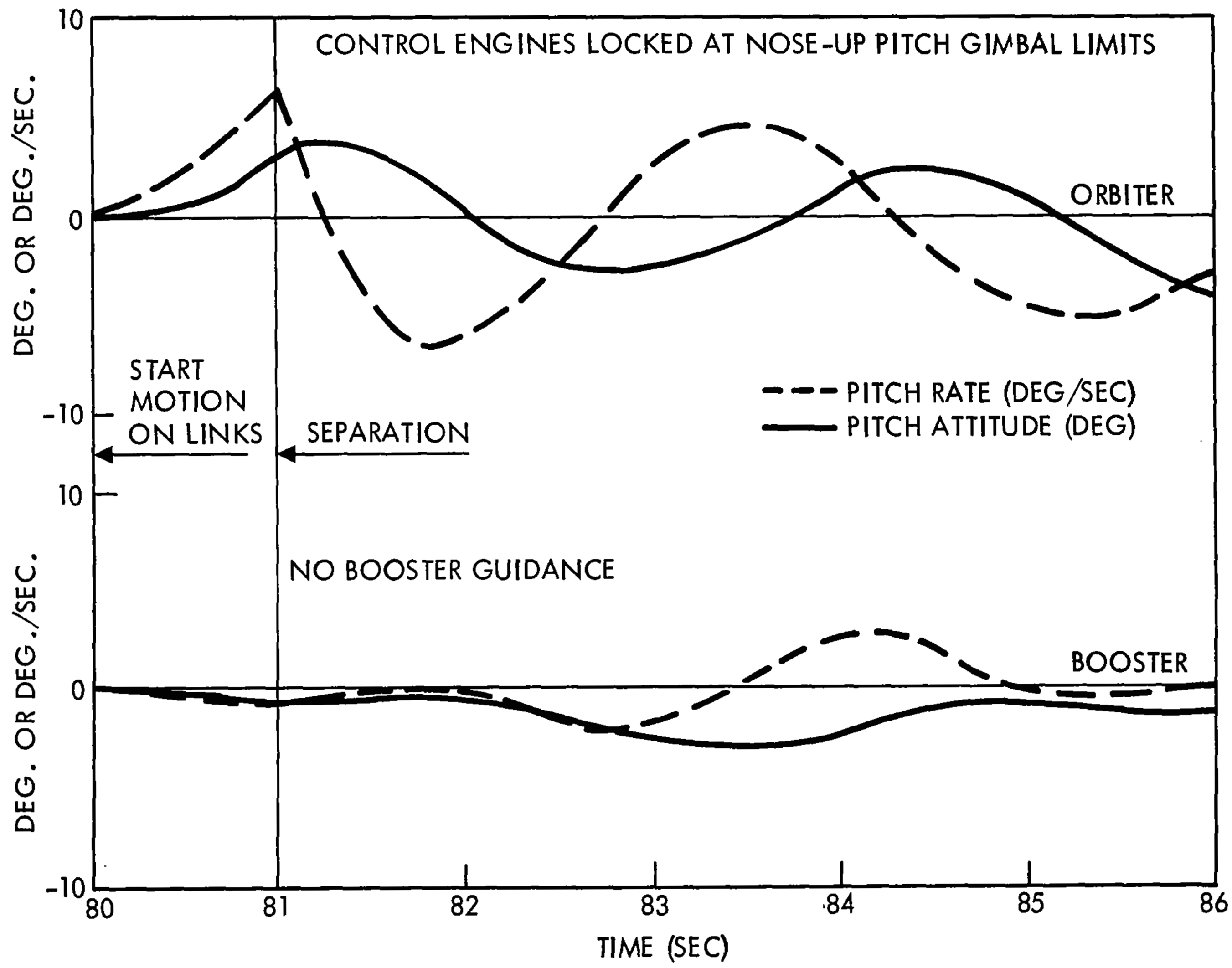

VARIATION OF αq at MAX. q

This figure summarizes αq histories as a function of flight time for the maximum q abort condition. Except for the +2-deg. α (angle of attack) case, the αq histories are well within the design limit. The +2-deg. α case is the design condition, with the orbiter reaching the limit at release and the booster slightly exceeding the limit on the first overshoot following release. Although it appears that biasing the angles of attack by a small amount negatively might balance the αq histories better, difficulty was encountered getting the linkage system under investigation to separate with angles of attack much below-1 deg.

VARIATION OF αq AT MAX q

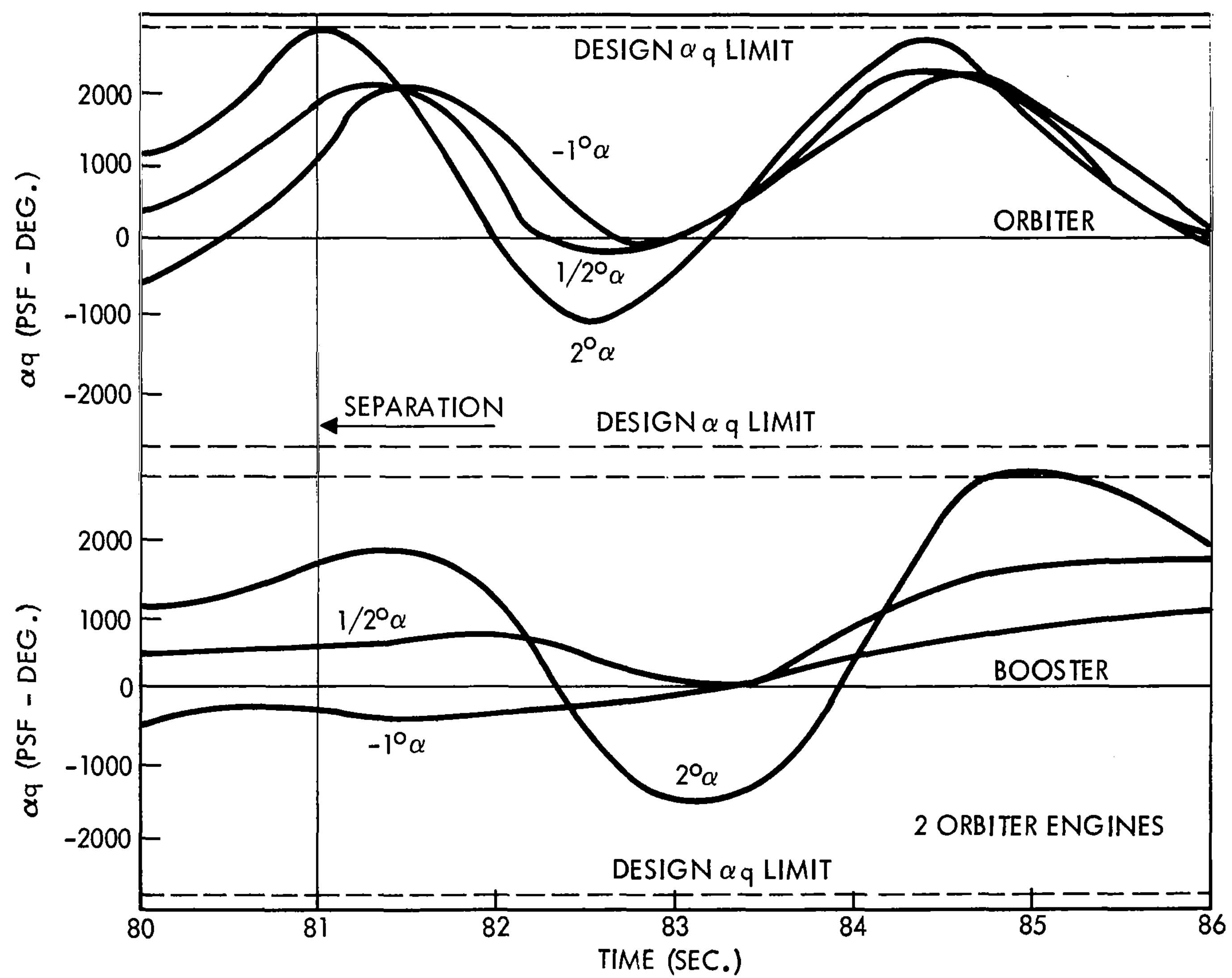

TRAJECTORY AT ABORT, OPTIONAL SEQUENCE

An optional sequence at maximum q is shown. This run was made only for 0.5-deg. α, and is merely meant to show flexibility at maximum q. This particular separation offers slightly lower load at separation and excellent tail clearance by comparison, but it has inherent disadvantages such as shutoff of four booster engines, reducing the attained distance versus time as shown in the figure. It also about doubles the time in close proximity during the crucial high aerodynamic interference region, again directly affecting the distance versus time separation between vehicles. For these reasons, the optional sequence is not recommended.

TRAJECTORY AT ABORT, MAX q, 0.5-DEG. α OPTIONAL SEQUENCE

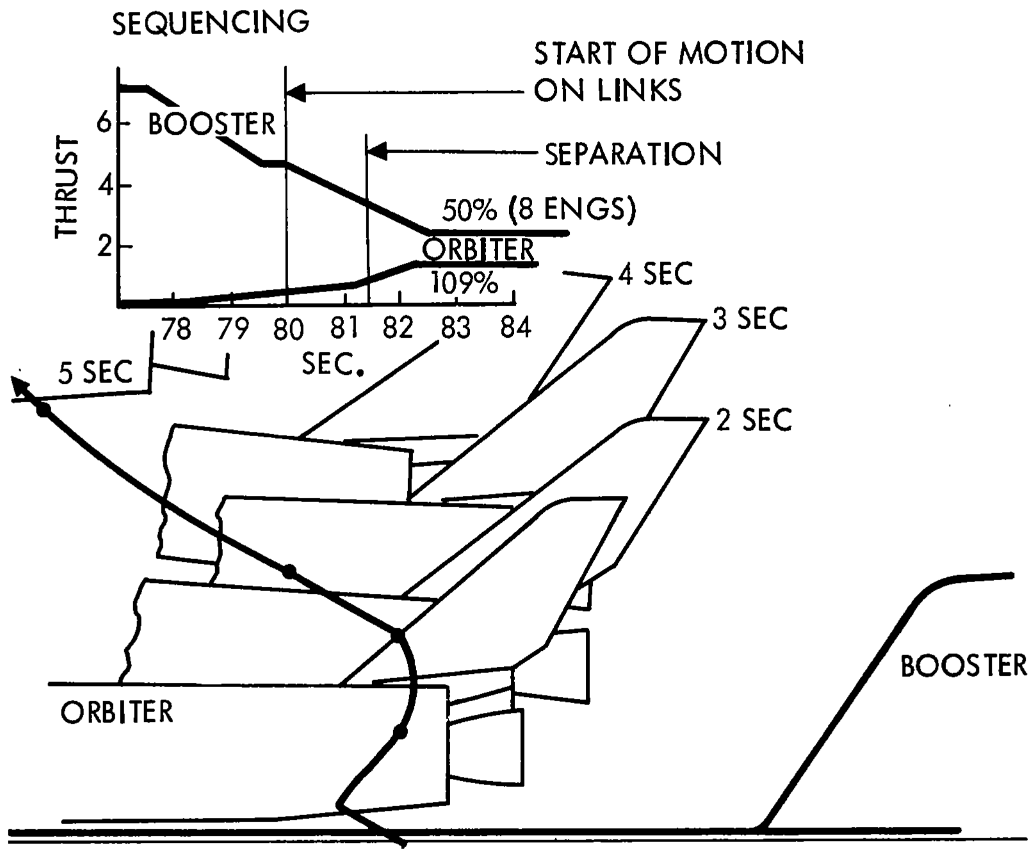

POST-LIFTOFF TRAJECTORY, TWO ORBITER ENGINES

The post-liftoff abort starts the motion on the links at 12 seconds after liftoff. The relative displacement of the vehicles versus time is shown. Advantage is taken at this point of the low dynamic pressure environment to obtain as much lateral displacement as possible to maximize vehicle separation. This is accomplished by guidance to obtain a 30-deg. relative attitude of both vehicles, using maximum thrust available until aerodynamic loading limits are attained.

Sequencing of the post-liftoff separation is similar to maximum q except that maximum available thrust of 109% (EPL, emergency power level) is used on both vehicles during and after sequencing. Maximum power can be used at separation because of the low q; both sequencing and the trajectory are shown.

The trajectory has good tail-clearance characteristics, but definitely has longer than normal tail plume heating during the separation. With atmospheric density high at this time, the plume will also be more concentrated (focused) than at normal staging and will adversely affect heating on the booster vertical tail.

The pitch rate and attitude indicate a very stable booster and a well-controlled orbiter, with the orbiter already responding to its preprogrammed 30-deg. attitude reorientation for the maximum distance versus time sequence. The oscillatory response of the orbiter is still obvious, but is not of concern at this low q.

POST-LIFTOFF TRAJECTORY, TWO ORBITER ENGINES

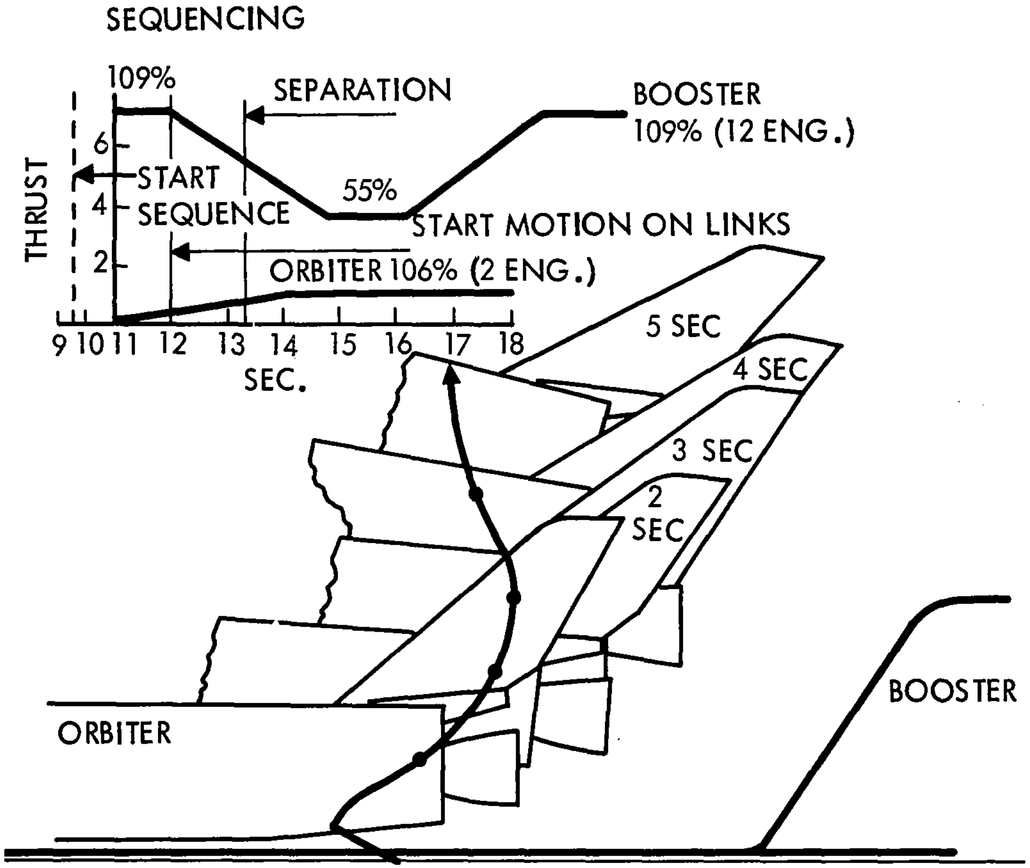

PAD FLYAWAY OF ORBITER

If there is a major system failure while the vehicles are on the pad, it is highly desirable to separate the Space Shuttle stages and fly the undamaged stage to safety. A major system failure, as used here, is a failure so serious as to assess the risk of explosion of one or the other stages as likely and eminent. Examples of such failures would be a major plumbing rupture in the engine compartment leading to a major fire, an engine explosion leading to potential secondary explosions and a major fire, or a chronic fire condition that cannot be controlled, leading to eventual stage destruction.

After initial measures to control the situation, the next best remedy is to get the system airborne and effect inflight stage separation, gaining the maximum lateral displacement per unit time (to mitigate the explosion hazard) and eventually recovering the undamaged stage (or both stages if conditions are favorable). However, it is recognized that the booster element is the most likely to sustain damage before lift off. Further, this is most likely to occur at engine ignition (which can best be described as a series of controlled explosions). In this event, it may be more prudent to initiate immediate engine cutoff and attempt to control the resulting fire (or fire potential). If fire control fails, subsequent engine ignition is probably undesirable (even if possible), and some means of flying the orbiter away from the incapacitated booster is desired.

The optimal stage separation sequence is as follows. The booster is not thrusting and an explosion is presumed inevitable. The orbiter ignites its engines and achieves a thrust level somewhat below one q earth relative. The linkage system is released for deployment and the orbiter moves out along the linkage trajectory arc under control of the orbiter engines, which are being throttled (for rate of deployment control) but not gimbaled (to prevent a feedback instability, since the orbiter rotational motions are fully constrained). At the appropriate time, the links are disconnected and the linkage system stowed; substantial clearance is thus obtained between the orbiter and the disconnected links in a fraction of a second. The orbiter engines are then gimbaled and stepped to their emergency power level (EPL or 109% thrust), and the orbiter begins the arduous task of flying to safety. The orbiter thrust-to-weight ratio at liftoff is 1.24g with the engines running at the emergency power level (EPL).

The pad flyaway capability is shown to demonstrate the feasibility of flying the orbiter off the pad, if desired. Analysis shows the ability to achieve 305 meters (1,000 feet) in 18.9 seconds, and 610 meters (2,000 feet) in 23.2 seconds from the decision to abort off the pad.

PAD FLYAWAY OF ORBITER

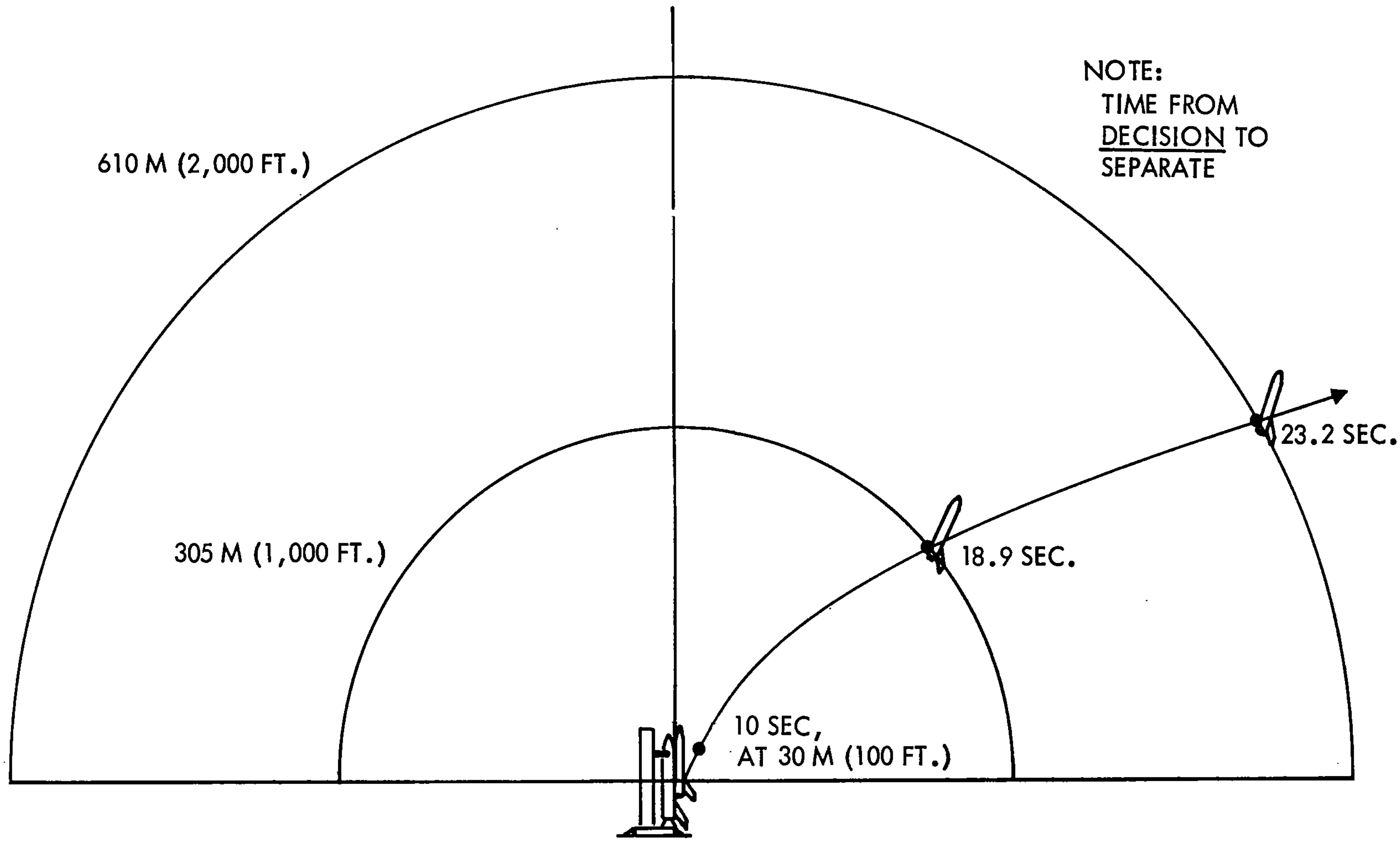

PAD FLYAWAY TRAJECTORY, TWO ORBITER ENGINES

Both the sequence and trajectory are shown here. EPL is used on the orbiter and maintained to maximize separation distance. The trajectory shows approximately a 10-second close proximity and plume impingement on the tail. The plume impingement is mitigated by the initial 3-deg. nose-up pitch gimbal angle on the orbiter engine preceeding and during motion on the links, but there are also greater than normal plume effects on the top portion of the booster, especially from the aft attachment forward. It is this sequence that would undoubtedly design the thermal protection system if abort off the pad is to be used.

PAD FLYAWAY TRAJECTORY, TWO ORBITER ENGINES

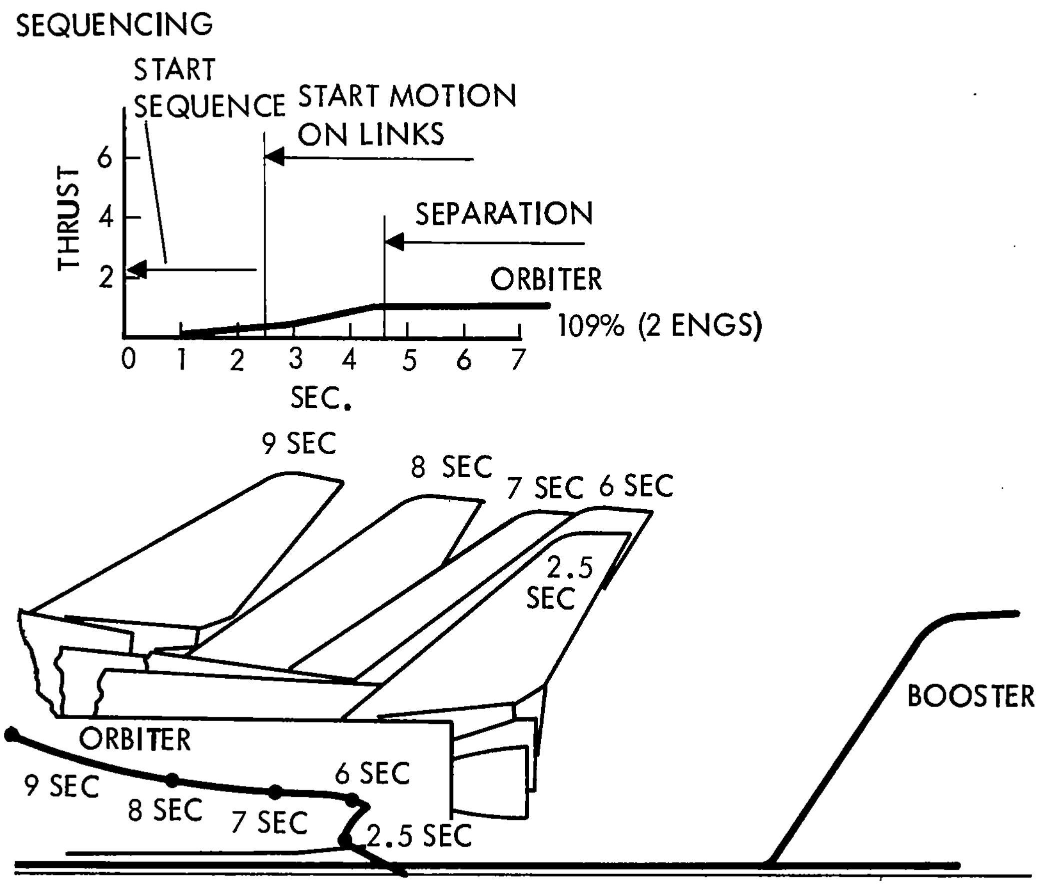

ORBITER ENGINE INLET ACCELERATIONS DURING SEPARATION SEQUENCE

This figure demonstrates that the longitudinal acceleration at the orbiter main propulsion engine inlets exceed the 0.2g guarantee in every case investigated. This ensures that sufficient propellants are available to the main engines to provide propellant settling and prevent cavitating the pumps.

ORBITER ENGINE INLET ACCELERATIONS DURING SEPARATION SEQUENCE

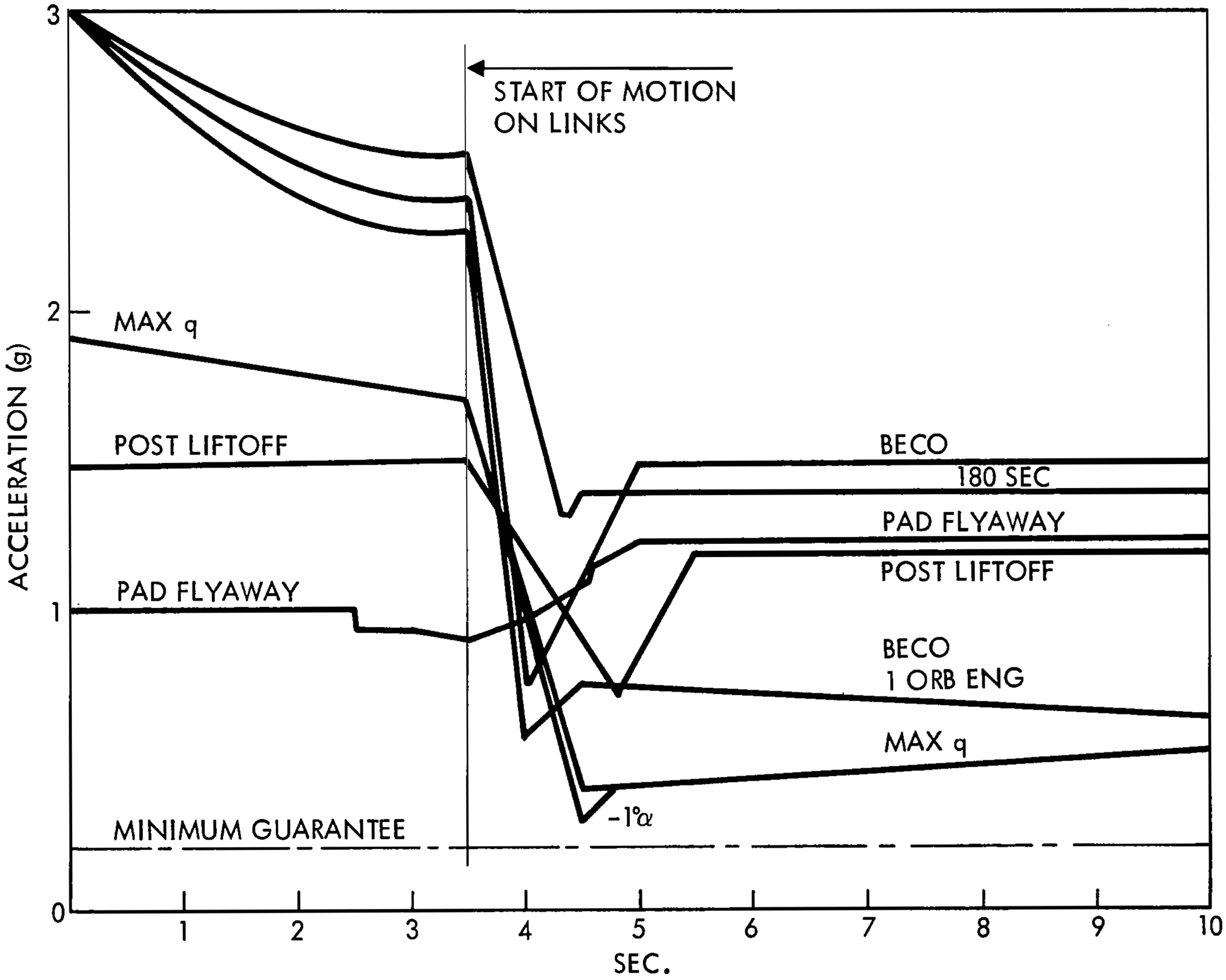

BOOSTER CREW ACCELERATIONS DURING SEPARATION SEQUENCE

This figure illustrates the rigid-body accelerations experienced by the booster's crew at the various abort conditions.

BOOSTER CREW ACCELERATIONS DURING SEPARATION SEQUENCE

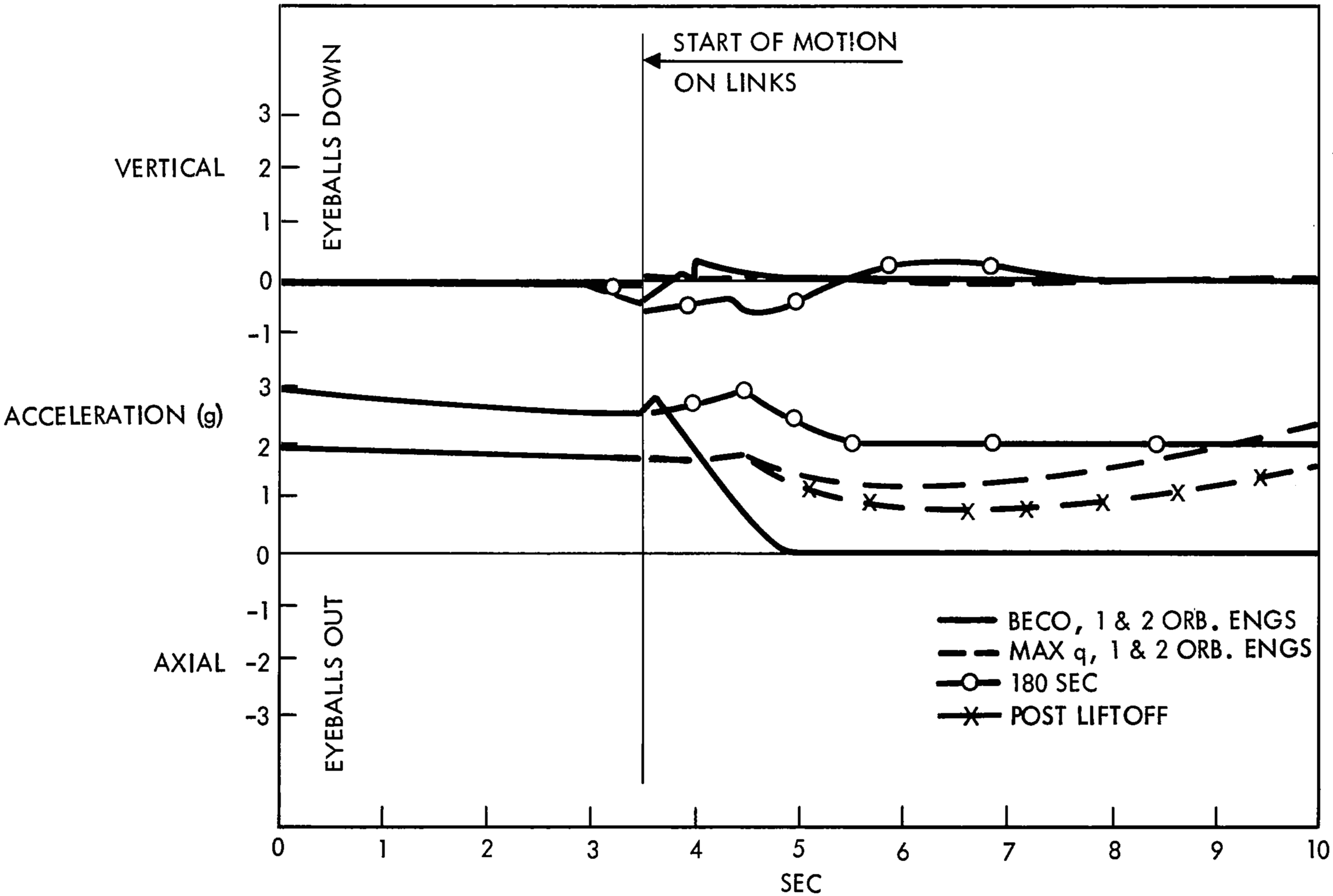

ORBITER CREW ACCELERATIONS DURING SEPARATION SEQUENCE

This figure illustrates the rigid-body accelerations experienced by the orbiter's crew and, with the preceding figure, demonstrates that, in spite of the speed at which separation takes place, the acceleration environment which the crew (hence, the payload) is subjected to is quite moderate.

ORBITER CREW ACCELERATIONS DURING SEPARATION SEQUENCE

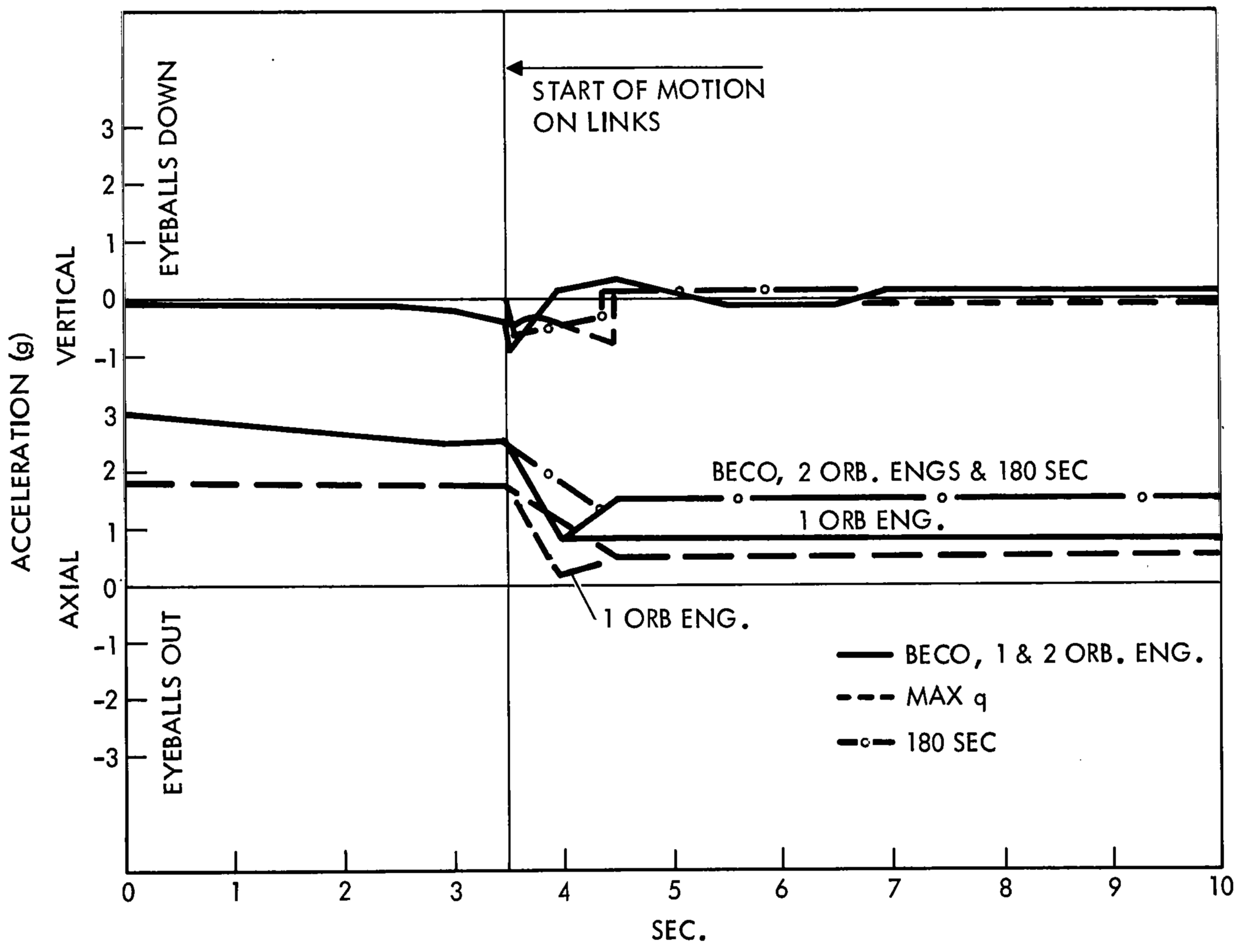

ENVELOPE OF ELAPSED TIME

The time required to achieve 305 and 610 meters (1,000 and 2,000 feet) of separation distance is measured from the decision to abort separate. Pre-liftoff and normal staging events have been added to the figure for reference. About 610 meters (2,000 feet) of separation is attained within 18 seconds anywhere during boost phase flight. Before liftoff, the orbiter can ignite its engines, separate from the booster, and achieve 610 meters (2,000 feet) of separation in 23.3 seconds (assuming its systems are ready). Following BECO, 24 seconds are required to achieve 610 meters (2,000 feet) of separation with one orbiter engine failed. History indicates that these times are generally sufficient to save one of the stages in the event of subsequent catastrophic destruction of the other stage.

ENVELOPE OF ELAPSED TIME TO 305 & 610 M (1,000 & 2,000 FT.) SEPARATION

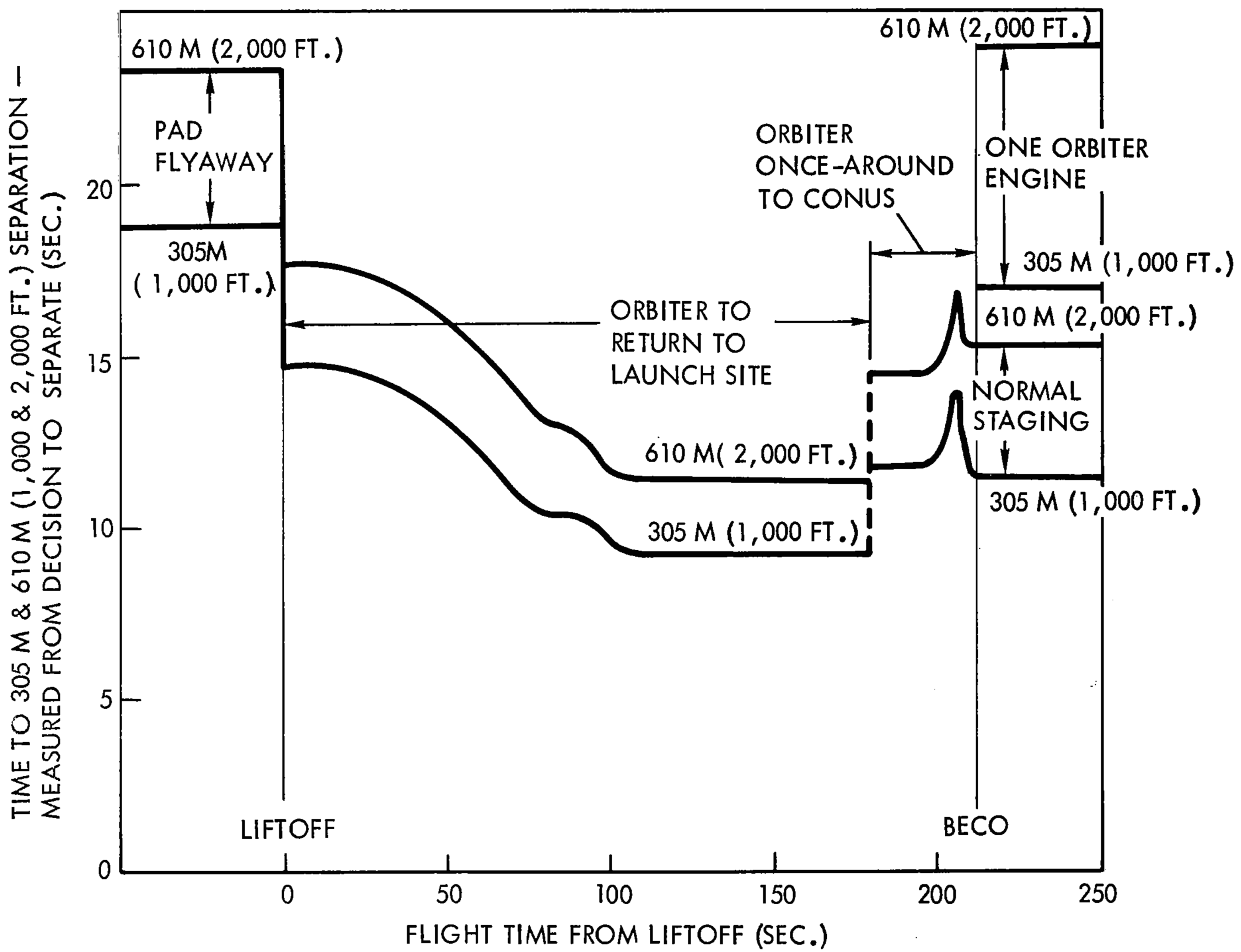

ABORT SEPARATION PENALTIES, AN ASSESSMENT

Definite penalties are associated with abort capabilities due to the additional system design requirements they impose. The most obvious areas are in increased structural loads (which imply increased weight), heating effects (which also include weight), program software, system complexity, etc. This section points out the most serious areas of consideration.

The structural loads that are directly chargeable to the separation system were analyzed. As previously mentioned, the interstage attachments and structure for ground handling and up-flight would be required regardless of the separation system.

All loads in relation to the separation system were derived from the computer simulation (P5255) as described in Ref. 3, which used rigid-body analysis.

The composite of the link resultant loads, both before and during separation, for the various abort and normal staging conditions are shown. It becomes obvious that Load A is a direct function of the booster thrust before release and that A is not designed by separation but rather by the up-flight 3g design limit. Link B functions before motion of the links and sees relatively low loads with very little spread for all conditions; again, it is not designed by separation but by the up-flight conditions at maximum q.

COMPOSITE OF INDIVIDUAL A&B RIGID-BODY LINK LOADS

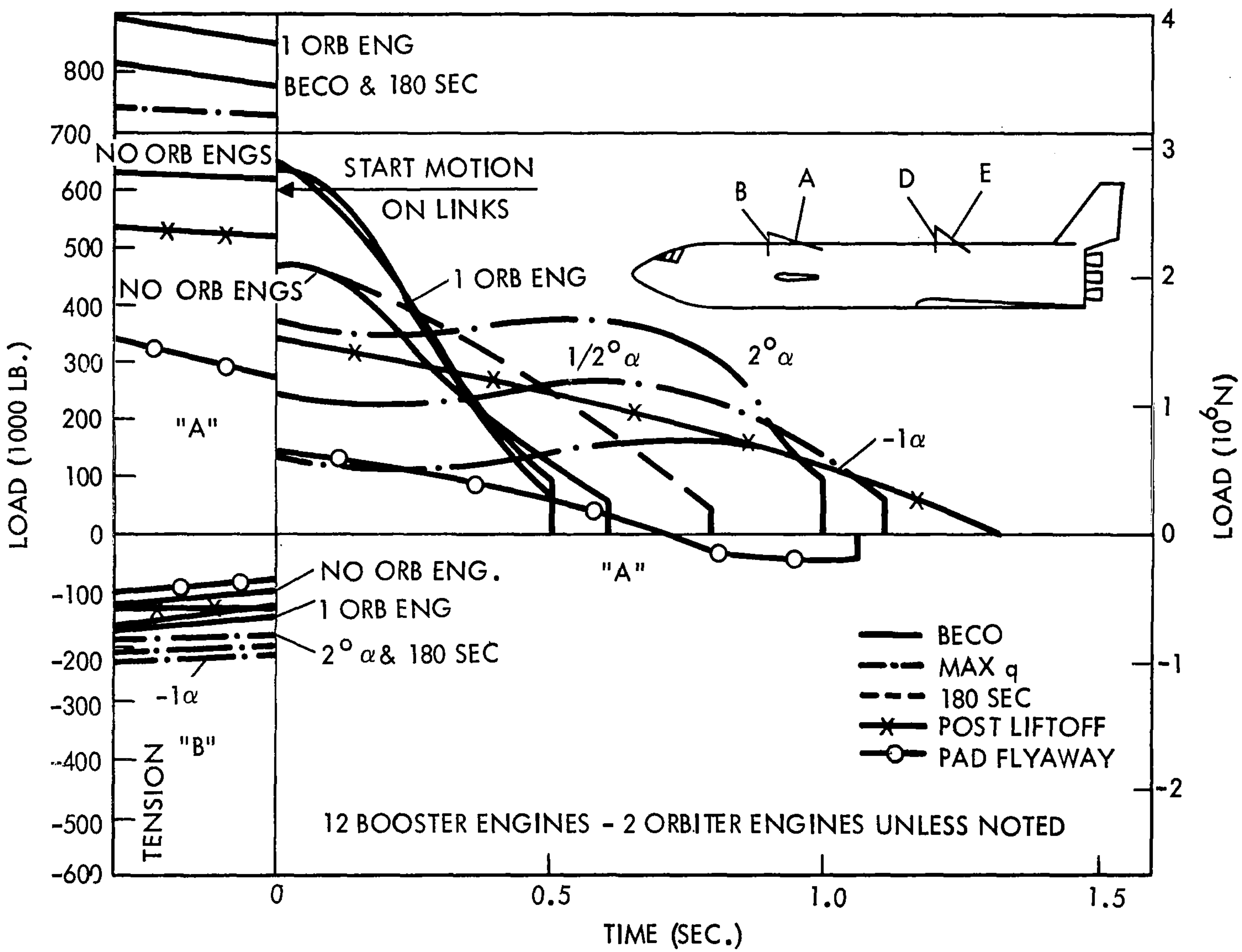

COMPOSITE OF INDIVIDUAL D&E RIGID BODY LINK LOADS

Links A and E are the only ones to sustain loads during motion on the links. At no time during the motion on the links does the vertical component in the booster or orbiter attachment exceed the initial load (which is considerably less than the design load), especially in the orbiter. Again the load in Link D only functions before motion of the links and is relatively low.

Attachment loads during ascent do not vary much once the orbiter cg and mass have been established. The 3g design limit load during ascent determines the main axial force to be reacted between attachments; therefore, the only other factor to consider is the coupling taken up by the forward and aft vertical attachments. The axial load may be taken out either at the forward or aft attachments, if desired, and the vertical reaction may be varied by increasing or decreasing the angle of the axial members between the booster and orbiter. It is feasible, within limits, to direct load forward or aft by varying link geometry. This must be done carefully, however, because it directly affects the trajectories at separation.

Link E, which is not a load-carrying member until separation, is totally designed by separation. Link E loads are shown and are directly affected by the separation condition, as shown in this composite. The time differential for each condition, until zero load is attained, is due to the time required for motion on the links. This time can also be expressed in terms of the angle theta (relative angle between centerlines of both vehicles). The purpose of the longer time on the links (or increase angle theta) is to provide good separation trajectories and is required for all conditions other than normal staging (where booster thrust is reduced to zero).

The normal staging load of Link E is relatively low, and the load shift from zero load to approximately 890,000 newtons (200,000 pounds) at the start of motion on the links is still low by comparison to that at the maximum q condition shown. It is obvious that the Link E penalty for maximum q abort is quite costly relative to normal staging, and elastic effects in this area are of concern. The orbiter and booster attachment loads (both horizontal and vertical components) show the overall effects due purely to abort separation, the largest being the axial load E_X at both orbiter and booster. This condition also gives rise to further study with the possibility of taking the main 3g axial load out through the aft member E. This would not penalize maximum q abort, but the forward link A load at normal staging must be traded against the weight penalties for both the orbiter and booster.

COMPOSITE OF INDIVIDUAL D & E RIGID BODY LINK LOADS

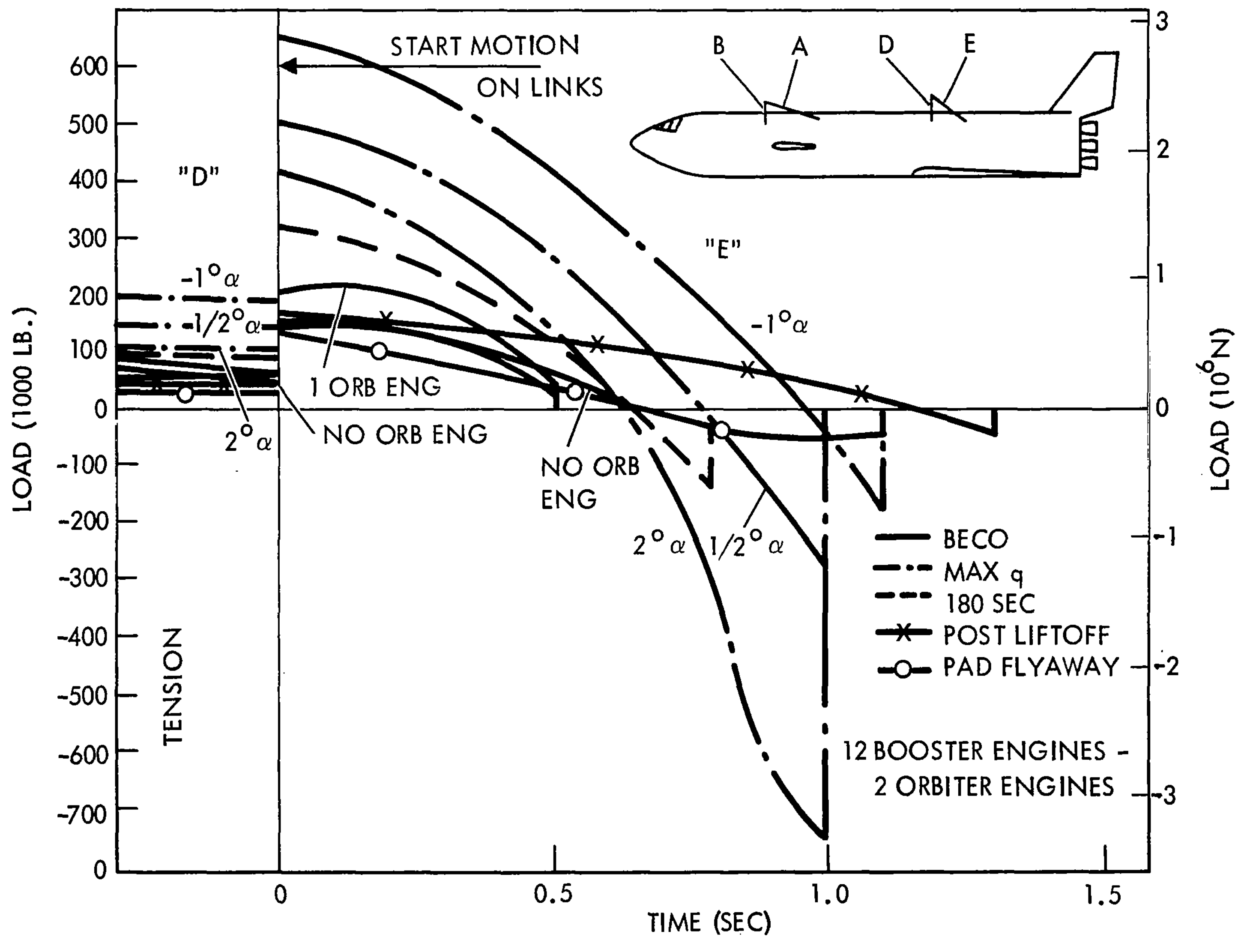

AFT LINK ASSEMBLY MASS PENALTY

Mass penalties for abort separation must be evaluated as those only directly chargeable to abort. To this end, a comparison has been made of each area affected.

The abort loads were analyzed and used to determine the mass penalty. In the review of the abort conditions it is quite apparent that the predominating area is abort at high q. Also apparent is the fact that it is solely the aft axial link (described as Link E) and its backup structure in both the booster and orbiter that inherits the majority of the mass penalty.

The figure shown gives a breakdown of the aft link assembly, comparing normal staging with abort at maximum q. A 550-kilogram (1,213-pound) mass penalty was assessed.

AFT LINK ASSEMBLY MASS PENALTY

	MASS IN KG (LB.) NORMAL STAGING	MAX q ABORT	Δ MASS
LONGITUDINAL TUBES	108 (237)	249 (550)	142 (313)
BOOSTER PIVOT FITTINGS & BEARINGS	109 (240)	259 (570)	150 (330)
CREEP CYLINDER & BEARING	127 (281)	255 (562)	127 (281)
RETRACT ACTUATORS (AFT)	53 (116)	76 (168)	24 (52)
PYROTECHNIC BOLTS	59 (129)	78 (172)	20 (43)
INSTALLATION BOLTS	11 (24)	33 (72)	22 (48)
RETRACT ACTUATORS (FWD)	249 (548)	315 (694)	66 (146)
	714 (1,575)	1,265 (2,788)	$\boxed{550}$ $\boxed{(1,213)}$

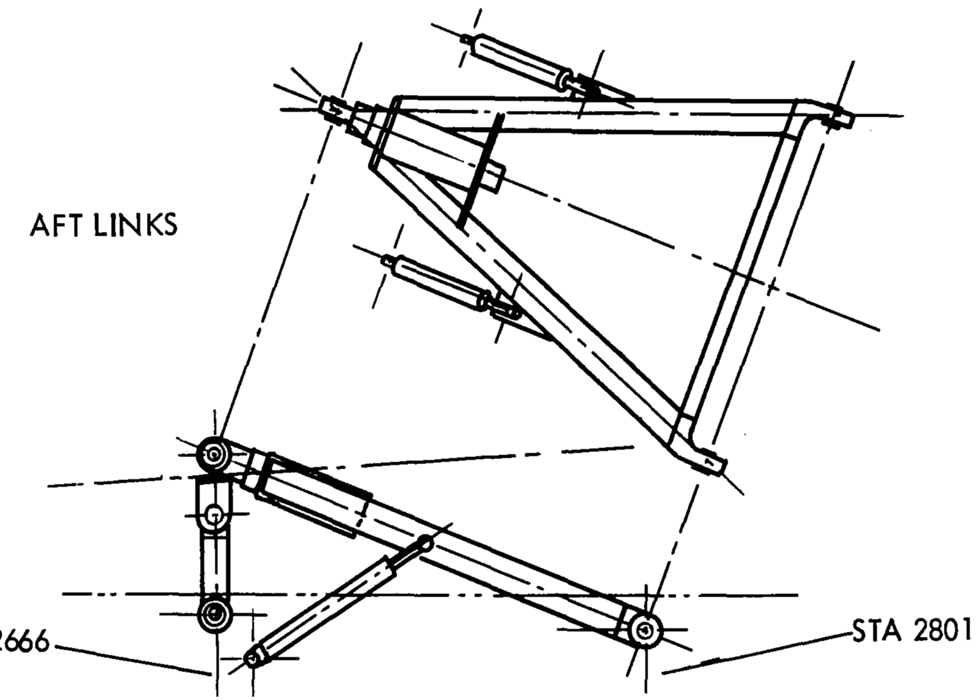

BOOSTER BULKHEAD MASS PENALTY

The resultant increase in the backup structural mass in the booster is shown. A comparison of actual resultant design load is also shown at the attachment at the top of the bulkhead. This increase is due to only the vertical load components and mounted to 1,318 kilograms (2,906 pounds) of inert mass.

BOOSTER BULKHEAD MASS PENALTY

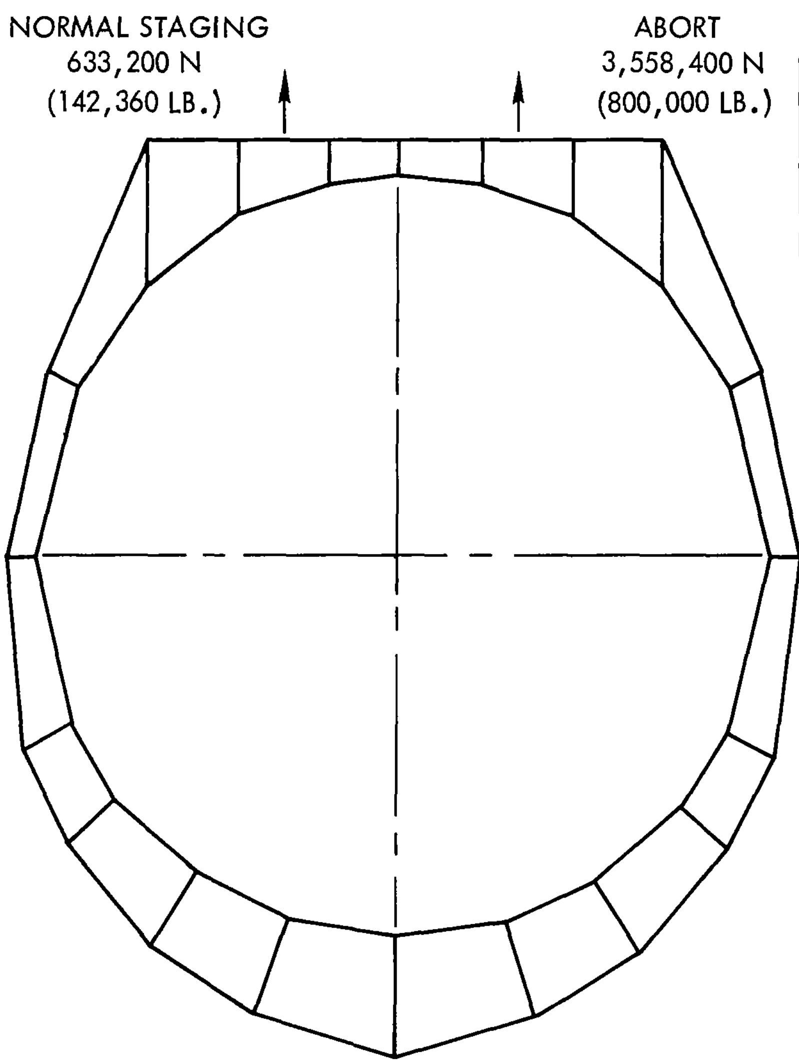

MASS IN KG (LB.)

	NORMAL STAGING	MAX αq ABORT	Δ MASS
CAPS	375 (826)	1,044 (2,301)	669 (1,475)
WEBS	316 (697)	897 (1,978)	581 (1,281)
FITTINGS	35 (77)	103 (227)	68 (150)
	726 (1,600)	2,044 (4,506)	$\boxed{1,318 (2,906)}$

BOOSTER SKIN AND LONGERON MASS PENALTY

The axial load results in an increase in mass in the longeron and skin (for shear transfer), of 138 and 193 kilograms (305 and 425 pounds), respectively.

BOOSTER SKIN & LONGERON MASS PENALTY

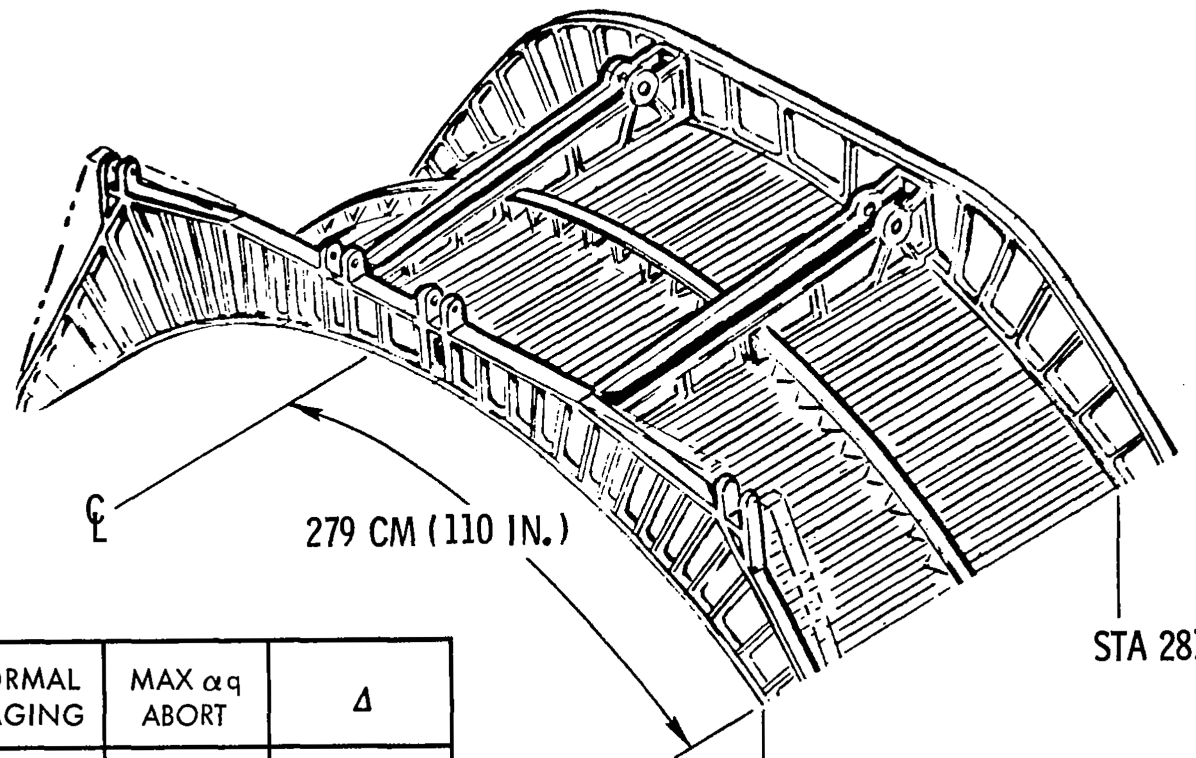

	NORMAL STAGING	MAX αq ABORT	Δ
AVG. CROSS SECTION IN CM^2 (SQ. IN.)	25.1 (3.9)	96.8 (15.0)	71.6 (11.1)
MASS IN KG (LB.)	49 (108)	187 (413)	$\boxed{138}$ $\boxed{(305)}$
SKIN GAGE IN CM (IN.)	0.432(0.170)	0.706(0.278)	0.274 (0.108)
MASS IN KG (LB.)	303 (668)	496 (1,093)	$\boxed{193}$ $\boxed{(425)}$

ORBITER MASS PENALTIES

Orbiter attachment penalties for the abort phase are shown and, in terms of payload, the 978-kilogram (2,155-pound) mass penalty appears quite high. Some alternatives could be examined to reduce this penalty, but they were not in the scope of this study.

One approach would be to attach the orbiter not through the aft payload bulkhead but through the engine mount structure, which should be quite massive. Another approach is to consider a push orbiter and possibly take the main 3g axial load through the aft attachment; this would not penalize maximum q abort and would probably eliminate all aft weight increases due to abort. However, consideration must be given to the forward attachment at normal separation, which would probably become penalized. Preliminary runs indicate that the forward axial link loads would be higher during normal separation than during maximum q abort, but a possible decrease of the booster mass penalty due to the smaller shear surface transfer area (due to the reduction of the forward link design condition, which would be reduced by about 50%) must also be considered.

Another factor would be the orbiter mass penalty due to a conversion from a pull to a push design, but this should be relatively small.

ORBITER MASS PENALTIES

MASS IN KG (LB.)

ITEM	NORMAL STAGING	MAX α q ABORT	Δ MASS
BULKHEAD	525 (1,158)	1,034 (2,280)	509 (1,122)
FUSELAGE FLOOR	232 (512)	624 (1,375)	391 (863)
FITTING	32 (70)	109 (240)	77 (170)
TOTAL	789 (1,740)	1,767 (3,895)	978 (2,155)

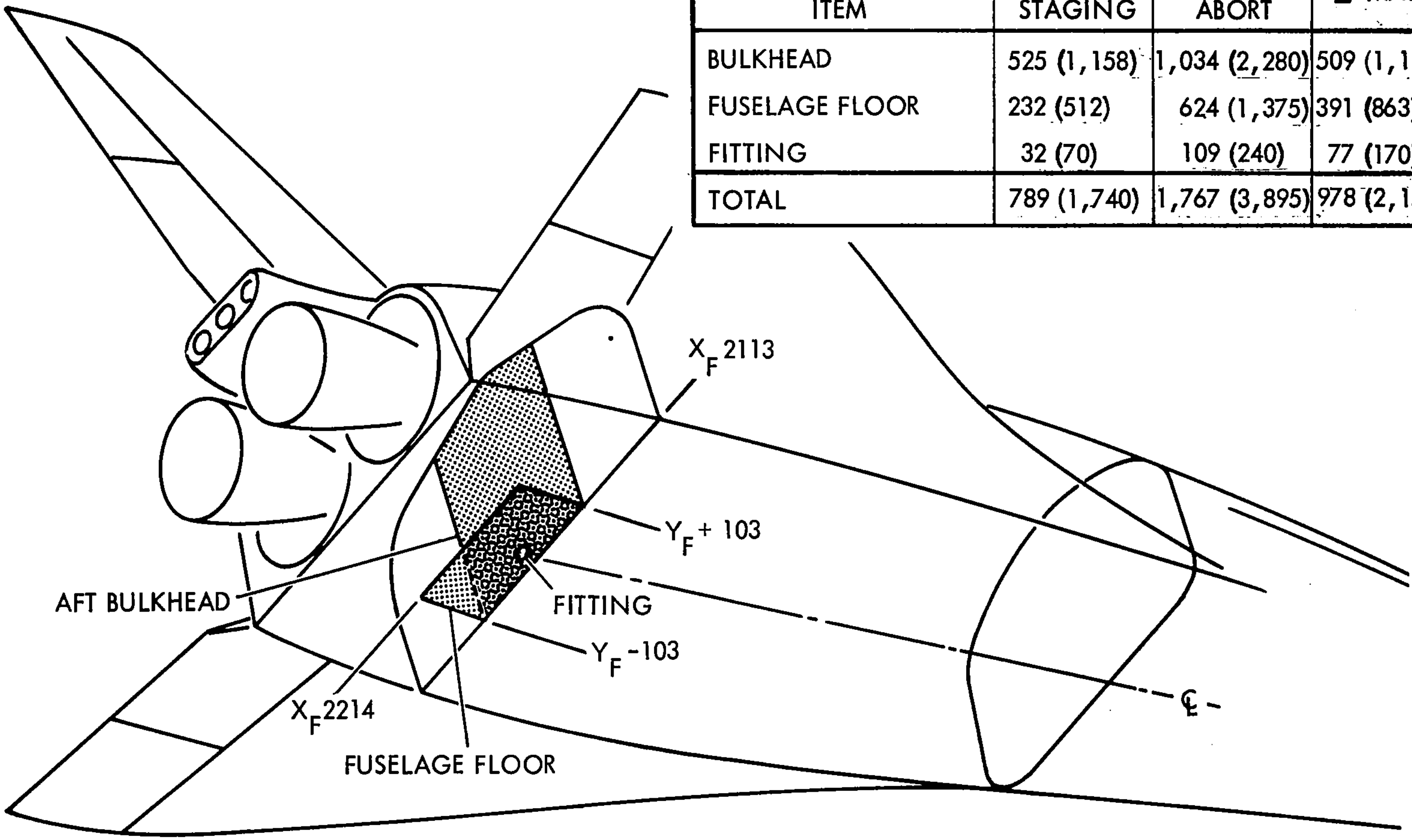

SUMMARY OF ABORT STRUCTURAL LOADS MASS PENALTIES

The following table summarizes structural loads mass penalties for abort. This converts to about 1,371 kilograms (3,023 pounds) of lost payload, (394 kilograms or 868 pounds of which is contributed by the booster).

The present baseline is designed for the plume effects of normal separation. This includes heating and acoustic conditions normally occurring while the orbiter engines are building up thrust during separation sequencing. The actual duration of plume impingement is meaningful only for approximately 5.5 seconds, of which 2.5 seconds is normally below the 20% thrust level. For abort, the condition on or near the pad becomes the design case because (1) maximum thrust of the orbiter is required for safe separation, and (2) the orbiter plume at sea level is more concentrated (focused). The orbiter plume will also sweep the top of the booster during the first few seconds after separation for this condition. It is estimated that an additional mass penalty of from 227 to 454 kilograms (500 to 1,000 pounds) on the booster would be required. This is equivalent to an additional 40 to 81 kilograms (89 to 178 pounds) of payload penalty.

Separation system sequence computer control and programming are strongly affected by any abort capability that would require considerable computer tasks and storage. Vehicle data must be pooled on a continuous basis and stored for sequence updating as required and, of course, new sequences would be required probably every 15 seconds of flight.

A larger scope for vehicle and subsystem control and monitoring would also be required with automatic and/or manual immediate separation upon detection of a critical failure. The penalties for this additional software capability are difficult to assess, but must certainly be considered.

SUMMARY OF ABORT STRUCTURAL LOADS MASS PENALTIES

		WEIGHT (LB.)	MASS (KG)
BOOSTER			
	LINKAGE, FITTINGS, ACTUATOR, CREEP CYLINDER , & BOLTS	1,213	550
	BULKHEAD, STATION 2801	2,906	1,318
	DRAG LONGERONS	305	138
	SKIN PANELS	425	193
	TOTAL	4,849	2,199
ORBITER			
	BULKHEAD, STATION 2113	1,122	509
	CAPS AND SKIN PANELS	863	391
	LOCAL FITTINGS	170	77
	TOTAL	2,155	977

Major conclusions and recommendations for future study are presented in this table.

REFERENCES

1. "Space Transportation Systems (STS) Study (U)," Section 19.12, "Separation System Analysis," Unclassified, SAMSO-TR-69-348, November 1969 (Confidential).
2. L.R. Bird, "Post-Test Report for Triamese Separation Test HST 284-0," Convair Aerospace Division of General Dynamics Aeroballistics Technical Note TN-69-AE-08, 10 December 1969.
3. M.J. Hurley, "Digital Program P5255, A Six-Degree, Multiple-Body Separation Simulation for Hinged and/or Linked Lifting-Entry Vehicles," Volumes I and II, Convair Aerospace Division of General Dynamics, Report GDC-ERR-1377, December 1969.
4. M.J. Lanfranco, "Wind-Tunnel Investigation of the Separation Maneuver of Equal-Sized Bodies," AIAA Paper 70-260, presented at AIAA Advanced Space Transportation Meeting, Cocoa Beach, Florida, February 1970.
5. M.J. Hurley and M.J. Lanfranco, "Separation Dynamics of Multibody Clusters of Hinged and/or Linked Lifting--Entry Vehicles," presented to the Seventh Space Congress, Cocoa Beach, Florida, April 1970.
6. R.H. Schuett, M.O. Clark, and M.J. Hurley, "Space Shuttle Staging Dynamics," as contained in NASA Technical Memorandum NASA-TM X-52876, "Space Transportation System Technology Symposium," Volume II, "Dynamics and Aeroelasticity," July 15-17 1970, pp 123-142.
7. F.E. Jarlett, "Separation System Trade Study," Convair Aerospace Division of General Dynamics, Report 76-546-10-002, November 1970.
8. J.M. De Bevoise, "Aerodynamic Interference Between Parallel and Staged Winged Space Launch Vehicles During Separation," Convair Aerospace Division of General Dynamics, Report GDC-ERR-1566, December 1970.
9. G.W. Carrie and M.J. Hurley, "Space Shuttle Separation System Analysis, A Capability Assessment," Convair Aerospace Division of General Dynamics Report 76-549-4-172, June 1971.
10. M.J. Hurley, "Booster Recovery Following Premature Space Shuttle Stage Separation," presented to the NASA Space Shuttle Aerothermodynamics Technology Conference held at the Ames Research Center, December 15 and 16, 1971.

STUDY SUMMARY

CONCLUSIONS

- ABORT SEPARATION IS FEASIBLE FROM PRE-LIFTOFF THROUGH NORMAL STAGING
- STRUCTURE MASS PENALTY FOR ABORT SEPARATION CAPABILITY IS APPROXIMATELY 1,371 KILOGRAMS (3,023 LB.) PAYLOAD (4,849 LB. ON THE BOOSTER AND 2,155 LB. ON THE ORBITER)
- ADDITIONAL THERMAL PROTECTION TO PROTECT AGAINST PLUME IMPINGEMENT CAN ADD UP TO AN ADDITIONAL 81 KILOGRAMS (178 POUNDS) PAYLOAD EQUIVALENT (1,000 POUNDS ON THE BOOSTER)

MAJOR FUTURE CONSIDERATIONS

- EVALUATE AFT STRUT FOR LOAD CARRYING DURING ASCENT
- EVALUATE ELASTIC EFFECTS OF LINKS AND INTERNAL PRIMARY STRUCTURE
- DESIGN MECHANICAL INTERFACE TO DISCONNECT CLEANLY AT VARIOUS LINK ROTATION ANGLES
- INVESTIGATE REQUIREMENTS ON COMPUTER SOFTWARE TO SUPPORT BOTH NORMAL AND ABORT SEPARATION

SPACE SHUTTLE BOOSTER FLYBACK SYSTEM SYNTHESIS

D. W. [illegible]es, W. J. Moran, and V. A. Lee

Convair Aerospace Division
General Dynamics Corporation
Fort Worth, Texas

SUMMARY

This paper is concerned with one particular aspect of configuration development and evaluation for an earth-to-orbit reusable space transportation system. It deals only with the first-stage booster element of the system. Furthermore, it is restricted to consideration of only those aspects of the booster which are associated with its capability to be recovered - i.e., the booster flyback system. The major portion of the discussion is concerned with a computerized synthesis approach for treating this problem. A more detailed development of the methodology is given in General Dynamics Report ERR-FW-1198, "Reusable Booster Flyback System Synthesis."

BOOSTER FLYBACK SYSTEM SYNTHESIS

(Figure 1)

The earth-to-orbit reusable space transportation system considered here utilizes a first-stage winged booster to propel a second-stage winged orbiter to part of its required mission velocity. Following staging, the booster enters the atmosphere and decelerates and turns aerodynamically toward a landing site (usually at the launch location). Then, powered by turbojet engines, it cruises to the landing site as a subsonic airplane and lands horizontally. The booster also has abort and ferry capabilities.

The system is configured and sized on the basis of efficiently delivering specified payloads to specified low earth orbits, and retrieving payloads from these orbits. These requirements coupled with the mission concept illustrated in the opposing figure define diverse, complex flight mechanics/performance considerations which in turn drive the system synthesis process.

The problem of synthesizing a "good" (hopefully "best" in some sense) configuration for the booster cannot, of course, be considered out of the context of the complete system - i.e., booster plus orbiter. A total-system synthesis function is obviously required. However, a separate (but closely coordinated) detailed booster synthesis process can be effectively used to compliment a less-detailed overall synthesis effort. Moreover, for many purposes, synthesis of those booster components which relate to the flyback (post-staging) aspects of the mission can, if properly coordinated, be handled separately to good advantage. These components - wing and other aerodynamic surfaces, air-breathing propulsion, and landing gear - are termed the flyback system.

Configuration synthesis of the booster fly-back system (in combination with given booster bodies) is the problem which is considered here.

BOOSTER FLY-BACK SYSTEM SYNTHESIS

● THE BOOSTER AFTER STAGING

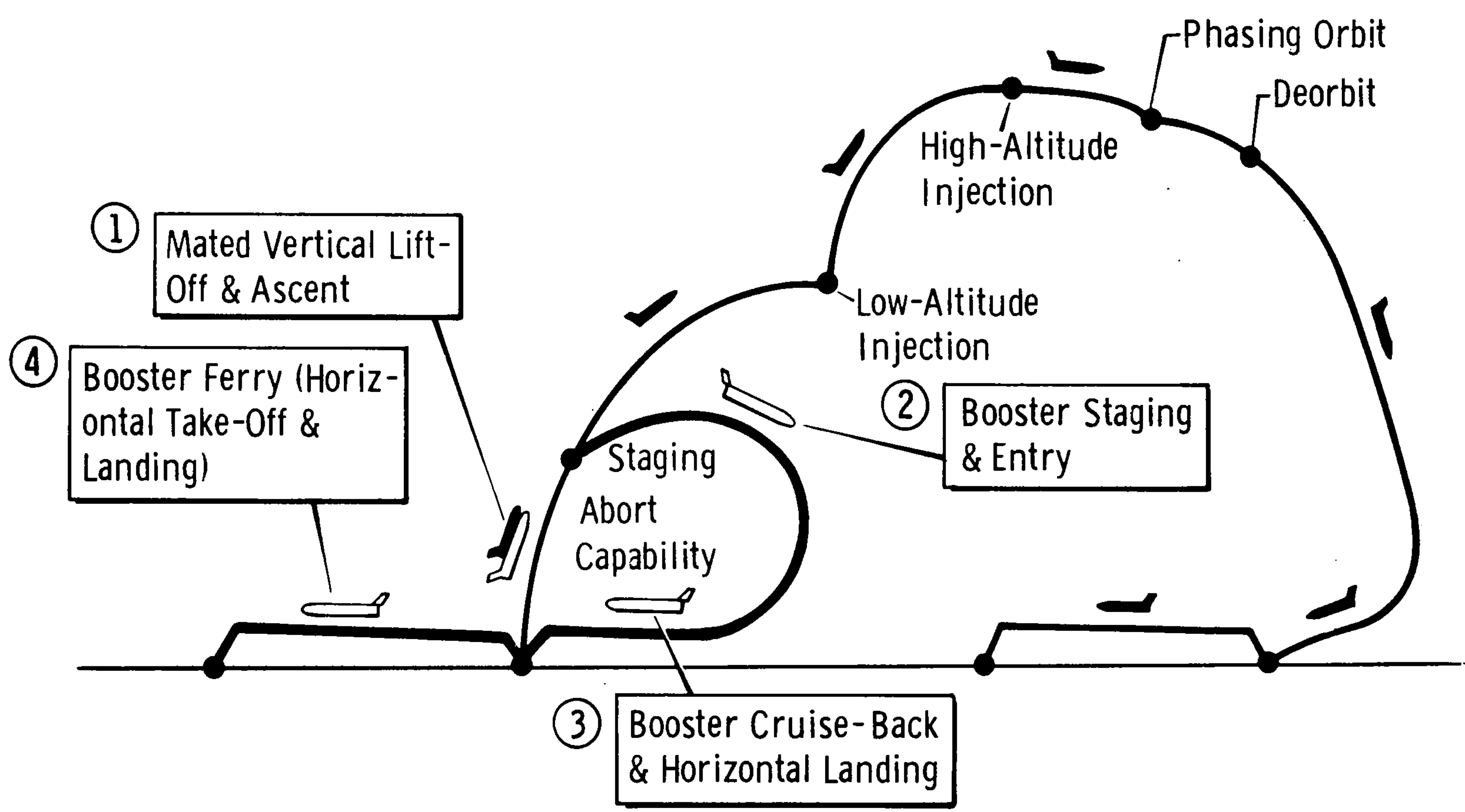

Figure 1

A TYPICAL DESIGN
(Figure 2)

The opposing figure illustrates the fly-back system components for a typical booster design. Note that the 12 air-breathing engines are stowed in the wing during entry, and deployed at the beginning of cruise.

A TYPICAL DESIGN - Flyback System Components

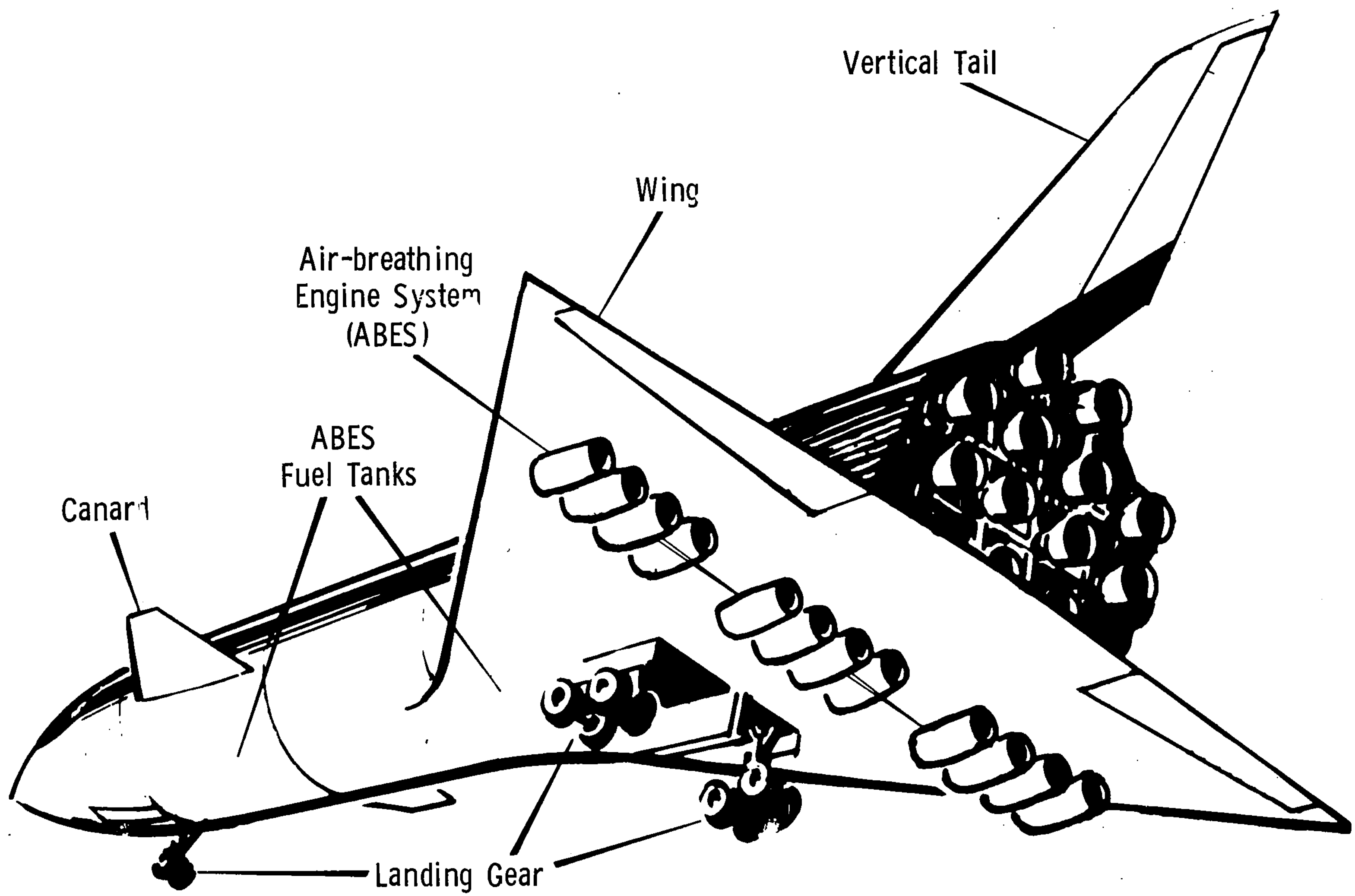

Figure 2

PROBLEM VARIABLES, PARAMETERS, AND OPTIONS
(Figure 3)

The basic synthesis problem is configuration definition corresponding to minimum fly-back system weight or cost or some combination of weight and cost - which in turn tends to minimize the total cost of the overall space transportation system. In addition, there are related problems involving sizing (e.g., in response to changes in payload requirements); sensitivities (e.g., required weight with respect to air-breathing propulsion specific fuel consumption); various trades and special studies (e.g., cost effectiveness and risk studies); and flight mechanics/performance/mission analysis studies (for fixed vehicles).

The opposing figure presents the independent configuration variables which were selected to be varied arbitrarily in the process of configuration optimization. In addition, canard area, vertical tail area, and fore-and-aft wing location were designated configuration variables but are defined by stability and control requirements, rather than available for arbitrary variation.

The figure also lists some of the configuration parameters and options which were selected to accommodate the treatment of various types of designs. Some of the flight mechanics/performance/mission analysis options which were selected to permit handling of essentially all types of situations in this area are also given.

PROBLEM VARIABLES, PARAMETERS, & OPTIONS

- INDEPENDENT CONFIGURATION VARIABLES
  - WING
    - Area (S) or Wing Loading (W/S)
    - Sweep (Λ)
    - Aspect Ratio (AR)
    - Thickness Ratio (t/c)
    - Taper Ratio (λ)
  - AIR-BREATHING ENGINE
    - Thrust Level (ϵ) or Thrust-to-Weight (T/W)
    - Number (N)
- OTHER CONFIGURATION VARIABLES
  - CANARD AREA
  - VERTICAL TAIL AREA
  - WING LOCATION
- CONFIGURATION PARAMETERS & OPTIONS
  - AIR-BREATHING ENGINE LOCATIONS
  - FUEL TANK LOCATIONS
  - LANDING GEAR LOCATIONS
  - WING-LOCATION CRITERIA AND LIMITS
  - VERTICAL TAIL CRITERIA
  - AND OTHERS
- FLIGHT MECHANICS/PERFORMANCE/ MISSION ANALYSIS OPTIONS
  - ENTRY FLIGHT PATH
  - CRUISE RULES
  - LANDING AND TAKEOFF RULES
  - ATMOSPHERE
  - WINDS
  - AND OTHERS

Figure 3

OVERALL APPROACH
(Figure 4)

The need to consider a large number of configuration variations, coupled with the complexity of this system, makes a computerized synthesis approach very desirable, if not mandatory. In response to this need, a booster flyback system synthesis computer procedure has been developed.

The two basic types of synthesis tasks which are accommodated by this procedure are (1) sizing (scaling a fixed-shape configuration in response to changes in mission/payload requirements, structural weight estimates, etc.); and (2) synthesis per se, involving changes in both size and shape (e.g., wing sweep, wing thickness ratio, engine thrust level, etc.). In addition, the procedure can be used to evaluate the flight mechanics/performance mission analysis capabilities and characteristics of fixed-configuration vehicles.

The overall approach to the booster flyback system synthesis computer procedure is summarized in the figure.

An arbitrary configuration is set by specification of (1) the independent configuration variables for the flyback system and (2) fixed booster body. The procedure then locates the wing in a fore-and-aft direction, and sizes the canard and vertical tail - on the basis of stability and control considerations. At this point, the configuration is completely specified, and the force-type data (aerodynamic forces, air-breathing propulsion data, and mass properties) are determined. The performance of the vehicle is then evaluated through the entry and cruise-back phases of the mission, with aerodynamic heating computations being carried out during entry. The cruise-back capability of the booster is compared with the range to the desired landing site at the end of entry, and if it does not agree, a new fuel weight is estimated by the procedure. This requires recomputation of the structural weights and stability and control considerations.

When the landing-location (or range) criterion is satisfied in this weight-sizing iteration, additional performance is computed as desired.

OVERALL APPROACH

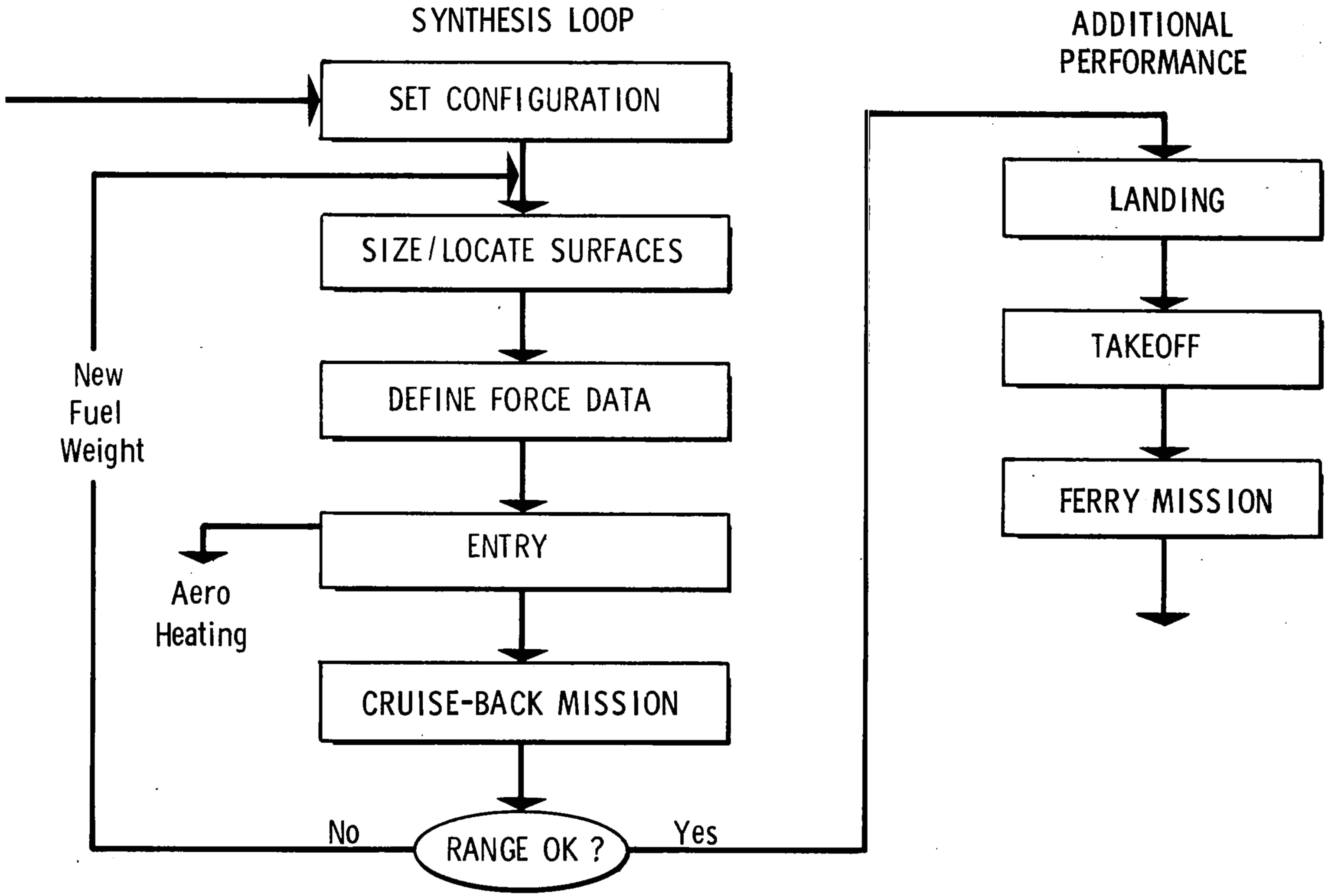

Figure 4

PROGRAM MODULES

(Figure 5)

As indicated in the figure, the procedure is concerned with two primary functions, technology data generation and flight mechanics/performance evaluation, and two secondary functions, geometry and procedure control. These are considered secondary from the standpoint of computational complexity.

The technology considerations which are involved in this problem cover all of the basic technology areas and all flight regimes. In addition, the complex interactions resulting from these technology considerations, superimposed on the flight mechanics/performance framework of the flyback mission, result in a very involved configuration synthesis process.

The following figures summarize each of the five technology areas, flight mechanics/performance, and geometry. Procedure control is not discussed per se, but is implied in the other discussions.

PROGRAM MODULES

- TECHNOLOGY DATA
  - Aerodynamic Forces
  - Air-Breathing Propulsion
  - Mass Properties
  - Stability & Control
  - Aerodynamic Heating
- FLIGHT MECHANICS/PERFORMANCE
  - Entry
  - Cruise-Back
  - Landing
  - Takeoff
  - (Ferry)
  - (Abort)
- GEOMETRY
- CONTROL

Figure 5

THE REFERENCE CONFIGURATION METHOD
(Figure 6)

The key element of a configuration synthesis computer procedure is the technology data generation function. The overall usefulness of the procedure is largely determined by how well this function is conceived and implemented.

The figure summarizes the technology data approach which is used. It is particularly well suited to the handling of synthesis studies for vehicles which are at a stage of their development such that they are receiving intensive treatment by the various functional areas of the engineering organization (e.g., aerodynamic analyses and wind tunnel tests, design layouts, stability and control evaluations, etc.). Provision is made for storing a reference configuration definition (usually the current baseline design) and its corresponding technology data (aerodynamic force data, propulsion data, etc.). In addition, provision is made for storing technology perturbation data (e.g., lift and drag variations as functions of the independent configuration variables).

When values of the independent configuration variables are specified which differ from the stored reference set, the technology data are determined by perturbing off of the stored set of reference configuration data, thus forcing the synthesis procedure to agree with the detailed external evaluation provided for the reference (baseline) configuration. In the figure, the Y's represent mission and operation-type variables, (e.g., Mach number, angle of attack, flap position. The X's represent the independent configuration variables (e.g., aspect ratio, sweep). An asterisk denotes reference conditions, and a tilde denotes perturbation data.

The reference configuration library can be changed whenever it is thought to be necessary (e.g., following a baseline configuration change or a wind tunnel test). Similarly, the perturbation libraries (e.g., mass properties) can be changed as is deemed appropriate, (although this will probably not be necessary with every reference library change). It is important to emphasize that the reference and perturbation library data are generated external to and independent of the synthesis procedure using whatever level of detail is available and appropriate (analysis and/or test data of any origin).

REFERENCE CONFIGURATION METHOD

REFERENCE DATA:

- Externally Generated, Internally Stored Configuration and Data as Functions of Flight Variables

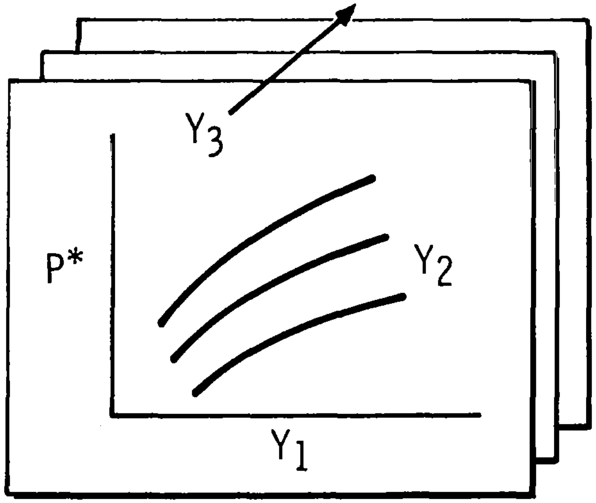

PERTURBATION DATA:

- Externally Generated, Internally Stored Data as Functions of Configuration Variables

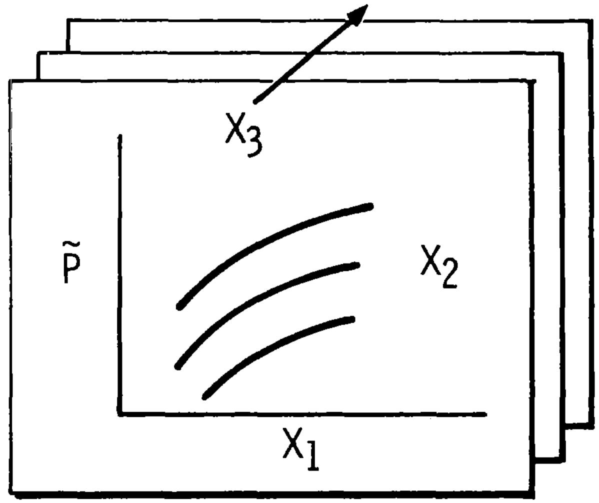

$$P(X, Y) = P^*(Y) + \overbrace{\left[\tilde{P}(X, Y) - \tilde{P}(X^*, Y)\right]}^{\Delta P}$$

Data for Current Configuration	Reference Configuration Data	Perturbation Data for Current Configuration	Perturbation Data for Reference Configuration

Figure 6

TECHNOLOGY FUNCTIONS AND METHODS

(Figure 7)

The opposing figure indicates (1) the type of data provided by each of the five technology areas, and (2) the computational approach used in each area.

TECHNOLOGY FUNCTIONS and METHODS

	PROVIDES	THROUGH
• AERODYNAMIC FORCES	Lift and Drag	Reference Configuration + Size and Shape Perturbation Data
• MASS PROPERTIES	Weight and C. G. Data	
• STABILITY AND CONTROL	Surface Location and Sizing	
• AIR-BREATHING PROPULSION	Thrust and Fuel Flow	Scaling of Reference Engine Data
• AERODYNAMIC HEATING	Heating Data (Information Only)	Several Analytical Models

Figure 7

AERODYNAMIC FORCES

(Figure 8(a))

The opposing figure presents the approach used in the procedure for generating lift and drag data of an arbitrary fly-back system configuration definition. As shown in the upper part of the figure, reference lift and drag data are stored in the aerodynamic forces portion of the reference configuration library. Note the provision for separate low speed/high lift data and for engine stowage and dèployment in terms of nacelle drag. Drag increments are also provided for gear deployment, drag chute deployment, etc. Perturbation data, of the type shown in the lower part of the figure, are used to perturb the reference lift and drag data when a configuration which differs from the reference configuration is called for.

For example, an aspect ratio of 3.0 is specified when the reference configuration aspect ratio is 2.5. In this case, the perturbation data account for all the changes in the reference data due to a change only in aspect ratio. If several configuration variables (e.g., aspect ratio, sweep, and engine thrust level) were specified different from their reference configuration values, then lift and drag perturbation data corresponding to the combined effect would be generated. Note the provision for different sets of lift and drag increments for each flow regime: low speed/high lift, subsonic, supersonic, and hypersonic.

The basis of the perturbation process for the aerodynamic data is the use of a linear lift curve and a parabolic drag polar. The parameters which define these familiar representations (α_{LO}, C_{L_α}, ΔC_L, $C_{D_{MIN}}$, K, etc.) are externally-generated data which are stored in the aerodynamic forces perturbation library. As is indicated in the figure, the parameters are stored as functions of (1) the independent configuration variables and (2) other configuration variables (e.g., canard area). In addition to the configuration variables (which are underlined in the figure), some other internally-generated variables also appear (e.g., C_{L_α}, e, etc.). The double asterisks denote subsonic data which are also used for low speed/high lift.

AERODYNAMIC FORCES

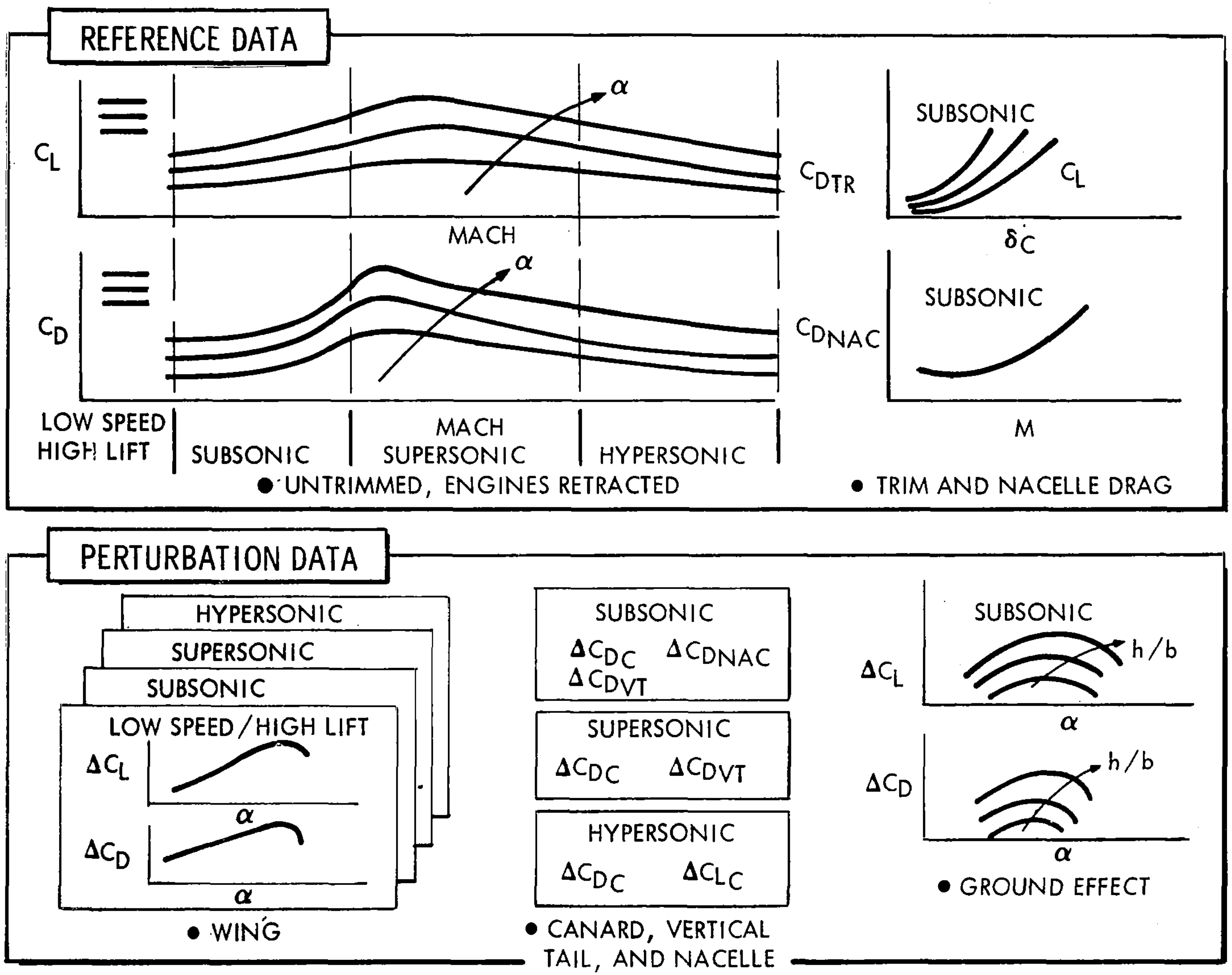

Figure 8(a)

AERODYNAMIC FORCES (Cont'd)
(Figure 8(b))

The process of generating the type of perturbation data shown in the lower part of the previous figure is as follows. The lift curves and polars are entered first at reference configuration conditions and then at perturbation conditions. The lift and drag differences between these two entries provide the perturbation increments which are then applied to the reference data to define the lift and drag characteristics of the new configuration.

It should be pointed out that the procedure assumes a linear lift curve and a parabolic drag polar only in the process of determining the perturbation data. The reference data are dependent on no such assumption. Furthermore, separate sets of lift curve and polar parameters are used for each speed regime.

AERODYNAMIC FORCES

- FUNCTIONAL DEPENDENCIES OF PERTURBATION DATA

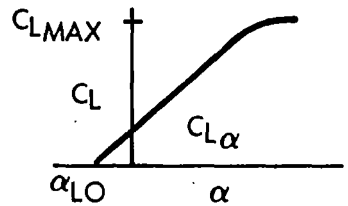

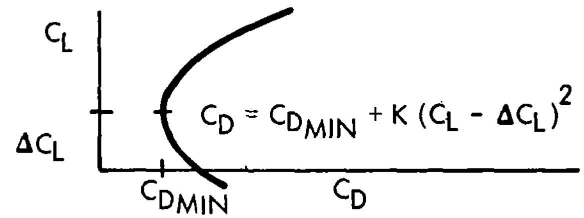

REGIME	WING	CANARD	VERTICAL TAIL	NACELLE
LOW SPEED / HIGH LIFT (Landing and Takeoff)	C_{LO} (AR, $C_{L\alpha}$) C_{LMAX} (AR, Λ, λ) ΔC_L ($C_{L\alpha}$, C_{LO}, e) C_{DFLAP} (AR, Λ, a) $\Delta\alpha$(h/b, AR, C_L) α^*_{PB} e^*_{MAX}	C_{DC} (S_C)	C_{DVT} (S_{VT})	C_{DNAC} ($S_{NAC_{WET}}$)
SUBSONIC (Cruise)	**C_{DMIN} (S, Λ, t/c) **$C_{L\alpha}$(AR, Λ, a, λ) α_{LO} (AR, Λ, λ) **K ($C_{L\alpha}$, AR) ΔC_L (AR, K)			
SUPERSONIC (Entry and Transition)				—
HYPERSONIC (Entry)	C_L (S, α) C_D (S,α)	C_{DC} (S_C) C_{LC} (S_C)	—	—

Figure 8(b)

MASS PROPERTIES
(Figure 9)

As summarized in the figure, the procedure accounts for both weight changes and longitudinal center of gravity changes as functions of the configuration variables. The general approach is the same as that employed for the aerodynamic forces. However, since the component weights are not functions of the mission variables (i.e., Mach number and angle of attack), the mass properties portion of the procedure is considerably less complex.

Reference weights and centers of gravity of the fly-back system components listed in the figure are stored in the mass properties portion of the reference configuration library. Parametric weight increments for the components listed in the figure are obtained by entering the parametric weight libraries twice (once with the reference values and once with the perturbed values of the configuration variables). Weight increments for other flyback system components are computed analytically (e.g., ABES tank weight as a function of ABES fuel weight). All vehicle components not included in the flyback system are included in a fixed body weight. A contingency weight may be computed internally from an analytical expression.

Longitudinal center of gravity perturbations are handled analytically (e.g., wing c.g. is assumed to move as a constant percentage of the mean aerodynamic cord as the wing planform changes).

MASS PROPERTIES

- WEIGHTS

• REFERENCE WEIGHTS FOR • Wing • Canard • Vertical Tail • Propulsion (ABES) √ Engine √ Nacelle • Gear √ Nose √ Main	PLUS	• Parametric Weight Increments for Flyback System Components • Fixed Body Weight • Contingency Weight

- Dry Fly-Back System (FBS) Weight + ABES Fuel
- Total FBS Weight

- LONGITUDINAL C.G.'s
  Reference Values + Analytical Variations = Total C.G.

Figure 9

STABILITY AND CONTROL

(Figure 10)

The stability and control functions are (1) to locate the wing fore-and-aft (wing size is an independent variable); (2) to size the canard (location is specified for a given reference configuration), and (3) to size the vertical tail (location is specified).

It should be noted that cruise balance can not be assured for an arbitrary configuration definition. The reason for this is that a minimum size canard is selected on the basis low-speed trim requirements, and this minimum size may be larger than the maximum size which is consistent with a desired positive static margin. In such a case, some other configuration change could be considered - e.g., wing size, fuel location (center of gravity, etc.).

Canard deflection during cruise and approach is determined for use in determining trim drag. In the overall synthesis process, the wing location affects the required canard size, and the resultant canard and vertical tail sizes affect the aerodynamic forces and the total weight.

The stability and control computations use reference values of aerodynamic forces and moments and other parameters, and perturbations off of these reference values. Both externally-generated, internally-stored data and analytical relationships are used.

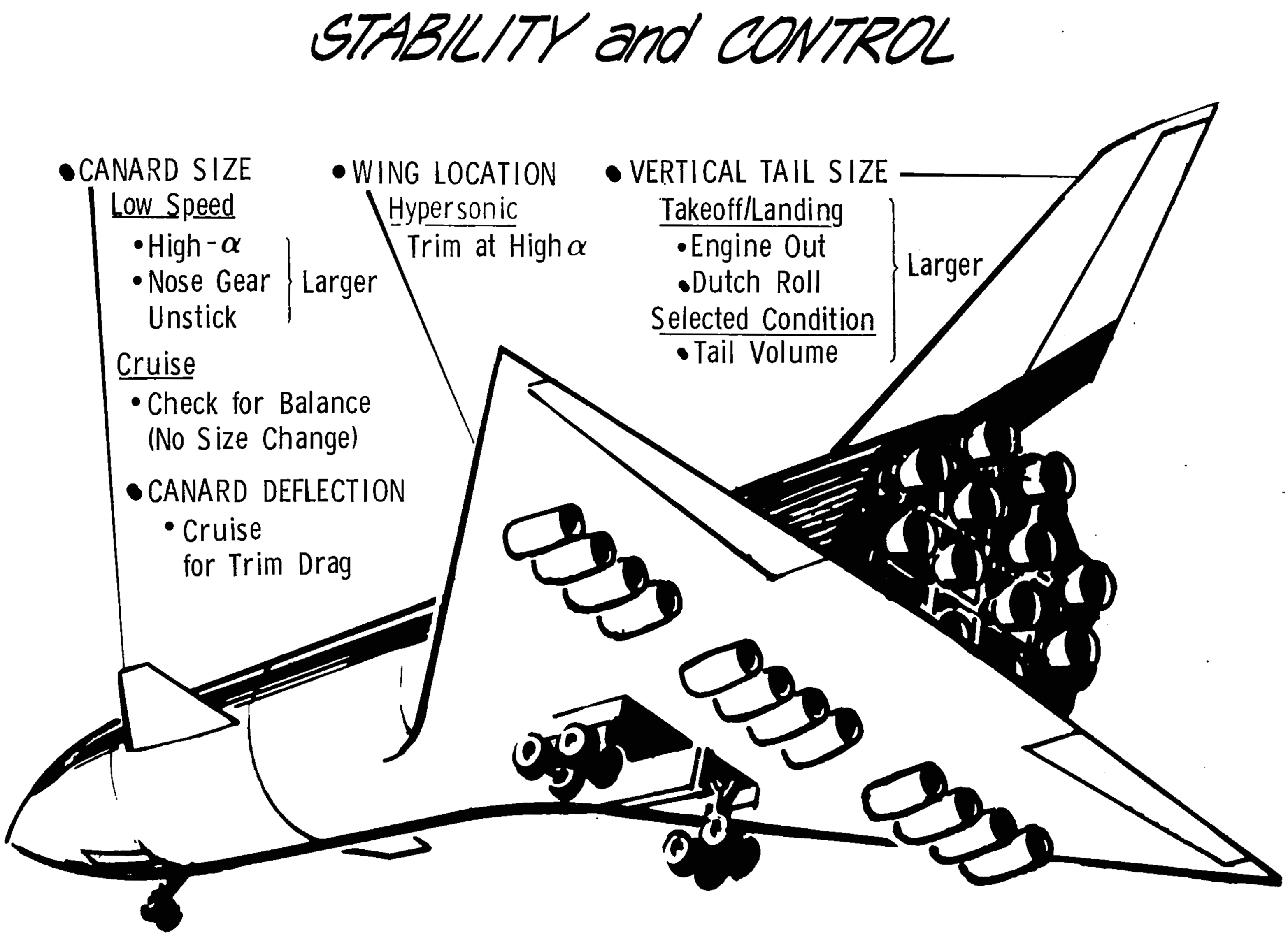
STABILITY and CONTROL
• CANARD SIZE
Low Speed
• High - α
• Nose Gear Unstick
Larger
Cruise
• Check for Balance (No Size Change)
• CANARD DEFLECTION
• Cruise for Trim Drag
• WING LOCATION
Hypersonic
Trim at High α
• VERTICAL TAIL SIZE
Takeoff/Landing
• Engine Out
• Dutch Roll
Selected Condition
• Tail Volume
Larger

Figure 10

AIR-BREATHING PROPULSION

(Figure 11)

Unlike the wing, which is permitted to change in both size and shape, the air-breathing engines are of fixed design (for a given reference configuration) and are only scaled up and down in size. The reference engine thrust and fuel flow data are stored in the propulsion library as functions of altitude and Mach number. The independent engine configuration variable is ϵ, the ratio of perturbed engine thrust level to reference engine thrust level. As shown in the figure, thrust and fuel flow for scaled engines (primed values) are obtained by multiplying the reference values by the scale factor ϵ. The scaling is performed under the assumption of constant specific fuel consumption. Nacelle diameter and length changes are computed on the basis of the expressions shown in the figure, where k can be either constant or a function of ϵ.

AIR-BREATHING PROPULSION

THRUST SCALING OF A FIXED CONFIGURATION

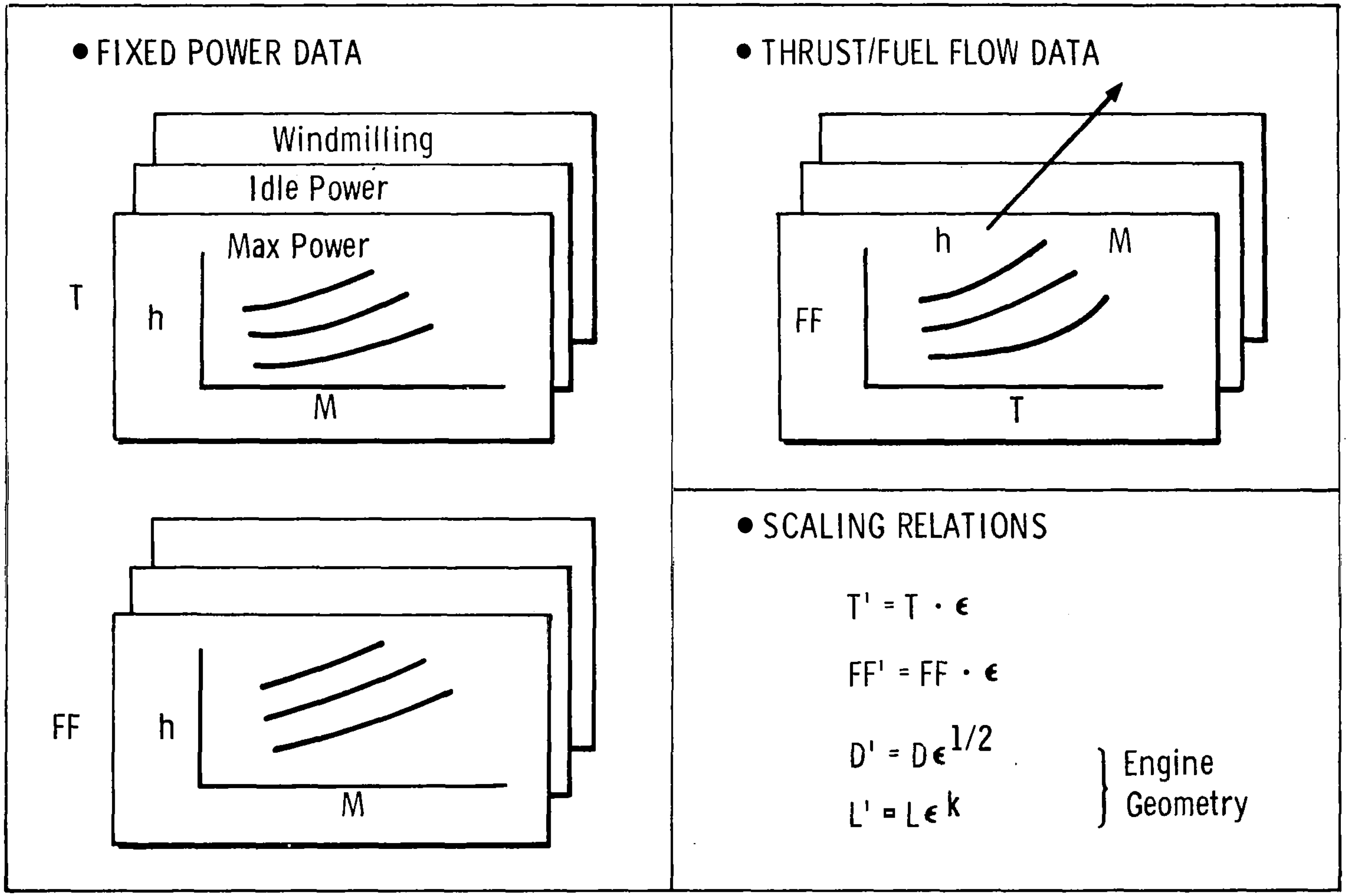

Figure 11

AERODYNAMIC HEATING

(Figure 12)

Changes in maximum temperatures and heating rates affect the synthesis process directly by influencing weight requirements. In addition, heating data provide guidance for materials selection; structural concept formulation (e.g., heat sink, hot structure, etc.); and general design (e.g., canard location to avoid severe shock-impingement heating). The heating/weight interaction could have been handled internally by making the weight perturbation data a function of the aerodynamic heating parameters. However, for simplicity, it was elected to treat this interaction external to the procedure. Therefore, the aerodynamic heating data are generated for information only and are used externally to (1) verify, or modify if necessary, the reference configuration weights and weight perturbation data, and (2) to provide design guidance.

A variety of generalized laminar, turbulent, and high angle of attack techniques are available to compute temperatures and heating rates at up to twelve locations over the vehicle. The appropriate method is selected internally by the program based on input switching values of Reynold's Number and angle of attack. Either a three-node or a one-node model may be specified at a given location. A radiation equilibrium calculation can be included in each model.

A typical problem may include (1) stagnation heating computations at selected points on the surface leading edges and on the nose, (2) surface heating computations at representative points on the body, wing and tail, and (3) surface heating of the upper and lower surfaces at given locations on the wing and canard using a three-node model.

AERODYNAMIC HEATING

- A VARIETY OF GENERALIZED LAMINAR, TURBULENT, AND HIGH - α TECHNIQUES AVAILABLE ALL OVER THE VEHICLE
  - 1- or 3-Node Thermal Model
  - Radiation Equilibrium Model
- TYPICAL LOCATIONS

● Stagnation Line/Point Heating

⬢ Surface Heating
Primary Locations

⬡ Upper Surface (Closed Lower)

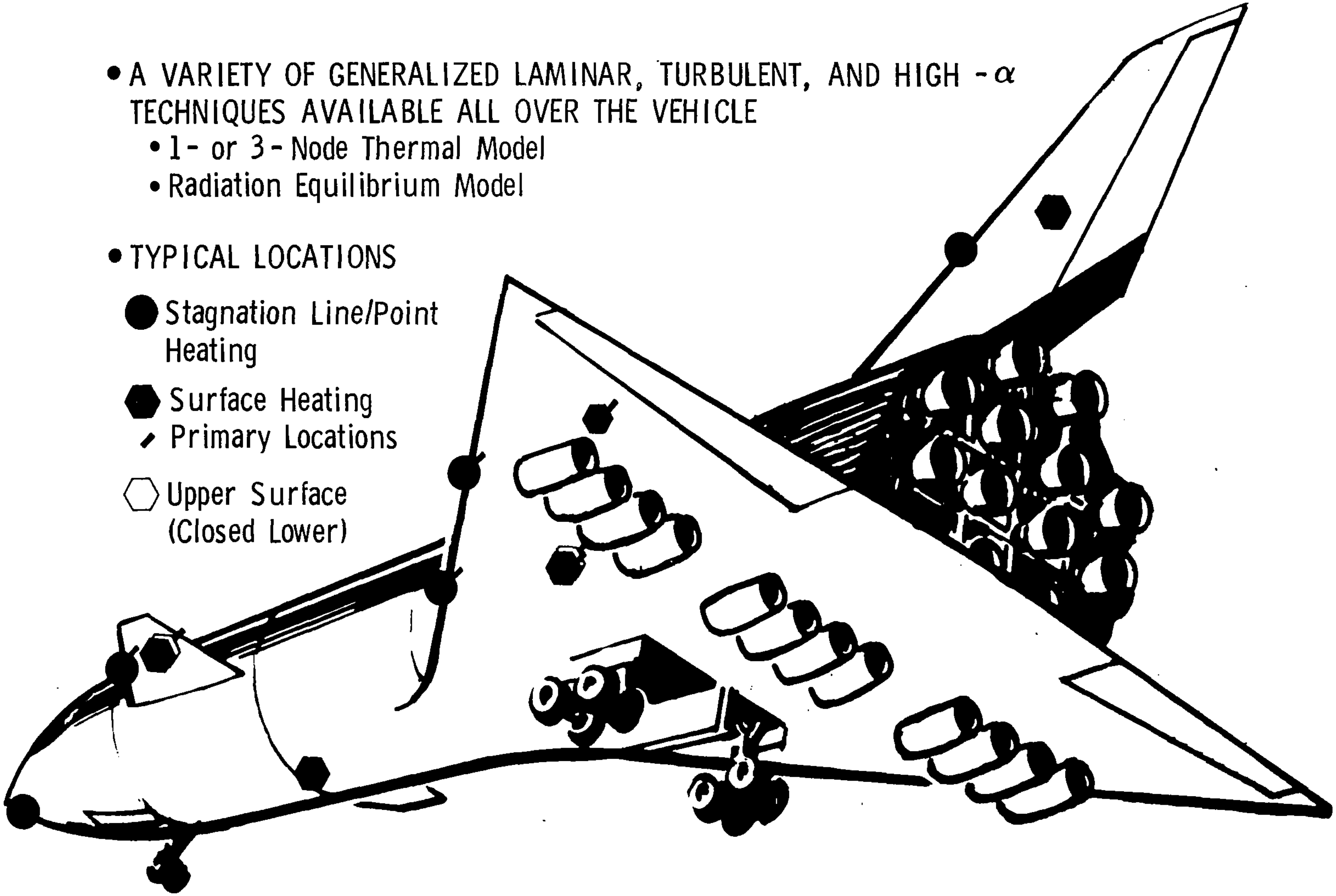

Figure 12

FLIGHT MECHANICS/PERFORMANCE/MISSION ANALYSIS

(Figure 13)

During each pass through the weight-sizing loop, the flyback capability of the vehicle is determined by integration of the path from landing back to the beginning of cruise. The required flyback range is determined by integration of the entry path from staging to engine deployment.

The entry path is integrated with a three-translational-degree-of-freedom procedure developed on another project. It assumes a spherical, rotating earth and a wind profile that varies in speed and direction with altitude. The procedure includes a set of transformations which allow the type of entry path to be specified as a series of segments with virtually any type of controls.

The cruise routines are based on quasi-steady-state equations of motion in two degrees of freedom. A head-wind profile and various engine-out options are provided. The cruise paths may be internally optimized on altitude and/or speed with ceiling contraints and cruise-climb corrections applied.

An optional descent path at idle power may be integrated if range credit is allowed. Landing reserves are computed from any combination of (1) a fixed fuel allowance, (2) a percentage of total fuel available, and (3) a specified duration at constant altitude and optimum or constant speed.

On the final pass through the sizing iteration, i.e., when the weight at entry satisfies the flyback requirement, the aerodynamic heating equations are integrated during the integration of the entry path. Other performance calculations are also made at this point. These include takeoff and landing simulations to determine runway length requirements and integration of a ferry mission to determine ferry range capability.

FLIGHT MECHANICS/PERFORMANCE/MISSION ANALYSIS

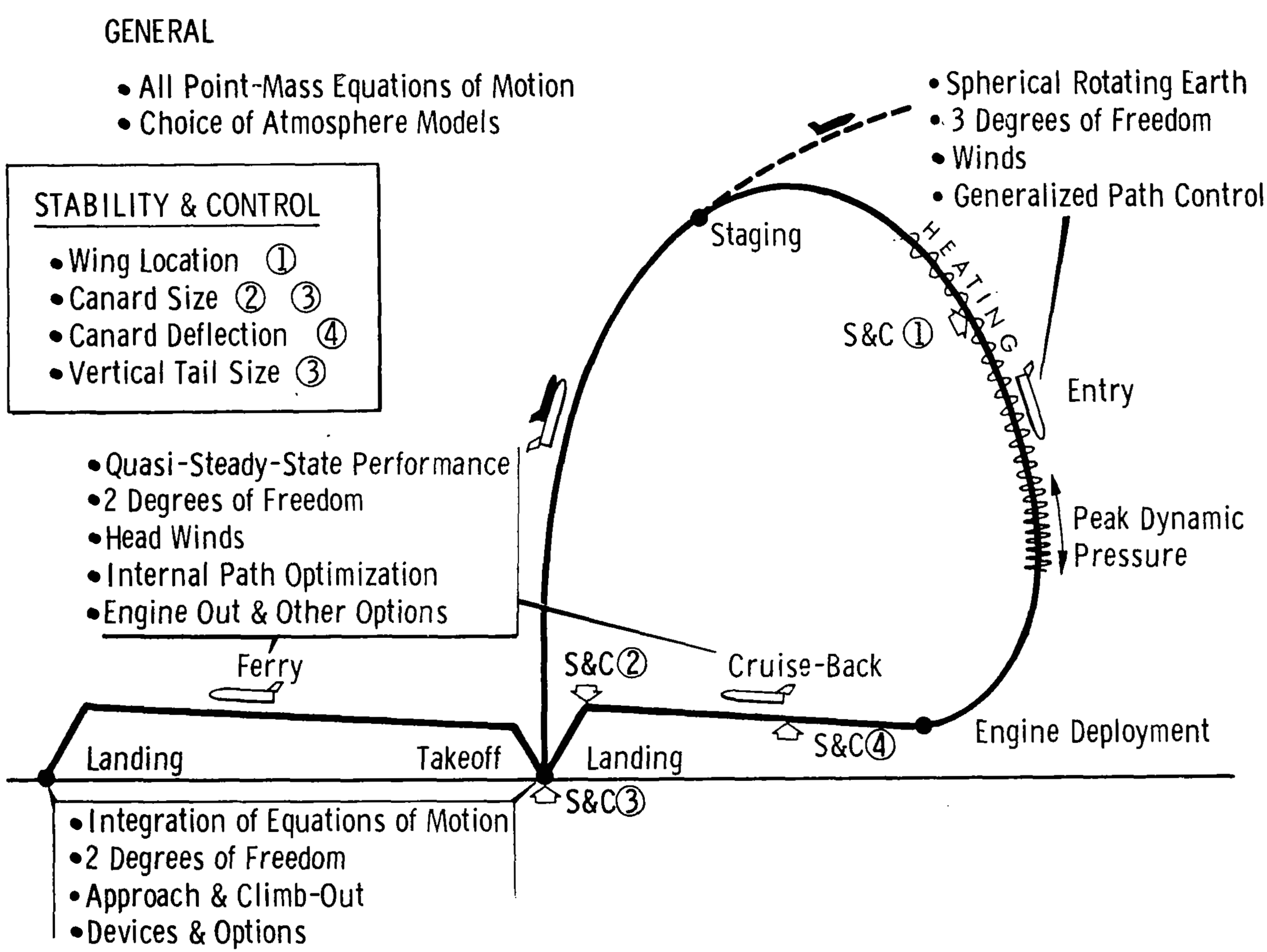

Figure 13

EXAMPLE GEOMETRY VARIABLES - PLANFORM

(Figure 14)

Numerous geometrical variables must be determined for use in the various technology computations (e.g., reference areas for aerodynamic forces, moment arms for stability and control, etc.) and in the computer graphics routines. Some of the planform variables involved in this process are illustrated in the figure. For example, secondary wing planform variables such as exposed and theoretical root chords, tip chord, exposed mean aerodynamic chord, etc., are computed from primary configuration variables such as exposed wing area, leading edge sweep, aspect ratio, and taper ratio.

Numerous options are available to accommodate a wide variety of configuration types. These options relate to such things as the locations of engines, cruise fuel tanks, and main landing gear and how each moves as the primary configuration variables are perturbed.

EXAMPLE GEOMETRY VARIABLES - PLANFORM

WING:

- Area - S_{Exp}
- Sweep - Λ
- Aspect Ratio - $AR = b^2/S$
- Thickness Ratio - t/c
- Taper Ratio - $\lambda = C_T/C_{R\,Exp}$

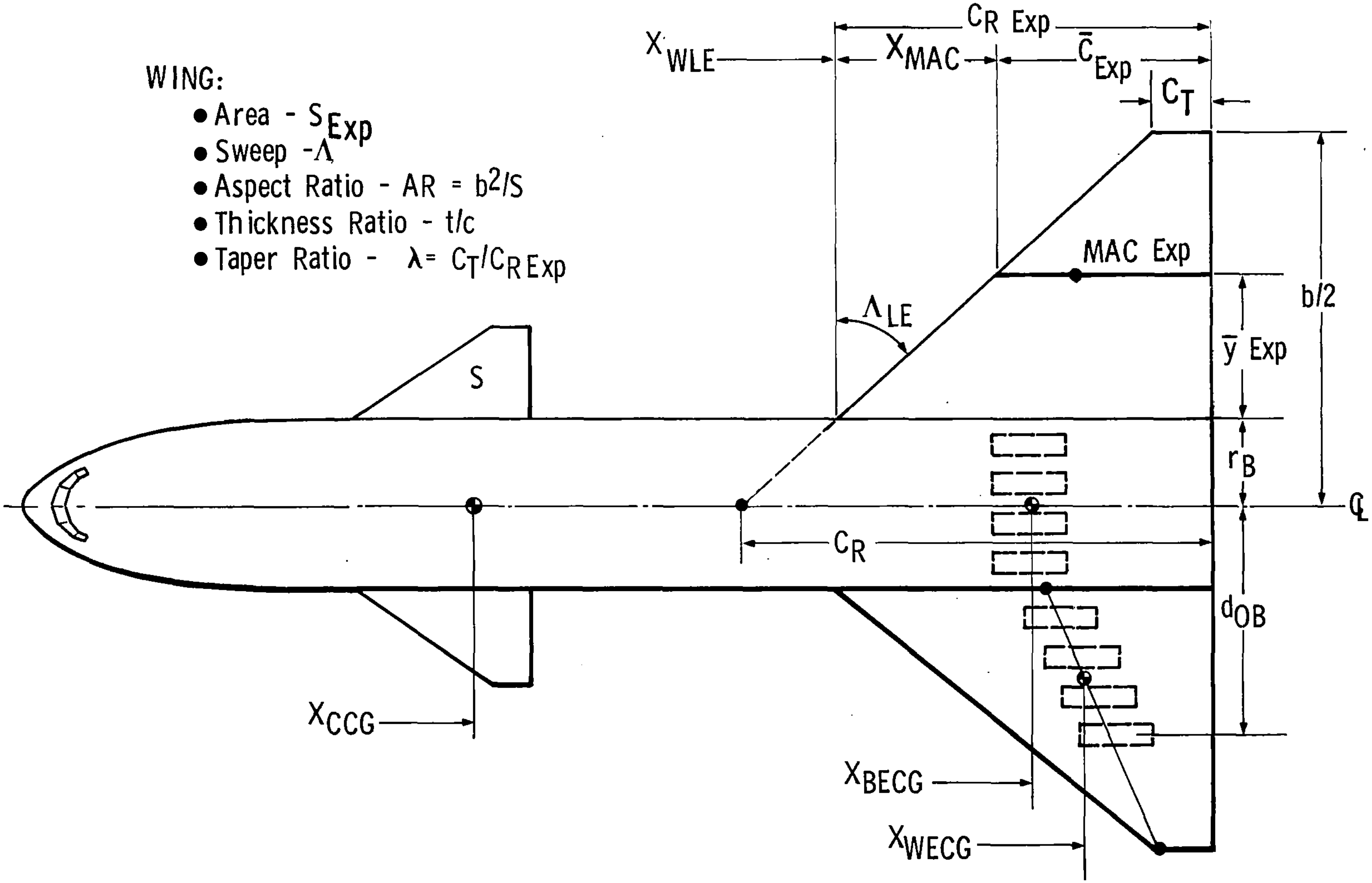

Figure 14

EXAMPLE GEOMETRY VARIABLES - PROFILE

(Figure 15)

In addition to the planform variables mentioned on the previous page, other geometry variables pertaining to the vehicle profile are computed. For example, ground interference angles for wing trailing edge root and tip chords and vehicle tail bump are computed for the purpose of determining the maximum pitch angle. Another example is the location and orientation of the resultant thrust vector with respect to the vehicle center of gravity which is provided for use in stability and control computations.

EXAMPLE GEOMETRY VARIABLES - PROFILE

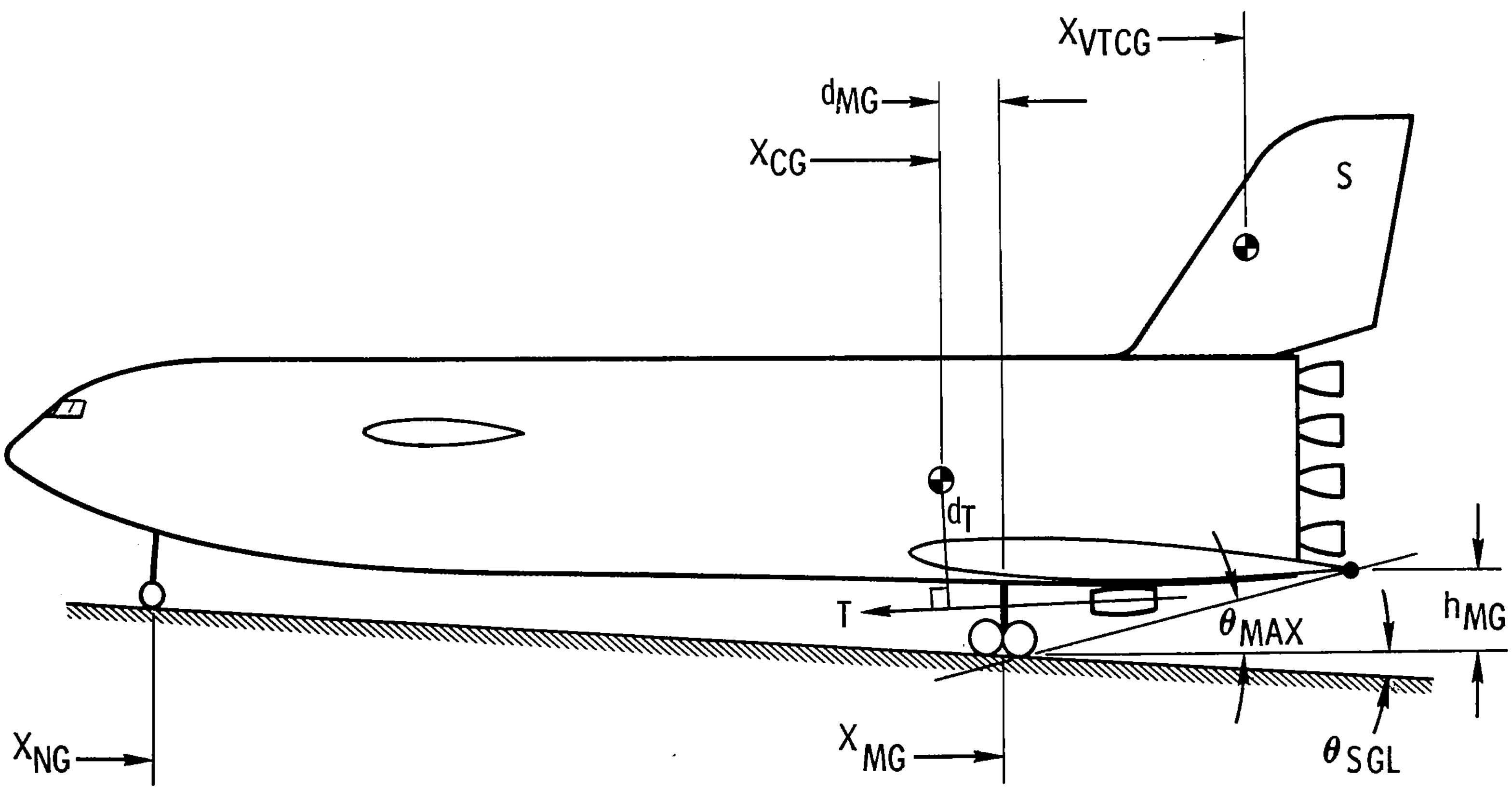

Figure 15

PROGRAM APPLICATIONS

(Figure 16)

The computer procedure which has been developed is designed to treat a number of different types of problems associated with configuration definition and evaluation for the booster flyback system of a reusable earth-to-orbit space transportation system.

The figure summarizes the principal areas of procedure application and the basis of its operation. For specified configurations, the procedure can be used simply as a flight mechanics/performance/aerodynamic-heating evaluation tool of considerable detail and versatility. However, its most powerful utilization is (1) to scale an existing configuration up or down (e.g., to accommodate a different payload weight); or (2) to synthesize a completely new configuration - to the point of optimizing it (e.g., minimum weight). In addition, the procedure can be applied to a number of special problems, including the generation of sensitivity data of all types. For all of these applications, constraints are applied to insure that the proper landing location is achieved and that stability and control criteria are met.

Surveys can be conducted on the seven independent configuration variables shown in the figure. For each point on the parametric curves the program provides a complete set of configuration and flight path definitions with geometry, aerodynamic, stability and control, aeroheating, mass properties and performance summaries.

The results of studies using this procedure will be integrated into overall booster studies, and ultimately into total system (booster plus orbiter) studies.

PROGRAM APPLICATIONS

- FLIGHT MECHANICS/PERFORMANCE/HEATING
- SCALING AN EXISTING CONFIGURATION
- SYNTHESIZING A NEW CONFIGURATION
- CONFIGURATION, MISSION, OTHER SENSITIVITIES
- CONFIGURATION OPTIMIZATION

- SATISFIED CONSTRAINTS
  - Landing Location (Fuel)
  - Trim
- INFORMATION
  - Cruise Balance
  - Aero Heating
  - Landing Performance
  - Takeoff Performance
  - Ferry Performance
  - Etc.

Perturbations on ...

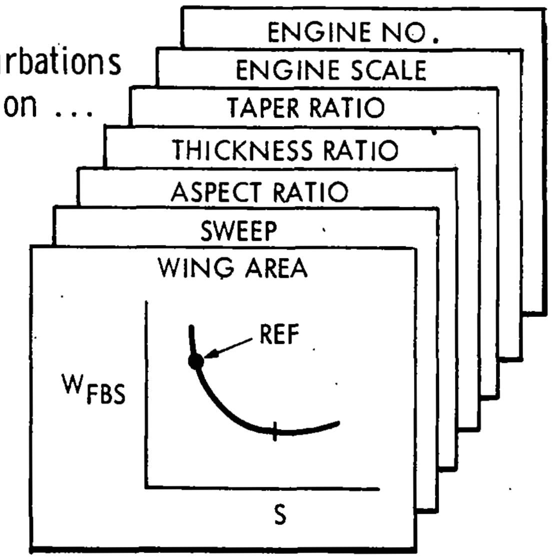

Figure 16

FLIGHT MECHANICS/PERFORMANCE

(Figure 17)

The computer procedure is currently in final checkout and intial operational evaluation. The final three figures present example results which have been obtained in checkout runs. To avoid the impression that these example results imply configuration guidance relative to some real design, several of the variables are plotted in normalized form, rather than as actual values.

The opposing figure presents a typical entry path, starting after staging. A roll program is initiated and a highly pitched, highly banked segment is flown until a load factor limit is reached. The load factor limit is followed by a stability limit specified by a Mach-alpha profile. The turn is continued until the heading to the landing site is achieved.

FLIGHT MECHANICS/PERFORMANCE

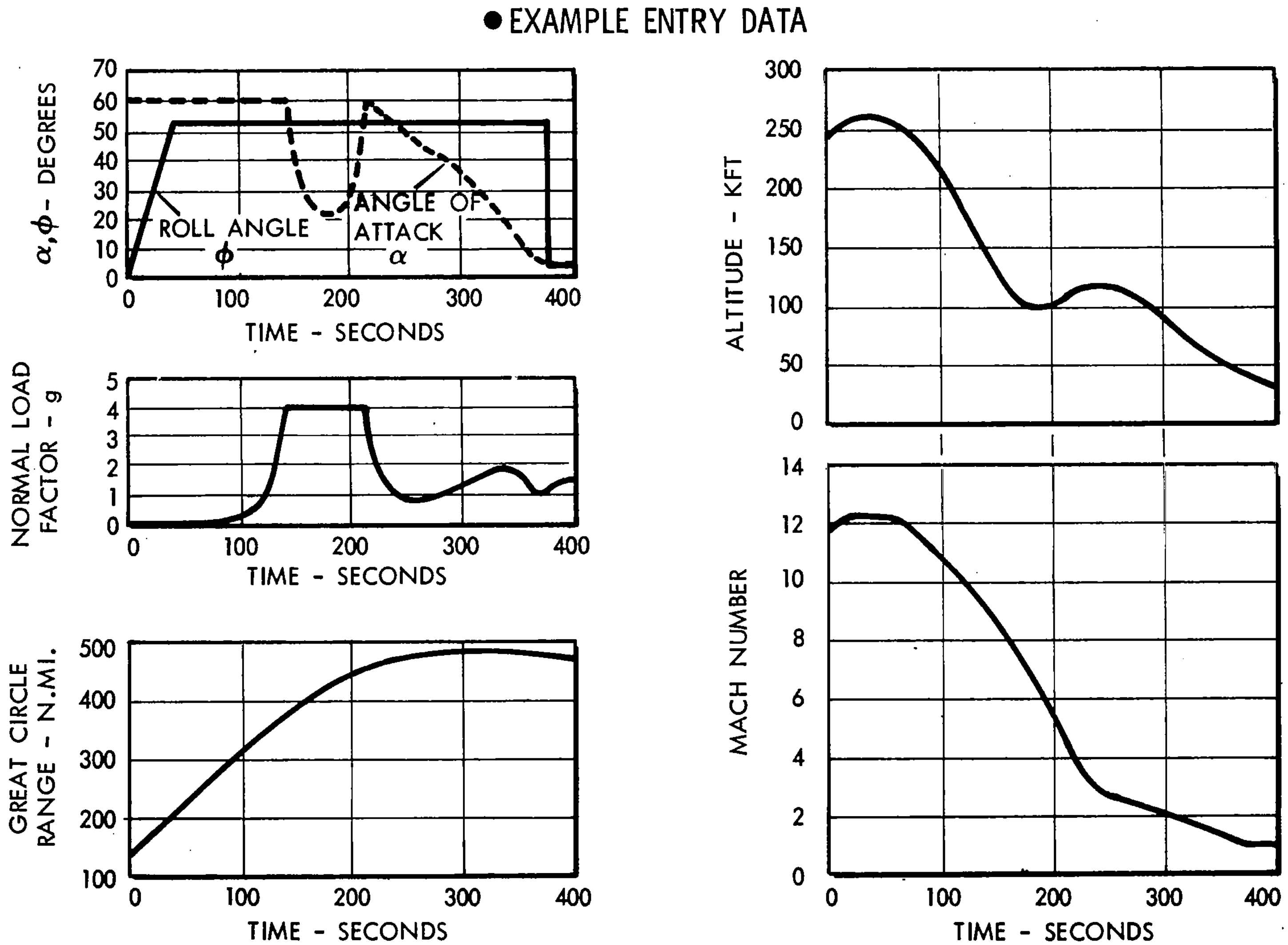

Figure 17

EXAMPLE SENSITIVITY DATA

(Figure 18)

The opposing figure presents the results of sizing two specific configurations with and without an assumed wind profile. This is a severe profile, and it acts essentially as a crosswind during entry and headwind during cruise. The effects of wind on both cruise-back range and flyback system weight are shown.

EXAMPLE SENSITIVITY DATA

- EFFECT OF WIND

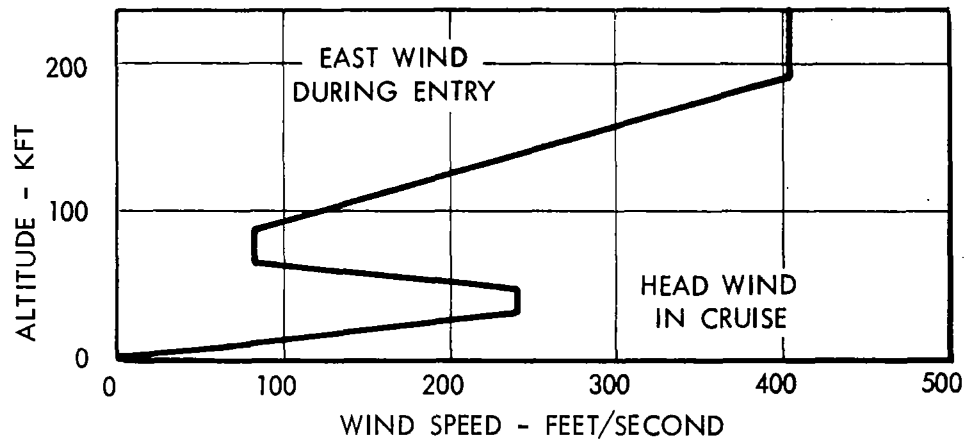

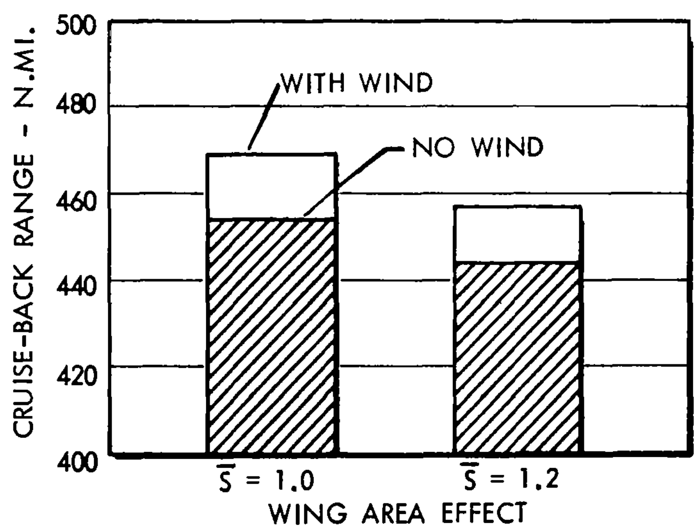

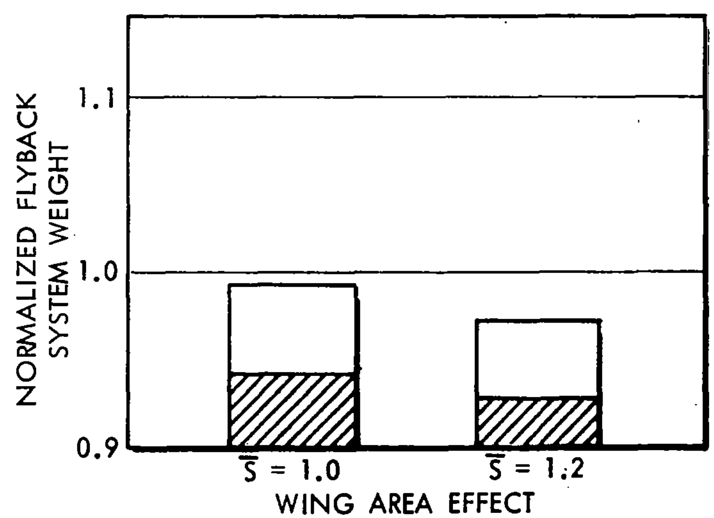

Figure 18

EXAMPLE SYNTHESIS DATA

(Figure 19)

The opposing figure shows the effects on cruise-back range and flyback system weight due to independent variations in aspect ratio, wing area, and engine scale factor. It can be seen that increasing either aspect ratio or wing area decreases flyback system weight. This is due to improved cruise efficiency in the case of aspect ratio, and due to improved deceleration and turning during entry in the case of wing area. The engine scale factor has little effect, because the scaling is done at constant specific fuel consumption.

EXAMPLE SYNTHESIS DATA

● CRUISE-BACK RANGE VARIATIONS

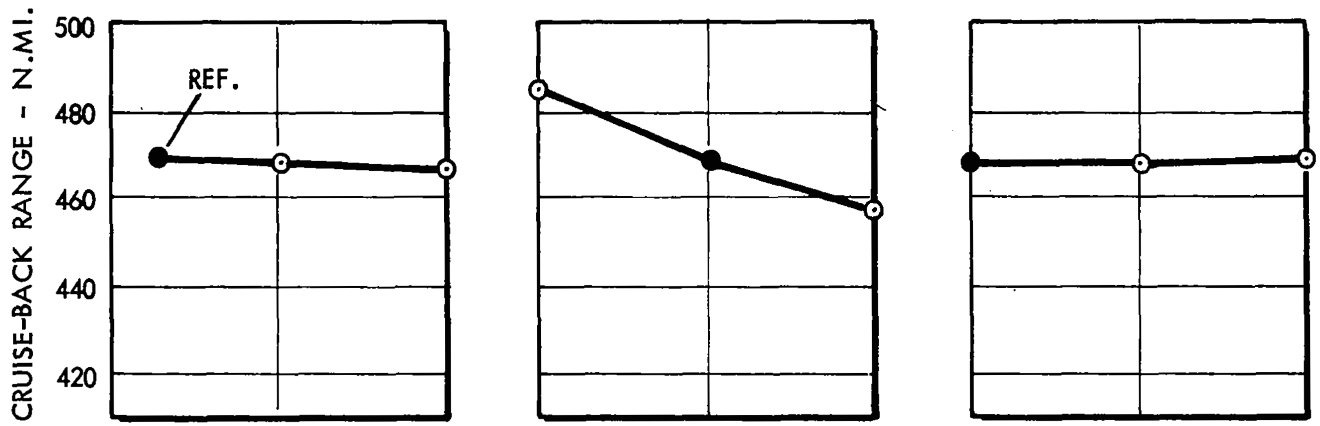

● FLY-BACK SYSTEM WEIGHT VARIATIONS

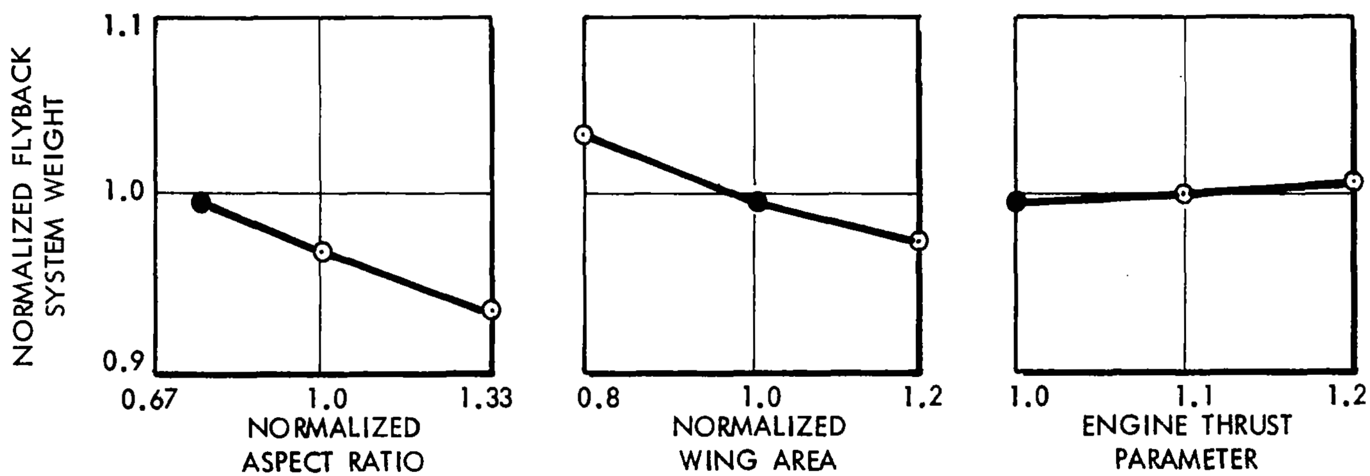

Figure 19

OPTIMIZED SPACE SHUTTLE TRAJECTORY SIMULATION

Louis Tramonti, Senior Aeroballistics Engineer
Trajectory Simulation, Vehicle Software Systems and Trajectories

Richard G. Brusch, Design Specialist
Optimization Technology, Launch Vehicle Programs

Convair Aerospace Division of General Dynamics
San Diego, California

INTRODUCTION

Current and anticipated aerospace vehicles have many trajectory degrees-of-freedom that can be optimized to maximize or minimize a performance measure such as payload, range, or cost. This feature is particularly true for lifting reusable space shuttle configurations where the inclusion of lift adds additional operational modes such as lifting dogleg maneuvers during ascent, aerodynamically-controlled entry maneuvers, and synergetic skipping maneuvers. Many trajectory constraints must be considered such as maximum heating, acceleration, angle of attack, and excluded or included overflight or impact regions. To synthesize lifting shuttle vehicle trajectories, it is necessary to have the capability to optimize highly constrained trajectories for all phases of flight.

A computer program, the General Trajectory Optimization Program (GTOP), is described in this paper. The program can handle the ascent, return, and synergetic maneuvers of lifting boosters and spacecraft. This generality also means that the GTOP program can be used for a large variety of aerospace vehicles and missions.

TRAJECTORY STRUCTURE

Trajectory sectioning is a method of subdividing the time history of a trajectory simulation into parts relevant to the description of the simulation. The simulation sections are defined to allow for the following types of changes in the simulation models:

1. Changes in the state equations (the flight equations).
2. Changes in the control model (those functions and parameters that the user is free to manipulate).
3. Changes in the various trajectory constraints.
4. Changes in the terms of the performance measure.
5. Requirement for an analytic trajectory segment (e.g. a weight discontinuity caused by jettisoning an expended stage or a conic trajectory arc).

A section is defined as any segment of the trajectory in which the mathematical model is of a given form and the state variables $x_{ij}(t)$, during the numerically integrated part, are continuous functions of time. Section endpoints are chosen to coincide with points at which the differential equations, the control model, or the trajectory constraints change form; or at which the state variables experience a discontinuity. Analytic trajectory segments are used whenever a state variable discontinuity is modeled or whenever it is possible to propagate the trajectory analytically, such as use of a conic trajectory. Trajectory sectioning provides a skeletal framework that may be molded by users with widely varying problems to facilitate the description of their particular problem to a general mathematical model.

Each trajectory section may consist of an analytic part and a numerically integrated part. The numerically integrated part of a section is governed by the set of nonlinear differential equations of motion (the state equations*) which must be numerically integrated in order to propagate the trajectory. The state equations have the form shown in Equation (1) in the illustration.

The analytic part of a section is that part for which analytic integrals of the motion may be used to propagate the trajectory. The four analytic methods currently available are: 1) state variable discontinuity by a specified value, 2) state variable discontinuity to a specified value, 3) conic trajectory propagation through a specified time, and 4) conic trajectory propagation through a specified central angle.

**The state equations (to be discussed later) define the position, velocity, and weight of the vehicle.*

STATE EQUATIONS

$$x_{ij}(t) = f_{ij}\left[x_{ij}(t),\ u_{kj}(t),\ d_p,\ t\right] \tag{1}$$

$i = 1, 2, \ldots n_i$ (state variable index)

$j = 1, 2, \ldots n_j$ (simulation section index)

$k = 1, 2, \ldots n_k$ (time varying control parameter index)

$p = 1, 2, \ldots n_p$ (time invariant design parameter index)

where:

$u_{kj}(t)$ is the kth time varying* control variable of the jth simulation section.

d_p is the pth time invariant design parameter

$x_{ij}(t)$ is the ith state variable of the jth simulation section

t is the time

**The procedure described here, and which is used in the GTOP Program, allows the use of any of a large number of parameters as the independent variable of a control function; however, these independent variables are themselves time varying; hence the representation $u_{ku}(t)$ is general*

For some problems it is necessary to be able to simulate a trajectory which branches at one or more points. For example, the optimization of a space shuttle ascent trajectory in which constraints are imposed during the booster return flight and during possible abort return flights (left half of figure) requires the capability to simulate a trajectory with multiple branching points. After each ascent trajectory simulation, the normal booster return flight and hypothetical abort trajectories which can be initiated at the beginning or end of any ascent simulation section (as shown in left half of figure) are then simulated. To meet the return flight constraints, the ascent trajectory must be modified; thus the hypothetical abort and booster return trajectories directly influence the optimization of the ascent trajectory. A generalized branching capability is provided in the GTOP system. This procedure allows the initiation of any simulation section at either the beginning or end of any integrated arc. This trajectory sectioning and general branching capability is shown in the right half of the figure.

TRAJECTORY STRUCTURE

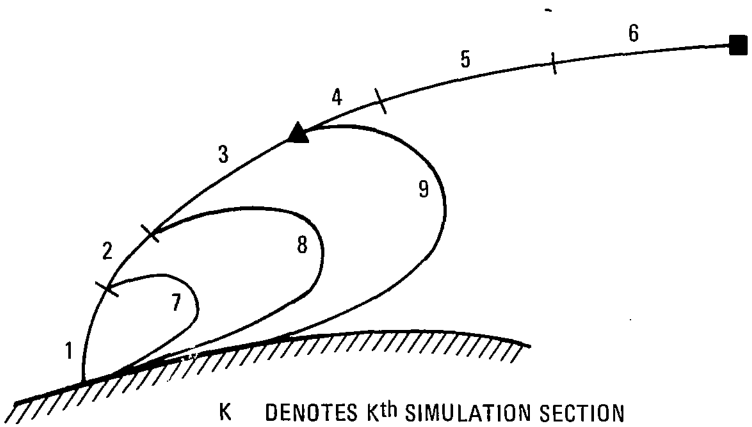

K DENOTES K^th SIMULATION SECTION
▲ STAGING
■ ORBITAL INSERTION

SIMULATION SECTION	FLIGHT PHASE
1 ⟶ 6	NOMINAL ASCENT
7	ABORT CASE 1
8	ABORT CASE 2
9	BOOSTER RETURN

TYPICAL ASCENT TRAJECTORY WITH BOOSTER ABORT/RETURN CONSTRAINTS

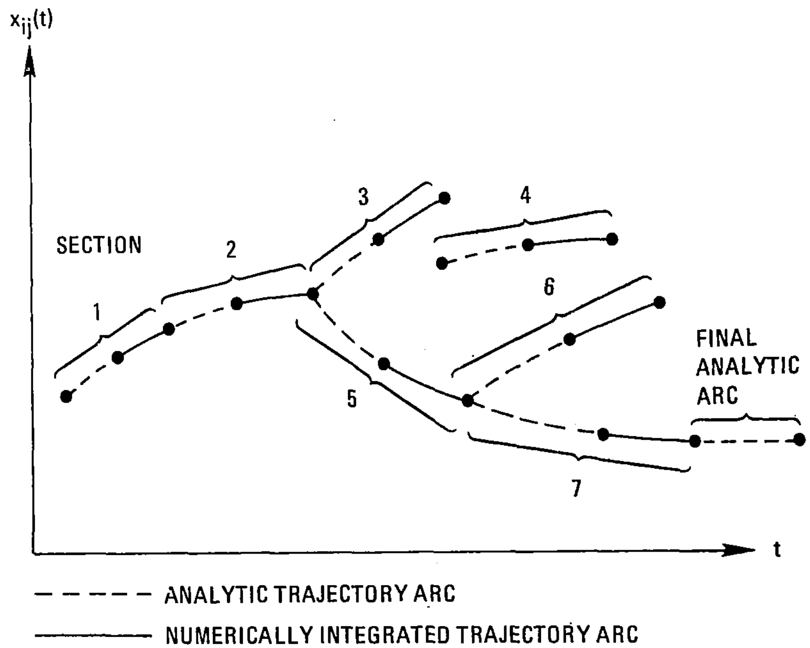

TRAJECTORY SECTIONING AND GENERAL BRANCHING CAPABILITY

Figure 1

GENERAL MATHEMATICAL PROBLEM

The mathematical problem is to extremize a performance measure which is a function of the vehicle and its trajectory when the vehicle/trajectory is constrained by up to six categories of constraints. The performance measure to be extremized has the form of Equation (2).

The problem, then, is to determine optimal $u_{kj}(t)$ and d_o such that J is extremized and such that the specified constraints are satisfied. The general mathematical model incorporates six types of problem-oriented equality and inequality constraints. Two fundamentally different types of constraints can be identified; those that are functions of the time-varying system variables (dynamic constraints), and those that are functions of the design parameters and the initial and final states of the trajectory sections (parametric constraints). For user convenience, two additional constraints depending upon integrals of the time-varying system variables are provided. These constraint categories are defined by equations (3) through (8).

The dynamic inequality constraints include the familiar state and control variable inequality constraints as a subset. The parametric equality constraints allow the specification of the boundary conditions on the differential equations as well as constraints on the time invariant design parameters. It is noted, however, that neither dynamic nor integral constraints can be defined on an analytic arc.

PERFORMANCE INDEX

$$J = \sum_{m=1}^{n_\phi} \Phi_m (t_j^o, t_j^f, x_{ij}^o, x_{ij}^f, d_p) + \sum_{j=1}^{n_j} \sum_{\ell=1}^{n_L} \int_{t_j^o}^{t_j^f} L_\ell \left[x_{ij}(t), u_{kj}(t), d_p, t\right] dt \qquad (2)$$

where Φ_m is the mth parametric performance term (e.g., net weight)

L_ℓ is the ℓth dynamic performance term (e.g., heating parameter)

n_ϕ is the number of parametric performance terms

n_L is the number of dynamic performance terms

and the superscripts "o" and "f" denote evaluation at the initial and final values of time during the corresponding section.

EQUATIONS FOR CONSTRAINT CATEGORIES

Dynamic inequality (e.g. specification of a maximum dynamic pressure during an interval):

$$\xi_{sj}\left[x_{ij}(t),\ u_{kj}(t),\ d_p,\ t\right] \geq 0 \qquad s = 1, 2, \ldots, n_\xi \tag{3}$$

Dynamic equality (e.g. specification of flight at a constant altitude during an interval):

$$\eta_{sj}\left[x_{ij}(t),\ u_{kj}(t),\ d_p,\ t\right] = 0 \qquad s = 1, 2, \ldots, n_\eta \tag{4}$$

Parametric inequality (e.g. exclusion of areas on the earth's surface from predicted impact for spent stages):

$$\zeta_s\,(t_j^o,\ t_j^f,\ x_{ij}^o,\ x_{ij}^f,\ d_p) \geq 0 \qquad s = 1, 2, \ldots, n_\zeta \tag{5}$$

Parametric equality (e.g. orbital insertion conditions):

$$\psi_s\,(t_j^o,\ t_j^f,\ x_{ij}^o,\ x_{ij}^f,\ d_p) = 0 \qquad s = 1, 2, \ldots, n_\psi \tag{6}$$

Integral inequality (e.g. specification of a maximum total heating parameter):

$$\sum_{j=1}^{n_j} \int_{t_j^o}^{t_j^f} Q_{sj} \left[x_{ij}(t), \mu_{kj}(t), d_p, t\right] dt - D_s \geqq 0 \qquad s = 1, 2, \ldots n_Q \tag{7}$$

Integral equality (e.g. total impulse):

$$\sum_{j=1}^{n_j} \int_{t_j^o}^{t_j^f} P_{sj} \left[x_{ij}(t), \mu_{kj}(t), d_{pj}, t\right] dt - C_s = 0 \qquad s = 1, 2, \ldots n_p \tag{8}$$

where ξ_{si}, η_{sj}, Q_{sj}, and P_{sj} *denote independent functions applicable during simulation section* j.

NONLINEAR PROGRAMMING TECHNIQUE

Nonlinear programming is a term applied to any algorithmic procedure seeking to extremize a function of N independent variables that are restricted to some subspace of Euclidian N-space. The problem then is to minimize J(y) as shown by Equations 9, 10, and 11.

The trajectory optimization problem is a nonlinear programming problem except for one feature: a continuous function of time is sought as the solution to the trajectory optimization problem, whereas the solution to the nonlinear programming problem is represented by a point in Euclidian N-space. This dissimilarity is resolved by approximating the continuous function of time by a function of n independent parameters. These n parameters then become a subset of the N independent variables in the nonlinear programming formulation.

There are two ways in which the n parameters can conveniently be chosen to describe the control. The n parameters can specify the control magnitude at specified points in time. An interpolation device, such as simple linear interpolation can be used to define the control at intermediate points in time. Alternately, the parameters can be regarded as coefficients of some mathematical model that is a function of time. The dynamic optimal control can be approximated to any desired accuracy by refining the parameterization of the control function.

The method of Fiacco-McCormick,[1-8] which is currently judged to be the best interior penalty function method* was selected as the nonlinear programming method to be employed to solve the highly constrained trajectory optimization problems. This method transforms the highly constrained trajectory optimization problem to a related sequence of unconstrained optimization problems in which the sequence is described by the positive real number r_k. The penalty function is the sum of the performance index J(y) and the Fiacco-McCormick penalty terms for inequality and equality constraints.

The algorithm begins at a point $y^{(0)}$ in Euclidian N-space at which all inequalities are satisfied (a feasible point). A systematic method for obtaining an initial feasible solution is given by Fiacco-McCormick[3] and is described later. The constant r_1 is selected and the point $y^{(1)}$ is found such that $P(y^{(1)}, r_1)$ is a minimum. A new value $r_2 < r_1$ is then selected and a point $y^{(2)}$ is found so that $P(y^{(2)}, r_2)$ is a minimum, etc. The limit approaches the solution to the nonlinear programming problem, Equations (9) to (11).

*An interior penalty function method starts with a solution estimate in the feasible region, that is in a region in which none of the inequality constraints are violated. A penalty term is added to the performance index, which keeps the solution in the feasible region at each stage in the iteration.

P — PROBLEM

$$\text{Minimize } J(y) \tag{9}$$

subject to

$$g_i(y) \geq 0 \qquad i = 1, 2, \ldots, m \tag{10}$$

$$h_j(y) = 0 \qquad j = 1, 2, \ldots, p \tag{11}$$

where $y = (y_1, y_2, \ldots, y_N)^T$ and the functions $g_i(y)$ and $h_j(y)$ are single-valued functions of y. To maximize $J(y)$, it is sufficient to minimize $-J(y)$.

$$P(y, r_k) = J(y) + r_k \sum_{i=1}^{m} \frac{1}{g_i(y)} + r_k^{-1/2} \sum_{j=1}^{p} h_j^2(y) \tag{12}$$

$$\lim_{r_k \to 0} \left[\min_{y} P(y^{(k)}, r_k) \right] \tag{13}$$

$$P(y^{(k)}, r_k) > P(y^{(k+1)}, r_{k+1}) \quad \text{for} \quad r_k > r_{k+1} \tag{14}$$

Each iteration requires minimization of the function P for a given value of r. This problem is termed the P-problem, and its solution is fundamental to the method of Fiacco-McCormick. The computational algorithm which was implemented minimizes the function P, using a Fletcher-Powell[9] function minimization algorithm in conjunction with the simultaneous golden section search/cubic curve fit, one dimensional search of Johnson and Meyers.[10]

It can be seen from the form of the penalty term that a minimization technique will avoid points y that cause $g_i(y)$ to go to zero and become negative since $1/g_i(y)$ would increase without bound. Clearly, the initial point $y^{(0)}$ must be feasible. It is also clear that the minimization of $P(y, r_k)$ will force $h_j \to 0$, since otherwise these terms would increase without bound as $r^{1/2}$ goes to zero.

A sequence of minimizations is performed with $r_1 > r_2 \ldots > r_k \ldots > r_f$, rather than just one minimization of $P(y, r_k)$, because the latter minimization problem is very difficult to solve from a numerical standpoint. The solution of the P-problem at each stage then provides a good initial estimate for the solution of the P-problem at the following stage.

Fiacco and McCormick[2] prove that their method is computationally stable for the inequality constrained problem because of Equation (14).

GENERATION OF A FEASIBLE SOLUTION – This section reviews the algorithm developed by A. V. Fiacco for generating initial feasible solutions. An arbitrary initial design vector y^o will result in general in $s<m$ of the inequality constraints being satisfied while the remainder will be in violation. With no loss in generality, assume the constraints to be reordered so that the first s constraints are the satisfied constraints. Constraint $s + 1$ can be brought into the feasible set while simultaneously guaranteeing that constraints $1, 2,\ldots,s$ remain in the feasible set by solving the following nonlinear programming problem:

$$\text{minimize} \quad J(y) \equiv -g_{s+1}(y)$$

$$\text{subject to} \quad g_j(y) \geqslant 0 \quad j = 1,\ldots,s$$

using the Fiacco-McCormick algorithm previously described. The minimization is terminated as soon as g_{s+1} becomes positive. This constraint is then a member of the feasible set and the procedure is repeated with the next violated constraint until all inequality constraints are satisfied. Note that both the equality constraints, Equation 11, and the original performance index, Equation 9, are temporarily ignored during the generation of the feasible solution.

CONSTRAINED OPTIMAL CONTROL AS A NONLINEAR PROGRAMMING PROBLEM

Implementation of the method of Fiacco-McCormick requires a solution to the P-problem defined in the previous section. Before exhibiting the function P for the trajectory optimization problem, it is convenient to transform the integral constraints, Equations (7) and (8), into parametric constraints on the final values of the following pseudo-state variables, Equations 15 through 18.

Now the P function for the general trajectory optimization problem may be formed by adding to the objective function, Equation 2, penalty terms for constraints, Equations 3 to 6, 16, and 18, in accordance with Equation 12, to yield Equation 19.

PSEUDO-STATE VARIABLES

$$\dot{x}_{(n+i),j} = P_{ij}\left[x_{ij}(t),\ u_{kj}(t),\ d_p,\ t\right] \qquad x^{o}_{(n+1),j} = 0 \qquad i = 1, 2, \ldots, n_p \tag{15}$$

with corresponding parametric constraints

$$x^{f}_{(n+i),} - C_i = 0 \qquad i = 1, 2, \ldots, n_p \tag{16}$$

and

$$\dot{x}_{(n+n_p+i),j} = Q_{ij}\left[x_{ij}(t),\ u_{ij}(t),\ d_p,\ t\right] \qquad x^{o}_{(n+n_p+i),j} = 0 \qquad i = 1, 2, \ldots, n_Q \tag{17}$$

with corresponding parametric constraints

$$x^{f}_{(n+n_p+i),j} - D_i \geq 0 \qquad i = 1, 2, \ldots, n_Q \tag{18}$$

$$P = G(t_j^o, t_j^f, x_{ij}^o, x_{ij}^f, d_p) + \sum_{j=1}^{n_j} \int_{t_j^o}^{t_j^f} L_j^* \left[x_{ij}(t), u_{kj}(t), d_{pj}, t \right] dt \tag{19}$$

where

$$\left.\begin{aligned}
G = {} & \sum_{m=1}^{n_\phi} \Phi_m (t_j^o, t_j^f, x_{ij}^o, x_{ij}^f, d_p) && \text{parametric performance} \\
& + r^{-1/2} \sum_{s=1}^{n_\Psi} \Psi_s^2 (t_j^o, t_j^f, x_{ij}^o, x_{ij}^f, d_p) && \text{parametric equality} \\
& + r^{-1/2} \sum_{i=1}^{n_p} \left[x_{(n+i),\ell}^f - C_i \right]^2 && \text{transformed integral quality} \\
& + r \sum_{s=1}^{n_\zeta} 1/\zeta_s (t_j^o, t_j^f, x_{ij}^o, x_{ij}^f, d_p) && \text{parametric inequality} \\
& + r \sum_{i=1}^{n_Q} 1\Big/\left[x_{(n+n_p+i),\ell}^f - D_i \right] && \text{transformed integral inequality}
\end{aligned}\right\} \tag{20}$$

and

$$\left.\begin{aligned}
L_j^* &= \sum_{\ell=1}^{n_L} L_\ell\left[x_{ij}(t),\, u_{kj}(t),\, d_p,\, t\right] dt && \text{integral performance} \\
&+ r^{-1/2} \sum_{s=1}^{n_\eta} \eta_{sj}^2 \left[x_{ij}(t),\, u_{kj}(t),\, d_p,\, t\right] && \text{dynamic equality} \\
&+ r \sum_{s=1}^{n_\xi} 1/\xi_{sj} \left[x_{ij}(t),\, u_{kj}(t),\, d_p,\, t\right] && \text{dynamic inequality}
\end{aligned}\right\} \quad (21)$$

GENERATING A FEASIBLE SOLUTION FOR STATE AND CONTROL VARIABLE VARIABLE INEQUALITY CONSTRAINTS [12]

The state and control variable inequality constraints, ξ_{sj} in Equation 3 must be satisfied over a continuous range of time.

An initial design estimate represented by the initial control function estimate $u^o(t)$ and the initial design parameter estimate d_p^o will result in general in $s < n_\xi$ of the dynamic inequality constraints being satisfied, while the remainder are violated during some time interval.

As before, assume the constraints to be reordered so that the first s constraints are those satisfied for the pertinent time interval, while the remainder are those in violation. Dynamic constraint s + 1 can then be brought into the feasible set while simultaneously guaranteeing that the first s constraints remain in the feasible set by solving the problem to the right.

The Fiacco-McCormick minimization algorithm is terminated as soon as $\xi_{(s+1)} \leqslant 0$ for all pertinent time intervals. This constraint is then a member of the feasible set and the procedure is repeated for the next violated dynamic inequality constraint until all inequality constraints have been satisfied.

NUMERICAL CONSIDERATIONS – The first term in Equation 22 is the integral of the current inequality constraint being satisfied, over all time at which it is in violation, (see figure). This term has minimum value of 0, which will be achieved when the constraint trajectory is driven out of the violated region. The second term prevents the constraint from going into violation at a time point at which the constraint was initially satisfied. The third term prevents constraints already in the feasible set from becoming violated.

Obviously it is impossible to integrate the second term to the time at which $\xi = 0$. To do so numerically causes trapped points during the minimization process. As ξ at point A in the figure moves the epsilon distance from being just violated to being just feasible the second penalty term experiences a sudden increase, although the move was in a desirable direction. The function minimization algorithm becomes trapped. To alleviate this problem the time intervals for the evaluation of the second term are fixed at integration time points just outside the violated region at the start of the function minimization.

Theoretically, these boundaries should remain frozen throughout the function minimization. Experience indicates, however, that the integration limits can be updated at the end of each one dimensional search. Such frozen limits on the first term are not required.

A DYNAMIC INEQUALITY CONSTRAINT TRAJECTORY

$$\underset{u(t)\, d_p}{\text{minimize}} \sum_{j=1}^{n_j} \int_{t_j^o}^{t_j^f} \Big\{ - \xi_{(s+1),j} U(- \xi_{(s+1),j}) \qquad (22)$$

$$+ r_k U(\xi_{(s+1),j}) / \xi_{(s+1),j} \quad + r_k \sum_{i=1}^{s} 1/ \xi_{ij} \Big\}\, dt$$

$$\text{where } U(x) = \begin{Bmatrix} 1 \text{ if } x > 0 \\ 0 \text{ if } x \leqq 0 \end{Bmatrix}$$

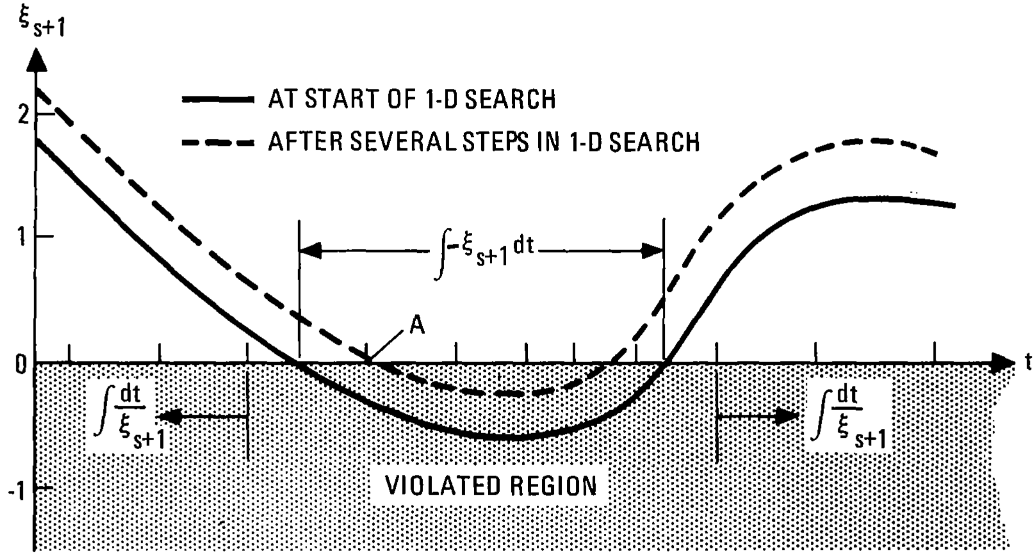

Figure 2

TRAJECTORY SIMULATION

To simulate and optimize Space Shuttle ascent and entry trajectories, a General Trajectory Optimization Program (GTOP) was developed.[11] This general-purpose computer program combines a flexible, high-speed, trajectory simulation module with a highly reliable nonlinear programming optimization driver. GTOP represents an implementation of all features of the general mathematical model presented previously.

The flight of the shuttle vehicle is described by a set of seven differential equations written in a relative velocity coordinate system. The first three elements of the state vector describe the current position of the vehicle with respect to a rotating earth: geocentric radius vector, r; geocentric latitude, θ; and geocentric longitude, ϕ.

DIFFERENTIAL EQUATIONS OF MOTION

$$\boxed{\dot{r} = v \sin\gamma}$$

$$\boxed{\dot{v} = \left[g_\theta(\cos\beta\cos\gamma) - g_r(\sin\gamma) + \frac{F_v g_0}{W} + \omega^2 r(\cos\theta)(\sin\gamma\cos\theta - \cos\beta\cos\gamma\sin\theta) \right]}$$

$$\boxed{\dot{\gamma} = \frac{v}{r}(\cos\gamma) + \left[\frac{1}{v}\right]\left[-g_\theta(\cos\beta\sin\gamma) - g_r(\cos\gamma) + \frac{F_\gamma g_0}{W} + 2\omega V(\sin\beta\cos\theta) + \omega^2 r(\cos\theta)(\cos\gamma\cos\theta + \cos\beta\sin\gamma\sin\theta) \right]}$$

$$\boxed{\dot{\beta} = \frac{1}{v(\cos\gamma)}\left[\frac{v^2}{r}(\sin\beta\cos^2\gamma\tan\theta) - g_\theta(\sin\beta) + \frac{F_\beta g_0}{W} + 2\omega V(\cos\gamma\sin\theta - \cos\beta\sin\gamma\cos\theta) + \omega^2 r(\sin\beta\sin\theta\cos\theta) \right]}$$

$$\boxed{\dot{\theta} = \frac{V\cos\beta\cos\gamma}{r}}$$

$$\boxed{\dot{\phi} = \frac{V\sin\beta\cos\gamma}{r\cos\theta}}$$

$$\boxed{\dot{w} = \text{tabular or analytic model}} \tag{23}$$

where

$$\left.\begin{aligned}
F_\beta &= (+\cos\lambda\sin\alpha\sin\sigma + \sin\lambda\cos\sigma)F_\xi + (-\sin\lambda\sin\alpha\sin\sigma + \cos\lambda\cos\sigma)F_\eta + (-\cos\alpha\sin\sigma)F_\zeta \\
F_v &= (+\cos\lambda\cos\alpha)F_\xi + (-\sin\lambda\cos\alpha)F_\eta + (+\sin\alpha)F_\zeta \\
F_\gamma &= (+\cos\lambda\sin\alpha\cos\sigma - \sin\lambda\sin\sigma)F_\xi + (-\sin\lambda\sin\alpha\cos\sigma - \cos\lambda\sin\sigma)F_\eta + (-\cos\alpha\cos\sigma)F_\zeta
\end{aligned}\right\} \tag{24}$$

g_r = the radial component of the gravitational acceleration vector

g_θ = the horizontal component of the gravitational acceleration vector (positive in local due north direction)

F = vector of aerodynamic and thrusting forces.

The velocity vector is described in a relative velocity coordinate system. The relative velocity coordinate system ($\hat{i}_\beta$ - $\hat{i}_V$ - $\hat{i}_\gamma$ axes) has its origin at the current position of the aerospace vehicle point mass and its axes aligned as shown in the left side of the figure.

The associated elements of the state vector (elements 4, 5, and 6) are the relative velocity magnitude* v; and, defining the orientation of the relative velocity vector, the relative flight path angle, γ, and the relative azimuth, β.

The seventh element of the state vector is the vehicle weight ($\dot{w}$). Analytic and Tabular models are available to define w.

Vehicle attitude is defined by three attitude angles: roll (bank) angle, σ; pitch angle of attack, α; and yaw angle of attack, λ. If the vehicle axes ($\hat{\xi}$, $\hat{\eta}$, $\hat{\zeta}$) shown in the right side of the figure are initially aligned with the relative velocity axes ($\hat{i}_V$, $\hat{i}_\beta$, and $\hat{i}_\gamma$, respectively) then the vehicle attitude is defined by a sequenced rotation around the $\hat{\xi}$-$\hat{\eta}$-$\hat{\zeta}$ axes, consisting of:

1. A first rotation around the roll ($\hat{\xi}$) axis through the bank roll angle (σ).
2. A second rotation about the pitch axis ($\hat{\eta}$) axis through the pitch angle of attack (α).
3. A final rotation about the yaw axis ($\hat{\zeta}$) axis through the yaw angle of attack (λ).

A typical rotation is shown in the right side of the figure.

**Relative here means relative to an earth fixed rotating coordinate system.*

COORDINATE SYSTEMS AND ATTITUDE ANGLES

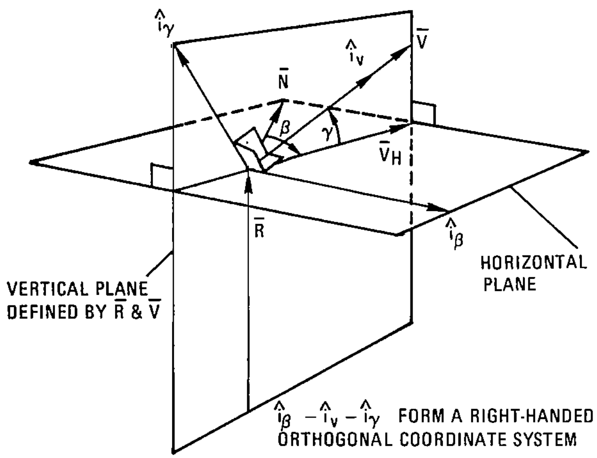

β = RELATIVE AZIMUTH
γ = RELATIVE FLIGHT PATH ANGLE
$\bar{N}$ = VECTOR IN HORIZONTAL PLANE POINTED NORTH
$\bar{R}$ = GEOCENTRIC RADIUS VECTOR
$\bar{V}$ = RELATIVE VELOCITY VECTOR
$\bar{V}_H$ = RELATIVE VELOCITY VECTOR PROJECTION IN HORIZONTAL PLANE

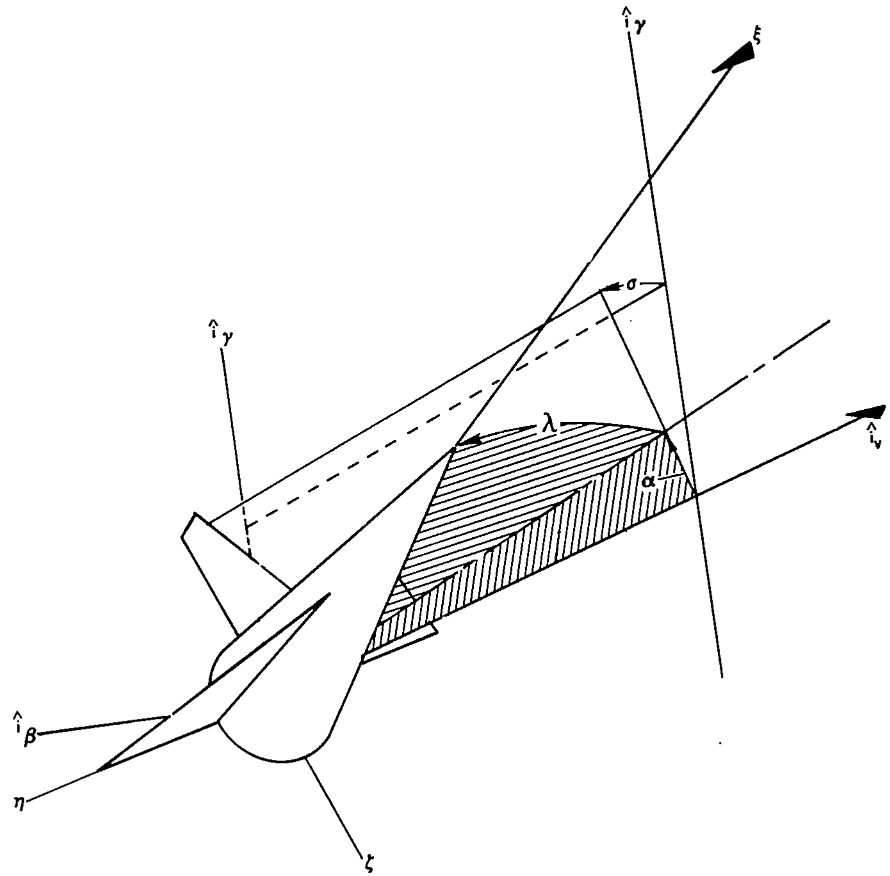

Figure 3

The central body total gravitational acceleration vector (g) is obtained directly from the central body gravitational potential energy function (U) by taking its gradient (∇U). The expression for U is shown in Equation 25.

The assumed gravity model includes up through the fourth harmonic term (N = 4) and assumes symmetry about the rotational axis. The corresponding expression for the gravitational components is $g_r = \partial U/\partial r$ and $g_\theta = -(\partial U/\partial \theta)/r$.

The local surface radius of the central body is defined by assuming the central body is an oblate spheroid with symmetry about the rotational axis and the equatorial plane shown at the bottom of the figure. This surface is described mathematically as a symmetric ellipsoid. The local surface radius (R_s) is then expressed as a function of the geocentric latitude (θ) from Equation 26 that defines the elliptic cross-section containing the rotational axis.

The atmosphere model is assumed to be static, that is, its characteristics are invariant with time. Two modeling methods are available. The first method utilizes n^{th} degree continuous expressions for the natural logarithm of the atmospheric density, the velocity of sound, and the atmospheric temperature, each as a function of altitude. The second method utilizes tables to define these quantities.

For suborbital velocities, the aerodynamic force coefficients are assumed to be dependent on Mach number (M_V) and the appropriate angle of attack (pitch or yaw angle of attack, α or λ, respectively). For near, or above, orbital velocities, the effects of viscosity can significantly affect the aerodynamic force. Examples of the latter occur during entry from orbit, synergetic maneuvers, and the terminal phases of ascent when the velocity is near orbital velocity. A realistic aerodynamic model that accounts for the effects of viscosity is available, as well as the standard velocity models. This model assumes that the aerodynamic force coefficients are dependent on the viscous parameter (P_V) and the appropriate angle of attack (α, or λ). The corresponding aerodynamic forces F_k are

$$F_k = C_k q A_k \qquad \text{for } k = \xi, \eta, \zeta$$

where A_k is the reference area

q is the dynamic pressure

C_k is the aerodynamic force coefficient

Several propulsion models are available. The models range from simplified models in which the vacuum thrust and propellant flow rate are constant to models in which the vacuum thrust, propellant flow rate, and engine throttling coefficient are tabular functions of generalized independent variables. Of particular use to the space shuttle ascent simulation is a model which automatically provides throttling to meet thrust acceleration constraints. For all models, the effective thrust is computed as a function of the atmospheric pressure.

CENTRAL BODY SURFACE GEOMETRY

$$U = -\frac{\mu_k}{r}\left[1 - \sum_{n=2}^{N} J_n \left(\frac{A}{R}\right)^n P_n\right] \tag{25}$$

where

A is the earth's equatorial radius
R is the geocentric radius magnitude
J_n is the n^{th} gravitational harmonic coefficient
P_n is the n^{th} Legendre polynominal in sin θ terms
μ_k is the gravitational field constant of the central body

$$R_s = \left[\left(\frac{\text{Cos}\,\theta}{A}\right)^2 + \left(\frac{\text{Sin}\,\theta}{B}\right)^2\right]^{-1/2} \tag{26}$$

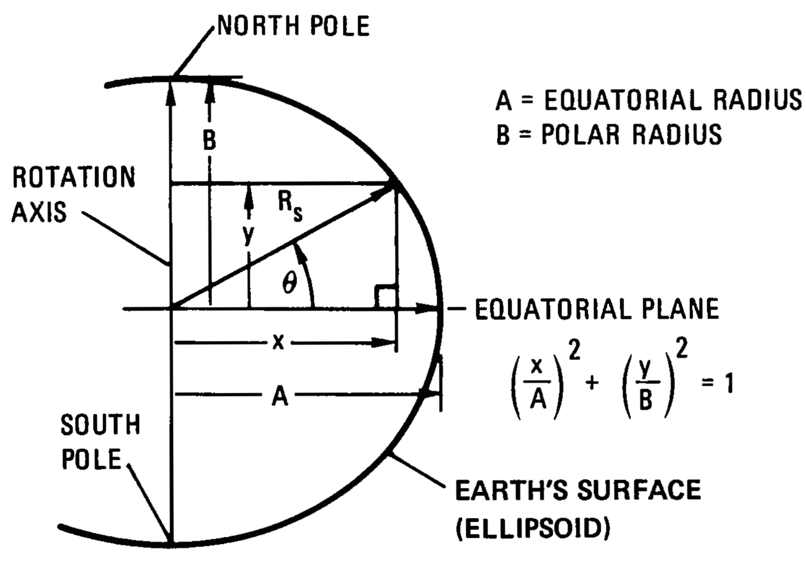

Figure 4

SPACE SHUTTLE BOOSTER RETURN EXAMPLE

An optimal space shuttle booster return trajectory was determined by using the GTOP computer program.[13] The trajectory was initiated at the staging point of a reference ascent trajectory. The following conditions were assumed:

Altitude = 74610.3 meters (244,784 ft.)

Velocity (relative) = 3299.2 meters/sec (10,824 fps)

Gamma (relative) = 5.654 deg.

Heading Azimuth (relative) = 182.495 deg.

Latitude = 32.788 deg.

Longitude = 239.343 deg.

Wing Area = 785.12 sq. meters (8,451 sq. ft.)

Weight = 349,942.9 kg (771,492 lb.)

Wing Loading (W/S) = 445.715 kg/sq. meter (91.29 psf)

Staging Time = 216.36 sec.

The aerodynamic force coefficients, C_ξ and C_ζ which were used are shown in the figure.

The problem is to minimize the distance of the Space Shuttle booster from the launch site after the booster has completed re-entry (altitude = 6096.0 meters (20,000 feet)). Minimizing this flyback distance minimizes the jet fuel required to execute the powered return to the launch site. Clearly, the less flyback fuel required, the grea he payload injected into orbit.

The entry trajectory for the Space Shuttle booster configuration was constrained by five state variable and control variable inequality constraints:

Total acceleration load factor $\leq$ 4g

Dynamic pressure $1/2\,\rho V^2 \leqslant 2441.2$ kg/sq. meter (500 lb./sq. ft.)

Instantaneous heating parameter $1/2\,\rho V^3 \leqslant 4.762 \times 10^6$ kg/sec. meter (3.2×10^6 lb./sec. ft.)

Angle of attack $\geqslant$ 0 deg.

Angle of attack $\leq$ 90 deg.

The last two constraints were due to the unavailability of aerodynamic data outside of this region.

C_ξ AND C_ζ AS FUNCTIONS OF MACH NUMBER AND ANGLE OF ATTACK

α		-90.	0.0	4.0	8.0	12.0	16.0	20.0	25.0	30.0	40.0	50.0	60.0	70.0	90.0
0	C_ζ	2.2761	-.0264	-.1524	-.2819	-.4240	-.5679	-.6911	-.8473	-1.0127	-1.3349	-1.6549	-1.9581	-2.2761	-2.2761
	C_ξ	.0000	-.0408	-.0309	-.0101	.0274	.0785	.1186	.1469	.1459	.1671	.1909	.1916	.1719	.0000
.6	C_ζ	2.2761	-.0264	-.1524	-.2819	-.4240	-.5679	-.6911	-.8473	-1.0127	-1.3349	-1.6549	-1.9581	-2.2761	-2.2761
	C_ξ	.0000	-.0408	-.0309	-.0101	.0274	.0785	.1186	.1469	.1459	.1671	.1909	.1916	.1719	.0000
.9	C_ζ	2.8706	-.0240	-.1879	-.3501	-.5183	-.6909	-.8914	-1.1200	-1.3066	-1.6810	-2.0687	-2.4506	-2.8706	-2.8706
	C_ξ	.0000	-.0580	-.0638	-.0698	-.0768	-.0838	-.0925	-.1067	- .1232	- .1364	- .1171	- .0754	- .0073	.0000
1.2	C_ζ	2.9920	-.0490	-.2183	-.3892	-.5736	-.7704	-.9860	-1.2103	-1.3993	-1.7694	-2.1582	-2.5534	-2.9920	-2.9920
	C_ξ	.0000	-.1555	-.1543	-.1540	-.1543	-.1509	-.1397	-.1583	- .1736	- .1796	- .1661	- .1174	- .0248	.0000
3.0	C_ζ	2.7028	-.0400	-.1533	-.2704	-.3986	-.5344	-.6788	-.8645	-1.0648	-1.4892	-1.8972	-2.2940	-2.7028	-2.7028
	C_ξ	.0000	-.0900	-.0995	-.1135	-.1197	-.1224	-.1254	-.1265	- .1243	- .1211	- .1037	- .0866	- .0153	.0000
5.0	C_ζ	2.5590	.0000	-.0764	-.1743	-.2826	-.4039	-.5372	-.7231	-.9265	-1.3656	-1.7869	-2.1521	2.5590	2.5590
	C_ξ	.0000	-.0500	-.0598	-.0765	-.0933	-.1026	-.1163	-.1262	- .1348	- .1464	- .1574	- .1225	- .0449	.0000
8.0	C_ζ	2.3935	.0000	-.0710	-.1561	-.2639	-.3848	-.5216	-.7065	- .9004	-1.3335	-1.7276	-2.0652	-2.3935	-2.3935
	C_ξ	.0000	-.0400	-.0552	-.0689	-.0870	-.0977	-.1028	-.1119	- .1095	- .1081	- .0724	- .0630	- .0901	.0000
50.0	C_ζ	2.3935	.0000	-.0710	-.1561	-.2639	-.3848	-.5216	-.7065	- .9004	-1.3335	-1.7276	-2.0652	-2.3935	-2.3935
	C_ξ	.0000	-.0400	-.0552	-.0689	-.0870	-.0977	-.1028	-.1119	- .1095	- .1081	- .0724	- .0630	- .0901	.0000

Reference Area = 785.12 sq. meters (8451 sq. ft.)

The initial angle of attack and bank angle were each modeled by 12 parameters as a function of Mach number, a monotonic function of time for the entry. This independent variable yields nearly uniform sensitivities of the performance index (flyback distance) to variations in the control modeling parameters. Time is unsatisfactory in this respect as an independent variable. The controls were tabulated at the following Mach numbers: 0, 0.6, 0.9, 1.2, 2, 3, 4, 5, 6, 7, 8, 9, 11, and 50.

The initial guess on the optimal control histories was intentionally poor (figures 5 and 6) to demonstrate the insensitivity of the algorithm to initial guesses. The trajectory corresponding to the initial control estimate resulted in a flyback distance of 756.91 km (408.7 n.mi.) and experienced a maximum acceleration load factor of 5.0g. Two one-dimensional minimization searches were required to obtain a solution satisfying all constraints (called "initial feasible solution" in figures 5 and 6. Since no attempt is made to maximize performance when generating the initial feasible solution, the flyback distance for the initial feasible solution was 862.29 km (465.6 n.mi.). However, after one unconstrained function minimization ($r = 1.0$) the flyback distance was reduced to 732.10 km (395.3 n.mi.).

After three more unconstrained function minimizations (with $r = 0.1$, 0.01, and 0.001, respectively) the final control history shown in figures 5 and 6 was obtained with a corresponding flyback range of 684.87 km (369.8 n.mi.). The relevant trajectory parameters are shown in figures 7 to 10. Note that both the acceleration load factor and the dynamic pressure state variable constraints are simultaneously active. The ripples in the load factor constraint are due to the discretization of the control.

ANGLE OF ATTACK VERSUS MACH NUMBER

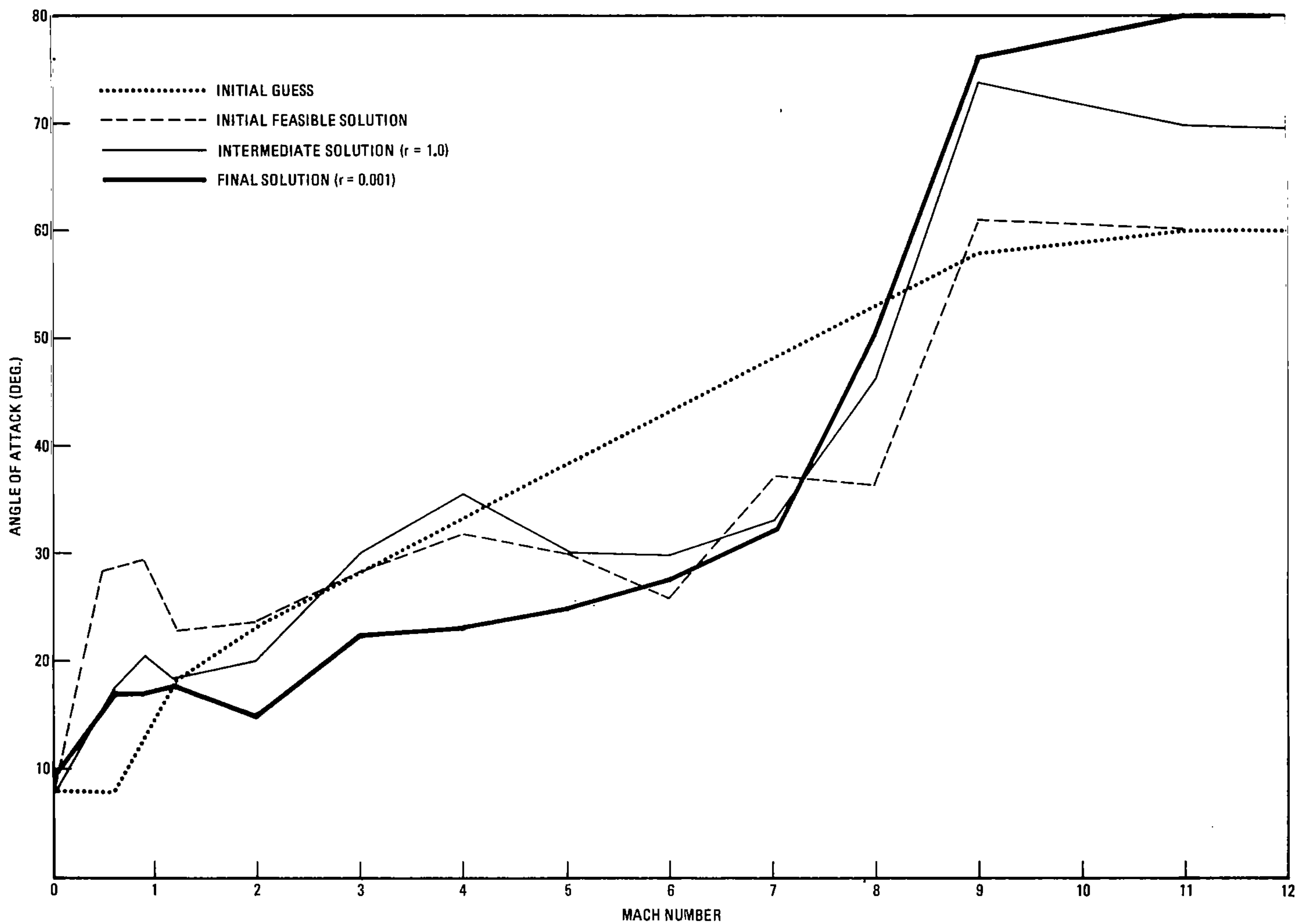

Figure 5

BANK ANGLE VERSUS MACH NUMBER

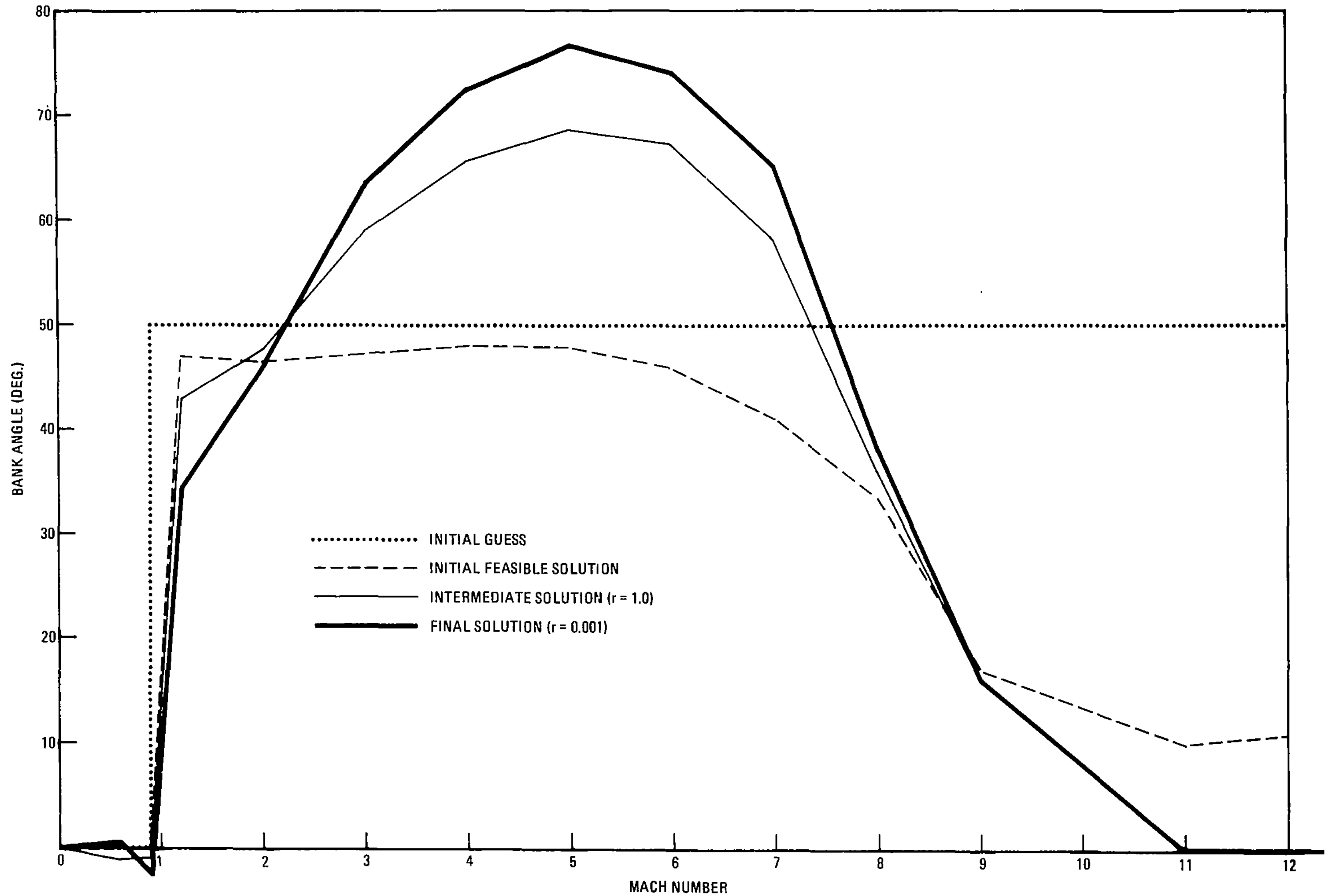

Figure 6

OPTIMAL MACH NUMBER AND CONTROL TIME HISTORIES

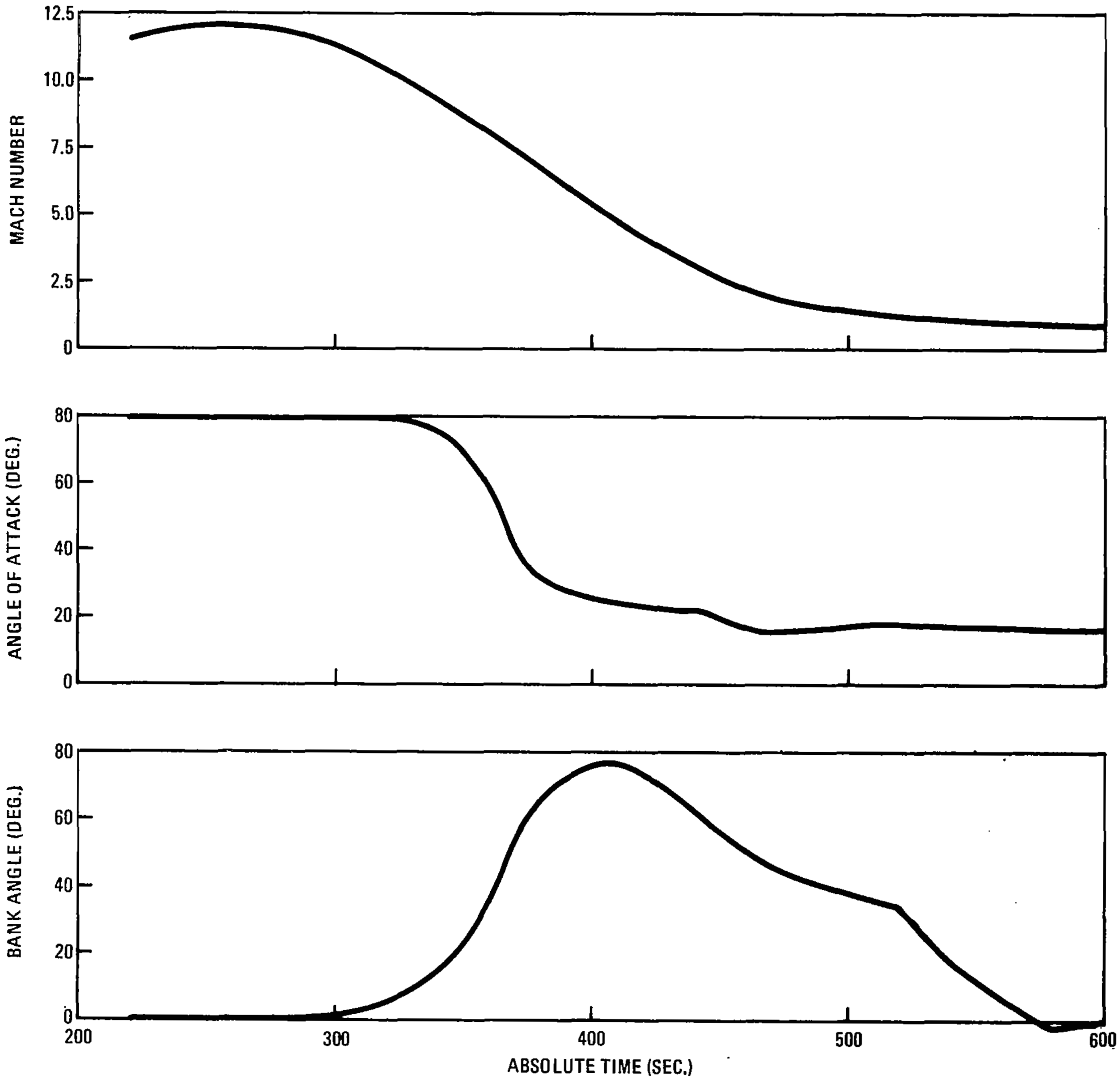

Figure 7

ACCELERATION LOAD FACTOR AND DYNAMIC PRESSURE CONSTRAINTS

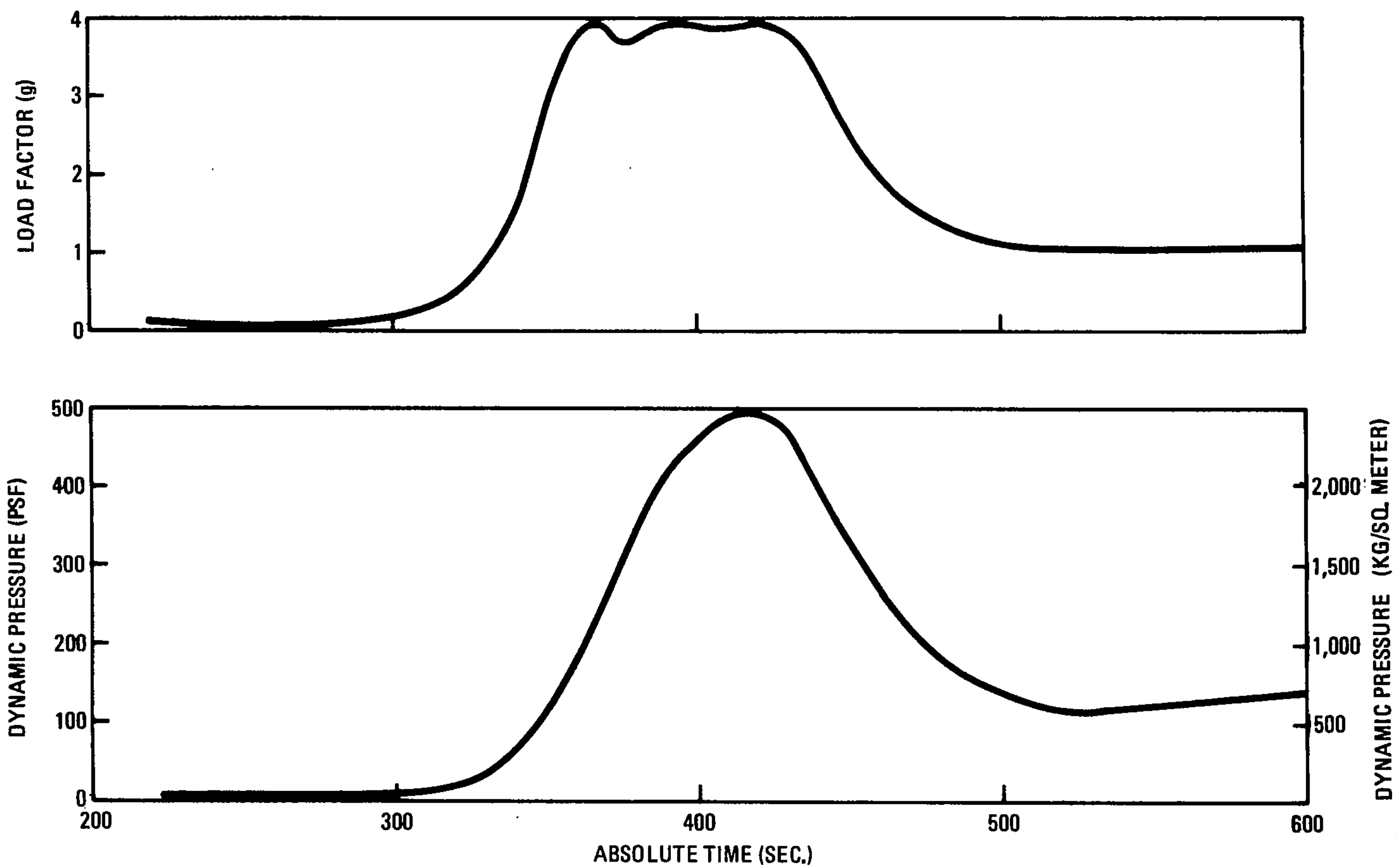

Figure 8

OPTIMIZED ALTITUDE AND RELATIVE VELOCITY TIME HISTORY

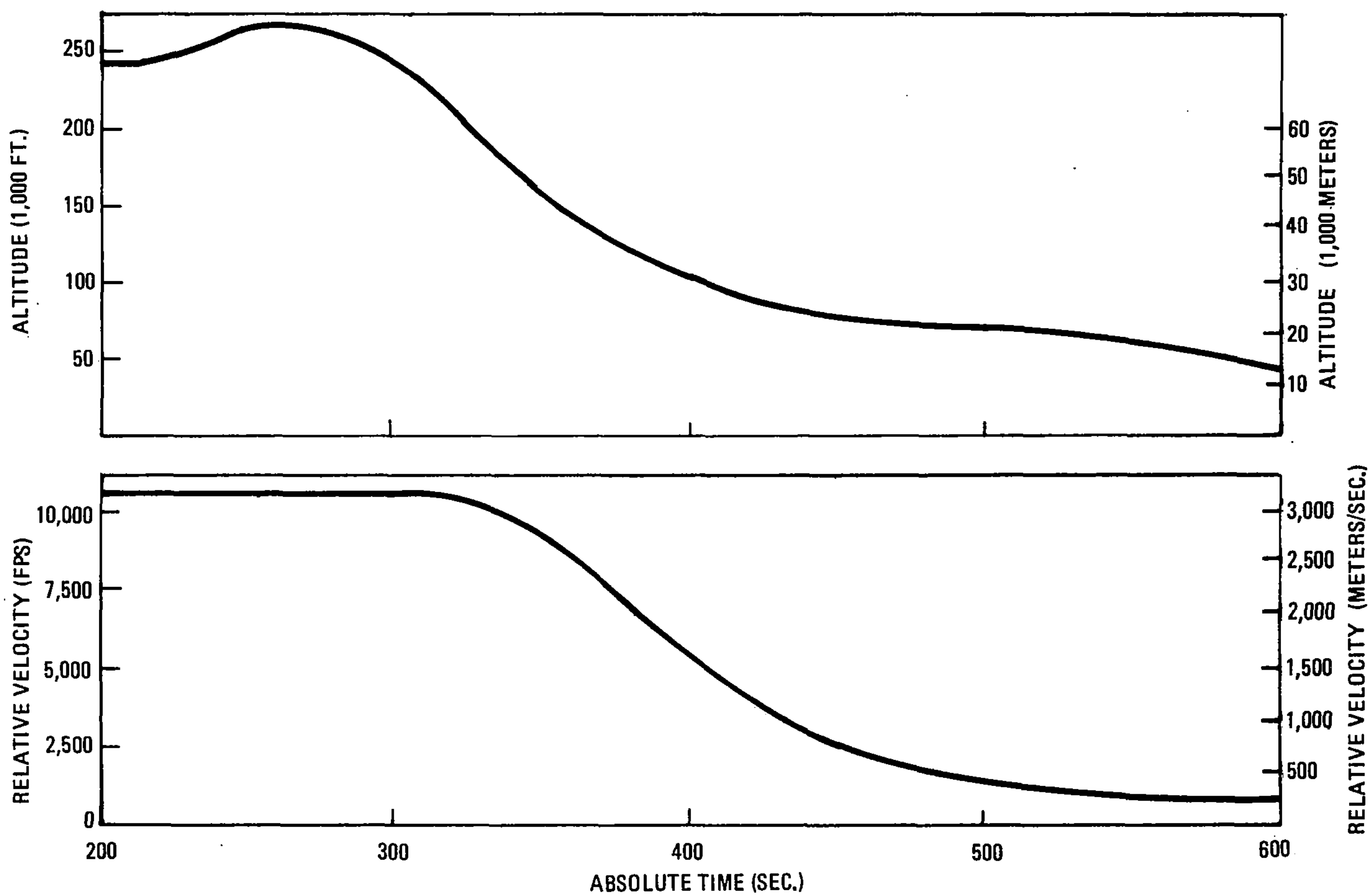

Figure 9

OPTIMIZED RELATIVE FLIGHT PATH ANGLE, AZIMUTH, AND DOWNRANGE DISTANCE

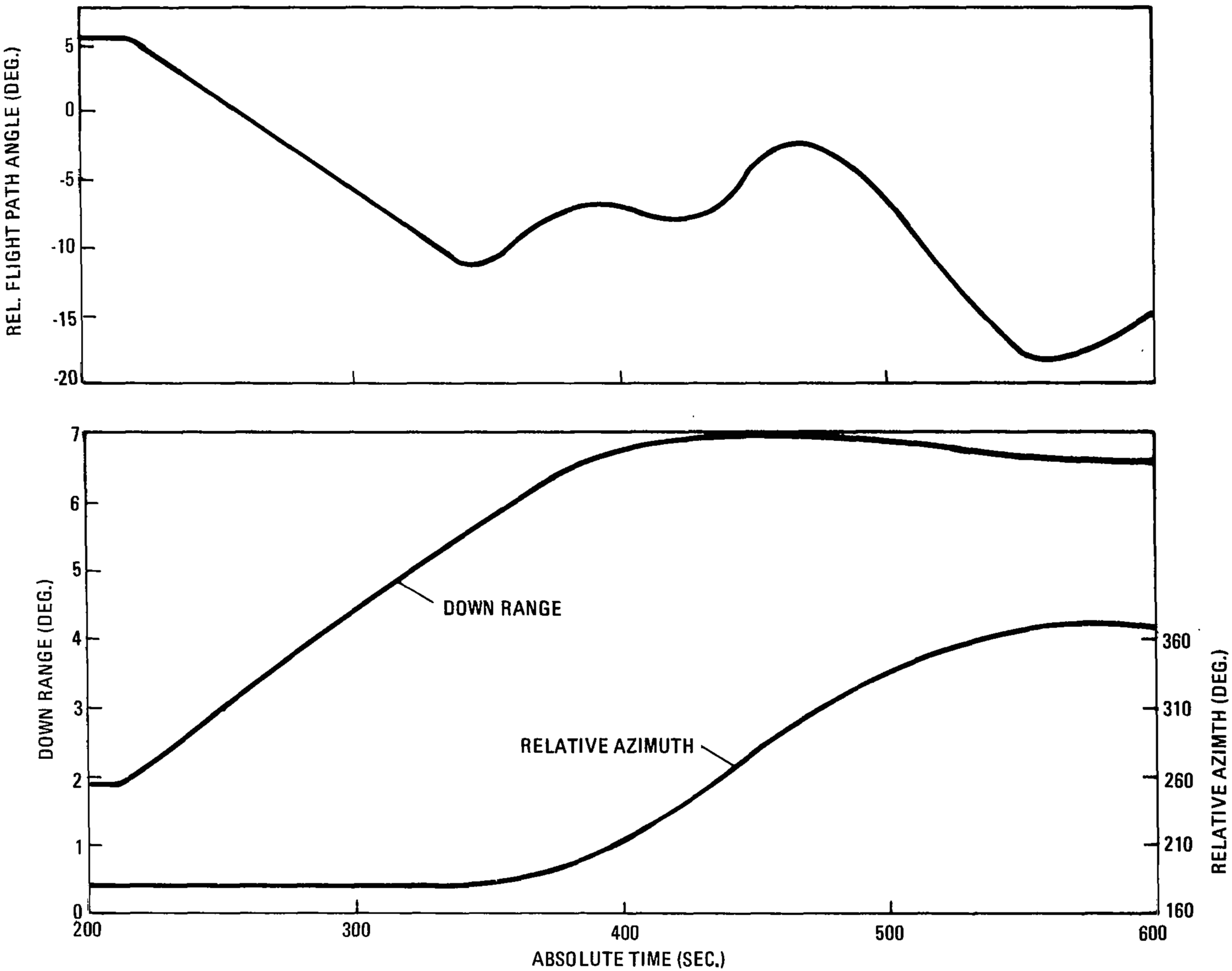

Figure 10

REFERENCES

1. Fiacco, A. V. and McCormick, G. P., *Nonlinear Programming: Sequential Unconstrained Minimization Techniques,* John Wiley & Sons, Inc., New York, 1968.
2. Fiacco, A. V., and McCormick, G. P., *Programming under Nonlinear Constraints by Unconstrained Minimization: A Primal-Dual Method,* RAC-TP-96, Research Analysis Corporation, September 1963.
3. Fiacco, A. V., and McCormick, G. P., "The Sequential Unconstrained Minimization Technique for Nonlinear Programming: A Primal-Dual Method," *Mgt. Sci.,* 10(2): 360-66 (1964).
4. Fiacco, A. V., and McCormick, G. P., "Computational Algorithm for the Sequential Unconstrained Minimization Technique for Nonlinear Programming," *Mgt. Sci.,* 10(4): 601-17 (1964).
5. Fiacco, A. V., and McCormick, G. P., "The Sequential Unconstrained Minimization Technique (SUMT) without Parameters," *Opns. Res.,* 15(5): 820-27 (1967).
6. Fiacco, A. V., and McCormick, G. P., "Extensions of SUMT for Nonlinear Programming: Equality Constraints and Extrapolation," *Mgt. Sci.,* 12(11): 816-29 (1966).
7. Fiacco, A. V., *Sequential Unconstrained Minimization Methods for Nonlinear Programming,* Ph.D. dissertation, Northwestern University, Evanston, Ill., June 1967.
8. Fiacco, A. V., *Penalty Methods for Mathematical Programming in E(N) with General Constraint Sets,* Research Analysis Corp. RAC-TP-385, 1969.
9. Fletcher, R., and Powell, M. J. D., "A Rapidly Convergent Descent Method for Minimization," *Computer Journal,* June 1963.
10. Guilfoyl, G., Johnson, I., and Wheatly P., "One-Dimensional Search Combining Golden Section and Cublc Techniques" *NASA* CR-65994, Jan. 1967.
11. Tramonti, L. G., Brusch, R. G., Schappelle, R. H., *Hypersonic Vehicle Trajectory Optimization,* Convair Aerospace Report GDC-ERR-1604, 1970.
12. Brusch, R. G. and Schappelle, R. H., "Obtaining Feasible Solutions to Inequality Constrained Control Problems," to be presented at the Fifth Hawaii International Conference on Systems Sciences, Honolulu, Hawaii Jan 11-13, 1972.
13. Brusch, R. G., "A Nonlinear Programming Approach to Space Shuttle Trajectory Optimization," *XXII Congress of the International Astronautical Federation,* Brussels, Belgium, Sept. 1971.